An Investigation of Droplet Evaporation Characteristics in an Ultrasound Environment

Mike Protheroe

A thesis submitted to Auckland University of Technology in fulfilment of the requirements for the degree of Doctor of Philosophy (PhD)

2014

Faculty of Design & Creative Technologies

School of Engineering

Institute of Biomedical Technologies (IBTec)

Primary Supervisor: Professor Ahmed Al-Jumaily

Abstract

This study investigates and quantifies the effect of an imposed ultrasound field on the evaporation of water droplets in, for example, humidifiers used in medical respiratory treatments. The purpose of the ultrasound field is to accelerate the droplet evaporation process. This would have benefits in terms of improved efficiencies, more compact equipment sizes and better process controllability. A preliminary investigation was carried out to identify the most promising mechanisms for the effect of the imposed ultrasound field on the evaporating droplets – this being the enhancement of the normal mass and heat transfer processes involved. From this, theoretical models of normal and ultrasound enhanced droplet evaporation were developed to predict the rates of water evaporation and also changes to the droplet size distribution during evaporation. An experimental investigation was carried out to measure water droplet evaporation rates and changes to the droplet size distribution under normal and ultrasound enhanced conditions. It was found that the ultrasound field improved droplet evaporation rates in all cases tested, even at very low power levels. Improvements varied from 1 – 30%. An increase in the strength of the ultrasound field increased the improvement in evaporation rate. However, air flow above a certain threshold diminished this improvement by disrupting the ultrasound field. Investigation of the changes to the droplet size distribution indicated that at high ultrasound power levels and low air flow rates a significant amount of droplet coalescence occurred which caused the droplet distribution for the remaining droplets to shift to much larger droplet sizes. Results from theoretical models compared well to the experimental results for most experimental conditions. Differences between model and experiment occurred for the very small droplet sizes and where the effect of the ultrasound field caused maximum droplet coalescence and heating of the air and these areas warrant further future investigation. It was concluded that the ultrasound enhancement of water droplet evaporation does occur by enhancing the heat and mass transfer processes involved, that improvements in evaporation rate up to 30% could be achieved and that this could be applied to medical respiratory equipment to improve its operation and efficiency.

Acknowledgments

Table of Contents

Attestation of Authorship

I hereby declare that this submission is my own work and that, to the best of my knowledge and belief, it contains no material previously published or written by another person (except where explicitly defined in the acknowledgements), nor material which to a substantial extent has been submitted for the award of any other degree or diploma of a university or other institution of higher learning.

_____

List of Figures

List of Tables

Nomenclature

Symbol	Property/Description and units
A	area (m²)
A_d	surface area of droplet (m²)
c	velocity of sound in the medium (m/s)
c_w	mass concentration of water vapour in air (kg/m³)
C_h	heat flux correction factor
C_m	mass flux correction factor
$C_{p,\infty}$	sp. heat capacity of the surrounding humid air (J/kg.K)
$C_{p,d}$	specific heat capacity of water in droplet (J/kg.K)
$C_{p,wvap}$	specific heat capacity of water vapour (J/kg.K)
d_d	droplet diameter (m), assuming spherical droplet
d_{tube}	diameter of tube (m)
$D[3,2]$	Sauter mean diameter (m) (see Table 2-1)
$D[4,3]$	volume mean diameter (m) (see Table 2-1)
$Dv10$	10th percentile diameter (m) (see Table 2-1)
$Dv50$	50th percentile diameter (m) (see Table 2-1)
$Dv90$	90th percentile diameter (m) (see Table 2-1)
D_w	diffusion coefficient for water vapour in air (m²/s)
$\dot{E}$	energy flow (W)
h	specific enthalpy (J/kg)
h_d	specific enthalpy of water in droplet (J/kg)
h_f	specific enthalpy of saturated liquid water (J/kg)
h_{fg}	specific enthalpy of vaporization of water (J/kg)
h_g	specific enthalpy of saturated water vapour (J/kg)
h_H	convection heat transfer coefficient (W/m².K)
h_M	convection mass transfer coefficient (m/s)
H	enthalpy (J)
j_w	mass flux of water vapour from droplet (kg/s.m²)
k	thermal conductivity (W/m.K)
k_f	thermal conductivity of the humid air (W/m.K)
K	mass transfer coefficient (kg/m²/s)

Symbol	Property/Description and units
Kn	Knudsen number ($= 2\lambda/d_d$)
Kn_h	thermal transport Knudsen number
Kn_m	mass transport Knudsen number
l	vibration mode number (2, 3, 4, …)
L	length of conduit (m)
m_a	mass of dry air (kg)
$\dot{m}_a$	mass flow rate of dry air in tube (kg)
m_d	mass of water in a single droplet (kg)
m_w	mass of water vapour (kg)
$\dot{m}_w$	mass flow rate of water vapour from droplet (kg/s)
m_∞	mass of surrounding humid air (kg)
$MMAD$	mass median aerodynamic diameter
M_w	molar mass of water = 18.015 (kg/kmol)
n	number of water droplets in distribution
N_{md}	droplet number concentration per kg dry air (/kg)
Nt	Number of discrete droplet sizes in droplet distribution
p	pressure, pressure amplitude (Pa)
p_0	total pressure inside conduit (= 101.325 kPa)
p_d	partial pressure of water vapour at the curved droplet surface (Pa)
p_s	partial pressure of water vapour above a flat surface (Pa)
p_∞	partial pressure of water vapour in the surrounding air (Pa)
Pr	Prandtl number
$\dot{Q}$	rate of heat flow (W)
r	radius (m)
r_d	droplet radius (m)
R_c	acoustic reflection coefficient
R_{th}	thermal resistance (°C/W)
R_u	the universal gas constant = 8,314.47 (J/kmol.K),
R_w	specific gas constant for water (J/kg.K),
Re	Reynolds number
Sc	Schmidt number
Sh	Sherwood number

Symbol	Property/Description and units
SMD	Sauter mean diameter (m) (see Table 2-1)
$Span$	measure of distribution width (see Table 2-1)
SPL	sound pressure level (dB)
t	time (s)
T_∞	temperature of surrounding humid air (K)
T_d	temperature of droplets and of humid air at the droplet surface (K)
T_w	temperature of water vapour (K)
v	velocity, velocity amplitude (m/s)
v_a	air specific volume (m^3/kg dry air)
V	volume (m^3)
$\dot{V}_a$	volume flow rate of air (m^3/s)
$\dot{V}_w$	volume flow rate of liquid water (m^3/s)
w_∞	specific humidity for surrounding air (kg water/kg dry air)
Z	acoustic impedance (Ns/m^3)
α_h	thermal accommodation coefficient
α_m	mass accommodation coefficient
ζ	air particle displacement amplitude (m)
λ	mean free path of gas molecules surrounding droplet (m)
μ	dynamic viscosity (Pa.s)
ξ_∞	dryness fraction of the surrounding air (= m_a/m_∞)
ρ	density (kg/m^3)
ρ_∞	density of the surrounding humid air (kg/m^3)
ρ_d	density of water droplet (kg/m^3)
ρ_w	partial density of water vapour in air (kg/m^3)
σ_d	surface tension of water (N/m)
ϕ_∞	relative humidity (RH) of the surrounding air
χ	mole fraction of solute
ω	frequency (rad/s)

Subscripts	
Symbol	**Property/Description and units**
d	relating to the droplet
f	final Value
i	initial value
j	Value for, or relating to, the jth sized droplet in the droplet distribution
∞	in the surrounding air, at some distance from
cond	conduction
conv	convection

Chapter 1 - Introduction

1.1 Introduction

This research investigates the effect of an imposed ultrasound field on the evaporation of water droplets. The purpose of the ultrasound field is to enhance or accelerate the evaporation process. Evaporation of liquid droplets is of key importance in, for example, spray humidifiers, spray driers, and liquid fuel combustors. By accelerating or enhancing the evaporation of the droplets then the time taken for this process could be reduced and this would have benefits in terms of improved efficiencies, more compact equipment sizes and better process controllability.

The proposed work involves imposing an ultrasound field on the droplets in the application so that the normal process of converting the liquid droplets to vapour is accelerated. It involves using ultrasound to produce micro-droplets (µm size-range) from water and using a second stage of ultrasound to assist in the subsequent conversion of these micro-droplets into vapour. Specifically, this research will investigate the effect of various ultrasound processes on the conversion of water from micro-droplets into vapour, for the purpose of humidifying an air stream.

1.2 Background

Current humidification methods used in many medical devices such as continuous positive airway pressure (CPAP) devices are based on a traditional convective heat transfer approach. However the industry desire is to seek an alternative method of humidification in the hope of achieving a more efficient and compact system. Humidification is essential in many medical therapy devices such as CPAP. This device is normally used for the treatment of sleep apnoea. Sleep apnoea is a condition where a person involuntarily stops breathing while they are asleep [1, 2]. This can occur when the soft tissues in the airways collapse and prevent the flow of air into and out of the lungs. The body responds by beginning to wake the person up so that they start breathing normally again. Usually the person does not fully wake but they do not remain in a deep sleep during the night so that when they do fully wake in the morning they still feel tired and are in fact lacking proper sleep. This can lead to health complications for the patient [2]. During treatment the patient wears a mask and is connected to the CPAP device via a breathing tube (Figure 1-1). The device consists of an air compressor, a

heater and a humidifier and supplies a flow of warm, moist air to the patient via the breathing tube and mask [3].

Figure 1-1: CPAP Device (courtesy F&P Healthcare Ltd)

By this means a positive pressure is maintained in the patient's respiratory tract which helps prevent the collapse of the airways and allows the patient to sleep normally. It has been found that warming and humidifying the air improves patient comfort and compliance [4]. Currently these devices are quite bulky and not particularly energy efficient. For example, to warm and humidify the air, in some CPAP devices, an uninsulated container of water is maintained at elevated temperatures and air is passed over the surface of the water. Heat transfer and moisture flow into the air provides the warmth and humidity for the air. This is simple and effective but not particularly energy efficient as heat is lost through the walls of the container to the environment and also the device is quite bulky. Controlling the air temperature and humidity to the correct levels can also be difficult, if changes occur in the environment or elsewhere, due to the thermal inertia of the mass of heated water. To improve the effectiveness of the CPAP devices it is desired to eliminate the large container of heated water and replace it with a system that is more compact, more controllable and more energy efficient.

1.2.1 Humidification methods

Most humidification processes involve contacting the unsaturated air with liquid water in such a way that some of the water evaporates into the air stream thus increasing the water content or humidity of the air. Energy is also supplied, usually in the form of heat, since the water is changing phase from a liquid to a gas. Simple methods of humidification involve passing the air over a bath of warm water or over a wetted surface. Often the wetted surface is of a porous or textured nature to give an extended

surface area and thus a greater rate of evaporation. In a medical environment, humidification of the air can be achieved by simply bubbling air through warm water. However, these methods tend to be large, bulky and not particularly energy efficient.

Another common method of humidification is to nebulise or atomise the water into small droplets and pass the air through a fine spray of these droplets. The large contact area between the small liquid droplets and the air allows for reasonably rapid transfer of water vapour into the air stream. The generation of the droplets can be achieved by several means including high pressure nozzles, spinning disks and so on but a more recently employed method involves the use of ultrasound transducers. These transducers are small, energy efficient and fast acting and were identified as the preferred method of droplet generation for this investigation. However, where nebulisation is used to humidify air in medical respiratory apparatus it is often important to ensure that all of the droplets have evaporated prior to inspiration by the patient. It takes a finite amount of time for the droplets to completely evaporate into the air and depending on the specific setup of the humidifier and the initial droplet size distribution it may require large chambers or lengths of delivery conduit to allow this to happen. By accelerating the droplet evaporation process it would be possible to reduce the chamber size or conduit length. In regard to this, it has been reported that the use of ultrasound techniques can enhance a number of chemical and physical processes [5, 6]. More specifically, subjecting large individual liquid droplets [7] and small vegetable pieces [8] to an ultrasound field has been found to accelerate the evaporation processes in these cases. Thus, in this current investigation it was proposed to pass the air and droplets from the nebuliser through an ultrasound field generated by a second ultrasound transducer in order to enhance or accelerate the conversion of these water droplets into vapour.

Physically, it is proposed that the air is flowing in a conduit, typically a breathing tube as used in medical respiratory apparatus. A nebuliser generates micro-droplets of water and these are combined with the air in the conduit. The air and water droplet mixture are then subject to an ultrasound field in order to accelerate the evaporation process. Such a system, that is nebulisation followed by evaporation enhancement, would be more compact in size and would eliminate the carryover of droplets to the patient. It also has the potential of being more energy efficient by eliminating the large mass of

heated water typically found in these devices. Furthermore, being fast acting, the system would enable more accurate control of the humidification process.

A system just like this, apparently, has not been proposed or studied before and with the benefits described give justification for the current investigation.

1.2.2 Other areas of application

A system like that described in the last section (1.2.1) could also have applications in other areas such as pulmonary drug delivery where medication is dissolved in water and nebulised into small droplets, combined with air and inhaled by the patient. The delivery of the medication to the ideal location in the respiratory system of the patient is dependent on droplet size [9], thus in this case it is not desired to evaporate all of the water droplets. However some evaporation will take place before the air becomes saturated and the droplet size distribution reaches an equilibrium state. The application of an ultrasound field to the mixture of air and droplets would enable the medicated droplet distribution to reach this equilibrium state more quickly and thus enable more compact and effective devices to be designed. Since droplet size is of critical importance in this application it would be important to be able to predict the droplet size distribution once it had reached equilibrium.

Also, changes to the droplet size distribution could be used to determine the progress of evaporation in other devices, such as humidifiers.

In liquid fuel combustion devices the liquid fuel is nebulised and the droplets must evaporate prior to combustion. The ultrasound field would enhance and accelerate the full evaporation of the liquid fuel prior to combustion taking place. This may well have implications for fuel efficiencies and improved performance.

In spray drying, liquids with dissolved solids are sprayed as small droplets into large chambers through which heated air is flowing. As the liquid droplets settle in the chamber the liquid portion evaporates so that at the base of the chamber only dry, solid particles remain. These chambers are typically of large proportions (depending on throughput) so acceleration of the drying process may have significant benefits in terms of reducing equipment sizes and costs.

1.3 Investigation

Liquid droplet evaporation and more specifically, water droplet evaporation has been studied in a range of scenarios. Also, although some studies have also been carried out on the effect of acoustic sound fields on evaporation it has usually involved individual, large (mm size range) water droplets or sprays of small liquid droplets other than water (e.g., liquid fuels). However the use of an imposed ultrasound field to enhance the evaporation of many small water droplets (such as that produced by an ultrasonic nebuliser) into air flowing in a conduit is relatively new.

This research focusses on using ultrasound in two stages to generate relatively small liquid droplets which evaporate and produce humidified air. Theoretical modelling as well as experimental work are to be undertaken to investigate the effect of an ultrasound field on droplet evaporation. The models would allow the determination of droplet lifetimes, characterisation of droplet size distributions as the droplets evaporate and determination of the effect of the evaporated liquid on the surrounding environment or carrier gas. It is intended that the models be used to quantify the energy requirements and operating parameters for use in the design of a new type of humidification apparatus and pulmonary drug delivery apparatus. It would also have possible application to other processes including liquid fuel combustion devices, spray driers and larger scale humidifiers.

1.4 Research objectives

Although the main objectives of this research will be detailed at the end of Chapter 2, this section gives an overview of the aims of the proposed investigation:

1. Preliminary investigation – investigate normal evaporation processes and then the proposed mechanisms for the enhancement of the water droplet evaporation using an ultrasound field. How is it going to work? Which mechanisms are more likely to occur or be most effective?

2. Quantify the evaporation process of the ultrasound generated droplets. Theoretical and experimental investigations will be used to achieve this objective.

3. Quantify the effect of a second stage ultrasound in enhancing the evaporation process. Theoretical and experimental investigations will be also used to achieve this objective.

Chapter 2 - Literature Review

2.1 Introduction

This study investigates the use of ultrasound techniques on water droplet generation and evaporation. The goal being to enhance or accelerate the evaporation of the water droplets and to predict changes in the droplet size distribution during the evaporation process. This has application to respiratory, humidification and pulmonary drug delivery devices in terms of efficiency, process controllability and equipment size.

In this chapter the background and prior research to this current study are detailed. It includes an explanation of water droplet generation, droplet evaporation and it details the mechanisms to be investigated for evaporation enhancement when the ultrasound field is imposed on the droplet and air mixture. Finally a summary of the detailed aims of the study are provided.

2.2 Water droplet generation (nebulisation) using ultrasonic transducers

The focus of this investigation is the use of ultrasound techniques in droplet generation and to accelerate the evaporation of these water droplets. Thus a thorough understanding of the mechanism of this nebulisation process could well provide insights into the subsequent enhancement of the evaporation of these droplets using an imposed ultrasound field. It also allows for the selection of the most suitable ultrasonic nebulisation technique for our study.

Nebulisation of a liquid (often referred to as atomisation in the literature) using ultrasonic techniques involves subjecting the liquid to mechanical vibrations at frequencies in the ultrasound range. The effect of the vibrations is to cause the water to break up into very small droplets. The mechanism for this break up depends on the technique used. The common techniques used in ultrasonic nebulisation involve the use of either flat plate or vibrating surface transducers [10-12] or transducers associated with micro-perforated plates [13-17]. Other, not so common techniques involve the use of ultrasound modulated two-fluid atomisation (UMTFA) devices [18], surface acoustic wave (SAW) devices [19], devices utilising the vibration of liquid in a small gap [20] and so on. These other, not so common techniques were not considered.

2.2.1 Flat plate transducers

Flat plate ultrasonic nebulisers exist in a range of geometries and be operated in different ways:

- The transducer consists of a flat circular plate (vibrating surface) submerged in a pool of liquid and during excitation a continuous fountain or column of liquid is ejected from the liquid surface [11, 21, 22]. Droplets are generated from the surface of the fountain into the surrounding air.

- In a similar arrangement the transducer consists of a flat circular plate (vibrating surface) open to the air. Small amounts of liquid are continuously dripped onto the plate where they disintegrate into many small droplets [23].

- The transducer is attached to one end of a shaft causing the shaft to vibrate in the axial direction [24, 25]. A capillary channel along the central axis of the shaft delivers liquid to the other end of the shaft (vibrating surface). Droplets are ejected directly from the vibrating end of the shaft.

In each of these cases very small liquid droplets are ejected from the surface of the liquid (that is, at the air-liquid interface). This phenomenon, along with other related ultrasonic phenomena was first reported in 1927 by Wood and Loomis [10]. Following their study, a number of researchers investigated the phenomenon in more detail in an effort to discover the mechanism of nebulisation. Some suggested that the mechanism by which the droplets were formed was due to the breakup of capillary waves on the liquid surface while others suggested that cavitation effects were the principle mechanism causing nebulisation. Later researchers [26-28] proposed that a combination of the two mechanisms, the so-called 'conjunction-theory', was most likely.

Capillary waves occur at and travel along the phase boundary or interface of two fluids where the form and propagation of the wave is mainly due to surface tension effects (rather than gravity effects). For example with water and air, small ripples forming on the surface of water as the result of a light breeze over the water are capillary waves. The action of ultrasound radiation on a liquid causes capillary waves to form at the liquid-air interface. If the intensity of the ultrasound is high enough, then the wave peaks disintegrate or break off and form small droplets. The capillary wave mechanism became firmly established after Lang's investigations in 1962 [21]. He investigated the

application of ultrasound to both thin films of liquid and to a deep pool of liquid and proposed that the median droplet size produced was proportional to the capillary wavelength on the liquid surface. He presented an equation in terms of fluid properties, driving frequency and an experimentally determined factor (0.34) which is still in use today:

$$D = 0.34 \left(\frac{8\pi\sigma}{\rho f^2}\right)^{1/3}$$

(2-1)

Where D = median droplet diameter, σ = surface tension, ρ = density and f = frequency of excitation.

Subsequent photographic studies [12, 29], experimental and theoretical studies [11, 12, 23-25, 28-30] confirm that capillary wave breakup is certainly a factor in the formation of droplets in ultrasonic nebulisation. Most of these researchers attribute the breakup of the capillary waves to some form of temporal instability of the wave such as Rayleigh-Taylor instabilities or Faraday instabilities.

Cavitation in a liquid is the formation and subsequent rapid collapse of a vapour bubble in a region of the liquid where the liquid pressure varies below and above the vapour pressure of the liquid. In this case the gas in the bubble is the vaporised liquid. The expansion and rapid collapse of gas bubbles in a liquid that is subject to pressure variations can also be due to the presence of dissolved gases or other microscopic gas bubbles in the liquid. In the case of ultrasonic nebulisation the applied acoustic field generates oscillations in the liquid which in turn cause pressure variations. If these oscillations are of a high enough intensity, the pressure at specific points in the liquid can vary above and below the vapour pressure of the liquid thus causing cavitation. Although the presence of cavitation processes during ultrasonic nebulisation has been established [23, 26, 28, 31], the exact role of cavitation in the formation of droplets is not well understood. Studies suggest that the hydraulic shock of the imploding bubbles initiates breakup of the liquid film and/or stimulates the formation of capillary waves [28, 30]. It has been noted that some ultrasonic nebulisation devices produce a wide range of droplet sizes and researchers have proposed that cavitation is the main reason for this [25, 30, 32]. Cavitation effects may dominate when the driving frequencies are higher (MHz range) and when large amplitudes of vibration are used [28, 33]. The way the liquid is supplied or attached to the transducer surface (thin film, pool of liquid or

drop by drop) can also affect the relative contributions of the cavitation and capillary wave break-up mechanisms.

These two mechanisms, droplet generation from capillary waves and cavitation, may also have significance in the application of the ultrasound field to enhance the subsequent conversion of the droplets into vapour and is considered in section 2.4 and also in the mechanisms considered for further droplet breakup in Chapter 3.

Furthermore the power consumption of ultrasonic nebulisation can be reduced, for a given nebulisation rate, by using pulsed rather than continuous excitation [34]. This is of interest to this investigation in terms of minimising energy requirements.

In the case of the submerged flat plate transducers, the droplets are typically generated into a chamber and a flow of air through the chamber contacts with the droplets and is humidified. Droplets tend to be carried over into the outlet stream and it is difficult to accurately determine the initial droplet size distribution generated in such a device. This initial droplet size distribution would be required for input to a theoretical model and for comparison purposes in this investigation. Thus this style of droplet generation was deemed unsuitable for our study. The vibrating shaft transducer would lend itself to miniaturisation and measurement of the generated droplet distribution however these devices were not commonly available.

2.2.2 Perforated Plate Transducers

Perforated plate nebulisers were developed from the principles used in ink-jet printing technology [35]. The nebuliser in this case usually consists of a small chamber filled with liquid where one wall of the chamber is comprised of a perforated plate. There are a number of perforations (100's – 1000's) in the plate which are usually circular and of very small diameter (μm – size). In one arrangement an ultrasonic transducer causes the wall opposite the perforated plate to vibrate at ultrasonic frequencies [36] and in another arrangement the ultrasonic transducer causes the perforated plate itself to vibrate [15]. In both cases, since the liquid in the chamber is virtually incompressible, the effect of the vibrations is to extrude or force the liquid through the perforations whereby they break up into small droplets on ejection. One other arrangement dispenses with the chamber and consists of the perforated plate supported in a cantilever arrangement [14, 37]. A transducer at the supported end of the plate causes the plate to vibrate at ultrasonic frequencies. Water (or other liquid) is fed onto the

vibrating plate and is extruded through the small holes thus generating a fine mist of small droplets.

The water extrusion process and the formation of the droplets after extrusion in these nebulisers are well studied [13, 35, 38] and a number of commercial medical devices are available [15]. These devices are compact, energy efficient and often used in medical respiratory equipment. As such they can be easily incorporated into situations similar to that being studied in this work. The method of generating droplets also lends itself to the accurate measurement of droplet sizes at the location they are being generated, which is a requirement for this investigation. Such a device was chosen as the means of droplet generation for our study and is detailed in Chapter 5.

2.3 Water droplet evaporation

The normal evaporation process of a water droplet into air is well understood and has been thoroughly studied [39-61]. As stated earlier one of the main applications of this research is biomedical lung supportive devices where humidity is essential for patients comfort. For such an application the water droplets and air are considered to be well mixed and flowing along a conduit. The conduit, for example being a breathing tube used in typical medical respiratory apparatus [62]. For this application it is assumed that initially the air and droplets are at the same temperature and since the droplets are very small it is assumed that they are stationary relative to the air and to each other. It is also assumed that the air surrounding the droplets is not saturated, thus allowing evaporation to take place. A water vapour concentration difference will exist between the air immediately adjacent to the surface of the droplets (which is usually assumed to be saturated) and the bulk air some distance away from the droplet surfaces. This concentration difference will cause diffusion of the water vapour away from the droplet surfaces to the bulk air. Liquid water at the droplet surfaces then evaporates to replace the vapour diffusing away from the surfaces (and maintain saturation conditions for the air at the droplet surface). The energy required to vaporise the liquid water initially comes from the internal energy of the droplets and so the droplet temperatures drop. Since a temperature difference now exists between the bulk air and the droplets, heat transfer by conduction occurs from the surrounding air to the droplets and in turn the air temperature also drops. This process continues until either the droplets completely

evaporate or equilibrium conditions are reached where the bulk air surrounding the droplets is saturated and at the same temperature as the remaining droplets.

If there is relative movement between the air and droplets then it may be necessary to consider conservation of momentum and the convection effects on the diffusion and heat transfer processes.

There is a large body of research in the area of droplet evaporation. The focus of our investigation is, regarding the droplets, on determining the amount of water evaporated from the droplets and changes to the droplet size distribution over time. Regarding the air surrounding the droplets the focus is on temperature and humidity changes. The outcome of the literature review for this section of the work is firstly to discover current understanding of the normal evaporation process and to give guidance in the development of suitable analytical modelling techniques for that process. Secondly, to discover currently recognised techniques for measuring the key parameters in this investigation, namely, droplet sizes and air temperature and humidity.

2.3.1 Single/Multiple Droplets

A significant amount of research has been carried out that involves the study of single droplets evaporating in a variety of scenarios, for example [51, 56, 63, 64]. In these cases it is usually assumed, since the droplet mass is relatively small, that the properties of the surrounding medium (usually air) do not change appreciably during the evaporation process. Thus the energy balance for the surrounding medium is ignored. Other studies involving multiple droplets and aerosols, for example [54, 65, 66], do allow for mass and energy changes in the surrounding medium. They allow for the coupling between the mass and energy balances for the droplets and the mass and energy balances for the medium surrounding the droplets. In our study where the many droplets are evaporating into air it is important that the coupling between mass and energy balances for the droplets and surrounding air is included in the model.

Some research focusses on the changes to the droplet size distribution between generation and after some time has passed [41, 67]. This has been identified as being of importance in, for example, aerosol drug delivery devices. Some of this research is experimental in nature and some analytical. Different methods of measuring droplet sizes have been investigated by various researchers [68-70] and the use of laser diffraction techniques is common in later research [67, 71].

2.3.2 Boundary Conditions

Since the proposed model will be used to primarily investigate medical breathing / drug delivery devices it is expected that the air and water droplets will be flowing along a suitable conduit, such as a tube. In reality the boundary conditions for the walls of the tube containing the evaporating water droplets and air are somewhere between adiabatic and isothermal conditions. Some studies assume isothermal conditions for the surrounding air [59, 72], especially if the water to air mass ratio is very small while others assume 'non-isothermal' conditions [45]. Adiabatic conditions are modelled for a limited number of cases in some research [73].

2.3.3 Fluid Properties

In any analysis, it must be decided how to handle the transport and thermodynamic properties of the fluids involved since temperatures and conditions can change during the process. Some studies [49, 59] assume that these properties remain constant for the duration of the evaporation process while others [72] appear to use variable values of these properties as the temperatures and humidities vary during the process. If constant properties are used then these properties must be evaluated at some suitable average temperature since the temperature of the air and the droplets will change during the evaporation process, depending on model assumptions and boundary conditions. Miller et al. [49] discuss in detail the importance of selecting an appropriate average temperature when determining fluid properties in a constant properties evaporation model if the accuracy of the solution is to be maintained. Often an iterative approach must be used to identify these suitable average values and this can be time consuming and subject to error.

Many studies do not clearly explain how they handle the determination of fluid properties or they may mention how one or two important properties are calculated. For example Dushin et al. [56] mention using the Clausius-Clapeyron equation to determine equilibrium vapour pressures and Xu et al. [74] mention using the Hyland and Wexler model for determining the thermodynamic properties of humid air.

For this investigation, to maintain accuracy, it was decided to determine all necessary fluid properties as temperatures and conditions changed during the evaporation process.

In regards to measuring fluid properties, measurement of air and water temperatures can be commonly achieved using RTD devices or thermocouples. A number of techniques are available to measure the humidity of air [75, 76] and it is commonly accepted that accurate measurement of the humidity near saturation is difficult. It is reported [77] that CMOS based sensors for measuring air humidity give reasonable accuracy near saturation and also include on chip calibration for added accuracy. A CMOS based sensor was used in this investigation and is described in detail in Chapter 5.

2.3.4 Droplet Size

For larger droplets (mm-size range) their mass is such that in a gaseous medium inertia will cause them to move relative to the gas and so the heat and mass transfer processes will be convective in nature [78, 79]. For very small droplets (μm-size range) the droplets remain entrained in the gas and there is little or no relative motion between droplet and gas. In this case the heat transfer is conductive in nature and the mass transfer is by normal (Fickian) diffusion [78].

Additionally for very small droplets the curvature of the droplet surface has an appreciable effect on the equilibrium water vapour pressure above the curved surface. This elevation in vapour pressure is known as the Kelvin effect [41]. Since this investigation considers the evaporation of micro-droplets the Kelvin effect will be considered in the theoretical formulation (see Chapter 4).

If a droplet completely evaporates then during the final stages of its 'life' it will become extremely small such that it approaches the size range of the gas molecules surrounding the droplet (air and water vapour) and the assumptions behind Fick's Law diffusion no longer apply. This non-continuum effect on water diffusion (and also on conduction heat transfer) as the droplets become very small can be compensated for by using correction factors [43, 48, 80]. These correction factors are based on the Knudsen number, Kn (where $\text{Kn} = 2\lambda/d_\text{d}$, and where λ is the mean free path of the gas molecules surrounding the droplet and d_d is the droplet diameter). The correction factors are also dependant on the mass and heat transfer accommodation coefficients, α_m and α_h [51]. They are described in detail in the theoretical formulation in Chapter 4.

2.3.5 Areas of Application

Research on evaporation of fuel droplets in combustion studies [53, 81, 82] often includes complicating factors such as the multicomponent nature of the fuel and the very high efflux rates of vapour issuing from the droplets. For the latter factor it is necessary to allow for Stefan flow in any analysis being undertaken. These factors can usually be ignored for water evaporation.

Research in the area of aerosol based drug delivery [9, 67, 83] focusses on maintaining the droplet size distribution as droplet size is an important factor in determining the location of deposition in the respiratory tract. Since the passages in the respiratory tract and lungs can be convoluted many evaporation models include loss of droplets as a result of wall deposition.

Spray drying research tends to focus on the evaporation processes occurring as a result of the free fall of the droplets through a heated gas stream and the resulting vapour flows inside the spray drying chamber [84-86]. Much of the later research uses CFD techniques [86].

2.3.6 Methods of Solution

Various systems of equations and methods of solution have been used to determine changes in droplet size, changes in air humidity and other parameters during the evaporation process. The more complex solutions involve the application of the Navier-Stokes equations (continuity, momentum and energy conservation) to the evaporation process using a variety of analytical and finite element solution techniques [7, 46, 87, 88]. The less complex solutions involve simplified equation schemes (continuity and energy balances) using empirical equations to describe the heat and mass transfer processes [66, 79, 89].

Plug flow techniques are commonly used to analyse chemical and physical processes occurring in certain types of flow reactors [90]. In a limited number of cases [55, 73] it has been used to analyse the evaporation of droplets in flow along a conduit. This analysis technique lends itself particularly to the physical situation being studied in this work.

Non-equilibrium considerations are included by some researchers [56, 58]. It is not always clear what the 'non-equilibrium' is referring to but in many cases [49] it is

referring to the non-continuum effects when the droplet sizes become very small as discussed above in Section 2.3.4.

In this investigation a theoretical formulation of the normal evaporation process for water droplets into air flowing along a conduit was needed that could be modified to incorporate the effects of an imposed ultrasound field. The method of approach taken in this investigation was to use a more simplified formulation, ignoring momentum effects, but including effects relating to micro-droplets discussed above. The formulation is described in detail in Chapter 4.

2.4 Ultrasound enhancement of droplet evaporation

Acoustic and ultrasound techniques have been used to enhance various physical and chemical processes [5, 91, 92] and the mechanism of this enhancement varies from process to process. It is proposed in this investigation to pass a water droplet and air flow through an ultrasound field for the purpose of enhancing or accelerating the water droplet evaporation process. A number of possible mechanisms for this evaporation enhancement have been identified.

Firstly, simplified droplet evaporation theory predicts that single droplets will evaporate according to the so called D^2 law [50, 51]. That is, the time for a single droplet to evaporate is proportional to the square of its diameter. In reality the evaporation process will be subject to complicating factors (for example, changes in the surrounding air conditions, Kelvin effect, non-continuum effects and so on) but it is still expected that the smaller droplets will evaporate and reduce in size more quickly than the larger droplets under the same conditions. Also, for a given volume of water converted into droplets the surface to volume ratio for smaller droplets is much greater than for larger droplets. The larger surface area allows for greater rates of heat and mass transfer in the evaporation processes. So, the normal evaporation process would be accelerated if the droplets were broken down into even smaller droplets. From the literature (references given in the following sections), three possible mechanisms were suggested for this disintegration process:

1. Excite the droplets in air at their resonant frequency and at large enough amplitudes to cause self-disintegration.

2. Squeeze the droplets in air: apply enough sound pressure to squeeze, flatten and ultimately disintegrate the droplets.

3. Impinge the droplets on a solid surface, either stationary or vibrating at an ultrasonic frequency, to disintegrate the droplets into even smaller droplets.

Secondly, rather than physically disintegrating the droplets, the ultrasound field could enhance the normal heat and mass transfer processes that occur during evaporation. This would occur by causing greater relative movement between the air and water droplets thus promoting convection mass and heat transfer processes. This would accelerate the evaporation processes.

Prior research for these mechanisms is considered in detail in the following sections

2.4.1 Resonant excitation and disintegration in air

It has been reported [93, 94] that a single droplet of water, acoustically levitated in air, can be made to oscillate (i.e. shape oscillations) and eventually self-disintegrate. The droplet was held suspended in air by means of an ultrasound levitator and the levitation signal was modulated with an acoustic signal close to one of the resonant frequencies of the droplet. The droplet was observed to oscillate and with a strong enough modulation signal it could be made to self-disintegrate into many smaller droplets.

Determining the modes of vibration and associated frequencies for a free liquid droplet has been the subject of a number of investigations. In 1879 Rayleigh [95] was the first to investigate this, both experimentally and theoretically. From a theoretical perspective he developed an equation for the frequency of small amplitude vibrations of a free, spherical inviscid liquid droplet

$$\omega = \left(\frac{l(l-1)(l+2)\sigma}{\rho R^3} \right)^{1/2} \tag{2-2}$$

Where ω = frequency of vibration, l = mode number = 2, 3, 4, ..., σ = surface tension, ρ = density, R = droplet radius.

Subsequently, other researchers have also studied the problem from an experimental and a theoretical perspective. From an analytical perspective a range of different numerical and computational methods for analysing oscillations of liquid drops have been developed. These include the Marker and Cell method [96], the boundary integral

method [97] and Galerkin's method [98, 99]. Each of these have their particular strengths and weaknesses but all give reasonable agreement between theory and experimental results.

Various studies in this area [97-102] have identified the following key points, which will influence the proposed disintegration process: aperiodic behaviour of the oscillations, resonant mode coupling phenomena (one mode of oscillation excites the droplet at another mode of oscillation), asymmetry of the oscillation amplitude, dependence of the oscillation frequency on the amplitude of oscillation and other non-linear oscillation effects. These effects have been thought to be caused by the influence of liquid viscosity, effects of the fluid surrounding the droplet and effect of fluid circulation within the droplet and as expected, on the amplitude of oscillation (i.e., large amplitude oscillations increase non-linear effects) [100]. Of particular interest are studies relating to large amplitude oscillation behaviour. In this case the large amplitude oscillations can lead to droplet breakup [97-100].

Some studies have considered the effects of viscosity, which influences the frequency and damping of the oscillations [101]. They also found that viscosity has less effect as the droplet gets smaller. Other studies have considered the effect of internal recirculation of fluid inside the droplet during oscillation [102].

Some theoretical studies have considered non-linear effects on the oscillating droplets [98, 99, 102]. Other studies have covered the range of small to medium and large oscillations, the latter leading to droplet breakup [98, 102]. These studies were confirmed experimentally [100, 103].

A common observation amongst these works is that as the amplitude of oscillation of the liquid droplet increases, the resonant frequency decreases and as the droplet size reduces, the effects of viscosity and internal circulation change (become less important). Another finding is that a pressure impulse may be more effective in causing droplet breakup than a steady irradiation of ultrasound.

All the studies mentioned have investigated individual, large (mm-size droplets) as these were more relevant to their investigation and of course easier to observe. In the current work it was necessary to investigate if an imposed ultrasound field could be used for the resonant break up of many, much smaller sized (~ 5 μm) micro-droplets. This is detailed in Chapter 3.

2.4.2 Acoustic squeezing and disintegration

It has also been reported in the literature [104, 105] that a single droplet of water, in a similar situation to that described in the previous section, can be acoustically squeezed to the point where it flattens out and eventually self-disintegrates. The ultrasound levitator produces an ultrasound standing wave which generates an upward ('levitation') force on the droplet if it is placed close to one of the pressure nodes of the standing wave. In the right conditions the levitation force balances the weight force of the droplet and it is held stationary, in air, in the device. The squeezing of the droplet is governed by the combined actions of the droplet surface tension, the acoustic pressure acting on the top and bottom of the droplet and suction stresses acting at the horizontal circumference of the droplet [104]. The latter suction stresses are caused by the Bernoulli effect of acoustic streaming flows around the droplet. It was found that disintegration involves the edge of the droplet being drawn out into a sheet which thins, vibrates and ultimately shatters – this process taking less than 0.5 ms [104]. It was also found that the onset of disintegration is determined by the critical acoustic Bond number, $B_{\text{a,cr}}$ (ratio of acoustic force to surface tension force),

$$B_{\text{a,cr}} = \frac{A^2 R_{\text{s}}}{\sigma \rho c^2}$$

(2-3)

where A = acoustic amplitude; R_{s} = spherical radius of the droplet; σ = surface tension of the droplet liquid; ρ = density of air and; c = sound speed in air [104].

This disintegration process can also be initiated on a stable, flattened droplet, in the levitator, by the application of an appropriate modulation frequency [94].

In the reported cases a single droplet was studied and the droplet was of relatively large (~ 1 mm size range) size. In the current work it was necessary to investigate if an imposed ultrasound field could be used for the acoustic squeezing and subsequent breakup of many, much smaller sized (~ 5 μm) micro-droplets. This is detailed in Chapter 3.

2.4.3 Solid surface excitation

In regard to the resonant excitation and disintegration of the droplets (as detailed in section 2.4.1) different means of improving the transfer of vibrations from the transducer to the droplet were considered. This could be achieved by bringing the

droplets into contact with a solid surface vibrating at ultrasonic frequencies. In fact this is one mechanism by which droplets can be generated using ultrasonic vibrations (see section 2.2.1). Exposure of these droplets to a second stage of ultrasound vibration from a solid surface may cause even smaller droplets to be generated.

A large body of work exists on the interaction that occurs when droplets come into contact with a solid surface [106-108] where a range of possible interactions can occur. These include attachment of the droplet to the surface, spreading out of the droplet over the surface, partial breakup of the droplet with partial attachment, bouncing of the droplet off the surface into several fragments (with possible partial attachment), disintegration of the droplet with some fragments remaining on the surface and some being ejected from the surface (bounce) and so on [107-109]. The interaction that occurs in a specific case depends on a range of factors and these include the droplet parameters: diameter, temperature, viscosity, density, surface tension and droplet impact velocity and impact angle. They also include the surface properties: surface roughness, surface temperature, surface hydrophobicity, surface compliance (elasticity) and so on. These parameters are usually combined into relevant dimensionless groups such as the Weber number, Reynolds number and the Ohnesorge number. Attempts have been made to correlate these numbers with the various interactions but in fact little correlation has been found [108]. However it is clear that under some circumstances the impact of a droplet alone on a solid surface can cause the droplet to break up into smaller pieces and be ejected from the surface. Also, if the surface is vibrating at ultrasonic frequencies this could well assist the further disintegration of the droplets. This needed to be investigated for the current work and is addressed in Chapter 3.

2.4.4 Enhance normal heat and mass transfer processes

It has been reported that the application of an acoustic field to a suspended droplet can enhance and accelerate the evaporation of that droplet. Early analytical and experimental research using an acoustic field in the audible range (< 20 kHz) indicated that the diffusion kinetics involved in evaporation can be intensified by the effect of these acoustic oscillations [110]. Increases of up to 90% in the Nusselt number were observed when large amplitude (relative to droplet size) acoustic waves were applied to large droplets evaporating in a gas flow [111]. In that study, a single large droplet (0.8

– 2 mm) was mechanically suspended in the gas flow in a low frequency (80 to 700 Hz) acoustic field applied transverse to the gas flow

For smaller droplets, where the evaporation process is dominated by conduction mechanisms (rather than convection) research has considered the relative motion between the oscillating gas particles and the small fluid droplet when subject to acoustic radiation. Provided the particles are dense relative to the gas, from Stokes law it can be shown that the ratio of droplet velocity amplitude to gas particle velocity amplitude is given [112] by

$$\frac{U_{p0}}{U_0} = \frac{1}{\sqrt{1 + (\omega \tau_d)^2}} \tag{ 2-4}$$

Where

$$\tau_d = \frac{D^2}{18 \nu \delta} \tag{ 2-5}$$

And where U_{p0} = droplet velocity amplitude, U_0 = gas particle velocity amplitude, ω = acoustic frequency, τ_d = dynamic relaxation time (of the droplet), D = droplet diameter, ν = kinematic viscosity of the gas, δ = ratio of gas to droplet density.

If the evaporating droplets were irradiated with an acoustic field of large enough amplitude and with a frequency that ensured maximum relative motion between the gas particles and the droplets (i.e., $U_{p0}/U_0 \approx 0$) then it was found that the evaporation rate increased significantly [82, 113-115]. These studies covered droplets in the size range of around 20 μm to 200 μm and used acoustic fields of low frequency (75 – 600 Hz).

For cases where the amplitude of ultrasound field is large relative to droplet size (small Strouhal number) then oscillating flow can be considered to be quasi-steady and normal steady flow correlations for the convection heat and mass transfer coefficients can be used [111, 115].

In a related area, power ultrasound was used to enhance the drying of small vegetable pieces. The aim of that work was to determine the effect of the ultrasound field on water evaporation from the vegetable pieces [116-120]. The methodology in each of these studies is similar and involves suspending a basket containing a number of pieces of the specific vegetable inside a cylinder. Warm, dry air flows through the cylinder and over the vegetable pieces causing water to evaporate from them. A transducer attached to

the cylinder is used to generate an intense ultrasound field within the cylinder, the purpose of which is to accelerate the water evaporation rate from the vegetable pieces. The frequency of this ultrasound field is set at 21.8 kHz and the intensity of the field inside the cylinder can be adjusted between 0 and 37 kW/m^3. A weigh scale attached to the basket records the loss of weight of the vegetable pieces due to water evaporation over time. The apparatus was thus used to determine the improvement in water evaporation from the vegetable pieces as a result of the ultrasound field. Improvements in evaporation were found to range from 10% to >100% depending on ultrasound power level, air velocity and vegetable type.

The effect of the ultrasound field on water evaporation from the vegetable pieces was found to be in two areas [117]. Firstly the ultrasound field affects the diffusion of water from inside the solid vegetable pieces to the surface of the solid. The physical structure of the vegetable is alternately stretched and compressed by the ultrasound field (the so called 'sponge effect') which assists water transport to the surface of the vegetable piece. Secondly the ultrasound field affects the transport of water vapour from the solid surface to the air through proposed mechanisms of pressure variations, reduced boundary layer thickness, oscillating air velocities and micro-streaming [117]. It is this second effect that is applicable to the process of evaporation being investigated in the current study.

It was also noted by researchers that when a (larger) spherical particle was suspended in an ultrasonic levitator localised gas flow was generated around the suspended particle. This so called acoustic streaming flow occurs as a result of non-linear interactions between the oscillating gas and the particle. It usually occurs when the Strouhal number (ratio of the droplet diameter to the air particle amplitude in the sound field) is small i.e., large droplet and small air particle amplitude. This flow is partially recirculating, axisymmetric and in the case of a liquid droplet, can increase the convection heat transfer and mass transfer processes for the droplet [7, 111, 121-125]. Physically, the Stokes layer is believed to play an important role in the generation of these streaming flow patterns. Figure 2-1 shows typical streaming flow patterns for three different cases. (In the diagram S is the Strouhal number).
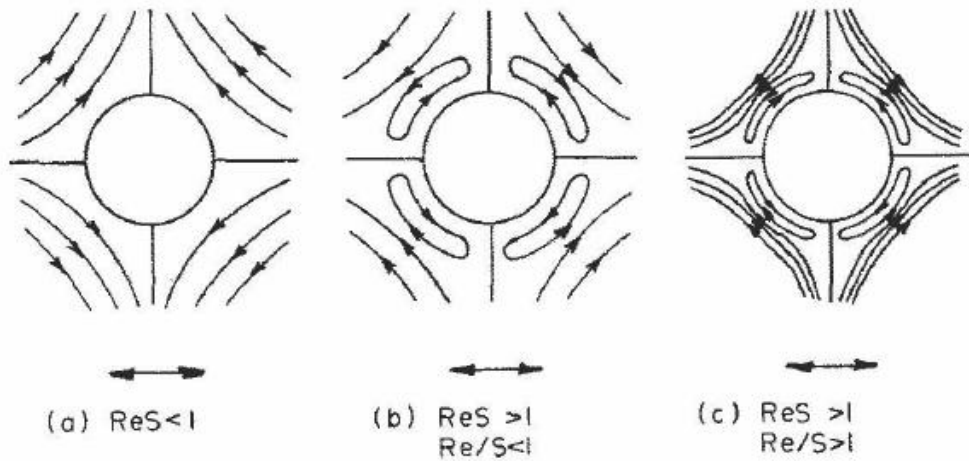
Figure 2-1: Flow patterns of steady streaming around a sphere [111]

In the case of evaporation of water droplets, significant increases in evaporation rate have been predicted and observed when the evaporating droplets are subjected to an acoustic field in an acoustic levitator. Most of these studies involved larger droplets. One study considered multi-droplet levitation and evaporation and it was found that the evaporation rate decreased as droplet spacing decreased [122].

When modelling the effects of the acoustic field on the evaporation processes some have attempted more analytical approaches [7, 110] while others have used approaches including empirical correlations [111, 115].

It is proposed in this research to investigate the possible enhancement of the evaporation of micro-droplets dispersed in air when irradiated with ultrasound at an appropriate frequency. It is noted in this case there is no problem with the impedance mismatch between air and water as the acoustic energy is being used to maintain air movement across the surface of the droplets rather than attempting to vibrate the droplets themselves.

2.5 Measurement of enhancement in evaporation

To experimentally investigate the enhancement in evaporation of the water droplets into air as they flow along a conduit and are subject to an ultrasound field this enhancement needs to be measured in some way. This could be achieved by measuring changes in the flow of the water droplets or by measuring changes to the humidity of the air however it may also be possible to determine the enhancement in water droplet evaporation by observing the changes to the droplet size distribution. In any case, measuring the droplet size distribution at the inlet and outlet of the conduit will give

some insight into the evaporation processes, for different sized droplets in the distribution and any enhancement that the application of ultrasound causes. Thus in this investigation it was decided to measure changes the droplet size distribution.

It should be noted that in the case of droplet evaporation, when comparing model results to experimental results, researchers [55, 59] tend to determine only one type of size distribution parameter (e.g.. the mass median aerodynamic diameter, $MMAD$ or $Dv50$) for comparison purposes. However in this investigation it was decided to determine a range of size distribution parameters so that further insight into the enhancement process for different droplet sizes could be determined.

2.6 Measurement and characterisation of droplet size distributions

In this section the accepted methods of determining the size distribution of an aerosol (small particles entrained in a gas) are discussed and the typical measures used to characterise such distributions are also detailed.

2.6.1 Droplet size distribution measuring techniques

In the case of aerosols, where the droplet sizes are in the micron range, as is the case in the current study, the measurement of the droplet size distribution presents a number of difficulties [126]. This is due to the small droplet sizes, their high number concentration and the fact that the droplets are moving with the aerosol. A range of methods have been used in the study of aerosols and include photographic techniques [69] impact/capturing techniques [127, 128] and optical techniques [71]. A summary of the range of techniques available is given by Black et al. [70]. A common method of determining the droplet size distribution, used in current research, is the use of a laser diffraction technique. In the laser diffraction technique particles are passed through a laser and the scattering pattern is measured by a number of detectors. These detectors are arranged at various scattering angles from the direction of the laser source. According to Mie light scattering theory for spherical particles a relationship exists between scattering angle, the intensity of the scattered light at that angle and the particle size distribution by volume. Such a device was selected for measurement of the droplet size distribution in this research and is detailed in Chapter 5.

2.6.2 Comparison of droplet size distributions

The laser diffraction technique generates percent volume data versus discrete droplet diameter for the droplet distribution. In the software that controls these devices it is possible for the user to select the number and range of discrete droplet diameters that are used in generating the droplet size distributions. The number of droplet size ranges (droplet size bins) in the distribution will vary depending on the distribution being measured or generated. After evaporation for example some of the smaller sized droplets will have completely evaporated and so disappear from the droplet size distribution.

In order to analyse changes in the droplet size distribution and also to compare experimental droplet size distributions with those generated by the theoretical evaporation models it was necessary to develop a valid means of comparing these distributions. This was achieved by comparing plots of percent volume versus droplet diameter and by comparing calculated distribution parameters

The percent volume and droplet size data can be plotted on semi-log axes and can be plotted in cumulative form. The cumulative form eliminates the effect of the different number of bin sizes (say when comparing a droplet size distribution at the inlet of the conduit with that at the outlet of the conduit when some droplet sizes will have disappeared from the distribution). However much of the finer detail for the different droplet sizes is lost in the cumulative distribution. Provided the change in the number of bin sizes is not too great then comparison between distributions using the normal non-cumulative plot is usually more informative.

Various distribution parameters can be determined for particle size, or in this case, droplet size distributions [50, 51, 129]. For the current study the following parameters have been chosen to describe the distribution: $Dv10$, $Dv50$, $Dv90$, $Span$, $D[3,2]$, $D[4,3]$ and are defined in Table 2-1.

These parameters have been chosen on the basis that they give information that is relevant to the current investigation. The $Dv10$ and $Dv90$ parameters give information about the tails of the distribution; the smallest and largest droplets. The $Dv50$ gives information about the median droplet diameter of the distribution (i.e., the middle sized droplets) and the $Span$ gives information about the spread of droplet sizes in the distribution.

Table 2-1: Droplet Size Distribution Parameters

Parameter	Definition
$Dv10$	The droplet diameter where 10 % of the volume of the droplets lies below this value. An indication of the size of the smallest droplets in the distribution.
$Dv50 - MMAD$	The droplet diameter where 50 % of the volume of the droplets lies below this diameter, that is, the median droplet size. For spherical droplets of water it is also known as the $MMAD$ or mass median aerodynamic diameter.
$Dv90$	The droplet diameter where 90 % of the volume of the droplets lies below this value. An indication of the size of the largest droplets in the distribution.
$Span$	$$Span = \frac{Dv90 - Dv10}{Dv50}$$ A measure of the width of the distribution
$D[3,2] - SMD$	$$D[3,2] = \frac{\sum_{j=1}^{Nt} n_j d_{d,j}^3}{\sum_{j=1}^{Nt} n_j d_{d,j}^2}$$ The weighted mean diameter based on surface area, also known as the SMD or Sauter mean diameter
$D[4,3]$	$$D[4,3] = \frac{\sum_{j=1}^{Nt} n_j d_{d,j}^4}{\sum_{j=1}^{Nt} n_j d_{d,j}^3}$$ The weighted mean diameter based on volume, also known as the mass mean diameter (since, in this case, all particles have same density)

A number of different mean values for a particle distribution can be determined but those selected for this study are the $D[3,2]$ and $D[4,3]$ which represent the mean droplet size based on surface area and the mean droplet size based on volume respectively. Both droplet volume and droplet surface area are important in evaporation studies.

2.7 Summary

The above literature review indicates the possibility of using an imposed ultrasound field to enhance the evaporation of water micro-droplets in air flowing along a conduit. Although a number of researchers have investigated the effect of ultrasound or acoustic

fields on the evaporation of liquid droplets none have considered the specific situation of the enhancing effect of ultrasound on the evaporation of a poly-disperse distribution of water droplets. Furthermore there are perceived gaps in current research in terms of, for example, accurate treatment of the fluid properties in the theoretical models.

The main objectives of this research, therefore are to investigate experimentally and theoretically the enhancing effect of an imposed ultrasound field on the evaporation of a poly-disperse distribution of water droplets into air as the air and droplets flow along a conduit. Specifically to quantify the changes in the amount of water evaporated and changes to the droplet size distribution as a result of the imposed ultrasound field.

The specific objectives of the research can be summarised as follows:

1. Investigate the mechanisms proposed in this chapter for the enhancement of the water droplet evaporation using an ultrasound field. This is detailed in Chapter 3.

2. Develop a theoretical model of the normal evaporation process for the situation being investigated – an air and water droplet mixture flowing along a conduit. The outputs from the model being used to determine the amount of water evaporated and changes to the droplet size distribution over the length of the conduit. This is detailed in Chapter 4.

3. Develop a theoretical ultrasound enhanced model to determine the effect of an imposed ultrasound field on the evaporation process for the situation being investigated. The outputs from the model being used to determine the amount of water evaporated and changes to the droplet size distribution over the length of the conduit. This is also detailed in Chapter 4.

4. Conduct an experimental investigation to quantify the amount of water evaporated and changes to the droplet size distribution for the normal evaporation of the ultrasound generated droplets and to compare these results with those of the theoretical model. This is detailed in Chapters 5 and 6.

5. Conduct an experimental investigation to quantify the effect of an imposed ultrasound field on the evaporation of the ultrasound generated droplets. Then to compare these results with the normal evaporation results and with results from the ultrasound enhanced model. This also is detailed in Chapters 5 and 6.

6. Analyse the results from the theoretical models and experimental investigations to better understand and to quantify the enhancement effect of the imposed ultrasound field on the evaporation of water droplets into air flowing along a conduit. This is detailed in Chapters 6 and 7.

Chapter 3 - Preliminary Investigation

3.1 Introduction

There is no clear trend in the literature regarding the effect of ultrasound on droplet evaporation especially in the context of many micro-droplets flowing in air along a conduit. While some literature focuses on single droplet size and breakup mechanisms, others focus on single droplet evaporation mechanisms. Therefore, it was felt that a thorough preliminary investigation is essential for better understanding of the whole process and to highlight the main contributing factors.

In Chapter 2 a number of possible mechanisms for the enhancement of water droplet evaporation as a result of an imposed ultrasound field were identified. This chapter details the preliminary investigation work on those mechanisms so that a suitable theoretical and experimental methodology could be developed. The first part of this chapter is a discussion arising from the literature review with respect to the development of a research approach. The research methodology is detailed at the end of this chapter.

3.2 Resonant excitation and disintegration in air

As detailed in Chapter 2 it has been reported that a large (mm size) droplet of water, acoustically levitated in air, can be made to oscillate (i.e., change shape) and eventually self-disintegrate. The droplet was held suspended in air by means of an ultrasound levitator and the levitation signal was modulated with an acoustic signal close to one of the resonant frequencies of the droplet. The droplet was observed to oscillate and with a strong enough modulation signal the droplet could be made to self-disintegrate into many smaller droplets. In the reported cases the droplets are relatively large so it was necessary in the current work to investigate the application of this air-excitation method to the resonant break up of much smaller sized (~ 5 µm) micro-droplets. The feasibility of this mechanism would depend on a number of factors: the droplet size and size range, the method of excitation, the droplet resonant frequencies and transmission of energy, by ultrasound, to the droplets. These factors are discussed in the following sections.

3.2.1 Droplet size range

Previous studies have dealt with only single droplets of a single size. However in this study many droplets with a range of droplet sizes are being dealt with. The method of exciting the droplets at their resonant frequencies has to be able to be applied to all of these droplets or at least a significant portion of them.

The droplet size range in the air/water droplet mixture depends on the specific device used to generate the droplets. A typical nebuliser like the Aerogen Aeroneb Solo nebuliser (see Chapter 5 for details) generates droplets that range in diameter from < 1 μm to around 60 μm with an $MMAD$ of around 4.5 μm, which is typical of ultrasonic nebulisers. A typical droplet size distribution for this device is shown in Figure 3-1 and associated droplet size distribution parameters for this distribution are given in Table 3-1. Thus, in this case, to excite a reasonable proportion of the droplets (80%) the method of excitation would need to be applied to droplets over a diameter range of around 1 – 10 μm.
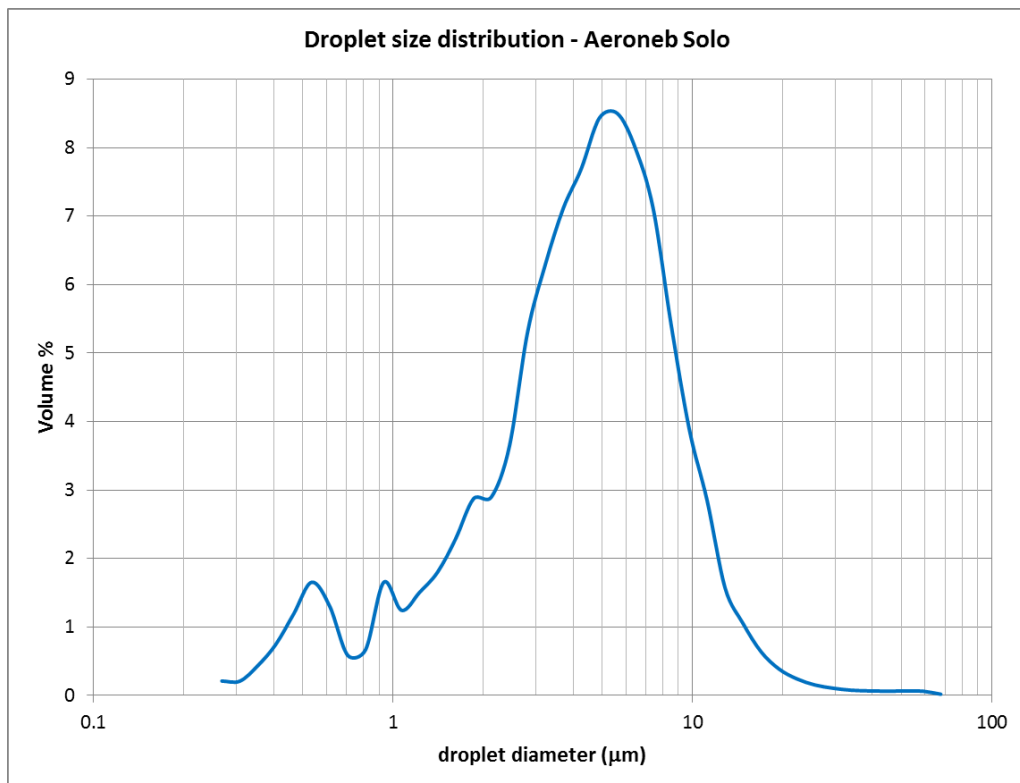
Figure 3-1: Typical droplet distribution for the Aeroneb Solo Nebuliser

Table 3-1: Droplet distribution parametersfor Aeroneb Solo nebuliser

Parameter	Value	
$Dv10$	1.15	μm
$Dv50$ - $MMAD$	4.46	μm
$Dv90$	9.53	μm
$Span$	1.88	
$D[3,2]$ - SMD	2.52	μm
$D[4,3]$	5.22	μm

3.2.2 Method of excitation

In the case of water micro-droplets in air, there is no need for acoustic levitation since the droplet sizes are such that they remain entrained in the air for reasonable periods of time. This can be shown by determining the terminal velocity of the droplets using Stokes law applied to a spherical particle settling in a gas [50] as follows

$$v_{\text{terminal}} = \frac{\rho_{\text{d}} d_{\text{d}}^2 g}{18\mu}$$

(3-1)

where v_{terminal} is the terminal velocity of the particle (m/s), d_{d} is the particle diameter, ρ_{d} is the density of the particle (kg/m³), g is the gravitational constant (9.81 m/s²) and μ is the dynamic viscosity of the gas (Pa.s). This equation is valid for particles of diameter 1 to 100 μm in air. For example, the terminal velocity of a 5 μm diameter water droplet in still air at 35°C is found to be around 0.7 mm/s. However the fewer larger droplets in the distribution will settle out more quickly, for example, for a 20 μm diameter water droplet in still air at 35°C the terminal velocity is around 11 mm/s.

To excite the droplets at one of their resonant frequencies it is considered that a suitable ultrasound air transducer be used. It would need to operate at a frequency close to the first or second resonant frequency of the droplets and be of sufficient power to induce large oscillations in the droplets. The majority of ultrasound transducers available use a piezoelectric element that is excited at one of its resonant frequencies. This means that a specific transducer would only be able to excite a small portion of the droplets at their resonant frequencies. A much smaller number of broadband transducers are available

that have a reasonable response over a range of frequencies and this type of transducer along with a suitable sweep signal would be required in this case.

3.2.3 Droplet resonant frequencies

As discussed in Chapter 2 the Rayleigh equation (2-2) gives the general relationship between a liquid droplet's diameter (or radius) and its resonant frequencies. It can be seen from that equation that the droplet resonant frequencies vary strongly with droplet diameter (d_d^3) and thus as the droplet diameter gets smaller the resonant frequencies increase rapidly.

Table 3-2 shows the Eigen frequencies for water droplets ranging in size from 1 to 10 μm in air. At smaller droplet diameters small changes in diameter lead to large changes in resonant frequency. For example, for droplets of water of say 5 μm and 4 μm diameter the resonant frequency for the fundamental mode ($l = 2$) is 973 kHz and 1360 kHz respectively.

Table 3-2: Eigenfrequencies (kHz) for water droplets in air

droplet diameter, d_d (μm)	Mode number (l)				
	2	3	4	5	6
1	10878.6	21066.2	32635.7	45508.3	59584.3
2	3846.2	7448.0	11538.5	16089.6	21066.2
3	2093.6	4054.2	6280.7	8758.1	11467.0
4	1359.8	2633.3	4079.5	5688.5	7448.0
5	973.0	1884.2	2919.0	4070.4	5329.4
6	740.2	1433.4	2220.6	3096.4	4054.2
7	587.4	1137.5	1762.2	2457.2	3217.3
8	480.8	931.0	1442.3	2011.2	2633.3
9	402.9	780.2	1208.7	1685.5	2206.8
10	344.0	666.2	1032.0	1439.1	1884.2

From the droplet distribution parameters in Table 3-1 it can be seen that 80% of the volume of water in the distribution lies between droplets of diameter 1.15 μm and 9.53 μm. For the fundamental mode of vibration this corresponds to a frequency range of around 400 kHz to 9 MHz which would be difficult to achieve even with a broadband

ultrasonic transducer. If just the larger sizes were targeted (e.g., 8 μm to 10 μm diameter), this would correspond to a frequency range of around 344 kHz to 740 kHz and this may be achievable by some broadband ultrasonic transducers.

3.2.4 Transmission of oscillations from transducer to droplets

There are three stages in the transmission of the excitations from the transducer to the droplets. Firstly from the transducer to the air, then transmission through the air to the droplets and finally from the air to the droplets. Each stage is now considered.

A number of manufacturers make piezoelectric and broadband transducers designed to operate in air. There is a large impedance difference between the transducer surface and the air. Thus, to maximise the transmission of ultrasound energy from the transducer to the air, impedance matching layers must be used on the surface of the transducer. However there are problems when used in an environment where water droplets are present, for example:

1. One manufacturer [130] of piezoelectric non-contact ultrasound (NCU) transducers designed to work in air states that their impedance matching layer is non-compatible with water/moisture so a special environmental protection layer would need be added. This reduces the efficiency of the ultrasound transmission to the air but does protect the transducer against water.

2. Another manufacturer [131] states that their NCU transducer will fail to work properly if any droplets or moisture condenses on the transducer surface. The surface will not be damaged (silicon) and once the moisture is removed it will return to its normal operation.

3. A manufacturer of a broadband non-piezoelectric transducers [132] states that their BAT transducers work well in air over a range of frequencies but can be damaged if the radiating surface comes in contact with the water droplets.

4. Many of these transducers are used in non-destructive testing (NDT) applications and so are of low power and may not be powerful enough to achieve droplet disintegration.

Thus, transducing ultrasound into the air is possible but the ultrasound energy transmitted may be limited.

Ultrasound transmittance through the air is attenuated significantly as the frequency of the ultrasound increases. Attenuation values for air at 35°C, 95% RH and 101.325 kPa are shown in Table 3-3 for a range of frequencies (from ISO 9613-1:1993 [133]):

Table 3-3: Attenuation of ultrasound in air

Frequency	Attenuation
50 kHz	1.24 dB/m
100 kHz	4.402 dB/m
500 kHz	52.73 dB/m
1000 kHz	179.9 dB/m

For ultrasound propagating at 1 MHz in air, the amplitude of air vibration (and hence energy of vibration) will reduce by 1.8 dB or to 66% of the original value over a distance of just 10 mm! Furthermore, the presence of liquid water droplets in the air will increase the attenuation significantly over these values. This means that the air/water droplet mixture would need to pass over the transducer in a thin layer, and be kept very close to the transducer, to maximise transmission of ultrasound to the droplets.

Finally the ultrasound energy transmitting through the air would need to be transmitted from the air to the water droplets. As with the transducer, there is a large impedance mismatch between air and water so only a small proportion of this ultrasound energy would be transmitted to the water droplet.

The acoustic impedance Z for a plane wave propagating through a medium is given by [134]

$$Z = \rho c \qquad\qquad (3\text{-}2)$$

where ρ is the density of the medium and c is the velocity of sound in the medium. For air at 35°C and ambient pressure $Z = 403.2$ Ns/m^3 and for water at 35°C and ambient pressure is $Z = 1.503 \times 10^6$ Ns/m^3. The reflection coefficient for transmission of plane acoustic wave from medium 1 to medium 2 with acoustic impedances of Z_1 and Z_2 respectively is given by [134]

$$R_c = \left(\frac{Z_2 - Z_1}{Z_2 + Z_1}\right)^2 \qquad\qquad (3\text{-}3)$$

Thus, for the transmission of a plane acoustic wave from air to water the reflection coefficient is $R_c = 0.9989$ i.e., only 0.1% of the energy will be transmitted to the water droplet!

3.2.5 Remarks – resonant excitation and disintegration in air

It seems clear that although the air-excitation of water droplets at their resonant frequency to induce self-disintegration is possible, especially for individual larger droplets, resonant disintegration becomes very difficult for water droplets that are very small (i.e., micro-droplets).

Firstly the excitation frequency varies strongly with droplet size (d_d^3) and the droplet sizes vary significantly for the output from a typical ultrasonic nebuliser. Thus a normal piezoelectric transducer (effectively 'one' resonant frequency) use to excite these droplets would be ineffective. Instead a special type of broadband transducer would be required to cover the range of frequencies needed.

Secondly the transmission of ultrasound from the transducer to the air, then through the air and finally from the air to the droplets suffers from significant attenuation at each stage of the transmission process. This is especially significant for the high frequency of ultrasound required to excite micro-droplets. Ultimately only a small fraction of the energy generated by the transducer is available to excite a water micro-droplet at its resonant frequency.

Resonant disintegration works for larger droplets because the resonant frequency required is low (in the audible range i.e., not ultrasonic) and although impedance issues still exist the attenuation in air over the distances involve (10's of cm) is negligible and reasonable transfer of energy to excite the larger water droplets is possible.

3.3 Acoustic squeezing and disintegration

It has also been reported in the literature [104, 105] that mm sized droplets of water, acoustically levitated in air, can be acoustically squeezed to the point where they flatten out and eventually self-disintegrate. The ultrasound levitator produces an ultrasound standing wave which generates an upward ('levitation') force on the droplet if it is placed close to one of the pressure nodes of the standing wave. In the right conditions the

levitation force balances the weight force of the droplet and it is held stationary, in air, in the device. The action of the acoustic levitation force in conjunction with the opposing weight force generates stresses that cause the droplet to deform in shape. If the amplitude of the levitation signal is increased the droplet is observed to change shape, flatten out until at some critical level the droplet disintegrates into many smaller droplets. This disintegration process could also be initiated on a stable, flattened droplet by the application of an appropriate modulation frequency [94].

In the reported cases the droplets are relatively large (~ 1 mm size range) and are individually levitated. However in the case of many water micro-droplets and air flowing along a tube it was difficult to envisage how an ultrasonic acoustic signal could be used to generate these squeezing forces over a large number of droplets or indeed if it was even possible. Furthermore, for larger (mm size) droplets the surface tension provides a very flexible surface to the droplet and inertia/viscous effects of the liquid inside the droplet tend to dominate. For micro-droplets the surface tension will provide a much stiffer, less flexible surface to the droplet relative to its mass and this will affect the ability to squeeze and disintegrate a micro-droplet. Therefore the application of this ultrasound mechanism to enhancing the evaporation process was not investigated any further.

3.4 Solid surface excitation and impact disintegration

It is apparent from section 3.2.4 that it is difficult to transfer enough energy from the transducer through the air to the droplets to achieve resonant disintegration. To overcome this problem it was proposed to use a solid surface (rather than air) vibrating at ultrasonic frequencies to transfer excitations to the droplets. When the micro-droplets come into contact with the surface they would either be excited at their resonant frequencies and at large enough amplitudes to cause self-disintegration or disintegrated into smaller droplets due to the velocity of vibration and impact. A further break up mechanism possibility is the generation of capillary waves or cavitation effects on the droplet as discussed in chapter 2. This technique has been used successfully to generate smaller droplets from single large (2 -3 mm diameter) droplets [135].

Of course the discussion in sections 3.2.1 on the droplet size range and in section 3.2.3 on the droplet resonant frequencies for air excitation applies to this case as well i.e., there is a large range of droplet sizes and a broadband transducer exciting the solid

surface would be required with a suitable sweep frequency generator to disintegrate a reasonable proportion of the droplets.

A second, related method of droplet disintegration, which could be called "impact disintegration", involves impinging the droplets onto a solid surface (not necessarily vibrating) at such a velocity that the droplets disintegrate and eject from the surface. This phenomena has been well studied [107, 108, 136-138] especially in regard to fuel droplets impacting on heated surfaces.

The feasibility of using a solid surface to excite the droplets or for impact disintegration depends on the interaction of the droplets with the solid surface and this is now considered.

3.4.1 Liquid droplet interactions with a solid surface

When a liquid droplet impinges on a dry solid surface (vibrating or stationary), a range of possible interactions can occur. These include attachment of the droplet to the surface, spreading out of the droplet over the surface, partial breakup of the droplet with partial attachment, bouncing of the droplet off the surface into several fragments (with possible partial attachment), disintegration of the droplet with some fragments remaining on the surface and some being ejected from the surface (bounce) and so on [107-109]. The interaction that occurs in a specific case depends on a range of factors and these include the droplet parameters: diameter, temperature, viscosity, density, surface tension and droplet impact velocity and impact angle as well as surface properties: surface roughness, surface temperature, surface hydrophobicity, surface compliance (elasticity) etc. These parameters are usually combined into relevant dimensionless groups such as the Weber number, Reynolds number and the Ohnesorge number and attempts have been made to correlate these numbers with the various interactions but little correlation has been found [108]. However at the low droplet velocities and surface temperatures, as is found in our study, the droplets will most likely attach to and spread out on the surface which will effectively prevent the droplet excitation process from occurring. Instead the vibrating surface will simply become covered with a layer of water. Preliminary calculations for the size of droplets used in our study confirmed this.

In the case of impact disintegration, the droplets would need to be impinged against the dry solid surface at much higher velocities to achieve droplet breakup, that is, a

'splashing' interaction. However even in the splashing regime a significant proportion of the droplet volume would remain attached to the solid surface [108] thus wetting the surface and preventing further droplet breakup. Once the solid surface is wetted then the droplet interaction with the surface changes and although analysis is easier (surface properties no longer influence the outcome) [108] and even though splashing will occur (generating smaller droplets) a significant proportion of the droplet volume remains on the wetted surface. The overall result is that in these situations evaporation will almost certainly be hindered rather than accelerated.

3.4.2 Experimentation

The expected outcomes for solid surface excitation and disintegration are investigated and confirmed by the results of three simple experiments. In each experiment the micro-droplets were impinged against solid surfaces.

- **Experiment 1**

In one experiment micro-droplets were ejected from a droplet generator (similar to that shown in Figure 3-3) and impinged directly against the inclined transmitting surface of a 1.45 MHz ultrasound nebulising transducer.

It was found that the droplets impinging on the transducer coalesced into larger droplets and either ran off the inclined face or were re-nebulised into droplets. The droplet size distribution downstream of the inclined transducer showed no significant changes from that measured at the outlet of the droplet generator. Since the droplet generator and inclined transducer operated at similar frequencies there were no size advantages gained from the small proportion of re-nebulised droplets.

- **Experiment 2**

In a second experiment the air/droplet mixture, from the droplet generator used in Experiment 1, was passed through a porous plug of aluminium excited at 1.45MHz. It was hoped that the porous nature of the aluminium would provide a large surface area that was vibrating and also allow free passage of the moist air.

It was found that the water droplets coalesced inside the porous plug and filled up the housing containing the plug. There was no detectable change in the droplet size distribution measure downstream of the porous plug compared to that measured upstream.

- **Experiment 3**

In a third experiment the air and water droplet mixture was delivered to the intake of a small, high speed (24,000 rpm) rotary compressor. The aim was to observe the effects of high impact velocities on the droplet distribution.

In this case it was found that the majority of the droplets attached to the impeller surfaces and very few droplets were discharged from the compressor outlet (too few to be measured for size). Liquid water dripped from the compressor casing. Thus it was evident that little if any droplet breakup had occurred.

3.4.3 Remarks – solid surface excitation and disintegration

From the initial investigation carried out in this section it also seems clear that using a solid surface to excite the many micro-droplets at their resonant frequency or impinging the many micro-droplets at high speeds against an ambient temperature solid surface will not result in further droplet disintegration. Rather, conditions are such that the droplets attach to and wet the solid surfaces. Although the mechanisms for droplet disintegration discussed in this section have been shown to occur for single, large droplets [135] or for many small droplets on heated surfaces [109] it is unlikely they will be effective in the enhancement of the evaporation of many micro-droplets in an air stream utilising ambient temperature surfaces.

3.5 Initial investigation of ultrasound enhanced evaporation

As discussed in section 3.2.2 the droplets generated from a typical ultrasonic nebuliser are small enough to remain entrained in the air flowing along a tube. Thus there is very little relative movement between the micro-droplets and the air. As mentioned in Chapter 2 many studies investigating the evaporation of these small micro-droplets into air [48, 52, 56, 59] assume that the heat transfer between droplet and air is conductive, rather than convective and the mass transfer between droplet and air is governed by Fick's law of diffusion rather than convective diffusion. Thus if it were possible to generate sufficient relative movement between the air and droplets it would be possible to promote both convective heat transfer and convective mass transfer. This would enhance and accelerate the evaporation process.

It may be possible to generate this relative movement between the droplets and the air by exciting the air and micro-droplet mixture using a suitable ultrasound signal. The air

particle displacement and velocity would need to be determined and the dynamic response of the droplets to the air movement would also need to be calculated.

The air particle displacement amplitude, ζ for a plane sinusoidal acoustic sound wave in a fluid is given by [134]

$$\zeta = \frac{v}{\omega} = \frac{p}{\rho c \omega}$$

(3-4)

where v is the particle velocity amplitude (m/s), p is the pressure amplitude of the acoustic signal (Pa), ρ is the density of the fluid (kg/m^3), c is the signal speed in the fluid (m/s) and ω is the frequency of the acoustic signal (rad/s). The rms value of the pressure amplitude, p_{rms} is related to the sound pressure level (SPL) by

$$SPL = 20 \log_{10} \left(\frac{p_{\text{rms}}}{p_{\text{ref}}} \right)$$

(3-5)

Where the reference rms pressure amplitude, p_{ref} is 20 µPa.

In Chapter 2 the dynamic response of a particle in a gas subject to a sinusoidal acoustic wave was discussed. Equation (2-4) gives the ratio of the particle velocity amplitude to the gas velocity amplitude and in the case of a harmonic (sinusoidal) acoustic signal the ratio of the displacement amplitudes will be the same as the ratio of the velocity amplitudes given in equation (2-4).

Thus, for example, for a 5 µm diameter water droplet in air at 20°C subjected to 160 dB of ultrasound at 100 kHz the displacement amplitude of the air molecules will be around 11 µm at a peak velocity of around 6.9 m/s. In this situation the displacement response of the water droplet to the air movement is around 2% (i.e., it remains relatively stationary relative to the air). Thus relative movement between air and droplet is generated from an ultrasound field and may be sufficient to enable convective heat and mass transfer.

3.5.1 Effect on different droplet sizes

A typical droplet size distribution from the ultrasonic nebuliser used in this study is presented in section 3.2.1. Table 3-4 shows results when the air and water droplet mixture is subjected to ultrasound in air at 20°C at 160 dB at frequencies of 20 kHz and 100 kHz for representative droplet sizes of 1, 5 and 20 µm. These droplet sizes represent the smaller, middle and larger sized droplets in the distribution. The peak air velocity in

all cases is 6.9 m/s. The results shown in the table are the amplitude of the air molecule vibration, the displacement response of the droplet and the peak Reynolds number (at maximum air velocity).

Table 3-4: Ultrasound effect, at 160 dB, on different droplet sizes

Droplet diameter (μm)	Amplitude of air molecule vibration (μm)		Droplet displacement response (%)		Peak Re	
	20 kHz	100 kHz	20 kHz	100 kHz	20 kHz	100 kHz
1	54	11	93	46	0.45	0.45
5	54	11	10	2.1	2.3	2.3
20	54	11	0.7	0.1	9.0	9.0

From Table 3-4 it can be seen that the convective enhancement effect will be lower for the smaller droplets since they tend to move with air oscillations and the Reynolds number is very low. Although the air particle displacement is large relative to droplet size. The convective enhancement effect is more significant for the large droplets, where it is needed, since they remain stationary relative to the air oscillations and the Reynolds numbers are larger. Lower frequencies are probably better for the larger droplets as the amplitude of air molecule vibration is larger. However this is partially offset by a greater droplet displacement response (i.e., droplet moves with the air more and so relative motion between droplet and air decrease slightly).

This simple analysis does not take into account the presence of a large number of droplets in the air and its effect on the acoustic wave nor the possibility that the acoustic wave could be a standing wave. Also, although the peak superficial Reynolds number based on these figures is still very low, due to the small droplet size, the enhancement of evaporation using this mechanism was considered worthy of further investigation. Preliminary experimental trials were conducted as detailed in the next section and a theoretical model for ultrasound enhanced evaporation is developed in Chapter 4.

3.5.2 Preliminary experimental work

Initial experimental work relating to the concept of using an ultrasound field to enhance the heat and mass transfer were carried out using a range of ultrasound transducers. This work was performed to evaluate the practical potential of the ideas that were previously developed.

Initially, low power piezoelectric based air transducers were used to generate the ultrasound field. Then more powerful broadband transducers were used. The frequency range of these latter transducers was varied in an attempt to see if different frequencies had any effect on the droplet evaporation process.

3.5.2.1 Low power air transducers

Initially the concept was tested by using low power ultrasonic air transducers in batch and continuous flow arrangements. This involved using a flat plat nebulising transducer mounted in the bottom of a chamber covered with a 2 cm layer of water so that droplets were generated into the chamber as shown in Figure 3-2 and Figure 3-3 . A second ultrasound air transducer was mounted in the top of the chamber. Two air transducers were used, one operated at 32.8 kHz and the second at 40 kHz. The chamber was also fitted with air inlet and outlet ports. Two scenarios were considered, batch mode and continuous mode.

In batch mode, the air supply was turned off and the nebulising transducer was run for a short period of time till droplets filled the chamber. This transducer was then turned off. Once turned off the droplets in the chamber would evaporate and/or condense and so ultimately disappear from view. This disappearance time was measured. The experiment was repeated but this time after the nebulising transducer was turned off the air transducer in the top of the chamber was turned on. The time taken for the droplets to evaporate/condense and disappear from view under the imposed ultrasound field was measured and the two times compared. Trials were run for the two different air transducers.
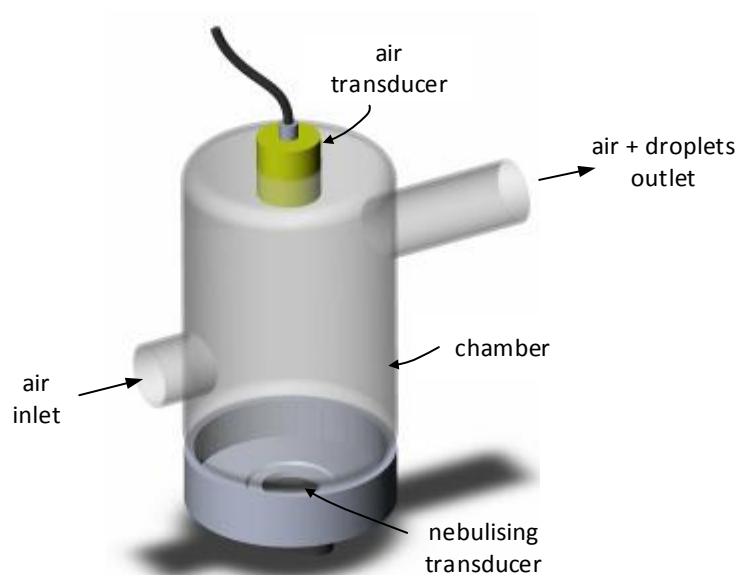
Figure 3-2: Schematic of initial experimental set up with low power ultrasonic air transducers
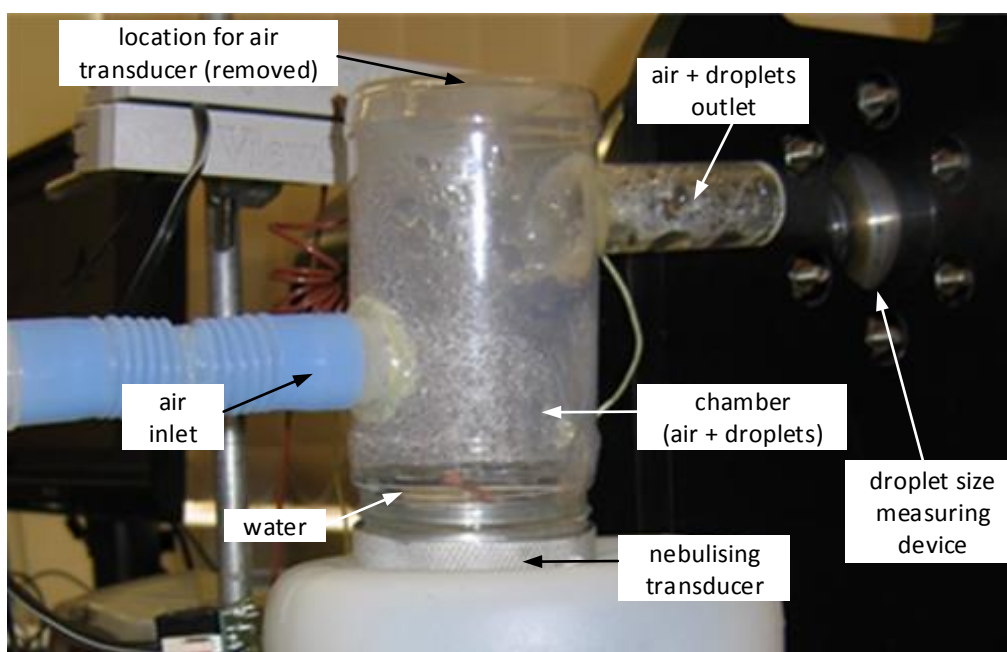
Figure 3-3: Experimental set up – continuous mode operation

In continuous mode the air supply was turned on at the same time as the flat plate nebuliser so that a stream of air and droplets issued from the outlet port of the chamber. A droplet size measuring device (Malvern Spraytec, described in detail in Chapter 5) was used to measure the droplet size distribution at the outlet port. The size distribution was measured with the top mounted air transducer turned off and again with it turned

on and the two distributions compared. Trials for both air transducers were carried out. Although no air properties were measured in these initial trials it was considered that even a small change in the droplet size distribution would indicate some enhancing effect from the ultrasound field. Additionally the Spraytec device output a % transmission value that was measure of the denseness of the spray so that any increase in evaporation could be seen as a change in the % transmission value.

However, no measureable effect was observed from the imposed ultrasound field in these initial trials. The times to disappearance in the batch mode trials for both air transducers were identical between normal and ultrasound cases. Also, there were no changes in the measured droplet size distributions or % transmission values in the continuous mode trials for both air transducers between normal and ultrasound cases.

The air transducer in the continuous mode set up was moved from the top of the chamber and mounted in the outlet port in an attempt to get a stronger ultrasound field, however the measured droplet size distributions and % transmission values again showed no changes between normal and ultrasound cases, for both air transducers.

The lack of any measurable change to the evaporation characteristics was considered to be either due to the low power input of the air transducers or possibly the frequency of operation of those transducers, which could not be altered.

Thus, an air ultrasound air transducer was sourced that had a much higher power output than those that had been used previously – a BAT transducer from MicroAcoustic Instruments Ltd. Additionally it was of a novel design (non-piezoelectric) that allowed true broadband operation over a wide range of frequencies (20 kHz – 2 MHz). The trials carried out with these transducers are described in the next section.

3.5.2.2 MicroAcoustic BAT transducers

At this stage the generation of droplets using the flat plat transducer and chamber described in the last section had been abandoned. With that system it was not possible to accurately measure the 'inlet' or input droplet size that would be needed as an input in the theoretical models that were being developed. A new method of nebulisation had been selected that used a perforated plate technique (described in Chapter 2) to generate the droplets. The device selected (Aeroneb Solo, described in detail in Chapter 5) allowed the inlet droplet size distribution to be easily measured and was more

suitable for incorporating into the proposed experimental apparatus for this investigation (see next section and Chapter 5).

Initially the experimental set up was as shown in in Figure 3-4 and Figure 3-5. Air was supplied to the conduit, droplets were generated directly into the air flow and the broadband BAT transducer was mounted just downstream of the nebuliser. The droplet size measuring device was mounted at the outlet of the conduit.
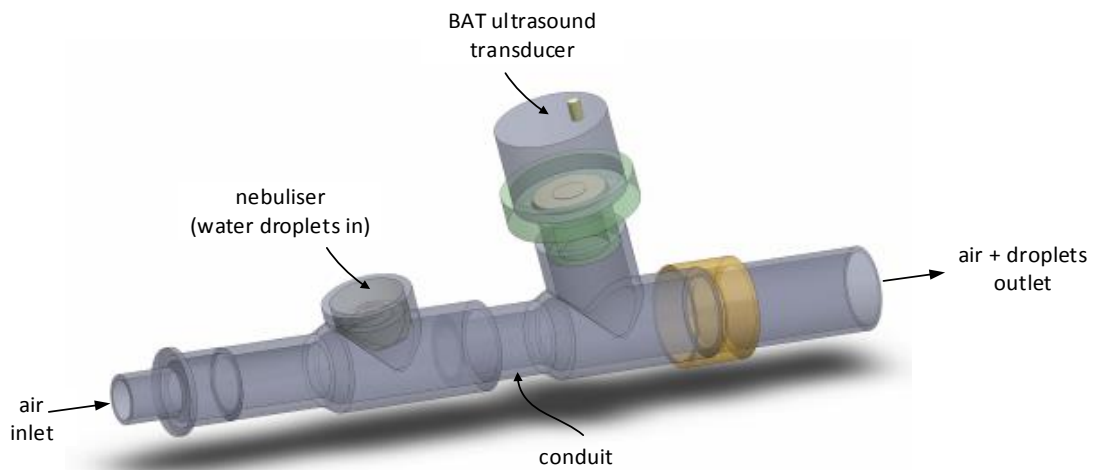
Figure 3-4:Experimental setup - BAT transducers
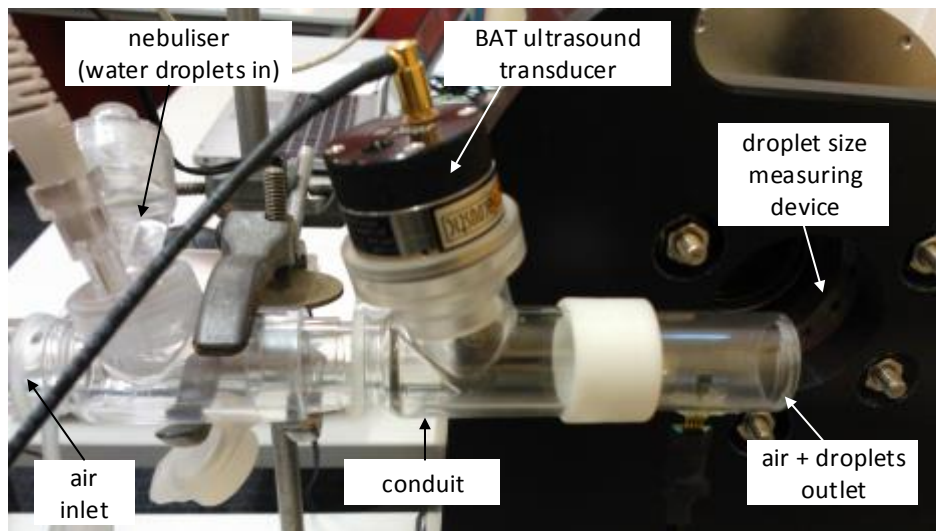
Figure 3-5: Experimental setup: BAT transducers

Trials consisted of turning on the air flow and nebuliser and measuring the droplet size distribution and % transmission values at the outlet of the conduit. Measurements were taken with the BAT transducer turned off and also taken with the BAT transducer turned on at different power inputs and frequencies. Again, in these initial trials, no air properties were measured as it was considered that even a small change in the droplet size distribution or % transmission values would indicate some enhancing effect from the imposed ultrasound field.

However at maximum power and over a wide range of frequencies no changes in the outlet droplet size distribution or % transmission values were observed.

It was also discovered that any water droplets that came into contact with the BAT transducer's active surface during high power operation destroyed the transducer!

Apparatus providing an alternative flow arrangement that minimised the risk of droplets coming into contact with the transducer active surface was designed and built and is shown in Figure 3-6 and Figure 3-7. However a complete set of trials (power levels, frequencies) with this new apparatus also failed to show any impact of the imposed ultrasound field on the outlet droplet size distribution.
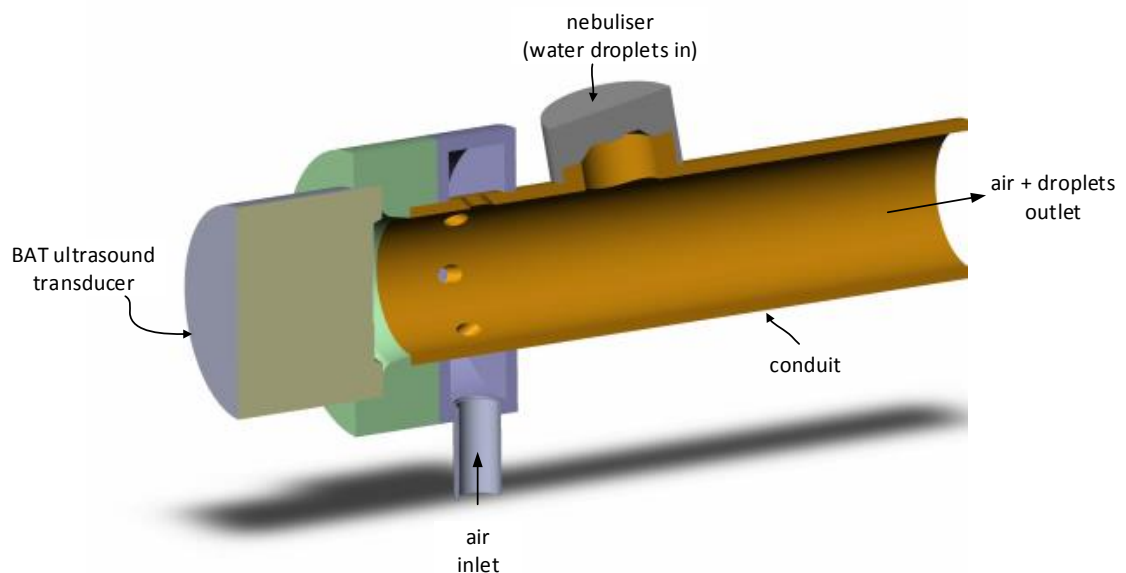
Figure 3-6: Cross-section of modified apparatus using BAT transducer

At this point it was realised that in fact much higher power levels would be needed in the imposed ultrasound field to achieve any evaporation enhancement. The power generated by the ultrasound transducers used so far were less than 1 W. Further

investigation in the area of 'power ultrasound' revealed that much higher power air ultrasound transducers were available and one such transducer was selected for the main investigation reported in this work (see Chapter 5).
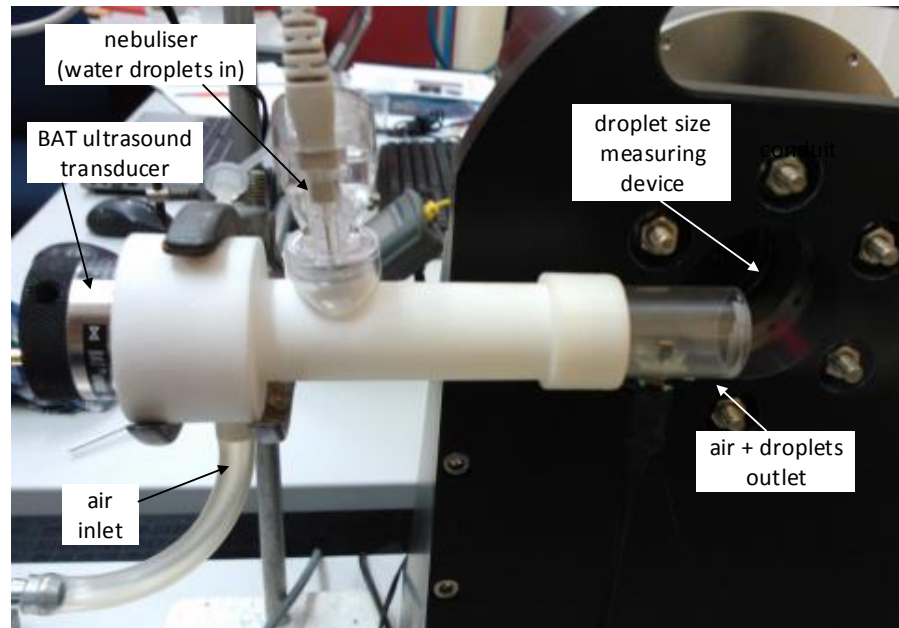
Figure 3-7: Modified experimental setup : BAT transducer

3.6 Methodology

From the initial investigations detailed in this chapter and from the literature review detailed in Chapter 2 a clear methodology for the experimental and theoretical investigation to be undertaken in this research was developed.

- A model of the normal evaporation process needed to be developed that accounted for all the significant physical and thermodynamic processes involved. It should allow for the droplet size distribution to be an input so that changes to that distribution could be determined. It should include explicit details of the mass and heat transfer processes involved as these will be modified for the ultrasound enhanced case. Outputs from the model should include the flow rate, temperature and size distribution of the water droplets and the flow rate, temperature and relative humidity of the air at the discharge of the conduit.

- Then a second ultrasound enhanced evaporation model would be developed. It would be substantially the same as the normal evaporation model but the heat and mass transfer processes would be modified to allow for the convection effect of the oscillating air molecules under the action of an imposed ultrasound field. Thus

results generated from these models could then be compared to experimental results to provide a better understanding of the ultrasound enhanced evaporation process and to quantify the effect of the ultrasound field on water droplet evaporation. Details of the development of the theoretical models are given in Chapter 4.

- The experimental investigation should clearly show any improvement in evaporation as the result of the imposed ultrasound field. Thus any apparatus used should be set up such that the amount of water evaporated over the length of the conduit could be determined and also any changes to the droplet size distribution could be determined. The general flow schematic for a suitable experimental set up to achieve these requirements is shown in Figure 3-8.
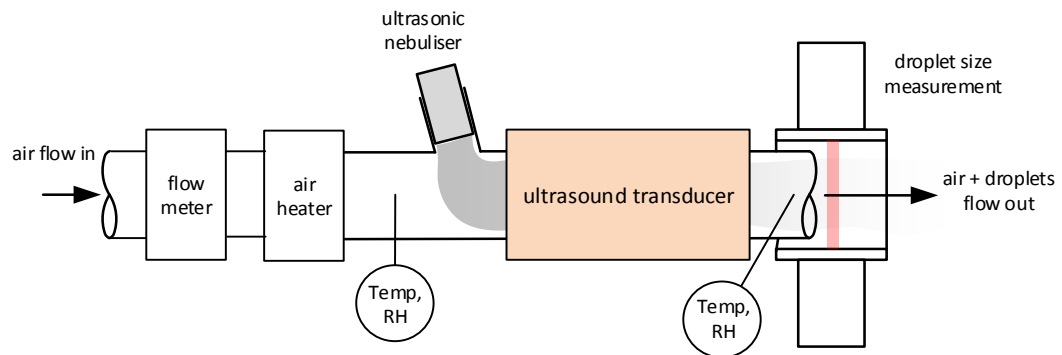
Figure 3-8: Schematic for experimental set up

In this set up, air of known temperature, pressure, relative humidity and flow rate flows along a conduit of known length and diameter. Water droplets of known temperature, flow rate and size distribution are generated by an ultrasonic nebuliser and combined with the flow of air in the conduit. The air and droplets can then be subjected to an intense ultrasound field of known frequency and amplitude which accelerates the droplet evaporation process. This ultrasound field can be turned off or on for comparison purposes. A flow of humidified air will discharge from the outlet of the conduit and also possibly a flow of water droplets (depending on the ratio of water flow to air flow at the inlet and depending on the length of conduit). Ideally all the conditions at the outlet of the conduit should be measured: temperature, flow rate and size distribution of the remaining water droplets (if any) and temperature, flow rate and relative humidity of the air.

- The experimental results generated would then be compared to the theoretical results to provide a better understanding of the ultrasound enhanced evaporation process and to quantify the effect of the ultrasound field on water droplet evaporation. Details of the actual experimental set up used are given in Chapter 5. Comparison and discussion of the results from both the theoretical models and the experimental investigation are given in Chapter 6 and Chapter 7.

Chapter 4 - Theoretical Formulation

4.1 Introduction

This thesis investigates and quantifies the improvement in evaporation of water droplets as a result of an imposed ultrasound field. An air and water droplet mixture flows along a conduit with the water droplets evaporating into the air. The mixture is then subject to an ultrasound field, the purpose of which is to accelerate the evaporation process. As the evaporation process depends significantly on the droplet size then changes to the droplet size distribution, are also of interest, as the droplet/air mixture travels along the conduit for both normal evaporation and when the ultrasound field is applied.

Conducting a purely experimental investigation has many limitations which come about as a result of the physical system and its surroundings. However, theoretical modelling has several advantages including wider general conclusions, change of any parameter, and so on. In this theoretical part of the investigation models are developed that simulate the droplet evaporation process. In the next section a model is developed that assumes the droplet size distribution is mono-disperse meaning that the water droplets are all of the same diameter. In later sections this model is modified to incorporate a more realistic poly-disperse droplet size distribution, where the droplet diameters vary in the size distribution. Finally the model is modified to incorporate the application of an ultrasound field to the air and poly-disperse droplets, with the intention of accelerating the droplet evaporation process. In each case the development of these theoretical models is described and their implementation in MATLAB® outlined.

4.2 Evaporation model – Mono-disperse droplets

As discussed in Chapter 2 and 3, it was decided to develop a water droplet evaporation model that can be modified to account for the application of an ultrasound field. This model is expected to be practical, easy to follow, and produces acceptable practical values. In this section a model is developed, comprised of the governing equations for the evaporation of mono-disperse water droplets into air as they flow along the conduit. Since there are many droplets evaporating into the air it is important that the coupling between the mass and energy balances for the droplets and for the surrounding air is included in the model. Thus these equations are based on the mass and energy balances

for the water droplets and for the surrounding air. Although others have developed similar models [55, 73]; nevertheless this model is expected to have the flexibility to account for a poly disperse droplet size distribution and to account for the effect of the imposed ultrasound field.

The key parameters in the evaporation process are: droplet size d_d, droplet temperature T_d, surrounding air humidity ϕ_∞ (in terms of the water vapour pressure p_∞) and surrounding air temperature T_∞. With these parameters it is possible to quantify the amount of water evaporated along the conduit. Although mono-disperse droplet distributions are rarely found in practice the mono-disperse droplet evaporation model represents a simpler initial case that, that when validated, would give confidence in the later more realistic and more complex evaporation models.

4.2.1 Physical situation to be modelled

The physical situation to be modelled consists of an air stream flowing along a conduit at flow rate $\dot{V}_{a,i}$, temperature $T_{\infty,i}$ and relative humidity $\phi_{\infty,i}$ (Figure 4-1) . An ultrasonic nebuliser attached to the conduit injects droplets into the air stream at a flow rate of $\dot{V}_{w,i}$ and uniform temperature $T_{d,i}$. The droplet size distribution for this model is considered to be mono-disperse with all the droplets having an initial uniform diameter of $d_{d,i}$. A representative thin plug or control mass of air and water droplets is considered and droplets begin to evaporate into the surrounding air in the plug as it moves along the conduit (Figure 4-2).
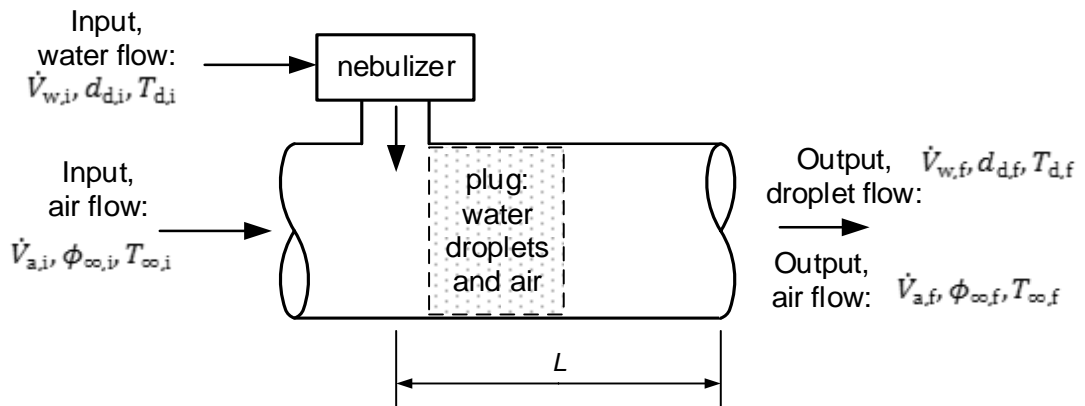
Figure 4-1: Physical situation of evaporation process – mono-disperse droplets
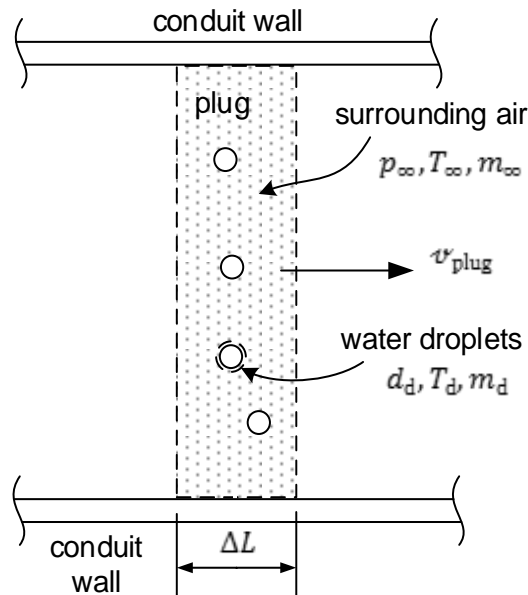
Figure 4-2 Plug flow model – mono-disperse droplets

4.2.2 Assumptions

The assumptions used in developing the theoretical mono-disperse droplet evaporation model are

1. The droplets are considered to consist of pure water only, i.e., there are no impurities or dissolved substances. The small amount of impurities in normal tap water will have little effect on the nebulisation or evaporation process.

2. The ratio of water droplets to air in the moving plug or control mass is low and is typical of that found in medical humidification devices.

3. The droplets generated by the ultrasonic nebuliser are of a single size (mono-disperse) typical of that produced by ultrasonic nebulisers and in the size range 2 – 20 μm.

4. The droplets are uniformly dispersed in the moving plug and due to the low liquid water to air ratio, they remain uniformly dispersed during their lifetime and therefore they do not coalesce. The droplets are ejected from the nebuliser at sufficient velocity so that they mix into the air in a uniform fashion.

5. Any interaction between the droplets and the conduit walls are ignored due to the low ratio of liquid water to air.

6. Due to the assumptions of low droplet concentration, and no interactions with conduit walls or other droplets it is assumed therefore that all the droplets behave uniformly.

7. Prior to complete evaporation the number concentration of the droplets (ie number of droplets per unit mass of dry air) remains constant in the moving plug.

8. The mass transfer mechanism is diffusion dominated (Fick's law) and the heat transfer mechanism is conduction dominated because the droplets are of a small size and remain approximately stationary relative to the air (see Chapter 3).

9. The droplet size is such that the time scales required for temperature uniformity within the droplet are much smaller than the evaporation time scales, therefore uniform temperature within the droplet is assumed.

10. The air immediately adjacent to the droplet surface has the same temperature as the droplet and has a water vapour pressure in the saturated condition.

11. Stefan flow is ignored since the saturation pressure at the droplet surface is much lower than the total pressure in the surrounding medium [51].

12. The conduit walls are assumed to be adiabatic which is approximately correct as the air flow along the conduit is relatively fast.

4.2.3 Droplet mass balance

Consider a system boundary that is located on the surface of a single water droplet (Figure 4-3) in the plug flowing along the conduit. Now considering conservation of mass over a small time period dt in the plug for the droplet, then

$$\left[\begin{pmatrix} \text{mass flow rate} \\ \text{into water} \\ \text{droplet} \end{pmatrix} - \begin{pmatrix} \text{mass flow rate} \\ \text{out of water} \\ \text{droplet} \end{pmatrix} \right] dt = \begin{pmatrix} \text{change of mass} \\ \text{of water} \\ \text{droplet} \end{pmatrix} \tag{4-1}$$

For an evaporating water droplet the first term in the above equation is zero and therefore

$$- \dot{m}_\text{w} = \frac{dm_\text{d}}{dt} \tag{4-2}$$

Where $\dot{m}_\text{w}$ is the mass flow rate of water evaporating from the droplet surface and m_d is the mass of the droplet. Considering the LHS of this equation, the evaporation rate of water vapour from the droplet surface to the surrounding air can be written as

$$\dot{m}_\text{w} = j_\text{w} A \tag{4-3}$$
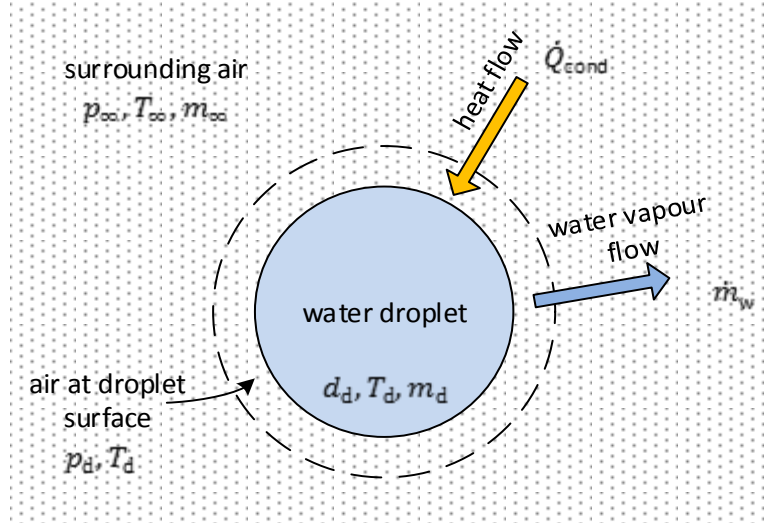
Figure 4-3 Mass and heat flows during evaporation

Where j_w is the mass flux and the surface area $A = 4\pi r^2$ for flux from a spherical droplet. Since diffusion of the water vapour is governed by Fick's law then the mass flux j_w is given by

$$j_w = -D_w \nabla c_w \qquad (4\text{-}4)$$

Where D_w is the diffusion coefficient for water vapour in air and c_w is the mass concentration of water vapour in the air. Also, since it is assumed that the water droplets are stationary relative to the air and there are large distances between the water droplets (relative to droplet size) then the concentration gradient is dependent on the radial distance, r alone so

$$\dot{m}_w = -D_w 4\pi r^2 \frac{dc_{w,}}{dr} \qquad (4\text{-}5)$$

In some situations the size of the droplets will become very small during evaporation such that they approach the size range of the gas molecules surrounding the droplets (air and water vapour) and the assumptions behind Fick's Law diffusion no longer apply. This non-continuum effect on water diffusion (and also conduction heat transfer) as the droplets become very small can be compensated for by using correction factors based on the Knudsen number ($\mathrm{Kn} = 2\lambda/d_d$, where λ is the mean free path of the gas molecules surrounding the droplet). The form of the correction factors used in our study are the same as those proposed by Fuchs & Sutugin [80], by Vesala et al. [48] and by Ferron & Soderholm [43] and are used to modify the mass and heat flux equations. The mass flux correction factor is

$$C_\text{m} = \frac{1 + \text{Kn}_\text{m}}{1 + \left(\frac{4}{3\alpha_\text{m}} + 0.377\right)\text{Kn}_\text{m} + \frac{4}{3\alpha_\text{m}}\text{Kn}_\text{m}^2} \tag{4-6}$$

And the heat flux correction factor is

$$C_\text{h} = \frac{1 + \text{Kn}_\text{h}}{1 + \left(\frac{4}{3\alpha_\text{h}} + 0.377\right)\text{Kn}_\text{h} + \frac{4}{3\alpha_\text{h}}\text{Kn}_\text{h}^2} \tag{4-7}$$

Where α_m and α_h are the mass accommodation coefficient and thermal (heat) accommodation coefficient respectively [51]. They are a measure of the effectiveness of the mass and heat transport processes occurring at the gas liquid interface during evaporation. Also, Kn_m and Kn_h are the mass transport Knudsen number and thermal transport Knudsen numbers respectively [43]. Thus equation (4-5) becomes

$$\dot{m}_\text{w} = -D_\text{w}4\pi r^2 \frac{dc_\text{w}}{dr}C_\text{m} \tag{4-8}$$

Solving equation (4-8) by separation of variables between the limits of $r = d_\text{d}/2$ and ∞ gives

$$\dot{m}_\text{w} = D_\text{w}.\,2\pi d_\text{d}(c_\text{d} - c_\infty)C_\text{m} \tag{4-9}$$

Where c_d and c_∞ are the mass concentrations of water vapour at the droplet surface and some distance away from the surface, respectively. Now this mass concentration of water vapour in the air, c_w is equivalent to the partial density, ρ_w of water vapour in the air, that is:

$$c_\text{w} = \rho_\text{w} = \frac{m_\text{w}}{V} \tag{4-10}$$

And, assuming that the water vapour behaves like an ideal gas then

$$p_\text{w}V = m_\text{w}R_\text{w}T_\text{w} \tag{4-11}$$

Rearranging gives

$$\frac{m_\text{w}}{V} = \frac{p_\text{w}}{R_\text{w}T_\text{w}} \tag{4-12}$$

Combining equations (4-12) and (4-10) and since the specific gas constant for the water vapour $R_\text{w} = R_\text{u}/M_\text{w}$ then

$$c_{\mathrm{w}} = \frac{p_{\mathrm{w}} M_{\mathrm{w}}}{R_{\mathrm{u}} T_{\mathrm{w}}} \tag{4-13}$$

Substituting equation (4-13) into (4-9) and writing the water vapour pressure and the air/water vapour temperatures in terms of the droplet surface and surrounding air, gives the mass flow rate of vapour diffusing from the droplet surface as (that is, LHS of equation (4-2))

$$\dot{m}_{\mathrm{w}} = \frac{D_{\mathrm{w}} 2\pi d_{\mathrm{d}} M_{\mathrm{w}}}{R_{\mathrm{u}}} \left(\frac{p_{\mathrm{d}}}{T_{\mathrm{d}}} - \frac{p_{\infty}}{T_{\infty}} \right) C_{\mathrm{m}} \tag{4-14}$$

Now, considering equation (4-2) the rate of change of mass of an individual water droplet in terms of the droplet diameter d_{d} then

$$\frac{dm_{\mathrm{d}}}{dt} = \frac{d}{dt} \left(\rho_{\mathrm{d}} \frac{\pi d_{\mathrm{d}}^{3}}{6} \right) \tag{4-15}$$

Where ρ_{d} is the density of water in the droplet. Therefore

$$\frac{dm_{\mathrm{d}}}{dt} = \frac{\rho_{\mathrm{d}} \pi d_{\mathrm{d}}^{2}}{2} \frac{dd_{\mathrm{d}}}{dt} \tag{4-16}$$

Substituting equations (4-16) and (4-14) into equation (4-2) and rearranging gives an expression for the rate of change of droplet diameter during the evaporation process.

$$\frac{dd_{\mathrm{d}}}{dt} = \frac{4 D_{\mathrm{w}} M_{\mathrm{w}}}{\rho_{\mathrm{d}} d_{\mathrm{d}} R_{\mathrm{u}}} \left(\frac{p_{\infty}}{T_{\infty}} - \frac{p_{\mathrm{d}}}{T_{\mathrm{d}}} \right) C_{\mathrm{m}} \tag{4-17}$$

Additionally, for the curved droplet surfaces there is an increase in vapour pressure due to the Kelvin effect [139] which can be expressed as

$$p_{\mathrm{d}} = p_{\mathrm{s}} \exp \left(\frac{4 \sigma_{\mathrm{d}} M_{\mathrm{w}}}{\rho_{\mathrm{d}} R_{\mathrm{u}} T_{\mathrm{d}} d_{\mathrm{d}}} \right) \tag{4-18}$$

Where p_{d} and p_{s} are the water vapour pressures above the curved droplet surface and a flat surface respectively. Also, σ_{d} is the surface tension of the water in the droplet.

4.2.4 Droplet energy balance

Considering now the energy balance for the droplet in Figure 4-3 then over a small time period dt

$$\left[\begin{pmatrix} \text{rate of energy} \\ \text{flow into water} \\ \text{droplet} \end{pmatrix} - \begin{pmatrix} \text{rate of energy} \\ \text{flow out of water} \\ \text{droplet} \end{pmatrix} \right] dt = \begin{pmatrix} \text{change of} \\ \text{energy of water} \\ \text{droplet} \end{pmatrix} \tag{4-19}$$

For conditions favouring evaporation, as will be typically found in medical breathing apparatus, then the surrounding air in the plug, some distance from the droplet, is at a higher temperature than the water droplet. Thus the energy flow into the droplet is by heat conduction, $\dot{Q}_{cond}$ and the energy flow out of the droplet is the latent energy associated with the water evaporating from the droplet, $\dot{E}_{out}$. The energy change of the droplet is the change in enthalpy of the droplet, dH_d. Thus equation (4-19) for a an evaporating droplet is

$$\dot{Q}_{cond} - \dot{E}_{out} = \frac{dH_d}{dt}$$

(4-20)

The rate of heat conduction from the air to the droplet for a spherical conduction layer is given by

$$\dot{Q}_{cond} = \frac{\Delta T}{R_{th,\,sphere}}$$

(4-21)

And the thermal conduction resistance of a spherical layer, $R_{th,\,sphere}$ is given by [140]

$$R_{th,\,sphere} = \frac{r_2 - r_1}{4\pi r_1 r_2 k}$$

(4-22)

where r_1 and r_2 are the inner and outer radii respectively and k is the thermal conductivity of the spherical layer. Thus, for a very thick spherical boundary layer (of air), as found in this case, then $r_2 \gg r_1$ and substituting $r_1 = d_d/2$, equation (4-22) reduces to

$$R_{th,\,boundary\,layer} = \frac{1}{2\pi d_d k_f}$$

(4-23)

Where k_f is the thermal conductivity of the air in the boundary layer surrounding the droplet. Substituting equation (4-23) into (4-21) and applying the non-continuum heat flux correction factor C_h, equation (4-7), gives the conduction heat transfer to a single droplet

$$\dot{Q}_{cond} = 2\pi d_d k_f (T_\infty - T_d) C_h$$

(4-24)

The air temperature at the surface of the droplet is assumed to be the same as the droplet temperature T_d and T_∞ is the air temperature in the bulk air surrounding all the droplets in the plug.

Now, the latent energy removed from the droplet in the form of a vapour flow (4-20), assuming the vapour is saturated at the droplet surface, is given by

$$\dot{E}_{out} = \dot{m}_w h_g \qquad (4\text{-}25)$$

where h_g is the enthalpy of the saturated water vapour at T_d. Combining equations (4-2) and (4-16) into (4-25) gives

$$\dot{E}_{out} = -\frac{\rho_d \pi d_d^2}{2} \frac{dd_d}{dt} h_g \qquad (4\text{-}26)$$

Finally, considering equation (4-20) the rate of change of energy (enthalpy) of a liquid droplet, can be written as

$$\frac{dH_d}{dt} = \frac{d(m_d h_d)}{dt} = h_d \frac{dm_d}{dt} + m_d \frac{dh_d}{dt} \qquad (4\text{-}27)$$

where h_d is the specific enthalpy of the liquid droplet. Substituting equations (4-27), (4-26) and (4-24) into the energy balance equation, (4-20) and simplifying gives

$$\frac{dh_d}{dt} = \frac{12 k_f (T_\infty - T_d) C_h + 3 \rho_d d_d (h_g - h_d) \frac{dd_d}{dt}}{\rho_d d_d^2} \qquad (4\text{-}28)$$

Also, the enthalpy of a liquid can be closely approximated [141] as follows

$$dh_d = C_{p,d} dT_d \qquad (4\text{-}29)$$

Where $C_{p,d}$ is the average specific heat capacity of the water in the droplet. The specific enthalpy h_d of the water in the droplet is approximately equal to the specific enthalpy of the saturated liquid h_f at the droplet temperature T_d, so the term $(h_g - h_d)$ in equation (4-28) can be written as the enthalpy of vaporisation h_{fg}. Thus substituting this simplification and equation (4-29) into equation (4-28) and rearranging gives an expression for the rate of change of droplet temperature during the evaporation process in the plug

$$\frac{dT_d}{dt} = \frac{12 k_f (T_\infty - T_d) C_h + 3 \rho_d d_d h_{fg} \frac{dd_d}{dt}}{\rho_d d_d^2 C_{p,d}} \qquad (4\text{-}30)$$

4.2.5 Surrounding air mass balance

Considering the mass balance for the region occupied by the surrounding air in the plug (see Figure 4-2 and Figure 4-3) then

$$\left[\begin{pmatrix} \text{mass flow rate} \\ \text{into region} \\ \text{occupied by} \\ \text{surrounding} \\ \text{air in plug} \end{pmatrix} - \begin{pmatrix} \text{mass flow rate} \\ \text{out of region} \\ \text{occupied by} \\ \text{surrounding} \\ \text{air in plug} \end{pmatrix}\right] dt = \begin{pmatrix} \text{change of mass} \\ \text{of region} \\ \text{occupied by} \\ \text{surrounding} \\ \text{air in plug} \end{pmatrix} \qquad (4\text{-}31)$$

The mass of dry air in the plug remains constant during the evaporation process and the mass flowing into the region occupied by the surrounding air in the plug is in the form of water vapour only (from all of the droplets) so that the mass balance is really a water balance. Furthermore, there is no mass flow out of the region occupied by the surrounding air in the plug. Applying this to equation (4-31) gives

$$n\dot{m}_{\mathrm{w}} = \frac{dm_{\mathrm{w},\infty}}{dt} \qquad (4\text{-}32)$$

Where n is the number of droplets in the plug and $m_{\mathrm{w},\infty}$ is the mass of water vapour in the surrounding air in the plug. Considering the mass flow rate of water vapour diffusing into the surrounding air from all of the droplets, and combining equations (4-2) and (4-16) for $\dot{m}_{\mathrm{w}}$ then

$$n\dot{m}_{\mathrm{w}} = n\frac{\rho_{\mathrm{d}}\pi d_{\mathrm{d}}^2}{2}\frac{dd_{\mathrm{d}}}{dt} \qquad (4\text{-}33)$$

Now, considering the rate of change of mass of water vapour in the region occupied by the surrounding air in the plug, it is assumed that the water vapour behaves like an ideal gas, and so from equation (4-12) for the surrounding air

$$m_{\mathrm{w},\infty} = \frac{p_\infty V}{R_{\mathrm{w}} T_\infty} \qquad (4\text{-}34)$$

Where p_∞ and T_∞ are the water vapour pressure and temperature respectively in the surrounding air in the plug. Differentiating with respect to time and assuming that the volume and temperature remain relatively constant compared to the water vapour pressure then

$$\frac{dm_{\mathrm{w},\infty}}{dt} = \frac{dp_\infty}{dt}\frac{V}{R_{\mathrm{w}} T_\infty} \qquad (4\text{-}35)$$

Now the volume of the plug can be expressed in terms of the mass of dry air, m_{a} and the air specific volume, v_{a}

$$V = m_{\mathrm{a}} v_{\mathrm{a}} \qquad (4\text{-}36)$$

And since the specific gas constant $R_w = R_u/M_w$ then

$$\frac{dm_{w,\infty}}{dt} = \frac{dp_\infty}{dt} \frac{M_w m_a v_a}{R_u T_\infty} \qquad (4\text{-}37)$$

Substituting equations (4-37) and (4-33) into equation (4-32), then simplifying and rearranging gives an expression for the rate of change of water vapour pressure in the surrounding air during the evaporation process in the plug

$$\frac{dp_\infty}{dt} = -\frac{\pi R_u T_\infty}{2 M_w v_a}\left(\rho_d d_d^2 N_{md} \frac{dd_d}{dt}\right) \qquad (4\text{-}38)$$

Where $N_{md} = n/m_a$, which is the number droplet concentration, i.e., number of droplets per kg of dry air in the plug. This number droplet concentration can also be expressed in terms of the input dry air flow rate $\dot{m}_a$ and water flow rate $\dot{V}_{w,i}$ into the conduit so for the plug

$$N_{md} = \frac{\dot{V}_{w,i}/(\pi d_{d,i}^3/6)}{\dot{m}_a} \qquad (4\text{-}39)$$

4.2.6 Surrounding air energy balance

Considering the energy balance for the region occupied by surrounding air in the plug:

$$\left[\begin{pmatrix}\text{rate of energy}\\ \text{flow into}\\ \text{region}\\ \text{occupied by}\\ \text{surrounding}\\ \text{air in plug}\end{pmatrix} - \begin{pmatrix}\text{rate of energy}\\ \text{flow out of}\\ \text{region}\\ \text{occupied by}\\ \text{surrounding}\\ \text{air in plug}\end{pmatrix}\right] dt = \begin{pmatrix}\text{change of}\\ \text{energy}\\ \text{of region}\\ \text{occupied by}\\ \text{surrounding}\\ \text{air in plug}\end{pmatrix} \qquad (4\text{-}40)$$

Assuming that the conduit walls containing the air/water droplet mixture are adiabatic and considering the plug as a closed system then this energy balance can also be considered as the constant pressure mixing of the humid surrounding air with the water vapour diffusing in to it from the droplets. This is combined with a conduction heat loss, to reach some equilibrium mixture temperature (Figure 4-4).

In this case, if a short finite time period Δt is now considered then this mixing process can be written as

$$\dot{Q}_{cond}\Delta t = \Delta H_{\text{humid air}} + \Delta H_{\text{water vapour}} \qquad (4\text{-}41)$$
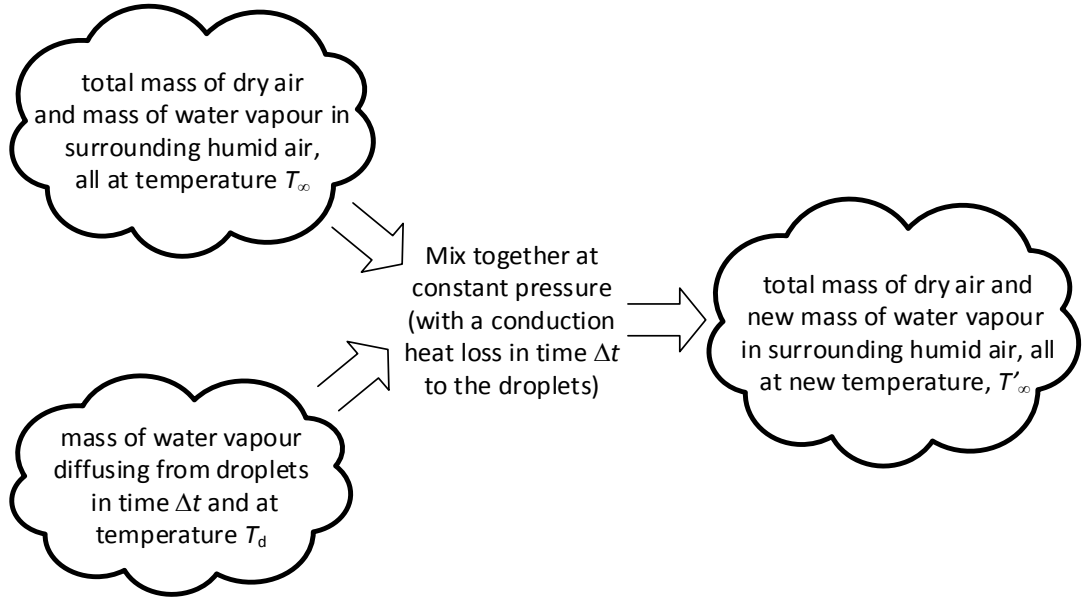
Figure 4-4: Mixing of humid air and diffusing water vapour

Since Δt is a very short time period there will be a very small change in the surrounding air temperature ΔT_∞ and the mass of water vapour diffusing into the surrounding air mass will also be very small, so

$$\dot{Q}_{\text{cond}}\Delta t = m_\infty C_{p,\infty}\Delta T_\infty + -n\Delta m_d C_{p,\text{wvap}}(T_\infty - T_d) \qquad (\,4\text{-}42)$$

Where m_∞ and $C_{p,\infty}$ are the mass and specific heat capacity, respectively, of the surrounding air in the plug. $C_{p,\text{wvap}}$ is the specific heat capacity of the water vapour alone in the boundary layer surrounding each droplet. Taking the limit $\Delta t \rightarrow 0$ in (\,4-42)

$$\dot{Q}_{\text{cond}} = m_\infty C_{p,\infty}\frac{dT_\infty}{dt} - n\frac{dm_d}{dt}C_{p,\text{wvap}}(T_\infty - T_d) \qquad (\,4\text{-}43)$$

Considering the heat conduction to a single droplet from equation (\,4-24), the heat conduction from the surrounding air to all of the droplets will be

$$\dot{Q}_{\text{cond}} = -n2\pi d_d k_f(T_\infty - T_d)C_h \qquad (\,4\text{-}44)$$

Substituting equation (\,4-44) into equation (\,4-43) and also substituting equation (\,4-16) into equation (\,4-43); since $dm_d/dt = -\dot{m}_w$ and rearranging gives an expression for the rate of change of surrounding air temperature during the evaporation process in the plug

$$\frac{dT_\infty}{dt} = \frac{\pi\xi_\infty N_{md}d_d(T_\infty - T_d)}{2C_{p,\infty}}\left(\rho_d d_d C_{p,\text{wvap}}\frac{dd_d}{dt} - 4k_f C_h\right) \qquad (\,4\text{-}45)$$

Where $\xi_\infty = m_a/m_\infty$, is the dryness fraction of the surrounding air in the plug.

Thus, the following four equations represent the governing equations for the evaporation of the mono-disperse water droplets into the air flowing along the conduit.

$$\frac{dd_d}{dt} = \frac{4D_w M_w}{\rho_d d_d R_u}\left(\frac{p_\infty}{T_\infty} - \frac{p_d}{T_d}\right)C_m \qquad (4\text{-}17)$$

$$\frac{dT_d}{dt} = \frac{12k_f(T_\infty - T_d)C_h + 3\rho_d d_d h_{fg}\frac{dd_d}{dt}}{\rho_d d_d^2 C_{p,d}} \qquad (4\text{-}30)$$

$$\frac{dp_\infty}{dt} = -\frac{\pi R_u T_\infty}{2M_w v_a}\left(\rho_d d_d^2 N_{md}\frac{dd_d}{dt}\right) \qquad (4\text{-}38)$$

$$\frac{dT_\infty}{dt} = \frac{\pi \xi_{air} N_{md} d_d (T_\infty - T_d)}{2C_{p,\infty}}\left(\rho_d d_d C_{p,wvap}\frac{dd_d}{dt} - 4k_f C_h\right) \qquad (4\text{-}45)$$

4.2.7 Initial and boundary conditions

As is normal for plug flow analysis there is no mass flow across the boundaries of the plug. Additionally the boundaries of the plug are considered to be adiabatic. That is, no heat flow through the conduit walls and no axial heat flow along the conduit. The velocity profile within the conduit may cause the plug to deform a little as it travels along the conduit but this will not significantly affect the boundary conditions.

The initial conditions for the model are the initial droplet diameters $d_{d,i}$ and temperatures $T_{d,i}$ and the initial water vapour pressure $p_{\infty,i}$, temperature $T_{\infty,i}$ and total pressure, p_0 of the inlet air stream. The initial water vapour pressure $p_{\infty,i}$ in the surrounding air is determined from the initial relative humidity $\phi_{\infty,i}$ of that air. Since the outlet of the conduit is open to atmosphere and flow rates are relatively low the total pressure is assumed to be 101.325 kPa. Although the total pressure does not appear in the equations it is used in the calculation of the various fluid and thermodynamic properties where appropriate.

Different outcomes can occur depending on the initial relative masses of water and air in the moving plug. If the relative mass of water is low enough, the evaporation process described by these equations continues until all of the droplets completely evaporate and the water content of the surrounding air reaches some final value (less than saturation). In this case a 'droplet lifetime' or 'evaporation distance' can be determined, that is: time or distance along conduit till the droplets completely evaporate. If the

water to air ratio is higher, then equilibrium can be reached where the water vapour concentration at the remaining droplet surfaces is in equilibrium with that in the surrounding air and the water droplets are at the same temperature as the surrounding air. In this latter case the droplets reach some final steady state size and an 'equilibrium' time or distance can be determined.

4.2.8 Method of solution and outputs

The governing differential equations with their initial and boundary conditions were solved simultaneously using numerical differentiation formulae (NDF's) and backward differentiation formulae (BDF's) typical of those used for solving 'stiff' sets of differential equations [142]. This was implemented using MATLAB® software as per the flow chart shown in Figure 4-5. Details of the MATLAB® code used for the mono-disperse droplet evaporation model is given in Appendix 3.

Initially, the differential equations were solved using a Runge-Kutta method, also implemented using MATLAB®, however, since this solution technique is not so suited to 'stiff' problems the solution times were very long. The numerical results from the 'stiff' solution technique were typically less than 1 % different from the Runge-Kutta results and solution times were significantly shorter.

Fluid transport and thermodynamic properties were determined using two software based property function libraries: LibHuAirProp and LibIF97. LibHuAirProp is the Library of Psychrometric, Thermodynamic and Transport properties for Real Humid Air, Steam, Water and Ice based on the ASHRAE Research Project RP-1485 [143]. LibIF97 is the Library of water and steam properties, calculated from the industrial formulation IAPWS-IF97 and all supplementary standards [144]. These libraries were utilized in the numerical solution of the governing equations by determining all property values at each time step of the numerical solution of the evaporation process.

The outputs from the mono-disperse model are matrices of the four dependant variables, the droplet diameter d_d, the droplet temperature T_d, the water vapour pressure in the surrounding air p_∞ and the surrounding humid air temperature T_∞, with respect to time as the plug moves along the conduit.
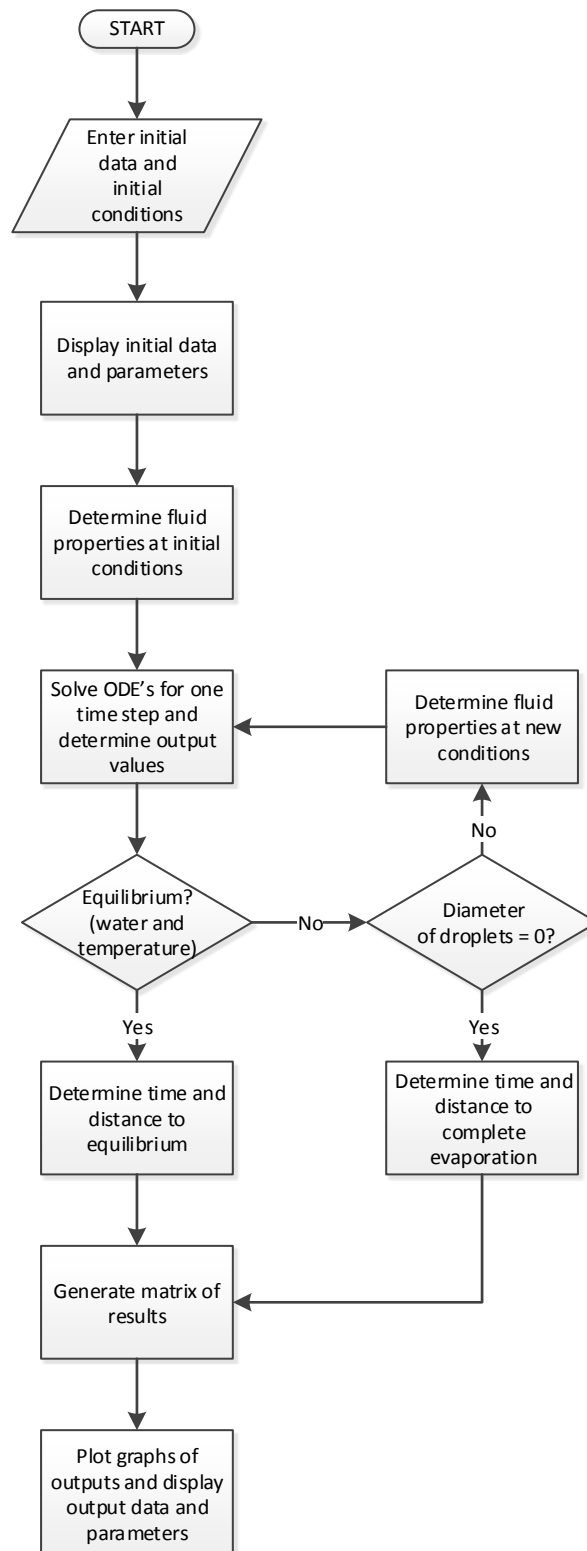
Figure 4-5 Flowchart for solution of governing equations – mono-disperse model

Assuming the plug does not deform significantly, the distance δL the plug has travelled along the conduit for each time step in the solution can be calculated from the conduit dimensions, the air (i.e., plug) velocity and air conditions during that time step

$$\delta L = \mathcal{v}_{\text{plug}}\Delta t_{\text{time step}} \qquad (\,4\text{-}46\,)$$

If the conduit was a tube of diameter d_{tube} then

$$\mathcal{v}_{\text{plug}} = \frac{\dot{m}v_{\text{a}}}{\pi d_{\text{tube}}^2/4} \qquad (\,4\text{-}47\,)$$

The air specific volume, v_{a} is determined at the average temperature and humidity of the air in that time step. Thus matrices of the four dependent variables with distance along the conduit are also determined.

From these matrices of results, the amount of water evaporated over a certain time or distance can be readily determined. This can then be used in comparison to the other models and eventually to experimental data to quantify the effect of ultrasound on water droplet evaporation.

4.2.9 Remarks – mono-disperse droplet evaporation model

In this section the governing equations for the evaporation process for mono-disperse water droplets in air flowing along a conduit were developed from mass and energy balances. The method used for solving these equations, using MATLAB®, was then outlined.

An initial investigation and validation was carried out using the mono-disperse model compared to overall mass and energy balances and also compared to another theoretical model and experimental results reported in the literature. Results from the mono-disperse model agreed well with results from the other sources and these are described in detail in Chapters 5 and 6.

This mono-disperse model forms the basis for a more realistic poly-disperse droplet evaporation model that is developed in the next section.

4.3 Evaporation model – Poly-disperse droplets

In this section the governing equations for the evaporation of the droplets into air as they flow along the conduit are developed, as for the previous model, from mass and energy balances for the water droplets and surrounding air in the plug. However, this case assumes the more realistic situation where the droplet size distribution is poly-disperse, meaning that the droplets are of varying sizes. The distribution of droplet sizes is described in terms of a discrete distribution of % volume of water for a specified

droplet diameter range, there being Nt droplet diameter ranges or 'bins' in the distribution.

Similarly to the previous model, the mass and energy balances are based on the key parameters in the evaporation process: droplet sizes $d_{\mathrm{d},j}$, droplet temperatures $T_{\mathrm{d},j}$, surrounding air humidity ϕ_∞ (in terms of the water vapour pressure p_∞) and surrounding air temperature T_∞ and total pressure, p_0. Where the subscript j refers to the jth diameter range or bin in the droplet size distribution. With these parameters it is possible to quantify the amount of water evaporated and quantify any changes to the droplet size distribution along the conduit. The method used for solving these equations, using MATLAB®, is also described.

4.3.1 Physical situation to be modelled

The physical situation to be modelled is the same as that for the mono-disperse model described in the previous section with the exception that the droplets injected into the air stream from the nebuliser are of varying sizes. The initial droplet size for the jth bin in the droplet size distribution is $d_{\mathrm{d},j,i}$. A representative thin plug or control mass of air and water droplets is considered and droplets begin to evaporate into the surrounding air in the plug as the plug moves along the conduit as shown in Figure 4-6, Figure 4-7 and Figure 4-8.
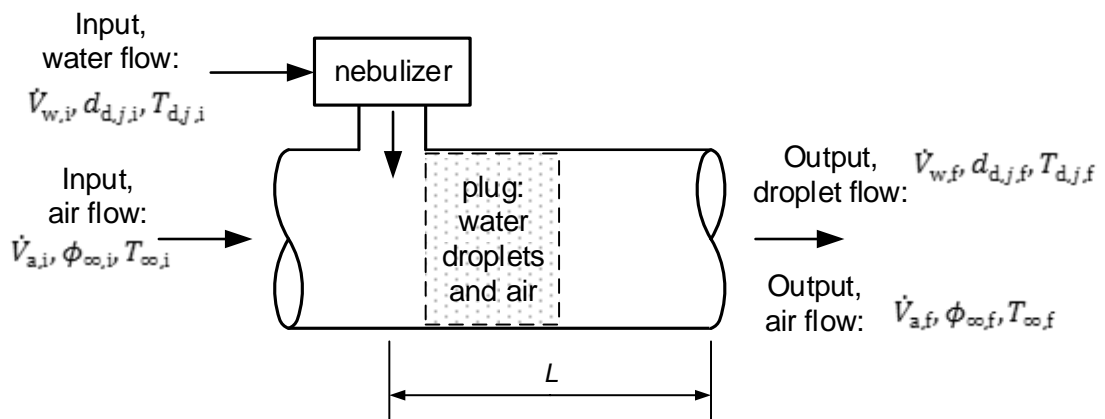
Figure 4-6: Physical model of evaporation process – poly-disperse droplets
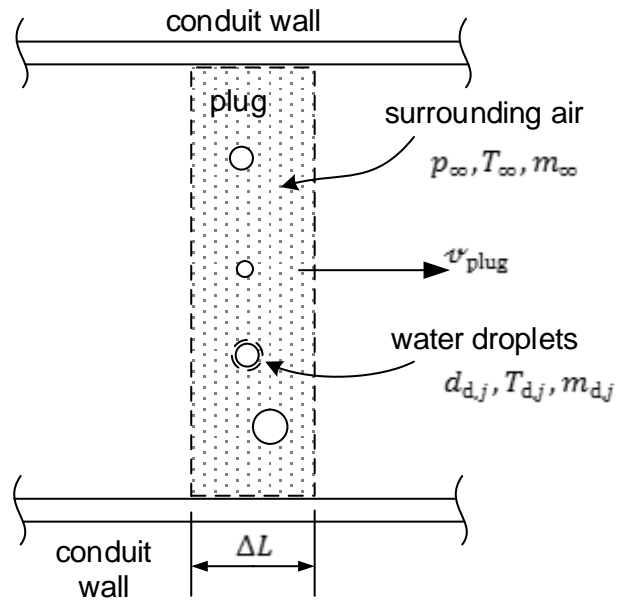
Figure 4-7 Plug flow model – poly-disperse droplets

4.3.2 Assumptions

The assumptions for this poly-disperse model are substantially the same as those for the mono-disperse model with the exception that assumptions 3, 6 and 7 are modified as follows:

3. The droplets generated by the ultrasonic nebuliser vary in size (poly-disperse size distribution) and can be described by a discrete size distribution in the size range of 0.2 to 70 μm.

6. Due to the assumptions of low droplet concentration, and no interactions with conduit walls or other droplets, it is assumed therefore that droplets of a particular initial size all behave uniformly.

7. Prior to complete evaporation the number concentration of the droplets in each size range (bin) remains constant in the moving plug.

4.3.3 Droplet mass balance

Consider a system boundary that is located on the surface of a single water droplet in the jth size range of the poly-disperse droplet size distribution (Figure 4-8). The conservation of mass over a small time period dt in the plug for the droplet will be identical to the mono-disperse case which is given in equation (4-1). For the evaporating water droplet, the first term in that equation is zero and therefore

66

$$-\dot{m}_{\text{w},j} = \frac{dm_{\text{d},j}}{dt} \qquad (4\text{-}48)$$

Which is similar to equation (4-2) for the mono-disperse case.
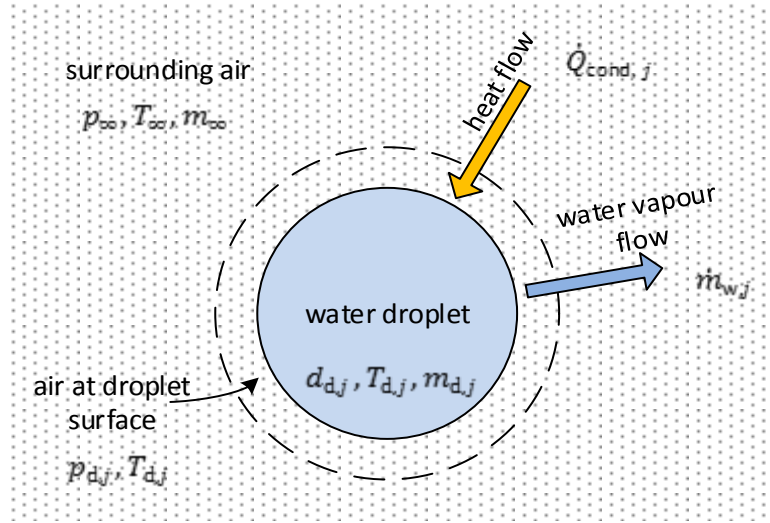
Figure 4-8 Mass and heat flows during evaporation

The droplet mass balance analysis for the poly-disperse case is similar to that for the mono-disperse case. Following that analysis, but applied to the poly-disperse case, an expression is derived for the rate of change of droplet diameter, for the jth droplet size in the distribution, during the evaporation process.

$$\frac{dd_{\text{d},j}}{dt} = \frac{4D_{\text{w},j}M_{\text{w}}}{\rho_{\text{d},j}d_{\text{d},j}R_{\text{u}}}\left(\frac{p_\infty}{T_\infty} - \frac{p_{\text{d},j}}{T_{\text{d},j}}\right)C_{\text{m},j} \qquad (4\text{-}49)$$

Which is similar to equation (4-17). As for the mono-disperse case there is an increase in the vapour pressure at the curved droplet surface due to the Kelvin effect and this is expressed in equation (4-18) and is used to determine water vapour pressure $p_{\text{d},j}$ in equation (4-49).

4.3.4 Droplet energy balance

The energy balance for the droplet in Figure 4-8 over a small time period dt will be identical to the mono-disperse case which is given in equation (4-19). Assuming the surrounding air in the plug, some distance from the droplet, is at a higher temperature than the water droplet then the energy flow is into the droplet and is by heat conduction, $\dot{Q}_{\text{cond},j}$. The energy flow out of the droplet is the latent energy associated with the water evaporating from the droplet, $\dot{E}_{\text{out},j}$. The energy change of the droplet

is the change in enthalpy of the droplet, $dH_{d,j}$. Thus equation (4-19) for a droplet in the jth size range becomes

$$\dot{Q}_{\text{cond, } j} - \dot{E}_{\text{out},j} = \frac{dH_{d,j}}{dt} \tag{4-50}$$

Which is similar to equation (4-20). The droplet energy balance analysis for the poly-disperse case is similar to that for the mono-disperse case. Following that analysis, but applied to the poly-disperse case, an expression is derived for the rate of change of droplet temperature during the evaporation process for the jth droplet size in the distribution in the plug

$$\frac{dT_{d,j}}{dt} = \frac{12k_{f,j}\left(T_\infty - T_{d,j}\right)C_{h,j} + 3\rho_{d,j}d_{d,j}h_{fg,j}\dfrac{dd_{d,j}}{dt}}{\rho_{d,j}d_{d,j}^2 C_{p,d,j}} \tag{4-51}$$

Which is similar to equation (4-30).

4.3.5 Surrounding air mass balance

The mass balance for the region occupied by the surrounding air in the plug (see Figure 4-7) is the same as for the mono-disperse case which is given in equation (4-31). The mass of dry air in the plug remains constant during the evaporation process and the mass flowing into the region occupied by the surrounding air in the plug is in the form of water vapour only (from all of the droplets) so that the mass balance is really a water balance. Furthermore, there is no mass flow out of the region occupied by the surrounding air. Applying this to equation (4-31) for all of the droplets in the plug gives

$$\sum_{j=1}^{Nt}\left(n_j\dot{m}_{w,j}\right) = \frac{dm_{w,\infty}}{dt} \tag{4-52}$$

Where Nt is the number of bins (droplet size ranges) in the droplet size distribution, and n_j is the number of droplets in the jth size range. The surrounding air mass balance analysis for the poly-disperse case is similar to that for the mono-disperse case. Following that analysis, but applied to the poly-disperse case, an expression is derived for the rate of change of water vapour pressure in the surrounding air during the evaporation process in the plug

$$\frac{dp_\infty}{dt} = -\frac{\pi R_u T_\infty}{2M_w v_a}\sum_{j=1}^{Nt}\left(\rho_{d,j}d_{d,j}^2 N_{md,j}\frac{dd_{d,j}}{dt}\right) \tag{4-53}$$

68

Where $N_{\text{md},j} = n_j/m_{\text{a}}$, which is the number droplet concentration, i.e., number of droplets in the jth size range per kg of dry air in the plug. This number droplet concentration can also be expressed in terms of the input air and water flow rates to the conduit. If $\dot{V}_{\text{w},j,i}$ is the volume flow rate of the jth sized water droplets at the point of injection into the conduit and $\dot{m}_{\text{a}}$ is the mass flow rate of dry air in the conduit then for the plug

$$N_{\text{md},j} = \frac{\dot{V}_{\text{w},j,i}/\left(\pi d_{\text{d},j,i}^3/6\right)}{\dot{m}_{\text{a}}} \qquad (4\text{-}54)$$

4.3.6 Surrounding air energy balance

The energy balance for the region occupied by the surrounding air in the plug (see Figure 4-7) is the same as that for the mono-disperse case which is given in equation (4-40). Assuming that the conduit walls containing the air/water droplet mixture are adiabatic and considering the plug as a closed system then this energy balance can also be considered as the constant pressure mixing of the humid surrounding air with the water vapour diffusing in to it from the droplets. This is combined with a conduction heat loss, to reach some equilibrium mixture temperature (Figure 4-4). As for the mono-disperse case, if a short finite time period Δt is now considered then this mixing process can be written as equation (4-41) and is repeated here

$$\dot{Q}_{\text{cond}}\Delta t = \Delta H_{\text{humid air}} + \Delta H_{\text{water vapour}} \qquad (4\text{-}41)$$

Since Δt is a very short time period there will be a very small change in the surrounding air temperature ΔT_∞ and the mass of water vapour diffusing into the surrounding air mass will also be very small, so

$$\dot{Q}_{\text{cond}}\Delta t = m_\infty C_{\text{p},\infty}\Delta T_\infty + \sum_{j=1}^{Nt} -n_j\Delta m_{\text{d},j}C_{\text{p,wvap},j}\left(T_\infty - T_{\text{d},j}\right) \qquad (4\text{-}55)$$

And taking the limit $\Delta t \to 0$

$$\dot{Q}_{\text{cond}} = m_\infty C_{\text{p},\infty}\frac{dT_\infty}{dt} + \sum_{j=1}^{Nt}\left[-n_j\frac{dm_{\text{d},j}}{dt}C_{\text{p,wvap},j}\left(T_\infty - T_{\text{d},j}\right)\right] \qquad (4\text{-}56)$$

The surrounding air energy balance analysis for the poly-disperse case is similar to that for the mono-disperse case. Following that analysis, but applied to the poly-disperse

case, an expression is derived for the rate of change of surrounding air temperature during the evaporation process in the plug

$$\frac{dT_\infty}{dt} = \frac{\pi \xi_\infty}{2C_{p,\infty}} \sum_{j=1}^{Nt} \left[N_{md,j} d_{d,j} \left(T_\infty - T_{d,j} \right) \left(\rho_{d,j} d_{d,j} C_{p,wvap,j} \frac{dd_{d,j}}{dt} \right) \right. \tag{4-57}$$
$$\left. - 4k_{f,j} C_{h,j} \right)\right]$$

Thus, the following equations represent the governing equations for the evaporation of the poly-disperse water droplets into the air flowing along the conduit. The number of discrete droplet sizes in the droplet size distribution is Nt, thus there are a total of $2Nt + 2$ ordinary differential equations to solve.

$$\frac{dd_{d,j}}{dt} = \frac{4D_{w,j} M_w}{\rho_{d,j} d_{d,j} R_u} \left(\frac{p_\infty}{T_\infty} - \frac{p_{d,j}}{T_{d,j}} \right) C_{m,j} \tag{4-49}$$

$$\frac{dT_{d,j}}{dt} = \frac{12 k_{f,j} \left(T_\infty - T_{d,j} \right) C_{h,j} + 3 \rho_{d,j} d_{d,j} h_{fg,j} \frac{dd_{d,j}}{dt}}{\rho_{d,j} d_{d,j}^2 C_{p,d,j}} \tag{4-51}$$

$$\frac{dp_\infty}{dt} = -\frac{\pi R_u T_\infty}{2 M_w v_a} \sum_{j=1}^{Nt} \left(\rho_{d,j} d_{d,j}^2 N_{md,j} \frac{dd_{d,j}}{dt} \right) \tag{4-53}$$

$$\frac{dT_\infty}{dt} = \frac{\pi \xi_\infty}{2C_{p,\infty}} \sum_{j=1}^{Nt} \left[N_{md,j} d_{d,j} \left(T_\infty - T_{d,j} \right) \left(\rho_{d,j} d_{d,j} C_{p,wvap,j} \frac{dd_{d,j}}{dt} \right) \right. \tag{4-57}$$
$$\left. - 4k_{f,j} C_{h,j} \right)\right]$$

4.3.7 Initial and boundary conditions

The initial and boundary conditions for the poly-disperse case will be the same as for the mono-disperse case explained in section 4.2.7. Thus there is no mass or heat flow across the boundaries of the plug. The initial conditions for the model are the initial droplet sizes $d_{d,j,i}$ and temperatures $T_{d,j,i}$ and the initial water vapour pressure $p_{\infty,i}$, temperature $T_{\infty,i}$ and total pressure p_0 of the inlet air stream. It is assumed that the initial temperatures of all the different sizes of droplets are the same. The initial water vapour pressure $p_{\infty,i}$ in the surrounding air is determined from the initial relative humidity $\phi_{\infty,i}$ of that air. Since the outlet of the conduit is open to atmosphere and flow

rates are relatively low the total pressure is assumed to be 101.325 kPa. Although the total pressure does not appear in the equations it is used in the calculation of the various fluid and thermodynamic properties where appropriate.

As for the mono-disperse case, different outcomes can occur depending on the initial relative masses of water and air in the moving plug. If the relative mass of water is low enough the evaporation process described by these equations continues until all of the droplets completely evaporate and the water content of the surrounding air reaches some final value (less than saturation). The smaller droplets will completely evaporate more quickly than the larger droplets and a 'droplet lifetime' or 'evaporation distance' can be determined for each initial droplet size in the droplet size distribution, i.e., the time or distance along conduit till that initial droplet size completely evaporates. If the water to air ratio is higher, then equilibrium can be reached where the water vapour concentration at the remaining droplet surfaces is in equilibrium with that in the surrounding air and the water droplets are at the same temperature as the surrounding air. In this latter case the droplets reach some final steady state size and an 'equilibrium' time or distance can be determined. Also in this latter case it is possible for some of the smaller initial droplet sizes to completely evaporate prior to equilibrium being reached and for these droplets a 'droplet lifetime' and 'evaporation distance' can be determined.

4.3.8 Method of solution and outputs

As for the mono-disperse model the governing differential equations with their initial and boundary conditions were solved simultaneously using numerical differentiation formulae (NDF's) and backward differentiation formulae (BDF's) typical of those used for solving 'stiff' sets of differential equations. This was implemented using MATLAB® software as per the flow chart shown in Figure 4-9. Details of the MATLAB® code used for the poly-disperse droplet evaporation model is given in Appendix 3.

As for the mono-disperse model, fluid transport and thermodynamic properties were determined using two software based property function libraries: LibHuAirProp and LibIF97. These libraries were utilized in the numerical solution of the governing equations by determining all property values at each time step of the numerical solution of the evaporation process (Figure 4-9).

Figure 4-9 Flowchart for solution of governing equations – poly-disperse model

The outputs from the poly-disperse model are matrices of the dependant variables, the droplet diameters $d_{\mathrm{d},j}$ and temperatures $T_{\mathrm{d},j}$ for each droplet size in the droplet size distribution, the water vapour pressure in the surrounding air p_∞ and the surrounding humid air temperature T_∞, with respect to time as the plug moves along the conduit.

Matrices of the dependent variables with respect to distance along the conduit can be determined using equations (4-46) and (4-47) as described in section 4.2.8 for the mono-disperse model.

From these matrices of results, the amount of water evaporated and changes to the droplet size distribution over a certain time or distance can be readily determined. These can then be used in comparison to the other models and to experimental data to (ultimately) quantify the effect of ultrasound on water droplet evaporation.

4.3.9 Remarks – poly-disperse droplet evaporation model

In this section the governing equations for the evaporation process for poly-disperse water droplets in air flowing along a conduit were developed from mass and energy balances. The method used for solving these equations, using MATLAB®, was then outlined. An investigation was carried out to validate and explore droplet evaporation using the poly-disperse model and this is detailed in Chapter 5.

This poly-disperse model forms the basis for a droplet evaporation model that incorporates the application of an ultrasound field to the air and droplet mixture, to enhance the evaporation process, and is detailed in the next section.

4.4 Evaporation model – Ultrasound – Poly-disperse droplets

This study investigates the effect of an ultrasound field on water droplet evaporation, with the goal of accelerating the evaporation of the droplets. In Chapter 3 it was proposed that the most likely mechanism for the acceleration of that evaporation process using ultrasound would be the enhancement of the normal heat and mass transfer processes that occur during normal droplet evaporation. Thus, in this section a theoretical formulation of the proposed ultrasound enhanced droplet evaporation process, based on convection heat and mass transfer processes, rather than conduction processes is described.

Since the droplets are considered to be poly-disperse the distribution of droplet sizes is described in terms of a discrete distribution of % volume of water for a specified droplet

diameter range, there being Nt droplet diameter ranges or 'bins' in the distribution, as for the previous poly-disperse model. The goal, again, is to develop equations for the key parameters in the ultrasound enhanced evaporation process. This includes those parameters used in the previous models: droplet size $d_{\mathrm{d},j}$, droplet temperature $T_{\mathrm{d},j}$, surrounding air humidity ϕ_∞ (i.e., vapour pressure p_∞) and surrounding air temperature T_∞. This now also includes parameters that describe the imposed ultrasound field: the ultrasound frequency, ω and the ultrasound amplitude (in terms of the sound pressure level or SPL). With these parameters it is possible to quantify the amount of water evaporated and quantify any changes to the droplet size distribution along the conduit and investigate their relationship to the imposed ultrasound field. The implementation of the model in MATLAB® is also outlined.

To our knowledge this is the first time that a model has been developed to describe the enhancing effect of an ultrasound field on the evaporation of many micro-droplets into air flowing along a conduit.

4.4.1 Physical situation to be modelled

The physical situation for the ultrasound enhanced evaporation model is substantially the same as the normal poly-disperse evaporation model in that it consists of an air stream flowing along a conduit at flow rate $\dot{V}_{\mathrm{a,i}}$, temperature $T_{\infty,\mathrm{i}}$ and relative humidity $\phi_{\infty,\mathrm{i}}$. An ultrasonic nebuliser attached to the conduit injects droplets into the air stream at a flow rate of $\dot{V}_{\mathrm{w,i}}$ and uniform temperature $T_{\mathrm{d,i}}$. However the section of tube downstream of the nebuliser is replaced by a cylindrical radiator driven by an ultrasonic transducer that creates a high intensity ultrasonic field through which the air and droplets flow (Figure 4-10).

A representative thin plug or control mass of air and water droplets is considered and droplets begin to evaporate into the surrounding air in the plug as the plug moves along inside the cylindrical radiator and through the imposed ultrasound field (Figure 4-11)
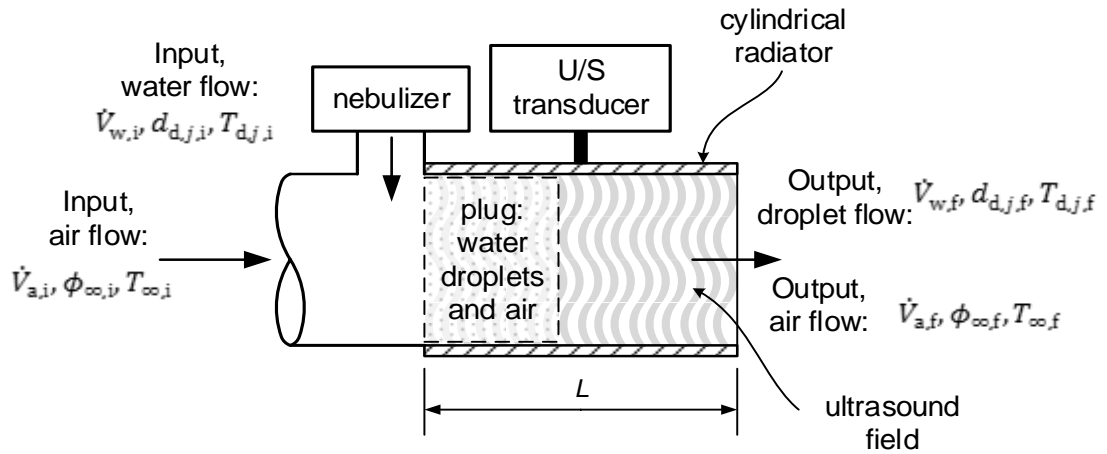
Figure 4-10: Physical model of evaporation process – ultrasound enhanced
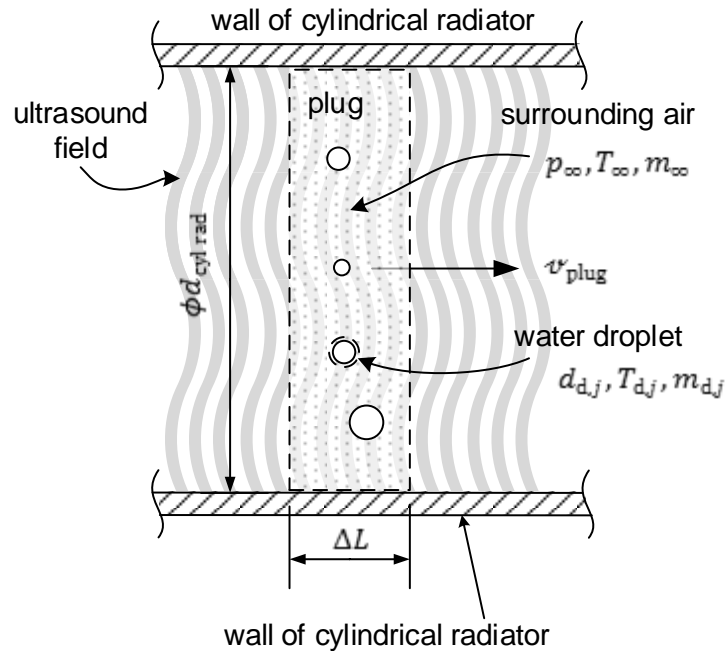
Figure 4-11 Plug flow model – poly-disperse droplets + ultrasound

4.4.2 Assumptions

The assumptions for the ultrasound enhanced evaporation model will be substantially the same as for the normal poly disperse evaporation model as per sections 4.2.2 and 4.3.2. However, with these additional assumptions regarding the imposed ultrasound field.

1. The ultrasound field has little heating effect on the air and droplets, so that the main effect of the ultrasound is to enhance the mass and heat transport processes occurring in the plug.

2. The magnitude of the air particle oscillation, due to the ultrasound field, is assumed to be large relative to the water droplet diameter, i.e., a small Strouhal number. Thus the air flow around each droplet can be considered to be quasi-steady [115].

4.4.3 Droplet mass balance

Consider a system boundary that is located on the surface of a single water droplet in the jth size range of the poly-disperse droplet size distribution (Figure 4-12). The conservation of mass over a small time period dt in the plug for the droplet will be identical to the mono-disperse and poly-disperse cases which is given in equation (4-1). Ignoring the first term in that equation for an evaporating droplet this can be written as

$$- \dot{m}_{w,j} = \frac{dm_{d,j}}{dt} \qquad (4\text{-}58)$$

In this case, the mass flow rate of water vapour from the droplet surface to the surrounding air is now assumed to be convection dominated due to the imposed ultrasound field. Thus, considering equation (4-58) and writing the mass flow in terms of mass convection [140], then

$$\dot{m}_{w,j} = h_{M,j} A_{d,j} \left(\rho_{w,s,j} - \rho_{w,\infty} \right) \qquad (4\text{-}59)$$

Where $h_{M,j}$ is the convection mass transfer coefficient for the droplets in the jth size range as a result of the imposed ultrasound field, $A_{d,j}$ is the surface area of a single droplet in the jth size range, $\rho_{w,s,j}$ is the partial density of water vapour at the surface of a droplet in the jth size range and $\rho_{w,\infty}$ is the partial density of water vapour in the air surrounding the droplets in the plug.

It was discussed in section 4.2.3 that, during evaporation, when the droplets become very small the non-continuum effect of the surrounding gas must be allowed for in determination of the evaporation rate. This was achieved using the correction factors stated in equations (4-6) and (4-7). These factors also apply in the case of convective evaporation [49, 56]. The mass flux correction factor for the poly-disperse case is

$$C_{m,j} = \frac{1 + \mathrm{Kn}_{m,j}}{1 + \left(\dfrac{4}{3\alpha_{m,j}} + 0.377 \right) \mathrm{Kn}_{m,j} + \dfrac{4}{3\alpha_{m,j}} \mathrm{Kn}_{m,j}^2} \qquad (4\text{-}60)$$
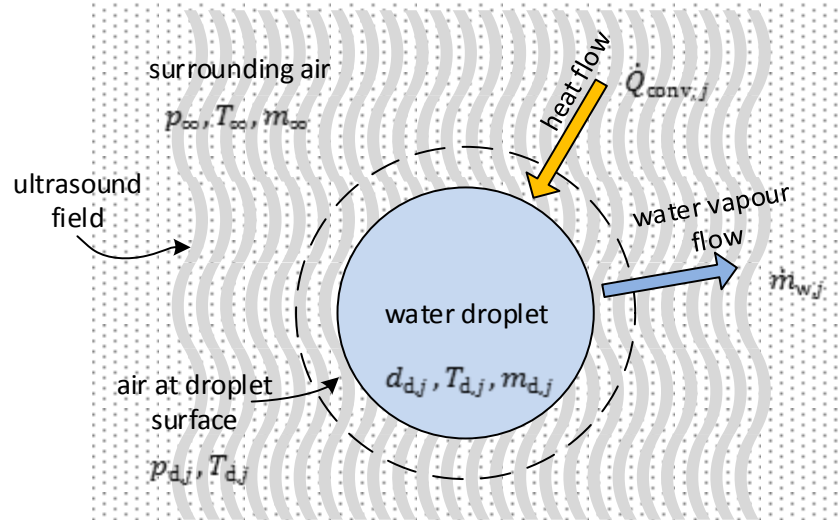
Figure 4-12 Mass and heat flows during evaporation - ultrasound enhanced

And the heat flux correction factor for the poly-disperse case is

$$C_{h,j} = \frac{1 + \mathrm{Kn}_{h,j}}{1 + \left(\dfrac{4}{3\alpha_{h,j}} + 0.377\right)\mathrm{Kn}_{h,j} + \dfrac{4}{3\alpha_{h,j}}\mathrm{Kn}_{h,j}^2}$$ (4-61)

Thus equation (4-59) becomes

$$\dot{m}_{w,j} = h_{M,j}A_{d,j}\left(\rho_{w,s,j} - \rho_{w,\infty}\right)C_{m,j}$$ (4-62)

From equations (4-10) and (4-12) the partial densities in this equation can be written generally as

$$\rho_w = \frac{p_w M_w}{R_u T_w}$$ (4-63)

A spherical droplet has a surface area $A_{d,j} = \pi d_{d,j}^2$ and also substituting equation (4-63) into equation (4-62) gives

$$\dot{m}_{w,j} = \frac{h_{M,j}\pi d_{d,j}^2 M_w}{R_u}\left(\frac{p_{d,j}}{T_{d,j}} - \frac{p_\infty}{T_\infty}\right)C_{m,j}$$ (4-64)

Now, the rate of change of mass of an individual water droplet (4-58) is the same as in the normal evaporation case (4-16) but here written for poly-disperse droplets.

$$\frac{dm_{d,j}}{dt} = \frac{\rho_{d,j}\pi d_{d,j}^2}{2}\frac{dd_{d,j}}{dt}$$ (4-65)

 Thus, substituting equations (4-65) and (4-64) into equation (4-58) and rearranging gives an expression for the rate of change of droplet diameter, for the jth droplet size in the distribution, during the ultrasound enhanced evaporation process

$$\frac{dd_{\mathrm{d},j}}{dt} = \frac{2h_{\mathrm{M},j}M_{\mathrm{w}}}{\rho_{\mathrm{d},j}R_{\mathrm{u}}}\left(\frac{p_\infty}{T_\infty} - \frac{p_{\mathrm{d},j}}{T_{\mathrm{d},j}}\right)C_{\mathrm{m},j} \tag{4-66}$$

For the curved droplet surfaces there is an increase in vapour pressure due to the Kelvin effect [139] as given in equation (4-18) and this is used to determine the partial water vapour pressure $p_{\mathrm{d},j}$ in equation (4-66).

It is assumed that the oscillating flow around the droplets is quasi-steady so the convection mass transfer coefficient, $h_{\mathrm{M},j}$ can be determined from steady flow correlations for convective mass transfer [115]. Modifying the correlation first developed by Ranz and Marshall [58] using the oscillating Reynolds Number gives

$$\mathrm{Sh}_j = 2 + 0.552\,\mathrm{Re}_{\mathrm{osc},j}^{1/2}\mathrm{Sc}_j^{1/3} \tag{4-67}$$

Where Sc is the Schmidt number and

$$\mathrm{Re}_{\mathrm{osc},j} = \frac{\mathscr{v}d_{\mathrm{d},j}}{\nu_j} \tag{4-68}$$

Where $\mathscr{v}$ = velocity amplitude of the ultrasound field and ν = the kinematic viscosity of the air. Thus from the Sherwood number [140] the convective mass transfer coefficient is

$$h_{\mathrm{M},j} = \frac{\mathrm{Sh}_j\,D_{\mathrm{w},j}}{d_{\mathrm{d},j}} \tag{4-69}$$

4.4.4 Droplet energy balance

The energy balance for the droplet in Figure 4-12 over a small time period dt will be identical to the mono-disperse and poly-disperse cases which is given in equation (4-19). Assuming the surrounding air in the plug, some distance from the droplet, is at a higher temperature than the water droplet then the energy flow into the droplet, in this case, is by heat convection from the surrounding air, $\dot{Q}_{\mathrm{conv},\,j}$. The energy flow out of the droplet is the latent energy associated with the water evaporating from the droplet $\dot{E}_{\mathrm{out},j}$. The energy change of the droplet is the change in enthalpy of the droplet, $dH_{\mathrm{d},j}$. Thus equation (4-19) for a droplet in the jth size range is

$$\dot{Q}_{\mathrm{conv},\,j} - \dot{E}_{\mathrm{out},j} = \frac{dH_{\mathrm{d},j}}{dt} \tag{4-70}$$

Considering equation (4-70), the rate of heat convection from the air to a single droplet in the jth size range, and applying the non-continuum heat flux correction factor (4-61), it can be written as [140],

$$\dot{Q}_{\text{conv},j} = h_{\text{H},j} A_{\text{d},j} (T_\infty - T_{\text{d},j}) C_{\text{h},j} \tag{4-71}$$

Where $h_{\text{H},j}$ is the convection heat transfer coefficient for the droplets in the jth size range as a result of the imposed ultrasound field. Also, the surface area for a spherical droplet $A_{\text{d},j} = \pi d_{\text{d},j}^2$ so

$$\dot{Q}_{\text{conv},j} = h_{\text{H},j} \pi d_{\text{d},j}^2 (T_\infty - T_{\text{d},j}) C_{\text{h},j} \tag{4-72}$$

Now, the latent energy removed from the droplet in the form of a vapour flow (4-70), assuming the vapour is saturated at the droplet surface, is given by

$$\dot{E}_{\text{out},j} = \dot{m}_{\text{w},j} h_{g,j} \tag{4-73}$$

where $h_{g,j}$ is the enthalpy of the saturated water vapour at $T_{\text{d},j}$. Combining equations (4-58) and (4-65) into (4-73) gives

$$\dot{E}_{\text{out},j} = -\frac{\rho_{\text{d},j} \pi d_{\text{d},j}^2}{2} \frac{dd_{\text{d},j}}{dt} h_{g,j} \tag{4-74}$$

Now the rate of change of energy (enthalpy) of a liquid droplet (4-70), can be written as

$$\frac{dH_{\text{d},j}}{dt} = \frac{d(m_{\text{d},j} h_{\text{d},j})}{dt} = h_{\text{d},j} \frac{dm_{\text{d},j}}{dt} + m_{\text{d},j} \frac{dh_{\text{d},j}}{dt} \tag{4-75}$$

Now, substituting equations (4-75), (4-74) and (4-72) into the energy balance equation, (4-70) and simplifying gives

$$\frac{dh_{\text{d},j}}{dt} = \frac{6h_{\text{H},j}(T_\infty - T_{\text{d},j}) C_{\text{h},j} + 3\rho_{\text{d},j}(h_{g,j} - h_{\text{d},j})\dfrac{dd_{\text{d},j}}{dt}}{\rho_{\text{d},j} d_{\text{d},j}} \tag{4-76}$$

Over a small temperature change, the enthalpy of a liquid can be closely approximated [141] as

$$dh_{\text{d},j} = C_{p,\text{d},j} dT_{\text{d},j} \tag{4-77}$$

Where $C_{p,\text{d},j}$ is the specific heat capacity of the water in a droplet in the jth size range. Also, the specific enthalpy $h_{\text{d},j}$ is approximately equal to the specific enthalpy of the

saturated liquid $h_{f,j}$ at the droplet temperature $T_{d,j}$, so the term $\left(h_{g,j} - h_{d,j}\right)$ in equation (4-76) can be written as the enthalpy of vaporisation $h_{fg,j}$. Thus substituting this simplification and equation (4-77) into equation (4-76) gives an expression for the rate of change of droplet temperature during the ultrasound enhanced evaporation process for the jth droplet size in the distribution in the plug

$$\frac{dT_{d,j}}{dt} = \frac{6h_{H,j}\left(T_\infty - T_{d,j}\right)C_{h,j} + 3\rho_{d,j}h_{fg,j}\dfrac{dd_{d,j}}{dt}}{\rho_{d,j}d_{d,j}C_{p,d,j}} \tag{4-78}$$

As mentioned in section 4.4.3 it is assumed that the oscillating flow around the droplets is quasi-steady so the convection heat transfer coefficient, $h_{H,j}$ can be determined from steady flow correlations for convective heat transfer. Modifying the correlation first developed by Ranz and Marshall [58] using the oscillating Reynolds Number (4-68).

$$\mathrm{Nu}_j = 2 + 0.552\,\mathrm{Re}_{osc,j}^{1/2}\,\mathrm{Pr}_j^{1/3} \tag{4-79}$$

and from the Nusselt number the convective heat transfer coefficient is

$$h_{H,j} = \frac{\mathrm{Nu}_j k_{d,j}}{d_{d,j}} \tag{4-80}$$

4.4.5 Surrounding air mass balance

The mass balance for the region occupied by the surrounding air in the plug (Figure 4-11) is the same as for the mono-disperse and poly-disperse cases which is given in equation (4-31). And the derivation of the governing equation based on the surrounding air mass balance is also the same as that for the poly-disperse droplet case, described in section 4.3.5. Thus equation (4-53) applies and is rewritten here for completeness

$$\frac{dp_\infty}{dt} = -\frac{\pi R_u T_\infty}{2M_w v_a} \sum_{j=1}^{Nt} \left(\rho_{d,j} d_{d,j}^2 N_{md,j} \frac{dd_{d,j}}{dt} \right) \tag{4-53}$$

Where $N_{md,j}$ is given by equation (4-54).

4.4.6 Surrounding air energy balance

The energy balance for the region occupied by the surrounding air in the plug (Figure 4-11) is the same as that for the mono-disperse case which is given in equation (4-40). Again, assuming that the conduit walls containing the air/water droplet mixture are adiabatic and considering the plug as a closed system then this energy balance can also

be considered as the constant pressure mixing of the humid surrounding air with the water vapour convection diffusing into it from the droplets. This is combined with a convection heat loss, to reach some equilibrium mixture temperature (Figure 4-13).
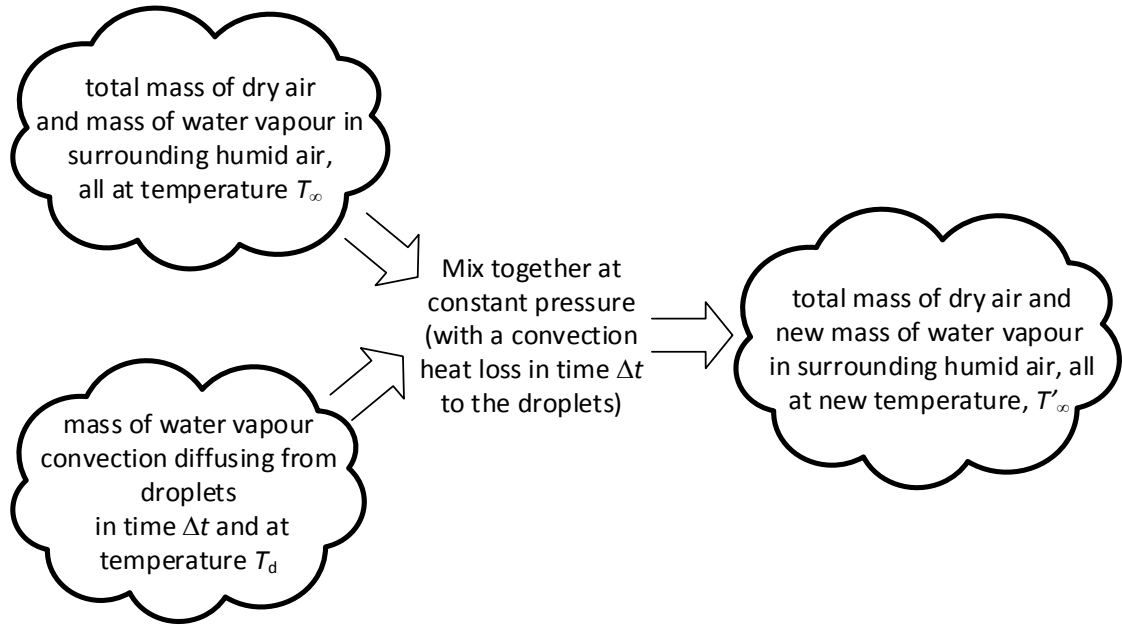
Figure 4-13: Mixing of humid air and diffusing water vapour – ultrasound case

In this case, if a short finite time period Δt is now considered then this mixing process can be written as

$$\dot{Q}_{\text{conv}}\Delta t = \Delta H_{\text{humid air}} + \Delta H_{\text{water vapour}} \tag{4-81}$$

Since Δt is a very short time period there will be a very small change in the surrounding air temperature ΔT_∞ and the mass of water vapour convection diffusing into the surrounding air mass will also be very small, so

$$\dot{Q}_{\text{conv}}\Delta t = m_\infty C_{\text{p},\infty}\Delta T_\infty + \sum_{j=1}^{Nt} -n_j \Delta m_{\text{d},j} C_{\text{p,wvap},j}\left(T_\infty - T_{\text{d},j}\right) \tag{4-82}$$

Taking the limit $\Delta t \to 0$

$$\dot{Q}_{\text{conv}} = m_\infty C_{\text{p},\infty}\frac{dT_\infty}{dt} + \sum_{j=1}^{Nt}\left[-n_j \frac{dm_{\text{d},j}}{dt} C_{\text{p,wvap},j}\left(T_\infty - T_{\text{d},j}\right)\right] \tag{4-83}$$

Considering the heat convection from the surrounding air to all of the droplets, then from equation (4-72)

$$\dot{Q}_{\mathrm{conv}} = -\sum_{j=1}^{Nt}\left[n_j h_{\mathrm{H},j}\pi d_{\mathrm{d},j}^2\left(T_\infty - T_{\mathrm{d},j}\right)C_{\mathrm{h},j}\right] \qquad (\,4\text{-}84)$$

Substituting equation (4-84) into equation (4-83) and also substituting equation (4-65) into equation (4-83); since $dm_{\mathrm{d},j}/dt = -\dot{m}_{\mathrm{w},j}$ and rearranging gives an expression for the rate of change of surrounding air temperature during the ultrasound enhanced evaporation process in the plug

$$\frac{dT_\infty}{dt} = \frac{\pi\xi_\infty}{2C_{\mathrm{p},\infty}}\sum_{j=1}^{Nt}\left[N_{\mathrm{md},j}d_{\mathrm{d},j}^2\left(T_\infty - T_{\mathrm{d},j}\right)\left(\rho_{\mathrm{d},j}C_{\mathrm{p},\mathrm{wvap},j}\frac{dd_{\mathrm{d},j}}{dt} - 2h_{\mathrm{H},j}\right)\right] \qquad (\,4\text{-}85)$$

Where $N_{\mathrm{md},j} = n_j/m_{\mathrm{a}}$ as before and $m_{\mathrm{a}}/m_\infty = \xi_\infty$ is the dryness fraction of the surrounding air in the plug.

Thus, the following equations represent the governing equations for the evaporation of the poly-disperse water droplets into the air flowing along the conduit with an imposed ultrasound field. The number of discrete droplet sizes in the droplet size distribution is Nt, thus there are a total of $2Nt + 2$ ordinary differential equations to solve.

$$\frac{dd_{\mathrm{d},j}}{dt} = \frac{2h_{\mathrm{M},j}M_{\mathrm{w}}}{\rho_{\mathrm{d},j}R_{\mathrm{u}}}\left(\frac{p_\infty}{T_\infty} - \frac{p_{\mathrm{d},j}}{T_{\mathrm{d},j}}\right)C_{\mathrm{m},j} \qquad (\,4\text{-}66)$$

$$\frac{dT_{\mathrm{d},j}}{dt} = \frac{6h_{\mathrm{H},j}\left(T_\infty - T_{\mathrm{d},j}\right)C_{\mathrm{h},j} + 3\rho_{\mathrm{d},j}\mathrm{h}_{\mathrm{fg},j}\dfrac{dd_{\mathrm{d},j}}{dt}}{\rho_{\mathrm{d},j}d_{\mathrm{d},j}C_{\mathrm{p},\mathrm{d},j}} \qquad (\,4\text{-}78)$$

$$\frac{dp_\infty}{dt} = -\frac{\pi R_{\mathrm{u}}T_\infty}{2M_{\mathrm{w}}v_{\mathrm{a}}}\sum_{j=1}^{Nt}\left(\rho_{\mathrm{d},j}d_{\mathrm{d},j}^2 N_{\mathrm{md},j}\frac{dd_{\mathrm{d},j}}{dt}\right) \qquad (\,4\text{-}53)$$

$$\frac{dT_\infty}{dt} = \frac{\pi\xi_\infty}{2C_{\mathrm{p},\infty}}\sum_{j=1}^{Nt}\left[N_{\mathrm{md},j}d_{\mathrm{d},j}^2\left(T_\infty - T_{\mathrm{d},j}\right)\left(\rho_{\mathrm{d},j}C_{\mathrm{p},\mathrm{wvap},j}\frac{dd_{\mathrm{d},j}}{dt} - 2h_{\mathrm{H},j}\right)\right] \qquad (\,4\text{-}85)$$

4.4.7 Initial and boundary conditions

The initial and boundary conditions for the ultrasound enhanced case will be the same as for the poly-disperse case explained in section 4.3.7. Thus there is no mass or heat flow across the boundaries of the plug. The initial conditions for the model are the initial droplet sizes $d_{\mathrm{d},j,\mathrm{i}}$ and temperatures $T_{\mathrm{d},j,\mathrm{i}}$ and the initial water vapour pressure $p_{\infty,i}$,

temperature $T_{\infty,i}$ and total pressure p_0 of the inlet air stream. It is assumed that the initial temperatures of all the different sizes of droplets are the same. The initial water vapour pressure $p_{\infty,i}$ in the surrounding air is determined from the initial relative humidity $\phi_{\infty,i}$ of that air. As in the previous models, since the outlet of the conduit is open to atmosphere and flow rates are relatively low the total pressure, p_0 is assumed to be 101.325 kPa. Although the total pressure does not appear in the equations it is used in the calculation of the various fluid and thermodynamic properties where appropriate.

4.4.8 Method of solution and outputs

As for the poly-disperse model the governing differential equations with their initial and boundary conditions were solved simultaneously using numerical differentiation formulae (NDF's) and backward differentiation formulae (BDF's) typical of those used for solving 'stiff' sets of differential equations. This was implemented using MATLAB® software as per the flow chart shown in Figure 4-14. Details of the MATLAB® code used for the ultrasound enhanced droplet evaporation model is given in Appendix 3.

As for the poly-disperse model, fluid transport and thermodynamic properties were determined using two software based property function libraries: LibHuAirProp and LibIF97. These libraries were utilized in the numerical solution of the governing equations by determining all property values at each time step of the numerical solution of the evaporation process (Figure 4-14).
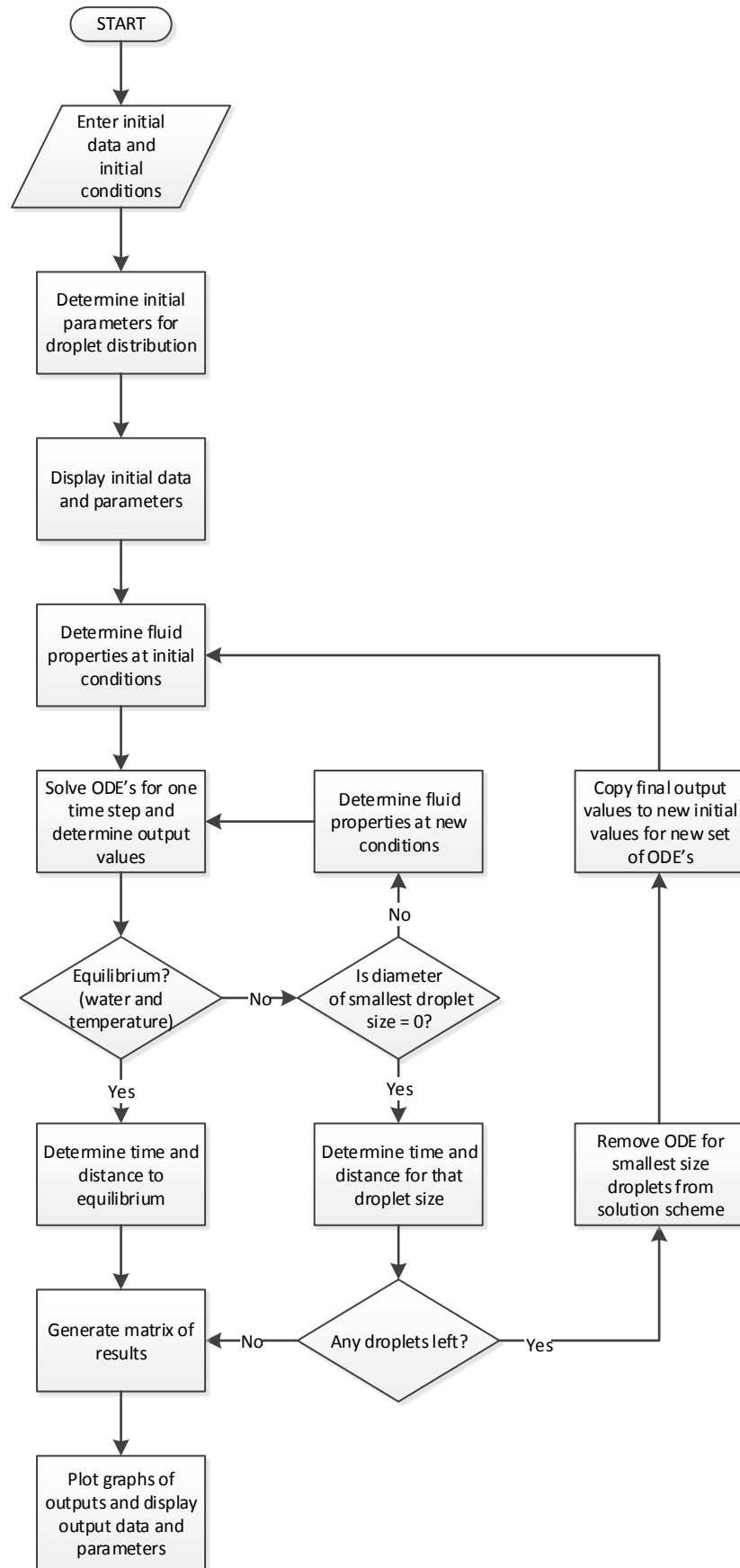
The outputs from the ultrasound enhanced model are matrices of the dependant variables, the droplet diameters $d_{d,j}$ and temperatures $T_{d,j}$ for each droplet size in the droplet size distribution, the water vapour pressure in the surrounding air p_∞ and the surrounding humid air temperature T_∞, with respect to time as the plug moves along the conduit.

Matrices of the dependent variables with respect to distance along the conduit can be determined using equations (4-46) and (4-47) as described in section 4.2.8 for the mono-disperse and poly-disperse models model.
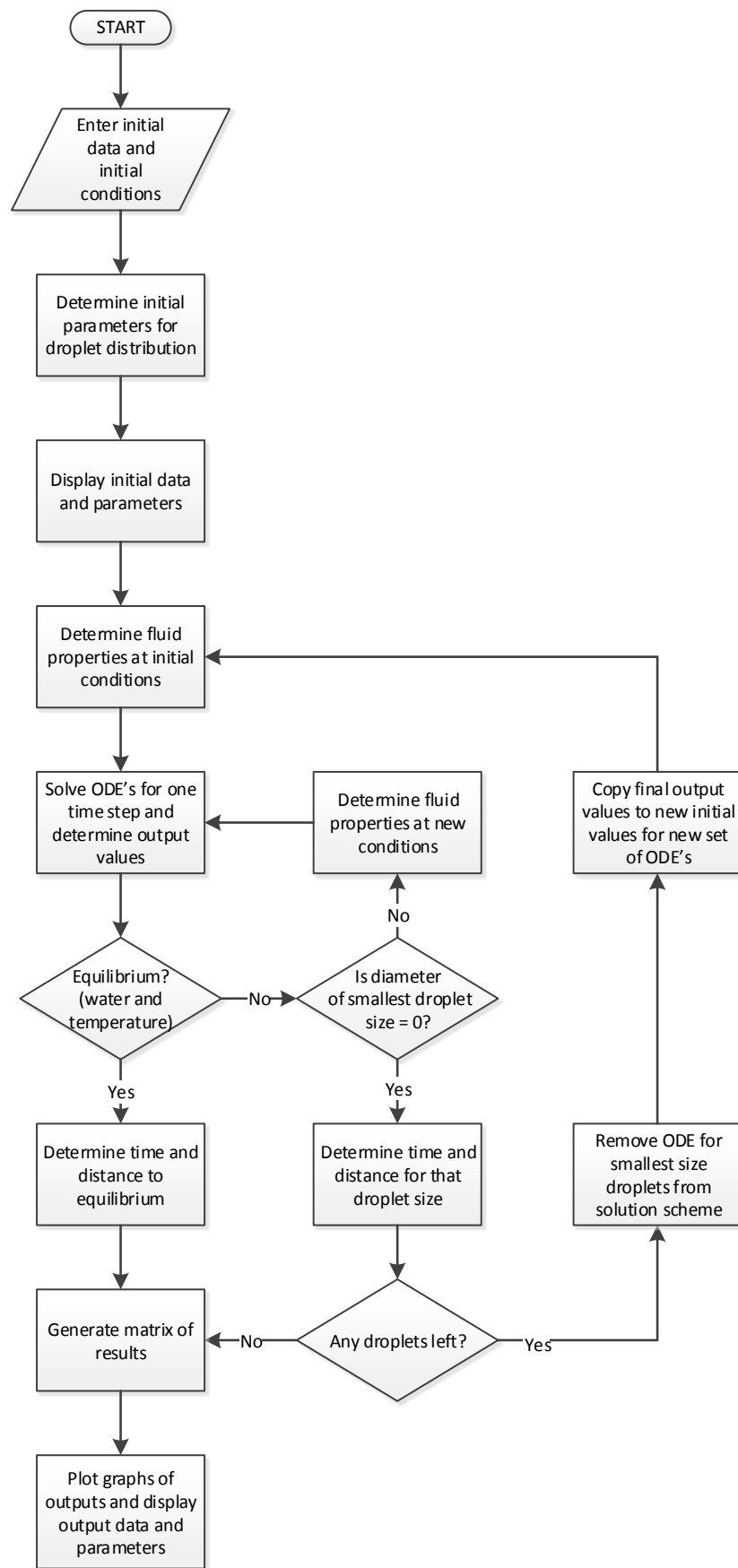
Figure 4-14 Flowchart for solution of governing equations – ultrasound enhanced evaporation

From these matrices of results, the amount of water evaporated and changes to the droplet size distribution over a certain time or distance can be readily determined. These can then be used in comparison to the other models and to experimental data to quantify the effect of ultrasound on water droplet evaporation.

In the same way as for the other models, the amount of water evaporated and changes to the droplet size distribution over a certain time or distance can be readily determined from these matrices of results. These can then be used in comparison to the other models and to experimental data to quantify the effect of the ultrasound field on water droplet evaporation.

4.4.9 Remarks – ultrasound enhanced evaporation model

In this section the governing equations for the ultrasound enhanced evaporation process for poly-disperse water droplets in air flowing along a conduit were developed from mass and energy balances. The method used for solving these equations, using MATLAB®, was then outlined.

An investigation was carried out to explore ultrasound enhanced droplet evaporation using this model along with experimental data and is detailed in Chapter 5.

4.5 Closure – theoretical formulation

In this chapter the following theoretical models were developed to describe the droplet evaporation process for a droplet and air mixture flowing along a conduit.

- Mono-disperse droplet distribution
- Poly-disperse droplet distribution
- Ultrasound enhanced evaporation

These models will be used to generate results for comparison with results from the experimental investigation. Together they will be used in the investigation, quantification and understanding of the enhancement of droplet evaporation due to an imposed ultrasound field.

Although the mono-disperse and poly-disperse droplet evaporation models have previously been described for general situations [51], nevertheless in this thesis they are developed specifically for a droplet and air mixture flowing along a conduit as is found

in medical respiratory devices. To the best of our knowledge the ultrasound enhanced evaporation model is developed for the first time in this thesis.

Chapter 5 - Experimental Investigation

5.1 Introduction

The experimental investigation detailed in this chapter focusses on determining the effect of the ultrasound field on the evaporation of water droplets into air as they flow along a conduit. In the previous chapter theoretical models were developed for this same purpose. To validate those models as well as to compare the theoretical results with practical values an experimental investigation has to be carried out. Thus this chapter has a two-fold experimental purpose: Firstly it investigates the rate of evaporation from water droplets under normal conditions. In principle this part validates the mono-disperse and poly-disperse models developed in the previous chapter. Secondly, it investigates changes in the rate of evaporation produced by the addition of an ultrasound field. As stated in the previous chapter, some of the inputs and boundary conditions for the models developed must be determined in advance. This is achieved in this chapter as various variables are measured and considered as inputs to the theoretical model. This gives terms of reference for comparing the theoretical and experimental results.

This chapter presents the methodology, experimental apparatus and sample results obtained in this work. The detailed experimental results for both normal and ultrasound enhanced evaporation can be found in Chapter 6 along with comparative results from the theoretical models.

5.2 Initial investigation – Mono-disperse droplet evaporation

As detailed in Chapter 4 the initial model that was developed assumed a mono-disperse droplet distribution. Since practical nebulisers do not generate truly mono-disperse droplet distributions, there are limitations in validating this model experimentally. However it is possible to compare outputs from the theoretical model with overall mass and energy balances and with appropriate experimental data from the literature.

The overall mass and energy balances were developed to give the final values of the four dependant variables d_d, T_d, p_∞ (or ϕ_∞) and T_∞, once steady state conditions had been achieved i.e., equilibrium reached or all the droplets had evaporated, for a given set of initial and operating conditions.

Considering the conduit as the thermodynamic system then the overall mass balance will consider both air and water flowing through the conduit. The mass flow of dry air will remain constant through the system, that is

$$\dot{m}_{a,inlet} = \dot{m}_{a,outlet} = \dot{m}_a \qquad (5\text{-}1)$$

Where $\dot{m}_a$ is the mass flow rate of dry air along the conduit.

The overall water mass balance consists of equating the total water entering the conduit with the total water leaving the conduit, assuming no holdup of water inside the conduit. Thus

$$\dot{m}_{w,inlet} + \dot{m}_a w_{\infty,\,inlet} = \dot{m}_{w,outlet} + \dot{m}_a w_{\infty,\,outlet} \qquad (5\text{-}2)$$

Where $\dot{m}_{w,inlet}$ and $\dot{m}_{w,outlet}$ are the inlet and outlet mass flow rate of water droplets respectively, and $w_{\infty,\,inlet}$ and $w_{\infty,\,outlet}$ are the specific humidities of the inlet and outlet air respectively. The overall energy balance, assuming adiabatic boundaries (conduit walls), consists of equating the total energy of the water and air entering the conduit with the total energy of the water (if any) and air leaving the conduit.

$$\dot{m}_{w,inlet} h_{w,inlet} + \dot{m}_a h_{a,inlet} = \dot{m}_{w,outlet} h_{w,outlet} + \dot{m}_a h_{a,outlet} \qquad (5\text{-}3)$$

Where $h_{w,inlet}$ and $h_{w,outlet}$ are the inlet and outlet specific enthalpies of the water droplets respectively and $h_{a,inlet}$ and $h_{a,outlet}$ are the inlet and outlet specific enthalpies of the air respectively.

The focus of this work is on the evaporation of the water droplets so the values of d_d, T_d, p_∞ (or ϕ_∞) and T_∞ were determined from these equations and then compared to the values determined from the theoretical mono-disperse evaporation model for the same initial and boundary conditions.

In other droplet evaporation research [59] a mono-disperse model has been developed and compared to experimental results. In that case the input and output droplet distributions in the experimental results, although poly-disperse, have been described in terms of a single droplet size (the $MMAD$ or $Dv50$). Thus their results would be suitable for comparison with results from the mono-disperse model in this work.

The results from the mass and energy balance comparisons along with a comparison of the model with relevant experimental data from the literature is detailed in Chapter 6.

5.3 Experimental design

In this section the aims of the experimental investigation and overall design of the experimental set-up are detailed. The actual apparatus and procedures used are described in subsequent sections.

5.3.1 Experimental aims

To achieve the overall aims of the investigation, as detailed in Chapters 1 - 3, the following experimental stages need to be carried out.

Over a fixed distance of conduit (effectively the outlet of the conduit):

- Determine the amount of water evaporation and changes to the droplet size distribution for the normal evaporation of droplets for a set of initial and boundary conditions.
- Determine the comparative amount of water evaporation and changes to the droplet size distribution for the ultrasound enhanced evaporation of droplets for the same initial and boundary conditions.

An ultrasound enhancement in evaporation rates may affect specific droplet size ranges and this would manifest as changes in the outlet water droplet size distribution. Thus it may be possible to measure or quantify the improvement in evaporation as a result of the imposed ultrasound field for different droplet size ranges.

For the ultrasound enhanced experimental stage it would be ideal if the apparatus enabled the investigation of the effect of frequency and amplitude of the ultrasound field on the evaporation process.

Furthermore equivalent results would be generated from the theoretical evaporation models (same initial and boundary conditions as the experimental cases) for additional comparison purposes.

5.3.2 Experimental parameters

The experimental parameters that needed to be measured in these trials were determined from the theoretical formulation of the evaporation process described in Chapter 4. These are listed in Table 5-1.

It was assumed that the total pressure in the conduit, p_0 was approximately constant at 101.325 kPa.

Table 5-1: Experimental Parameters

Parameter	Symbol
AIR PROPERTIES	
Air flow rate	$\dot{V}_\mathrm{a}$
Air temperature	T_∞
Air relative humidity (water vapour pressure)	$\phi_\infty\,(p_\infty)$
Total pressure	p_0
WATER DROPLET PROPERTIES	
Water droplet size distribution	$d_{\mathrm{d},j}$
Water droplet flow rate	$\dot{V}_\mathrm{w}$
Water droplet temperature	T_d
CONDUIT PROPERTIES	
Size (cross sectional area, diameter)	d_tube
Length	L
Thermal properties	adiabatic
ULTRASOUND FIELD	
Frequency	ω
Amplitude	SPL

Thus it was necessary in the design of the experiments that these parameters be measured and a decision made as to which parameters be varied (and which held constant) to achieve the aims of the investigation. The initial and boundary conditions for the theoretical models could also be determined from these parameters.

5.3.3 Variation of parameters

To quantify the effect of the ultrasound field on the evaporation rate of the water droplets the primary measurements would be the change in mass flow rate of the water droplets along the conduit. It would be possible to measure the mass flow rate of water droplets from the nebuliser (and this would be the inlet water mass flow rate) but it would be difficult to measure the mass flow rate of water droplets at some distance

along the conduit. Alternatively, the surrounding air properties (temperature and RH) at some distance along the conduit could be measured and would enable the evaporation rate to be determined. Measurement of the changes in the droplet size distribution would also give additional insight to how the ultrasound field affected the evaporation of the different droplet sizes.

Since this was a new application of an ultrasound field and the focus of the investigation was to quantify the effect of the ultrasound field on the evaporation process it was decided to vary a few key parameters only: the ultrasound field parameters (frequency and amplitude), the ratio of water droplets to air flowing through the conduit and the inlet air temperature. Future studies could investigate the effect of the other parameters on the enhancement in evaporation.

Air and water inlet temperatures would be mainly used at ambient conditions as this is typically what is found in medical respiratory equipment. Having the ability to vary the air temperature would give an additional understanding of the evaporation process. The inlet air relative humidity would be set at a low value (say around 10%) to maximise the amount of water droplet evaporation and minimise measurement errors. Each of these parameters (air temperature and RH, water temperature) would not be controlled but measured for each experiment.

Typically the ultrasonic nebulisers used in respiratory equipment do not allow for the flow rate and droplet size distribution to be altered. Normally these parameters would remain fairly constant for a given brand and model of nebuliser but may change with extended use or as a result of abnormal ambient conditions. Flow rate and size distribution would need to be measured for each experimental run.

Changes in the water droplet to air ratio would be achieved by varying the air flow rate through the conduit.

The conduit used in respiratory equipment is typically made of plastic and tubular in shape with a diameter range of 15 mm to 25 mm. Thus, polycarbonate tube of 22 mm ID was selected to be used in this experimental work.

The frequency and amplitude of the imposed ultrasound field would be determined by suitable equipment and instrumentation being available.

The first experimental investigation was carried out for the normal evaporation of water droplets into air in the conduit. The methodology and apparatus for this investigation is described in the next section.

5.4 Experimental apparatus – normal evaporation

To achieve the experimental design requirements detailed in the previous section for normal droplet evaporation trials, the apparatus in Table 5-2 was set up as per the flow schematic, Figure 5-1 and equipment layout Figure 5-2.
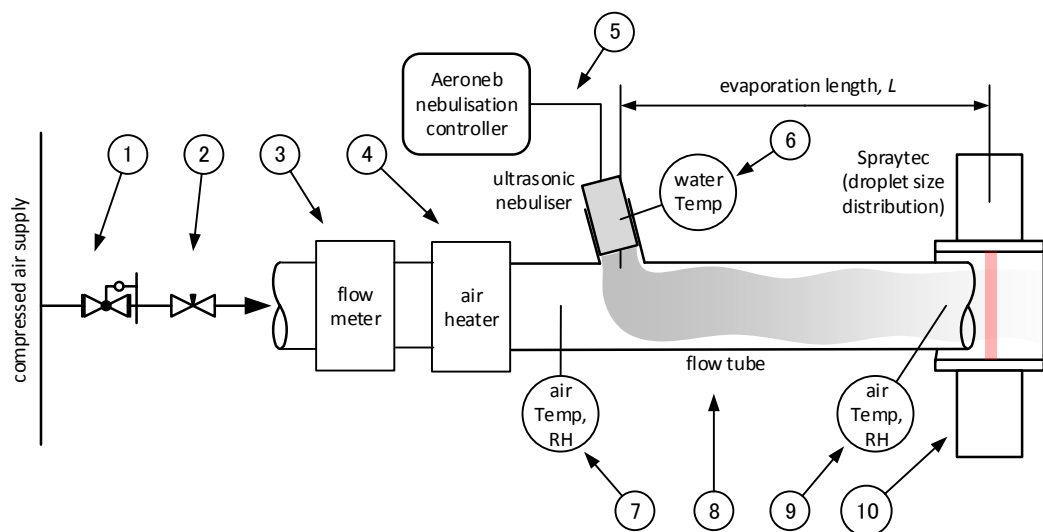
Figure 5-1: Flow schematic - normal evaporation
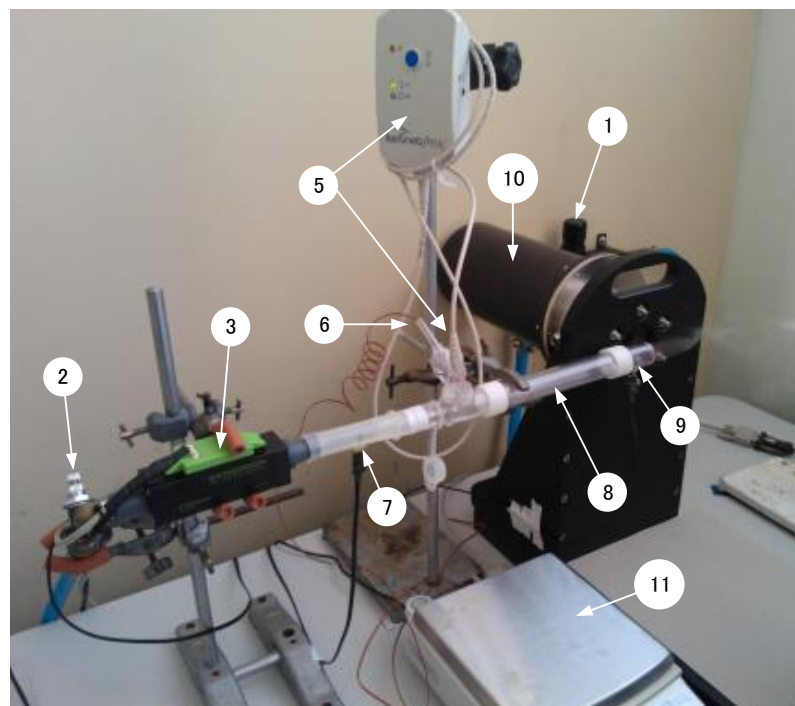
Figure 5-2: Layout of experimental apparatus - normal evaporation (air heater not shown)

5.4.1 List of apparatus

The list of apparatus used in the experimental trials for normal evaporation is given in Table 5-2

Table 5-2: List of apparatus - normal evaporation

Item	Description	Details
①	air supply, filter regulator	Existing air supply. B72G Filter/Regulator, F72G 5 micron filter. Norgren Ltd, NZ.
②	needle valve	TC1000C2800 Flow regulator, 1/4", BSP. Norgren, NZ.
③	air flow meter	CMOSens® EM1 Mass flow meter for gases. Model No. EM1NV4R0V_1A suitable for $0 - 200$ l/min. Sensirion AG, Switzerland
④	air heater	35 W tubular resistance heater. Electrical Engineering Dept, AUT.
⑤	water nebulisation transducer and controller	Aeroneb Solo nebuliser, Aeroneb Pro-X Controller. Aerogen Ltd, Ireland
⑥	Inlet water temperature sensor	Type K, thermocouple. Center 305 Digital temperature logger.
⑦	inlet air temperature and RH sensor	SHT71 CMOS sensor. EK-H4 interface. Sensirion AG, Switzerland
⑧	flow tube	25.4 x 22 mm polycarbonate tube. Mulford Engineering Plastics, NZ.
⑨	outlet air temperature and RH sensor	SHT71 CMOS sensor. EK-H4 interface. Sensirion AG, Switzerland
⑩	droplet size distribution measurement	Spraytec97 laser diffraction droplet sizer, RTSizer software. Malvern Instruments Ltd, England.
⑪	mass balance	Shimadzu UW4200. Shimadzu Scientific Instruments, NZ.

The more important items of apparatus are now described in more detail

5.4.2 Air flow meter ③

The air flow meter used, Figure 5-3, is a CMOSens® EM1 Mass flow meter for gases. Model No. EM1NV4R0V_1A supplied by Sensirion AG, Switzerland. The flow meter uses a thermal dispersion principle to measure the gas flow. Temperature sensors are mounted symmetrically upstream and downstream from a controllable heater element. The temperature difference between the upstream and downstream sensors relates to the gas mass flow. Circuitry is included on the device to integrate, amplify and linearize the sensor signals and generate a digital output. The output from the flow meter is connected via a proprietary cable and USB port to a laptop computer. Sensirion supplied software, SensiViewer v2.3 is used to view and log flow data.

The device has a measuring range of 0 – 200 l/min. Over the air flow range used in these experiments the device has a stated accuracy of 5% of measured value and a repeatability of 0.5% of measured value.

Figure 5-3: Air flow meter (courtesy Sensirion AG)

5.4.3 Air heater ④

The air is heated when required by a simple custom built resistance heater unit. It is rated at 35 W. A variable Lab power supply capable of providing up to 14 V at 3 A is connected to the heater unit.

5.4.4 Ultrasonic nebuliser ⑤

The ultrasonic nebulising system used to generate water droplets is an Aeroneb Solo nebuliser and Aeroneb Pro-X Controller, Figure 5-4, supplied by Aerogen Ltd, Ireland. The reservoir in the Solo nebuliser, Figure 5-5 is filled with water before each run and the controller is set to run for a maximum time of 30 minutes (normal mode). The

controller can be connected to its own power supply (AC/DC adapter) or can run off internal rechargeable batteries.

The operation of the nebuliser is based on the vibration of a perforated aperture plate. The aperture plate is dome shaped and contains over 1,000 precision formed tapered holes. It is embedded in the middle of a vibrational element and sits at the base of the water reservoir. Energy is applied to the vibrational element from the controller which causes the aperture plate to vibrate at around 128 kHz. This rapid vibration causes each hole in the plate to act as a micro-pump, extruding liquid through the holes to form uniformly sized droplets. The result is a low velocity aerosol discharged from the device.

Figure 5-4: Ultrasonic nebuliser - Controller and nebuliser (courtesy Aerogen Ltd)
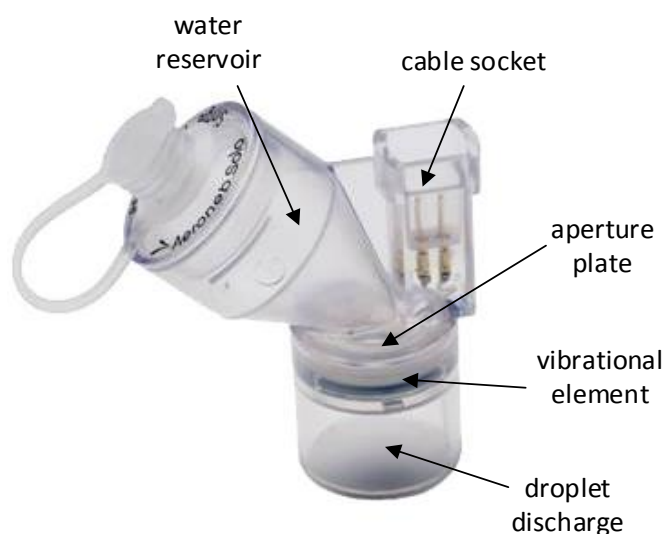
Figure 5-5: Nebuliser (courtesy Aerogen Ltd)

5.4.5 Air temperature and relative humidity measurement ⑦, ⑨

The sensors use to measure temperature and relative humidity of the air flow are SHT71 sensors, Figure 5-6, supplied by Sensirion AG, Switzerland. They consist of a capacitive sensing element for relative humidity and a band-gap sensor for temperature. Both sensors are coupled to a 14-bit analogue to digital converter and serial interface circuit. Each sensor is individually calibrated and the calibration coefficients programmed into memory on the sensor chip. Externally, they are connected via an EK-H4 interface (also supplied by Sensirion) to a laptop computer which enables the temperature and humidity data to be viewed and logged.
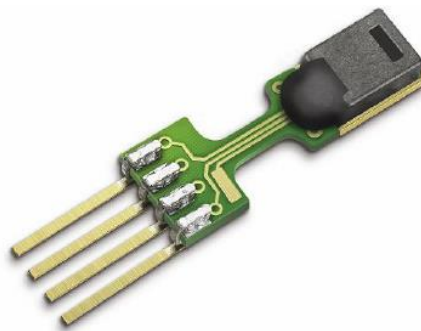
Figure 5-6: Sensirion SHT71 Humidity and Temperature Sensor (courtesy Sensirion AG)

Regarding relative humidity the sensors operate over a range of 0 – 100% RH with a typical accuracy of 3% of reading and repeatability of 0.1% of reading. At very low (~10% RH) and very high humidities (~90%) the accuracy is 4%. Regarding temperature, the sensors operate over a range of -40 – 100°C with a typical accuracy of ± 0.4°C and repeatability of ± 0.1°C. At the temperatures measured in these experiments the accuracy is the same as the typical values stated.

5.4.6 Droplets size distribution measurement ⑩

The droplet size distribution from the nebuliser and from the outlet of the flow tube is measured using a Spraytec laser diffraction device, Figure 5-7, supplied by Malvern Instruments Ltd, England. In the laser diffraction technique, see Figure 5-8, particles are passed through a laser and the scattering pattern is measured by a number of detectors (photodiodes). These detectors are arranged at various scattering angles from the direction of the laser source. According to Mie light scattering theory for spherical particles a relationship exists between scattering angle, the intensity of the scattered light at that angle and the particle size distribution by volume. The Spraytec RTSizer

software uses a patented algorithm, based on the Mie light scattering theory, to generate an accurate droplet size distribution from the detector readings. The software was set up for measuring water droplets in air.
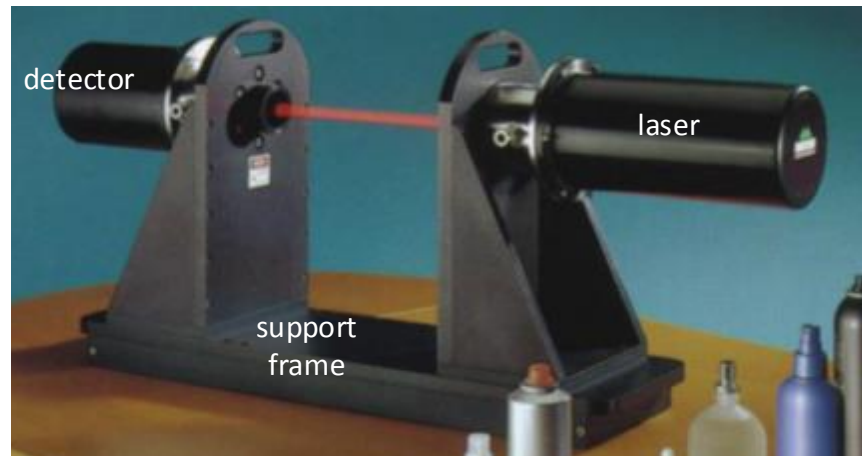
Figure 5-7: Spraytec. Droplet size measurement device (courtesy Malvern Instruments Ltd)
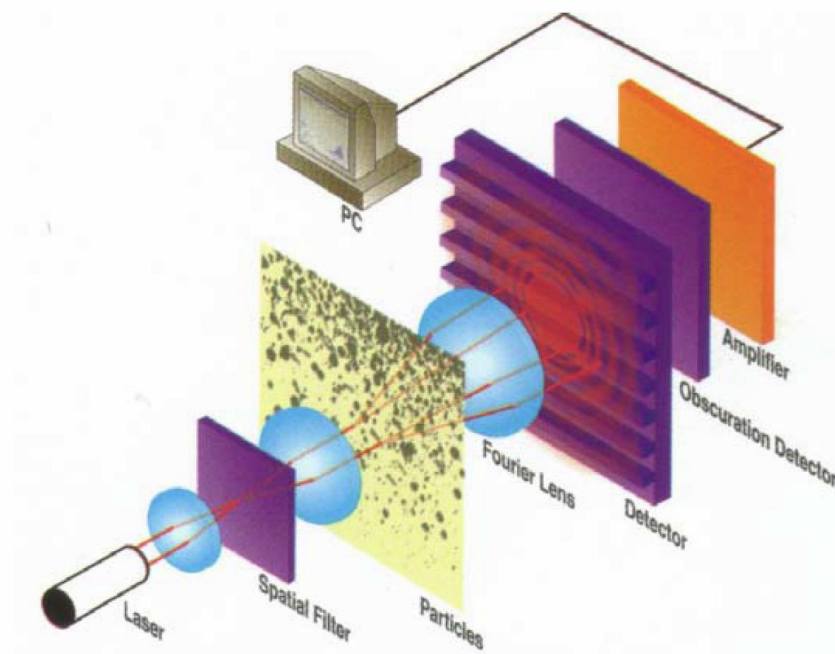
Figure 5-8: Laser scattering principle [145]

The Spraytec device is set up with the standard 100 mm lens that enables it to measure droplets in the 0.1 to 100 μm diameter range. The device can measure sprays with obscurations of between 2% and 95%. Accuracy is stated at 3% with a precision of 0.5%.

5.4.7 Mass balance ⑪

The nebulisation rate from the Aeroneb Solo nebuliser is measured by weight loss using a Shimadzu model UW4200H scale, Figure 5-9, supplied by Shimadzu Corporation, Japan. It is connected via an RS232 cable to a laptop and MATLAB® code is used to log the weight values and calculate the mass flow rate.

Figure 5-9: Mass Balance (courtesy Shimadzu Corporation)

The scale has a measuring range of 0 – 4200 g and a display resolution of 0.01 g. The repeatability is ≤ 0.01 g and linearity is ± 0.02 g.

5.4.8 General operation of the apparatus

- Air is supplied to the apparatus from a reticulated compressed air supply, ① through a filter/regulator and final micron filter and water trap. This ensures that the air is clean and relatively dry.

- A needle valve ② allows the flow rate of air into the apparatus to be adjusted. This flow rate is measured by an air flow meter ③. The air then passes through a resistance heater ④ connected to a variable power supply so that the inlet air temperature can be adjusted prior to entering the flow tube ⑧. The temperature and relative humidity of the inlet air is measure by a miniature CMOS sensor ⑦.

- A spray of water droplets is introduced into the air stream flowing along the tube from an ultrasonic nebuliser ⑤ fitted to a Y-piece that is connected to the flow tube. A controller supplies power to the ultrasonic nebuliser and water for nebulisation is added to a small receptacle in the nebuliser. A thermocouple ⑥ measures the water temperature in the water supply receptacle.

- A second miniature CMOS sensor ⑨ measures the temperature and relative humidity of the air at the outlet of apparatus.

- A laser diffraction device ⑩ measures the outlet droplet size distribution. It is also used, offline, to measure the inlet droplet size distribution i.e., the distribution at the discharge of the ultrasonic nebuliser ⑤.

- A mass balance ⑪ (not shown in schematic) is used, offline, to measure the droplet nebulisation rate of the ultrasonic nebuliser ⑤.

5.5 Experimental procedure – normal evaporation

Prior to the installation of the ultrasound field generation equipment, trials were run in the apparatus described above to provide a baseline for the normal evaporation process and thus enable comparison with the ultrasound enhanced evaporation process.

5.5.1 Input water droplet size distribution and flow rate

These experiments are carried out to determine initial conditions for the water droplet size distribution and flow rate. These parameters are measured at the discharge from the ultrasonic nebuliser. It is not possible to measure them during the trial so the nebuliser is removed from the apparatus to determine these measurements. This procedure is carried out at the beginning and end of each evaporation trial (see next section 5.5.2).

1. The nebuliser and controller are removed from the main apparatus (Figure 5-1) and set up on a lab stand on the mass balance.

2. The mass balance and lab stand are arranged so that the droplet discharge from the nebuliser is just above the measuring laser beam of the Spraytec device.

3. A laptop PC is connected to the mass balance to log the mass readings.

4. Droplets are generated from the nebuliser. The laptop PC captures mass loss data and the RTSizer software captures droplet size distribution data.

5. The trial runs for a period of around 3 minutes.

6. At the completion of the trial the nebuliser and controller are fitted back onto the main apparatus as shown in Figure 5-1.

MATLAB® code on the laptop PC is used to determine a water mass flow rate. The RTSizer software for the Spraytec device is used to generate an average droplet size distribution, and average distribution parameters ($Dv50$, $D[4.3]$ etc) for the period of the trial.

5.5.2 Evaporation trials

The purpose of these experiments are to determine the baseline for the normal evaporation of water droplets in the apparatus for a range of air flow rates, air temperatures and tube lengths. The results from these trials (water evaporation rates and changes to the droplet size distribution) will be firstly compared with the results from the theoretical model and then compared with experimental trials when the ultrasound field is applied to the evaporating water droplets.

1. The apparatus is set up with a flow tube of the desired length as per Figure 5-1 and the outlet of the flow tube is arranged as close as possible to the measuring laser beam of the Spraytec device.

2. The controller for the nebuliser is set to run from its external power supply and the reservoir that supplies the nebuliser is filled with clean water.

3. Each of the measuring devices is set up to log its readings onto a laptop PC. This includes the air flow meter, the nebuliser water temperature thermocouple and the two air temperature and RH sensors.

4. The RTSizer software for the Spraytec is set to measure and log the droplet size distribution data from the discharge of the flow tube.

5. The air flow into the apparatus is adjusted to the desired flow rate using the needle valve.

6. The air heater power supply is adjusted to give the desired air temperature into the apparatus. For ambient air trials the air heater is removed from the experimental setup.

7. Water droplets are generated from the nebuliser into the air stream and the apparatus allowed to stabilize for a period of 30 – 60 s.

8. Measurements from the various sensors are then recorded for a period of 3 – 5 minutes. These include:
   - inlet air temperature, RH and flow rate
   - inlet water temperature
   - outlet air temperature and RH
   - outlet droplet size distribution

9. If necessary a new set of parameters (air flow, air temperature, tube length) can be set and the above steps repeated.

10. At the end of a set of trials the nebuliser is removed from the apparatus and its discharge flow rate and droplet size distribution are checked according to the procedure described in section 5.5.1.

From the recorded data the various parameters were checked to ensure approximately steady conditions were achieved for each trial. Average values for all of the measured parameters were then determined for each individual trial and recorded (See Appendix 4). From these average values the initial and boundary conditions for the theoretical models were determined and the experimental amount of water evaporated was also calculated and recorded.

It was found that the Spraytec device needed a certain concentration of droplets in the air stream from the outlet of the apparatus to be able to give a reading of the droplet size distribution (i.e., % transmission < 95%). Also, the outlet air stream needed to be of sufficient velocity to prevent recirculation of the air stream and false size distribution readings. Thus it was found that the air flow rate in this apparatus needed to be between 6 and 25 lpm at ambient conditions. These air flows are also typical of what is found in medical respiratory apparatus. The trials in this section were run for the following cases

- Air flow: 6 lpm, 10 lpm, 15 lpm, 20 lpm, 25 lpm
- Tube lengths: 245 mm, 340 mm
- Air temperatures: ambient (~20°C), 34°C, 48°C

5.5.3 Typical results

The complete set of results for the trials are given in Appendix 4 and summarized in Chapter 6 for further discussion and comparison. For each trial the following typical results were generated:

- Amount of water evaporation (measured in terms of the moisture content of the air at the inlet and outlet, kg of water per kg of dry air)
- Table of size distribution parameters: $Dv10$, $Dv50$, $Dv90$, $Span$, $D[3,2]$, $D[4,3]$ (at both inlet and outlet)
- Graph of droplet size distribution: % Volume versus droplet diameter at inlet and at outlet

The initial and boundary conditions for each trial were also entered into the poly-disperse droplet evaporation model described in Chapter 4 and comparative values for

the droplet size distribution, distribution parameters and amount of water evaporation were determined. These were included along with the experimental results. Model results have been calculated for two cases, where the accommodation coefficients are set to a value of 0.04 and a value of 0.001. Figure 5-10 shows a typical set of results, in this for the case where L = 245 mm, $T_{\infty,i}$ = ambient, $V_{a,i}$ = 15 lpm.

5.6 Experimental apparatus – Ultrasound enhanced evaporation

To achieve the experimental design requirements for ultrasound enhanced evaporation as detailed in section 5.3 it was necessary to select an ultrasound device that was powerful enough to have a measurable effect on the droplet evaporation. Ideally, this device would also allow for its frequency to be varied so a more thorough investigation could be carried out. At the beginning of this research it was unknown what frequency and strength (amplitude) of ultrasound field would be necessary to produce a measurable effect on the evaporation process of the water droplets. The theoretical model developed in Chapter 4 indicated a reasonably high SPL would be required. It was also shown in Chapter 3 that the ideal frequency of oscillation would be that which maximised the relative movement of air across the surface of the water droplets for a wide range of droplet sizes in the droplet size distribution. Higher frequencies (~100 kHz) would be more effective but even at lower frequencies (~20 kHz) there is still an acceptable level of relative motion for medium to large size droplets, and it is these larger droplets that will take longer to evaporate.

In the course of the investigation a number of reasonably powerful transducers with variable frequency characteristics were tried in various configurations. However, these transducers and flow arrangements produced no measurable change on the evaporation process of the droplets and it became apparent that a much higher level of ultrasound field intensity would be required in order to see any effect on evaporation process. See Chapter 3 for a summary of the different transducers and configurations that were investigated.

Research into ultrasound enhanced drying of vegetable pieces, mentioned in Chapter 2, utilised an experimental set up consisting of a metal cylinder excited by a powerful ultrasound transducer.

Droplet size distributions

Air Flow rate: 15 lpm
Air Temp.: ambient
Conduit length: 245 mm

Legend: Input — Outlet (Expt.) — Outlet (Model: α = 0.04) — Outlet (Model: α = 0.001)

Experiment Date	28/03/2013
Time	15:19:00-15:23:05

Conduit Properties	Unit	Value
Diameter	mm	22.5
Length	mm	245

Parameter	Unit	INLET	Experimental Results at OUTLET	Model Results at OUTLET	
				α = 0.04	α = 0.001
Air Properties					
Flow rate	lpm	15.1	---	14.57	14.60
Temperature	°C	25	14.5	11.8	12.5
RH		0.138	0.888	1.00	0.93
Sp. Humidity	g/kg	2.708	9.172	8.669	8.394
Water Droplet Properties					
Flow rate	ml/min	0.338	---	0.233	0.238
Temperature	°C	28	---	11.8	11.8
Length to end of calculation				55.7	627

Parameter	Unit	Input	Outlet (Expt.)	Outlet (Model: α = 0.04)	Outlet (Model: α = 0.001)
Dv(10)	(μm)	1.04	1.29	2.18	1.88
Dv(50)	(μm)	4.34	4.49	5.30	4.98
Dv(90)	(μm)	9.38	8.98	10.38	10.23
Span		1.92	1.72	1.55	1.68
D[3][2]	(μm)	2.39	2.62	3.78	3.28
D[4][3]	(μm)	5.02	4.99	5.82	5.56
% Transm.		71.9%	80.8%		
Conc. (Cv)	ppm	19	14		

Figure 5-10: Sample result for normal evaporation: $\dot{V}_{a,i}$ = 15 lpm, L = 245 mm , $T_{\infty,i}$ = ambient.

The cylinder was excited at ultrasound frequencies to investigate the effect of the ultrasound field on the drying times of the vegetable pieces inside the cylinder. The configuration used in their work generated high amplitude standing waves inside the cavity of the cylinder, in the order of 150 dB at full power.This put the apparatus into the so-called 'power ultrasound' regime (i.e., 10 – 1000 W/cm^2) [146]. According to the theoretical model developed in Chapter 4 this would be adequate to provide an enhancement in the evaporation rates of the droplets.

Thus, the apparatus used in their experimental research [147-149] was obtained for use in the current experimental investigation since it provided a high intensity of ultrasound inside the cylindrical portion. The disadvantage with this apparatus was that the cylinder diameter was much larger than the flow tube used in this investigation, and it did not allow for the variation of ultrasound frequency. However it was deemed suitable to investigate the effect of an imposed ultrasound field on water droplet evaporation.

5.6.1 Apparatus to generate ultrasound field

The additional apparatus used to impose the ultrasound field on the flow of air and droplets was comprised of equipment supplied by Pusonics S.L. listed in Table 5-3. The set up for this equipment is shown as a schematic in Figure 5-11

Table 5-3: List of additional apparatus - ultrasound enhanced evaporation

Item	Description	Details
⑫	Sonotrode	Cylindrical tube, titanium, 300 mm long x 100 mm internal diameter x 5 mm wall thickness. Pusonics S.L.
⑬	Ultrasonic transducer	Proprietary design. Langevin bolt clamped, 21.7 kHz. Pusonics S.L.
⑭	Power amplifier and dynamic resonance controller	Proprietary design. Pusonics S.L.
⑮	Impedance matching unit	Proprietary design. Pusonics S.L.
⑯	Transition piece (inlet)	Custom made. AUT Workshop.
⑰	Transition piece (outlet)	Custom made. AUT Workshop.

5.6.2 Ultrasonic transducer and sonotrode ⑫ ⑬

The sonotrode (Figure 5-12) consists of a titanium cylinder of dimensions 300 mm long x 100 mm internal diameter and wall thickness 5 mm. The ultrasonic transducer, designed to operate at a resonant frequency of around 22 kHz, is custom built by Pusonics S.L. and is bolted to the wall of the cylinder at its mid-point. The dimensions and thickness of the cylinder are such that when excited by the transducer at a frequency of 22 kHz it vibrates in a mode that maximises the intensity of the ultrasound field inside the cylinder.
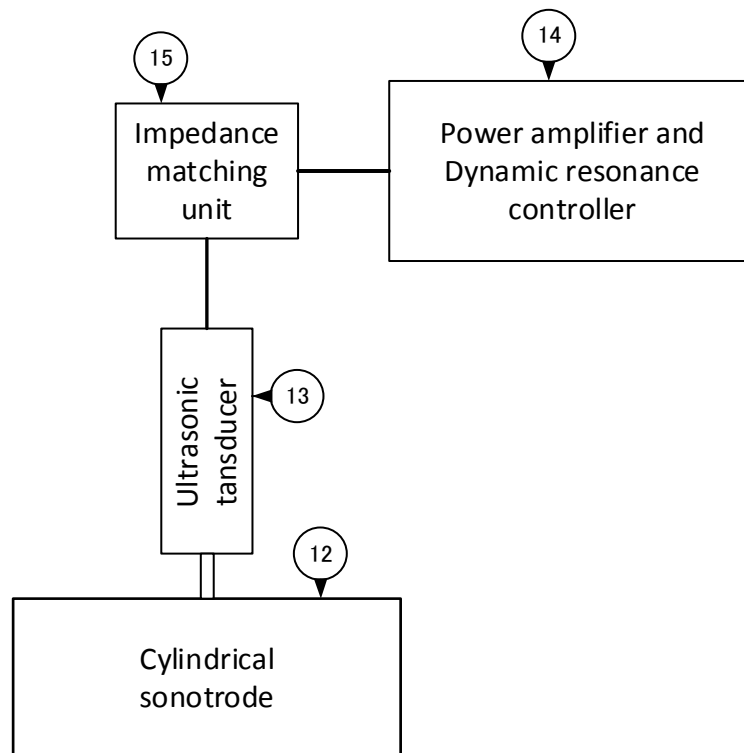
Figure 5-11: Schematic of Ultrasound field generation equipment

5.6.3 Power amplifier and dynamic resonance controller ⑭

The power amplifier and the dynamic resonance controller (Figure 5-13) is custom built by Pusonics S.L. and provides power to the ultrasonic transducer. The power level to be supplied to the transducer can be preselected. Once the power is turned on the dynamic resonance controller maintains the operation of the transducer at the selected power level.
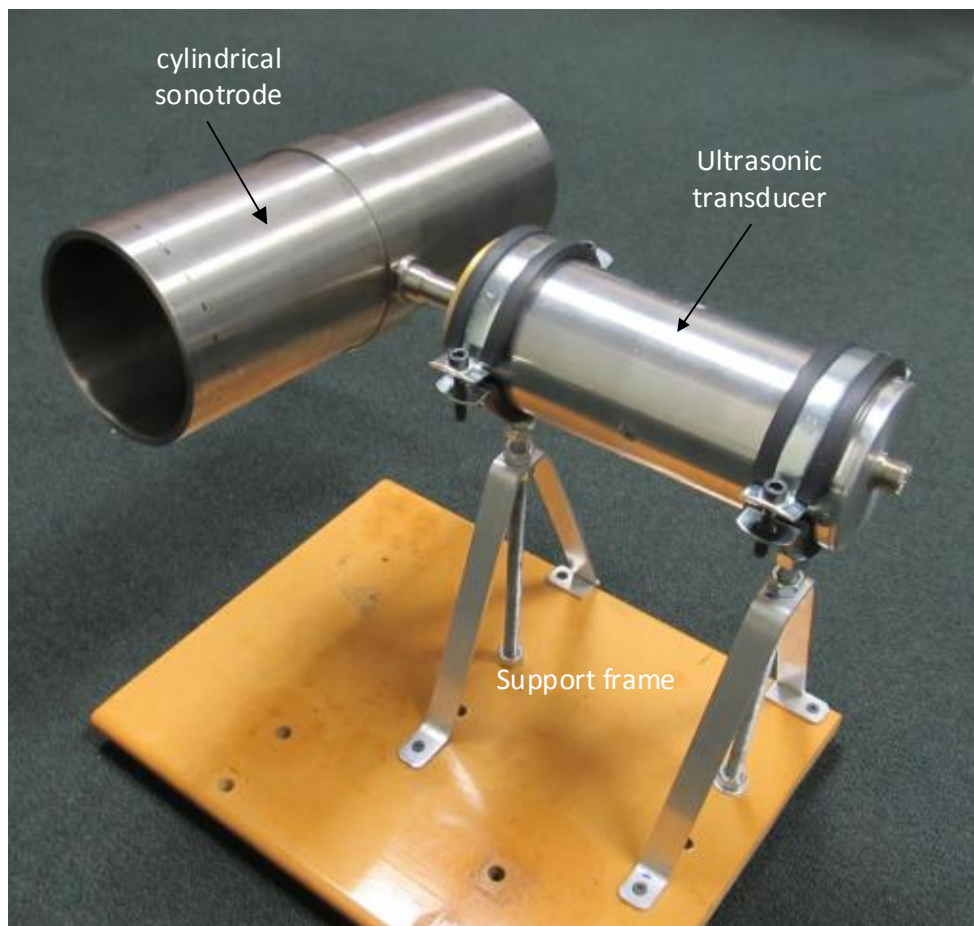
Figure 5-12: Sonotrode and Ultrasonic transducer

Figure 5-13: Power supply and resonance control system

5.6.4 Impedance matching unit ⑮

This unit, Figure 5-14, combined with the power amplifier and dynamic resonance controller maintains optimum resonance conditions and operation at the selected power level for the transducer and sonotrode. The unit is custom built by Pusonics S.L.
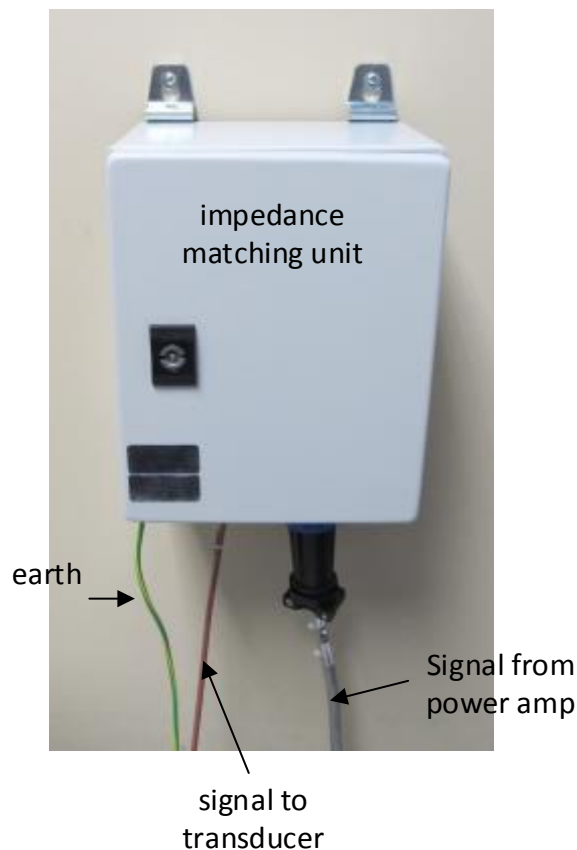
Figure 5-14: Impedance matching unit

5.6.5 General set up of ultrasound enhanced evaporation apparatus

It was necessary to incorporate the ultrasound field generation apparatus into the existing apparatus for the investigation of the enhancement in water droplet evaporation. Thus it was necessary to pass the droplets and air through the cylinder (sonotrode) and then to measure the effect of the ultrasound field on the droplet size distribution and air conditions at the exit of the cylinder. Since the cylinder was significantly larger than the flow tubes used in the existing apparatus it was incorporated into the apparatus using transition pieces, ⑯ and ⑰.

It was also important that the vibrations of the cylindrical sonotrode not be damped to any great degree so the transition pieces could not be attached directly to it. And, it was important for there to be an air tight seal between the transition pieces and the cylinder. These two requirements were achieved by using a thin plastic film covering the small

gap between the cylinder and the transition piece and held in place by two rubber bands, see Figure 5-15. The rubber band on the cylinder side was placed at a known vibrational node to minimise impact on the cylinder vibrations.
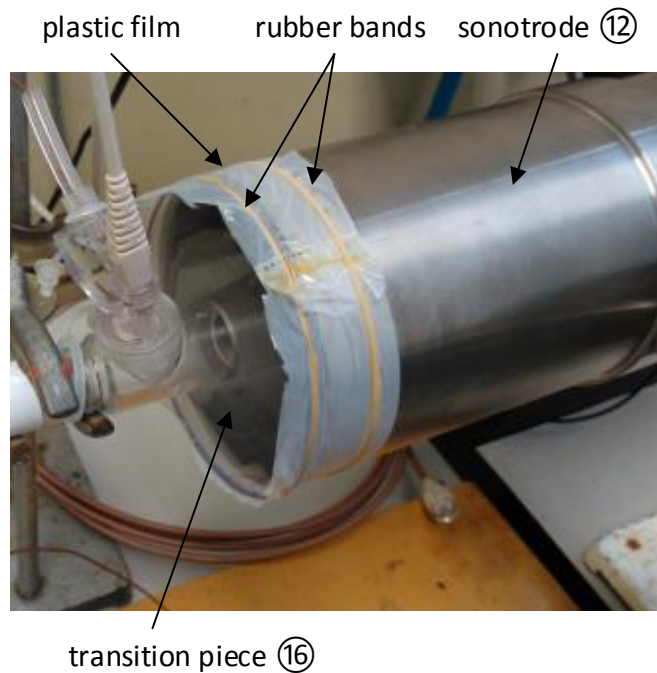
Figure 5-15: Sealing of transition piece to sonotrode

The overall setup of the experimental apparatus to investigate the effect of ultrasound on the evaporation of water droplets, incorporating the ultrasound field generation equipment is shown in Figure 5-16 and Figure 5-17.

The Pusonics equipment allows the cylinder to be driven at approximately 21.7 kHz at user selectable input transducer powers (2 W to 70 W). Although the frequency of the ultrasound could not be altered, the operating frequency of around 22 kHz would give enhancement to the evaporation process, especially for the larger droplets, as discussed earlier in this section.

In order to focus on the effect of the ultrasound field on evaporation of droplets into ambient air, the air heater was not incorporated into the experimental set up.

5.6.6 General operation of the apparatus

The apparatus, as shown in Figure 5-16 and Figure 5-17 is operated generally as described in section 5.4.8 for normal evaporation trials but with the additional operation of the equipment used to generate the ultrasound field.
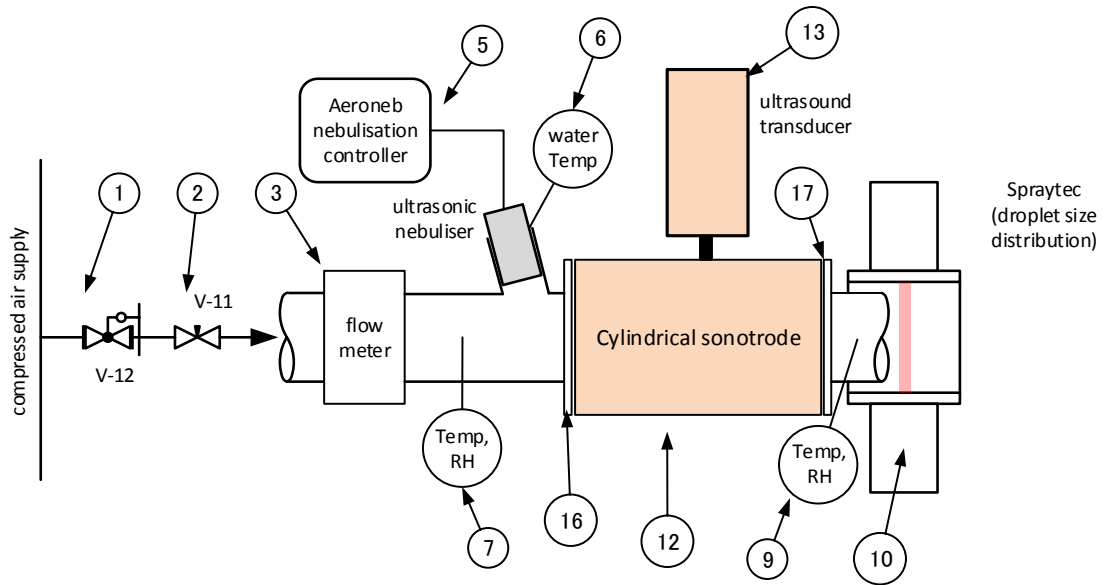
Figure 5-16: Schematic of Ultrasound Enhanced experimental setup

To operate the ultrasound field generation equipment the desired power level to be supplied to the ultrasonic transducer ⑬ is preselected on the power supply ⑭. This will determine the approximate SPL of the ultrasound field inside the cylindrical sonotrode ⑫. The relationship between input power level and ultrasound field amplitude (SPL) inside the cylinder has been measured by the manufacturer and a table provided, see Appendix 1. Once air and water droplets are flowing through the apparatus then the power supply ⑭ can be switched on which causes an ultrasound field to be generated in the cylindrical sonotrode. The resonance control system ⑭ and impedance matching unit ⑮ ensure that the transducer and sonotrode operate continuously at the selected power input.

5.7 Experimental procedure – Ultrasound enhanced evaporation

This section details the procedure used to generate experimental data for both normal evaporation and ultrasound enhanced evaporation with the ultrasound field generation apparatus in place. Since the ultrasound field generation apparatus was of a different diameter from the flow tube that it replaced, both normal and ultrasound enhanced evaporation trials needed to be run so that direct comparisons could be made between the two cases.
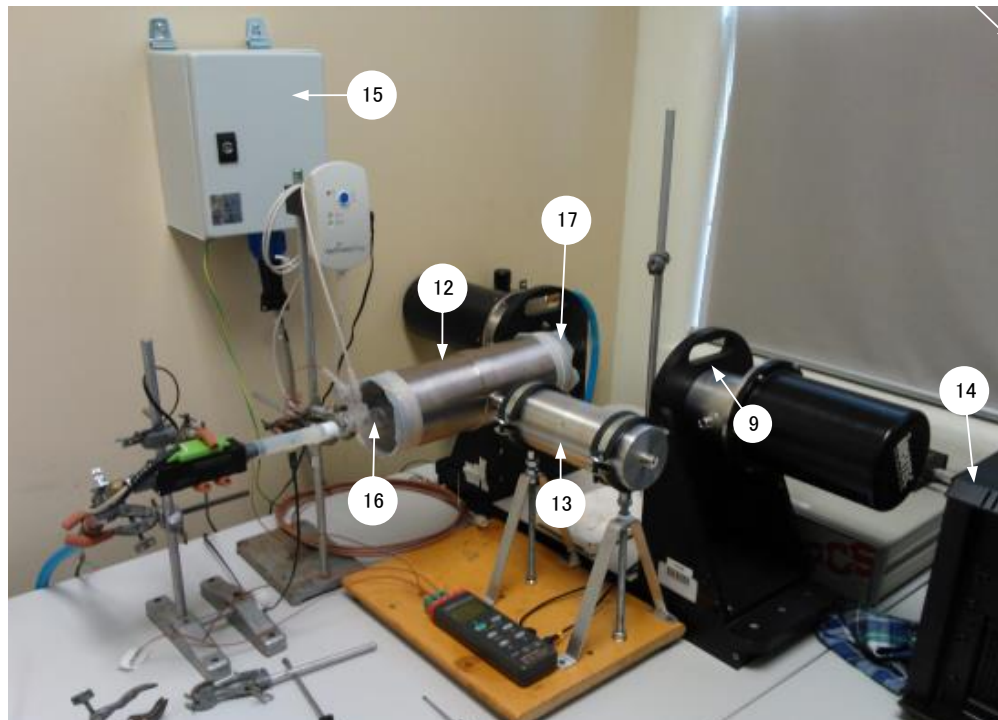
Figure 5-17: Layout of Ultrasound field generation equipment

5.7.1 Input water droplet size distribution and flow rate

It was necessary to determine the initial droplet size distribution and water droplet flow rate before each of the ultrasound enhanced evaporation trials. The procedure followed was identical to that described in section 5.5.1 for the normal evaporation trials.

5.7.2 Ultrasound enhanced evaporation trials

The purpose of these experiments is to determine the water evaporation rates and changes in the droplet size distribution using the ultrasound enhanced apparatus. Since the diameter of the ultrasound cylinder is larger than the flow tube used in the earlier normal evaporation trials (detailed in section 5.4) it was not possible to use the results from those earlier trials for compare with the current ultrasound trials. Thus these trials were run, initially with the ultrasound field off and then with the ultrasound field on to enable comparison between normal and ultrasound enhanced evaporation for the large flow cylinder size. The tube length (cylindrical sonotrode) could not be varied and the air inlet temperature was maintained at ambient. The results from these trials will also be compared with the results from the theoretical model for ultrasound enhanced evaporation.

1. The apparatus is set up with the discharge from the outlet transition piece
    arranged as close as possible to the measuring laser beam of the Spraytec device.

2. The controller for the nebuliser is set to run from its external power supply and the reservoir that supplies the nebuliser is filled with clean water.

3. Each of the measuring devices is set up to log its readings onto a laptop PC. This includes the air flow meter, the nebuliser water temperature thermocouple and the two air temperature and RH sensors.

4. The RTSizer software for the Spraytec is set to measure and log the droplet size distribution data from the discharge of the outlet transition piece.

5. The air flow into the apparatus is adjusted to the desired flow rate using the needle valve.

6. Water droplets are generated from the nebuliser into the air stream and the apparatus allowed to stabilize for a period of 30 – 60 s.

7. Measurements from the various sensors are then recorded for a period of around three minutes with the ultrasound power turned OFF.

8. The power supply to the ultrasound transducer is turned ON at a preselected power level and measurements from the various sensors continue to be recorded for a further period of three minutes.

9. The power supply to the ultrasound transducer is then turned OFF and measurements recorded for a further two minutes

10. The recorded measurements include:

    − inlet air temperature, RH and flow rate
    − inlet water temperature
    − outlet air temperature and RH
    − outlet droplet size distribution

11. If necessary a new set of parameters (air flow, ultrasound power level) can be set and the above steps repeated.

12. At the end of a set of trials the nebuliser is removed from the apparatus and its discharge flow rate and droplet size distribution are checked according to the procedure described in section 5.5.1.

From the recorded data the various parameters were checked to ensure approximately steady conditions were achieved for each trial. Average values for all of the measured parameters were then determined for each trial. From these average values the initial

and boundary conditions for the theoretical models were determined and the experimental amount of water evaporation was also calculated.

As for the earlier normal evaporation trials it was found that the Spraytec device needed a certain concentration of droplets in the air stream from the outlet of the apparatus to be able to give a reading of the droplet size distribution. Also, the outlet air stream needed to be of sufficient velocity to prevent recirculation of the air stream and false size distribution readings. Thus it was found that the air flow rate in this ultrasound enhanced apparatus needed to be between 6.5 and 20 lpm at ambient conditions. These air flows are also typical of what is found in medical respiratory apparatus.

Initial trials indicated that at power levels above 20 W, supplied to the ultrasonic transducer, there was insufficient quantity of droplets remaining in the outlet flow from the apparatus for the Spraytec device to reliably measure the droplet size distribution. The lowest setting possible on the power supply was 2 W, thus a range of power values between 2 and 20 W was chosen for these trials.

The trials in this section were run for the following cases

- Air flow: 6, 8, 10, 12, 15, 18, 20 lpm
- Tube length: 300 mm (length of cylindrical sonotrode)
- Air temperature: ambient (~20°C)
- Ultrasound Power level: 2, 5, 7, 10, 12, 15, 17, 20 W at a frequency of 21.7 kHz

5.7.3 Typical results

The complete set of results for the trials are given in Appendix 4 and summarized in Chapter 6 for further discussion and comparison. For each trial the following typical results were generated from the recorded data for both normal and ultrasound enhanced evaporation cases:

- Amount of water evaporation (measured in terms of the moisture content of the air at the inlet and outlet, kg of water per kg of dry air)
- Table of size distribution parameters: $Dv10, Dv50, Dv90, Span, D[3,2], D[4,3]$ (at both inlet and outlet)
- Graph of droplet size distribution: % Volume versus droplet diameter at inlet and at outlet

The initial and boundary conditions for each trial were also entered into the ultrasound enhanced droplet evaporation model described in Chapter 4 and comparative values for the droplet size distribution, distribution parameters and amount of water evaporation were determined. These were included along with the experimental results. Model results have been calculated for two cases, where the accommodation coefficients are set to a value of 0.04 and a value of 0.001.

Figure 5-18 shows a typical set of results, in this for the case where the airflow = 10 lpm and the ultrasound power level is 10 W.

A dramatic change in the droplet size distribution can be seen as a result of the ultrasound field in Figure 5-18. The increase in evaporation can be clearly seen in the increase of the experimental specific humidity for the ultrasound enhanced case also in Figure 5-18. These results are discussed in full in Chapter 7, along with all the other results presented in Chapter 6 for further discussion and comparison.

5.8 Closure

This chapter presents the experimental investigation into the improvements in evaporation of water droplets into air flowing along a conduit as a result of an imposed ultrasound field. It presents the design of the investigation and describes the experimental apparatus and procedures for both the normal evaporation investigation and the ultrasound enhanced evaporation investigation. Typical sample results for both investigations are also presented.

Droplet size distributions - Effect of Ultrasound

U/S Power: **10 W**
Air flow: **10 lpm**

Legend: Inlet — Outlet, U/S Off (Expt.) — Outlet, U/S On (Expt.)

Droplet size distributions - Expt. and Model

U/S Power: **10 W**
Air flow: **10 lpm**

Legend: Inlet — Outlet, U/S On (Expt.) — Outlet, U/S On (Model α=0.04) — Outlet, U/S On (Model α=0.001)

Experiment Date	30/05/2014
Time	11:16:45 - 11:18:53

Conduit Properties	Unit	Value
Diameter	mm	100
Length	mm	300

U/S Field	Unit	Value
Frequency	kHz	21.7
Power	W	10

Parameter	Unit	INLET	Experimental Results at OUTLET		Model Results at OUTLET			
			U/S Off	U/S On	U/S Off		U/S On	
					α = 0.04	α = 0.001	α = 0.04	α = 0.001
Air Properties								
Flow rate	lpm	10	---	---	9.67	9.67	9.67	9.67
Temp.	°C	21.85	18	19.9	9.4	9.4	9.6	9.6
Rel. Hum.		0.09925	0.931	0.934	1.002	1.000	1.002	1.000
Sp. Humidity	g/kg	1.61	12.08	13.68	7.35	7.35	7.44	7.44
Water Droplet Properties								
Flow rate	ml/min	0.331	---	---	0.263	0.263	0.262	0.262
Temp.	°C	24.55	---	---	9.4	9.4	9.6	9.6
Length to end of calculation					2	10	1	9

Parameter	Unit	INLET	Experimental Results at OUTLET		Model Results at OUTLET			
			U/S Off	U/S On	U/S Off		U/S On	
					α = 0.04	α = 0.001	α = 0.04	α = 0.001
Dv(10)	(µm)	0.96	1.83	7.46	1.61	1.44	1.59	1.42
Dv(50)	(µm)	3.99	4.81	12.79	4.56	4.47	4.55	4.45
Dv(90)	(µm)	8.68	8.76	21.02	9.21	9.12	9.21	9.11
Span		1.93	1.44	1.06	1.67	1.72	1.67	1.73
D[3][2]	(µm)	2.24	3.15	10.56	3.02	2.69	2.96	2.66
D[4][3]	(µm)	4.65	5.22	14.14	5.13	4.98	5.11	4.96
% Transm.		72.1%	75.7%	94.7%	---	---	---	---
Conc. (Cv)	ppm	17.7	21.7	15.2	---	---	---	---

Figure 5-18: Sample results, ultrasound enhanced evaporation: $\dot{V}_{a,i}$ = 10 lpm, L = 300 mm , $T_{\infty,i}$ = ambient, U/S power = 10 W

Chapter 6 - Results

6.1 Introduction

This research focusses on determining the improvement in evaporation of water droplets in air flowing along a conduit as a result of the application of an ultrasound field. In the previous chapters the aims, methodology, theoretical models and experimental apparatus were described in detail. In this chapter the detailed results from the theoretical and experimental investigation are reported.

Firstly results from the initial investigation of the mono-disperse droplet evaporation model are presented. This includes a comparison of the results generated from that model with theoretical overall mass and energy balances and a comparison with another mono-disperse model and experimental data from the literature.

Secondly results from the experimental and theoretical investigation of the evaporation of water droplets flowing along a conduit (no ultrasound field present) are presented. This includes experimental results and corresponding theoretical results generated from the poly-disperse model described in Chapter 4. These results are intended to provide insight into the droplet evaporation process and to provide a baseline for comparison with the second part of the experimental investigation. They are also used to validate the theoretical model.

Finally results from the experimental and theoretical investigation of ultrasound enhanced evaporation are presented. This includes experimental results from the literature, experimental results from this work and corresponding theoretical results from the ultrasound enhanced model described in Chapter 4. From these results it is possible to quantify the improvements in evaporation as the result of the imposed ultrasound field and also to compare the theoretical model with experimental results.

6.2 Mono-disperse droplets – Model validation

A mono-disperse evaporation model was developed as a proof of concept model that would form the foundation of a more complex but realistic poly-disperse droplet evaporation model. As mentioned in Chapter 5, practical nebulisers do not generate truly mono-disperse droplet distributions so there are limitations in validating this model experimentally. Thus, to validate the model it was compared with theoretical

overall mass and energy balances and also compared with results from the literature. Initially the results from the mono-disperse model were compared with the overall mass and energy balances described in Chapter 5 section 5.2.

6.2.1 Comparison with theoretical overall mass and energy balances

The mono-disperse model uses mass and energy balance equations to calculate the changes in the dependant variables over small time steps until equilibrium is reached or the plug reaches the end of the conduit (outlet). The overall mass and energy balances consider just the conditions at the inlet and conditions at the outlet of the conduit. Thus comparing the results from the model with the overall mass and energy balances is a reasonable method of theoretically validating the model.

Results from the mono-disperse model are given in Table 6-1 and Table 6-2 for a selection of initial conditions and are compared with the results from the theoretical overall mass and energy balances described in Chapter 5. The initial or inlet conditions that are varied are the water droplet flow rate (0.08 – 0.3 ml/min) and the initial temperature of the water droplets (10°C and 20°C). In each case the air flow rate is fixed at 30 l/min, the initial air temperature and relative humidity is fixed at 25°C and 40% respectively, and the initial water droplet size is fixed at 5 μm. These conditions represent typical values for medical respiratory equipment.

In Table 6-1 the % error between the model and overall mass and energy balance are shown for the calculated outlet air temperature and RH. In Table 6-2 the % error between the model and overall mass and energy balance are shown for the calculated outlet water droplet temperature and diameter. It can be seen that the calculated final values of the dependant variables generated by the mono-disperse model are on average < 1 % of the values generated by the theoretical overall mass and energy balances. Where the ratio of water to air is close to the critical value, that required to just saturate the incoming air stream (0.13 ml/min of water to 30 l/min of air in this case), the errors are larger (2 – 3%).

6.2.2 Comparison with results from the literature

To further validate the mono-disperse model it was compared with other model results and experimental data from the literature. The model of Rao et al [59] assumed that the temperature of the air surrounding the droplets remains constant (i.e. isothermal).

Their model was primarily used for the purpose of predicting droplet evaporation trends in drug delivery systems so that the performance of a typical cascade impact sizing device could be improved. Thus their focus was on the final droplet diameter after evaporation had taken place.

Table 6-1: Comparison of results from mono-disperse evaporation model (Model) and overall mass and energy balances (Balance). Air conditions at outlet.

Trial	Initial Conditions Water Droplets		Calculated Final Conditions Surrounding Air at Outlet					
	Flow rate $\dot{V}_{w,i}$ (ml/min)	Initial Temp. $T_{d,i}$ (°C)	Outlet Temperature $T_{\infty,f}$ (°C)			Outlet RH $\phi_{\infty,f}$		
			Balance	Model	% diff	Balance	Model	% diff
1	0.08	25	19.6	19.6	0.0	0.713	0.713	0.0
2	0.12	25	16.9	17.0	0.6	0.937	0.935	0.2
3	0.14	25	16.3	16.3	0.0	1.000	1.000	0.0
4	0.30	25	16.3	16.4	0.6	1.000	1.000	0.0
5	0.08	10	19.4	19.5	0.5	0.721	0.720	0.1
6	0.12	10	16.7	16.2	3.0	0.952	0.946	0.6
7	0.14	10	16.2	16.2	0.0	1.000	1.000	0.0
8	0.30	10	16.1	16.2	0.6	1.000	1.000	0.0

Table 6-2: Comparison of results from mono-disperse evaporation model (Model) and overall mass and energy balances (Balance). Water conditions at outlet

Trial	Initial Conditions Water Droplets		Calculated Final Conditions Water Droplets at Outlet					
	Flow rate $\dot{V}_{w,i}$ (ml/min)	Initial Temp. $T_{d,i}$ (°C)	Outlet Temperature $T_{d,f}$ (°C)			Outlet Diameter $d_{p,f}$ (µm)		
			Balance	Model	% diff	Balance	Model	% diff
1	0.08	25	NA	NA	NA	0	0	NA
2	0.12	25	NA	NA	NA	0	0	NA
3	0.14	25	16.3	16.3	0.0	2.09	2.05	1.9
4	0.30	25	16.3	16.4	0.6	4.12	4.12	0.0
5	0.08	10	NA	NA	NA	0	0	NA
6	0.12	10	NA	NA	NA	0	0	NA
7	0.14	10	16.2	16.2	0.0	1.000	1.000	0.0
8	0.30	10	16.1	16.2	0.6	1.000	1.000	0.0

They allowed for the presence of a small amount of drug (solute) in the water droplets. So, for comparison purposes, a version of the mono-disperse evaporation model was adjusted to match the model of Rao et al. This was done by setting $dT_\infty/dt = 0$ in equation (4-45) to simulate isothermal conditions and by adding equation (6-1) to allow for the depression of vapour pressure at the droplet surface due to the presence of a non-volatile solute.

$$p'_d = \chi_s p_d \qquad\qquad (6\text{-}1)$$

Where p'_d is the water vapour pressure at surface of droplet containing solute and χ_s is the mole fraction of solute. Also included in the model calculations is a correction factor of 1.35 that was utilised in their paper to match their model results with the experimental droplet sizing data from an impact sizing device.

Figure 6-1 and Figure 6-2 show graphs for two typical cases of final droplet size as a function of initial relative humidity (RH) of the surrounding air for two different model configurations. The model results shown in both these graphs are for a water flow rate of 0.296 ml/min with a solute concentration of 120 mg/ml and an initial droplet size of 5 μm. Model results have been generated for the normal case with adiabatic boundary conditions and for the case of isothermal boundary conditions.
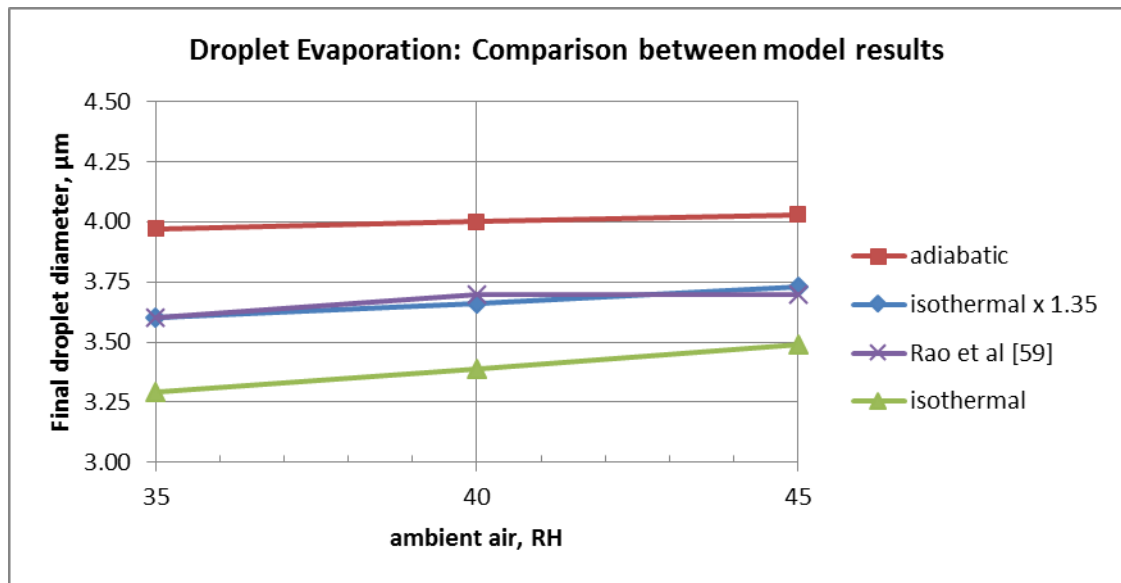
Figure 6-1: Model results of final droplet size as a function of surrounding air initial relative humidity for the case of $\dot{V}_{a,i}$ = 15 l/min, $T_{\infty,i}$ = 20°C
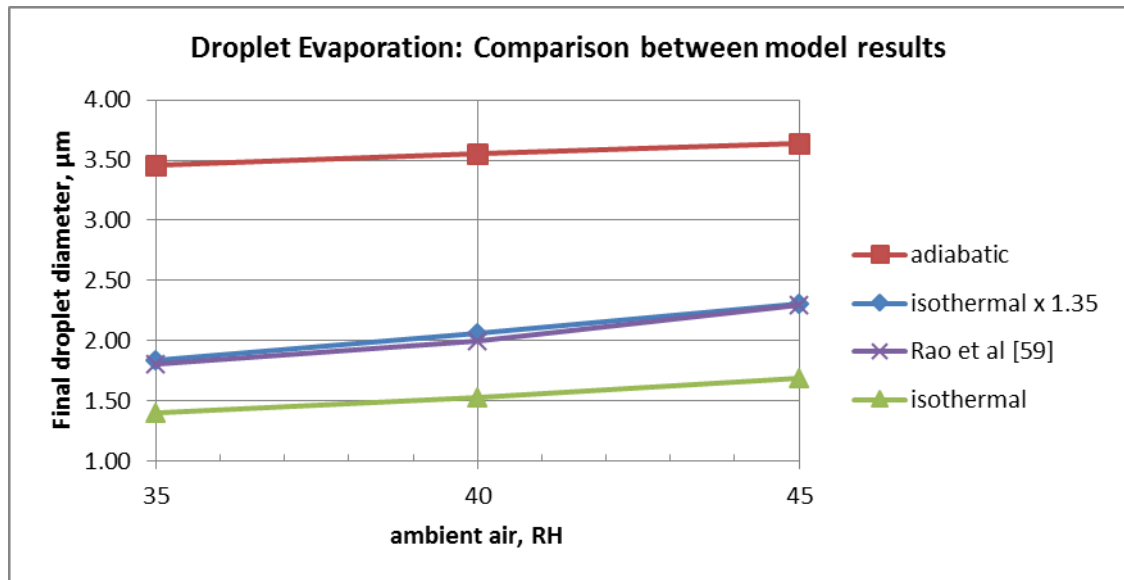
Figure 6-2: Model results of final droplet size as a function of surrounding air initial relative humidity for the case of $\dot{V}_{a,i}$ = 30 l/min and $T_{\infty,i}$ = 25°C.

Figure 6-1 and Figure 6-2 show that the isothermal and adiabatic results from the mono-disperse droplet evaporation model sit on either side of the results of Rao et al. In their set up they checked their model results against experimentally determined results (that is the $MMAD$) from an impact sizing device. They included a correction factor of 1.35 so that their model results were very close to the experimental $MMAD$ results. Assuming that the experimental $MMAD$ for the actual droplet size distribution can be equated to the diameters of a mono-dispersed droplet distribution then it seems clear that the actual evaporation process in their setup is somewhere between the isothermal case and the adiabatic case. It can also be seen from Figure 6-1 and Figure 6-2 that when the correction factor of 1.35 is included in the mono-disperse model from this work then the results almost exactly match the results of Rao et al.

Furthermore the mono-disperse model was validated against experimental data from Rao et al. The experimental data was in the form of final droplet sizes ($MMAD$) determined from an impact sizing device for a range of input conditions [59]. In Figure 6-3 this experimental data has been plotted against predicted final droplet sizes from the mono-disperse model for the same input conditions for both the adiabatic case (circles) and the isothermal case (solid squares).
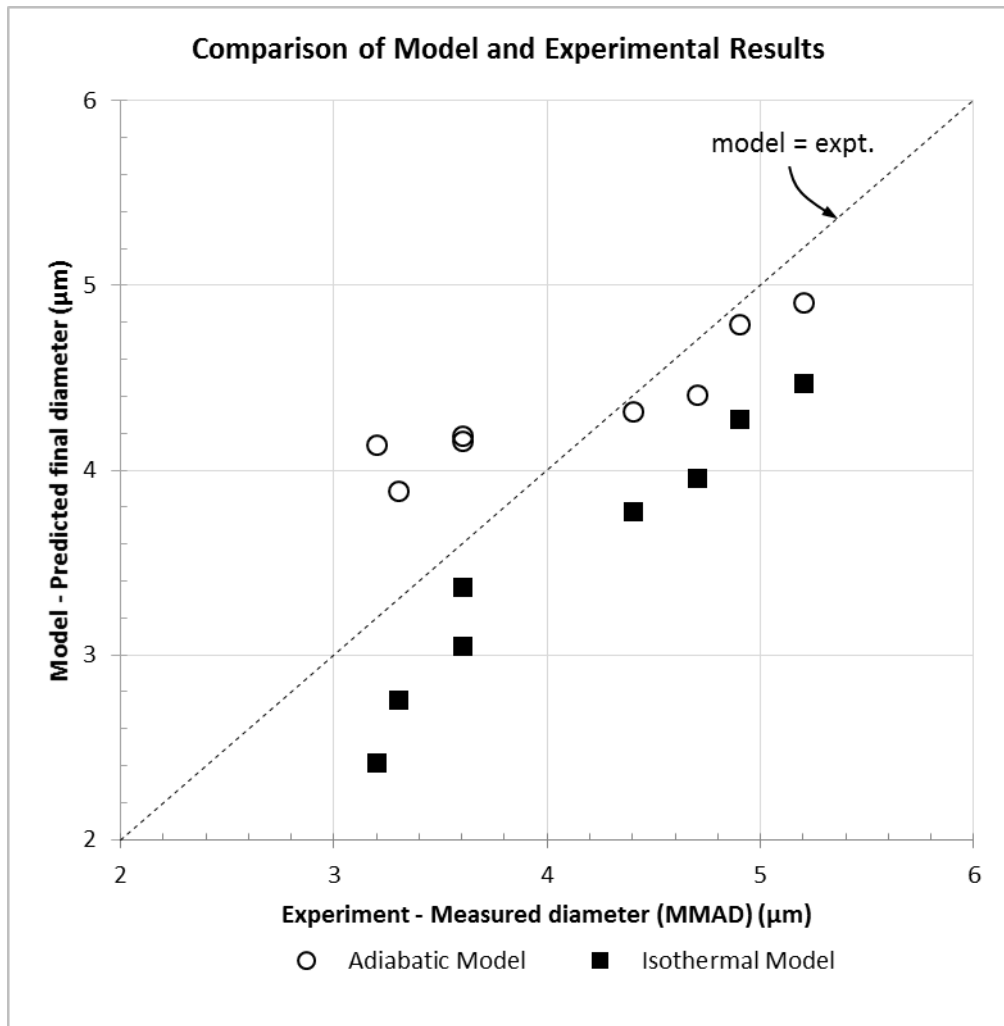
Figure 6-3: Comparison between final droplet sizes from experimental data (from an impact measuring device) and predicted final droplet diameters from the mono-disperse droplet evaporation model: Isothermal case ■, Adiabatic case ○

For final measured droplet diameters ($MMAD$) between 3 and 4 μm the results from the mono-disperse model sit on either side of the experimental data (as indicated by their relationship to the dashed 45° line in Figure 6-3). This suggests the validity of the mono-disperse model and also indicates that the experimental evaporation process probably reached equilibrium and is somewhere between the isothermal and adiabatic cases. However for final measured diameters between 4.2 and 5.2 μm the mono-disperse model results indicate smaller final diameters in both the isothermal and adiabatic cases. Further discussion of these results is presented in Chapter 7.

These comparisons suggest that the mono-disperse model is in fact providing reliable results regarding the evaporation of micrometre-size mono-disperse water droplets in air flowing in a tube. Thus the model is a suitable foundation for the development of the poly-disperse evaporation model, described in Chapter 4.

6.3 Normal evaporation – Poly-disperse droplets

The aim of this part of the investigation is to provide insight into the droplet evaporation process, to provide a baseline for comparison with ultrasound enhanced evaporation and to investigate the validity of the poly-disperse theoretical model. In the following two sections the experimental and theoretical results from the normal evaporation of water droplets flowing in air along a conduit are presented.

Experimental trials were carried out in accordance with the procedures detailed in Chapter 5 for the different cases shown in Table 6-3.

Table 6-3: Experimental Cases for which results were generated

Air flow $\dot{V}_a$ (lpm)	Air Temp, T_∞ ~22°C		Air Temp, T_∞ ~35°C		Air Temp , T_∞ ~48°C	
	Conduit Length, L		Conduit Length, L		Conduit Length, L	
	245 (mm)	340 (mm)	245 (mm)	340 (mm)	245 (mm)	340 (mm)
6.5	✓	✓	✓	-	✓	-
10	✓	✓	✓	-	✓	-
15	✓	✓	✓	-	✓	-
20	✓	✓	✓	-	✓	-
25	✓	✓	-	-	-	-

In each case the experimental parameters noted in Chapter 5, Table 5.1 were measured and recorded.

Raw results for each case are a presented in Appendix 4 and include

- Amount of water evaporation (measured in terms of the moisture content, specific humidity, of the air at the inlet and outlet)
- Table of size distribution parameters: $Dv10$, $Dv50$, $Dv90$, $Span$, $D[3,2]$, $D[4,3]$ (at both inlet and outlet)
- Graph of droplet size distribution: % Volume versus droplet diameter at inlet and at outlet

In the next section results are presented regarding the effect of air temperature, conduit length and air flow rate on the evaporation characteristics of the water droplets.

The initial and boundary conditions that were recorded for each trial were also entered into the poly-disperse droplet evaporation model described in Chapter 4. Thus comparative theoretical values were generated for the droplet size distribution, distribution parameters and amount of water evaporation. In section 6.5 these results are compared with their associated experimental results.

In all of the following figures the data points are joined by lines, they don't necessarily represent a trend but are included for clarification purposes, especially where there are many trials plotted on the one graph.

6.4 Variables affecting normal water droplet evaporation

In this section the effect of air flow rate, inlet air temperature and conduit length on the amount of water evaporated over the length of the conduit and the changes in droplet sizes in the droplet distribution, for normal evaporation conditions, are presented.

6.4.1 Amount of water evaporated

The amount of water evaporated is measured by the difference in the specific humidity of the air between the inlet and the outlet of the conduit. Values for this difference in specific humidity were determined from the raw data presented in Appendix 4 as a percentage of the inlet specific humidity according to

$$\Delta\% \, w = \frac{w_{\text{outlet}} - w_{\text{inlet}}}{w_{\text{inlet}}} \times 100\% \qquad (6\text{-}2)$$

Where w is the specific humidity of the air (kgw/kga). The difference in specific humidity is presented as a percentage change for conformity with the remainder of the results presented in this chapter.

These values are plotted in Figure 6-4 and Figure 6-5. Figure 6-4 shows, as expected, that for a given length of conduit (245 mm), the higher the inlet air temperature the greater the amount of water evaporated from the droplets. There are no clear trends with increasing air flow rate. Water evaporation decreases a little with air flow rate for the lower temperatures (20°C and 34°C) but initially increases for the highest air temperature (48°C). When considering the effect of conduit length it is apparent from Figure 6-5 that there is generally a larger amount of water evaporated over the longer length for different air flow rates.
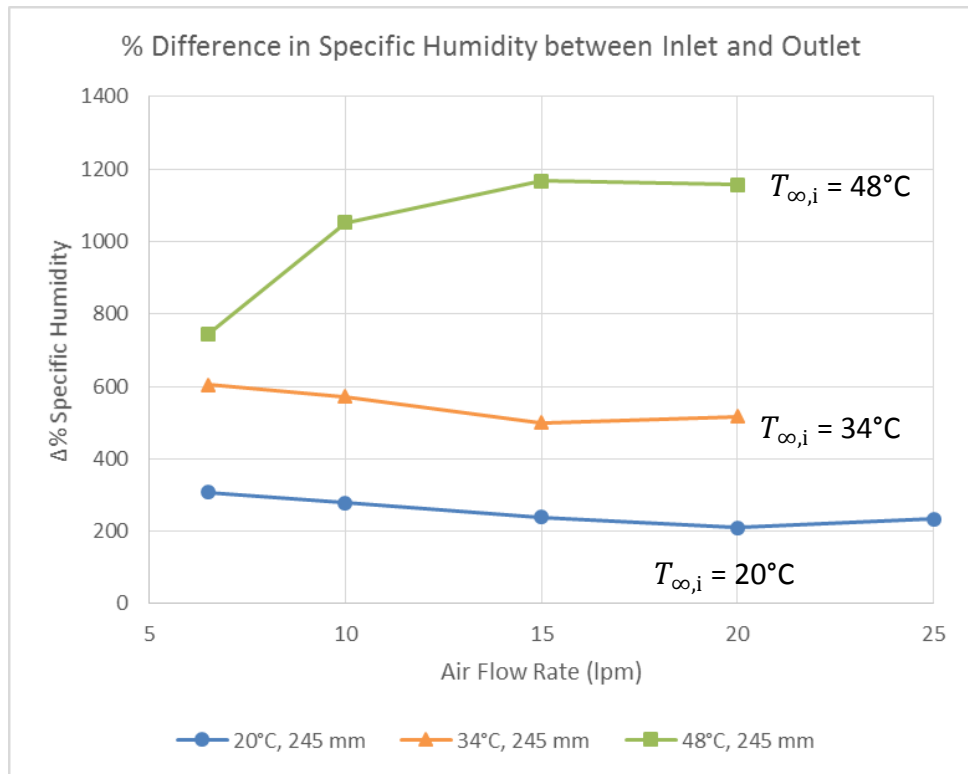
Figure 6-4: Effect of air temperature and air flow rate on water evaporation
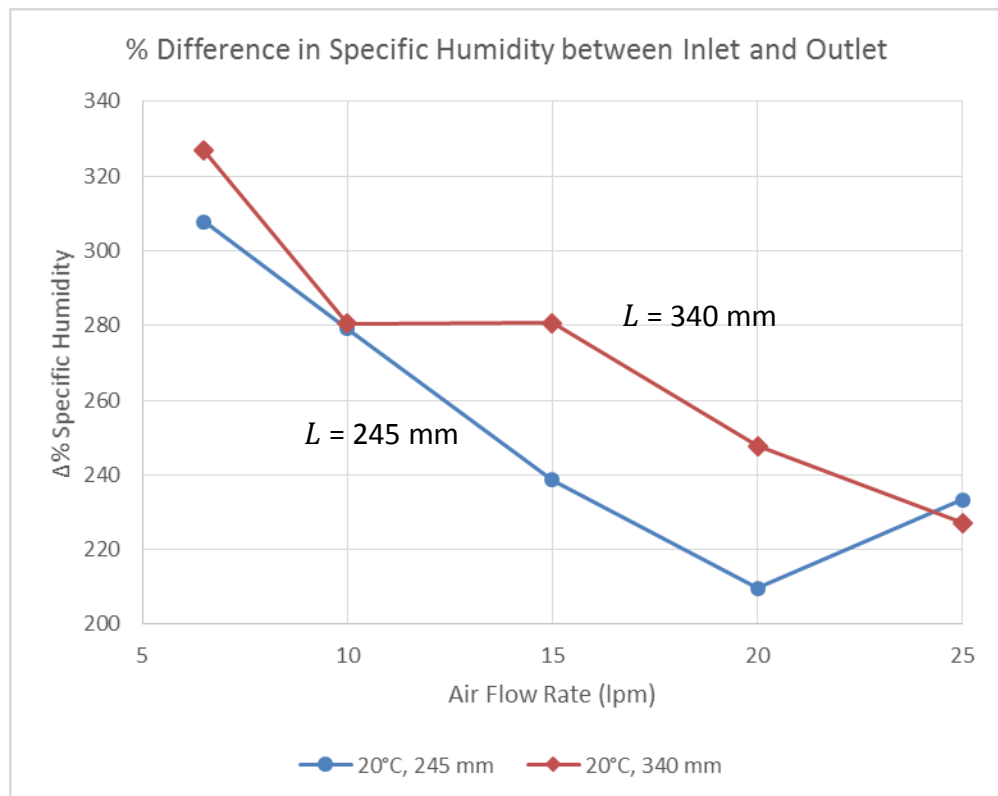
Figure 6-5: Effect of conduit length and air flow rate on water evaporation

This is expected as the residence time of the droplets and air inside the tube will increase with increasing length of tube. This gives greater time for evaporation to occur. For a given length the amount of water evaporated decreases with increasing air flow rate for the same reasons, that is the residence time of the droplets and air inside the tube will decrease with increasing air flow rate for a given length of tube.

6.4.2 Changes to the droplet size distribution

For a poly-disperse water droplet size distribution evaporating into air flowing along a conduit it is expected that the smaller droplets will decrease in size and completely evaporate more quickly than the larger droplets. This can be seen by considering a typical plot, Figure 6-6, showing the droplet size distributions at the inlet and at the outlet of the conduit. In this case the conduit length is 340 mm, the inlet air temperature is at ambient and the input air flow rate is 20 lpm. By comparing the inlet droplet size distribution (blue line) with the experimental outlet droplet size distribution (red line) it can be seen that the percent volume of the smaller sized droplets (d_{d} < 2 µm) is decreasing, the percent volume of the largest droplets (d_{d} > 10 µm) remains relatively the same and as a result the percent volume of the middle sized droplets (3 µm < d_{d} < 10 µm) actually increases.

This phenomenon can be presented in more detail by considering the droplet size distribution parameters: the $Dv10$, $Dv50$, and $Dv90$ which are the 10th percentile, 50th percentile and 90th percentile droplet diameters respectively. As described in Chapter 2 these parameters represent the smaller, middle and larger size droplets, respectively in the droplet size distribution. For the expected droplet evaporation scenario just described it is thus expected that the $Dv10$ will increase by a large amount, the $Dv50$ will increase by a moderate amount and the $Dv90$ will increase by a small amount. The values for $Dv10$, $Dv50$, and $Dv90$ recorded for each trial in Appendix 4 were used to determine a percentage difference for that parameter between the inlet and outlet droplet size distributions. The percentage difference in the $Dv10$ parameter, for example, is calculated as

$$\Delta\% \, Dv10 = \frac{Dv10_{\mathrm{outlet}} - Dv10_{\mathrm{inlet}}}{Dv10_{\mathrm{inlet}}} \times 100\% \qquad (6\text{-}3)$$

These % differences were then used to produce Figure 6-7 to Figure 6-12.
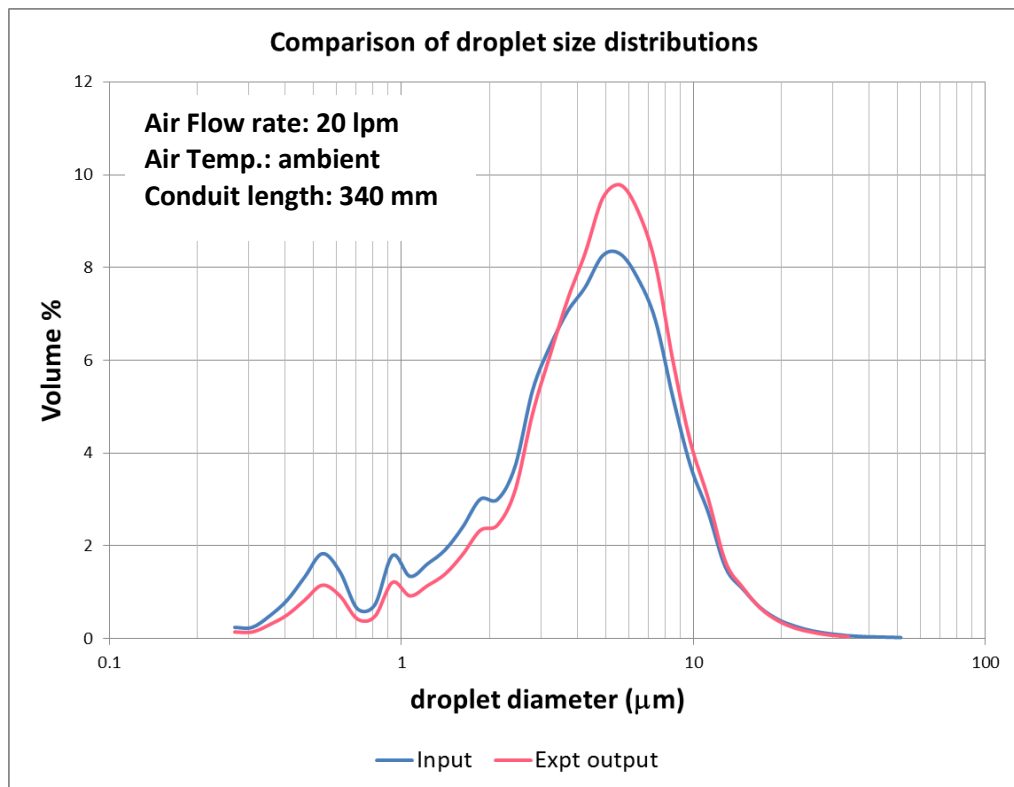
Figure 6-6: Comparison between inlet and outlet droplet size distributions – typical case
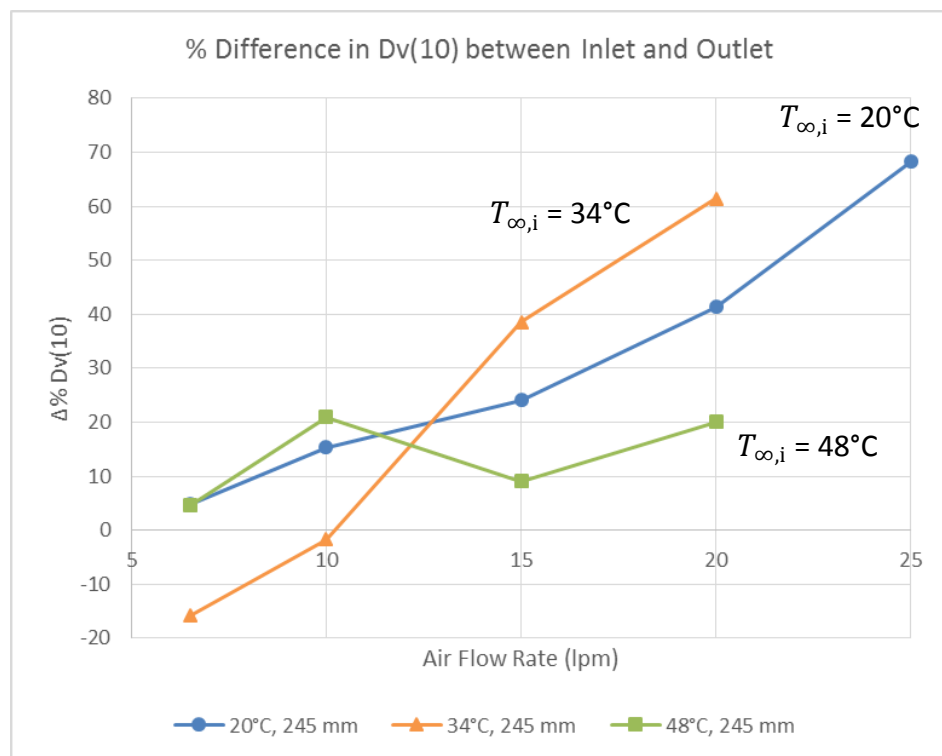
Figure 6-7 Effect of air temperature and air flow rate on changes to the smallest droplet sizes ($Dv10$) in the distribution

If the value of the $Dv10$ increases between the inlet and outlet of the conduit it means that there are less (lower volume percent) of the smallest droplets in the distribution at the outlet as a result of the evaporation process. Figure 6-7 shows generally that there is an increase in the $Dv10$ in the outlet droplet size distribution (only two cases in all the data where there was a decrease) and that this increase increases with air flow rate. The effect of air inlet temperature on the smallest droplets is not so clear.

However from Figure 6-8 it is clear that the increase in conduit length at ambient air temperatures increases the $Dv10$ and hence there is a decrease in the volume percent of the smallest droplet sizes at the outlet of the conduit.
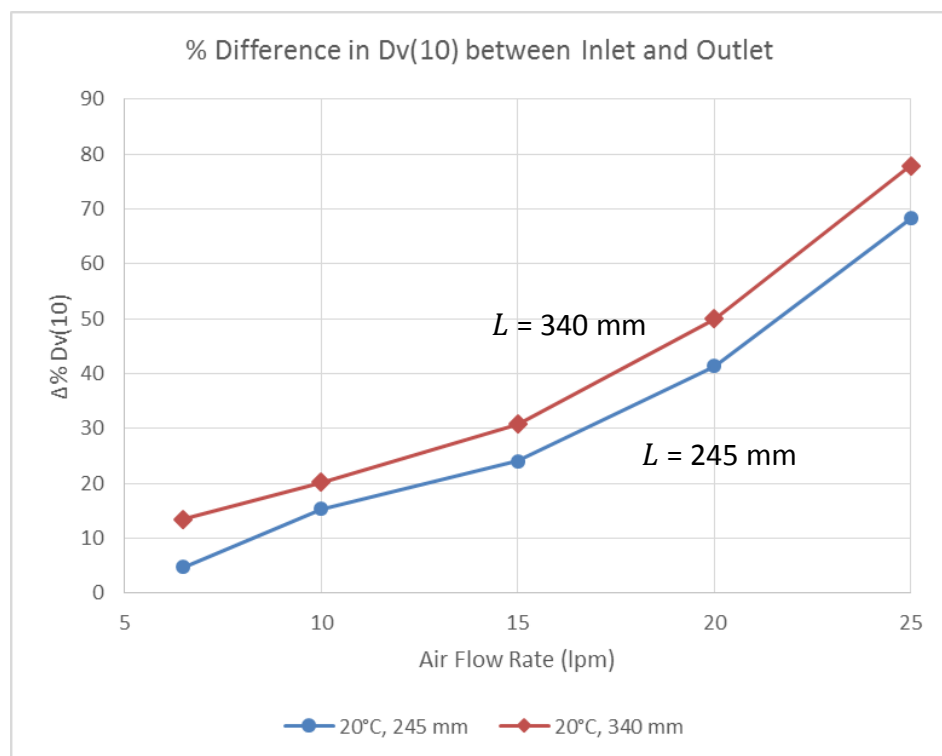
Figure 6-8: Effect of conduit length and air flow rate on changes to the smallest droplet sizes ($Dv10$) in the distribution

In the case of the $Dv50$ it can be seen from Figure 6-9 that for the lower air flow rates the $Dv50$ decreases a little (negative % difference) but this % difference becomes positive and increases with increasing air flow rate. An increase in the $Dv50$ could be due to two things: a decrease in the % volume of the droplet sizes in the lower half of the distribution or possibly an increase in the % volume of the droplet sizes in the upper half of the distribution. The latter is unlikely as conditions in the conduit favour evaporation and it is unlikely that any droplet coalescence, generating larger size droplets is taking place. As for the smaller droplets ($Dv10$) the effect of air temperature

on the middle size droplets is not so clear although a trend towards increasing $Dv50$ with increasing temperature is apparent, especially at the higher air flow rates.
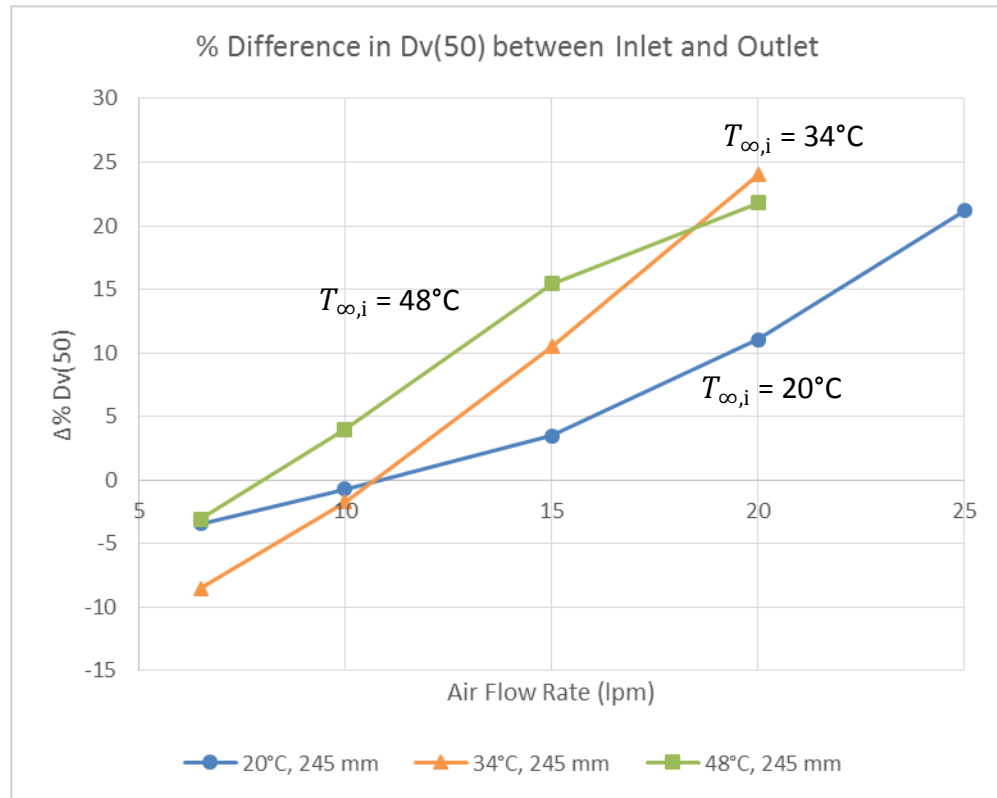
Figure 6-9: Effect of air temperature and air flow rate on changes to the middle of the distribution ($Dv50$)

The effect of the conduit length on the middle sized droplets is not so clear with a small increase in the % difference in $Dv50$ for all but the highest air flow rate as is shown in Figure 6-10

Figure 6-11 shows that for over half of the cases measured (all at lower air flow rates) the change in $Dv90$ is negative. This means that the % volume of the largest droplets in the distribution has decreased at the outlet of the conduit. This is unexpected and further investigation of the actual droplet size distributions (Appendix 4) for each case implies that the very largest droplets are somehow disappearing altogether from the outlet distribution. This is unlikely due to evaporation and the possible reasons for this are discussed in Chapter 7. However it is clear that, as for the smallest droplets and the middle sized droplets, increasing air flow rate causes the % difference in $Dv90$ to become increasingly positive.
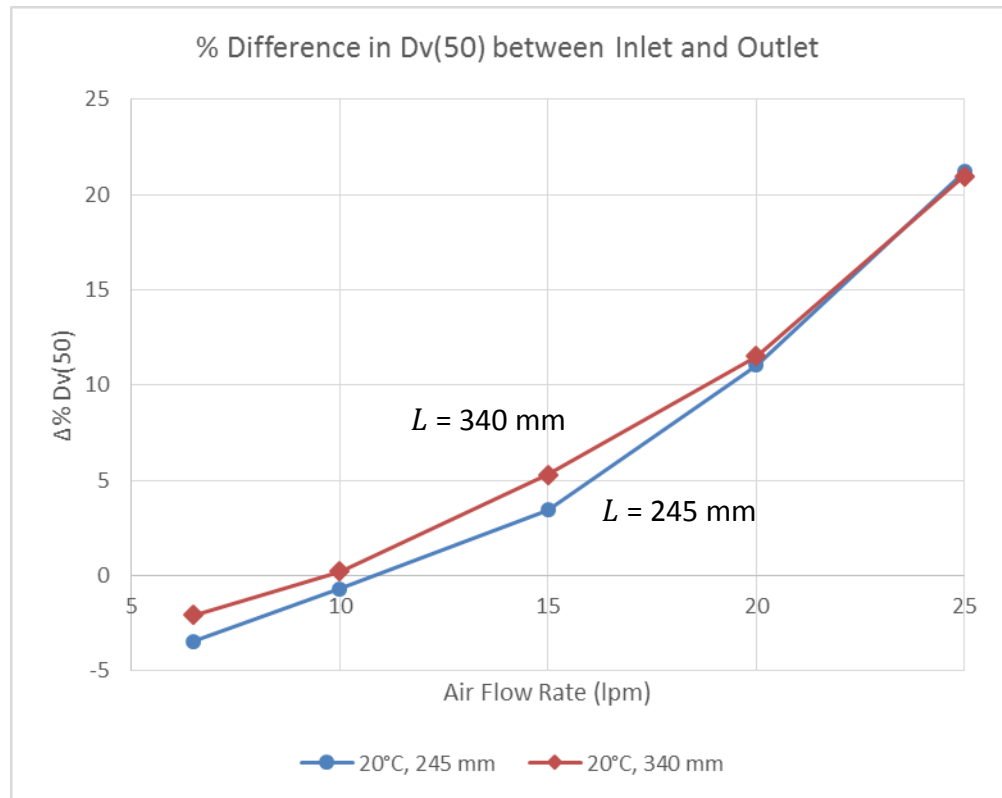
Figure 6-10: Effect of conduit length and air flow rate on changes to the middle of the distribution ($Dv50$)
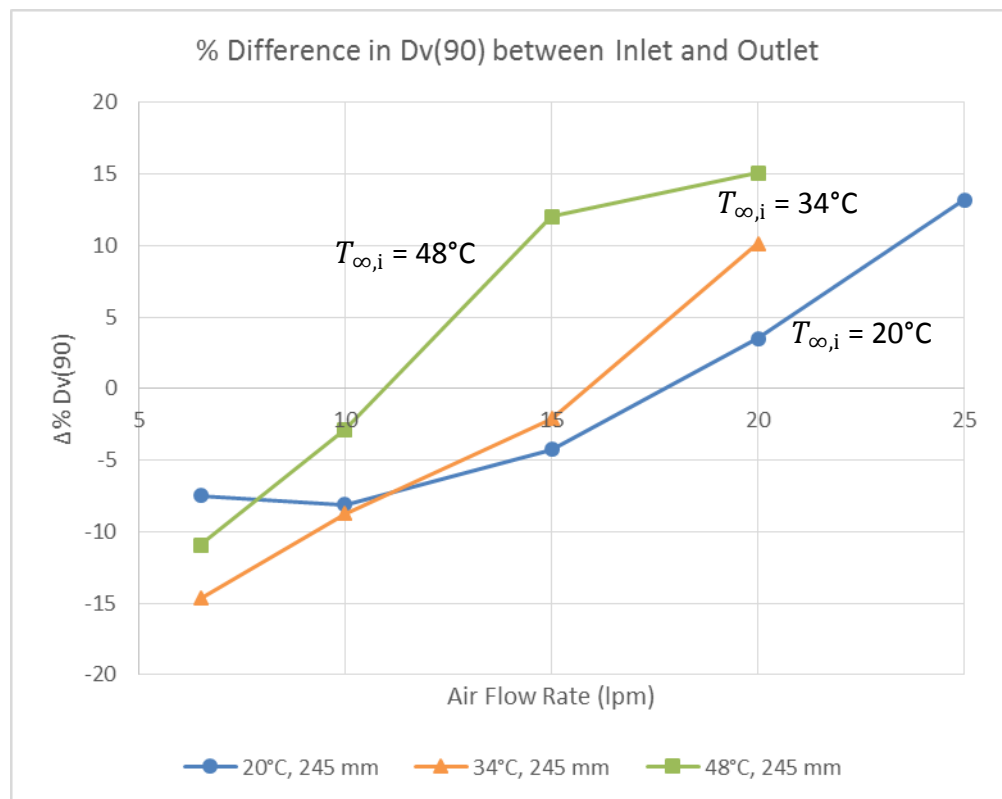
Figure 6-11: Effect of air temperature and air flow rate on changes to the largest droplet sizes ($Dv90$) in the distribution

This implies that at the higher air flow rates, for a given length of conduit, even though the amount of water evaporating over that length is less, the expected changes in the droplet size distribution become more pronounced. That is the $Dv10$ increases a large amount, the $Dv50$ increases a moderate amount and the $Dv90$ increases a small amount. The effect of the conduit length on the largest droplets is not so clear as shown in Figure 6-12.
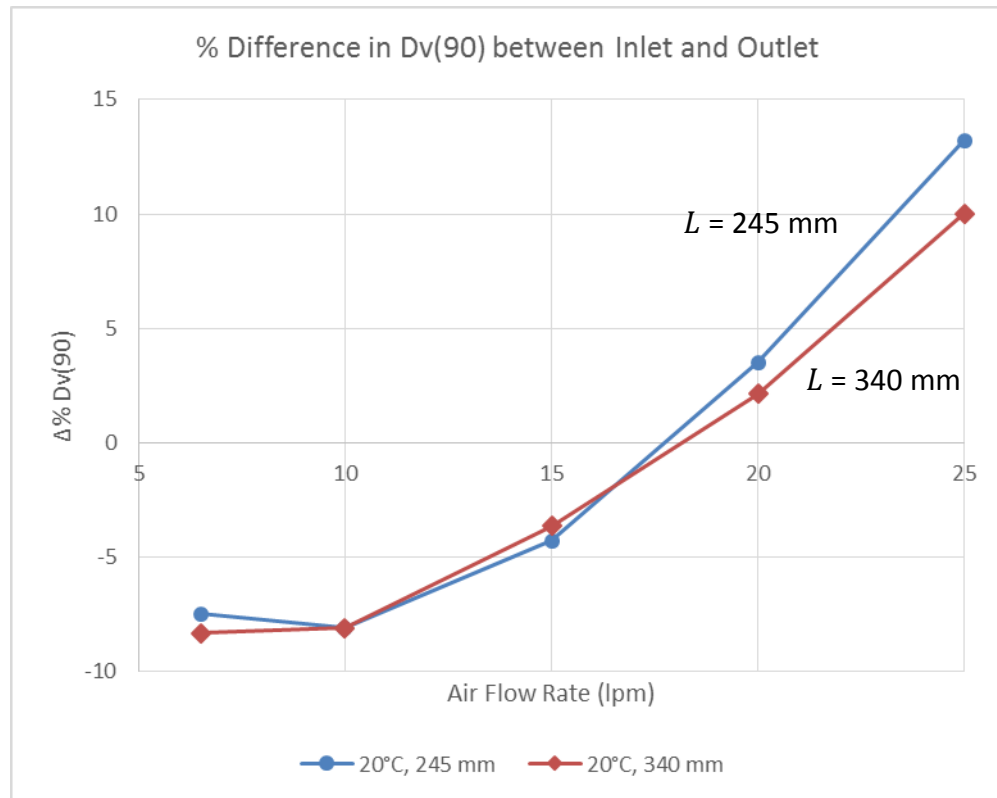
Figure 6-12: Effect of conduit length and air flow rate on changes to the largest droplet sizes ($Dv90$) in the distribution

6.5 Comparison with model results

As stated in section 6.3 the initial and boundary conditions for each trial were also entered into the poly-disperse droplet evaporation model (see Chapter 4). Thus values for the amount of water evaporation, changes to the droplet size distribution, and changes to the distribution parameters were determined from the model for comparison with the experimental results. A reasonable correlation between experimental and model results would give confidence in the theoretical model as a predictive tool and give confidence that the model was suitable for further modification to describe the effects of an imposed ultrasound field on droplet evaporation.

The mass accommodation coefficient and the thermal accommodation coefficient, α_{m} and α_{h} respectively are two of the inputs to the theoretical models as detailed in Chapter 4. These coefficients are used in the mass and heat flux correction factors respectively. Values for the coefficients range between 0 and 1. Much debate has occurred over the correct values to use and although values of 1 or 0.04 are commonly used, values as low as 0.001 have been used in the literature [58, 150]. In this research values of 0.04 and 0.001 have both been used for the mass and thermal accommodation coefficients to generate comparative results from the theoretical models.

6.5.1 Amount of water evaporated

As detailed in the section 6.4.1 the difference in specific humidity in the air stream between the inlet and outlet of the conduit is a measure of the amount of water that has evaporated. Since the inlet water flow and inlet air specific humidity is relatively constant in each trial, comparing just the specific humidity in the air outlet stream between the experimental and theoretical cases will give an indication of the accuracy of the theoretical model. The percentage difference in outlet air specific humidity for the experimental cases and corresponding theoretical cases was determined from the raw results in Appendix 4 according to

$$\Delta\% \, w = \frac{w_{\text{outlet, expt.}} - w_{\text{outlet, model}}}{w_{\text{outlet, expt.}}} \times 100\% \qquad (\,6\text{-}4)$$

These values are presented in Figure 6-13 and Figure 6-14. The model results are calculated using accommodation coefficients of 0.04 which were found to give more accurate results when considering the amount of water evaporated.

Figure 6-13 shows that the % difference in air specific humidity between the experimental results and theoretical results is at a maximum of around 21% for the case of ambient air and lowest air flow rate of 6.5 lpm. But is well within 5% for the higher air flow rates and temperatures. Over half of the trials had a difference of < 5.5% between theoretical model and experimental results. This indicates that the model is giving reasonable results for the amount of water evaporated, in the majority of cases.

With regards to the conduit length Figure 6-14 shows the % difference between the model and experimental result for the amount of water evaporated is greater for the longer conduit length. But also that this % error decreases with increasing air flow rate.
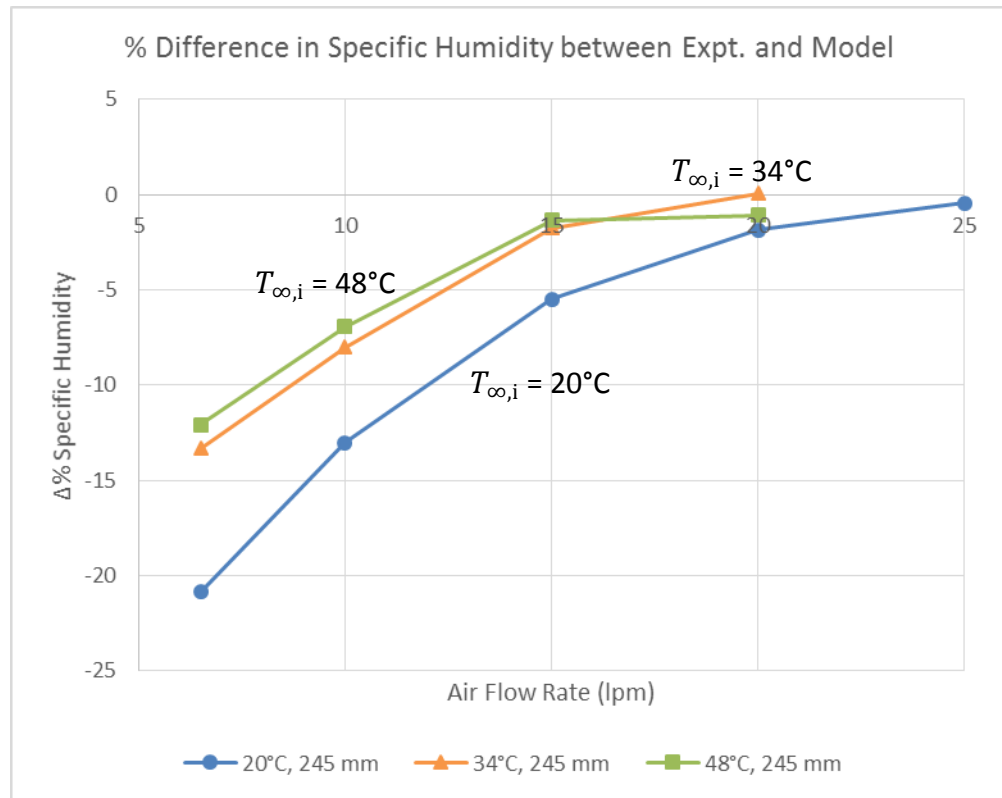
Figure 6-13: Specific humidity of outlet air: Comparison between experimental and theoretical results for various air temperatures vs air flow rate ($\alpha_m = \alpha_h = 0.04$)
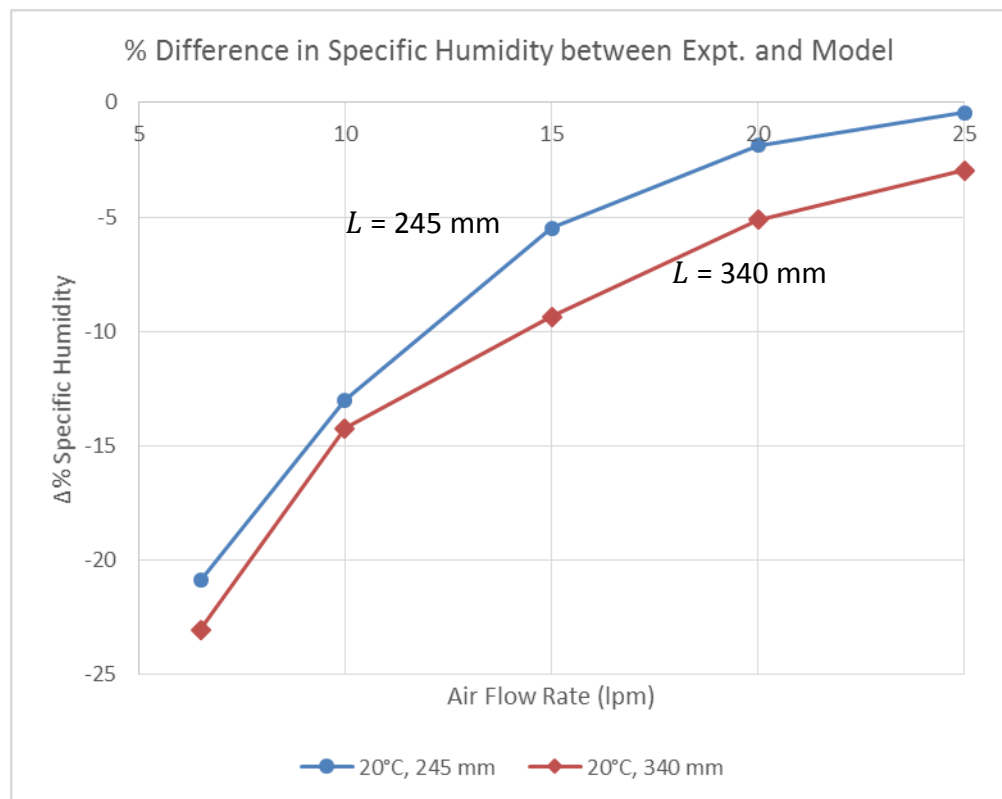
Figure 6-14: Specific humidity of outlet air: Comparison between experimental and theoretical results with respect to conduit length and air flow rate: ($\alpha_m = \alpha_h = 0.04$)

In all cases the theoretical model is predicting more water is evaporating than what was measured experimentally.

6.5.2 Droplet size distribution and parameters at outlet

By considering the droplet size distribution generated by the theoretical model and comparing it to the experimentally measured droplet size distribution for each trial it is possible to see if the model is more or less accurate for predicting evaporative changes to the different droplet size ranges.

Consider Figure 6-15. This is for the same trial as Figure 6-6 but now also shows the theoretical droplet size distribution data, at the outlet of the conduit (in addition to the inlet and experimental outlet droplet size distributions). The purple line represents the theoretical model output for accommodation coefficients of $\alpha_m = \alpha_h = 0.04$ and the green line represents the theoretical model output for accommodation coefficients of $\alpha_m = \alpha_h = 0.001$. Comparing these two lines with the experimental droplet size distribution (red line) at the outlet of the conduit shows that:

- The theoretical model using accommodation coefficients $\alpha_m = \alpha_h = 0.001$ (green curve) appears to give a more accurate prediction of the actual droplet size distribution (red curve) and this is generally true for all trials.
- The theoretical model is less accurate for the smaller droplet sizes.

These observations can be examined in more detail by again considering the distribution parameters: the $Dv10$, $Dv50$, and $Dv90$ for all trials. The values for $Dv10$, $Dv50$, and $Dv90$ recorded for each trial in Appendix 4 were used to determine a % Difference for that parameter between the experimental outlet and theoretical model outlet droplet size distributions. The percentage difference in the $Dv10$ parameter, for example, is calculated as

$$\Delta\% \, Dv10 = \frac{Dv10_{\text{outlet, expt.}} - Dv10_{\text{outlet, model}}}{Dv10_{\text{outlet, expt}}} \times 100\% \tag{6-5}$$

These percentage differences, for each parameter, were then used to produce Figure 6-16 to Figure 6-21. The model values for each parameter are calculated using accommodation coefficients of 0.001 in these cases.
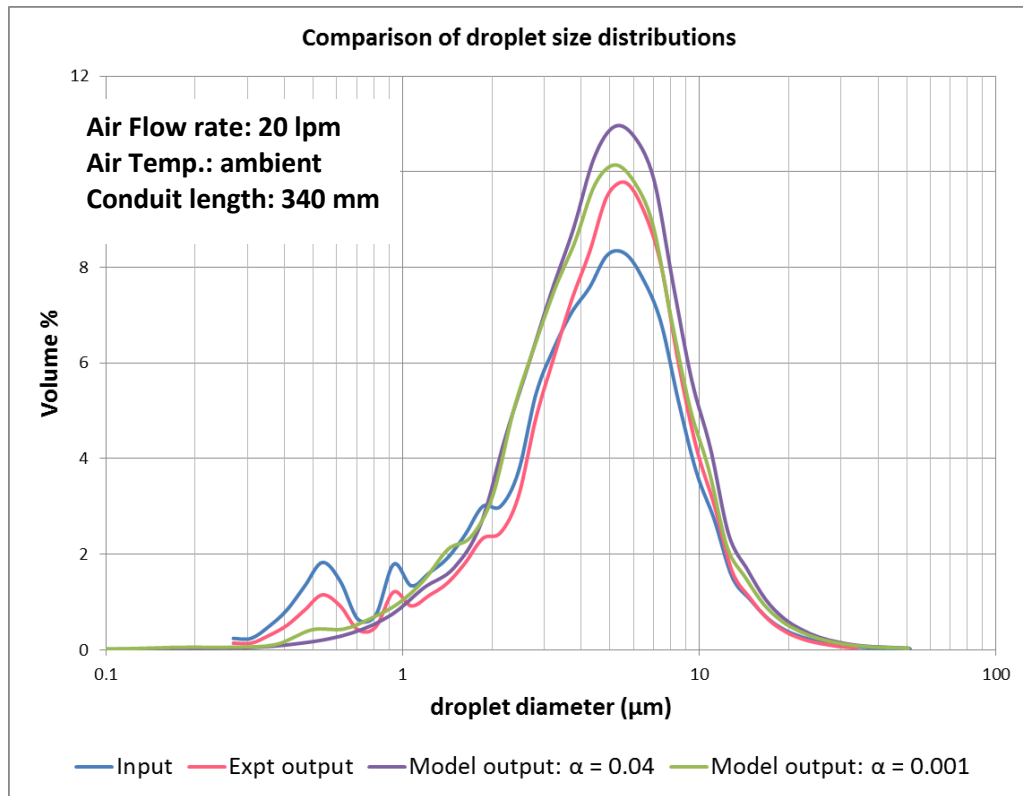
Figure 6-15: Comparison between experimental and theoretical (model) outlet droplet size distributions – typical case

Figure 6-16 shows that for the smaller droplet sizes the difference between the experimental result and the theoretical result is quite large (between +20 and +85%). This indicates that the model is not accurately predicting the evaporation characteristics of the smaller droplets. The model is over predicting the evaporation of the smaller droplets (that is, under predicting the size of the smaller droplets) and the possible reasons for this are discussed in Chapter 7. There appears to be little correlation between model accuracy and inlet air temperature or air flow rate.

Regarding conduit length Figure 6-17 shows that the model is more accurate for the longer conduit case although errors are still large (up to 40%) for the smaller droplet sizes. For ambient air the model appears to be least accurate in predicting the smaller droplet sizes for medium air flow rates (15 lpm) and more accurate at very low and very high air flow rates.
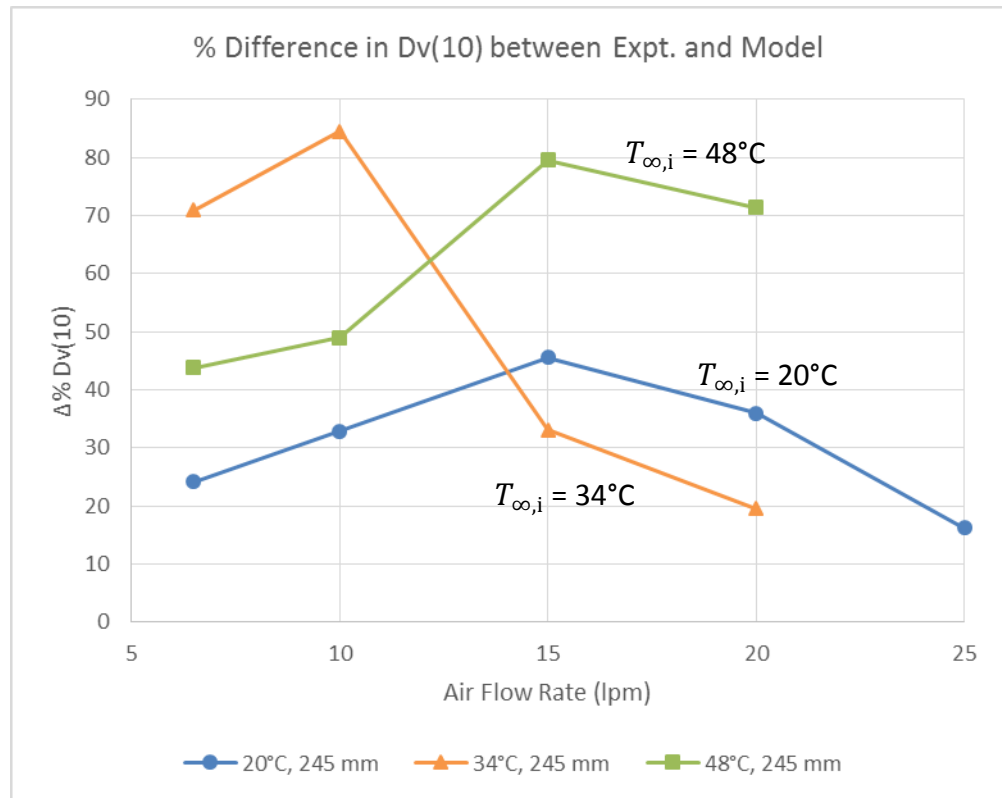
Figure 6-16: Comparison between experimental and theoretical results with respect to air temperature and air flow rate: smaller droplet sizes ($Dv10$)
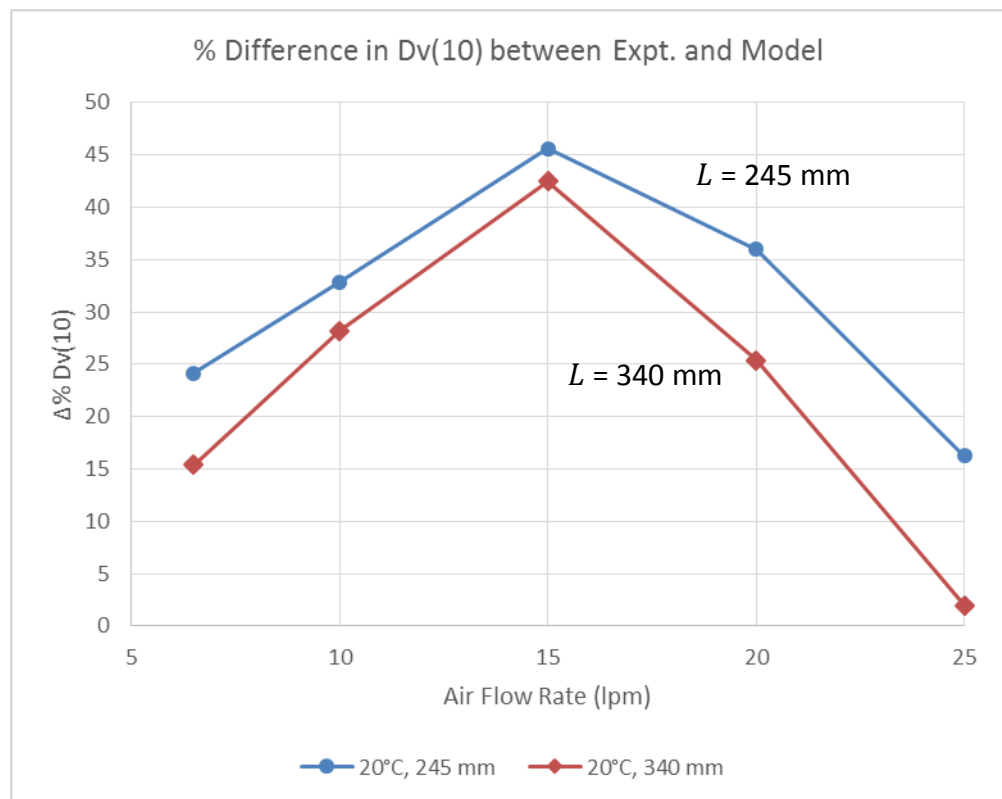
Figure 6-17: Comparison between experimental and theoretical results with respect to conduit length and air flow rate: smaller droplet sizes ($Dv10$)

Figure 6-18 shows that in the case of the $Dv50$, which represents the middle of the droplet size distribution, the accuracy of the model is much better than for the smallest droplet sizes ($Dv10$). Differences range between +22% and -14%. Accuracy is best around medium air flow rates (15 and 20 lpm), where differences are less than 5% for all air temperatures. There appears to be no correlation of model accuracy for the middle sized droplets with air temperature. For increasing air flow rate, the difference between model and experiment for the middle sized droplets is positive and decreasing for the lower air flow rates and negative and increasing for the higher air flow rates.

In regards to conduit length (Figure 6-19) the difference between model and experimental results for the middle droplet sizes is similar for both lengths apart from the trial where the air flow rate was 15 lpm. In this case the difference is significant (11% compared to -2%).

For the larger droplet sizes (represented by the $Dv90$) Figure 6-20 shows that the model is over predicting the changes in droplet size. As noted in the previous section it appears that the large droplets are physically disappearing from the droplet distribution (not evaporating) as they travel along the conduit. If indeed this is the case then the experimental value of $Dv90$ will be artificially lowered and explains why the model is over predicting this value. The effect decreases at higher air flow rates, that is, the model becomes more accurate for predicting the effect on the larger droplet sizes at the higher air flow rates. There appears to be little or no correlation with temperature.

Regarding conduit length Figure 6-21 the differences between model and experiment for the larger droplet sizes are relatively small.

In the previous two sections, results from water droplet evaporation trials have been presented and compared with results from the theoretical models. This has shown in general that the evaporation behaviour of the water droplets is as expected in terms of the amount of water evaporated and in terms of changes to the droplet size distribution. Comparison of the experimental results with corresponding theoretical model results have generally been good and discussion on reasons for some of the larger differences are presented in Chapter 7.
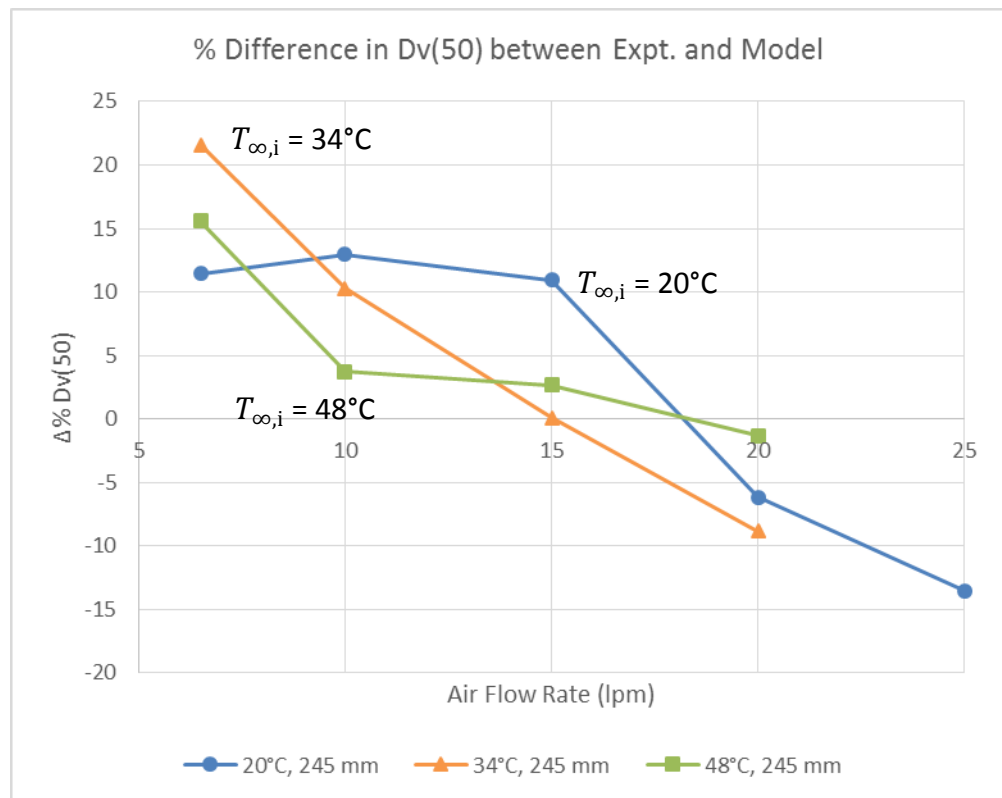
Figure 6-18: Comparison between experimental and theoretical results with respect to air temperature and air flow rate: middle droplet sizes ($Dv50$)
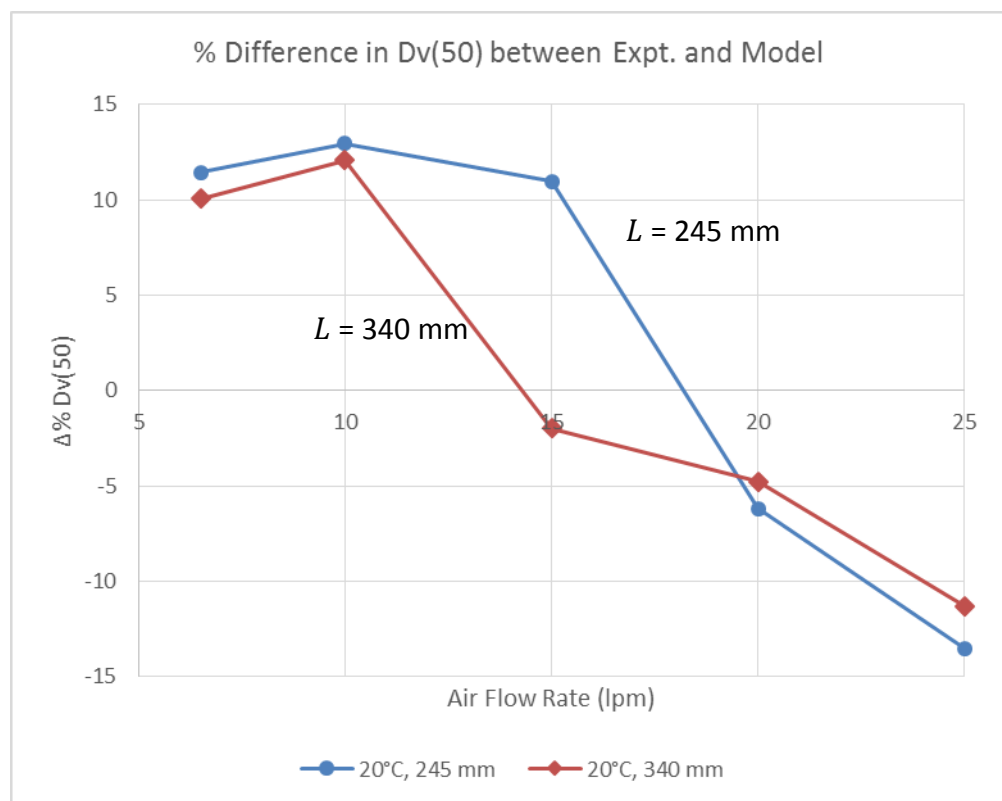
Figure 6-19: Comparison between experimental and theoretical results with respect to conduit length and air flow rate: middle droplet sizes ($Dv50$)
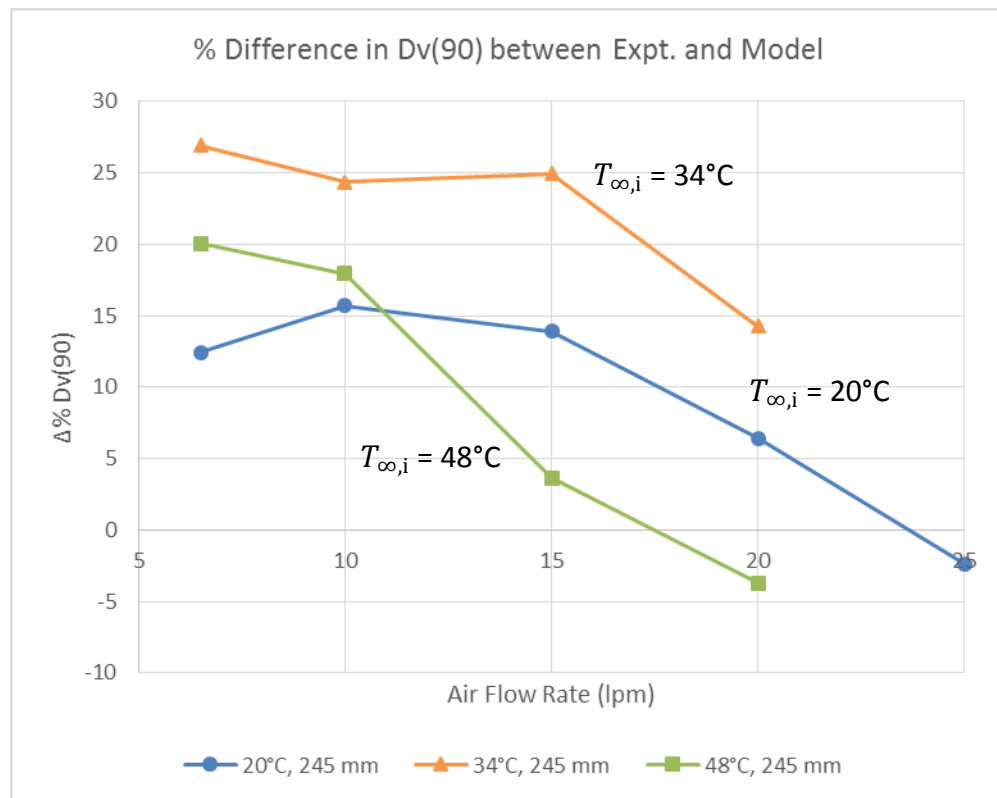
Figure 6-20: Comparison between experimental and theoretical results with respect to air temperature and air flow rate: larger droplet sizes ($Dv90$)
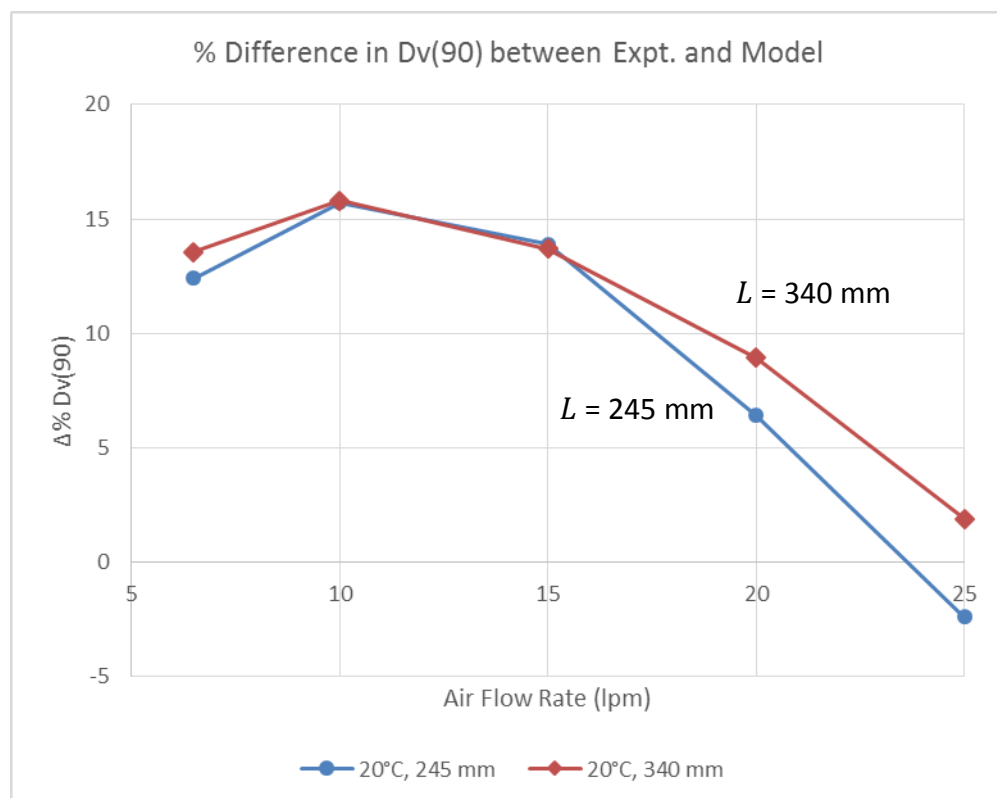
Figure 6-21: Comparison between experimental and theoretical results with respect to conduit length and air flow rate: larger droplet sizes ($Dv90$)

6.6 Ultrasound enhanced evaporation

The aim of this part of the investigation is to provide insight into the ultrasound enhanced evaporation process, to quantify the improvement in droplet evaporation as a result of the imposed ultrasound field and to investigate the validity of the theoretical model.

In the following three sections the experimental and theoretical results are presented from the investigation of the ultrasound enhanced evaporation process.

In the next section, experimental results reported in the literature for an increase in water evaporation due to an imposed ultrasound field are compared with those generated from the theoretical model.

In section 6.8, the experimental results from the ultrasound enhanced evaporation process are compared to corresponding experimental results for the normal evaporation process. The effect of air flow rate and ultrasound power level on the amount of water evaporated and the droplet size distribution are presented.

And finally in section 6.9 the initial and boundary conditions for each experimental trial were also entered into the ultrasound enhanced droplet evaporation model described in Chapter 4 and comparative values for the droplet size distribution, distribution parameters and amount of water evaporation were determined. These were compared to the corresponding experimental results.

6.7 Comparison with the literature

Although the use of an acoustic field to enhance the evaporation of water in a variety of different situations has been reported in the literature [111, 115, 121, 151-153], very few were in situations comparable to that being investigated in the current work. The situation investigated in this work is comprised of an ultrasound field applied to a poly-dispersion of many droplets evaporating into air flowing along a conduit. As discussed in Chapter 2, in most other cases the sound field was applied to single, large (mm size range) droplets and in most cases the acoustic field used was not in the ultrasound region. In cases where an ultrasound field was used, its main purpose was to levitate the one or two large droplets and then to investigate the evaporation due to the acoustic streaming flows, generated by the ultrasound field, around these droplets.

However experimental data was available for the drying of various vegetable pieces in a power ultrasound environment, similar to the physical situation modelled in this work [117]. As described in Chapter 2 the effect of the ultrasound field on water evaporation from the vegetable pieces was found to be in two areas. Firstly the ultrasound field affects the diffusion of water from inside the solid vegetable pieces to the surface of the solid. Secondly the ultrasound field affects the transport of water vapour from the solid surface to the air through proposed mechanisms of pressure variations, reduced boundary layer thickness, oscillating air velocities and micro-streaming. It is this latter effect that is applicable to the process of evaporation being investigated in the current study. Thus if the effect of the ultrasound on the water evaporation from the surface of the vegetable pieces to the air can be quantified this data could be compared with results from the ultrasound enhanced model. Results from the model would be estimates rather than accurate values nevertheless they are indicative values which could be used as terms of reference for comparison.

6.7.1 Power ultrasound drying results

In the research investigating the effect of an ultrasound field on vegetable drying detailed in Chapter 2, a 'mass transfer coefficient', K (units kg/m^2/s) was determined. This coefficient quantifies the magnitude of the water vapour transport from the surface of the vegetable pieces to the air. It was discovered that generally, the magnitude of this external mass transfer coefficient increased with increasing intensity of the ultrasound field. In that research, values of K were determined for a variety of different situations (ultrasound power levels, air flow rates, vegetable packing densities etc) for a variety of different vegetable types. Table A 1 to Table A 7 in Appendix 2 show the results from this research for different vegetable types subject to air flowing through the cylinder at a velocity of 1 m/s and inlet temperature of 40°C. Although different ultrasound intensities inside the cylinder were investigated only the results from the maximum ultrasound power intensity of 37 kW/m^3 are shown. Three parameters are extracted from their data that indicate the rate of water evaporation from the vegetable pieces: the overall drying time (to a pre-set moisture content for the vegetable pieces), the initial moisture removal rate and the mass transfer coefficient, K. These are shown in the tables for each vegetable type for the case of no applied ultrasound and for the case of maximum applied ultrasound (37 kW/m^3). To quantify the effect of the

ultrasound field on the water evaporation and for comparison with the outputs from the model of the current work, improvement factors are defined in this work. In the case of overall drying times the improvement factor is defined as

$$IF_{time} = \frac{\text{drying time with NO ultrasound}}{\text{drying time WITH ultrasound}} \qquad (6\text{-}6)$$

In the case of initial drying rates, the improvement factor is defined as

$$IF_{rate} = \frac{\text{initial drying rate WITH ultrasound}}{\text{initial drying rate with NO ultrasound}} \qquad (6\text{-}7)$$

In the case of the mass transfer coefficient, K, the improvement factor is defined as

$$IF_k = \frac{\text{mass transfer coefficient WITH ultrasound}}{\text{mass transfer coefficient with NO ultrasound}} \qquad (6\text{-}8)$$

These factors were calculated from the extracted data and are also tabulated in Appendix 2. Figure 6-22 plots the three improvement factors determined for each vegetable type. Note, for strawberry [120] the experimental conditions are slightly different (air velocity is 2 m/s and ultrasound power is 25 kW/m^2). Note also, mass transfer coefficients were not determined in the carrot and lemon peel studies [118].
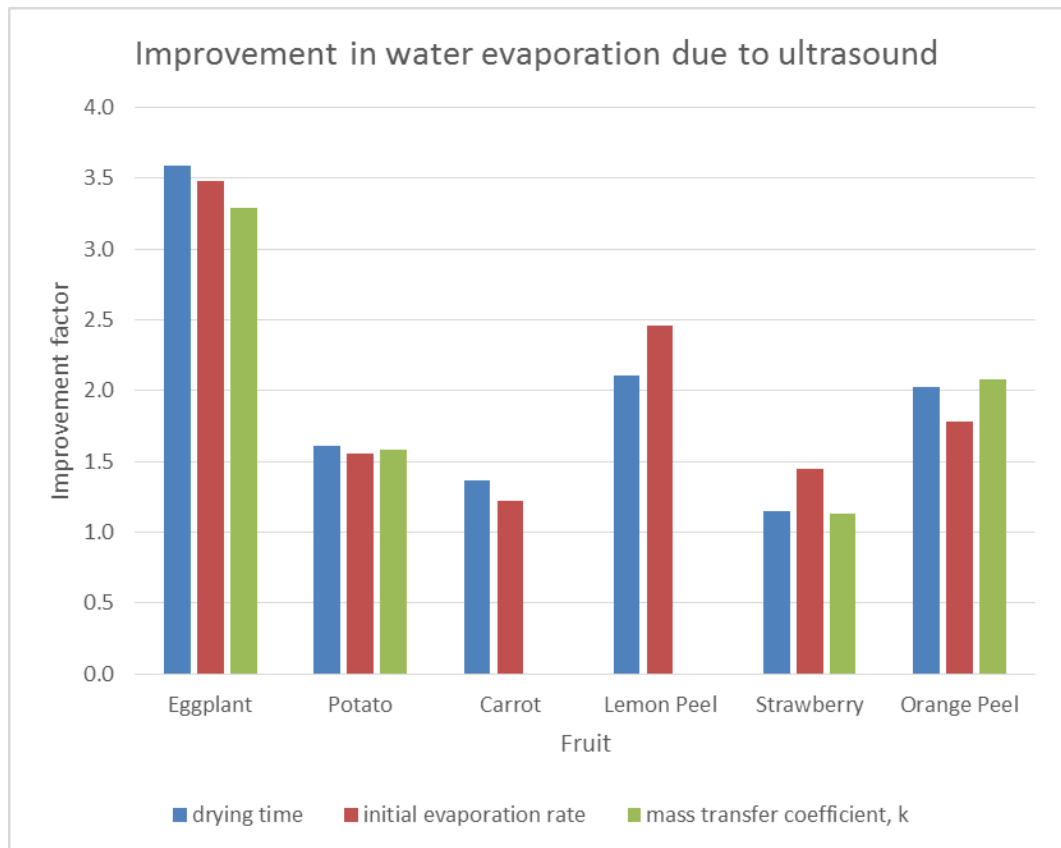
Figure 6-22: Improvement in water evaporation from vegetable pieces due to the application of an ultrasound field – Experimental data.

From Figure 6-22 it can been seen that the value of the improvement factor varies greatly with vegetable type. Vegetables with a porous solid structure tend to have a large improvement factor (for example, eggplant) and vegetables with a denser solid structure (for example, potato and carrot) tend to have lower improvement factors. It can also be seen that the three different improvement factors are reasonably consistent for a specific vegetable type. The overall drying time figures in Table A 1 to Table A 7 in Appendix 2 depend on both the water diffusion through the solid as well as the water mass transfer from the surface of the solid to the air whereas the mass transfer coefficient (K) figures in those same tables depend only on the latter effect. Yet the two improvement factors based on these different parameters are similar for a specific vegetable type. This means that whatever data is available (external mass transfer coefficient, initial evaporation rate, or just the overall drying times) that data can be used to estimate the effect of the ultrasound on the external mass transfer coefficient.

The improvement factor, generally, ranges from 1.15 for the denser vegetables to 3.5 for the more porous vegetables. On average, the improvement factor in the external mass transfer coefficient is around 1.5 across all vegetable types. This corresponds to an improvement of around 50% in the water evaporation from the surface of the vegetable pieces as a result of the ultrasound field. These results can now be compared to equivalent results generated from the theoretical ultrasound enhanced evaporation model.

6.7.2 Comparative model outputs

This part of the experimental investigation compares outputs from the theoretical ultrasound enhanced evaporation model with the published experimental data detailed in the previous section. To achieve this it is necessary to set up the model and its inputs to match as closely as possible the physical situation described in the vegetable drying research. The small pieces of vegetable from that research are physically and thermodynamically different from the droplets of water being studied in this investigation. However, the effect of the ultrasound field on heat transfer and water transport between the air and the surface of the droplets should be the similar to that between the air and surface of the vegetable pieces. In a similar way for the vegetable pieces, it is expected that the ultrasound field will reduce the convective boundary layer,

generate pressure and air velocity variations over the droplet surfaces and cause micro-streaming [119] thus enhancing both heat and mass transfer for the water droplets.

For comparison purposes the ultrasound enhanced evaporation model was set up with input data taken from measured input data in earlier trials of the apparatus described in section 6.3. While the input water droplet flow rate was held approximately constant, the air flow rate was varied to give a variance in the ratio of air to water droplets flowing along the tube. This being roughly analogous to the different vegetable types (hard and soft). Two parameters are calculated in the model in order to determine the effect of the ultrasound field on the evaporation of the water droplets. Firstly, the amount of water evaporated over a set distance along the conduit is determined and secondly the time taken for the air and water droplets to reach equilibrium is also determined. Here, equilibrium is defined as either all of the droplets evaporating or the relative humidity of the air surrounding the droplets reaching unity and the temperatures of the droplets and air becoming equal. These two parameters, drying time and time to equilibrium, were determined for the case of no ultrasound and for the case of an applied ultrasound field. It was reported in the vegetable drying research that the maximum ultrasound power of 37 kW/m^3 generated an SPL of around 154.5 dB of pressure inside the cylinder and this value was used in the model to determine the magnitude of air oscillation of the ultrasound field.

Table A 8 and Table A 9 in Appendix 2 show the amount of water evaporated over two different distances (245 mm and 340 mm) and the time taken to reach equilibrium for air at different velocities and temperatures. To quantify the effect of the ultrasound field on the water evaporation from the droplets and for comparison with the experimental results generated in section 6.3, improvement factors are defined. In the case of the amount of water evaporated over a set distance, the improvement factor is defined as

$$IF_{\text{amt}} = \frac{\text{amount evaporated with NO ultrasound}}{\text{amount evaporated WITH ultrasound}}$$

(6-9)

And in the case of time to reach equilibrium, the improvement factor is defined as

$$IF_{\text{time}} = \frac{\text{time to reach equilibrium with NO ultrasound}}{\text{time to reach equilibrium WITH ultrasound}}$$

(6-10)

These improvement factors were calculated and are presented in Table A 10 in Appendix 2 and plotted in Figure 6-23. Thus, this graph shows the improvement in water evaporation due to the presence of an ultrasound field of similar intensity as to that used in the generation of the experimental data in section 6.7.1. When considering the times to equilibrium for the theoretical model these improve by a factor of around 1.22 (or 22%) except for the low air flow rate case (6.4 lpm) where the improvement factor is around 1.6 or 60%. This larger value for the low air flow rate is probably due to the longer residence time for the droplets in the tube, that is, longer exposure to the ultrasound field. When considering the amount of water evaporated over a fixed distance in the conduit, the improvement factors are somewhat less at around 1.03 or 3%.
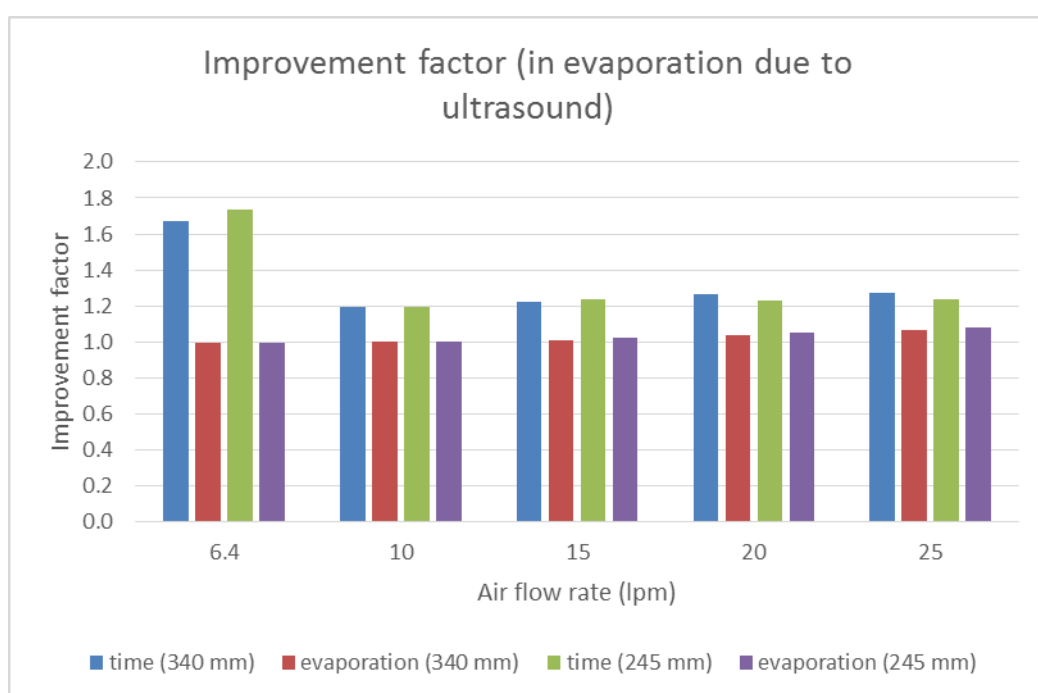
Figure 6-23: Improvement in water evaporation due to presence of ultrasound field
- Theoretical Model

6.7.3 Remarks – comparison with the literature

The improvement factor determined from the time to equilibrium for the theoretical model was found to be on average about 1.2 (or 20%). This compares favourably with the improvement factors for water evaporation presented in the previous section (Figure 6-22) at around 1.5 (or 50%). Thus, the theoretical model is giving a good indication of the enhancement of the water evaporation from the water droplets in this current study.

6.8 Variables affecting improvement in evaporation

In this section results are presented for the case of an ultrasound field imposed on the water droplets evaporating in air as they flow along a conduit. Results presented focus on the effect of air flow rate and ultrasound power level on the amount of water evaporated and on changes to the droplet size distribution over the length of the conduit.

Results were generated from trials detailed in Chapter 5 for the following different cases

- Air flow: 6, 8, 10, 12, 15, 18, 20 lpm
- Ultrasound Power level: 2, 5, 7, 10, 12, 15, 17, 20 W at a frequency of 21.7 kHz

The conduit tube length remained constant at 300 mm (could not be altered) and the inlet air temperature was kept approximately constant at ambient conditions.

In each trial the experimental parameters noted in Chapter 5, Table 5.1 were measured and recorded in accordance with the procedures laid out in that chapter. Raw results for each case are a provided in the Appendix 4 and include:

- Amount of water evaporation (measured in terms of the moisture content, specific humidity, of the air at the inlet and outlet).
- Table of size distribution parameters: $Dv10$, $Dv50$, $Dv90$, $Span$, $D[3,2]$, $D[4,3]$ (at both inlet and outlet)
- Graph of droplet size distribution: % Volume versus droplet diameter at inlet and at outlet

6.8.1 Amount of water evaporated

As detailed in the section 6.4.1 the % difference in specific humidity in the air stream between the inlet and outlet of the conduit is a measure of the amount of water that has evaporated. Since the inlet water flow and inlet air specific humidity is relatively constant in each trial, comparing just the specific humidity in the air outlet stream when the ultrasound field is off and when it is on will give an indication of the improvement in evaporation as a result of the ultrasound field. The specific humidity of the air at the outlet of the conduit is shown in the following two tables. Table 6-4 shows values for the specific humidity when the ultrasound field is turned off and Table 6-5 shows values, for the same trials, when the ultrasound field is turned on.

The percentage difference between the values in these two tables is then calculated for each trial according to

$$\Delta\% \, w = \frac{w_{\text{outlet, US on}} - w_{\text{outlet, US off}}}{w_{\text{outlet, US off}}} \times 100\% \qquad (6\text{-}11)$$

These percentage difference values are shown in Table 6-6 and plotted in Figure 6-24 and Figure 6-25. Figure 6-24 plots the values against air flow rate for each ultrasound power level and Figure 6-25 plots the percentage differences vs ultrasound power level for each air flow rate. The percentage difference plotted in these graphs is a measure of the improvement in evaporation due to the presence of the ultrasound field.

Table 6-4: Measured Specific Humidity of air (g/kg) at conduit outlet. Ultrasound OFF

Air flow rate (lpm)	Ultrasound Power (W)							
	2	5	7	10	12	15	17	20
6.5	13.13	12.60	12.25	12.84	12.71	12.66	13.48	12.34
8	12.13	12.00	11.43	12.38	12.40	12.27	14.00	12.42
10	11.57	11.57	10.98	12.08	11.86	11.67	12.90	12.43
12	10.78	11.07	10.51	11.56	11.58	11.19	12.14	11.35
15	10.15	10.53	10.19	10.82	10.66	10.59	11.31	10.95
18	9.61	9.79	9.60	10.16	10.09	9.78	10.54	10.40
20	9.35	9.38	9.35	9.83	9.76	9.42	10.24	9.94

Table 6-5: Measured Specific Humidity of air (g/kg) at conduit outlet. Ultrasound ON

Air flow rate (lpm)	Ultrasound Power (W)							
	2	5	7	10	12	15	17	20
6.5	13.94	13.45	13.69	14.25	14.48	14.65	15.98	14.32
8	12.77	13.08	12.84	14.09	14.55	14.65	16.81	15.02
10	11.82	12.12	11.70	13.68	14.27	14.22	16.08	15.01
12	11.02	11.49	11.28	13.09	13.82	13.45	15.34	14.57
15	10.25	11.00	10.67	11.86	11.62	11.80	13.46	13.43
18	9.73	10.01	9.97	10.83	10.88	10.59	11.60	11.99
20	9.39	9.55	9.50	10.43	10.57	10.15	10.95	10.68

Table 6-6: Change in Specific Humidity of air (g/kg) at conduit outlet as a result of the imposed ultrasound field.

Air flow rate (lpm)	Ultrasound Power (W)							
	2	5	7	10	12	15	17	20
6.5	6.2%	6.7%	11.8%	11.0%	13.9%	15.7%	18.6%	16.0%
8	5.3%	9.0%	12.3%	13.8%	17.3%	19.4%	20.1%	21.0%
10	2.2%	4.7%	6.6%	13.2%	20.3%	21.9%	24.6%	20.7%
12	2.3%	3.9%	7.3%	13.3%	19.4%	20.2%	26.3%	28.4%
15	1.0%	4.4%	4.7%	9.6%	9.0%	11.4%	19.0%	22.7%
18	1.2%	2.2%	3.8%	6.6%	7.8%	8.3%	10.0%	15.3%
20	0.4%	1.8%	1.5%	6.1%	8.3%	7.7%	7.0%	7.4%

From the above Tables and from Figure 6-24 it can be seen that the application of the ultrasound field has had a significant effect on the evaporation of water from the droplets into the airstream. This improvement in evaporation ranges from around 0.5% up to 28% depending on air flow rate and power level. Generally, the higher the ultrasound power level, the greater the improvement in evaporation. For the lower ultrasound power levels (< 10 W) an increase in air flow rate reduces the improvement and for the higher power levels (>10 W) the improvement peaks at an air flow rate of around 10 to 12 lpm.

Figure 6-25 confirms the trend that the higher ultrasound power levels give greater improvement in water droplet evaporation. It also shows that at any particular air flow rate, increasing the ultrasound power level will increase the evaporation of water from the droplets. It also confirms that at the higher power levels the improvement peaks at an air flow rate of around 10 to 12 lpm.

It was also noted on inspection of the apparatus after each trial that for certain trials there were droplets of water attached to the inside walls of the conduit. At each ultrasound power level a critical air flow rate was found such that droplets of water were present on the walls for air flows below this critical value. Table 6-7 lists values of the critical air flow rate for each input ultrasound power level. It was not possible to determine the mass of water that was held up in the apparatus under these conditions however at a given power level it was greater at the lower air flow rates.
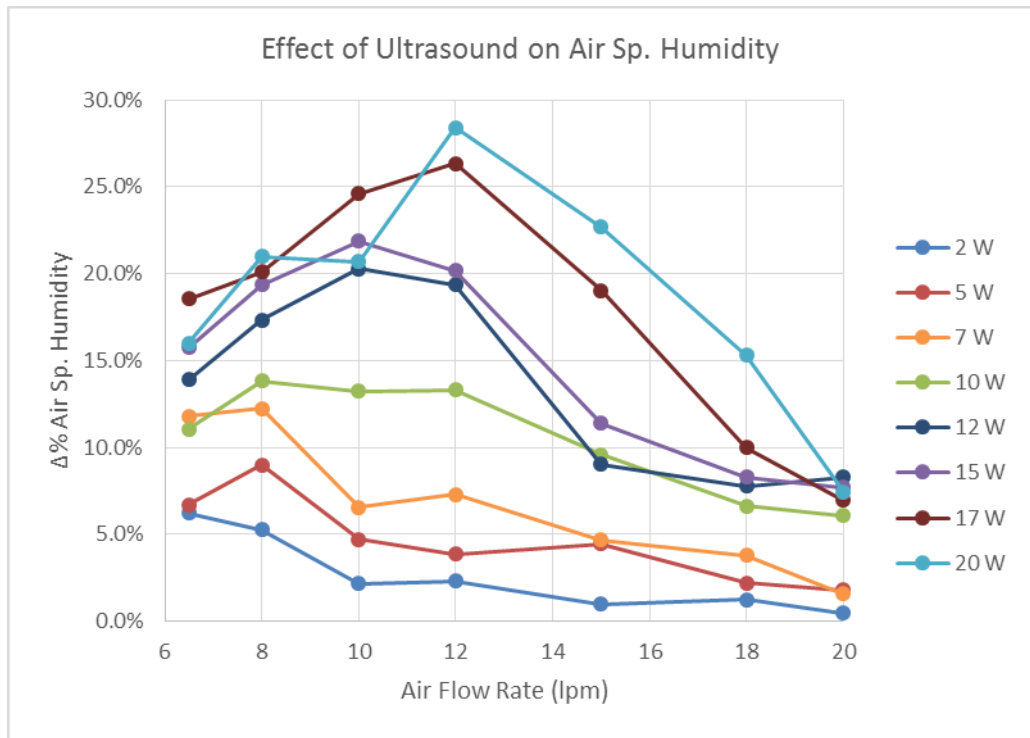
Figure 6-24: Percent change in Specific Humidity at conduit outlet as a result of the ultrasound field, at various power levels – vs air flow rate.
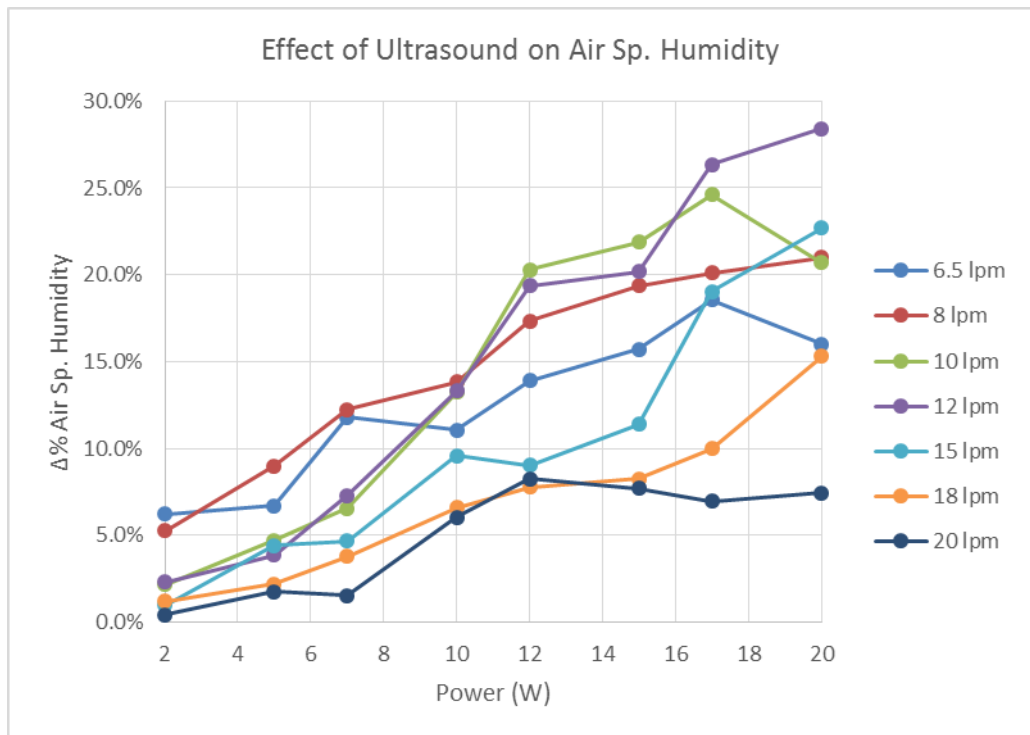
Figure 6-25: Percent change in Specific Humidity at conduit outlet as a result of the ultrasound field, at various air flow rates – vs ultrasound power level.

147

It is clear from Table 6-7 that at the lowest air flow rates (6.5 and 8 lpm) there was some hold up of water in the apparatus for all ultrasound power levels. Also, the hold up of water increased as the ultrasound power level increased. Although this hold up of water would have affected the overall water balance for each trial, it did not affect the measurement of the water vapour in the air at the outlet of the conduit. That is the calculation of the improvement in water evaporation presented at the beginning of this section is still valid.

Table 6-7: Critical air flow rates for water droplet hold up in the apparatus

Ultrasound Power Level (W)	Critical air flow rate (lpm)
2	8
5	10
7	10
10	12
12	12
15	15
17	15
20	15

It was also noted that power levels higher than 25 W and air flow rates greater than 15 lpm that there were no droplets visible at all at the conduit outlet and there was no holdup of droplets in the conduit (sonotrode). Under these conditions complete evaporation of the droplets was occurring over the length of the conduit.

6.8.2 Changes to the droplet size distribution

It was expected that the changes to the droplet size distribution as a result of an imposed ultrasound field would be an enhancement of the changes resulting from normal evaporation. These latter changes have been presented in section 6.4.2.

Figure 6-26 and Figure 6-27 show typical changes to the droplet size distribution when the evaporating droplets and air are subject to an ultrasound field. In this case the input power to the device generating the ultrasound field is 5 W and the air flow rates are 8 lpm and 18 lpm respectively for the two graphs.
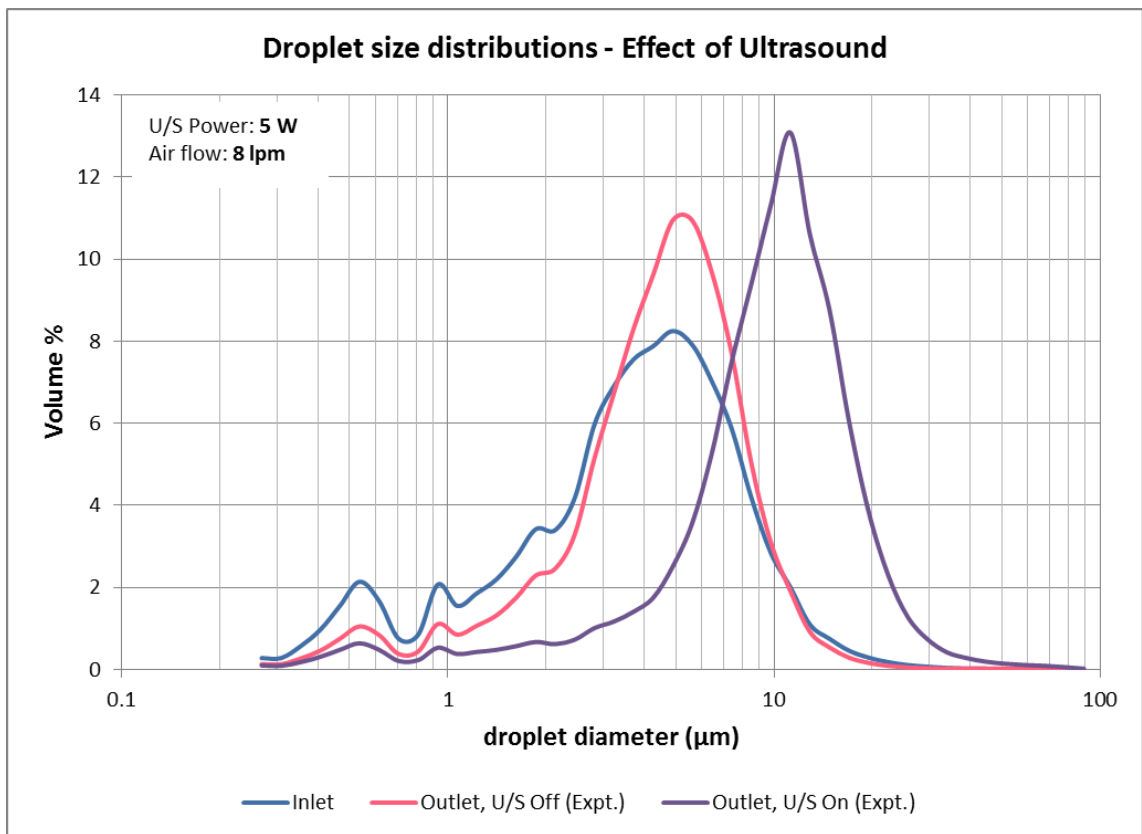
Figure 6-26: Droplet size distributions, low air flow
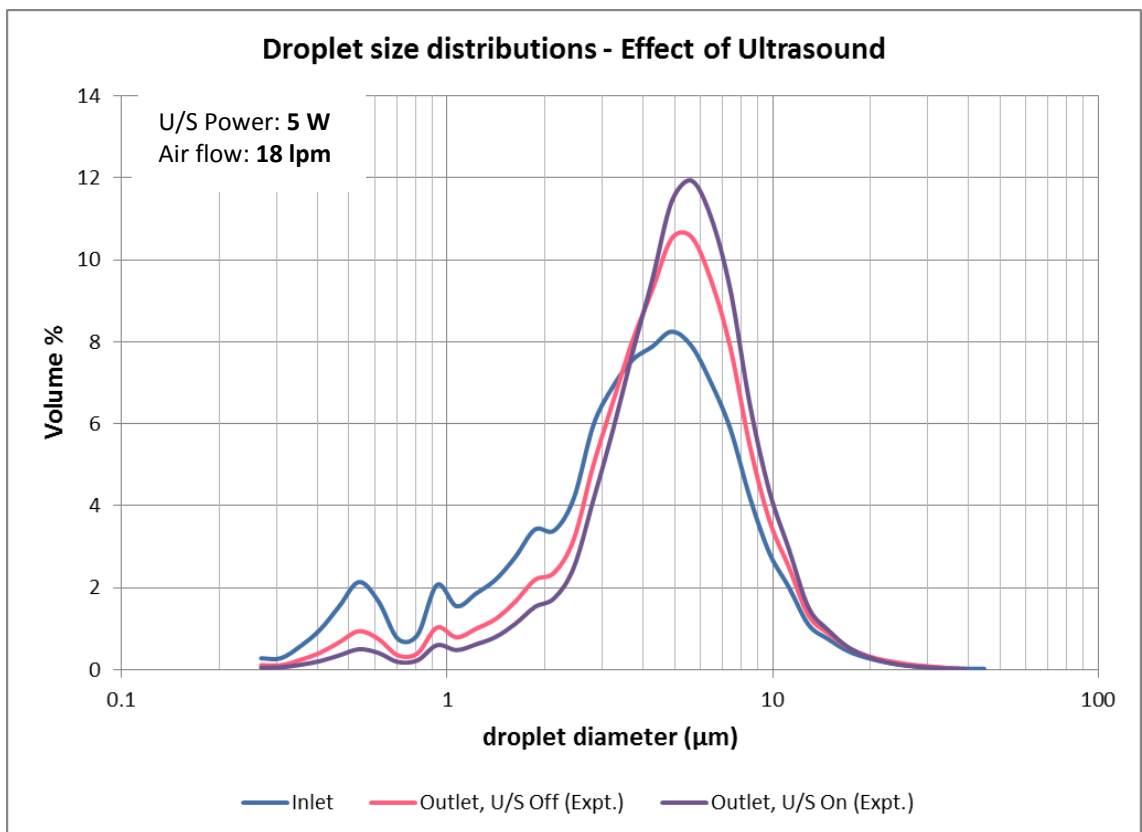
Figure 6-27: Droplet size distributions, high air flow

149

The blue curve represents the droplet size distribution at the inlet to the conduit and the red curve represents the distribution at the outlet of the conduit, under normal evaporation conditions. The purple curve represents the droplet size distribution at the outlet of the conduit when the ultrasound field is turned on.

In the low air flow case the change in droplet size distribution at the outlet of the conduit when the ultrasound field is applied is marked when compared to the normal distribution at the outlet. The distribution has shifted significantly to larger droplet sizes. In the case of higher air flow the change in size distribution at the outlet as a result of the ultrasound field is still apparent but not so marked.

Although the change in droplet size distribution is marked in the low air flow case the corresponding improvement in evaporation is only modest at 5.3% improvement. A thorough discussion of these results is provided in Chapter 7.

To investigate the changes in the outlet droplet size distribution in more detail, as a result of the ultrasound field, the size distribution parameters $Dv10$, $Dv50$ and $Dv90$ representing the smaller , middle sized and larger droplets respectively are again considered. The values for these parameters, recorded for each trial in Appendix 4, were used to determine a percentage difference for that parameter at the outlet of the conduit. The difference being between the value of the parameter with the ultrasound field turned off and with the ultrasound field turned on. The percentage difference in the $Dv10$ parameter, for example, is calculated as

$$\Delta\% \, Dv10 = \frac{Dv10_{\text{outlet, US on}} - Dv10_{\text{outlet, US off}}}{Dv10_{\text{outlet, US off}}} \times 100\% \qquad (\,6\text{-}12)$$

These percentage differences, for each parameter, were then used to produce Figure 6-28 to Figure 6-33

Figure 6-28 shows the effect of the ultrasound field on the smaller droplets ($Dv10$) in the distribution at the outlet of the conduit for various ultrasound power levels versus air flow rate. In all cases except one the ultrasound field has increased the value of $Dv10$ significantly compared to normal evaporation. Positive changes range from 10% to over 300%. This means that there is a lower volume percentage of the smaller droplets present in the distribution at the outlet of the conduit as a result of the imposed ultrasound field. The reasons for this could be due to evaporation of those droplets or other effects discussed in Chapter 7.
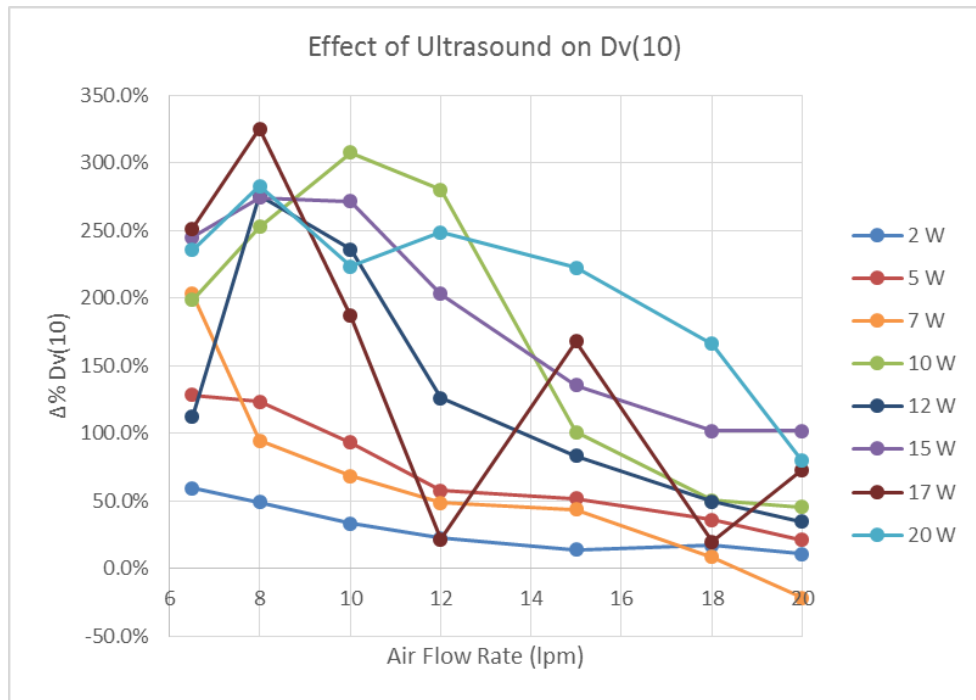
Figure 6-28: Percent change in $Dv10$ at conduit outlet as a result of the ultrasound field, for various power levels – vs air flow rate

Although results for some trials (for example, 17 W and 10 W) show high variance the general trend is that the change in $Dv10$ decreases with increasing air flow rate for a specific ultrasound power level. Also, the effect of the ultrasound on $Dv10$ is greater at higher ultrasound power levels.

Figure 6-29 shows the same information plotted at various air flow rates versus ultrasound power level. This shows that at a specific air flow rate, increasing the power level tends to increase the positive change in $Dv10$, that is, decrease the volume percentage of smaller droplets in the distribution.

Figure 6-30 shows the effect of the ultrasound field on the middle of the droplet size distribution ($Dv50$) at the outlet of the conduit for various ultrasound power levels versus air flow rate. In all cases the ultrasound field has increased the value of $Dv50$ significantly compared to normal evaporation although not as greatly as for the smaller droplets. Changes range from 1% to just under 180%. This means that, at the outlet of the conduit, there is a lower volume percentage of smaller droplets present in the distribution and possibly a greater volume percentage of larger droplets in the distribution as a result of the imposed ultrasound field. The reasons for this could be due to evaporation of the smaller droplets and other effects discussed in Chapter 7. The general trend is similar to that for the changes to the smaller droplets ($Dv10$), that is

the $Dv50$ decreases with increasing air flow rate for a specific ultrasound power level. The effect of the ultrasound on $Dv50$ is greater at higher ultrasound power levels.
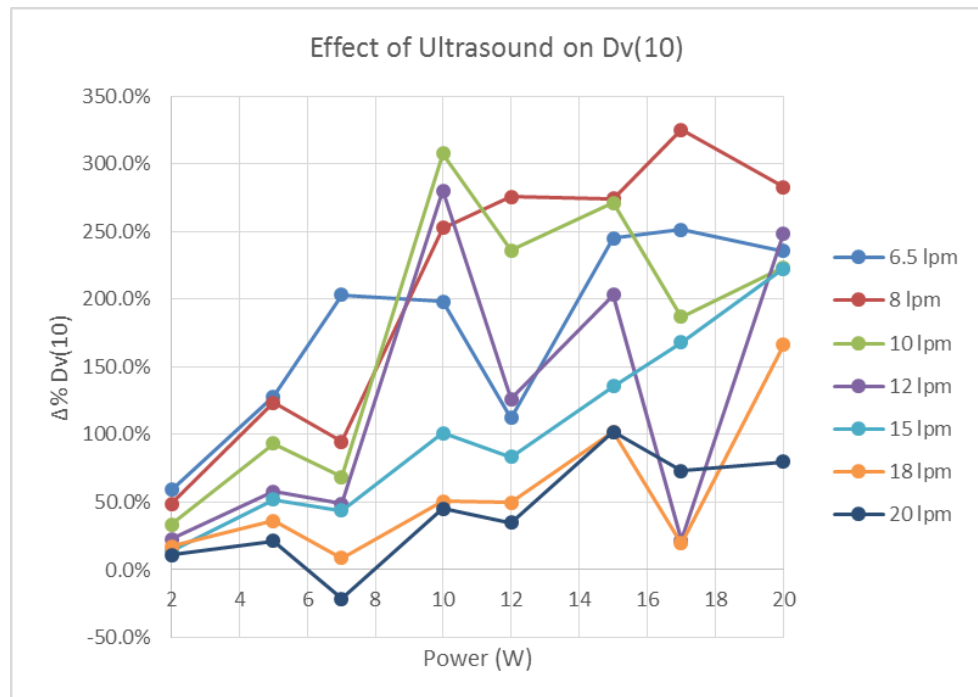
Figure 6-29: Percent change in $Dv10$ at conduit outlet as a result of the ultrasound field, for various air flow rates – vs ultrasound power level
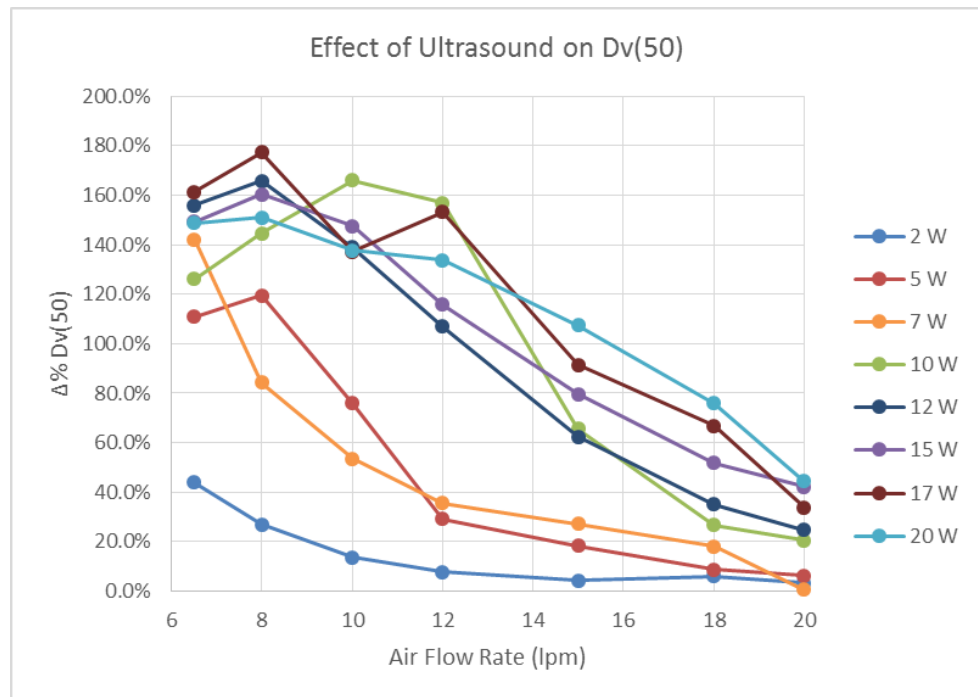
Figure 6-30: Percent change in $Dv50$ at conduit outlet as a result of the ultrasound field, for various power levels – vs air flow rate

Figure 6-31 shows the same information plotted at various air flow rates versus ultrasound power level. This shows that at a specific air flow rate, increasing the power level tends to increase the change in the middle sized droplets in the distribution, which is the middle of the distribution is at a larger droplet size. This could be due to a lower percentage volume of the smaller droplets (as shown considering the $Dv10$ above) or possibly a greater volume percentage of the larger droplets. The increase in $Dv50$ is more consistent at the higher air flow rates (15, 18 and 20 lpm). At the lower air flow rates the changes in $Dv50$ tend to fluctuate somewhat with increasing ultrasound power level.
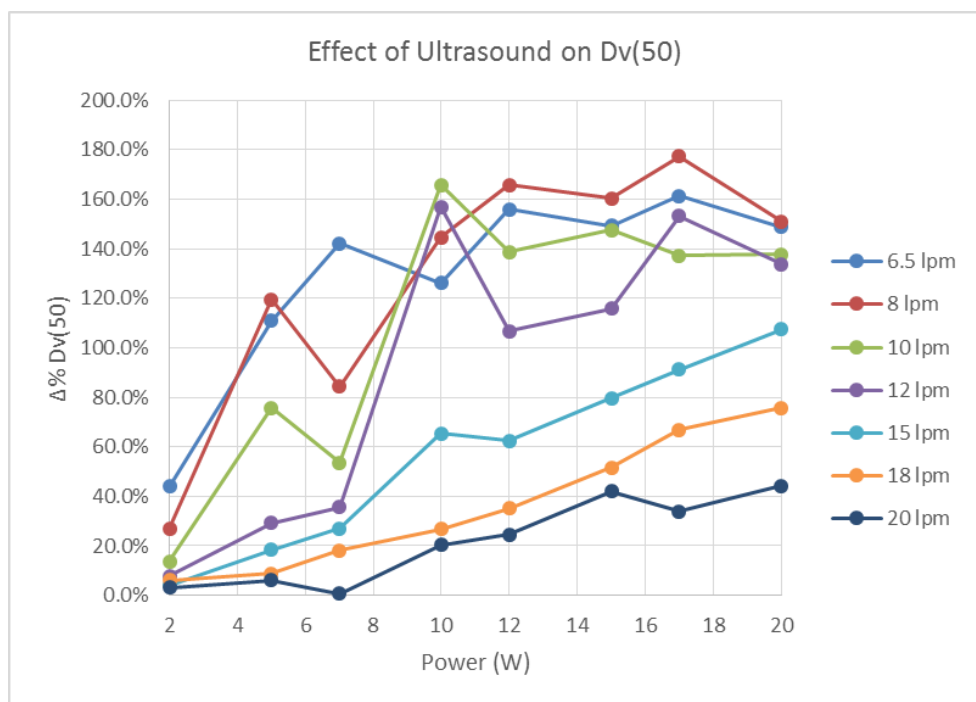
Figure 6-31: Percent change in $Dv50$ at conduit outlet as a result of the ultrasound field, for various air flow rates – vs ultrasound power level

Figure 6-32 shows the effect of the ultrasound field on the larger droplet sizes ($Dv90$) at the outlet of the conduit for various ultrasound power levels versus air flow rate. In all cases the ultrasound field has increased the value of $Dv90$ significantly compared to normal evaporation to almost the same degree as for the middle of the distribution ($Dv50$). Changes range from 0% to just under 160%. This means that, at the outlet of the conduit, there is a greater volume percentage of larger droplets present in the distribution as a result of the imposed ultrasound field. The level of change for these larger droplets is unexpected and indicates that the ultrasound field is having effects on the distribution other than just enhancing the evaporation. For example some

coalescence could be occurring and this is discussed in more detail in Chapter 7. The general trend is similar to that for the changes to the smaller droplets ($Dv10$) and for the $Dv50$ that is, the $Dv90$ decreases with increasing air flow rate for a specific ultrasound power level. Also, the effect of the ultrasound on $Dv90$ is greater at higher ultrasound power levels.
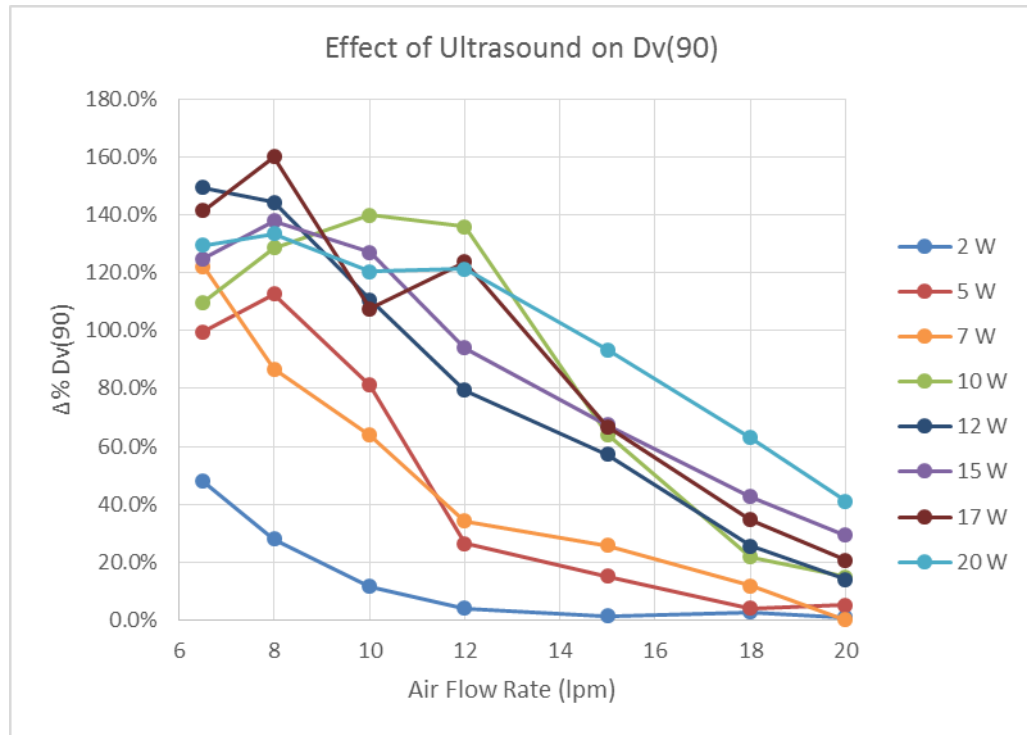
Figure 6-32: Percent change in $Dv90$ at conduit outlet as a result of the ultrasound field, for various power levels – vs air flow rate

Figure 6-33 shows the same information plotted at various air flow rates versus ultrasound power level. The trend is very similar to that for the smaller droplets and to that for the middle of the distribution, that is, at a specific air flow rate, increasing the power level tends to increase the volume percentage of larger droplets in the distribution. As for the $Dv50$ the increase in $Dv90$ is more consistent at the higher air flow rates (15, 18 and 20 lpm). At the lower air flow rates the changes in $Dv90$ tend to fluctuate somewhat with increasing ultrasound power level.

This confirms that the change in $Dv50$ (increase) is due to the changes in $Dv10$ (less smaller droplets) and to the changes in the $Dv90$ (more of the larger droplets). The combination of these effects is to shift the droplet size distribution to larger droplet sizes as clearly shown in Figure 6-26. These changes are discussed more fully in Chapter 7.
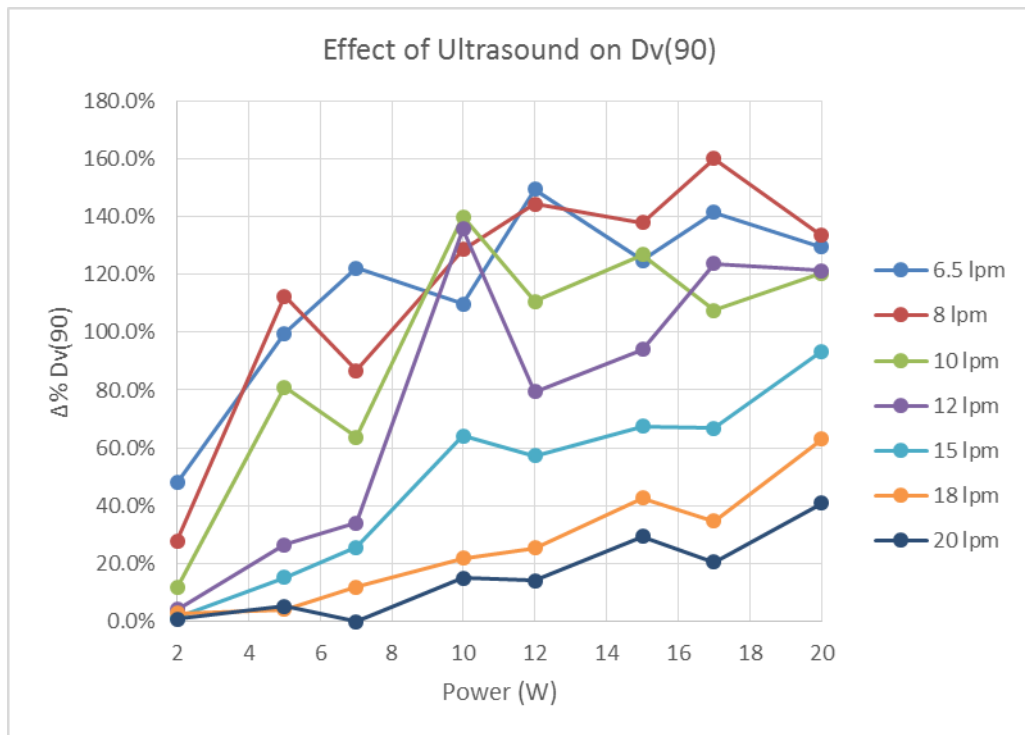
Figure 6-33: Percent change in $Dv90$ at conduit outlet as a result of the ultrasound field, for various air flow rates – vs ultrasound power level

In this section the results show that the ultrasound field has had a marked effect on the sizes of droplets in the distribution at the outlet of the conduit. The ultrasound field has caused the distribution to shift to larger droplet sizes and this effect is most prominent at lower air flow rates and higher ultrasound power levels. These changes are much greater than that indicated by the increased amount of water evaporated from the droplets as presented in the previous section (6.8.1). It is apparent that the ultrasound field is having other effects on the droplets apart from just enhancing their evaporation. The ultrasound field may be causing droplet coalescence and this is discussed more fully in Chapter 7.

6.9 Comparison with model results

As stated in section 6.6 the initial and boundary conditions for each ultrasound enhanced evaporation trial were also entered into the ultrasound enhanced droplet evaporation model (described in Chapter 4). Thus values for the amount of water evaporation, changes to the droplet size distribution, and changes to the size distribution parameters were determined from the model for comparison with the experimental results. A reasonable correlation between experimental and model results

would give confidence in the theoretical ultrasound enhanced evaporation model as a predictive tool.

Similar to the poly-disperse droplet evaporation model, the mass accommodation coefficient and the thermal accommodation coefficient, α_m and α_h respectively are also two of the inputs to the ultrasound enhanced evaporation model as detailed in Chapter 4. As for the poly-disperse model (see the introduction to section 6.5) values of 0.04 and 0.001 for mass and thermal accommodation coefficients have been used (for comparison purposes) in the ultrasound enhanced evaporation model.

6.9.1 Amount of water evaporated

In each of the poly-disperse droplet evaporation trials the inlet water flow, and inlet air specific humidity is relatively constant and this is the same for the ultrasound enhanced evaporation trials. Thus comparing just the specific humidity in the air outlet stream between the experimental and theoretical cases will give an indication of the accuracy of the theoretical model in terms of the amount of water evaporated. The percentage difference in outlet air specific humidity for the experimental cases and corresponding theoretical cases was determined from the raw results in Appendix 4 according to equation (6-4).

These values are presented in Figure 6-13 and Figure 6-14. It is immediately apparent that there are significant differences between the experimental amount of water evaporated and that being predicted by the theoretical model. The model is under-predicting the amount of water evaporated for the ultrasound enhanced evaporation trials. Error values range between 25% and 54%. It is possible that the ultrasound field, in practice, is having additional effects on the evaporating water droplets other than those included in the theoretical model. These effects are discussed in Chapter 7. It should also be noted that the results from the theoretical model are very similar, no matter what values of the accommodation coefficients (α_m and α_h) are used.

From Figure 6-34 the error between experimental results and theoretical model results in terms of water evaporation decreases with increasing air flow rate at a particular power level. Also, the error is least at the lower power levels.

From Figure 6-35 it can be seen that at a particular air flow rate the error between model and experiment increases slightly with increasing power level. Also, the error is least at the higher air flow rates. These results are discussed in detail in Chapter 7.
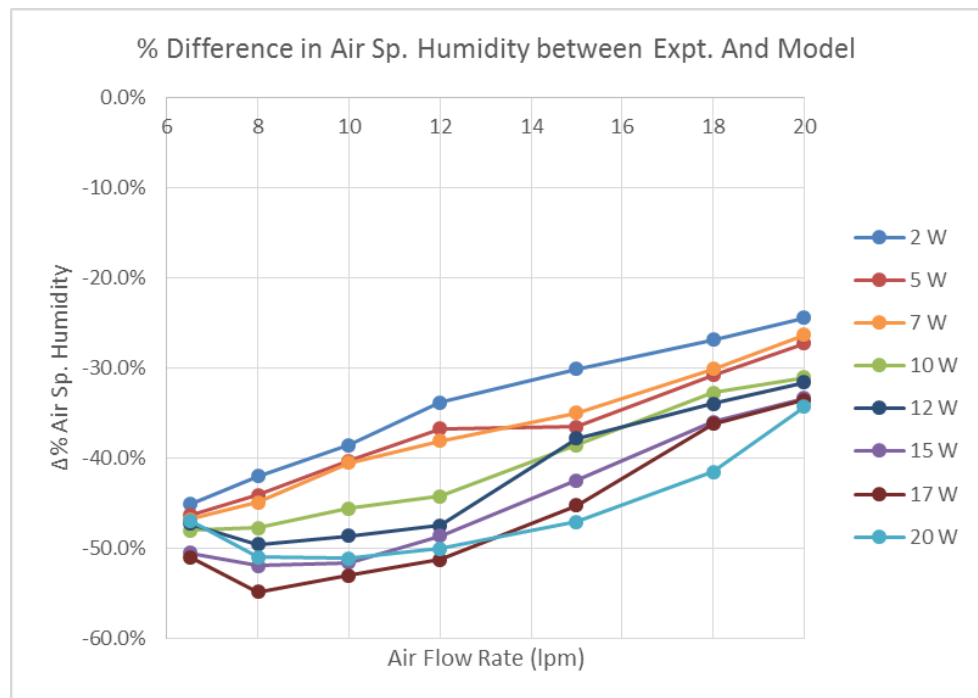
Figure 6-34: Amount of water evaporated: Comparison between experimental and theoretical results for various ultrasound power levels vs air flow rate
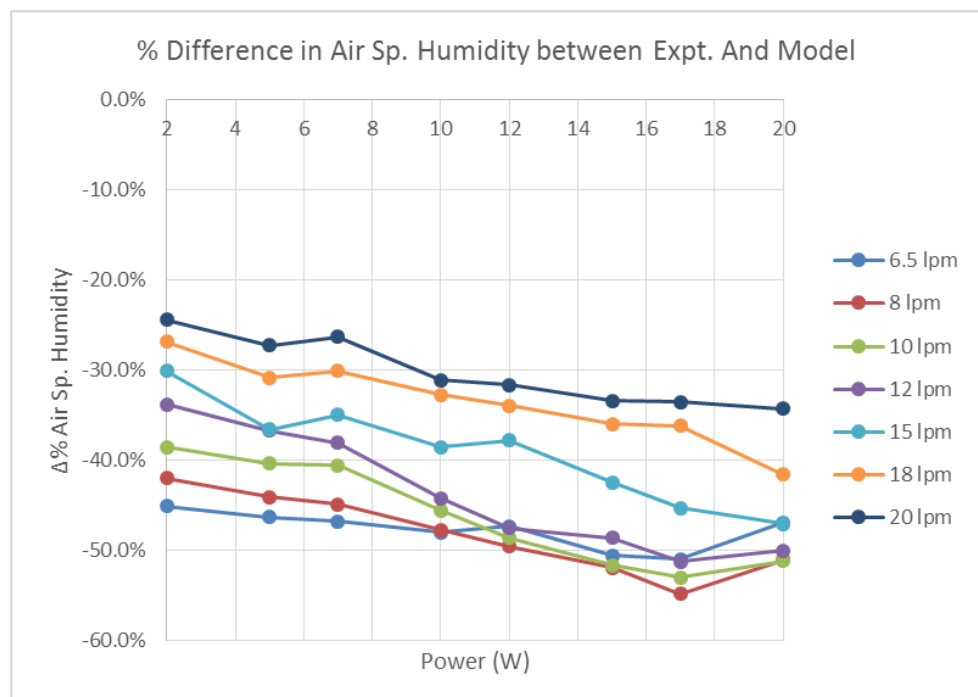
Figure 6-35: Amount of water evaporated: Comparison between experimental and theoretical results for various air flow rates vs ultrasound power level.

6.9.2 Droplet size distribution and parameters at outlet

By considering the droplet size distribution generated by the ultrasound enhanced theoretical model and comparing it to the experimentally measured droplet size distribution for each trial it is possible to see if the model is more or less accurate for predicting evaporative changes to the different droplet size ranges.

Consider Figure 6-36 and Figure 6-37. These are for the same trials as Figure 6-26 and Figure 6-27 respectively but now also show the theoretical droplet size distribution data, at the outlet of the conduit (in addition to the inlet and experimental outlet droplet size distributions). The orange lines represent the theoretical model output for accommodation coefficients of $\alpha_m = \alpha_h = 0.04$ and the light blue lines represent the theoretical model output for accommodation coefficients of $\alpha_m = \alpha_h = 0.001$. Comparing these two lines with the experimental droplet size distribution (purple lines) at the outlet of the conduit shows that:

- For low air flow rates the theoretical model using accommodation coefficients $\alpha_m = \alpha_h = 0.001$ or = 0.04 do not accurately represent the changes in droplet size distribution.
- At higher air flow rates the theoretical model becomes more accurate.

These observations can be examined in more detail by again considering the size distribution parameters: the $Dv10$, $Dv50$, and $Dv90$ for all trials. The values for these parameters were recorded for each trial in Appendix 4 and are used to determine a % Difference for that parameter between the experimental outlet and theoretical model outlet droplet size distributions.

Although there are some differences in the values of the theoretical parameters generated by the model depending on what value of the accommodation coefficient is used, the differences are small. In the following results the theoretical values for each parameter have been generated using accommodation coefficients of 0.001. The percentage difference in the $Dv10$ parameter, for example, is calculated using equation (6-5). These percentage differences, for each parameter, were then used to produce Figure 6-38 to Figure 6-43.
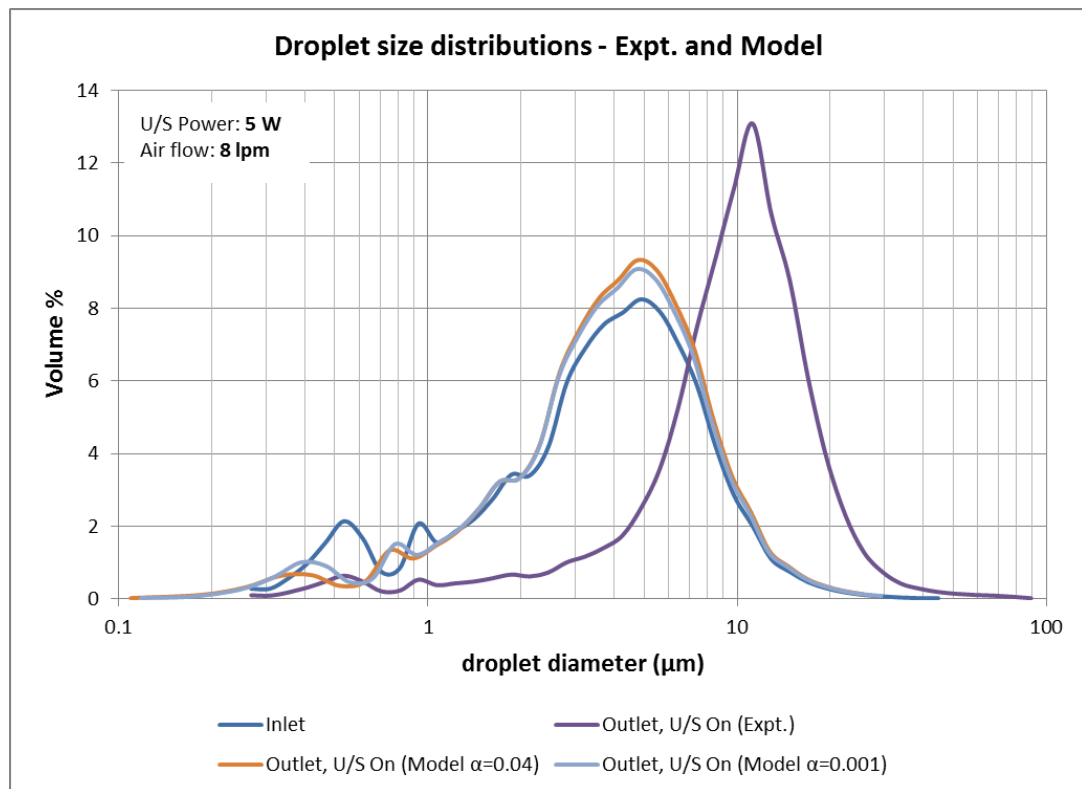
Figure 6-36: Comparison between experimental and theoretical (model) outlet droplet size distributions – typical case, low air flow rate
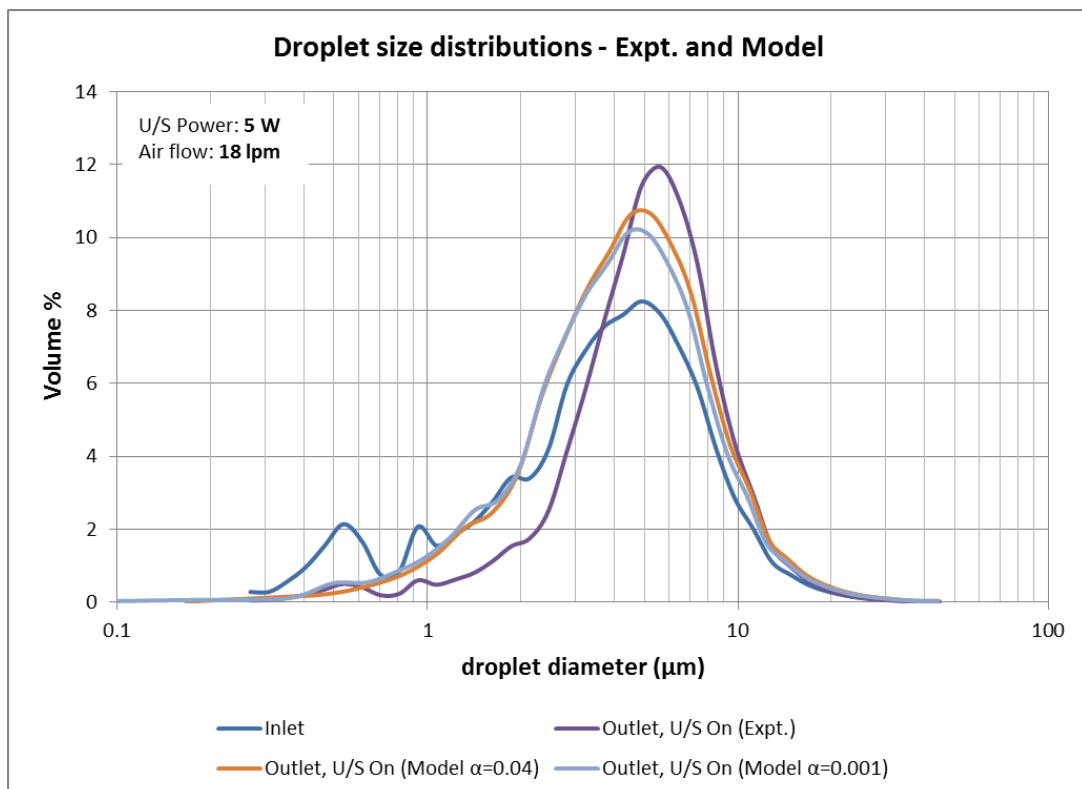
Figure 6-37: Comparison between experimental and theoretical (model) outlet droplet size distributions – typical case, high air flow rate

Figure 6-38 shows that for the smaller droplet sizes the difference between the experimental result and the theoretical result is quite large. Apart from some trials showing high variance in their results (for example, for the 7 and 15 W trials) the errors generally range between 0 and -85%.

This means that the model is under-predicting evaporation characteristics of the smaller droplets. Thus there are less of the smaller droplets in the experimental size distribution compared to that predicted by the model. The model is most accurate for high air flow rates and lower ultrasound power levels. The possible reasons for this are discussed in Chapter 7. For a given ultrasound power level the accuracy of the model tends to improve with increasing air flow rate. Also, model results at lower ultrasound power levels, for the smaller droplets, are more accurate.
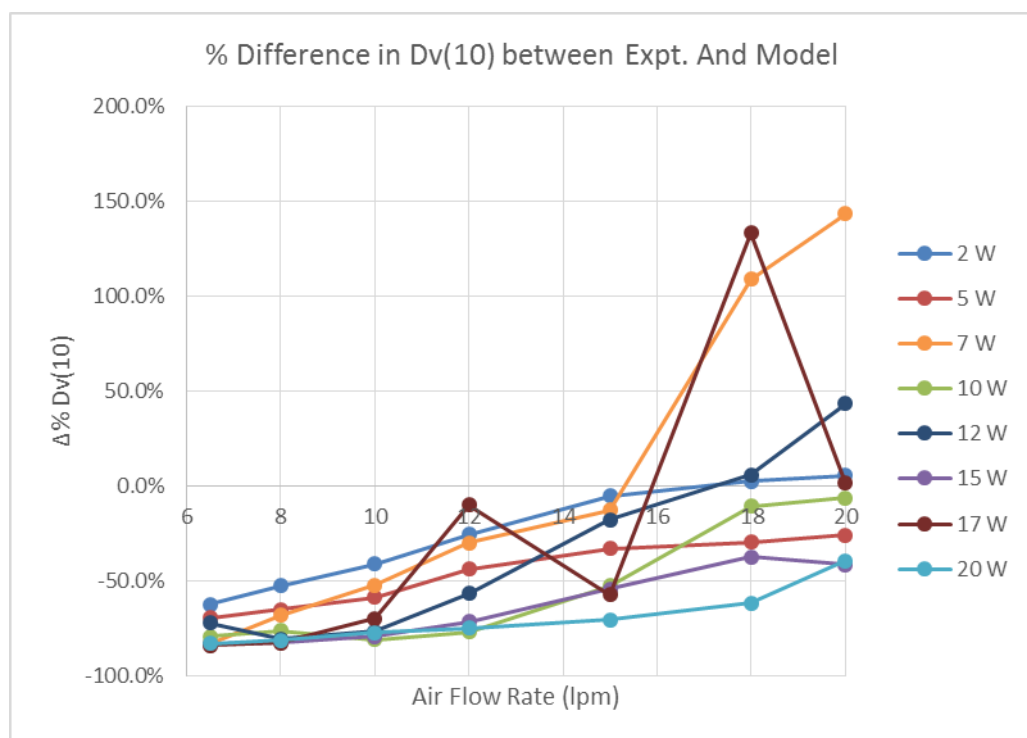
Figure 6-38: Comparison between experimental and theoretical outlet distributions - smaller droplet sizes ($Dv10$) for various ultrasound power levels vs air flow rate

Figure 6-39 shows results from some of the high air flow rate trials with a high variance. However, for a given air flow rate the accuracy of the model generally decreases with increasing power level for the smaller droplets.
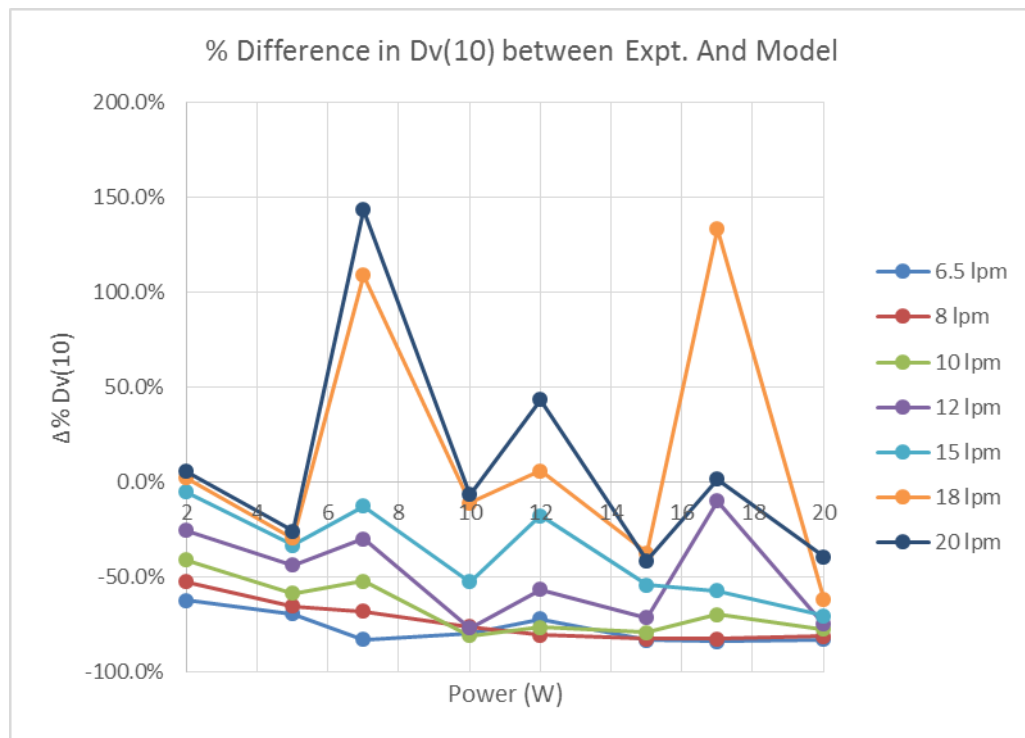
Figure 6-39: Comparison between experimental and theoretical outlet distributions - smaller droplet sizes ($Dv10$) for various air flow rates vs ultrasound power level

Figure 6-40 shows that in the case of the $Dv50$, which represents the middle of the droplet size distribution, the model is generally under-predicting its value in the droplet size distribution at the outlet of the conduit. The value of the $Dv50$ is affected by changes in the % volume of the smaller and larger droplet sizes combined. Since the value of the $Dv50$ in the experimental droplet size distribution is generally higher than that predicted by the model it shows that there is probably a lower percentage volume of the smaller droplets and a higher percentage volume of the larger droplets in the experimental trials. Comparing Figure 6-40 to Figure 6-38 shows that the accuracy of the model for the middle droplet sizes is a little better than for the smallest droplet sizes ($Dv10$). Differences between experiment and model results range between +3% and -66%. As for the smaller droplets, accuracy is best for high air flow rates and lower power levels, where differences are less than -20%. At a given ultrasound power level the accuracy of the model, for the middle droplet sizes, tends to improve with increasing air flow rate. Also, model results at lower ultrasound power levels are more accurate.

Figure 6-41 shows some high variance in results but generally for a given air flow rate the accuracy of the model, for middle droplet sizes, decreases with increasing power level. The model tends to be more accurate at the higher flow rates.

161
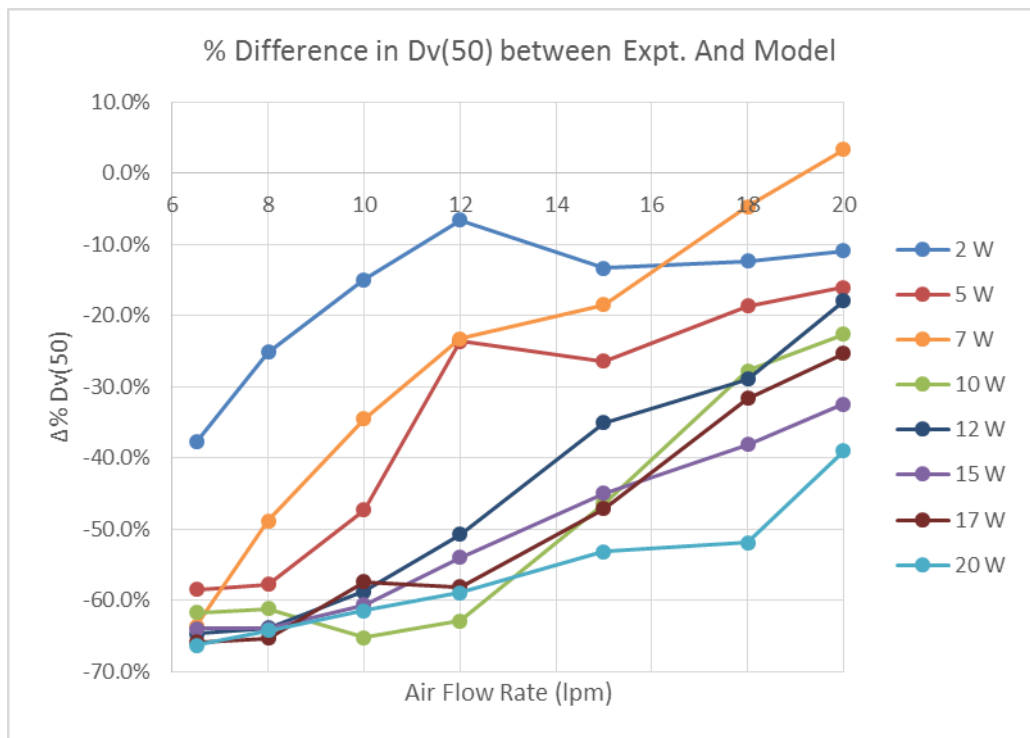
Figure 6-40: Comparison between experimental and theoretical outlet distributions - middle droplet sizes ($Dv50$) for various ultrasound power levels vs air flow rate
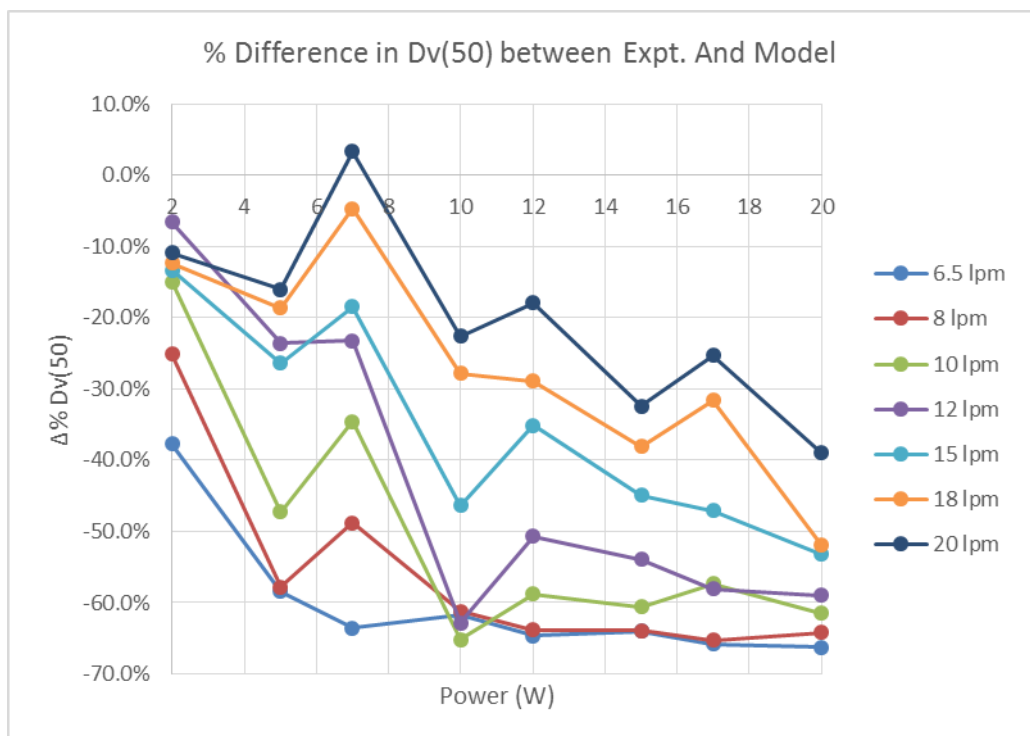
Figure 6-41: Comparison between experimental and theoretical outlet distributions - middle droplet sizes ($Dv50$) for various air flow rates vs ultrasound power level

For the larger droplet sizes Figure 6-42 shows that the model tends to under-predict the value of the $Dv90$. This is similar to the results for the $Dv10$ and for the $Dv50$. In the case of the $Dv90$, under prediction of its value means that is there is a greater volume percent of the larger droplets in the experimental droplet size distribution at the outlet of the conduit compared to what the model is predicting. Comparing Figure 6-42 with Figure 6-40 shows that the accuracy of the model for the larger droplet sizes is a little better again than for the middle sized droplets ($Dv50$). Differences between experiment and model results range between +9% and -57%. As for the smaller and middle sized droplets, accuracy is best for higher air flow rates and lower power levels, where differences are less than +/-10%. . At a given ultrasound power level the accuracy of the model, for the larger droplet sizes, tends to improve with increasing air flow rate. Also, model results at lower ultrasound power levels are more accurate.
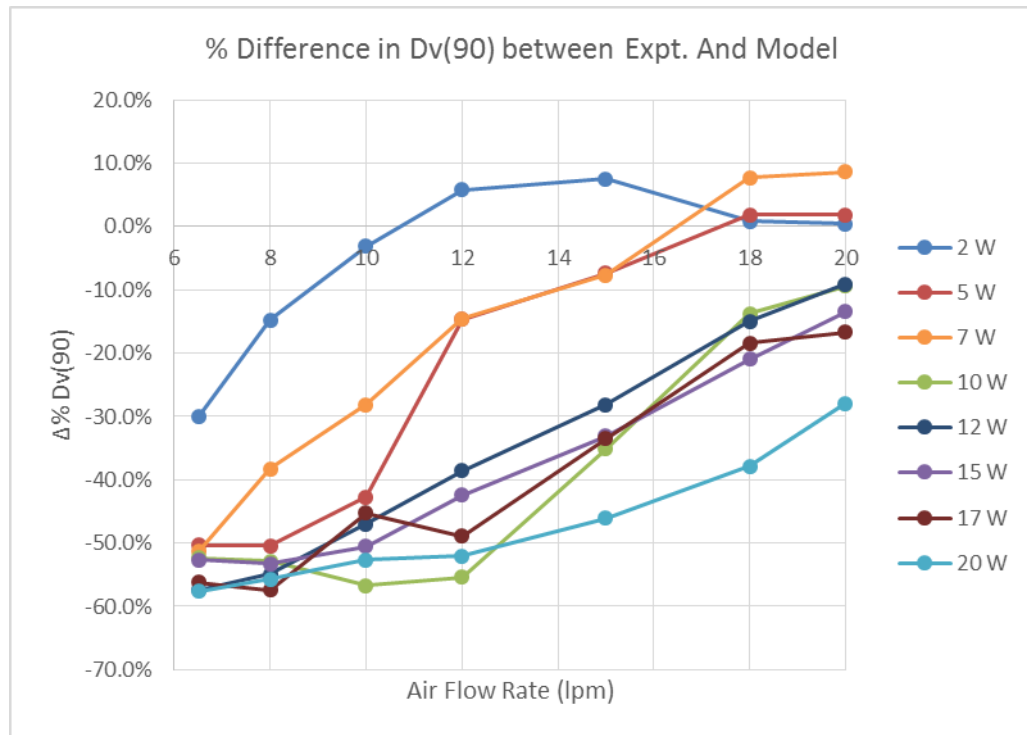
Figure 6-42: Comparison between experimental and theoretical outlet distributions - larger droplet sizes ($Dv90$) for various ultrasound power levels vs air flow rate

Figure 6-43 shows some high variance in results but generally for a given air flow rate the accuracy of the model, for middle droplet sizes, decreases with increasing power level. The model tends to be more accurate at the higher flow rates.

In this section the experimental results from the ultrasound enhanced evaporation trials have been compared with results from the theoretical ultrasound enhanced

evaporation model. The amount of water evaporated and changes to the droplet size distribution were considered. Generally there are large differences between the experimental results and the equivalent model results and this indicates that there are factors appearing in the experimental trials that may not be allowed for in the theoretical model. These factors are discussed in detail in the next Chapter.
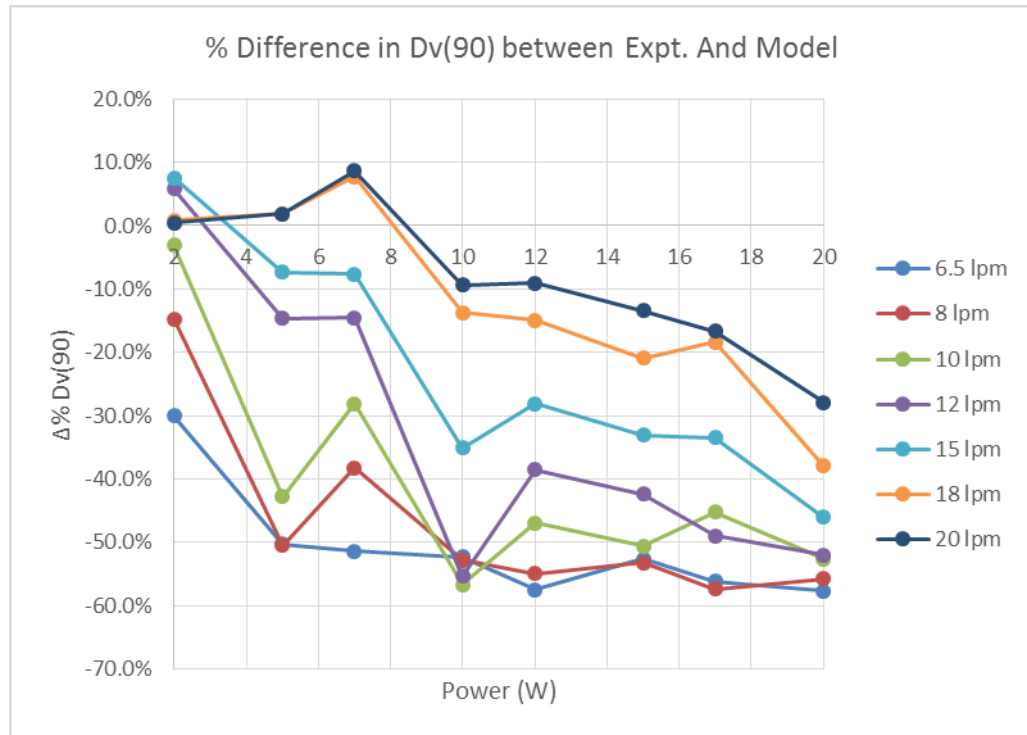
Figure 6-43: Comparison between experimental and theoretical outlet distributions - larger droplet sizes ($Dv90$) for various air flow rates vs ultrasound power level

6.10 Closure

This chapter presents the results of the experimental and theoretical investigation into the improvements in evaporation of water droplets into air flowing along a conduit as a result of an imposed ultrasound field. It shows that the imposed ultrasound field does in fact improve the evaporation characteristics of the droplets. It also shows that the mono-disperse and poly-disperse models generally are able to predict normal evaporation characteristics reasonably well. The ultrasound enhanced model is able to give reasonable predictions of evaporation performance in some circumstances. When the ultrasound power levels are high and air flow rates are low, other factors are influencing the evaporation process and so the model results differ significantly from experimental results in those situations.

Chapter 7 - Discussion and Conclusions

7.1 Introduction

This chapter discusses in detail the results from the experimental and theoretical investigation presented in Chapter 6. The section headings in this chapter generally match the section headings in Chapter 6. Thus, from this chapter, reference from the discussion can be easily made to the relevant results in Chapter 6.

Firstly results from the initial investigation of the mono-disperse droplet evaporation model are discussed. This part of the investigation shows that the results from the mono-disperse model compare very well with overall theoretical heat and mass balances as well as theoretical results from another model and experimental data reported in the literature.

Secondly results from the experimental and theoretical investigation of the evaporation of water droplets flowing along a conduit (no ultrasound field present) are discussed. This also shows reasonable a reasonable comparison between model and experiment.

Finally results from the experimental and theoretical investigation of ultrasound enhanced evaporation are discussed. Differences between model and experiment are shown to be due to additional effects not accounted for in the model.

A section is included outlining the significance, innovation and contribution of this work followed by a detailed conclusion and discussion of possibilities for future investigation.

7.2 Mono-disperse droplets – Model validation

The mono-disperse evaporation model was developed in the early stages of the research as a pre-cursor to the more complex but realistic poly-disperse evaporation model. The results presented in Chapter 6 show generally that the mono-disperse evaporation model accurately predicts the evaporation characteristics for theoretical mono-disperse droplet size distributions.

7.2.1 Comparison with theoretical overall mass and energy balances

Differences between the model and the theoretical overall mass and energy balances were very small (< 3% in all cases and < 1% for many cases). The larger errors occurred where the ratio of water droplets to air was close to the value required to just saturate

the incoming air. Although this was a comparison of a theoretical result with another theoretical result it did show that there were no anomalies or errors in the equations used in the model. It also showed that there were no errors in the implementation of those equations in MATLAB and thus it would serve as a good foundation for the implementation of the poly-disperse model.

7.2.2 Comparison with results from the literature

The mono-disperse model was also compared to results for final droplet size from an alternative model and experimental results reported in the literature [59]. When the correction factor, that was used by the authors in the literature model, was applied to the mono-disperse model in this work the results generated for final droplet size were almost identical to the literature model.

Experimental results from the same study for the final droplet sizes fell in between the two cases of isothermal and adiabatic boundary conditions generated by the mono-disperse droplet model for lower ratios of water droplets to air as shown in Figure 6-3. (The ratio of water to air is not shown in the results in Chapter 6 but can be seen in Table 2 of reference [59]). This is as expected as real experimental conditions will in fact most likely be somewhere between isothermal and adiabatic boundary conditions. However when the ratio of water to air is higher both cases of isothermal and adiabatic boundary conditions in the mono-disperse model predict smaller final droplet sizes than what was measured experimentally. It is possible that when the water droplet to air ratio is higher, then, in the experimental set up used by those researchers [59], the droplet/air mixture had not reached evaporative equilibrium prior to deposition on the stages of the impact sizing device used to measure the median droplet diameter. Since the mono-disperse model assumes evaporation has reached equilibrium, the results from the impact sizing device would therefore be larger than that predicted by the mono-disperse model for this data as seen in Figure 6-3.

An alternative conclusion can be drawn from the results shown in Figure 6-3, if it is assumed that all of the experimental results represent equilibrium droplet sizes. Then, it can be seen from the graph that the predicted results from the mono-disperse evaporation model with adiabatic boundary conditions correlate more closely with the experimental data than the results from the isothermal boundary condition case. This indicates that in fact the experimental boundary conditions may be closer to being

adiabatic rather than isothermal. Either way, there is not much time for heat transfer from the walls to occur since the transit time is so short.

Although the poly-disperse droplet evaporation model could be modified to allow for both isothermal and adiabatic boundary conditions, it was mainly used with adiabatic boundary conditions, as this was considered to be closer to real conditions.

7.3 Normal evaporation – poly-disperse droplets

One of the intentions of this part of the investigation was to provide a baseline of normal evaporation results that could be compared with ultrasound enhanced evaporation results. However the equipment ultimately procured to provide the ultrasound field was significantly different in dimensions to the conduit used in this poly-disperse droplet evaporation investigation. Thus the results gathered here could not be used in direct comparison with the ultrasound enhanced results reported in section 6.6 to 6.9. Nevertheless valuable insight was gained into the evaporation process as a consequence of this part of the investigation

7.4 Variables affecting normal water droplet evaporation

Insights were gained from the results in this section regarding the effect of air temperature, conduit length and air flow rate (really ratio of water droplets to air) on the evaporation of the water droplets.

7.4.1 Amount of water evaporated

It was found in the results (section 6.4) that increasing the inlet air temperature increased the amount of water evaporating from the droplets over the length of the conduit. This is expected because there are larger temperature differences between the air and water droplets to drive heat transfer and more energy available in the warmer air for droplet evaporation. Furthermore, for a given quantity of water vapour in the air, if the air is heated then the mass concentration of this water vapour decreases and thus the driving force for diffusion of water vapour (evaporation) will be greater at higher air temperatures.

Increasing the length of the conduit also increased the amount of water evaporated and this also is as expected since there is a longer time available for evaporation to take place.

Increasing the air flow rate has two implications for the evaporation of the water droplets. Firstly, since the water droplet flow rate is relatively constant for each trial, increasing the air flow rate decreases the ratio of water droplets to air in the conduit. It would be expected that for a lower ratio of water droplets to air that increased evaporation would take place. If the ratio of water droplets to air is high then the surrounding air quickly moves towards saturation which would slow down the evaporation process. In the case of lower water droplet to air ratios the difference in moisture content between the droplet surfaces and the bulk air would (that is, the driving force for water diffusion) would remain relatively large and the rate of evaporation would not slow down over the length of the conduit. Secondly, since air velocities are higher the residence time of the droplets and air over the length of the conduit decreases. This would have the effect of decreasing the amount of water evaporated. Therefore, as air velocities increase these two effects work against each other and tend to cancel each other out in terms of changing the amount of water evaporated.

It was observed from the results from this section (Figure 6-4) that in most trials the amount of water evaporated decreased with increasing air flow rate. This implies that the residence time effect is greater than the water/air ratio effect for these cases. However in the case of the higher air temperature the amount of water evaporated increased with increasing air flow rate. Increasing air temperature would not affect the residence time appreciably (a little due to density changes) but would probably have a greater effect on the evaporation rate when the ratio of water droplets to air was lower (that is, when air flow rates were higher). At lower water/air ratios the higher air temperature would remain higher for longer giving a greater driving force for evaporation.

In summary it can be said from these results that heating the air for droplet evaporation can improve the amount of water evaporated over a given length of conduit. Also, by adjusting the water/air ratio the rate of water evaporation can be optimized.

7.4.2 Changes to the droplet size distribution

Simplified droplet evaporation theory predicts that single droplets will evaporate according to the so called D^2 law [50, 51] as discussed in Chapter 2. That is, the time for a single droplet to evaporate is proportional to the square of its diameter. As a result

the smaller droplets will evaporate and reduce in size more quickly than the larger droplets.

Thus for a given droplet size distribution at the inlet of the conduit it would be expected that at the outlet it would generally change shape as shown in Figure 7-1. The right hand side of the outlet size distribution (larger droplets) does not change appreciably but there are less of the smaller droplets so that the distribution is compressed towards the right and so becomes taller and narrower. Considering the size distribution parameters as a result of these changes, all of the percentile size parameters ($Dv10$, $Dv50$, $Dv90$) and mean size parameters ($D[4,3]$, $D[3,2]$) would increase in value between the inlet and outlet size distributions. However the $Span$ of the distribution (refer to Table 2-1) would become smaller at the outlet (that is, its width is narrower at the outlet of the conduit). Generally speaking this behaviour is evident from the results for this section of the investigation and can be seen for a typical case in Figure 6-6. In the next sections the effect of air flow rate, air temperature and conduit length on the droplet size distribution at the outlet of the conduit will be discussed
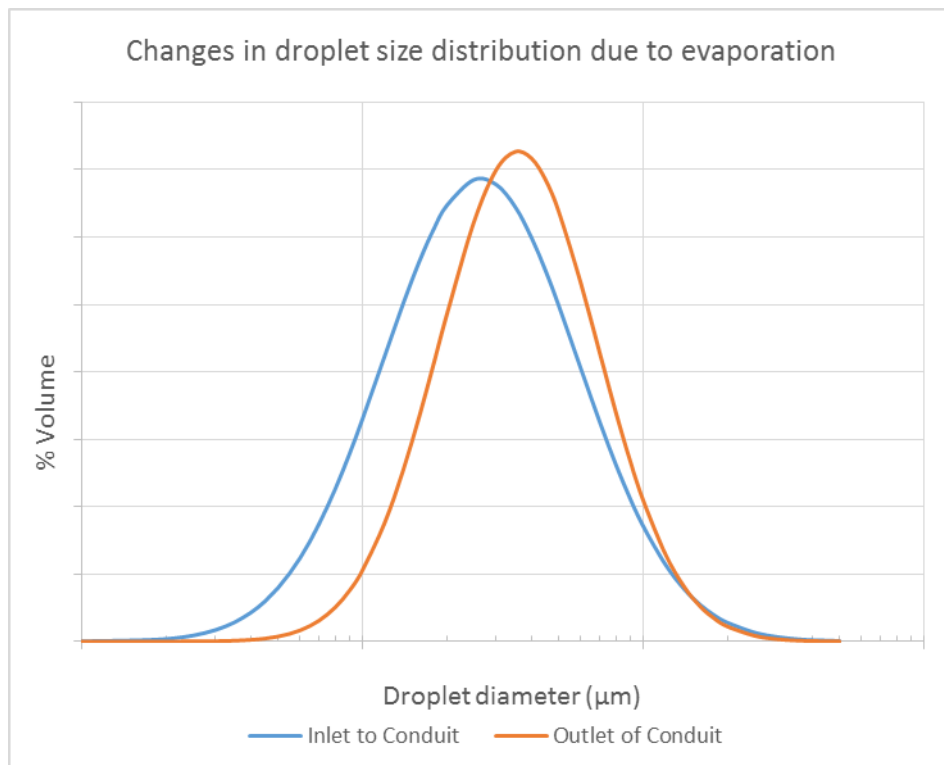
Figure 7-1: Expected changes to the droplet size distribution as a result of droplet evaporation along the conduit

From the experimental results reported in section 6.4.2 and Figure 6-7 it can be seen that apart from two results the change in $Dv10$ from inlet to outlet is positive indicating

that the volume % of smaller droplets is decreasing as expected. However the change in $Dv10$ increases with air flow rate. Although the change in water evaporation with air flow rate (Figure 6-4) is relatively small the change in the % volume of smaller droplets in the droplet distribution, with air flow rate, is much larger. At higher air flow rates an increase in minor air turbulence will possibly affect the smaller droplets to a greater degree (due to lower inertia) causing them to evaporate more quickly relative to the larger droplets. This would cause a decrease in their volume % relative to the larger droplets at the higher air flow rates.

At low air flow rates the change in $Dv50$ is negative (see Figure 6-9). Above an air flow rate of around 10 lpm, the change becomes positive (shift in median droplet size to larger values) as expected. Changes in the median droplet size ($Dv50$) tend to be more sensitive to the changes in the other parts of the distribution. A large negative shift in the volume % of the larger droplets, for example, will also impact the median droplet size (see following discussion on changes to the $Dv90$ parameter). Similarly to the smaller droplets, as the air flow rate increases above 10 lpm the median droplet sizes increase with increasing air flow rate. The slopes of the Δ% $Dv50$ vs air flow rate curves in Figure 6-7 are significantly less than the slopes of the Δ% $Dv10$ vs air flow rate curves so the same phenomenon (increasing minor turbulence with air flow rate) that is possibly affecting the smaller droplets could be affecting the whole distribution. However this effect on the larger droplets in the distribution will reduce in inverse proportion to droplet size.

When considering changes to the larger droplets in the distribution Figure 6-11 shows that for over half of the trials, the change in $Dv90$ is negative. This implies that there is a lower % volume of the larger droplets at the outlet of the conduit compared to the inlet. The effect is greatest at the lowest air flow rates. This is unexpected and indicates that the larger droplets are possibly being 'removed' from the distribution rather than just evaporating. The larger droplets will settle in the air stream more quickly than the smaller droplets and possibly settle out on the sides of the conduit. At lower air flow rates there is greater time to do this and so the effect is greater at these flow rates. Above an air flow rate of 15 lpm the change in $Dv90$ becomes positive (as would be expected) and increases with increasing air flow rate. The slopes of the Δ% $Dv90$ vs air flow rate curves in Figure 6-11 are less again than the slopes of the Δ% $Dv50$ vs air flow

rate curves in Figure 6-9. Therefore, the same phenomenon of minor turbulence affecting the evaporation of the other droplet sizes, mentioned earlier, is also possibly affecting the larger droplets but to a lesser degree, as would be expected.

Overall the effect of air flow rate on the droplet size distribution is generally to shift the distribution as shown in Figure 7-1 and in greater amounts as the air flow rate increases. Thus the width of the distribution would be expected to decrease with increasing air flow rate. Figure 7-2 shows a plot of the % change in $Span$ vs air flow rate for all trials. All results apart from two, at the higher air temperature, show that as the air flow rate increases the change in $Span$ becomes increasingly negative. This means that indeed the distribution does tend to become narrower as the air flow rate increases.
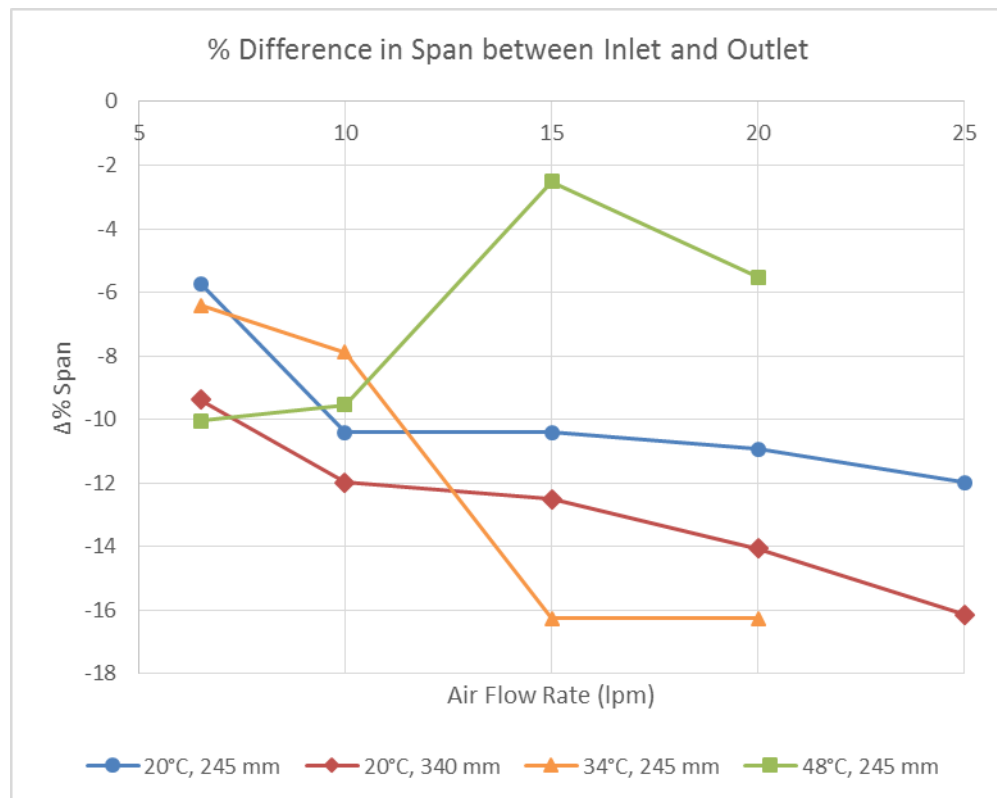
Figure 7-2: Changes to the width of the distribution vs air flow rate for all trials

The case where the span increases is for the higher air temperature (green curve) and, as noted in the previous section, the amount of water evaporation increases with air flow rate at this air temperature. It is not possible from the experimental results to determine water evaporation of the different parts of the droplet distribution, but it is possible that the increase in evaporation rate occurs in droplet sizes that cause the $Span$ to increase.

From the results there seems to be little correlation with air temperature and changes to the droplet size distribution. For the smaller droplet sizes ($Dv10$, Figure 6-7) this is especially so. For the middle and larger droplet sizes in the distribution (Figure 6-9 and Figure 6-11) there is more of a correlation. At higher flow rates the higher air temperature tends to cause a greater positive change in $Dv50$ and $Dv90$. This means that the middle and upper parts of the droplet size distribution are moving more to larger droplet sizes as the air temperature increases. It was noted previously that the higher air temperature increases the amount of evaporation and it would appear that this effect occurs mainly for the middle and larger sized droplets.

It was noted in the results that for the smaller droplets an increase in conduit length caused a decrease in the volume % of those droplets. This effect was not so apparent for the middle of the distribution and for the larger droplets their volume % actually decreased in some trials. Since greater evaporation occurs over longer conduit lengths (as discussed in the previous section) it is expected that there will be a decrease in all sizes of droplets at greater conduit lengths. This is the case for smaller and middle sized droplets but not so for the larger droplets. As discussed earlier, it is apparent that the larger droplets are being removed from the distribution, possibly settling out onto the conduit walls due to their greater mass and greater terminal velocities. This effect would be accentuated as the conduit length increases and so there are less of the larger droplets in the distribution for the longer conduit trials.

Thus generally the longer the conduit the more pronounced the changes to the droplet distribution illustrated in Figure 7-1 will be i.e., becoming taller and narrower. Additionally the removal of the larger droplets due to possible settling onto the conduit walls will remove the largest droplets from the right hand tail of the distribution.

7.5 Comparison with model results

The initial and boundary conditions for each experimental trial were entered into the poly-disperse droplet evaporation model. Thus values for the amount of water evaporation, the droplet size distribution and the size distribution parameters were determined from the model for comparison with the experimental results. In this section the accuracy of the model with regards to these values are discussed in detail.

7.5.1 Amount of water evaporated

In regards to the amount of water evaporated it is apparent from Figure 6-13 and Figure 6-14 the model is more accurate for higher air flow rates, higher air temperatures and shorter conduit lengths. Under these conditions the assumptions of the model (described in Chapter 4) are apparently more applicable. In half of the trials the errors are less than 5.5% which indicates the model is reasonably accurate in predicting the amount of water evaporated under those conditions.

At low air flow rates the water droplet to air ratio increases and so interactions between droplets and between droplets and conduit wall are more likely. Also it is less likely that the droplets will be uniformly distributed throughout the air in the conduit as the water droplet to air ratio increases. These effects will cause greater differences between the model results and experimental results at low air flow rates.

At higher air temperatures the evaporation process causes the air to cool so that the bulk air temperature in the conduit is probably closer to ambient conditions and the adiabatic boundary conditions assumed in the model are more closely achieved.

At longer conduit lengths any errors in the model are accentuated due to the longer time period over which they are occurring.

Generally speaking the errors between the experimental results and the model results are negative which indicates that the model is under predicting the amount of water evaporated. It was found that using mass and thermal accommodation coefficients of 0.04 were more accurate in regards to the amount of water evaporated but values of 0.001 gave a more accurate result regarding changes to the droplet distribution. The accommodation coefficients are a measure of the efficiency of the interaction of the gas molecules and the liquid surface during evaporation or condensation. They have a direct effect on the rate at which the evaporation process proceeds. Therefore, larger values of the accommodation coefficients may well give better results in terms of amount of water evaporated over the length of the conduit, but smaller values give a better overall result for changes to the droplet size distribution.

7.5.2 Droplet size distribution and parameters at outlet

Comparing a typical example of an experimental size distribution curve at the outlet of the conduit with curves generated by the model (see Figure 6-15 for example) it appears

that the model is giving best results for very low values of the accommodation coefficients (that is, values around 0.001). It is not clear why this is the case but the effect of the accommodation coefficients on the non-continuum correction factors (see Chapter 4) is dependent on droplet size. Thus the lower accommodation coefficients more accurately predict changes to the overall size distribution but are not so accurate for the total amount of water evaporated.

The model tends to be less accurate for the very small droplet sizes: the model predicts that these much smaller sizes will change in size and completely evaporate more quickly than what is happening in reality. The reasons for this could be that the smaller droplets, once injected into the air stream do not disperse particularly well but rather remain stratified in the air stream. Consequently the local air conditions around the smaller droplets become saturated (the rest of the air in the plug is still not yet saturated) and this hinders further evaporation of the smallest droplets.

For the smaller droplets, from Figure 6-16, there appears to be little correlation between model accuracy and air flow rate or air temperature. Perhaps a little more accurate at the lower temperatures. From Figure 6-17 the model is slightly more accurate for the longer conduit length. It is possible that the correction factors used that apply when the droplets become very small are not particularly accurate. Although the ones used as described in Chapter 4 are used by a number of other researchers there are other formulations that may be more accurate. For the middle of the droplet size distribution the accuracy of the model is improved significantly. From Figure 6-18 accuracy is best around the middle of the flow rate range and at higher air temperatures. At the larger droplet sizes (Figure 6-20 and Figure 6-21) the accuracy again falls away and this probably due to the larger droplets settling out in the experimental apparatus as described in the previous section.

7.5.3 Remarks

In this section, and the previous two sections, the results for the investigation of the normal evaporation of water droplets into air flowing along a conduit have been discussed. Experimentally it was found for a fixed flow rate of water droplets that increasing the conduit length and increasing the air temperature improved the quantity of water evaporated into the air stream. It was also found that the water droplet size distribution changed during evaporation. The smaller droplets evaporate and reduce in

size more quickly than the larger droplets so that the size distribution shifts towards the larger droplets (as shown in Figure 7-1). Changes to the droplet size distribution can be minimised by decreasing the air flow rate (or maintaining a high water droplet to air ratio) and keeping the air temperature at ambient or cooler.

These findings have implications for medical respiratory equipment design. For humidifying air and ensuring no droplets are carried over to the patient then the air should be preheated and conduit length should be as long as practically possible. For drug delivery via aerosol then the air should be as cool as possible, conduit lengths kept as short as possible and air supplied at ambient or cooler. Obviously using saturated air would also help. In this way minimal evaporation will occur and changes to the droplet size distribution will also be minimal.

The poly-disperse droplet evaporation model is a reasonably accurate simulation of the actual evaporation process. Comparison between inlet and outlet distributions and model results with experimental results showed that the model is over predicting the evaporation of the smaller droplets and experimentally the very largest droplets are possibly settling out in the conduit. This also has implications for medical respiratory equipment design. Increasing air flow rates and reducing conduit lengths will minimise the settling out of the largest droplets.

7.6 Ultrasound enhanced evaporation

The aim of this part of the investigation was to provide insight into the ultrasound enhanced evaporation process, to quantify the improvement in droplet evaporation as a result of the imposed ultrasound field and to investigate the validity of the theoretical model. In previous sections the theoretical and experimental results of normal evaporation of water from droplets as they flow in air along a conduit have been discussed. In the following three sections the results from the experimental and theoretical investigation of ultrasound enhanced evaporation are discussed.

In the next section, the comparison of experimental results reported in the literature for improvements in water evaporation due to an imposed ultrasound field with those generated from the theoretical model are discussed.

In section 7.8, the comparison of experimental results from the ultrasound enhanced evaporation process with corresponding experimental results for the normal

evaporation process are discussed. The effect of air flow rate and ultrasound power level on the amount of water evaporated and the droplet size distribution are discussed.

And finally in section 7.9 comparison of results from the theoretical ultrasound evaporation model with corresponding experimental results are discussed.

7.7 Comparison with the literature

As detailed in section 6.7 very few situations are reported in the literature similar to what is being investigated in this work, namely application of ultrasound to water droplets evaporating into air as they flow along a conduit. However experimental data was available for the drying of various small vegetable pieces in a power ultrasound environment, similar to the physical situation modelled in this work.

In section 6.7 it was explained that the effect of the ultrasound field on the evaporation of water from the surface of the small vegetable pieces was considered to be similar to the effect of the ultrasound field on the evaporation of water from the droplet surfaces being studied in this work.

An improvement factor was calculated for the different vegetable pieces which indicated the increase in water evaporation as a result of the application of the ultrasound field. For the maximum ultrasound power supplied to their apparatus the improvement factors varied from 1.2 to 3.5 depending on the vegetable type. On average the improvement factor was around 1.5. That is, the application of the ultrasound field improved the water evaporation rate from the vegetable pieces by about 50% on average.

Although not directly comparable, results were generated from the ultrasound enhanced evaporation model for a range of flow rates and conditions comparable with those stated in the literature. The improvement factors for time to equilibrium (average of around 1.2 or 20% improvement) compare reasonably well with the literature improvement factors. The main conclusion from this comparison is that the presence of an ultrasound field does improve the evaporation of water in both cases and by roughly similar amounts. Areas of similarity between the literature study and our study are:

- That the nature of the ultrasound field is similar in both cases – being a standing wave generated in a cylindrical transducer.

- That the ultrasound field is affecting the diffusion processes of the water from the solid or liquid surface to the air in a similar manner.

The main points of difference being:

- The size of the surface from which water is evaporating.
- The interaction of the ultrasound field with the structure beneath the surface in the case of the literature study

In regards to the latter difference, for a porous and flexible solid the ultrasound field can cause an increase in the water diffusion rate through the solid as a result of the alternate compressions and stretching of the solid structure. This does not occur in the case of a water droplet.

In regards to the former difference it has been pointed out by a number of researchers [110, 111, 115, 154] and discussed in Chapter 2 that the size of the object evaporating relative to the displacement amplitude of the ultrasound field does have an effect on the evaporation characteristics. In the case of a relatively large object (e.g., vegetable piece) and small displacement amplitude the ultrasound causes streaming flows around the object which enhance evaporation. In the case of a small object (water droplet) and relatively larger displacement amplitude the effect of the ultrasound is similar to quasi-steady flow convection which also enhances the evaporation process. Thus the convective flows around the droplets are inherently different from the convective flows around the vegetable pieces but nonetheless both flows will enhance the water evaporation rate.

Thus, although there are differences between our study and the literature study the ultrasound enhanced theoretical model developed in our study is giving a favourable indication of the enhancement of the water evaporation from the water droplets, when compared to the literature study results.

7.8 Variables affecting improvement in ultrasound enhanced evaporation

In this section results are discussed for the effect of an ultrasound field imposed on the water droplets evaporating in air as they flow along a conduit. Discussion focusses on the effect of air flow rate and ultrasound power level on the amount of water evaporated and on changes to the droplet size distribution over the length of the

conduit. As mentioned previously, it was not possible to use the normal evaporation results reported in Chapter 6, section 6.4 as a baseline for comparison with these results since the dimensions of the conduit used in this part of the investigation were so different. Instead normal evaporation results were generated for each trial prior to switching on the ultrasound field. Thus a direct comparison could be made between normal and ultrasound enhanced evaporation results.

7.8.1 Amount of water evaporated

It is apparent from Figure 6-24 and Figure 6-25 that the effect of an imposed ultrasound field is to improve the amount of water evaporated from the droplets for all air flow rates and ultrasound power levels. At a given air flow rate, increasing the displacement amplitude of the imposed ultrasound field (that is, increasing the ultrasound input power level) increases the amount of water evaporated. Under normal evaporation conditions the mass and heat transfer processes for the evaporating droplets are expected to be conductive in nature, as discussed in Chapter 2. The effect of the ultrasound field is to generate localised air movement and pressure variations that will cause the mass and heat transfer processes to become convective in nature. It would be expected that as the amplitude of the air movements and pressure variations increased that the convection processes would be enhanced and thus the rate of evaporation would also increase.

In the experimental trials the specific humidity or water content of the air is determined from a measurement of the air temperature and the relative humidity of the air. Figure 6-24 and Figure 6-25 in Chapter 6 show the difference in specific humidity in the air at the outlet of the conduit as a result of the imposed ultrasound field. In comparison, Figure 7-3 and Figure 7-4 show the difference in air temperature at the outlet of the conduit and are very similar to the difference in air specific humidity graphs.

This indicates that the effect of the ultrasound is not only enhancing the mass and heat transfer processes during evaporation it is also imparting energy into the air and droplet mixture causing the air temperature to increase. This increases the moisture content capacity of the air and is a factor in the increase in the amount of water evaporated as a result of the imposed ultrasound field.

It was noted that for the lower ultrasound power levels (< 10 W) an increase in air flow rate reduces the improvement in evaporation. This negative effect of the air flow rate

was also noted in similar research [147]. It is thought that the increased air flow rate disrupts the ultrasound field and reduces its effect on the convective heat and mass transfer processes.
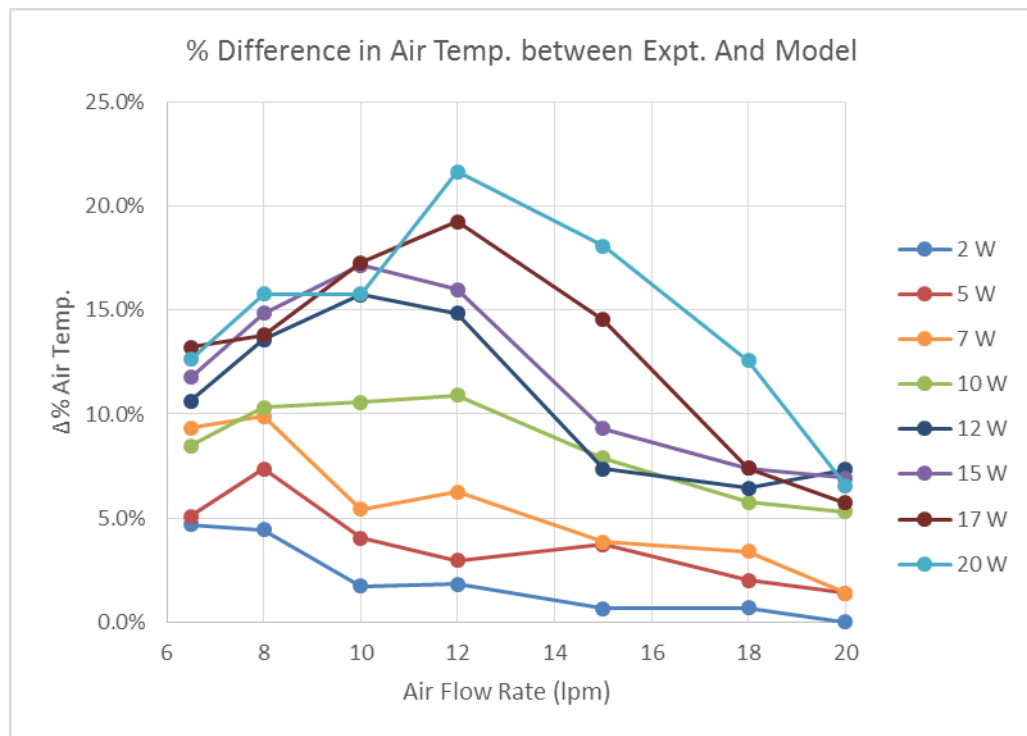
Figure 7-3: Percent change in Air Temperature at conduit outlet as a result of the ultrasound field, at various power levels – vs air flow rate.
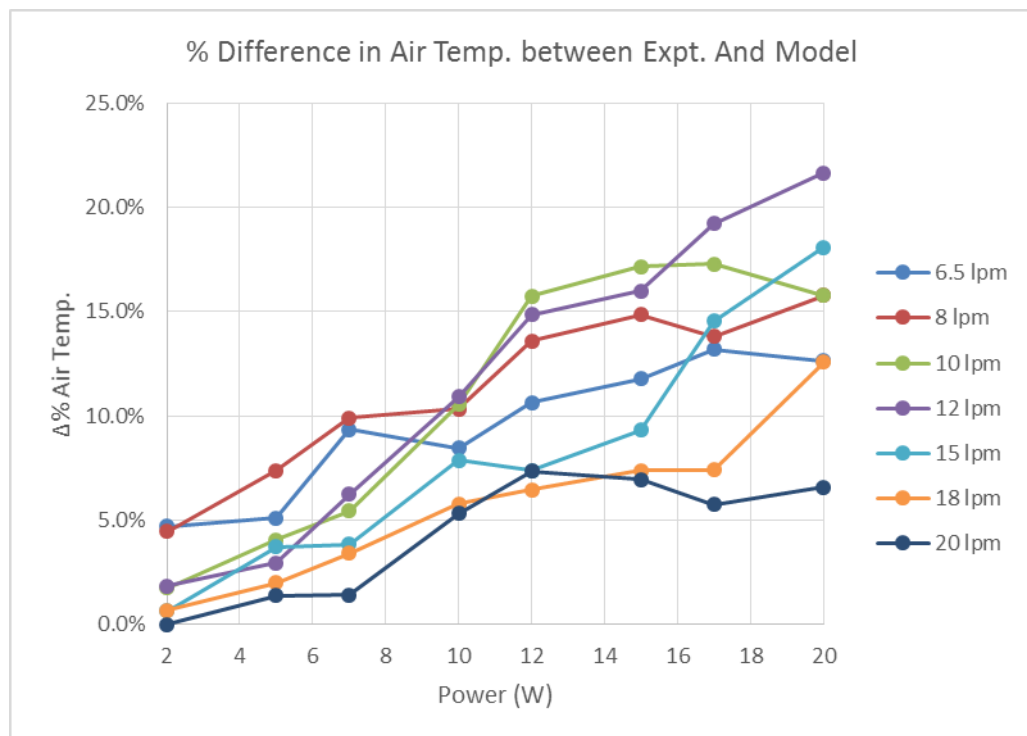
Figure 7-4: Percent change in Air Temperature at conduit outlet as a result of the ultrasound field, at various air flow rates – vs ultrasound power level.

179

For the higher power levels (>10 W) the improvement in evaporation peaks at an air flow rate of around 10 to 12 lpm. Therefore, at the higher power levels, when the air flow rate is low, the ultrasound field is not disturbed appreciably, so that increasing the air flow rate actually improves the overall convection effects and improves the rate of water evaporation. At 10 – 12 lpm this combined effect reaches a maximum. At even higher air flow rates the ultrasound field begins to be adversely affected by the air velocity and the improvement in evaporation decreases as is seen at the lower power levels.

It was also noted in the results (Table 6-7) that under lower air flow and higher ultrasound power conditions that visible droplets of water were present on the walls of the conduit at the end of the trial. It is possible that at the higher power levels the amplitude of excitation of the air molecules was such that it caused the smaller droplets travelling close to the walls of the conduit to be impacted against the walls. On impact they would attach to the wall and after many such events the droplets would coalesce and become visible. If the air flow rates were high enough (greater than the critical value) then the air velocities reduced the effect of the ultrasound field and droplet hold up on the walls was prevented.

It was also noted in the results that at high ultrasound power levels (>25 W) and high air flow rates that there was no liquid water hold up in the conduit (sonotrode) and no visible sign of droplets in the conduit outlet. Thus the water droplets were completely evaporated. The experiments carried out were done so at lower power levels so that the size distribution of the droplets in the conduit outlet could be measured and changes observed. However it is clear that at higher power levels it is possible to accelerate the droplet evaporation process so that it compete evaporation occurs over relatively short distances.

7.8.2 Changes to the droplet size distribution

It was expected that the changes to the droplet size distribution, between inlet and outlet of the conduit, as a result of the imposed ultrasound field would be an enhancement of the changes resulting from normal evaporation. These latter changes have been discussed in section 6.4.2 above.

At the higher air flow rates, where the effect of the ultrasound is somewhat reduced, this is indeed the case as can be seen in Figure 6-27. The blue curve represents the

droplet size distribution at the inlet of the conduit and the red curve represents the droplet size distribution at the outlet of the conduit under normal evaporation conditions. The changes to the outlet size distribution are in line with those changes discussed in section 6.4.2. The smaller droplets are evaporating and reducing in size more quickly than the larger droplets so that the distribution curve at the outlet is compressed to the right and becomes taller and narrower. The effect of the ultrasound should be to enhance this so that the purple curve, representing the droplet size distribution at the outlet with the ultrasound field turned on, should compress further to the right and become even taller and narrower than the normal outlet curve, which is indeed the case. The improvement in water evaporation for this case is relatively low at 2.2%.

However at low air flow rates, where the effect of the ultrasound field is greater the effect on the droplet size distribution is more dramatic as can be seen in Figure 6-26. In this case the outlet droplet size distribution has moved significantly towards the larger droplet sizes. The improvement in evaporation in this case is much better at 9.0%. The movement in the shape and position of the outlet droplet size distribution with the ultrasound field applied, at low air flow rates, is far greater than would be expected as a result of an improvement in the evaporation processes alone. The size distribution at the outlet indicates that indeed there is a lower volume % of the smaller droplets, as expected but also there is a greater volume % of the larger droplets. This seems to indicate that as well as the enhanced evaporation processes the ultrasound field is also causing the droplets to collide with one another and coalesce together to form larger droplets. It was noted in Chapter 2 that the ultrasound field will cause some movement in the droplets relative to the surrounding air. Less for the larger (greater inertia) droplets and more for the smaller droplets. It was shown there that the dynamic response of a 5 μm diameter water droplet, subjected to an ultrasound field of 22 kHz and SPL of 150 dB would experience a response of 9.5% where the air particle movement has an amplitude of 15.7 μm. For smaller droplets, say 1 μm the response is 92%. Thus, it is possible that the smaller droplets, moving with the air particle oscillations, collide with one another and collide with larger more stationary droplets. This causes coalescence and the creation of even larger droplets in the distribution.

Additionally, it was noted in the previous section and in the results that water droplets were present on the walls of the apparatus under high power and low air flow conditions. As just described, it is more likely that the smaller droplets would be moved by the imposed ultrasound field and those droplets nearest the conduit walls would impact and attach to the walls. This would accentuate the removal of the smaller droplets from the distribution and add to the movement of the size distribution to larger droplet sizes as noted earlier in this section.

When the specific droplet sizes in the distribution are considered, these observations are confirmed. Considering the effect of the ultrasound field on the $Dv10$, (Figure 6-28) representing the smaller droplets in the distribution, the change in this value for low flow rates and high ultrasound power levels is over 300% for some trials! This means that there is a much lower volume % of the smaller droplets in the outlet distribution as a result of the ultrasound field. Also, as the air flow rate increases this change in the volume % of the smaller droplets decreases. As mentioned in the previous section the increased air flow rate is believed to disrupt the ultrasound field and thus its effect on the droplet size distribution is reduced.

And, similarly for the amount of water evaporated, an increase in ultrasound power level at a given air flow rate tends to increase the effect on the smaller droplets in the distribution. That is, the $Dv10$ increases as shown in Figure 6-29 which implies that the volume % of the smaller droplets in the outlet distribution decreases with increasing ultrasound power level.

These same trends can be seen for the middle sized and large sized droplets (Figure 6-30 to Figure 6-33). For the $Dv50$ the increase due to the ultrasound field ranges from 1% to 180%. Thus the change on the middle sized droplets is not as dramatic as for the smaller droplets. However for the $Dv90$ it would be expected that the percent change would decrease further but the change is almost at the same level as for the $Dv50$. Thus the coalescing effect of the ultrasound field is generating a significant increase in the volume % of the larger droplets as well.

The ultrasound field causes a significant change to the droplet size distribution. Some of this change is due to increased evaporation of water but other effects, such as coalescence of the water droplets and impact of the water droplets on the walls of the conduit must also be occurring. These changes increase with increasing ultrasound

power level but are attenuated by increasing air flow rate which disrupts the ultrasound field.

It is clear that the ultrasound field improves the evaporation of water from the droplets as they flow in air along the conduit, however the ultrasound field also has a significant and potentially unwanted effects on the droplet size distribution. This being the coalescence of smaller droplets into larger droplets

7.9 Comparison with model results

The initial and boundary conditions for each ultrasound enhanced experimental trial were entered into the ultrasound enhanced droplet evaporation model. Thus values for the amount of water evaporation, changes to the droplet size distribution, and changes to the distribution parameters were determined from the model for comparison with the experimental results. It is apparent, however, from the discussion of the experimental results in the previous section that other effects are occurring as a result of the imposed ultrasound field that have not been allowed for in the theoretical model. It is expected then that there will be significant differences between model and experimental results especially in regards to changes in the droplet size distribution. These differences and the specific reasons for them are discussed in the next two sections.

7.9.1 Amount of water evaporated

As noted in the results and shown in Figure 6-34 and Figure 6-35 there is a significant difference between the experimental amount of water evaporated and that being predicted by the theoretical model. The model is under-predicting the amount of water evaporated for the ultrasound enhanced evaporation trials by between 25% and 45%. As discussed in the previous section regarding the experimental improvement in water evaporation, it is observed that the temperature of the air at the outlet of the conduit increases. It is apparent then that the ultrasound field is doing more than just enhancing the mass and heat transfer processes during evaporation. It is also imparting energy into the air and droplet mixture which in turn is enhancing the evaporation of water from the droplets. There is no allowance for additional energy input into the air and water droplets in the model and this could account for the negative discrepancy in results between model and experiment.

Also, the model assumes that plug flow occurs in the conduit. With the ultrasound apparatus and set up used for these trials this was probably not the case. The ultrasound apparatus that was available and used for the trials in this section is described in Chapter 5. The conduit (sonotrode) used in the ultrasound trials had a much larger diameter compared to the conduit used in earlier (normal evaporation) trials. The droplet generation device had a relatively small diameter and it was necessary to inject the droplets into the air stream as close to the inlet to the conduit as possible. Thus the set up described in Chapter 5 was used. However, during use, flow patterns as depicted in Figure 7-5 were observed through the transparent transition pieces.
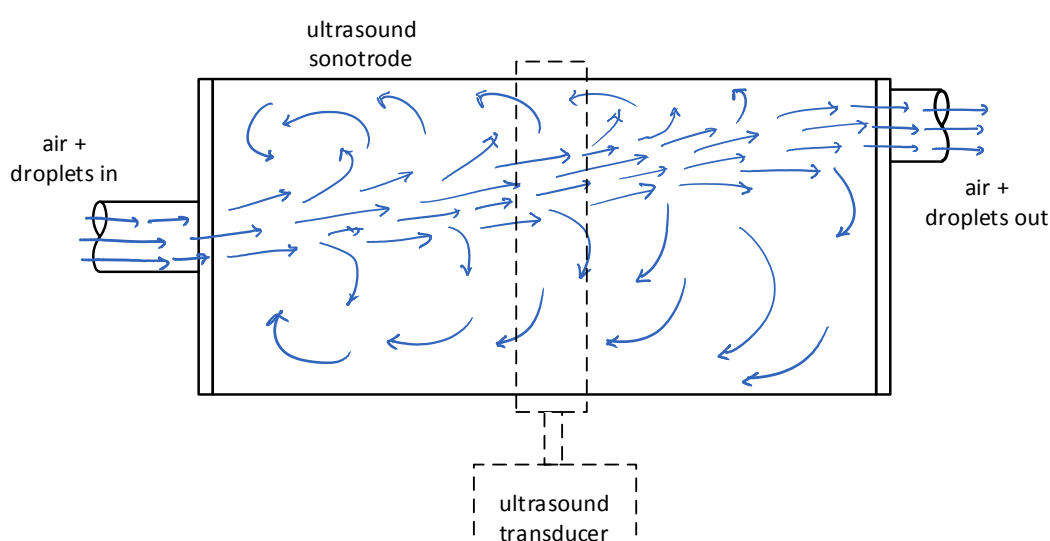
Figure 7-5: Flow patterns observed inside conduit (ultrasound sonotrode)

The air flow thought the droplet generator and into the conduit causes a central flow channel of air and droplets to form inside the conduit with some flow recirculation occurring at the outer extremities of the conduit. This obviously is far from the ideal plug flow assumed in the theoretical model. Attempts were made to recalculate the model results based on a smaller 'pseudo-diameter'. However, the results for the model based on the smaller pseudo diameter were not that much different from the results based on the full diameter of the conduit. Furthermore, this difference between model and experiment would tend to suggest that the plug flow theoretical model would give greater amounts of water evaporated compared to the experimental data (where the bulk of the flow is channelling through the device more quickly than expected). But in fact the model is understating the amount of water evaporated. The effect of added energy into the air and water droplets is apparently much greater than the non-plug flow recirculating air currents effect.

It was noted in the results (Figure 6-34 and Figure 6-35) that the discrepancy between model and experimental results for the amount of water evaporated tended to decrease with air flow rate (at a given power level) and increase with power level (at a given air flow rate). Increasing air flow rate tends to decrease the effectiveness of the ultrasound field as has been discussed already. Therefore, this would tend to decrease the energy input into the evaporation process and thus the difference between model and experimental results would decrease. However as the power level of the ultrasound field increase then it is expected that the energy input into the evaporation process would increase and thus cause a greater discrepancy between model and experimental results.

7.9.2 Droplet size distribution and parameters at outlet

It was noted in Chapter 6 that the differences between the experimental droplet size distribution curves and the theoretical curves is significant in some cases but improves at lower ultrasound powers and higher air flow rates.

Two theoretical results were generated from the model for each trial using two different values (0.04 and 0.001) for the accommodation coefficients α_m and α_h. From the detailed results in Appendix 4 it is observed that for virtually every trial the difference between the two theoretical curves is minimal. That is the model results appear to be independent of the value used for the accommodation coefficient. The reason for this is that, theoretically (according to the model), equilibrium conditions are being achieved prior to the outlet of the conduit for all values of the accommodation coefficients used. The effect of the accommodation coefficient is to slow down or speed up the theoretical evaporation process, especially for the very small droplets. Thus for a given set of inlet and boundary conditions, once equilibrium is achieved, those equilibrium conditions are very similar irrespective of the values of the accommodation coefficients used. Thus, for a 'long' conduit, it is possible that theoretical equilibrium conditions will be achieved prior to the outlet of the conduit, no matter what value of the accommodation coefficient is used. This is the case for all ultrasound enhanced evaporation trials.

Considering the droplet size distribution parameters as reported in Chapter 6 in Figure 6-38 to Figure 6-43 it was noted that for all parts of the droplet size distribution the accuracy of the model improved with air flow rate and decreased with increasing power levels. So that, at an ultrasound power level of 2 W and air flow rate of 20 lpm the

accuracy of theoretical model in predicting the $Dv10$, $Dv50$ and $Dv90$ is with an error of 5.4%, -10.9% and 0.5% respectively. However at the other extreme, at an ultrasound power level of 20 W and an air flow rate of 6.5 lpm the accuracy of theoretical model in predicting the $Dv10$, $Dv50$ and $Dv90$ is with an error of -83%, -66.3% and 57.6% respectively. Again, as discussed previously the effect of the air velocity on the ultrasound field is to lessen its effects on the evaporation process. Thus the input of energy, not allowed for in the model, is reduced at higher air flow rates and increased at higher ultrasound power levels.

7.10 Uncertainty in experimental results

The physical processes involved in the ultrasound enhancement of droplet evaporation include heat and mass transfer, multi-phase fluid flow and ultrasound propagation through an aerosol. Measurement of the changes to the droplet distribution involves a laser diffraction technique and determination of the droplet evaporation involves the measurement of the air flow rate, air temperature and humidity and water droplet flowrate. Quantifying the contribution of all of these sources to an overall uncertainty in the experimental measurements is beyond the scope of this investigation,

However during the experimental phase of the investigation a number of trials were repeated several times (in some cases 5 – 6 times) under the same conditions to provide an estimation of the random errors involved in the measurements. Although these errors were not quantified in a systematic fashion they were estimated to be consistent within 10 – 20% maximum.

7.11 Conclusion

The aim of this investigation was to experimentally and theoretically investigate the improvement in evaporation of water droplets into air flowing along a conduit as a result of an imposed ultrasound field. Also, to quantify that improvement. From the experimental and theoretical investigation it has been shown:

- That indeed the ultrasound field does improve the evaporation of the water droplets up to around 30% compared to normal evaporation.
- That the improvement in evaporation as a result of the imposed ultrasound field increased with ultrasound power level. But even at very low power levels (2 W)

there was an increase in evaporation rates of around 5% at the lower air flow rates.

- That the maximum improvement in water evaporation occurred at mid-range air flow rates of around 10 and 12 lpm for this set up. At lower air flow rates it was apparent the air flow had little impact on the ultrasound field but at higher air flow rates the air flow disrupted the ultrasound field so its effects on the evaporating droplets were diminished.

- That the changes in the droplet distribution between the inlet and outlet of the conduit, apparent in normal evaporation, were accentuated when the ultrasound field was applied. The effect of the ultrasound field was greatest on the smallest droplets in the distribution. They moved with the air particles in the ultrasound field causing them to coalesce with other droplets and thus shifting the droplet distribution to larger sizes.

- That the ultrasound field had additional effects on the evaporation processes other than just enhancing the heat and mass transfer processes. The outlet air temperature was observed to increase which indicates the ultrasound field was transferring energy into the air, which in itself would enhance droplet evaporation. Also, as mentioned in the previous point, the significant shift of the droplet distribution sizes from smaller to larger indicating that the ultrasound field was causing coalescence of droplets. These affects being most noticeable at high ultrasound power levels and low air flow rates when the strength of the ultrasound field is at its greatest

- When results from the theoretical model were compared to the experimental results it generally confirmed the conclusions mentioned above. Since some of these effects (e.g., energy input and coalescence) were not allowed for in the theoretical model there were large discrepancies between the theoretical results and experimental results. This was especially so when these effects were at their maximum, that is at high ultrasound power levels and low air flow rates. Conversely, when the air flow rates were high and ultrasound power levels low, the model results were more accurate. This indicates that when the unaccounted for effects were at their lowest the model was providing more accurate results suggesting that indeed the improvement in evaporation is due to the

enhancement of the heat and mass transfer processes. Thus the model could be used in these situations to predict the effects of the imposed ultrasound field.

The implication of this research is that imposing an ultrasound field on evaporating droplets can have a significant effect on the droplets. It certainly improves evaporation rates, due to enhanced heat and mass transfer processes and energy input, and this could have beneficial application to medical breathing devices and related applications. The fact that the ultrasound also causes a shift in the droplet distribution, probably as a result of droplet coalescence, is not so beneficial for evaporative applications where smaller droplet sizes are better (evaporate more quickly). However by managing the process conditions, air flow rate and ultrasound power this coalescence could be minimised.

7.12 Significance, Innovation and Contribution

The significance and contribution of this investigation is that it furthers the development of smaller more energy efficient humidification elements used in lung supportive respiratory devices. The focus of the investigation was the use of ultrasound techniques to enhance the humidification process. Although the use of ultrasound in droplet generation is well known this work investigates, for the first time, the application of a second stage of ultrasound to enhance the evaporation of the water droplets. By accelerating or enhancing the evaporation of the droplets then the time taken for this process could be reduced and this would have benefits in terms of improved efficiencies, more compact equipment sizes and better process controllability.

Although the models developed in this investigation for normal droplet evaporation have been used by other researchers for general situations. Nevertheless, in this investigation, they have been developed from first principles specifically in relation to medical respiratory apparatus. Furthermore the model for ultrasound enhanced evaporation of water droplets is developed for the first time in this investigation.

This investigation also presents for the first time experimental results from the application of a power ultrasound transducer to the evaporation of water droplets flowing along a conduit.

7.13 Future work

From this research it is clear that an imposed ultrasound field has a significant positive effect on the evaporation of water droplets flowing with air along a conduit. It also has potentially unwanted effects such as droplet coalescence. Future work in this area is proposed as follows:

- The theoretical model could be further developed to include the heating effect of the ultrasound field on the air.

- The theoretical model could also be developed to include a coalescence model to account for any droplet-to-droplet and droplet-to-wall interactions.

- Investigate the evaporation (normal and ultrasound enhanced) of the smaller droplets in more detail as these seem to behave differently from the larger droplets in the distribution.

- Regarding experimental work, the apparatus could be developed to better match the intended area of application, being biomedical respiratory apparatus. That is, designing and building an ultrasound transducer that is of a more appropriate size that would have benefits in terms of lower power requirements and lower equipment costs.

- Investigate the effects of other parameters such as air temperature and conduit length on the ultrasound enhanced evaporation of the water droplets

- Different ultrasound transducers and transducer arrangements could be investigated to optimise the effect of the ultrasound field on the water droplet evaporation.

Appendices

Appendix 1 - *SPL* level in Ultrasound Sonotrode

In order to compare the ultrasound enhanced model results with the measured experimental results it was necessary to know the amplitude or sound pressure level (*SPL*) of the ultrasound field generated inside the cylindrical sonotrode. The equipment used to generate the ultrasound field, as described in detail in Chapter 5, allows the selection of the input power to the ultrasonic transducer but the resulting *SPL* of the ultrasound field inside the cylindrical sonotrode was not known.

The supplier of the power ultrasound equipment, Pusonics S.L., carried out measurements of the average *SPL* inside the cylinder with a 1/8" diameter GRAS microphone and measured the values shown in Table A 1.

Table A 1: Measured *SPL* at different power inputs

Electrical Power Applied (W)	*SPL* (dB)
75	153.29
1	134.32

From this data the following equation was derived to determine the *SPL* at any power level between 1 and 75 W.

$$SPL = 134.32 + 10.117 \log_{10} P \qquad \text{(A 1-1)}$$

Where P is the input power level (W).

Appendix 2 - Results from the Literature

In Chapter 6 results from the ultrasound enhanced model in this work were compared with results from the literature. The results from the literature were extracted from graphs and tables in various works and are collated and presented here. Comparative model results are presented in the section

A 2.1 Literature results

The results relate to the use of power ultrasound in the drying of small vegetable pieces, Table A 2 to Table A 7. In all cases the power ultrasound was generated at 21.78 kHz and at a power of 90 W (equivalent to 37 kW/m^3), except for the strawberry pieces, where the power was 25 kW/m^3. The results extracted consist of drying times, the initial evaporation rate and the mass transfer coefficient. Each of these is determined for the normal drying case (no ultrasound power applied) and for the case with maximum ultrasound power applied.

Table A 2: Results for eggplant pieces: Ref [116]

Eggplant Air: 40°, 1 m/s	ultrasound power (kW/m^3)	drying times (s)	initial evap. rate (x 10^{-3}) (kgw/s/kgdm)	mass transfer coefficient (kgw/s/m^2)
No ultrasound	0	24250	0.9188	1.87
Ultrasound	37	6750	3.196	6.16
Change/Improvement		-72.2%	247.8%	229.4%
Improvement Factor		**3.593**	**3.478**	**3.294**

Table A 3: Results for potato pieces: Ref [117]

Potato Air: 40°, 1 m/s	ultrasound power (kW/m^3)	drying times (s)	initial evap. rate (x 10^{-3}) (kgw/s/kgdm)	mass transfer coefficient (kgw/s/m^2)
No ultrasound	0	12640	0.4234	2.03
Ultrasound	37	7850	0.6604	3.21
Change/Improvement		-37.9%	56.0%	58.1%
Improvement Factor		**1.610**	**1.560**	**1.581**

Table A 4: Results for carrot pieces: Ref [118]

Carrot Air: 40°, 1 m/s	ultrasound power (kW/m^3)	drying times (s)	initial evap. rate (x 10^{-3}) (kgw/s/kgdm)	mass transfer coefficient (kgw/s/m^2)
No ultrasound	0	11870	1.215	--
Ultrasound	37	8670	1.483	--
Change/Improvement		-27.0%	22.1%	--
Improvement Factor		**1.369**	**1.221**	**--**

Table A 5: Results for lemon peel pieces: Ref [118]

Lemon Peel Air: 40°, 1 m/s	ultrasound power (kW/m^3)	drying times (s)	initial evap. rate (x 10^{-3}) (kgw/s/kgdm)	mass transfer coefficient (kgw/s/m^2)
No ultrasound	0	31680	0.3215	--
Ultrasound	37	15055	0.7903	--
Change/Improvement		-52.5%	145.8%	--
Improvement Factor		**2.104**	**2.458**	**--**

Table A 6: Results for strawberry pieces: Ref [120]

Strawberry Air: 40°, 2 m/s	ultrasound power (kW/m^3)	drying times (s)	initial evap. rate (x 10^{-3}) (kgw/s/kgdm)	mass transfer coefficient (kgw/s/m^2)
No ultrasound	0	19100	0.9183	1.446
Ultrasound	25	16640	1.326	1.633
Change/Improvement		-12.9%	44.4%	12.9%
Improvement Factor		**1.148**	**1.444**	**1.129**

Table A 7: Results for orange peel pieces: Ref [119]

Orange Peel Air: 40°, 1 m/s	ultrasound power (kW/m^3)	drying times (s)	initial evap. rate (x 10^{-3}) (kgw/s/kgdm)	mass transfer coefficient (kgw/s/m^2)
No ultrasound	0	34800	0.1979	1.17
Ultrasound	37	17200	0.3524	2.43
Change/Improvement		-50.6%	78.1%	107.7%
Improvement Factor		**2.023**	**1.781**	**2.077**

A 2.2 Comparative model results

The comparative ultrasound enhanced model results (see section 6.7.2) are given in Table A 8 and Table A 9.

Table A 8: Model results for L = 245 mm

Case #	Nominal Air flow (l/min)	Ultrasound	time to equilibrium (s)	distance to equilibrium (mm)	amount evaporated at L (kg/s) x 10^{-6}
1	6.4	None	0.4139	108.28	0.7728
		U/S ON	0.2381	62.4	0.7708
2	10	None	0.5182	211.6	1.181
		U/S ON	0.4337	177.1	1.181
3	15	None	1.0228	627.3	1.654
		U/S ON	0.827	507.3	1.689
4	20	None	1.7649	1440.1	1.842
		U/S ON	1.4321	1168.6	1.941
5	25	None	2.8749	2925.5	1.905
		U/S ON	2.3196	2360.5	2.051

Table A 9: Model results for *L* = 340 mm

Case #	Nominal Air flow (l/min)	Ultrasound	time to equilibrium (s)	distance to equilibrium (mm)	amount evaporated at L (kg/s) x 10^{-6}
1	6.4	None	0.4039	107	0.7866
		U/S ON	0.2416	63.3	0.7848
2	10	None	0.5234	215	1.198
		U/S ON	0.4395	180.5	1.198
3	15	None	1.0563	647.1	1.74
		U/S ON	0.8649	529.9	1.758
4	20	None	1.83	1491.9	2.031
		U/S ON	1.4482	1180.9	2.112
5	25	None	2.8809	2938.3	2.131
		U/S ON	2.27	2315.5	2.269

From the previous two tables the following improvement factors are calculated and shown in Table A 10.

Table A 10: Improvement factors

Air flow rate (lpm)	*L* = 340 mm		*L* = 245 mm	
	time	evap'n	time	evap'n
6.4	1.67	1.00	1.74	1.00
10	1.19	1.00	1.19	1.00
15	1.22	1.01	1.24	1.02
20	1.26	1.04	1.23	1.05
25	1.27	1.06	1.24	1.08

Appendix 3 - MATLAB code for models

The MATLAB code for the three theoretical models is provided here:

A 3.1 Mono-disperse droplet evaporation model

Main body of code

```matlab
% Adds fourth ODE to track changes in air temperature.
% But CORRECTED fourth ODE to include the energy of heating/cooling the
% water vapour to match the surrounding air temp.
%
% All fluid properties are calculated at actual temperature of fluids
% as solution progresse ie variable properties
%
% Includes Kelvin effect factor to adjust the saturation vapour pressure
% at the curved droplet surface.
% Uses surface tension and density values at the input average temperature
%
% Droplet temp (and hence droplet vap. pressure) drop off as droplet
% dissapears so display max value over last part of results.
%
% Also includes Knudsen correction factors for heat and mass transfer
%
global K1 K6 K7 K8 Po KLm KLh alpham alphah
%
starttime = ['--- ', datestr(now), ' ----------START-- Rv10_3 --------'];
disp (starttime)
tic
%-----------------------------------------------------------
% Parameters that remain constant for this version
%
% Initial coditions for the air
Va = 30;            % total Volume of air per minute (litres)
Tinf_i = 25;      % Initial bulk mean temperature of air (C)
RHinf_i = 0.4;    % Initial relative humidity
% Initial Conditions for the water
Vw = 0.08;          % total volume of water per minute nebulised (ml)
Td_i = 25;        % initial droplet temperature (C)
dd_i = 5e-6;      % Initial droplet diameter (m)
%
Nd = Vw*6*1000/(1e6*pi*dd_i^3*Va); % droplet number concentration
%
M_w = 18.015;       % molecular weight of water (kg/kmol)
Ru = 8314.5;        % Universal gas constant (J/kmol.K)
NA = 6.0221367e26;  % Avogadro constant (/kmol)
Po = 101.325;       % Ambient total pressure (kPa)
%
% Determine Pinf_i initial condition from RHinf_i (Pa):
winf_i = W_ptphi_HAP_SI(Po,Tinf_i,RHinf_i);
Pinf_i = pH2O_ptW_HAP_SI(Po, Tinf_i, winf_i)*1000; % initial air...
                                        % vap pressure (Pa)
%
% Knudsen Correction Factors - Constant parts
dH2O = 310e-12;  % effective diameter of water molecule (m)
dAir = 360e-12;  % effective diameter of air molecule (m)
KLm = Ru/(sqrt(2)*pi*dH2O^2*NA*Po*1000); % mean free path - constant parts
KLh = Ru/(sqrt(2)*pi*dAir^2*NA*Po*1000); % mean free path - constant parts
alpham = 1; % accomodation coefficient (mass transfer)
alphah = 1; % accomodation coefficient (heat transfer)
%
% ODE Constant parts
K1 = 4*M_w/Ru;              % constant for ODE 1
K6 = -pi*Ru*Nd/(2*M_w);       % constant for ODE 3
K8 = pi*Nd/2;              % constant for ODE 4
K7 = 4*M_w/Ru;  % constant parts of Kelvin effect factor
%
% Display input parameters
instr1 = sprintf('Air    : Temp = %4.1f C, RH = %4.2f, Flow = %5.2f l/min',...
    Tinf_i, RHinf_i, Va);
instr2 = sprintf('Droplet: Temp = %4.1f C, diam. = %6.1e m, Flow = %6.4f ml/min',...
    Td_i, dd_i, Vw);
instr3 = sprintf('Po = %7.3f kPa,  Knudsen: alpha(m) = %3.1f, alpha(h) = %3.1f',...
    Po, alpham, alphah);
```

```matlab
disp(instr1)
disp(instr2)
disp(instr3)
%
%-----------------------------------------------------------
% ODE solver and options
options = odeset('Events', @finish1, 'Refine', 4, 'RelTol', 1e-4);
%
[t,soln,te,xe,ie] = ode15s(@Rao10_3ODE,[0,100000],[dd_i, Td_i, Pinf_i,...
    Tinf_i], options);
%-----------------------------------------------------------
% Display of output: Various graphs of the key parameters as they vary with
% time
subplot(3,2,1)
plot(t,soln(:, 1)), xlabel('time (s)'),ylabel('droplet diameter (m)')
subplot(3,2,2)
Temps = [soln(:, 2) soln(:, 4)];  % array of droplet and air temps
plot(t, Temps), xlabel('time (s)'),ylabel('droplet/air temperature (C)')
subplot(3,2,3)
rho_w = arrayfun(@(Tda) 1/vliq_pt_97_SI(Po, Tda), soln(:, 2));  % density of water
droplet (kg/m^3)
% Surface Tension lookup to enable calc. of Kelvin effect factor
sigma_w = arrayfun(@(Tda) Sigma_t_97(Tda)/1000, soln(:, 2));
Pd_plt = arrayfun(@(Tda) pH2Os_pt_HAP_SI(Po,Tda)*1000, soln(:, 2)).*...
    exp(K7.*sigma_w./((soln(:, 2) + 273.15).*rho_w.*soln(:, 1)));
plot(t,Pd_plt), xlabel('time (s)'),ylabel('droplet vapour pressure (Pa)')
subplot(3,2,4)
plot(t,soln(:, 3)), xlabel('time (s)'),...
    ylabel('air vapour pressure(Pa)')
winf = arrayfun(@(Tinf, Pinf) W_ptpH2O_HAP_SI(Po,Tinf,Pinf),...
    soln(:, 4), soln(:, 3)/1000);
RHinf_plt = arrayfun(@(Tinf, winff) phi_ptW_HAP_SI(Po,Tinf,winff),...
    soln(:, 4), winf);
subplot(3,2,5)
plot(t,RHinf_plt), xlabel('time (s)'),...
    ylabel('air relative humidity')
subplot(3,2,6)
plot(t,winf), xlabel('time (s)'),...
    ylabel('air humidity ratio (kgw/kgda)')
% Print out (display) the various parameters valuse at the end of the
% solution process
if ie == 2  % If second 'finish' event has stopped the solver ie RH = 1
    outstr1 = sprintf('\rfinal droplet diameter = %11.4e m\r\rtime to approx. steady
state = %7.4f seconds\r',...
        soln(end, 1), te);
    outstr2 = sprintf('final droplet temperature = %6.3f deg. C\r',...
        max (soln(int32(length(soln)*0.5):end , 2)));% Find max value
    outstr6 = sprintf('final air temperature = %6.3f deg. C\r', soln(end, 4));
    outstr5 = sprintf('final air relative humidity = %f \r', RHinf_plt(end));
    outstr7 = sprintf('final air humidity ratio = %f kgw/kgda \r', winf(end));
else    % If first 'finish' event has stopped the solver ie drop diameter = 0
    outstr1 = sprintf('\rdroplet lifetime = %9.6f seconds\r', te);
    outstr2 = sprintf('final droplet temperature = %6.3f deg. C\r',...
        max (soln(int32(length(soln)*0.5):end , 2)); % find max value
    outstr3 = sprintf('final droplet vapour pressure = %7.2f Pa\r',...
        max (Pd_plt(int32(length(soln)*0.5):end , 1))); % find max value
    outstr6 = sprintf('final air temperature = %6.3f deg. C\r', xe(4));
    outstr4 = sprintf('final air vapour pressure = %7.2f Pa\r', xe(3));
    outstr5 = sprintf('final air relative humidity = %f \r', RHinf_plt(end));
    outstr7 = sprintf('final air humidity ratio = %f kgw/kgda \r', winf(end));
end
et = toc;
headerstr = ['--- ', datestr(now), ' -----COMPLETE---- ',num2str(et),' s -----'];
disp (headerstr)
disp (outstr1)
disp (outstr2)
disp (outstr6)
disp (outstr5)
disp (outstr7)
```

ODE function

```matlab
function [dTP_dot] = Rao10_3ODE(t, dTP)
% dTP(1) = droplet diameter, dd (m)
% dTP(2) = droplet temperature, Td (C)
% dTP(3) = water vapour pressure in ambient air, Pinf (Pa)
% dTP(4) = ambient humid air temperature (C)
```

```matlab
%
global K1 K6 K7 K8 Po KLm KLh alpham alphah Pd
%
% Fluid Property data and calculated initial conditions
% Liquid water properties at Td ie dTP(2)
rho_w = 1/vliq_pt_97_SI(Po, dTP(2));  % density of water droplet (kg/m^3)
Cp_w = cp_ptx_97(Po/100, dTP(2), -1)*1000;
h_w = (hvaps_t_97_SI(dTP(2)) - hliqs_t_97_SI(dTP(2)))*1000;
                                    % latent heat of vaporisation (J/kg)
% Surface Tension to enable calculation of Kelvin effect factor
sigma_w = Sigma_t_97(dTP(2))/1000; % surface tension (N/m)
% droplet sat. vapour pressure , including Kelvin effect
Pd = pH2Os_pt_HAP_SI(Po,dTP(2))*1000*...
    exp(K7*sigma_w/((dTP(2)+273.15)*rho_w*dTP(1)));
%
% Humid Air - Transport properties (k or lambda and Dw)at Tfilm
Tfilm = (dTP(2) + dTP(4))/2;     % Film temperature
D_w = 1.8948e-8/Po*(Tfilm + 273.15)^2.072;    % Diff coeff. (m^2/s)
RHinf = dTP(3)/(pH2Os_pt_HAP_SI(Po,dTP(4))*1000);
if RHinf > 1     % set RH to 1 if it goes over 1 as air becomes saturated
    RHinf = 1;
end
wfilm = W_ptphi_HAP_SI(Po,Tfilm,(1 + RHinf)/2);
lam_a = Lambda_ptW_HAP_SI(Po, Tfilm, wfilm);  %thermal conductivity (W/m.K)
%
% Humid Air - remaining properties at Tinf ie dTP(4)
winf = W_ptpH2O_HAP_SI(Po, dTP(4), dTP(3)/1000);
% winf = W_ptphi_HAP_SI(Po, dTP(4),RHinf);
rhoinf = Rho_ptW_HAP_SI(Po, dTP(4), winf);  % density of humid air (kg/m^3)
Cpinf = cp_ptW_HAP_SI(Po, dTP(4), winf)*1000;    % sp. ht cap of humid air (J/kg.C)
%
Pfilm = (Pd + dTP(3))/2;
Cpwvap = cp_ptx_97(Pfilm/100000, Tfilm, -1)*1000; % sp ht capacity of the...
% water vapour(J/kg.C) at average film temp and pressure
%
% Knudsen Correction factors
Lm = KLm*(Tfilm + 273.15);  % mean free path - mass transfer
Lh = KLh*(Tfilm + 273.15);  % mean free path - heat transfer
Cm = (1 + 2*Lm/dTP(1))/(1 + (4/(3*alpham)+0.377)*2*Lm/dTP(1) + ...
    4/(3*alpham)*(2*Lm/dTP(1))^2);
Ch = (1 + 2*Lh/dTP(1))/(1 + (4/(3*alphah)+0.377)*2*Lh/dTP(1) + ...
    4/(3*alphah)*(2*Lh/dTP(1))^2);
%
%
dd_dot = K1*Cm*D_w/(dTP(1)*rho_w)*(dTP(3)/(dTP(4)+273.15)...
    - Pd/(dTP(2)+273.15)); % first ODE
% Td_dot = -12/(rho_w*Cp_w*dTP(1)^2)*(K4*D_w*h_w*Cm*(Pd/(dTP(2)+273.15)...
%     - dTP(3)/(dTP(4)+273.15)) + lam_a*Ch*(dTP(2) - dTP(4)));
Td_dot = (12*lam_a*Ch*(dTP(4) - dTP(2)) + 3*rho_w*dTP(1)*h_w*dd_dot)...
    /(rho_w*Cp_w*dTP(1)^2); % second ODE
Pinf_dot = K6*rho_w*(dTP(4)+273.15)*dTP(1)^2*dd_dot;
%Tinf_dot = 0;  % use this when simulating Rao's model
Tinf_dot = K8*dTP(1)*(dTP(4) - dTP(2))/(rhoinf*Cpinf)*(rho_w*dTP(1)*...
    Cpwvap*dd_dot - 4*lam_a*Ch);
dTP_dot = [dd_dot; Td_dot; Pinf_dot; Tinf_dot];
```

Completion function

```matlab
function [value,isterminal,direction] = finish1(t,y)
% Stop (Finish!) the integration when the diameter of the droplet
% passes through zero (ie evaporates) OR when the diameter of the droplet
% no longer changes (ie environment is saturated, RH = 1).
% Stop the integration in both cases.
%
global Po
RH = y(3)/(pH2Os_pt_HAP_SI(Po,y(4))*1000); % easier to use RH = 1
value = [y(1) - .00000001 ; RH - 0.9999999]; % Detect diam. = 0 or RH = 1
isterminal = [1; 1];   % Stop the integration in both cases
direction = [-1; 0];    % Negative direction only for diameter
```

A 3.2 Poly-disperse droplet evaporation model

Main body of code:

```
% ITERATIVE version of Ms_11_5xj_main to process lots of input data sets at
% once.  So dispense with any output to command window... just calculate
% and save results. Reads input data in.
% Need to specify values of alpha to be used, any notes that apply and the
% Model input data to be used
%
% Also changed the way you set the length: Now L is set to the experimental
% value and if L < L(calc end) the distribution at L will be different from
% the final (end) values. If L > L(calc end) rather than stopping it sets
% the distribution values at L EQUAL to the final (end) values (since
% equilibrium has been reached so values shouldn't change...)
%
% Multi size droplet evaporation model - Any number(Nt)sizes of droplets
% originally based on single size droplet evaporation model: Rv10_3, but
% directly based on Ms_10_3_xj_main. Ver 11 adds distance calculation based
% on inside diameter of tubing... Also adds droplet MEAN and MEDIAN calcs
%
% v11_5 allows for the calculation to continue in cases where although
% RH=1, temperature equilibrium has not yet been reached... so calculation
% stops when droplets and air temperature are the same.
%
% v11_4 allows for the changing volume flowrate (dry air mass flow rate
% remains constant) along the tube (as temperature of air changes) So need
% to input tubing diameter ID and target distance L...  to determine
% droplet distribution at some specified length along the tube -
% interpolates to find values at that distance.
%
% This means that the ODE's also had to be adjusted... and the droplet
% number concentration defined as number per kg of dry air (rather than
% kg/m^3)
%
% ODE 1: Nt mass balance ODE's (one for each droplet size).
% ODE 2: Nt energy balance ODE's (one for each droplet size).
% ODE 3: One mass balance ODE for the surrounding Air.
% ODE 4: One energy balance ODE for the surrounding Air.
%
% All fluid properties are calculated at actual temperature of fluids
% as solution progresses ie variable properties
%
% Includes Kelvin effect factor to adjust the saturation vapour pressure
% at the curved droplet surface.
%
% Also includes Knudsen correction factors for heat and mass transfer
%
clear
% ######## Input any notes relating to these set of runs...
notes1 = 'Power Ultrasound Trials - Period prior to turning U/S on';
notes2 = 'U/S OFF. Data from 29/5/2014. 5 W. Trying alpha = 1, 0.5';
%
global K1 K6 Po KLm KLh alpham alphah Nmd N
%
% ######## Input here the values of alpha to be used
alphas = [1, 0.5];
maxloopk = length(alphas);
%
% ######## Input the Model input data file o be used
input_datafile = 'Input Data\Model input data 2014-05-29 PU 5W';
% this datafile contains all input parameters
load(input_datafile)
maxloopj = size(input_data,1);
%
for nj = 2:maxloopj
    msgdata = sprintf('Data loop %d of %d', nj - 1, maxloopj - 1);
    disp(msgdata) % feedback to Command Window on progress
    %
    for nk = 1:maxloopk
        alpha = alphas(nk);
        msgalpha = sprintf('   Alpha loop %d of %d', nk, maxloopk);
        disp(msgalpha) % feedback to Command Window on progress
        %
        expt_date = input_data{nj,1}and ; % Actual date experiment was
        %                                   run and data recorded
        %
        starttime = ['--- ', datestr(now),...
```

```matlab
    ' --------- START -------- Ms_11_5xj ------'];
% disp (starttime)
% tic
%----------------------------------------------------------------
% INPUT parameters
% ----------------------------------------------------------------
% Air
Tinf_i = input_data{nj,2}; % Initial bulk mean temperature of air (C)
RHinf_i = input_data{nj,3};  % Initial relative humidity
Va_i = input_data{nj,4};   % total Volume of air per minute (litres)
% Water
Td_ic = input_data{nj,5};% initial droplet temp.for all droplet sizes (C)
Vw = input_data{nj,6}; % total volume of water per minute nebulised (ml)
in_drop_distbn = ['Input Distributions\input drop dist ',...
    input_data{nj,7}];
% input droplet distribution
%
% Accommodation coefficents Set above as part of for loop...
% Set both alpha-m and alpha-h to same value
%
% Tubing
ID = input_data{nj,9};         % Internal diameter of tubing (mm)
L = input_data{nj,8};    % target distance along tube where droplet
% distribution is desired to be known (mm)
%---------------------------
% Set up droplet distribution
% ---------------------------
% Multi size droplet details.  MUST be from larger to smaller
load (in_drop_distbn)  % loads droplet distribution into the
% variable: drop_dist. Original data in mat file is small to LARGE,
% needs to be reordered LARGE to small.
Nt = size(drop_dist,2);     % number of droplet sizes or bins
dd_i = 1e-6*fliplr(drop_dist(1,:));
Vol_pct_i = 100 * fliplr(drop_dist(2,:));
Td_i = Td_ic*ones(1, Nt);          % initial droplet temperatures (C)
%
% Basic error checking of distribution
if length(dd_i) ~= Nt, disp('no. of droplet sizes incorrect'),...
        return, end
if length(Vol_pct_i) ~= Nt, disp('no. of %vols incorrect'),...
        return,  end
Total = single(sum (Vol_pct_i));
if abs(Total-100) >= 0.03
    errormsg = sprintf(...
        'Total volume percent is not equal to 100.0, %6.2f\r'...
        , Total);
    disp (errormsg)
    return
end
for j = 1:(Nt-1)
    if dd_i(j) <= dd_i(j + 1),...
            disp ('sizes not in descending order'), return, end
end
% ----------------------
% Constants
M_w = 18.015;      % molecular weight of water (kg/kmol)
Ru = 8314.5;       % Universal gas constant (J/kmol.K)
NA = 6.0221367e26;  % Avogadro constant (/kmol)
Po = 101.325;      % Ambient total pressure (kPa)
%
% Determine initial AIR conditions
winf_i = W_ptphi_HAP_SI(Po,Tinf_i,RHinf_i); % humid. ratio (kgw/kga)
Pinf_i = pH2O_ptW_HAP_SI(Po, Tinf_i, winf_i)*1000; % vap press. (Pa)
vinf_i = v_ptW_HAP_SI(Po, Tinf_i,winf_i); % air sp. volume (m^3/kga)
%
% Mass flow rate of DRY AIR - assuming Va is vol.flowrate of MOIST air
m_a = Va_i/1000/60/vinf_i; % mass flow rate of dry air for
%                          number concentrations (kg/s)
% Droplet number concentrations - based on mass flow rate of dry air
% Nd = Vw/100*6*1000/(1e6*pi*Va)*Vol_pct_i./dd_i.^3; OLD DEFINITION
Nmd = Vw*6/(1e6*60*pi*m_a)*Vol_pct_i/100./dd_i.^3; % (no. of drops/kga)
%
% Droplet Mean diameters (D32, D43) and Dv10, Dv50 (= MMAD), Dv90
D32_i = sum(Nmd.*dd_i.^3)/sum(Nmd.*dd_i.^2);
D43_i = sum(Nmd.*dd_i.^4)/sum(Nmd.*dd_i.^3);
Vol_pct_i_cum = cumsum(drop_dist(2,:)*100); % smallest to largest
% Spraytech calc for Dv10, Dv50 etc (uses Dupper rather than Davg)
Dv10_i = interp1(Vol_pct_i_cum, drop_dist(3,:), 10, 'linear');
Dv50_i = interp1(Vol_pct_i_cum, drop_dist(3,:), 50, 'linear');
Dv90_i = interp1(Vol_pct_i_cum, drop_dist(3,:), 90, 'linear');
```

```matlab
span_i = (Dv90_i - Dv10_i)/Dv50_i;
%
%
% Initial conditions
initial_condxi = [dd_i Td_i Pinf_i Tinf_i];
%
% Knudsen Correction Factors - Constant parts
dH2O = 310e-12;  % effective diameter of water molecule (m)
dAir = 360e-12;  % effective diameter of air molecule (m)
KLm = Ru/(sqrt(2)*pi*dH2O^2*NA*Po*1000); % mean free path - const. parts
KLh = Ru/(sqrt(2)*pi*dAir^2*NA*Po*1000); % mean free path - const. parts
alpham = alpha; % accomodation coefficient (mass transfer)
alphah = alpha; % accomodation coefficient (heat transfer)
%
% ODE Constant parts
K1 = 4*M_w/Ru;     % constant for ODE 1 and for Kelvin effect factor
K6 = -pi*Ru/(2*M_w);   % constant for ODE 3's
%
% Flow parameters
Flow_area = pi*ID^2/4;      % tube flow area (m^2)
Vel_ai = Va_i/60/1000/Flow_area*1e6;  % initial velocity of air
% and droplets along tube (m/s)
%
% -----------------------------------------------------------------
% Begin SOLUTION of ODE equations for all Nt droplet sizes
% -----------------------------------------------------------------
% Preallocate cell arrays
ctxj = cell(1, Nt); csolnxj = cell(1, Nt); ciexj = zeros(1, Nt);
for j = 1:Nt  % loop around if smallest droplet size evaporates and
    % reduce the number of ODE's
    N = Nt - j + 1;
    %-----------------------------------------------------------
    % ODE solver and options
    options = odeset('Events', @finish5xj, 'Refine', 4,...
        'RelTol', 1e-4);
    %
    [txj,solnxj,texj,xexj,iexj] = ode15s(@Ms_11_5xjODE,[0,100], ...
        initial_condxi, options);
    %-----------------------------------------------------------
    % Display current droplet-size bin number to see progress...
    msgstr = sprintf('Processed droplet-size bin no. %d of %d',...
        N, Nt);
    h = msgbox(msgstr, 'Progress', 'help', 'replace');
    %
    % Store results in cell arrays (where necessary)
    ctxj(1,N) = {txj};
    csolnxj(1,N) = {solnxj};
    % ctexj(1,N) = texj;
    % cxexj(1,N) = {xexj};
    ciexj(1,N) = iexj;
    % Continue solving for larger diameters if smallest diameter
    % has evaporated - set final values from last solution to
    % initial values for next solution
    if iexj == 1  % smallest diam. droplet has completely evaporated
        Tinf_ij = solnxj(end, (2*N+2)); % Initial bulk mean
        %                              temperature of air (C)
        Pinf_ij = solnxj(end, (2*N+1)); % initial air vap press.(Pa)
        % Multi size droplet details
        dd_ij = solnxj(end, 1:(N-1));      % Initial droplet diams.(m)
        Td_ij = solnxj(end, (N + 1):(2*N - 1)); % initial droplet
        %                                    temperatures (C)
        %Initial conditions
        initial_condxi = [dd_ij Td_ij Pinf_ij Tinf_ij];
    else break  % if RHinf = 1 (ie iexj = 2) then stop solving ODE's
    end
end
%
% -----------------------------------------------------------------
% RESULTS: Set up cells and vectors for plotting and display of
% FINAL results
% -----------------------------------------------------------------
% Indices for generating results and preallocate cells and arrays
j = 1; k = 1; t = cell(1, Nt); dd = cell(1, Nt); Td = cell(1, Nt);
life = zeros(1,Nt); Pinf = zeros(1, Nt); Tinf = zeros(1, Nt);
L_t = cell(1,Nt); dist = zeros(1, Nt);
dd_f = zeros(1,Nt);  % Length cell array and final values
for j = 1:N
    t{1,j} = ctxj{1,Nt};
    dd{1,j} = csolnxj{1,Nt}(:,j);
    Td{1,j} = csolnxj{1,Nt}(:,(Nt + j));
```

```matlab
        for k = 1:(Nt - N)
            t{1,j} = [t{1,j}; (t{1,j}(end) + ctxj{1,(Nt - k)}(2:end))];
            dd{1,j} = [dd{1,j}(:); csolnxj{1,(Nt - k)}(2:end,j)];
            Td{1,j} = [Td{1,j}(:);...
                csolnxj{1,(Nt - k)}(2:end,(Nt + j - k))];
        end
        if ciexj(1,1) == 1, life(j) = t{1,j}(end);...
            else life(j) = 99.9999; end
    end
    for j = (N + 1):Nt
        t{1,j} = ctxj{1,Nt};
        dd{1,j} = csolnxj{1,Nt}(:,j);
        Td{1,j} = csolnxj{1,Nt}(:,(Nt + j));
        for k = 1:(Nt - j)
            t{1,j} = [t{1,j}; (t{1,j}(end) + ctxj{1,(Nt - k)}(2:end))];
            dd{1,j} = [dd{1,j}(:); csolnxj{1,(Nt - k)}(2:end,j)];
            Td{1,j} = [Td{1,j}(:); csolnxj{1,(Nt - k)}(2:end,...
                (Nt + j - k))];
        end
        life(j) = t{1,j}(end);
    end
    Pinf = csolnxj{1,Nt}(:,(2*Nt + 1));
    Tinf = csolnxj{1,Nt}(:,(2*Nt + 2));
    for k = 1:(Nt - N)
        Pinf = [Pinf; csolnxj{1,(Nt-k)}(2:end,(2*Nt + 1 - 2*k))];
        Tinf = [Tinf; csolnxj{1,(Nt-k)}(2:end,(2*Nt + 2 - 2*k))];
    end
    % Calculate array of moisture content and RH of surrounding air
    winf = arrayfun(@(Tinfa, Pinfa) W_ptpH2O_HAP_SI(Po,Tinfa,Pinfa),...
        Tinf, Pinf/1000);
    % RHinf = arrayfun(@(Tinfa, winfa) phi_ptW_HAP_SI(Po,Tinfa,winfa),...
    %    Tinf, winf);
    % When RH reaches 1 if winf goes above the saturation pressure at
    % that temperature then RHinf is invalid... so calculate RHinf from
    % ratio of winf to winf_sat
    RHinf = arrayfun(@(Tinfa, Pinfa) Pinfa/pH2Os_pt_HAP_SI(Po,Tinfa),...
        Tinf, Pinf/1000);
    %
    % Final volume flow rate and velocity of air
    Va_f = m_a*v_ptW_HAP_SI(Po, Tinf(end), winf(end))*1000*60; % (l/min)
    Vel_af = Va_f/60/1000/Flow_area*1e6; % (m/s)
    %
    % Determine distances taking into account the change in
    % temperature, density and relative humidity of the air.  Use dry
    % air mass flow rate as the constant
    N_L = length(t{1,1});   % length of time vector
    L_tm = zeros(N_L, 1);   % initialise distance vector
    for j = 2:N_L
        Tinf_m = (Tinf(j - 1, 1) + Tinf(j, 1))/2;  % average air temp (C)
        winf_m = (winf(j - 1, 1) + winf(j, 1))/2;  % avg humidity (kgw/kga)
        vinf_m = v_ptW_HAP_SI(Po, Tinf_m, winf_m); % sp. volume (m^3/kga)
        Vel_m = m_a*vinf_m/Flow_area*1e6;          % velocity (m/s)
        DeltaL = Vel_m*(t{1,1}(j, 1) - t{1,1}(j-1, 1));  % extra distance
        L_tm(j,1) = L_tm(j - 1, 1) + DeltaL;  % distance vector
    end
    %
    % Generate cell array of times for plotting lengths, and final
    % values of droplet sizes and final lengths and final temperatures
    for k = 1:Nt
        L_t{1,k} = L_tm(1:length(t{1,k}));
        dd_f(1,k) = dd{1,k}(end);   % vector of final droplet sizes
        dist(1,k) = L_t{1,k}(end);  % vector of final distances for
        %                             each droplet size
        Td_f(1,k) = Td{1,k}(end);   % vector of final droplet temperatures
    end
    %
    % Vector of final droplet volumes and % volumes
    Vol_f = Nmd*pi.*dd_f.^3/6; % volume of droplets (m^3) per kg dry air
    Vol_pct_f = Vol_f/sum(Vol_f)*100;
    Vw_f = sum(Vol_f)*m_a*1e6*60; % volume flowrate (ml/min) for
    %                               remaining droplets
    %
    % Calculations for final droplet distribution and mean/median values
    %  Remove zeros from final values for plotting
    dd_fp = dd_f(1:N);
    Vol_pct_fp = Vol_pct_f(1:N); % ignore the volumes of the
    %                              'evaporated' droplets
    Vol_pct_fp_cum = cumsum(fliplr(Vol_pct_fp)); % cumul Vol in ascending order
    %
    if ciexj(1,1) == 0 % Only compute mean/median values if two
```

```
%                    or more bins remaining
% Droplet Mean diameters (D32, D43) and Dv10, Dv50 (= MMAD), Dv90
D32_f = sum(Nmd(1:N).*dd_fp.^3)/sum(Nmd(1:N).*dd_fp.^2);
D43_f = sum(Nmd(1:N).*dd_fp.^4)/sum(Nmd(1:N).*dd_fp.^3);
% Spraytech calc for Dv10, Dv50 etc uses Dupper rather than
% Davg so set up vector of Dupper sizes that match dd_fp sizes
dd_fv = fliplr(dd_fp)*1e6;
ind_SP = find(drop_dist(3,:)> dd_fv(1,1),1,'first'); %index
%                               of matching droplet size
dd_fSP = drop_dist(3,ind_SP(1,1)); % Dupper droplet size
for j = 2:N % create vectors of indices and Dupper droplet sizes
    ind_SP = [ind_SP, find(drop_dist(3,:)> dd_fv(1,j),1,'first')];
    dd_fSP = [dd_fSP, drop_dist(3,ind_SP(1,j))];
end
Dv10_f = interp1(Vol_pct_fp_cum, dd_fSP, 10, 'linear');
Dv50_f = interp1(Vol_pct_fp_cum, dd_fSP, 50, 'linear');
Dv90_f = interp1(Vol_pct_fp_cum, dd_fSP, 90, 'linear');
span_f = (Dv90_f - Dv10_f)/Dv50_f;
else
    D32_f = 0; D43_f = 0; Dv10_f = 0; Dv50_f = 0;
    Dv90_f = 0; span_f = 0;
end
%
% ----------------------------------------------------------------
% RESULTS: Determine values of results at DISTANCE L
% ----------------------------------------------------------------
% Check experimental length L with length at end of calculations.
% If L > L(calc end) then set L values to end values
% If L < L(calc end) then calc L values and save along with end
% values
%
if L > L_t{1,1}(end)*1000 % L > L(calc end) so set L values to end values
    t_L = NaN;
    Tinf_fL = Tinf(end);
    winf_fL = winf(end);
    RHinf_fL = RHinf(end);
    Va_fL = Va_f;  % (l/min)
    Vel_afL = Vel_af;  % (m/s)
    %
    dd_fL = dd_f;
    dd_fLp = dd_fp;
    Td_fL = Td_f;
    %
    Nmd_L = Nmd; % just Nmds for the droplets that remain
    Vol_fL = Vol_f;
    Vol_pct_fL = Vol_pct_f;
    Vol_pct_fLp = Vol_pct_fp;
    % Vol_pct_fL_cum = cumsum(fliplr(Vol_pct_fL)); % cumul Vol in
    % ascending order
    Vw_fL = Vw_f; % volume flowrate (ml/min) for remaining droplets
    %
    D32_fL = D32_f;
    D43_fL = D43_f;
    Dv10_fL = Dv10_f;
    Dv50_fL = Dv50_f;
    Dv90_fL = Dv90_f;
    span_fL = span_f;
else
    % If L < L(calc end) then calculate values at L
    %
    % Vector of droplet sizes and temperatures at some distance L
    % from the initial mixing point
    %
    % Time at distance L
    t_L = interp1(L_tm, t{1,1}, L/1000, 'linear'); % time to
    % location L (s)
    % Air properties, flow rate and velocity at L
    Tinf_fL = interp1(t{1,1}, Tinf, t_L,'linear');
    winf_fL = interp1(t{1,1}, winf, t_L,'linear');
    RHinf_fL = interp1(t{1,1}, RHinf, t_L,'linear');
    Va_fL = m_a*v_ptW_HAP_SI(Po, Tinf_fL, winf_fL)*1000*60;  % (l/min)
    Vel_afL = Va_fL/60/1000/Flow_area*1e6;  % (m/s)
    %
    % Calculate volumes for final %-volume distribution at distance
    % L.  Interpolate (linear) to find droplet sizes at L
    dd_fL = interp1(t{1,1}, dd{1,1}, t_L,'linear');
    Td_fL = interp1(t{1,1}, Td{1,1}, t_L,'linear');
    for j = 2:Nt
        if t{1,j}(end) > t_L  ;
            dd_fL = [dd_fL, interp1(t{1,j}, dd{1,j}, t_L,'linear')];
```

203

```matlab
            Td_fL = [Td_fL, interp1(t{1,j}, Td{1,j}, t_L,'linear')];
        end
    end
    dd_fLp = dd_fL; % for plotting bar graph
    %
    Nmd_L = Nmd(1, 1:length(dd_fL)); % just Nmds for the droplets
    %                                  that remain
    Vol_fL = Nmd_L*pi.*dd_fL.^3/6;
    Vol_pct_fL = Vol_fL/sum(Vol_fL)*100;
    Vol_pct_fLp = Vol_pct_fL; % for plotting bar graph
    Vol_pct_fL_cum = cumsum(fliplr(Vol_pct_fL)); % cumul Vol in
    %                                      ascending order
    Vw_fL = sum(Vol_fL)*m_a*1e6*60; % volume flowrate (ml/min)
    %                                 for remaining droplets
    %
    if length(dd_fL) >= 2 % Only compute mean/median values if
        %                     two or more bins remaining
        % Droplet Mean diams.(D32, D43) and Dv10, Dv50 (= MMAD), Dv90
        D32_fL = sum(Nmd(1:length(dd_fL)).*dd_fL.^3)/...
            sum(Nmd(1:length(dd_fL)).*dd_fL.^2);
        D43_fL = sum(Nmd(1:length(dd_fL)).*dd_fL.^4)/...
            sum(Nmd(1:length(dd_fL)).*dd_fL.^3);
        % Spraytech calc for Dv10, Dv50 etc uses Dupper rather than
        % Davg so set up vector of Dupper sizes that match dd_fp
        % sizes
        dd_fLv = fliplr(dd_fL)*1e6;
        ind_SPL = find(drop_dist(3,:)> dd_fLv(1,1),1,'first');
        %index of matching droplet size
        dd_fSPL = drop_dist(3,ind_SPL(1,1));
        % Dupper droplet size
        for j = 2:length(dd_fL) % create vectors of indices and
            %                       Dupper droplet sizes
            ind_SPL = [ind_SPL, find(drop_dist(3,:)> dd_fLv(1,j), ...
                1,'first')];
            dd_fSPL = [dd_fSPL, drop_dist(3,ind_SPL(1,j))];
        end
        Dv10_fL = interp1(Vol_pct_fL_cum, dd_fSPL, 10, 'linear');
        Dv50_fL = interp1(Vol_pct_fL_cum, dd_fSPL, 50, 'linear');
        Dv90_fL = interp1(Vol_pct_fL_cum, dd_fSPL, 90, 'linear');
        span_fL = (Dv90_fL - Dv10_fL)/Dv50_fL;
    else
        D32_fL = 0; D43_fL = 0; Dv10_fL = 0; Dv50_fL = 0;
        Dv90_fL = 0; span_fL = 0;
    end
end


%
% ----------------------------------------------------------------
% Set up array of MODEL OUTPUT DISTRIBUTION (droplet size and vol%)
% for easy export to Excel.  At END of calculation and at L
% ----------------------------------------------------------------
%
m_o_d_end = flipud([dd_fp'*1000000, Vol_pct_fp']); % in ascending order
m_o_d_L = flipud([dd_fLp'*1000000, Vol_pct_fLp']);
%
% Array of Final Droplet distribution parameters for easy export to
% Excel. At END of calculation and at L
%
dist_param_end = [Dv10_f Dv50_f Dv90_f span_f D32_f*1e6 D43_f*1e6 ...
    0 Tinf(end) RHinf(end) L L_t{1,1}(end)*1000]';
dist_param_L = [Dv10_fL Dv50_fL Dv90_fL span_fL D32_fL*1e6 D43_fL*1e6 ...
    0 Tinf_fL RHinf_fL L L_t{1,1}(end)*1000]';
%
% ----------------------------------------------------------------
% SAVE RESULTS
% ----------------------------------------------------------------
% Finished all calculations: Write Workspace (all variables) to file
filedate = datestr(now, 'yyyy-mm-dd HH-MM-SS');
[~, comp_name] = system('hostname');
filename = ['Saved Runs\', filedate,' ', num2str(Nt),...
    ' bins ', comp_name(1:6)];
save(filename)
%
% Write summary data to an Excel Spreadsheet for easy transfer to
% distribution comparison spreadheets etc
xlsfilename = [filename, '.xlsx'];
dist_param_L_cell(:,1) = {'Expt Date' 'Calc Date'...
    'Notes 1' 'Notes 2' 'INPUTS' ...
    'Tinf_i' 'RHinf_i' 'Va_i' 'Td_ic' 'Vw' 'alphas' 'L' 'ID' ...
    'Distbn' '' 'OUTPUTS - Distbn Parameters at L' 'Dv10' 'Dv50'...
```

204

```
            'Dv90' 'span' 'D[32]' 'D[43]' '' '' '' 'Tinf(L)'...
            'RHinf(L)' 'L' 'Length(end)' '' 'OUTPUTS - Distbn at L'...
            'Diameter'};
        dist_param_L_cell(:,2) = {expt_date...
            [filedate, ' - (NORMAL model)'] ...
            notes1 notes2 '' Tinf_i RHinf_i ...
            Va_i Td_ic Vw alpha L ID in_drop_distbn '' '' Dv10_fL ...
            Dv50_fL Dv90_fL span_fL D32_fL*1e6 D43_fL*1e6 '' '' '' ...
            Tinf_fL RHinf_fL L L_t{1,1}(end)*1000 '' '' '% Volume'};
        dist_param_L_cell(:,3) = {'' '' '' '' '' 'C' '' 'l/min' 'C' 'ml/min' ...
            '' 'mm' 'mm' '' '' '' 'um' 'um' 'um' '' 'um' ...
            'um' '' '' '' 'C' '' 'mm' 'mm' '' '' ''};
        xlswrite(xlsfilename, dist_param_L_cell)
        xlswrite(xlsfilename, m_o_d_L, 1, 'A33')
    end
end
disp('  ***** Calculations Complete *****   ')
```

ODE function

```
function [dTP_dot] = Ms_11_5xjODE(t, dTP)
% Modified for change in droplet concentration to number per kg dry air
% (Note: No different from Ms_11_4xjODE just change name to match main
% program)
% dTP(j) = droplet diameters, dd(j) (m)
% dTP(N + j) = droplet temperatures, Td(j) (C)
% dTP(2N + 1) = water vapour pressure in ambient air, Pinf (Pa)
% dTP(2N + 2) = ambient humid air temperature, Tinf (C)
%
global K1 K6 Po KLm KLh alpham alphah Nmd N
%
%
RHinf = dTP(2*N + 1)/(pH2Os_pt_HAP_SI(Po,dTP(2*N + 2))*1000);
if RHinf > 1    % set RH to 1 if it goes over 1 as air becomes saturated
    RHinf = 1;
end
% Humid Air - remaining properties at Tinf ie dTP(2N + 2)
winf = W_ptpH2O_HAP_SI(Po, dTP(2*N + 2), dTP(2*N + 1)/1000);
% winf = W_ptphi_HAP_SI(Po, dTP(N + i),RHinf);
vinf = v_ptW_HAP_SI(Po, dTP(2*N + 2), winf);  % air sp. vol (m^3/kga)
Cpinf = cp_ptW_HAP_SI(Po, dTP(2*N + 2), winf)*1000;    % sp. ht cap of humid air
(J/kg.C)
massfrac = XiAir_W_HAP_SI(winf); % mass fraction of dry air in moist air
%
% ------------ Set up property arrays --------------
% Preallocate arrays for speed...
rho_w = zeros(1,N); Cp_w = zeros(1,N); h_w = zeros(1,N);
sigma_w = zeros(1,N); Pd = zeros(1,N); Tfilm = zeros(1,N); D_w = zeros(1,N);
wfilm = zeros(1,N); lam_a = zeros(1,N); Pfilm = zeros(1,N);
Cpwvap = zeros(1,N); Lm = zeros(1,N); Lh = zeros(1,N);Cm = zeros(1,N);
Ch = zeros(1,N);
%
for j = 1:N
% Liquid water properties at relevant Td's
% density of water droplet (kg/m^3)
rho_w(j) = 1/vliq_pt_97_SI(Po, dTP(N + j));  % density of water droplet (kg/m^3)
% specific heat capacity of water droplets (J/kg.C)
Cp_w(j) = cp_ptx_97(Po/100, dTP(N + j), -1)*1000;
% latent heat of vaporisation (J/kg)
h_w(j) = (hvaps_t_97_SI(dTP(N + j)) - hliqs_t_97_SI(dTP(N + j)))*1000;
% Surface Tension to enable calculation of Kelvin effect factor (N/m)
sigma_w(j) = Sigma_t_97(dTP(N + j))/1000;
% droplet sat. vapour pressure , including Kelvin effect (Pa)
Pd(j) = pH2Os_pt_HAP_SI(Po,dTP(N + j))*1000*...
    exp(K1*sigma_w(j)/((dTP(N + j)+273.15)*rho_w(j)*dTP(j)));
% Humid Air - Transport properties (k or lambda and Dw)at Tfilm's
% Film temperatures (C)
Tfilm(j) = (dTP(N + j) + dTP(2*N + 2))/2;
% Diffusion coefficients (m^2/s)
D_w(j) = 1.8948e-8/Po*(Tfilm(j) + 273.15)^2.072; % Correct values
% Specific humidity of film (kg/kgda)
wfilm(j) = W_ptphi_HAP_SI(Po,Tfilm(j),(1 + RHinf)/2);
% thermal conductivity of film (W/m.K)
lam_a(j) = Lambda_ptW_HAP_SI(Po, Tfilm(j), wfilm(j));
%
```

205

```matlab
% partial pressure of water vapour in the film (Pa)
Pfilm(j) = (Pd(j) + dTP(2*N + 1))/2;
% specific heat capacity of water vapour (J/kg.C) at film temp and pressure
Cpwvap(j) = cp_ptx_97(Pfilm(j)/100000, Tfilm(j), -1)*1000;
%
% Knudsen Correction factors
% mean free paths
Lm(j) = KLm*(Tfilm(j) + 273.15);
Lh(j) = KLh*(Tfilm(j) + 273.15);
Cm(j) = (1 + 2*Lm(j)/dTP(j))/(1 + (4/(3*alpham)+0.377)*2*Lm(j)/dTP(j) + ...
    4/(3*alpham)*(2*Lm(j)/dTP(j))^2);
Ch(j) = (1 + 2*Lh(j)/dTP(j))/(1 + (4/(3*alphah)+0.377)*2*Lh(j)/dTP(j) + ...
    4/(3*alphah)*(2*Lh(j)/dTP(j))^2);
end
%
% ODE's
dd_dot = K1*Cm.*D_w./(dTP(1:N)'.*rho_w).*(dTP(2*N + 1)/(dTP(2*N + 2)+273.15)...
    - Pd./(dTP((N + 1):2*N)' + 273.15)); % first ODE,  all droplet
Td_dot = (12*lam_a.*Ch.*(dTP(2*N + 2) - dTP((N + 1):2*N)') + 3*rho_w.*dTP(1:N)'.*...
    h_w.*dd_dot)./(rho_w.*Cp_w.*dTP(1:N)'.^2); % second ODE, all droplets
Pinf_dot = K6/vinf*(dTP(2*N + 2)+273.15)*sum(Nmd(1:N).*rho_w.*dTP(1:N)'.^2.*dd_dot);
% Tinf_dot = 0;  % use this when simulating Rao's model
Tinf_dot = pi*massfrac/(2*Cpinf)*...
    sum(Nmd(1:N).*dTP(1:N)'.*(dTP(2*N + 2) - dTP((N + 1):2*N)').*(rho_w.*dTP(1:N)'.*...
    Cpwvap.*dd_dot - 4*lam_a.*Ch));
dTP_dot = [dd_dot'; Td_dot'; Pinf_dot; Tinf_dot];
%
```

Completion function

```matlab
function [value,isterminal,direction] = finish5xj(t,y)
% Stop (Finish!) the integration when the diameter of the smallest droplet
% passes through zero (ie evaporates) OR when environment is saturated,
% (ie RH = 1)AND the temperature of the largest droplets is in equilibrium
% with the air temperature.
% STOP the integration in both cases.
%
global Po N
% Calculate RH from its definition rathr than using the LibHuAir prop
% function (problems if if goes just above 1)
RH = y(2*N + 1)/(pH2Os_pt_HAP_SI(Po,y(2*N + 2))*1000);
%
T_eqlbm = 1; % Set T_eqlbm = Td - Tinf to 1 until RH is close to 1
%
if RH > 0.999999 % when RH close to 1 then stop integration when T_eqlbm = 0
    T_eqlbm = y(N+1) - y(2*N + 2)-0.05;
end
%
value = [y(N) - .00000001 ; T_eqlbm]; % Detect diam. = 0 or temp equilibrium
isterminal = [1; 1];   % Stop the integration in both cases
direction = [-1; 0];   % Negative direction only for diameter
```

A 3.3 Ultrasound enhanced droplet evaporation model

Main body of code:

```matlab
% ITERATIVE version of Ms_11_5xj_US_main to process lots of input data sets
% at once.  So dispense with any output to command window... just calculate
% and save results. Reads input data in. Need to specify values of alpha to
% be used, any notes that apply and the Model input data to be used
%
% Also changed the way you set the length: Now L is set to the experimental
% value and if L < L(calc end) the distribution at L will be different from
% the final (end) values. If L > L(calc end) rather than stopping it sets
% the distribution values at L EQUAL to the final (end) values (since
% equilibrium has been reached so values shouldn't change...)
%
% Multi size droplet evaporation model - Any number(Nt)sizes of droplets
% originally based on single size droplet evaporation model: Rv10_3, but
% directly based on Ms_10_3_xj_main. Ver 11 adds distance calculation based
% on inside diameter of tubing... Also adds droplet MEAN and MEDIAN calcs
%
% v11_5 allows for the calculation to continue in cases where although
```

```matlab
% RH=1, temperature equilibrium has not yet been reached... so calculation
% stops when droplets and air temperature are the same.
%
% v11_4 allows for the changing volume flowrate (dry air mass flow rate
% remains constant) along the tube (as temperature of air changes) So need
% to input tubing diameter ID and target distance L...  to determine
% droplet distribution at some specified length along the tube -
% interpolates to find values at that distance.
%
% This means that the ODE's also had to be adjusted... and the droplet
% number concentration defined as number per kg of dry air (rather than
% kg/m^3)
%
% ODE 1: Nt mass balance ODE's (one for each droplet size).
% ODE 2: Nt energy balance ODE's (one for each droplet size).
% ODE 3: One mass balance ODE for the surrounding Air.
% ODE 4: One energy balance ODE for the surrounding Air.
%
% All fluid properties are calculated at actual temperature of fluids
% as solution progresses ie variable properties
%
% Includes Kelvin effect factor to adjust the saturation vapour pressure
% at the curved droplet surface.
%
% Also includes Knudsen correction factors for heat and mass transfer
%
clear
% ######## Input any notes relating to these set of runs...
notes1 = 'Running US model with alpha = 1 to see effect';
notes2 = 'Nu Correlation: Nu(j) = 2 + 0.55*Re_osc(j)^0.5*Pr_film(j)^(1/3);';
%
global K1 K6 Po KLm KLh alpham alphah Nmd N p_amp omega
%
% ######## Input here the values of alpha to be used
alphas = [1];
maxloopk = length(alphas);
%
% ######## Input the Model input data file o be used
input_datafile = 'Input Data\Model input data 2014-05-29 US 5W';
% this datafile contains all input parameters
load(input_datafile)
maxloopj = size(input_data,1);
%
for nj = 2:maxloopj
    msgdata = sprintf('Data loop %d of %d', nj - 1, maxloopj - 1);
    disp(msgdata) % feedback to Command Window on progress
    %
    for nk = 1:maxloopk
        alpha = alphas(nk);
        msgalpha = sprintf('   Alpha loop %d of %d', nk, maxloopk);
        disp(msgalpha) % feedback to Command Window on progress
        %
        expt_date = input_data{nj,1}; % Actual date experiment was
        %                               run and data recorded
        %
        starttime = ['--- ', datestr(now),...
            ' --------- START -------- Ms_11_5xj ------'];
        % disp (starttime)
        % tic
        %-----------------------------------------------------------------
        % INPUT parameters
        % ----------------------------------------------------------------
        % Air
        Tinf_i = input_data{nj,2}; % Initial bulk mean temperature of air (C)
        RHinf_i = input_data{nj,3};  % Initial relative humidity
        Va_i = input_data{nj,4};   % total Volume of air per minute (litres)
        % Water
        Td_ic = input_data{nj,5};% initial droplet temp.for all droplet sizes (C)
        Vw = input_data{nj,6}; % total volume of water per minute nebulised (ml)
        % input droplet distribution
        in_drop_distbn = ['Input Distributions\input drop dist ',...
            input_data{nj,7}];
        %
        % Accommodation coefficients Set above as part of for loop...
        % Set both alpha-m and alpha-h to same value
        %
        % Tubing
        ID = input_data{nj,9};        % Internal diameter of tubing (mm)
        L = input_data{nj,8};    % target distance along tube where droplet
        % distribution is desired to be known (mm)
```

207

```matlab
%
% Ultrasound **************
freq = input_data{nj,10};    % Frequency of applied ultrasound (kHz)
Power = input_data{nj,11};   % Power readout from Pusonics gear (W)
%
%---------------------------
% Set up droplet distribution
% ---------------------------
% Multi size droplet details.  MUST be from larger to smaller
load (in_drop_distbn)  % loads droplet distribution into the
% variable: drop_dist. Original data in mat file is small to LARGE,
% needs to be reordered LARGE to small.
Nt = size(drop_dist,2);      % number of droplet sizes or bins
dd_i = 1e-6*fliplr(drop_dist(1,:));
Vol_pct_i = 100 * fliplr(drop_dist(2,:));
Td_i = Td_ic*ones(1, Nt);          % initial droplet temperatures (C)
%
% Basic error checking of distribution
if length(dd_i) ~= Nt, disp('no. of droplet sizes incorrect'),...
        return, end
if length(Vol_pct_i) ~= Nt, disp('no. of %vols incorrect'),...
        return,  end
Total = single(sum (Vol_pct_i));
if abs(Total-100) >= 0.03
    errormsg = sprintf(...
        'Total volume percent is not equal to 100.0, %6.2f\r'...
        , Total);
    disp (errormsg)
    return
end
for j = 1:(Nt-1)
    if dd_i(j) <= dd_i(j + 1),...
            disp ('sizes not in descending order'), return, end
end
% ----------------------
% Constants
M_w = 18.015;      % molecular weight of water (kg/kmol)
Ru = 8314.5;       % Universal gas constant (J/kmol.K)
NA = 6.0221367e26; % Avogadro constant (/kmol)
Po = 101.325;      % Ambient total pressure (kPa)
% Ultrasound Constants
omega = 2*pi*freq*1000; % ultrasound frequency (rad/s)
% Sound Pressure Level of ultrasound (dB) related to Power (Pusonics)
SPL = 134.32 + log10(Power)*(153.29 - 134.32)/log10(75); % from Pusonics
p_amp = 10^(SPL/20)*0.00002*sqrt(2); % ultrasnd press amplitude (Pa)
% Note: * sqrt(2) since SPL formula is for RMS pressure... we want
% pressure amplitude...
%
% Determine initial AIR conditions
winf_i = W_ptphi_HAP_SI(Po,Tinf_i,RHinf_i); % humid. ratio (kgw/kga)
Pinf_i = pH2O_ptW_HAP_SI(Po, Tinf_i, winf_i)*1000; % vap press. (Pa)
vinf_i = v_ptW_HAP_SI(Po, Tinf_i,winf_i); % air sp. volume (m^3/kga)
%
% Mass flow rate of DRY AIR - assuming Va is vol.flowrate of MOIST air
m_a = Va_i/1000/60/vinf_i; % mass flow rate of dry air for
%                            number concentrations (kg/s)
% Droplet number concentrations - based on mass flow rate of dry air
% Nd = Vw/100*6*1000/(1e6*pi*Va)*Vol_pct_i./dd_i.^3; OLD DEFINITION
Nmd = Vw*6/(1e6*60*pi*m_a)*Vol_pct_i/100./dd_i.^3; % (no. of drops/kga)
%
% Droplet Mean diameters (D32, D43) and Dv10, Dv50 (= MMAD), Dv90
D32_i = sum(Nmd.*dd_i.^3)/sum(Nmd.*dd_i.^2);
D43_i = sum(Nmd.*dd_i.^4)/sum(Nmd.*dd_i.^3);
Vol_pct_i_cum = cumsum(drop_dist(2,:)*100); % smallest to largest
% Spraytech calc for Dv10, Dv50 etc (uses Dupper rather than Davg)
Dv10_i = interp1(Vol_pct_i_cum, drop_dist(3,:), 10, 'linear');
Dv50_i = interp1(Vol_pct_i_cum, drop_dist(3,:), 50, 'linear');
Dv90_i = interp1(Vol_pct_i_cum, drop_dist(3,:), 90, 'linear');
span_i = (Dv90_i - Dv10_i)/Dv50_i;
%
%
% Initial conditions
initial_condxi = [dd_i Td_i Pinf_i Tinf_i];
%
% Knudsen Correction Factors - Constant parts
dH2O = 310e-12;  % effective diameter of water molecule (m)
dAir = 360e-12;  % effective diameter of air molecule (m)
KLm = Ru/(sqrt(2)*pi*dH2O^2*NA*Po*1000); % mean free path - const. parts
KLh = Ru/(sqrt(2)*pi*dAir^2*NA*Po*1000); % mean free path - const. parts
alpham = alpha; % accomodation coefficient (mass transfer)
```

```matlab
alphah = alpha; % accomodation coefficient (heat transfer)
%
% ODE Constant parts
K1 = 2*M_w/Ru;    % constant for ODE 1 and for Kelvin effect factor
K6 = -pi*Ru/(2*M_w);   % constant for ODE 3's
%
% Flow parameters
Flow_area = pi*ID^2/4;      % tube flow area (m^2)
Vel_ai = Va_i/60/1000/Flow_area*1e6;  % initial velocity of air
% and droplets along tube (m/s)
%
% -----------------------------------------------------------------
% Begin SOLUTION of ODE equations for all Nt droplet sizes
% -----------------------------------------------------------------
% Preallocate cell arrays
ctxj = cell(1, Nt); csolnxj = cell(1, Nt); ciexj = zeros(1, Nt);
for j = 1:Nt  % loop around if smallest droplet size evaporates and
    % reduce the number of ODE's
    N = Nt - j + 1;
    %-------------------------------------------------------------
    % ODE solver and options
    options = odeset('Events', @finish5xj, 'Refine', 4,...
        'RelTol', 1e-4);
    %
    [txj,solnxj,texj,xexj,iexj] = ode15s(@Ms_11_5xj_US_ODE_f,...
        [0,100], initial_condxi, options);
    %-------------------------------------------------------------
    % Display current droplet-size bin number to see progress...
    msgstr = sprintf('Processed droplet-size bin no. %d of %d',...
        N, Nt);
    h = msgbox(msgstr, 'Progress', 'help', 'replace');
    %
    % Store results in cell arrays (where necessary)
    ctxj(1,N) = {txj};
    csolnxj(1,N) = {solnxj};
    % ctexj(1,N) = texj;
    % cxexj(1,N) = {xexj};
    ciexj(1,N) = iexj;
    % Continue solving for larger diameters if smallest diameter
    % has evaporated - set final values from last solution to
    % initial values for next solution
    if iexj == 1  % smallest diam. droplet has completely evaporated
        Tinf_ij = solnxj(end, (2*N+2)); % Initial bulk mean
        %                               temperature of air (C)
        Pinf_ij = solnxj(end, (2*N+1)); % initial air vap press.(Pa)
        % Multi size droplet details
        dd_ij = solnxj(end, 1:(N-1));     % Initial droplet diams.(m)
        Td_ij = solnxj(end, (N + 1):(2*N - 1)); % initial droplet
        %                               temperatures (C)
        %Initial conditions
        initial_condxi = [dd_ij Td_ij Pinf_ij Tinf_ij];
    else break  % if RHinf = 1 (ie iexj = 2) then stop solving ODE's
    end
end
%
% -----------------------------------------------------------------
% RESULTS: Set up cells and vectors for plotting and display of
% FINAL results
% -----------------------------------------------------------------
% Indices for generating results and preallocate cells and arrays
j = 1; k = 1; t = cell(1, Nt); dd = cell(1, Nt); Td = cell(1, Nt);
life = zeros(1,Nt); Pinf = zeros(1, Nt); Tinf = zeros(1, Nt);
L_t = cell(1,Nt); dist = zeros(1, Nt);
dd_f = zeros(1,Nt);  % Length cell array and final values
for j = 1:N
    t{1,j} = ctxj{1,Nt};
    dd{1,j} = csolnxj{1,Nt}(:,j);
    Td{1,j} = csolnxj{1,Nt}(:,(Nt + j));
    for k = 1:(Nt - N)
        t{1,j} = [t{1,j}; (t{1,j}(end) + ctxj{1,(Nt - k)}(2:end))];
        dd{1,j} = [dd{1,j}(:); csolnxj{1,(Nt - k)}(2:end,j)];
        Td{1,j} = [Td{1,j}(:);...
            csolnxj{1,(Nt - k)}(2:end,(Nt + j - k))];
    end
    if ciexj(1,1) == 1, life(j) = t{1,j}(end);...
    else life(j) = 99.9999; end
end
for j = (N + 1):Nt
    t{1,j} = ctxj{1,Nt};
    dd{1,j} = csolnxj{1,Nt}(:,j);
```

```
        Td{1,j} = csolnxj{1,Nt}(:,(Nt + j));
        for k = 1:(Nt - j)
            t{1,j} = [t{1,j}; (t{1,j}(end) + ctxj{1,(Nt - k)}(2:end))];
            dd{1,j} = [dd{1,j}(:); csolnxj{1,(Nt - k)}(2:end,j)];
            Td{1,j} = [Td{1,j}(:); csolnxj{1,(Nt - k)}(2:end,...
                (Nt + j - k))];
        end
        life(j) = t{1,j}(end);
    end
    Pinf = csolnxj{1,Nt}(:,(2*Nt + 1));
    Tinf = csolnxj{1,Nt}(:,(2*Nt + 2));
    for k = 1:(Nt - N)
        Pinf = [Pinf; csolnxj{1,(Nt-k)}(2:end,(2*Nt + 1 - 2*k))];
        Tinf = [Tinf; csolnxj{1,(Nt-k)}(2:end,(2*Nt + 2 - 2*k))];
    end
    % Calculate array of moisture content and RH of surrounding air
    winf = arrayfun(@(Tinfa, Pinfa) W_ptpH2O_HAP_SI(Po,Tinfa,Pinfa),...
        Tinf, Pinf/1000);
    % RHinf = arrayfun(@(Tinfa, winfa) phi_ptW_HAP_SI(Po,Tinfa,winfa),...
    %     Tinf, winf);
    % When RH reaches 1 if winf goes above the saturation pressure at
    % that temperature then RHinf is invalid... so calculate RHinf from
    % ratio of winf to winf_sat
    RHinf = arrayfun(@(Tinfa, Pinfa) Pinfa/pH2Os_pt_HAP_SI(Po,Tinfa),...
        Tinf, Pinf/1000);
    %
    % Final volume flow rate and velocity of air
    Va_f = m_a*v_ptW_HAP_SI(Po, Tinf(end), winf(end))*1000*60; % (l/min)
    Vel_af = Va_f/60/1000/Flow_area*1e6; % (m/s)
    %
    % Determine distances taking into account the change in
    % temperature, density and relative humidity of the air.  Use dry
    % air mass flow rate as the constant
    N_L = length(t{1,1});   % length of time vector
    L_tm = zeros(N_L, 1);   % initialise distance vector
    for j = 2:N_L
        Tinf_m = (Tinf(j - 1, 1) + Tinf(j, 1))/2;  % average air temp (C)
        winf_m = (winf(j - 1, 1) + winf(j, 1))/2;  % avg humidity (kgw/kga)
        vinf_m = v_ptW_HAP_SI(Po, Tinf_m, winf_m); % sp. volume (m^3/kga)
        Vel_m = m_a*vinf_m/Flow_area*1e6;          % velocity (m/s)
        DeltaL = Vel_m*(t{1,1}(j, 1) - t{1,1}(j-1, 1));  % extra distance
        L_tm(j,1) = L_tm(j - 1, 1) + DeltaL;  % distance vector
    end
    %
    % Generate cell array of times for plotting lengths, and final
    % values of droplet sizes and final lengths and final temperatures
    for k = 1:Nt
        L_t{1,k} = L_tm(1:length(t{1,k}));
        dd_f(1,k) = dd{1,k}(end);   % vector of final droplet sizes
        dist(1,k) = L_t{1,k}(end);  % vector of final distances for
        %                             each droplet size
        Td_f(1,k) = Td{1,k}(end);   % vector of final droplet temperatures
    end
    %
    % Vector of final droplet volumes and % volumes
    Vol_f = Nmd*pi.*dd_f.^3/6; % volume of droplets (m^3) per kg dry air
    Vol_pct_f = Vol_f/sum(Vol_f)*100;
    Vw_f = sum(Vol_f)*m_a*1e6*60; % volume flowrate (ml/min) for
    %                               remaining droplets
    %
    % Calculations for final droplet distribution and mean/median values
    %  Remove zeros from final values for plotting
    dd_fp = dd_f(1:N);
    Vol_pct_fp = Vol_pct_f(1:N); % ignore the volumes of the
    %                              'evaporated' droplets
    Vol_pct_fp_cum = cumsum(fliplr(Vol_pct_fp)); % cumul Vol in ascending order
    %
    if ciexj(1,1) == 0 % Only compute mean/median values if two
        %                or more bins remaining
        % Droplet Mean diameters (D32, D43) and Dv10, Dv50 (= MMAD), Dv90
        D32_f = sum(Nmd(1:N).*dd_fp.^3)/sum(Nmd(1:N).*dd_fp.^2);
        D43_f = sum(Nmd(1:N).*dd_fp.^4)/sum(Nmd(1:N).*dd_fp.^3);
        % Spraytech calc for Dv10, Dv50 etc uses Dupper rather than
        % Davg so set up vector of Dupper sizes that match dd_fp sizes
        dd_fv = fliplr(dd_fp)*1e6;
        ind_SP = find(drop_dist(3,:)> dd_fv(1,1),1,'first'); %index
        %                                    of matching droplet size
        dd_fSP = drop_dist(3,ind_SP(1,1)); % Dupper droplet size
        for j = 2:N % create vectors of indices and Dupper droplet sizes
            ind_SP = [ind_SP, find(drop_dist(3,:)> dd_fv(1,j),1,'first')];
```

210

```matlab
            dd_fSP = [dd_fSP, drop_dist(3,ind_SP(1,j))];
        end
        Dv10_f = interp1(Vol_pct_fp_cum, dd_fSP, 10, 'linear');
        Dv50_f = interp1(Vol_pct_fp_cum, dd_fSP, 50, 'linear');
        Dv90_f = interp1(Vol_pct_fp_cum, dd_fSP, 90, 'linear');
        span_f = (Dv90_f - Dv10_f)/Dv50_f;
    else
        D32_f = 0; D43_f = 0; Dv10_f = 0; Dv50_f = 0;
        Dv90_f = 0; span_f = 0;
    end
%
% --------------------------------------------------------------
% RESULTS: Determine values of results at DISTANCE L
% --------------------------------------------------------------
% Check experimental length L with length at end of calculations.
% If L > L(calc end) then set L values to end values
% If L < L(calc end) then calc L values and save along with end
% values
%
if L > L_t{1,1}(end)*1000 % L > L(calc end) so set L values to end values
    t_L = NaN;
    Tinf_fL = Tinf(end);
    winf_fL = winf(end);
    RHinf_fL = RHinf(end);
    Va_fL = Va_f;  % (l/min)
    Vel_afL = Vel_af;  % (m/s)
    %
    dd_fL = dd_f;
    dd_fLp = dd_fp;
    Td_fL = Td_f;
    %
    Nmd_L = Nmd; % just Nmds for the droplets that remain
    Vol_fL = Vol_f;
    Vol_pct_fL = Vol_pct_f;
    Vol_pct_fLp = Vol_pct_fp;
    % Vol_pct_fL_cum = cumsum(fliplr(Vol_pct_fL)); % cumul Vol in
    % ascending order
    Vw_fL = Vw_f; % volume flowrate (ml/min) for remaining droplets
    %
    D32_fL = D32_f;
    D43_fL = D43_f;
    Dv10_fL = Dv10_f;
    Dv50_fL = Dv50_f;
    Dv90_fL = Dv90_f;
    span_fL = span_f;
else
    % If L < L(calc end) then calculate values at L
    %
    % Vector of droplet sizes and temperatures at some distance L
    % from the initial mixing point
    %
    % Time at distance L
    t_L = interp1(L_tm, t{1,1}, L/1000, 'linear'); % time to
    % location L (s)
    % Air properties, flow rate and velocity at L
    Tinf_fL = interp1(t{1,1}, Tinf, t_L,'linear');
    winf_fL = interp1(t{1,1}, winf, t_L,'linear');
    RHinf_fL = interp1(t{1,1}, RHinf, t_L,'linear');
    Va_fL = m_a*v_ptW_HAP_SI(Po, Tinf_fL, winf_fL)*1000*60;  % (l/min)
    Vel_afL = Va_fL/60/1000/Flow_area*1e6;  % (m/s)
    %
    % Calculate volumes for final %-volume distribution at distance
    % L.  Interpolate (linear) to find droplet sizes at L
    dd_fL = interp1(t{1,1}, dd{1,1}, t_L,'linear');
    Td_fL = interp1(t{1,1}, Td{1,1}, t_L,'linear');
    for j = 2:Nt
        if t{1,j}(end) > t_L  ;
            dd_fL = [dd_fL, interp1(t{1,j}, dd{1,j}, t_L,'linear')];
            Td_fL = [Td_fL, interp1(t{1,j}, Td{1,j}, t_L,'linear')];
        end
    end
    dd_fLp = dd_fL; % for plotting bar graph
    %
    Nmd_L = Nmd(1, 1:length(dd_fL)); % just Nmds for the droplets
    %                                  that remain
    Vol_fL = Nmd_L*pi.*dd_fL.^3/6;
    Vol_pct_fL = Vol_fL/sum(Vol_fL)*100;
    Vol_pct_fLp = Vol_pct_fL; % for plotting bar graph
    Vol_pct_fL_cum = cumsum(fliplr(Vol_pct_fL)); % cumul Vol in
    %                                               ascending order
```

211

```matlab
        Vw_fL = sum(Vol_fL)*m_a*1e6*60; % volume flowrate (ml/min)
        %                                 for remaining droplets
        %
        if length(dd_fL) >= 2 % Only compute mean/median values if
            %                         two or more bins remaining
            % Droplet Mean diams.(D32, D43) and Dv10, Dv50 (= MMAD), Dv90
            D32_fL = sum(Nmd(1:length(dd_fL)).*dd_fL.^3)/...
                sum(Nmd(1:length(dd_fL)).*dd_fL.^2);
            D43_fL = sum(Nmd(1:length(dd_fL)).*dd_fL.^4)/...
                sum(Nmd(1:length(dd_fL)).*dd_fL.^3);
            % Spraytech calc for Dv10, Dv50 etc uses Dupper rather than
            % Davg so set up vector of Dupper sizes that match dd_fp
            % sizes
            dd_fLv = fliplr(dd_fL)*1e6;
            ind_SPL = find(drop_dist(3,:)> dd_fLv(1,1),1,'first');
            %index of matching droplet size
            dd_fSPL = drop_dist(3,ind_SPL(1,1));
            % Dupper droplet size
            for j = 2:length(dd_fL) % create vectors of indices and
                %                       Dupper droplet sizes
                ind_SPL = [ind_SPL, find(drop_dist(3,:)> dd_fLv(1,j), ...
                    1,'first')];
                dd_fSPL = [dd_fSPL, drop_dist(3,ind_SPL(1,j))];
            end
            Dv10_fL = interp1(Vol_pct_fL_cum, dd_fSPL, 10, 'linear');
            Dv50_fL = interp1(Vol_pct_fL_cum, dd_fSPL, 50, 'linear');
            Dv90_fL = interp1(Vol_pct_fL_cum, dd_fSPL, 90, 'linear');
            span_fL = (Dv90_fL - Dv10_fL)/Dv50_fL;
        else
            D32_fL = 0; D43_fL = 0; Dv10_fL = 0; Dv50_fL = 0;
            Dv90_fL = 0; span_fL = 0;
        end
end


%
% ------------------------------------------------------------------
% Set up array of MODEL OUTPUT DISTRIBUTION (droplet size and vol%)
% for easy export to Excel.  At END of calculation and at L
% ------------------------------------------------------------------
%
m_o_d_end = flipud([dd_fp'*1000000, Vol_pct_fp']); % in ascending order
m_o_d_L = flipud([dd_fLp'*1000000, Vol_pct_fLp']);
%
% Array of Final Droplet distribution parameters for easy export to
% Excel. At END of calculation and at L
%
dist_param_end = [Dv10_f Dv50_f Dv90_f span_f D32_f*1e6 D43_f*1e6 ...
    0 Tinf(end) RHinf(end) L L_t{1,1}(end)*1000]';
dist_param_L = [Dv10_fL Dv50_fL Dv90_fL span_fL D32_fL*1e6 D43_fL*1e6 ...
    0 Tinf_fL RHinf_fL L L_t{1,1}(end)*1000]';
%
% ------------------------------------------------------------------
% SAVE RESULTS
% ------------------------------------------------------------------
% Finished all calculations: Write Workspace (all variables) to file
filedate = datestr(now, 'yyyy-mm-dd HH-MM-SS');
[~, comp_name] = system('hostname');
filename = ['Saved Runs\', filedate,' ', num2str(Nt),...
    ' bins ', comp_name(1:6)];
save(filename)
%
% Write summary data to an Excel Spreadsheet for easy transfer to
% distribution comparison spreadheets etc
xlsfilename = [filename, '.xlsx'];
dist_param_L_cell(:,1) = {'Expt Date' 'Calc Date'...
    'Notes 1' 'Notes 2' 'INPUTS' ...
    'Tinf_i' 'RHinf_i' 'Va_i' 'Td_ic' 'Vw' 'alphas' 'L' 'ID' ...
    'Distbn' '' 'ULTRASOUND' 'Frequency' 'SPL' 'Power' ''...
    'OUTPUTS - Distbn Parameters at L' 'Dv10' 'Dv50'...
    'Dv90' 'span' 'D[32]' 'D[43]' '' '' '' 'Tinf(L)'...
    'RHinf(L)' 'L' 'Length(end)' '' 'OUTPUTS - Size Distribution at L'...
    'Diameter'};
dist_param_L_cell(:,2) = {expt_date [filedate, ' - (ULTRASOUND model)'] ...
    notes1 notes2 '' Tinf_i RHinf_i ...
    Va_i Td_ic Vw alpha L ID in_drop_distbn '' '' freq SPL Power '' ''...
    Dv10_fL Dv50_fL Dv90_fL span_fL D32_fL*1e6 D43_fL*1e6 '' '' '' ...
    Tinf_fL RHinf_fL L L_t{1,1}(end)*1000 '' '' '% Volume'};
dist_param_L_cell(:,3) = {'' '' '' '' '' 'C' '' 'l/min' 'C' 'ml/min' ...
    '' 'mm' 'mm' '' '' '' 'kHz' 'dB' 'W' '' '' 'um' 'um' 'um' '' 'um' ...
    'um' '' '' '' 'C' '' 'mm' 'mm' '' '' ''};
```

212

```matlab
        xlswrite(xlsfilename, dist_param_L_cell)
        xlswrite(xlsfilename, m_o_d_L, 1, 'A38')
    end
end
disp('  ***** Calculations Complete *****    ')
```

ODE function

```matlab
function [dTP_dot] = Ms_11_5xj_US_ODE_f(t, dTP)
% Modified for Ultrasound enhancement, f version for speed enhancements
%
% Modified for change in droplet concentration to number per kg dry air
%
% dTP(j) = droplet diameters, dd(j) (m)
% dTP(N + j) = droplet temperatures, Td(j) (C)
% dTP(2N + 1) = water vapour pressure in ambient air, Pinf (Pa)
% dTP(2N + 2) = ambient humid air temperature, Tinf (C)
%
global K1 K6 Po Nmd N p_amp omega KLm KLh alpham alphah
%
%
RHinf = dTP(2*N + 1)/(pH2Os_pt_HAP_SI(Po,dTP(2*N + 2))*1000);
if RHinf > 1    % set RH to 1 if it goes over 1 as air becomes saturated
    RHinf = 1;
end
% Humid Air - remaining properties at Tinf ie dTP(2N + 2)
winf = W_ptpH2O_HAP_SI(Po, dTP(2*N + 2), dTP(2*N + 1)/1000);
% winf = W_ptphi_HAP_SI(Po, dTP(N + i),RHinf);
vinf = v_ptW_HAP_SI(Po, dTP(2*N + 2), winf);  % air sp. vol (m^3/kga)
Cpinf = cp_ptW_HAP_SI(Po, dTP(2*N + 2), winf)*1000;  % sp. ht cap of humid
% air (J/kg.C)
massfrac = XiAir_W_HAP_SI(winf); % mass fraction of dry air in moist air
%
% ============== Set up property arrays ==============
% Preallocate arrays for speed...
rho_w = zeros(1,N); Cp_w = zeros(1,N); h_w = zeros(1,N);
sigma_w = zeros(1,N); Pd = zeros(1,N); Tfilm = zeros(1,N); D_w = zeros(1,N);
wfilm = zeros(1,N); lam_a = zeros(1,N); rho_film = zeros(1,N);
c_film = zeros(1,N); nu_film = zeros(1,N); Pr_film = zeros(1,N);
Sc_film = zeros(1,N); Pfilm = zeros(1,N); Cpwvap = zeros(1,N);
v_amp = zeros(1,N); Re_osc = zeros(1,N); Nu = zeros(1,N); h_H = zeros(1,N);
h_M = zeros(1,N); Sh = zeros(1,N);
Lm = zeros(1,N); Lh = zeros(1,N);Cm = zeros(1,N); Ch = zeros(1,N);
%
for j = 1:N
% -------- Liquid water properties at relevant Td's
% density of water droplets (kg/m^3)
rho_w(j) = 1/vliq_pt_97_SI(Po, dTP(N + j)); % density of water drop (kg/m^3)
% specific heat capacity of water droplets (J/kg.C)
Cp_w(j) = cp_ptx_97(Po/100, dTP(N + j), -1)*1000;
% latent heat of vaporisation (J/kg)
h_w(j) = (hvaps_t_97_SI(dTP(N + j)) - hliqs_t_97_SI(dTP(N + j)))*1000;
% Surface Tension to enable calculation of Kelvin effect factor (N/m)
sigma_w(j) = Sigma_t_97(dTP(N + j))/1000;
% droplet sat. vapour pressure , including Kelvin effect (Pa)
Pd(j) = pH2Os_pt_HAP_SI(Po,dTP(N + j))*1000*...
    exp(2*K1*sigma_w(j)/((dTP(N + j)+273.15)*rho_w(j)*dTP(j)));
% -------- Humid Air - Transport properties (k or lambda and Dw)at Tfilm's
% Film temperatures (C)
Tfilm(j) = (dTP(N + j) + dTP(2*N + 2))/2;
% Diffusion coefficients (m^2/s)
D_w(j) = 1.8948e-8/Po*(Tfilm(j) + 273.15)^2.072; % Correct values
% from Marrero & Martin 1972
% Specific humidity of humid air in film (kg/kgda)
wfilm(j) = W_ptphi_HAP_SI(Po,Tfilm(j),(1 + RHinf)/2);
% thermal conductivity of humid air in film (W/m.K)
lam_a(j) = Lambda_ptW_HAP_SI(Po, Tfilm(j), wfilm(j));
% density of humid air in film (kg/m^3)
rho_film(j) = Rho_ptW_HAP_SI(Po,Tfilm(j),wfilm(j));
% speed of sound in humid air in film (m/s)
c_film(j) = c_ptW_HAP_SI(Po,Tfilm(j),wfilm(j));
% dynamic viscosity of humid air in film (Pa s)
eta_film(j) = Eta_ptW_HAP_SI(Po,Tfilm(j),wfilm(j));
% kinematic viscosity of humid air in film (m^2/s)
% nu_film(j) = Ny_ptW_HAP_SI(Po,Tfilm(j),wfilm(j));
nu_film(j) = eta_film(j)/rho_film(j); % faster
% Specific heat capacity of humid air in film (J/kg.K)
Cp_film(j) = cp_ptW_HAP_SI(Po,Tfilm(j),wfilm(j))*1000;
```

213

```matlab
% Prandtl No. of humid air in film
% Pr_film(j) = Pr_ptW_HAP_SI(Po,Tfilm(j),wfilm(j));
Pr_film(j) = Cp_film(j)*eta_film(j)/lam_a(j); % faster
% Schmidt No. for the humid air in the film
Sc_film(j) = nu_film(j)/D_w(j);
% partial pressure of water vapour in the film (Pa)
Pfilm(j) = (Pd(j) + dTP(2*N + 1))/2;
% specific heat capacity of water vapour (J/kg.C) at film temp and pressure
Cpwvap(j) = cp_ptx_97(Pfilm(j)/100000, Tfilm(j), -1)*1000;
%
% -------- Convection coefficients in the film, h_M and h_H ------
% Velocity amplitude of the ultrasound wave (m/s)
v_amp(j) = p_amp/(rho_film(j)*c_film(j));
% Reynolds No. (oscillating)
Re_osc(j) = v_amp(j)*dTP(j)/nu_film(j);
% Re_s(j) = v_amp(j)^2/(nu_film(j)*freq_rad); % Gopinath & Mills 1993 eqn (8)
% Nusselt Number
% Nu(j) = 2; % Normal conduction (for sphere) For checking with Non U/S model
% Nu(j) = 1.413*Pr_film(j)^0.7*Re_s(j)^0.5; % Gopinath & Mills 1993 eqn (48)
% Nu(j) = 5.1; % Burdukov
Nu(j) = 2 + 0.55*Re_osc(j)^0.5*Pr_film(j)^(1/3); %Larsen, normal correlation
h_H(j) = Nu(j)*lam_a(j)/dTP(j);
% Sherwood number
% Sh(j) = 2; % Normal conduction (for sphere) For checking with Non U/S model
% Sh(j) = Nu(j); % Heat & Mass Transfer analogy
% Sh(j) = 5.1; % Burdukov For checking with Normal model
Sh(j) = 2 + 0.55*Re_osc(j)^0.5*Sc_film(j)^(1/3); %Larsen, normal correlation
h_M(j) = Sh(j)*D_w(j)/dTP(j);

% Knudsen Correction factors
% mean free paths
Lm(j) = KLm*(Tfilm(j) + 273.15);
Lh(j) = KLh*(Tfilm(j) + 273.15);
Cm(j) = (1 + 2*Lm(j)/dTP(j))/(1 + (4/(3*alpham)+0.377)*2*Lm(j)/dTP(j) + ...
    4/(3*alpham)*(2*Lm(j)/dTP(j))^2);
Ch(j) = (1 + 2*Lh(j)/dTP(j))/(1 + (4/(3*alphah)+0.377)*2*Lh(j)/dTP(j) + ...
    4/(3*alphah)*(2*Lh(j)/dTP(j))^2);
end
%
% ODE's
dd_dot = K1*Cm.*h_M./rho_w.*(dTP(2*N + 1)/(dTP(2*N + 2)+273.15)...
    - Pd./(dTP((N + 1):2*N)' + 273.15)); % ODE 1, all droplet sizes
Td_dot = (6*h_H.*Ch.*(dTP(2*N + 2) - dTP((N + 1):2*N)') + 3*rho_w.*...
    h_w.*dd_dot)./(rho_w.*Cp_w.*dTP(1:N)'); % ODE 2, all droplet sizes
Pinf_dot = K6*(dTP(2*N + 2)+273.15)/vinf*sum(Nmd(1:N).*...
    rho_w.*dTP(1:N)'.^2.*dd_dot); % ODE 3,
% Tinf_dot = 0;  % use this when simulating Rao's model
Tinf_dot = pi*massfrac/(2*Cpinf)*...
    sum(Nmd(1:N).*dTP(1:N)'.^2.*(dTP(2*N + 2) - dTP((N + 1):2*N)').*...
    (rho_w.*Cpwvap.*dd_dot - 2*h_H.*Ch));
dTP_dot = [dd_dot'; Td_dot'; Pinf_dot; Tinf_dot];
%
```

Completion function

```matlab
function [value,isterminal,direction] = finish5xj(t,y)
% Stop (Finish!) the integration when the diameter of the smallest droplet
% passes through zero (ie evaporates) OR when environment is saturated,
% (ie RH = 1)AND the temperature of the largest droplets is in equilibrium
% with the air temperature.
% STOP the integration in both cases.
%
global Po N
% Calculate RH from its definition rathr than using the LibHuAir prop
% function (problems if if goes just above 1)
RH = y(2*N + 1)/(pH2Os_pt_HAP_SI(Po,y(2*N + 2))*1000);
%
T_eqlbm = 1; % Set T_eqlbm = Td - Tinf to 1 until RH is close to 1
%
if RH > 0.999999 % when RH close to 1 then stop integration when T_eqlbm = 0
    T_eqlbm = y(N+1) - y(2*N + 2)-0.05;
end
%
value = [y(N) - .00000001 ; T_eqlbm]; % Detect diam. = 0 or temp equilibrium
isterminal = [1; 1];   % Stop the integration in both cases
direction = [-1; 0];   % Negative direction only for diameter
```

Appendix 4 - Detailed Results

A 4.1 Introduction

Experimental and theoretical model results are recorded in this appendix for each evaporation trial that was carried out.

A 4.2 Detailed results – Normal evaporation

Experimental data was recorded for each trial as described in Chapter 5, section 5.5. From this data the following results were generated for normal evaporation:

- Amount of water evaporation (measured in terms of the moisture content of the air at the inlet and outlet, kg of water per kg of dry air)

- Table of size distribution parameters: $Dv10$, $Dv50$, $Dv90$, $Span$, $D[3,2]$, $D[4,3]$ (at both inlet and outlet)

- Graph of droplet size distribution: % Volume versus droplet diameter at inlet and at outlet

The initial and boundary conditions for each trial were also entered into the poly-disperse droplet evaporation model described in Chapter 4 and comparative values for the droplet size distribution, distribution parameters and amount of water evaporation were determined. These were included along with the experimental results. Model results have been calculated for two cases, where the accommodation coefficients are set to a value of 0.04 and a value of 0.001.

Trial 4.2.1 Air flow: 6 lpm, Length: 245 mm, Temperature: ambient

Droplet size distributions

Air Flow rate: 6 lpm
Air Temp.: ambient
Conduit length: 245 mm
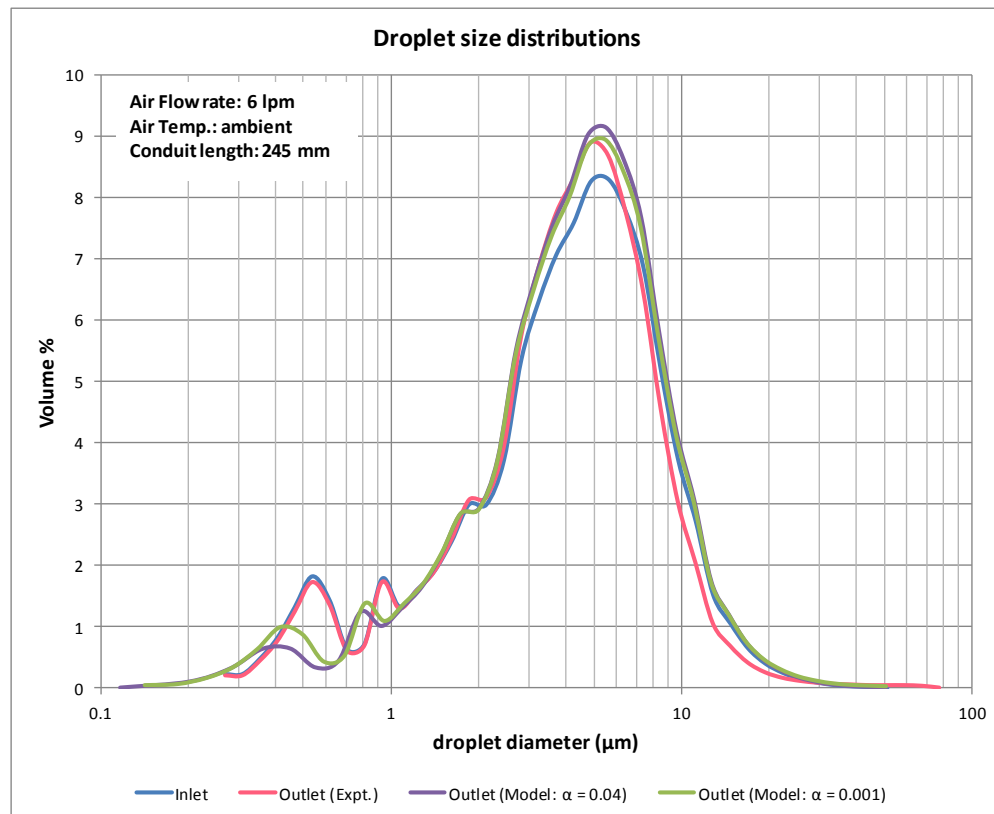
| Experiment Date | 28/03/2013 |
| Time | 15:01:55 - 15:05:48 |

Conduit Properties	Unit	Value
Diameter	mm	22.5
Length	mm	245

Parameter	Unit	INLET	Experimental Results at OUTLET	Model Results at OUTLET	
				α = 0.04	α = 0.001
Air Properties					
Flow rate	lpm	6.43	---	6.22	6.22
Temperature	°C	25.2	17.5	12.6	12.6
RH		0.142	0.916	1.00	1.00
Sp. Humidity	g/kg	2.821	11.504	9.103	9.105
Water Droplet Properties					
Flow rate	ml/min	0.338	---	0.291	0.291
Temperature	°C	26.5	---	12.6	12.6
Length to end of calculation				24.6	108

Parameter	Unit	Inlet	Outlet (Expt.)	Outlet (Model: α = 0.04)	Outlet (Model: α = 0.001)
Dv(10)	(μm)	1.04	1.09	1.50	1.35
Dv(50)	(μm)	4.34	4.19	4.75	4.67
Dv(90)	(μm)	9.38	8.68	9.81	9.76
Span		1.92	1.81	1.75	1.80
D[3][2]	(μm)	2.39	2.40	2.96	2.70
D[4][3]	(μm)	5.02	4.88	5.38	5.26
% Transm.		71.9%	50.5%		
Conc. (Cv)	ppm	19	40		

Trial 4.2.2 Air flow: 10 lpm, Length: 245 mm, Temperature: ambient

Droplet size distributions

Air Flow rate: 10 lpm
Air Temp.: ambient
Conduit length: 245 mm
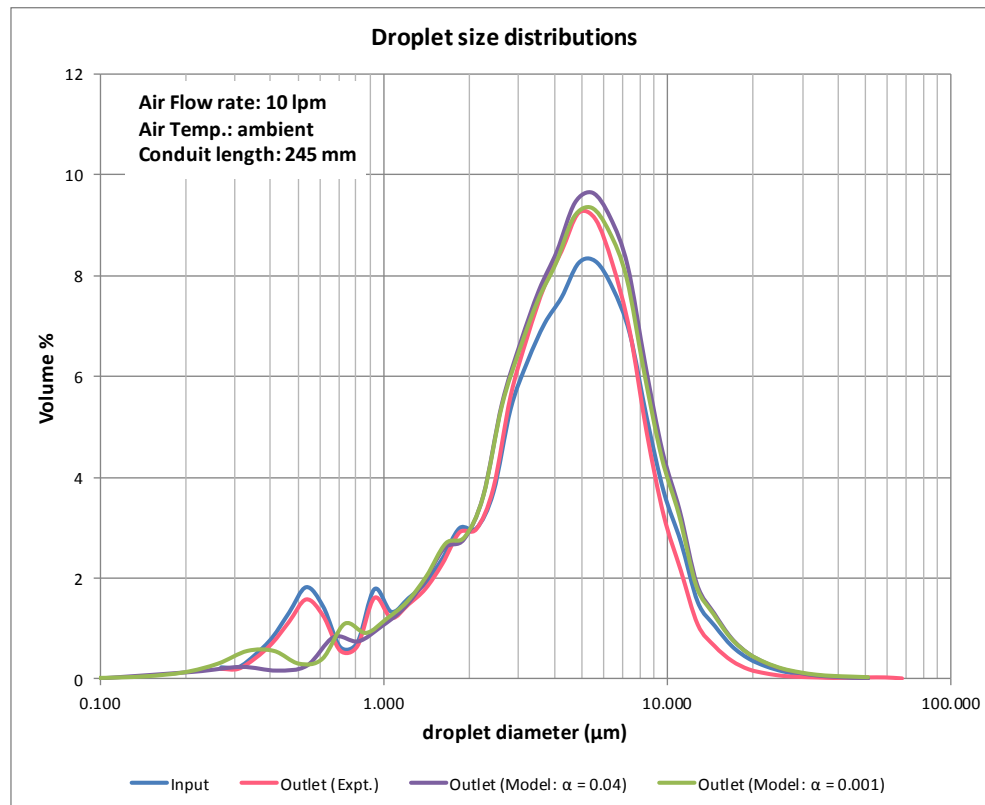
Experiment Date	28/03/2013
Time	15:12:05-15:16:09

Conduit Properties	Unit	Value
Diameter	mm	22.5
Length	mm	245

Parameter	Unit	INLET	Experimental Results at OUTLET	Model Results at OUTLET	
				α = 0.04	α = 0.001
Air Properties					
Flow rate	lpm	10.04	---	9.69	9.69
Temperature	°C	25.1	15.7	12.0	12.0
RH		0.135	0.904	1.00	1.00
Sp. Humidity	g/kg	2.665	10.102	8.789	8.789
Water Droplet Properties					
Flow rate	ml/min	0.338	---	0.266	0.266
Temperature	°C	27	---	12.0	12.0
Length to end of calculation				38.4	212

Parameter	Unit	Input	Outlet (Expt.)	Outlet (Model: α = 0.04)	Outlet (Model: α = 0.001)
Dv(10)	(µm)	1.04	1.20	1.79	1.59
Dv(50)	(µm)	4.34	4.31	4.98	4.87
Dv(90)	(µm)	9.38	8.62	10.05	9.98
Span		1.92	1.72	1.66	1.72
D[3][2]	(µm)	2.39	2.51	3.36	2.95
D[4][3]	(µm)	5.02	4.81	5.58	5.41
% Transm.		71.9%	67.2%		
Conc. (Cv)	ppm	19	24		

Trial 4.2.3 Air flow: 15 lpm, Length: 245 mm, Temperature: ambient

Droplet size distributions

Air Flow rate: 15 lpm
Air Temp.: ambient
Conduit length: 245 mm

Legend: Input — Outlet (Expt.) — Outlet (Model: α = 0.04) — Outlet (Model: α = 0.001)

Experiment Date	28/03/2013	
Time	15:19:00-15:23:05	

Conduit Properties	Unit	Value
Diameter	mm	22.5
Length	mm	245

Parameter	Unit	INLET	Experimental Results at OUTLET	Model Results at OUTLET	
				α = 0.04	α = 0.001
Air Properties					
Flow rate	lpm	15.1	---	14.57	14.60
Temperature	°C	25	14.5	11.8	12.5
RH		0.138	0.888	1.00	0.93
Sp. Humidity	g/kg	2.708	9.172	8.669	8.394
Water Droplet Properties					
Flow rate	ml/min	0.338	---	0.233	0.238
Temperature	°C	28	---	11.8	11.8
Length to end of calculation				55.7	627

Parameter	Unit	Input	Outlet (Expt.)	Outlet (Model: α = 0.04)	Outlet (Model: α = 0.001)
Dv(10)	(µm)	1.04	1.29	2.18	1.88
Dv(50)	(µm)	4.34	4.49	5.30	4.98
Dv(90)	(µm)	9.38	8.98	10.38	10.23
Span		1.92	1.72	1.55	1.68
D[3][2]	(µm)	2.39	2.62	3.78	3.28
D[4][3]	(µm)	5.02	4.99	5.82	5.56
% Transm.		71.9%	80.8%		
Conc. (Cv)	ppm	19	14		

Trial 4.2.4 Air flow: 20 lpm, Length: 245 mm, Temperature: ambient

Droplet size distributions

Air Flow rate: 20 lpm
Air Temp.: ambient
Conduit length: 245 mm

Legend: Input, Outlet (Expt.), Outlet (Model: α = 0.04), Outlet (Model: α = 0.001)
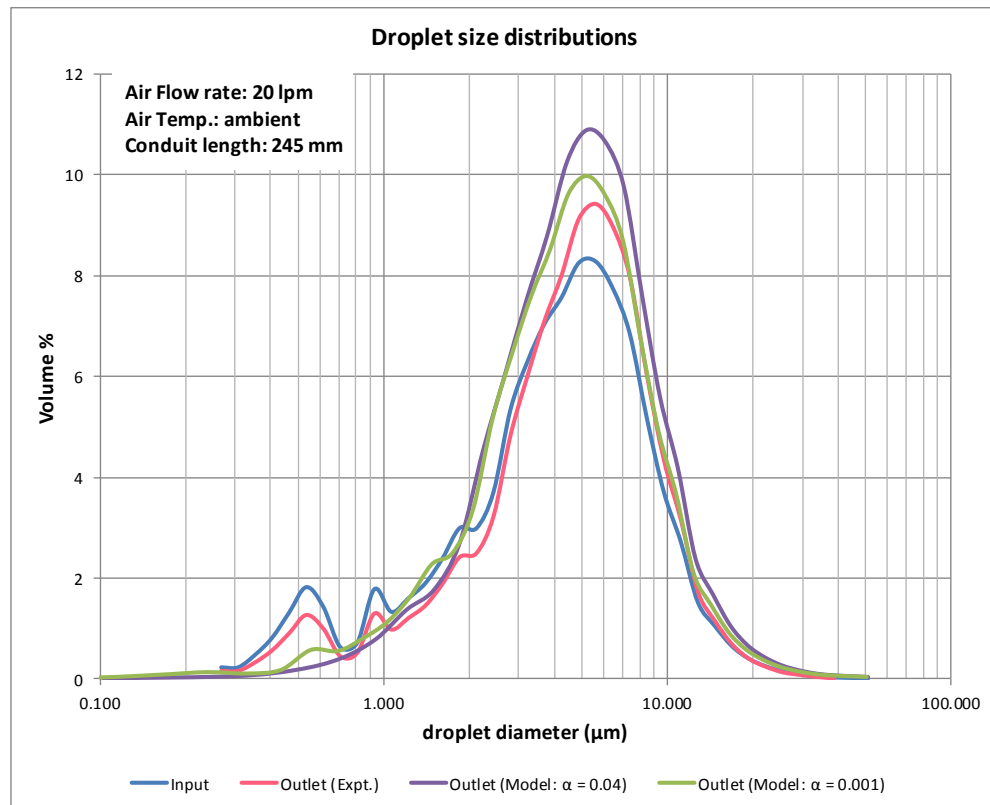
Experiment Date: 28/03/2013
Time: 15:25:31-15:29:34

Conduit Properties	Unit	Value
Diameter	mm	22.5
Length	mm	245

Parameter	Unit	INLET	Experimental Results at OUTLET	Model Results at OUTLET	
				α = 0.04	α = 0.001
Air Properties					
Flow rate	lpm	20.1	---	19.39	19.53
Temperature	°C	24.8	13.8	11.7	14.2
RH		0.146	0.889	1.00	0.75
Sp. Humidity	g/kg	2.832	8.770	8.607	7.574
Water Droplet Properties					
Flow rate	ml/min	0.338	---	0.202	0.226
Temperature	°C	27.2	---	11.7	11.8
Length to end of calculation				70.6	1440

Parameter	Unit	Input	Outlet (Expt.)	Outlet (Model: α = 0.04)	Outlet (Model: α = 0.001)
Dv(10)	(µm)	1.04	1.47	2.17	2.00
Dv(50)	(µm)	4.34	4.82	4.90	4.52
Dv(90)	(µm)	9.38	9.71	10.82	10.33
Span		1.92	1.71	1.76	1.84
D[3][2]	(µm)	2.39	2.84	4.06	3.41
D[4][3]	(µm)	5.02	5.38	6.04	5.61
% Transm.		71.9%	87.5%		
Conc. (Cv)	ppm	19	9		

Trial 4.2.5 Air flow: 25 lpm, Length: 245 mm, Temperature: ambient

Droplet size distributions

Air Flow rate: 25 lpm
Air Temp.: ambient
Conduit length: 245 mm

Legend: Input — Outlet (Expt.) — Outlet (Model: α = 0.04) — Outlet (Model: α = 0.001)
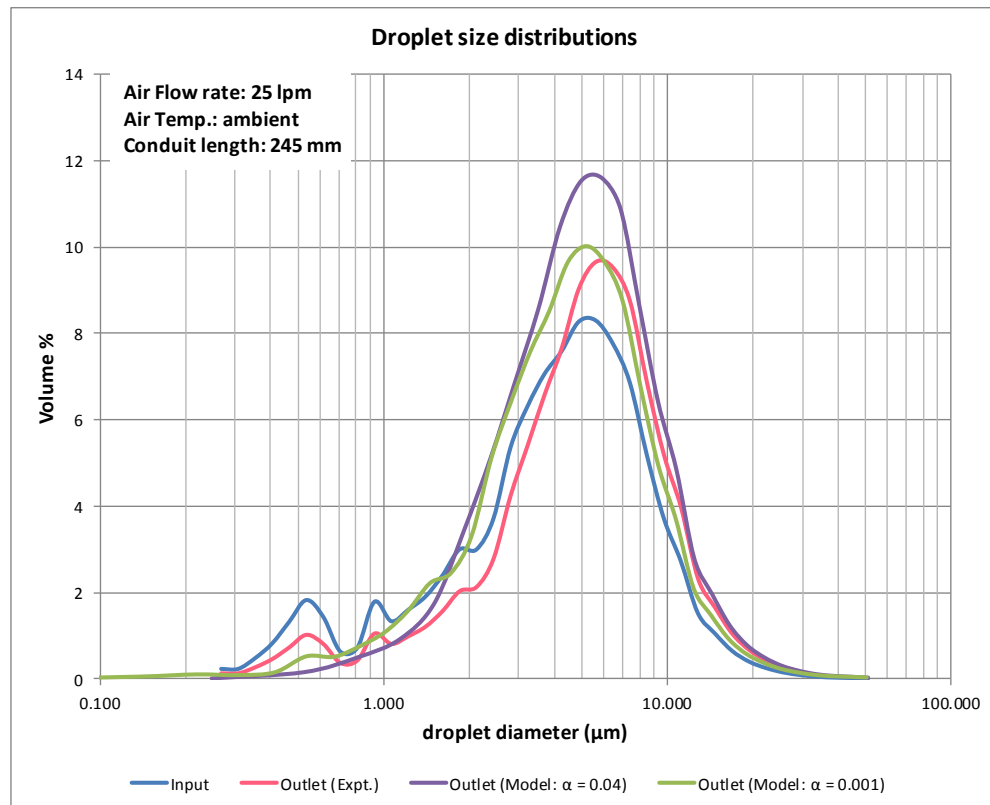
Experiment Date	28/03/2013
Time	15:31:11-15:35:34

Conduit Properties	Unit	Value
Diameter	mm	22.5
Length	mm	245

Parameter	Unit	INLET	Experimental Results at OUTLET	Model Results at OUTLET α = 0.04	α = 0.001
Air Properties					
Flow rate	lpm	25.1	---	24.19	24.51
Temperature	°C	24.6	13.1	11.2	15.8
RH		0.131	0.886	1.00	0.57
Sp. Humidity	g/kg	2.509	8.344	8.330	6.427
Water Droplet Properties					
Flow rate	ml/min	0.338	---	0.167	0.223
Temperature	°C	27.2	---	11.2	11.5
Length to end of calculation				136.8	2926

Parameter	Unit	Input	Outlet (Expt.)	Outlet (Model: α = 0.04)	Outlet (Model: α = 0.001)
Dv(10)	(µm)	1.04	1.75	2.38	2.03
Dv(50)	(µm)	4.34	5.26	5.27	4.55
Dv(90)	(µm)	9.38	10.62	11.39	10.37
Span		1.92	1.69	1.71	1.83
D[3][2]	(µm)	2.39	3.20	4.36	3.45
D[4][3]	(µm)	5.02	5.93	6.32	5.63
% Transm.		71.9%	91.4%		
Conc. (Cv)	ppm	19	7		

Trial 4.2.6 Air flow: 6 lpm, Length: 340 mm, Temperature: ambient

Droplet size distributions

Air Flow rate: 6 lpm
Air Temp.: ambient
Conduit length: 340 mm

Legend: Input — Outlet (Expt.) — Outlet (Model: α = 0.04) — Outlet (Model: α = 0.001)
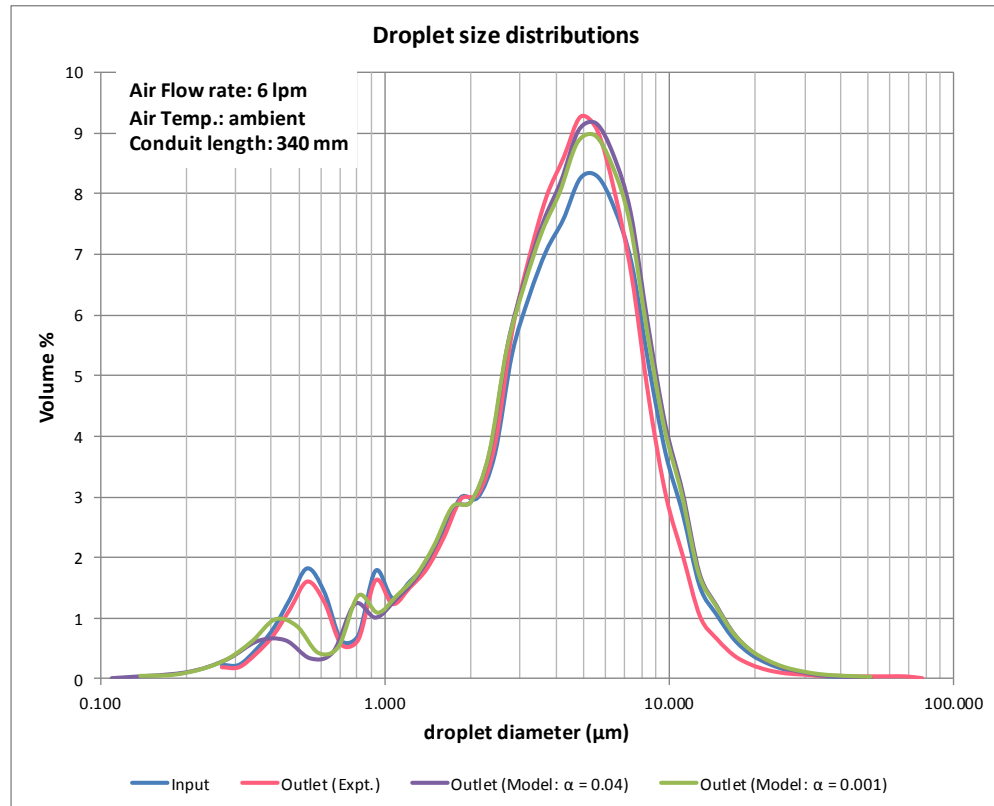
| Experiment Date | 28/03/2013 |
| Time | 16:04:05 - 16:08:48 |

Conduit Properties	Unit	Value
Diameter	mm	22.5
Length	mm	340

Parameter	Unit	INLET	Experimental Results at OUTLET	Model Results at OUTLET	
				α = 0.04	α = 0.001
Air Properties					
Flow rate	lpm	6.43	---	6.21	6.21
Temperature	°C	25.7	18.2	12.7	12.7
RH		0.137	0.911	1.00	1.00
Sp. Humidity	g/kg	2.803	11.966	9.208	9.208
Water Droplet Properties					
Flow rate	ml/min	0.338	---	0.290	0.290
Temperature	°C	26.4	---	12.7	12.7
Length to end of calculation				24.3	107

Parameter	Unit	Input	Outlet (Expt.)	Outlet (Model: α = 0.04)	Outlet (Model: α = 0.001)
Dv(10)	(µm)	1.04	1.18	1.52	1.36
Dv(50)	(µm)	4.34	4.25	4.75	4.68
Dv(90)	(µm)	9.38	8.60	9.82	9.77
Span		1.92	1.74	1.74	1.80
D[3][2]	(µm)	2.39	2.48	2.97	2.70
D[4][3]	(µm)	5.02	4.88	5.39	5.27
% Transm.		71.9%	52.0%		
Conc. (Cv)	ppm	19	39		

Trial 4.2.7 Air flow: 10 lpm, Length: 340 mm, Temperature: ambient

Droplet size distributions

Air Flow rate: 10 lpm
Air Temp.: ambient
Conduit length: 340 mm

Legend: Input; Outlet (Expt.); Outlet (Model: a = 0.04); Outlet (Model: a = 0.001)
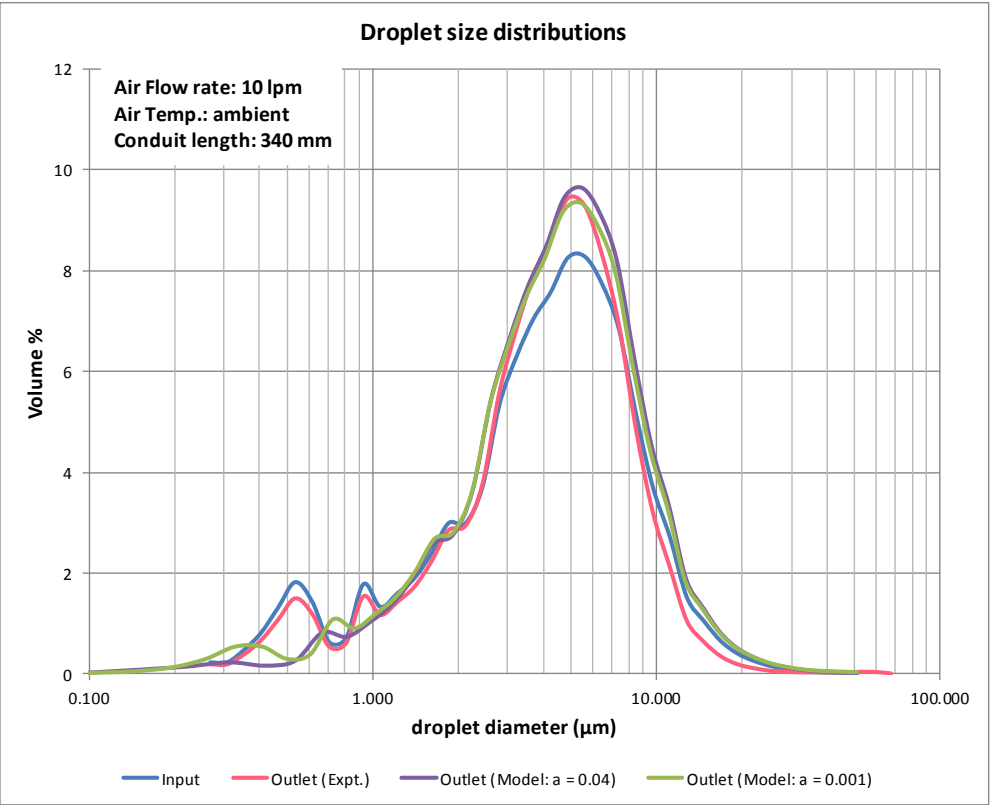
Experiment Date	28/03/2013	
Time	16:12:08 - 16:16:42	

Conduit Properties	Unit	Value
Diameter	mm	22.5
Length	mm	340

Parameter	Unit	INLET	Experimental Results at OUTLET	Model Results at OUTLET α = 0.04	α = 0.001
Air Properties					
Flow rate	lpm	10.1	---	9.75	9.75
Temperature	°C	25.4	16.2	12.3	12.3
RH		0.136	0.901	1.00	1.00
Sp. Humidity	g/kg	2.733	10.401	8.921	8.921
Water Droplet Properties					
Flow rate	ml/min	0.338	---	0.265	0.265
Temperature	°C	27.9	---	12.3	12.2
Length to end of calculation				38.4	215

Parameter	Unit	Input	Outlet (Expt.)	Outlet (Model: a = 0.04)	Outlet (Model: a = 0.001)
Dv(10)	(µm)	1.04	1.25	1.80	1.60
Dv(50)	(µm)	4.34	4.35	4.99	4.88
Dv(90)	(µm)	9.38	8.62	10.06	9.98
Span		1.92	1.69	1.66	1.72
D[3][2]	(µm)	2.39	2.56	3.37	2.96
D[4][3]	(µm)	5.02	4.86	5.58	5.41
% Transm.		71.9%	68.9%		
Conc. (Cv)	ppm	19	23		

Trial 4.2.8 Air flow: 15 lpm, Length: 340 mm, Temperature: ambient

Droplet size distributions

Air Flow rate: 15 lpm
Air Temp.: ambient
Conduit length: 340 mm

Legend: Input — Outlet (Expt.) — Outlet (Model: α = 0.04) — Outlet (Model: α = 0.001)
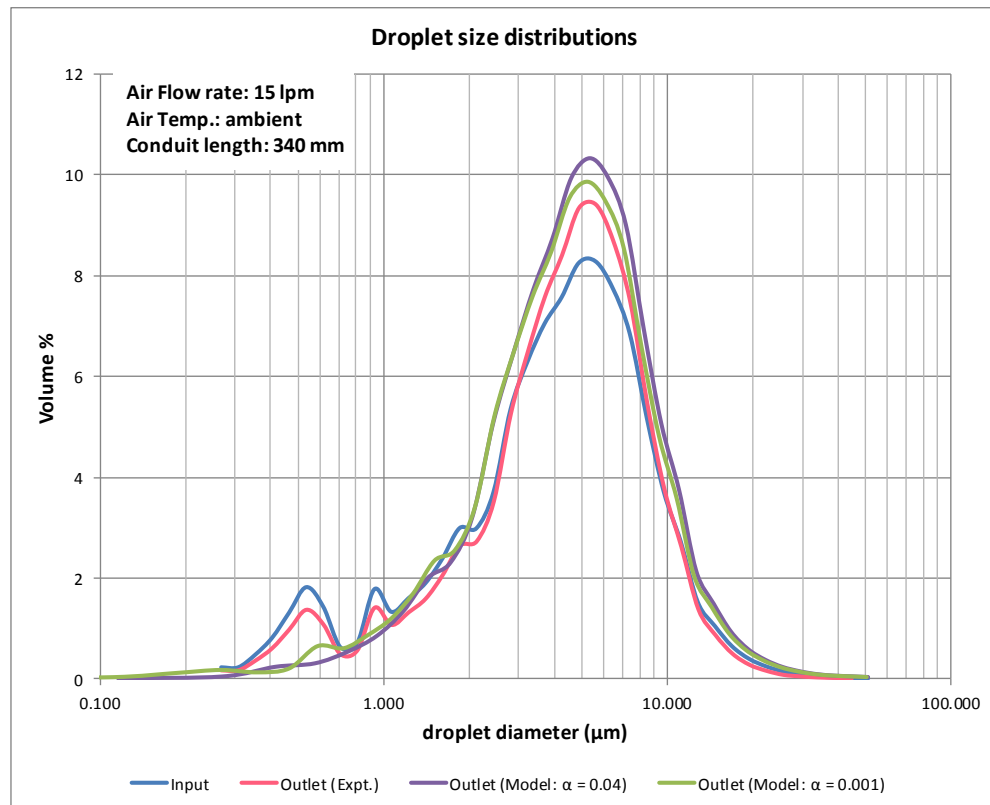
| Experiment Date | 28/03/2013 |
| Time | 16:19:16 - 16:23:28 |

Conduit Properties	Unit	Value
Diameter	mm	22.5
Length	mm	340

Parameter	Unit	INLET	Experimental Results at OUTLET	Model Results at OUTLET	
				α = 0.04	α = 0.001
Air Properties					
Flow rate	lpm	15.1	---	14.55	14.56
Temperature	°C	25.2	14.9	11.7	11.9
RH		0.125	0.891	1.00	0.97
Sp. Humidity	g/kg	2.482	9.448	8.565	8.455
Water Droplet Properties					
Flow rate	ml/min	0.338	---	0.230	0.233
Temperature	°C	26.9	---	11.6	11.6
Length to end of calculation				55.5	647

Parameter	Unit	Input	Outlet (Expt.)	Outlet (Model: α = 0.04)	Outlet (Model: α = 0.001)
Dv(10)	(µm)	1.04	1.36	2.14	1.94
Dv(50)	(µm)	4.34	4.57	5.32	4.48
Dv(90)	(µm)	9.38	9.04	10.40	10.28
Span		1.92	1.68	1.55	1.86
D[3][2]	(µm)	2.39	2.70	3.81	3.36
D[4][3]	(µm)	5.02	5.07	5.84	5.59
% Transm.		71.9%	81.5%		
Conc. (Cv)	ppm	19	14		

Trial 4.2.9 Air flow: 20.1 lpm, Length: 340 mm, Temperature: ambient

Droplet size distributions

Air Flow rate: 20 lpm
Air Temp.: ambient
Conduit length: 340 mm

Legend: Input, Outlet (Expt.), Outlet (Model: α = 0.04), Outlet (Model: α = 0.001)
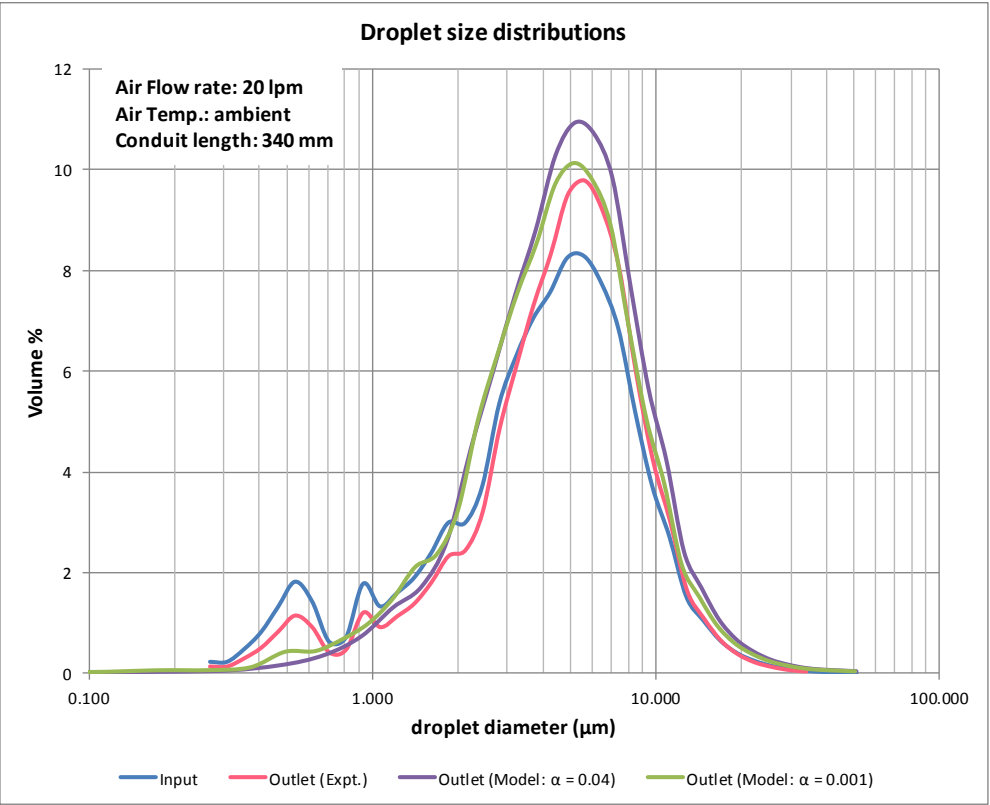
Experiment Date	28/03/2013	
Time	16:25:19 - 16:29:30	

Conduit Properties	Unit	Value
Diameter	mm	22.5
Length	mm	340

Parameter	Unit	INLET	Experimental Results at OUTLET	Model Results at OUTLET α = 0.04	α = 0.001
Air Properties					
Flow rate	lpm	20.1	---	19.38	19.46
Temperature	°C	24.8	13.87	11.4	13.0
RH		0.132	0.898	1.00	0.83
Sp. Humidity	g/kg	2.559	8.901	8.445	7.780
Water Droplet Properties					
Flow rate	ml/min	0.338	---	0.199	0.215
Temperature	°C	26.9	---	11.4	11.5
Length to end of calculation				71.0	1492

Parameter	Unit	Input	Outlet (Expt.)	Outlet (Model: α = 0.04)	Outlet (Model: α = 0.001)
Dv(10)	(µm)	1.04	1.56	2.19	1.96
Dv(50)	(µm)	4.34	4.84	4.93	4.61
Dv(90)	(µm)	9.38	9.58	10.86	10.44
Span		1.92	1.65	1.76	1.84
D[3][2]	(µm)	2.39	2.93	4.09	3.54
D[4][3]	(µm)	5.02	5.38	6.06	5.67
% Transm.		71.9%	88.7%		
Conc. (Cv)	ppm	19	9		

Trial 4.2.10 Air flow: 25 lpm, Length: 340 mm, Temperature: ambient

Droplet size distributions

Air Flow rate: 25 lpm
Air Temp.: ambient
Conduit length: 340 mm

Legend: Input — Outlet (Expt.) — Outlet (Model: α = 0.04) — Outlet (Model: α = 0.001)
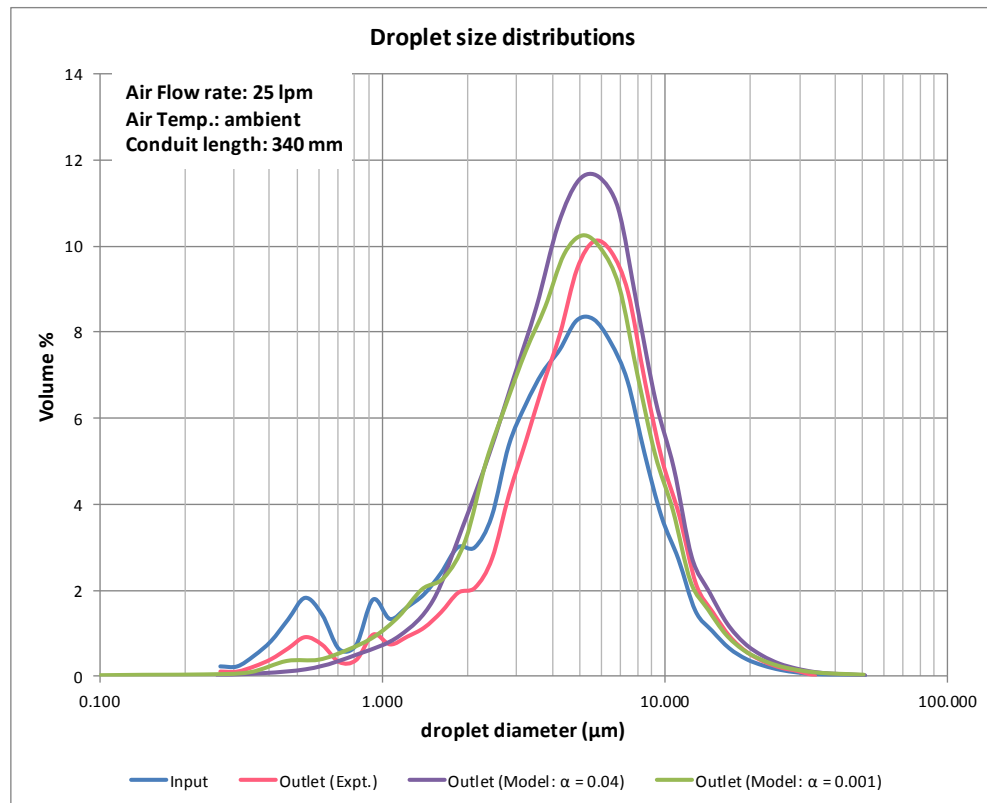
Experiment Date 28/03/2013
Time 16:30:43 - 16:35:04

Conduit Properties	Unit	Value
Diameter	mm	22.5
Length	mm	340

Parameter	Unit	INLET	Experimental Results at OUTLET	Model Results at OUTLET	
				α = 0.04	α = 0.001
Air Properties					
Flow rate	lpm	25.15	---	24.25	24.48
Temperature	°C	24.7	13.43	11.4	14.8
RH		0.138	0.904	1.00	0.67
Sp. Humidity	g/kg	2.660	8.704	8.447	7.037
Water Droplet Properties					
Flow rate	ml/min	0.338	---	0.168	0.209
Temperature	°C	27.8	---	11.4	11.6
Length to end of calculation				135.7	2938

Parameter	Unit	Input	Outlet (Expt.)	Outlet (Model: α = 0.04)	Outlet (Model: α = 0.001)
Dv(10)	(µm)	1.04	1.85	2.36	1.89
Dv(50)	(µm)	4.34	5.25	5.26	4.66
Dv(90)	(µm)	9.38	10.32	11.37	10.52
Span		1.92	1.61	1.71	1.85
D[3][2]	(µm)	2.39	3.29	4.35	3.58
D[4][3]	(µm)	5.02	5.86	6.31	5.70
% Transm.		71.9%	93.0%		
Conc. (Cv)	ppm	19	6		

Trial 4.2.11 Air flow: 6 lpm, Length: 245 mm, Temperature: 34 °C

Droplet size distributions

Air Flow rate: 6 lpm
Air Temp.: 34°C
Conduit length: 245 mm

Legend: Inlet — Outlet (Expt.) — Outlet (Model: α = 0.04) — Outlet (Model: α = 0.001)

X-axis: droplet diameter (µm)
Y-axis: Volume %
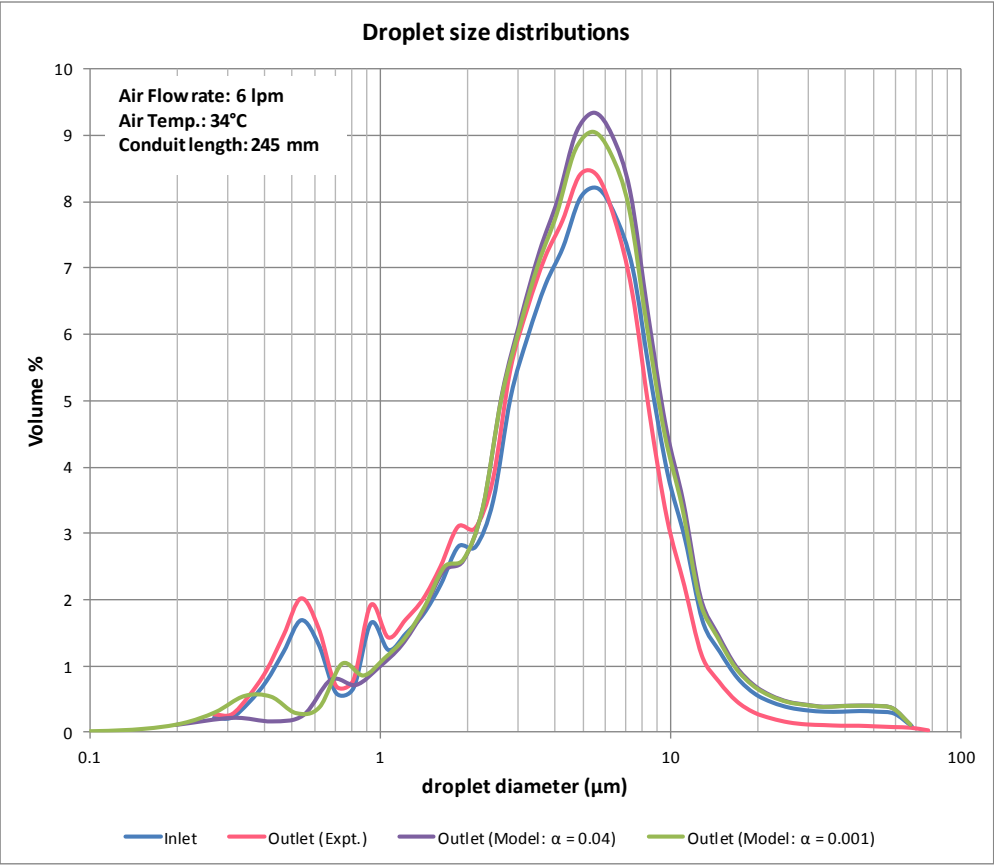
Experiment Date 29/11/2014
Time 10:27:03 - 10:33:06

Conduit Properties	Unit	Value
Diameter	mm	22.5
Length	mm	245

Parameter	Unit	INLET	Experimental Results at OUTLET	Model Results at OUTLET	
				α = 0.04	α = 0.001
Air Properties					
Flow rate	lpm	6.06	---	5.75	5.75
Temperature	°C	35.4	18.7	15.3	15.4
RH		0.0503	0.93	1.00	1.00
Sp. Humidity	g/kg	1.790	12.617	10.938	10.942
Water Droplet Properties					
Flow rate	ml/min	0.328	---	0.265	0.265
Temperature	°C	25.8	---	15.4	15.3
Length to end of calculation		0		32.7	121

Parameter	Unit	Inlet	Outlet (Expt.)	Outlet (Model: α = 0.04)	Outlet (Model: α = 0.001)
Dv(10)	(µm)	1.14	0.96	1.86	1.64
Dv(50)	(µm)	4.58	4.19	5.20	5.09
Dv(90)	(µm)	10.43	8.90	11.38	11.30
Span		2.03	1.90	1.83	1.89
D[3][2]	(µm)	2.53	2.28	3.58	3.10
D[4][3]	(µm)	5.96	4.98	6.68	6.50
% Transm.		72.8%	53.6%		
Conc. (Cv)	ppm	20	34		

Trial 4.2.12 Air flow: 10 lpm, Length: 245 mm, Temperature: 34 °C

Droplet size distributions

Air Flow rate: 10 lpm
Air Temp.: 34°C
Conduit length: 245 mm

Legend: Inlet — Outlet (Expt.) — Outlet (Model: α = 0.04) — Outlet (Model: α = 0.001)
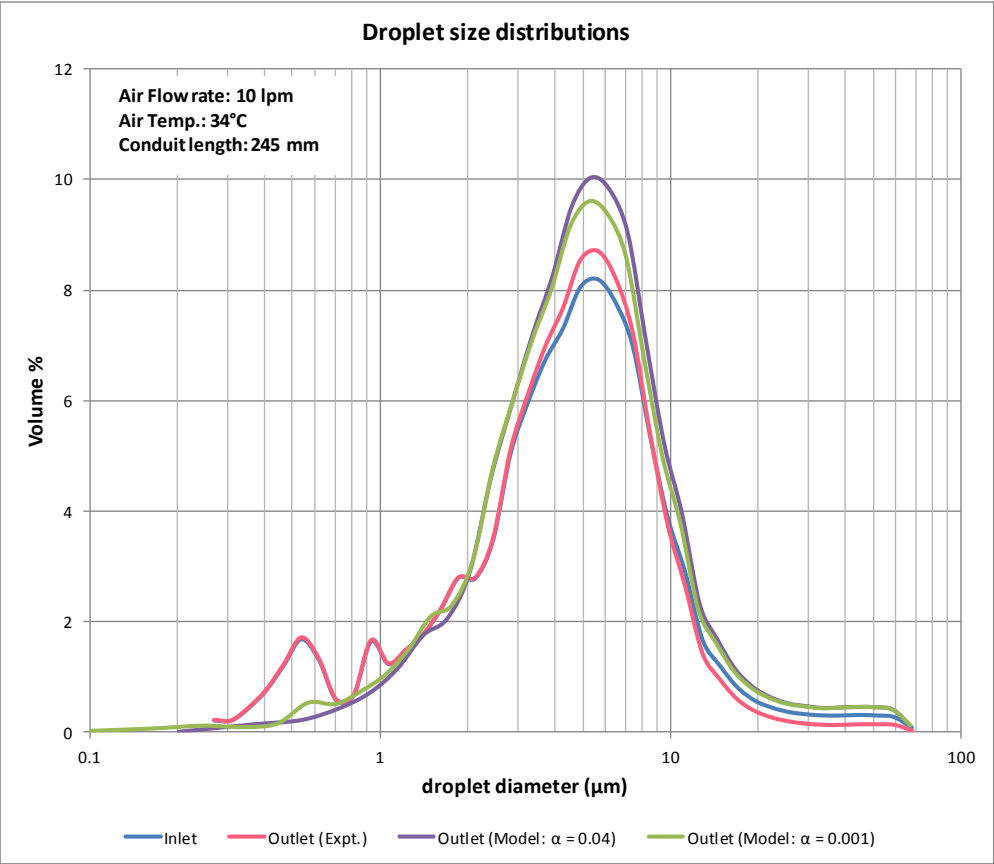
| Experiment Date | 29/11/2014 |
| Time | 10:12:17 - 10:18:05 |

Conduit Properties	Unit	Value
Diameter	mm	22.5
Length	mm	245

Parameter	Unit	INLET	Experimental Results at OUTLET	Model Results at OUTLET	
				α = 0.04	α = 0.001
Air Properties					
Flow rate	lpm	10	---	9.48	9.48
Temperature	°C	35.1	17.5	14.9	15.0
RH		0.0491	0.92	1.00	1.00
Sp. Humidity	g/kg	1.718	11.555	10.631	10.617
Water Droplet Properties					
Flow rate	ml/min	0.328	---	0.227	0.227
Temperature	°C	26.4	---	14.9	14.9
Length to end of calculation		0		53.0	308

Parameter	Unit	Inlet	Outlet (Expt.)	Outlet (Model: α = 0.04)	Outlet (Model: α = 0.001)
Dv(10)	(µm)	1.14	1.12	2.33	2.07
Dv(50)	(µm)	4.58	4.50	5.62	4.96
Dv(90)	(µm)	10.43	9.52	11.97	11.84
Span		2.03	1.87	1.72	1.97
D[3][2]	(µm)	2.53	2.49	4.08	3.62
D[4][3]	(µm)	5.96	5.38	7.12	6.85
% Transm.		72.8%	73.3%		
Conc. (Cv)	ppm	20	19		

Trial 4.2.13 Air flow: 15 lpm, Length: 245 mm, Temperature: 34 °C

Droplet size distributions

Air Flow rate: 15 lpm
Air Temp.: 34°C
Conduit length: 245 mm
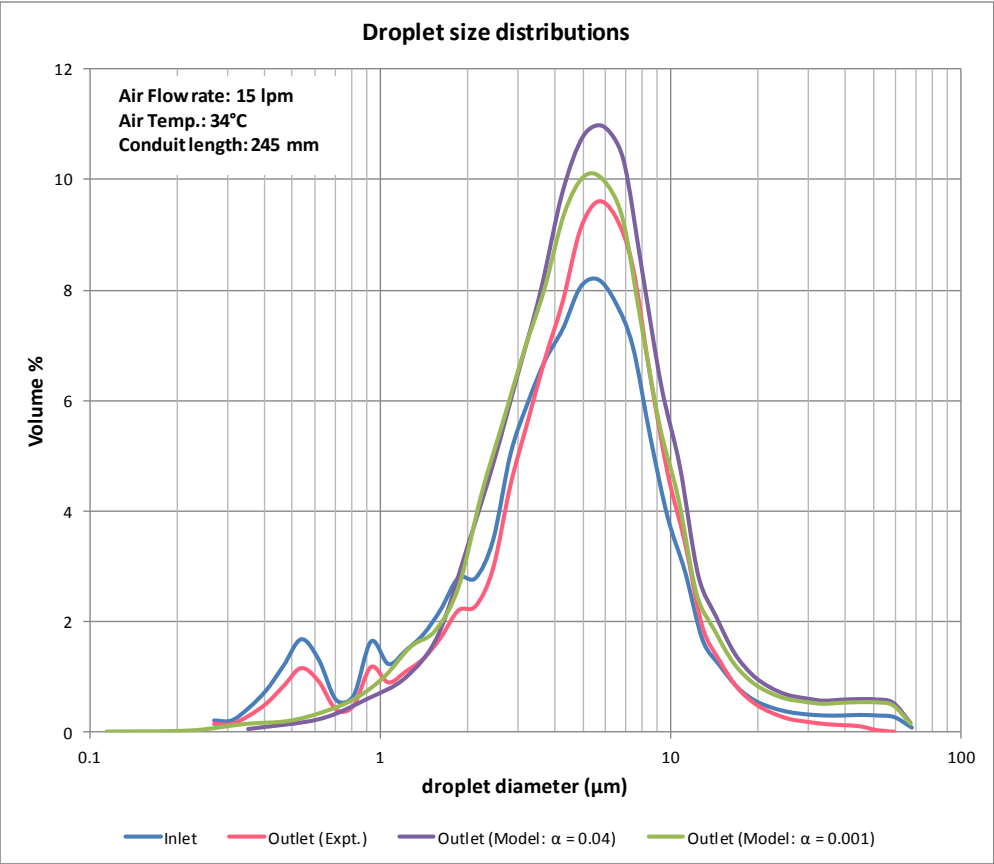
| Experiment Date | 29/11/2014 |
| Time | 09:45:51 - 09:52:01 |

Conduit Properties	Unit	Value
Diameter	mm	22.5
Length	mm	245

Parameter	Unit	INLET	Experimental Results at OUTLET	Model Results at OUTLET	
				α = 0.04	α = 0.001
Air Properties					
Flow rate	lpm	15.1	---	14.30	14.38
Temperature	°C	35.4	16.7	15.0	16.9
RH		0.0508	0.91	1.00	0.81
Sp. Humidity	g/kg	1.808	10.852	10.661	9.815
Water Droplet Properties					
Flow rate	ml/min	0.328	---	0.177	0.191
Temperature	°C	26.9	---	15.0	15.0
Length to end of calculation		0		77.1	1049

Parameter	Unit	Inlet	Outlet (Expt.)	Outlet (Model: α = 0.04)	Outlet (Model: α = 0.001)
Dv(10)	(µm)	1.14	1.58	2.50	2.10
Dv(50)	(µm)	4.58	5.06	5.46	5.06
Dv(90)	(µm)	10.43	10.21	13.54	12.76
Span		2.03	1.70	2.02	2.10
D[3][2]	(µm)	2.53	3.00	4.59	3.96
D[4][3]	(µm)	5.96	5.79	7.80	7.19
% Transm.		72.8%	86.9%		
Conc. (Cv)	ppm	20	10		

Trial 4.2.14 Air flow: 20 lpm, Length: 245 mm, Temperature: 34 °C

Droplet size distributions

Air Flow rate: 20 lpm
Air Temp.: 34°C
Conduit length: 245 mm

Legend: Inlet, Outlet (Expt.), Outlet (Model: α = 0.04), Outlet (Model: α = 0.001)

Conduit Properties	Unit	Value
Diameter	mm	22.5
Length	mm	245

Parameter	Unit	INLET	Experimental Results at OUTLET	Model Results at OUTLET	
				α = 0.04	α = 0.001
Air Properties					
Flow rate	lpm	20	---	18.91	19.20
Temperature	°C	35.8	16.2	14.9	20.5
RH		0.0474	0.92	1.00	0.55
Sp. Humidity	g/kg	1.724	10.624	10.632	8.298
Water Droplet Properties					
Flow rate	ml/min	0.328	---	0.127	0.179
Temperature	°C	25.7	---	14.9	15.1
Length to end of calculation		0		137.6	2778

Parameter	Unit	Inlet	Outlet (Expt.)	Outlet (Model: α = 0.04)	Outlet (Model: α = 0.001)
Dv(10)	(µm)	1.14	1.84	2.71	2.20
Dv(50)	(µm)	4.58	5.68	6.22	5.18
Dv(90)	(µm)	10.43	11.49	16.23	13.13
Span		2.03	1.70	2.17	2.11
D[3][2]	(µm)	2.53	3.36	5.12	4.05
D[4][3]	(µm)	5.96	6.43	8.81	7.33
% Transm.		72.8%	93.3%		
Conc. (Cv)	ppm	20	6		

Trial 4.2.15 Air flow: 6 lpm, Length: 245 mm, Temperature: 48 °C

Droplet size distributions

Air Flow rate: 6 lpm
Air Temp.: 48°C
Conduit length: 245 mm

Inlet — Outlet (Expt.) — Outlet (Model: α = 0.04) — Outlet (Model: α = 0.001)
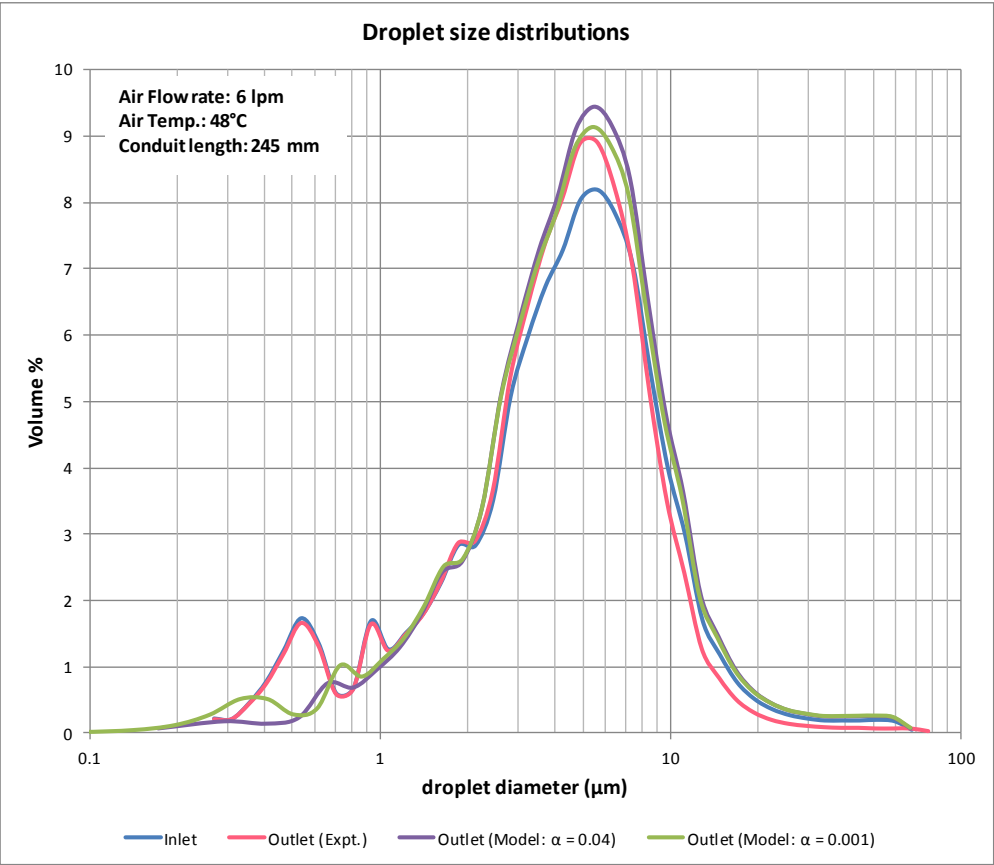
Experiment Date   29/11/2014
Time   14:50:35 - 14:54:50

Conduit Properties	Unit	Value
Diameter	mm	22.5
Length	mm	245

Parameter	Unit	INLET	Experimental Results at OUTLET	Model Results at OUTLET	
				α = 0.04	α = 0.001
Air Properties					
Flow rate	lpm	6.13	---	5.77	5.77
Temperature	°C	39.2	19.6	16.5	16.5
RH		0.0362	0.931	1.00	1.00
Sp. Humidity	g/kg	1.584	13.376	11.758	11.759
Water Droplet Properties					
Flow rate	ml/min	0.345	---	0.275	0.275
Temperature	°C	25.2	---	16.5	16.4
Length to end of calculation		0		30.5	115

Parameter	Unit	Inlet	Outlet (Expt.)	Outlet (Model: α = 0.04)	Outlet (Model: α = 0.001)
Dv(10)	(µm)	1.10	1.15	1.87	1.65
Dv(50)	(µm)	4.54	4.40	5.20	5.09
Dv(90)	(µm)	10.15	9.04	10.95	10.85
Span		1.99	1.79	1.75	1.81
D[3][2]	(µm)	2.49	2.49	3.58	3.10
D[4][3]	(µm)	5.66	5.13	6.35	6.16
% Transm.		70.8%	50.6%		
Conc. (Cv)	ppm	21	41		

Trial 4.2.16 Air flow: 10 lpm, Length: 245 mm, Temperature: 48 °C

Droplet size distributions

Air Flow rate: 10 lpm
Air Temp.: 48°C
Conduit length: 245 mm

Legend: Inlet — Outlet (Expt.) — Outlet (Model: α = 0.04) — Outlet (Model: α = 0.001)
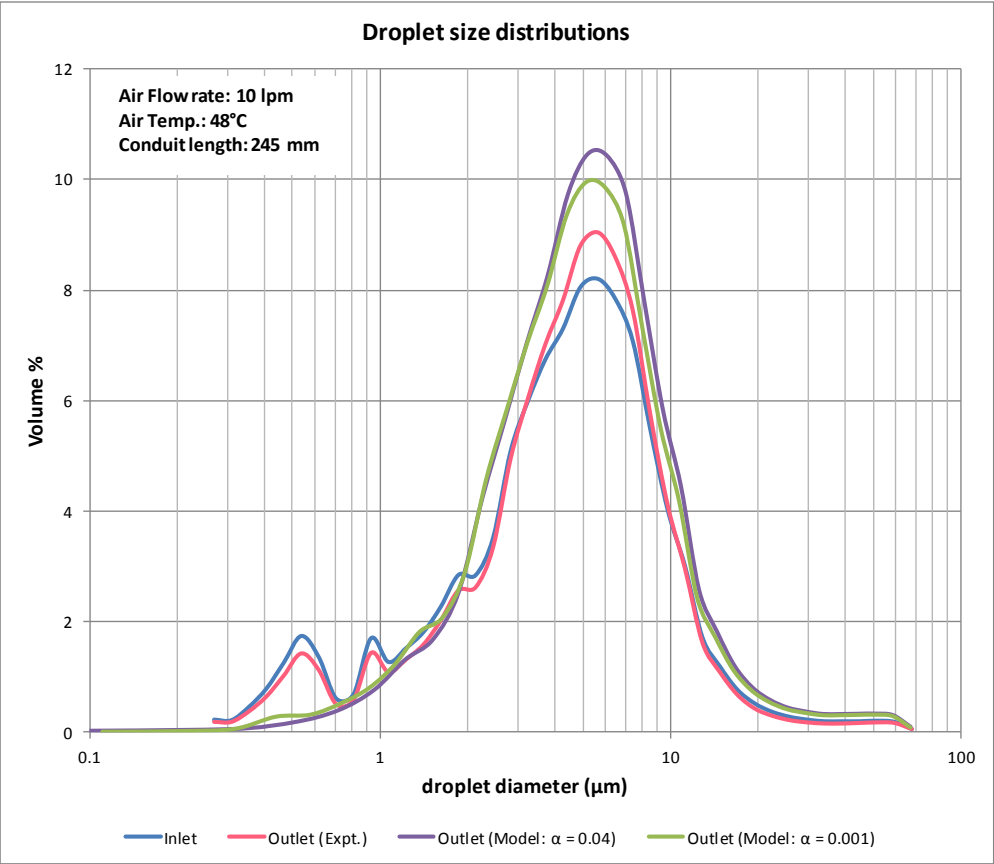
| Experiment Date | 29/11/2014 |
| Time | 14:38:19 - 14:43:24 |

Conduit Properties	Unit	Value
Diameter	mm	22.5
Length	mm	245

Parameter	Unit	INLET	Experimental Results at OUTLET	Model Results at OUTLET	
				α = 0.04	α = 0.001
Air Properties					
Flow rate	lpm	10.14	---	9.46	9.46
Temperature	°C	44.7	20.3	17.9	18.0
RH		0.0206	0.923	1.00	0.99
Sp. Humidity	g/kg	1.203	13.860	12.897	12.856
Water Droplet Properties					
Flow rate	ml/min	0.345	---	0.215	0.215
Temperature	°C	28.5	---	17.9	17.9
Length to end of calculation		0		46.1	355

Parameter	Unit	Inlet	Outlet (Expt.)	Outlet (Model: α = 0.04)	Outlet (Model: α = 0.001)
Dv(10)	(µm)	1.10	1.33	2.21	1.98
Dv(50)	(µm)	4.54	4.72	5.08	4.90
Dv(90)	(µm)	10.15	9.86	11.80	11.63
Span		1.99	1.80	1.89	1.97
D[3][2]	(µm)	2.49	2.72	4.26	3.80
D[4][3]	(µm)	5.66	5.63	6.93	6.60
% Transm.		70.8%	73.0%		
Conc. (Cv)	ppm	21	21		

Trial 4.2.17 Air flow: 15 lpm, Length: 245 mm, Temperature: 48 °C

Droplet size distributions

Air Flow rate: 15 lpm
Air Temp.: 48°C
Conduit length: 245 mm

Legend: Inlet — Outlet (Expt.) — Outlet (Model: α = 0.04) — Outlet (Model: α = 0.001)
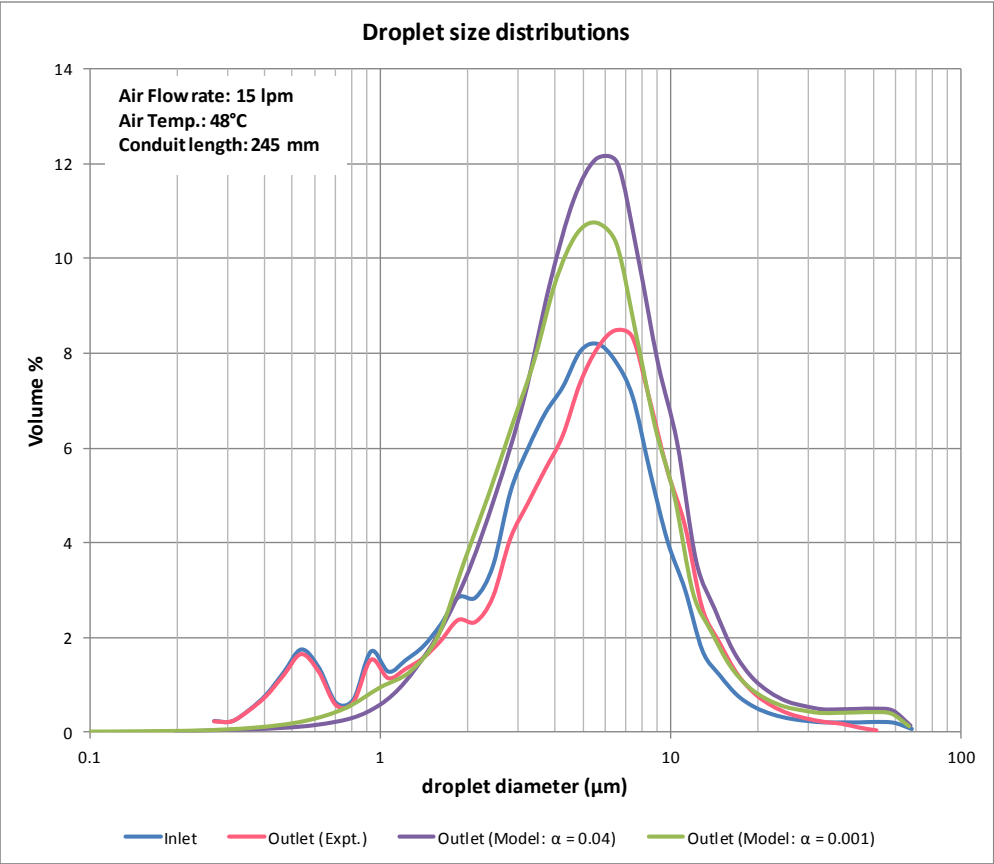
Experiment Date   29/11/2014
Time   14:20:45 - 14:28:11

Conduit Properties	Unit	Value
Diameter	mm	22.5
Length	mm	245

Parameter	Unit	INLET	Experimental Results at OUTLET	Model Results at OUTLET α = 0.04	α = 0.001
Air Properties					
Flow rate	lpm	15.03	---	13.93	14.05
Temperature	°C	47.8	20.2	18.6	21.8
RH		0.0158	0.918	1.00	0.74
Sp. Humidity	g/kg	1.081	13.696	13.512	12.144
Water Droplet Properties					
Flow rate	ml/min	0.345	---	0.142	0.164
Temperature	°C	27	---	18.6	18.7
Length to end of calculation		0		66.0	1308

Parameter	Unit	Inlet	Outlet (Expt.)	Outlet (Model: α = 0.04)	Outlet (Model: α = 0.001)
Dv(10)	(µm)	1.10	1.20	2.55	2.16
Dv(50)	(µm)	4.54	5.24	5.98	5.38
Dv(90)	(µm)	10.15	11.37	13.82	11.78
Span		1.99	1.94	1.88	1.79
D[3][2]	(µm)	2.49	2.69	4.93	4.15
D[4][3]	(µm)	5.66	6.11	7.91	7.03
% Transm.		70.8%	89.1%		
Conc. (Cv)	ppm	21	8		

Trial 4.2.18 Air flow: 20 lpm, Length: 245 mm, Temperature: 48 °C

Droplet size distributions

Air Flow rate: 20 lpm
Air Temp.: 48°C
Conduit length: 245 mm

Legend: Inlet — Outlet (Expt.) — Outlet (Model: α = 0.04) — Outlet (Model: α = 0.001)
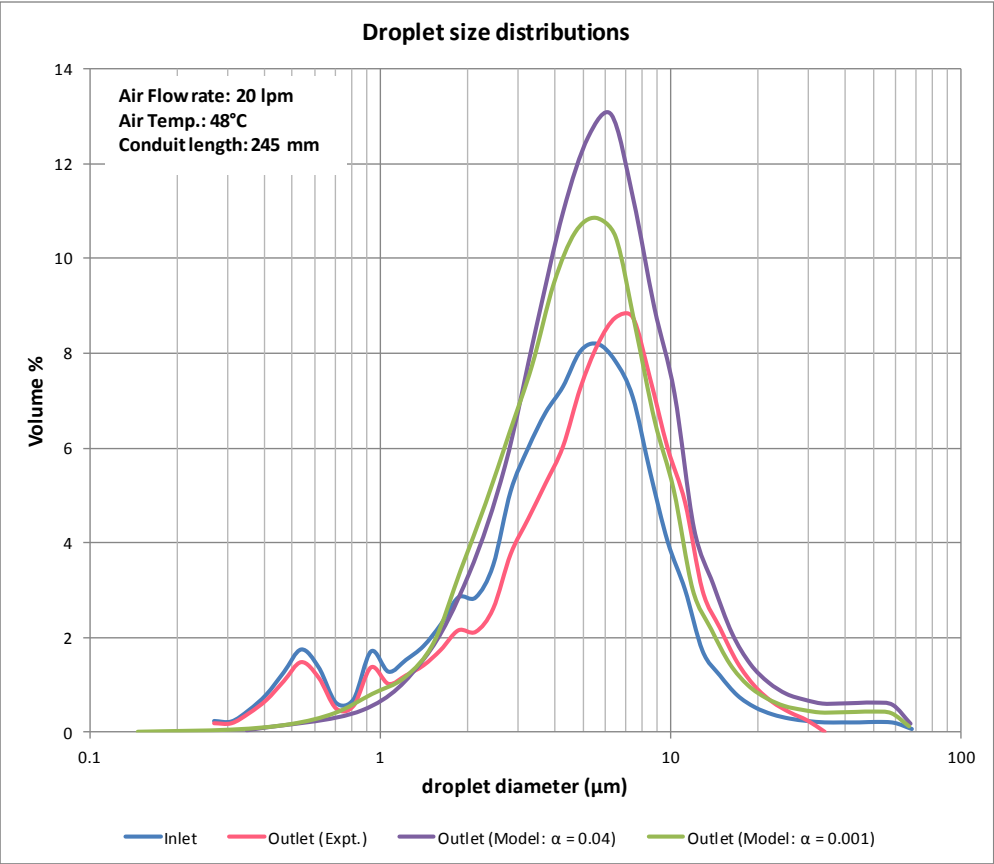
Experiment Date   29/11/2014
Time   14:11:36 - 14:13:16

Conduit Properties	Unit	Value
Diameter	mm	22.5
Length	mm	245

Parameter	Unit	INLET	Experimental Results at OUTLET	Model Results at OUTLET	
				α = 0.04	α = 0.001
Air Properties					
Flow rate	lpm	17.33	---	16.07	16.32
Temperature	°C	47.3	20.5	18.4	23.9
RH		0.0161	0.888	1.00	0.59
Sp. Humidity	g/kg	1.074	13.492	13.345	11.014
Water Droplet Properties					
Flow rate	ml/min	0.345	---	0.113	0.157
Temperature	°C	27.2	---	18.4	18.5
Length to end of calculation		0		116.0	2244

Parameter	Unit	Inlet	Outlet (Expt.)	Outlet (Model: α = 0.04)	Outlet (Model: α = 0.001)
Dv(10)	(µm)	1.10	1.32	2.88	2.26
Dv(50)	(µm)	4.54	5.53	6.13	5.46
Dv(90)	(µm)	10.15	11.68	15.28	11.24
Span		1.99	1.88	2.02	1.65
D[3][2]	(µm)	2.49	2.85	5.23	4.19
D[4][3]	(µm)	5.66	6.26	8.50	7.10
% Transm.		70.8%	94.2%		
Conc. (Cv)	ppm	21	4		

A 4.3 Detailed Results – Ultrasound Enhanced Evaporation

For each trial, using the ultrasound enhance apparatus, the following typical results were generated from the recorded data for both normal and ultrasound enhanced evaporation cases:

- Amount of water evaporation (measured in terms of the moisture content of the air at the inlet and outlet, kg of water per kg of dry air)
- Table of size distribution parameters: $Dv10$, $Dv50$, $Dv90$, $Span$, $D[3,2]$, $D[4,3]$ (at both inlet and outlet)
- Graph of droplet size distribution: % Volume versus droplet diameter at inlet and at outlet

The initial and boundary conditions for each trial were also entered into the ultrasound enhanced droplet evaporation model described in Chapter 4 and comparative values for the droplet size distribution, distribution parameters and amount of water evaporation were determined. These were included along with the experimental results. Model results have been calculated for two cases, where the accommodation coefficients are set to a value of 0.04 and a value of 0.001.

Trial 4.3.1 Ultrasound Power: 2 W, Air Flow: 6.5 lpm

Droplet size distributions - Effect of Ultrasound

Droplet size distributions - Expt. and Model
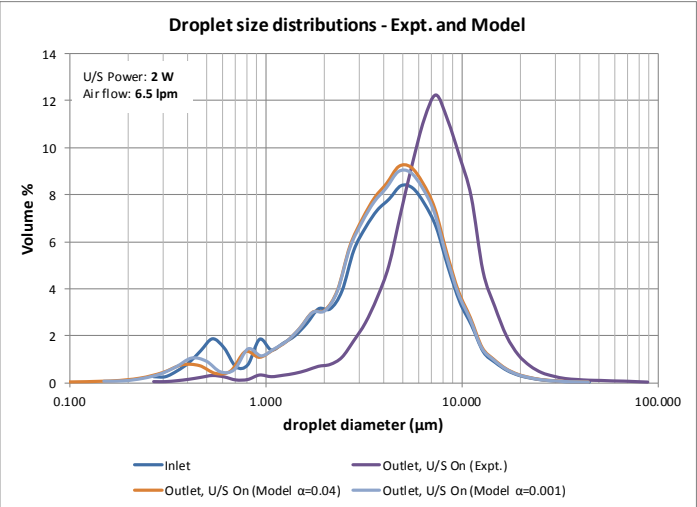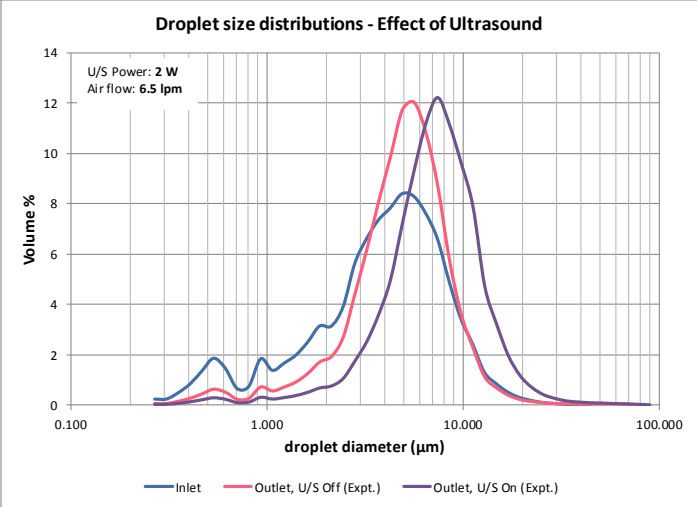
Experiment Date	9/06/2014
Time	14:40:33 - 14:49:03

Conduit Properties	Unit	Value
Diameter	mm	100
Length	mm	300

U/S Field	Unit	Value
Frequency	kHz	21.7
Power	W	2

Parameter	Unit	INLET	Experimental Results at OUTLET		Model Results at OUTLET			
			U/S Off	U/S On	U/S Off		U/S On	
					α = 0.04	α = 0.001	α = 0.04	α = 0.001
Air Properties								
Flow rate	lpm	6.515	---	---	6.30	6.30	6.31	6.31
Temp.	°C	21.95	19.2	20.1	9.8	9.8	10.0	10.0
Rel. Hum.		0.101	0.937	0.94	1.003	1.001	1.003	1.000
Sp. Humidity	g/kg	1.65	13.13	13.94	7.58	7.58	7.65	7.65
Water Droplet Properties								
Flow rate	ml/min	0.323	---	---	0.277	0.277	0.277	0.277
Temp.	°C	24.4	---	---	9.8	9.8	10.0	10.0
Length to end of calculation					1	5	1	4

Parameter	Unit	INLET	Experimental Results at OUTLET		Model Results at OUTLET			
			U/S Off	U/S On	U/S Off		U/S On	
					α = 0.04	α = 0.001	α = 0.04	α = 0.001
Dv(10)	(µm)	1.02	2.19	3.49	1.46	1.33	1.45	1.31
Dv(50)	(µm)	4.19	5.02	7.23	4.58	4.51	4.57	4.50
Dv(90)	(µm)	8.91	8.89	13.15	9.26	9.20	9.26	9.20
Span		1.88	1.33	1.33	1.70	1.75	1.71	1.75
D[3][2]	(µm)	2.34	3.51	5.30	2.86	2.63	2.82	2.61
D[4][3]	(µm)	4.78	5.54	8.10	5.12	5.01	5.11	4.99
% Transm.		76.9%	63.3%	78.6%	---	---	---	---
Conc. (Cv)	ppm	14.9	40.0	32.6	---	---	---	---

Trial 4.3.2 Ultrasound Power: 2 W, Air Flow: 8 lpm

Droplet size distributions - Effect of Ultrasound

Droplet size distributions - Expt. and Model
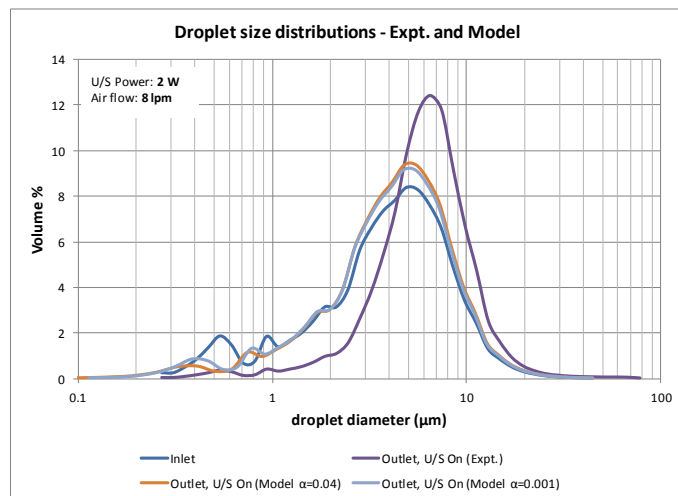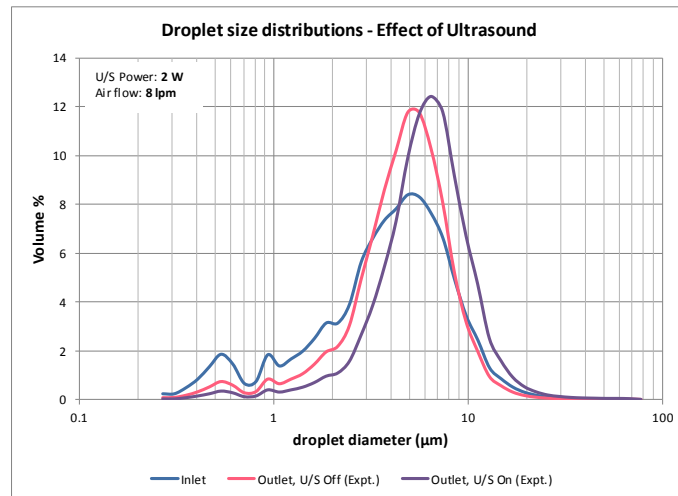
Experiment Date	9/06/2014
Time	15:01:58 - 15:07:59

Conduit Properties	Unit	Value
Diameter	mm	100
Length	mm	300

U/S Field	Unit	Value
Frequency	kHz	21.7
Power	W	2

Parameter	Unit	INLET	Experimental Results at OUTLET		Model Results at OUTLET			
			U/S Off	U/S On	U/S Off		U/S On	
					α = 0.04	α = 0.001	α = 0.04	α = 0.001
Air Properties								
Flow rate	lpm	8.1	---	---	7.84	7.84	7.83	7.83
Temp.	°C	21.75	18	18.8	9.5	9.5	9.5	9.5
Rel. Hum.		0.0966	0.935	0.935	1.003	1.000	1.003	1.000
Sp. Humidity	g/kg	1.56	12.13	12.77	7.39	7.39	7.40	7.40
Water Droplet Properties								
Flow rate	ml/min	0.323	---	---	0.267	0.267	0.267	0.267
Temp.	°C	23.75	---	---	9.5	9.5	9.5	9.5
Length to end of calculation					1	7	1	6

Parameter	Unit	INLET	Experimental Results at OUTLET		Model Results at OUTLET			
			U/S Off	U/S On	U/S Off		U/S On	
					α = 0.04	α = 0.001	α = 0.04	α = 0.001
Dv(10)	(µm)	1.02	2.00	2.98	1.58	1.43	1.57	1.41
Dv(50)	(µm)	4.19	4.82	6.12	4.68	4.59	4.67	4.58
Dv(90)	(µm)	8.91	8.53	10.91	9.37	9.31	9.37	9.30
Span		1.88	1.36	1.30	1.66	1.72	1.67	1.72
D[3][2]	(µm)	2.34	3.30	4.51	3.02	2.72	2.97	2.70
D[4][3]	(µm)	4.78	5.20	6.80	5.20	5.06	5.19	5.05
% Transm.		76.9%	68.2%	75.2%	---	---	---	---
Conc. (Cv)	ppm	14.9	31.4	32.6	---	---	---	---

Trial 4.3.3 Ultrasound Power: 2 W, Air Flow: 10 lpm

Droplet size distributions - Effect of Ultrasound

U/S Power: **2 W**
Air flow: **10 lpm**

Legend: Inlet — Outlet, U/S Off (Expt.) — Outlet, U/S On (Expt.)

Droplet size distributions - Expt. and Model

U/S Power: **2 W**
Air flow: **10 lpm**

Legend: Inlet — Outlet, U/S On (Expt.) — Outlet, U/S On (Model α=0.04) — Outlet, U/S On (Model α=0.001)
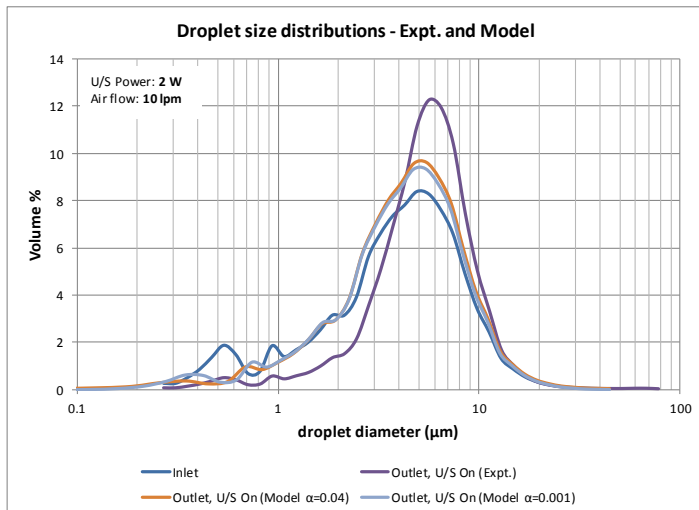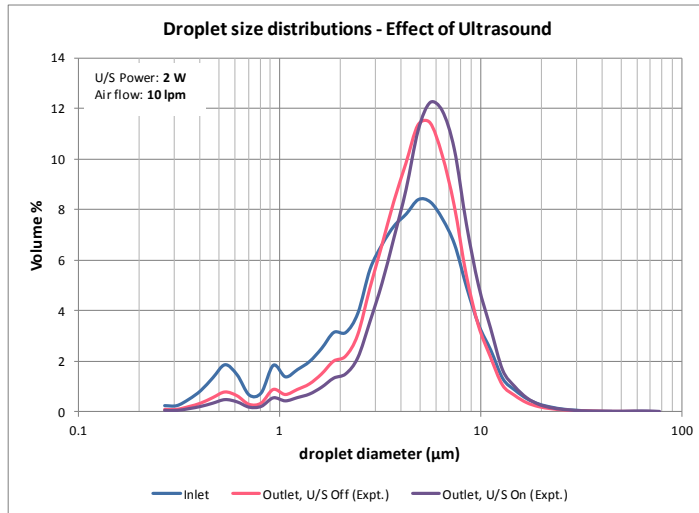
| Experiment Date | 9/06/2014 |
| Time | 15:37:00 - 15:43:30 |

Conduit Properties	Unit	Value
Diameter	mm	100
Length	mm	300

U/S Field	Unit	Value
Frequency	kHz	21.7
Power	W	2

Parameter	Unit	INLET	Experimental Results at OUTLET		Model Results at OUTLET			
					U/S Off		U/S On	
			U/S Off	U/S On	α = 0.04	α = 0.001	α = 0.04	α = 0.001
Air Properties								
Flow rate	lpm	9.96	---	---	9.64	9.64	9.62	9.62
Temp.	°C	21.5	17.3	17.6	9.1	9.1	9.2	9.2
Rel. Hum.		0.09465	0.933	0.935	1.002	1.000	1.002	1.000
Sp. Humidity	g/kg	1.50	11.57	11.82	7.22	7.22	7.26	7.27
Water Droplet Properties								
Flow rate	ml/min	0.323	---	---	0.255	0.255	0.255	0.255
Temp.	°C	24.05	---	---	9.1	9.1	9.2	9.2
Length to end of calculation					2	11	1	10

Parameter	Unit	INLET	Experimental Results at OUTLET		Model Results at OUTLET			
					U/S Off		U/S On	
			U/S Off	U/S On	α = 0.04	α = 0.001	α = 0.04	α = 0.001
Dv(10)	(µm)	1.02	1.94	2.59	1.71	1.54	1.70	1.53
Dv(50)	(µm)	4.19	4.84	5.50	4.79	4.69	4.78	4.68
Dv(90)	(µm)	8.91	8.70	9.71	9.50	9.42	9.50	9.41
Span		1.88	1.40	1.29	1.63	1.68	1.63	1.69
D[3][2]	(µm)	2.34	3.26	3.95	3.21	2.85	3.16	2.82
D[4][3]	(µm)	4.78	5.24	5.98	5.29	5.13	5.27	5.11
% Transm.		76.9%	74.6%	76.9%	---	---	---	---
Conc. (Cv)	ppm	14.9	23.8	26.2	---	---	---	---

Trial 4.3.4 Ultrasound Power: 2 W, Air Flow: 12 lpm
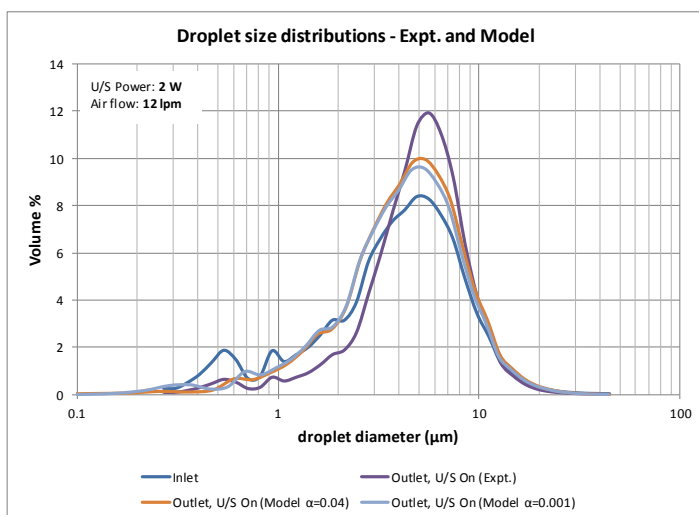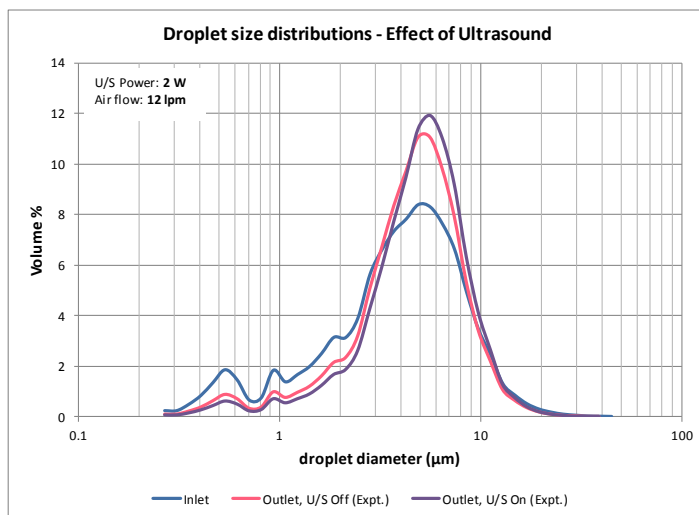
Experiment Date	9/06/2014	
Time	15:52:26 - 15:57:47	

Conduit Properties	Unit	Value
Diameter	mm	100
Length	mm	300

U/S Field	Unit	Value
Frequency	kHz	21.7
Power	W	2

Parameter	Unit	INLET	Experimental Results at OUTLET		Model Results at OUTLET			
					U/S Off		U/S On	
			U/S Off	U/S On	α = 0.04	α = 0.001	α = 0.04	α = 0.001
Air Properties								
Flow rate	lpm	12.1	---	---	11.69	11.69	11.69	11.69
Temp.	°C	21.9	16.3	16.6	9.2	9.2	9.3	9.3
Rel. Hum.		0.09405	0.927	0.93	1.002	1.000	1.002	1.000
Sp. Humidity	g/kg	1.53	10.78	11.02	7.28	7.28	7.29	7.29
Water Droplet Properties								
Flow rate	ml/min	0.323	---	---	0.240	0.241	0.240	0.240
Temp.	°C	24.4	---	---	9.3	9.2	9.3	9.2
Length to end of calculation					2	18	1	17

Parameter	Unit	INLET	Experimental Results at OUTLET		Model Results at OUTLET			
					U/S Off		U/S On	
			U/S Off	U/S On	α = 0.04	α = 0.001	α = 0.04	α = 0.001
Dv(10)	(μm)	1.02	1.82	2.23	1.90	1.68	1.87	1.66
Dv(50)	(μm)	4.19	4.76	5.13	4.93	4.81	4.92	4.79
Dv(90)	(μm)	8.91	8.67	9.03	9.67	9.57	9.66	9.56
Span		1.88	1.44	1.33	1.58	1.64	1.58	1.65
D[3][2]	(μm)	2.34	3.13	3.57	3.43	3.03	3.38	2.98
D[4][3]	(μm)	4.78	5.13	5.50	5.39	5.21	5.37	5.18
% Transm.		76.9%	80.8%	82.3%	---	---	---	---
Conc. (Cv)	ppm	14.9	16.6	17.4	---	---	---	---

Trial 4.3.5 Ultrasound Power: 2 W, Air Flow: 15 lpm
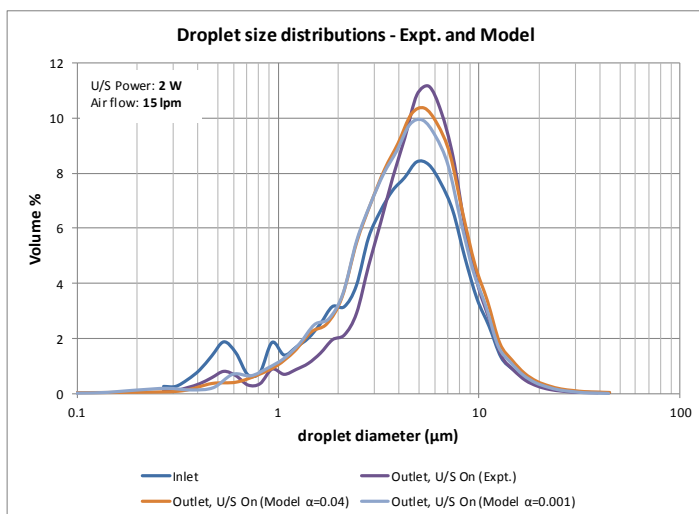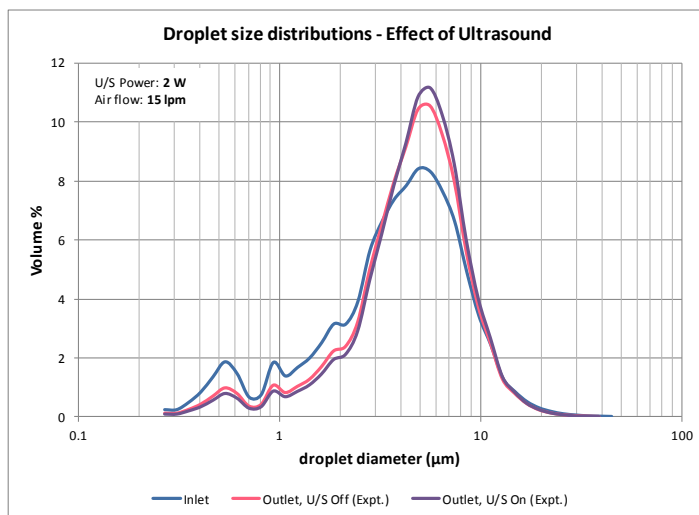
Experiment Date	9/06/2014	
Time	16:03:36 - 16:08:11	

Conduit Properties	Unit	Value
Diameter	mm	100
Length	mm	300

U/S Field	Unit	Value
Frequency	kHz	21.7
Power	W	2

Parameter	Unit	INLET	Experimental Results at OUTLET		Model Results at OUTLET			
			U/S Off	U/S On	U/S Off		U/S On	
					α = 0.04	α = 0.001	α = 0.04	α = 0.001
Air Properties								
Flow rate	lpm	14.95	---	---	14.48	14.48	14.38	14.38
Temp.	°C	21.9	15.5	15.6	9.1	9.1	9.0	9.0
Rel. Hum.		0.0892	0.92	0.923	1.001	1.000	1.001	1.000
Sp. Humidity	g/kg	1.45	10.15	10.25	7.23	7.23	7.17	7.17
Water Droplet Properties								
Flow rate	ml/min	0.323	---	---	0.221	0.222	0.221	0.221
Temp.	°C	25.15	---	---	9.1	9.1	9.0	9.0
Length to end of calculation					2	33	2	30

Parameter	Unit	INLET	Experimental Results at OUTLET		Model Results at OUTLET			
			U/S Off	U/S On	U/S Off		U/S On	
					α = 0.04	α = 0.001	α = 0.04	α = 0.001
Dv(10)	(μm)	1.02	1.72	1.96	2.11	1.88	2.10	1.86
Dv(50)	(μm)	4.19	4.78	4.98	5.01	4.33	5.00	4.31
Dv(90)	(μm)	8.91	8.95	9.07	9.88	9.76	9.87	9.75
Span		1.88	1.51	1.43	1.55	1.82	1.56	1.83
D[3][2]	(μm)	2.34	3.05	3.31	3.65	3.26	3.61	3.22
D[4][3]	(μm)	4.78	5.21	5.40	5.52	5.30	5.50	5.27
% Transm.		76.9%	85.3%	87.4%	---	---	---	---
Conc. (Cv)	ppm	14.9	12.0	11.1	---	---	---	---

Trial 4.3.6 Ultrasound Power: 2 W, Air Flow: 18 lpm

Droplet size distributions - Effect of Ultrasound

U/S Power: **2 W**
Air flow: **18 lpm**

Legend: Inlet — Outlet, U/S Off (Expt.) — Outlet, U/S On (Expt.)

Droplet size distributions - Expt. and Model

U/S Power: **2 W**
Air flow: **18 lpm**

Legend: Inlet — Outlet, U/S On (Expt.) — Outlet, U/S On (Model α=0.04) — Outlet, U/S On (Model α=0.001)
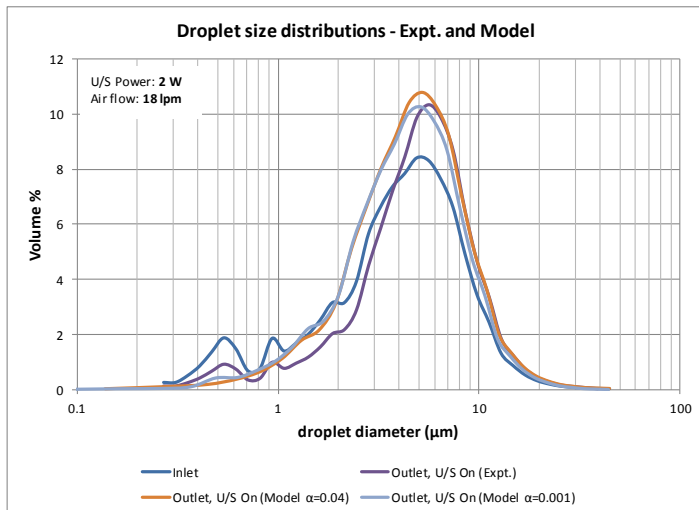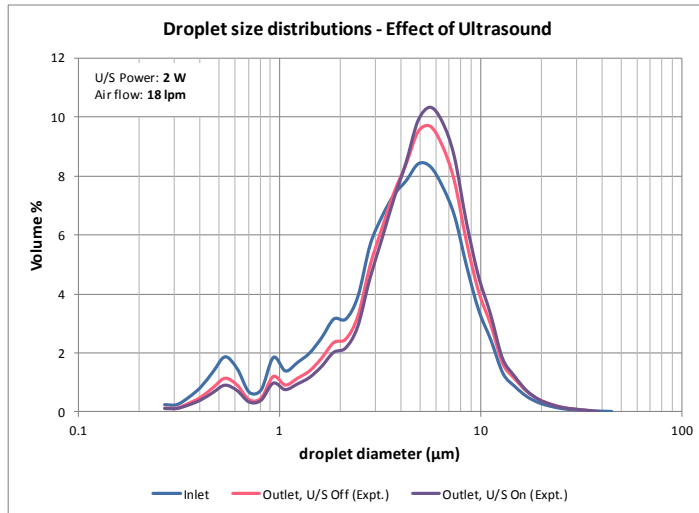
| Experiment Date | 9/06/2014 |
| Time | 16:13:34 - 16:18:38 |

Conduit Properties	Unit	Value
Diameter	mm	100
Length	mm	300

U/S Field	Unit	Value
Frequency	kHz	21.7
Power	W	2

Parameter	Unit	INLET	Experimental Results at OUTLET		Model Results at OUTLET			
					U/S Off		U/S On	
			U/S Off	U/S On	α = 0.04	α = 0.001	α = 0.04	α = 0.001
Air Properties								
Flow rate	lpm	18.1	---	---	17.46	17.46	17.46	17.46
Temp.	°C	21.8	14.7	14.8	8.9	8.9	8.9	8.9
Rel. Hum.		0.0858	0.918	0.923	1.000	1.000	1.000	1.000
Sp. Humidity	g/kg	1.39	9.61	9.73	7.10	7.10	7.11	7.11
Water Droplet Properties								
Flow rate	ml/min	0.323	---	---	0.200	0.200	0.200	0.200
Temp.	°C	26.05	---	---	8.9	8.9	8.9	8.9
Length to end of calculation					3	58	2	53

Parameter	Unit	INLET	Experimental Results at OUTLET		Model Results at OUTLET			
					U/S Off		U/S On	
			U/S Off	U/S On	α = 0.04	α = 0.001	α = 0.04	α = 0.001
Dv(10)	(µm)	1.02	1.56	1.83	2.10	1.93	2.06	1.87
Dv(50)	(µm)	4.19	4.80	5.09	4.74	4.48	4.71	4.46
Dv(90)	(µm)	8.91	9.61	9.87	10.11	9.98	10.10	9.95
Span		1.88	1.68	1.58	1.69	1.79	1.71	1.81
D[3][2]	(µm)	2.34	2.93	3.24	3.84	3.48	3.79	3.43
D[4][3]	(µm)	4.78	5.39	5.64	5.66	5.39	5.63	5.35
% Transm.		76.9%	89.8%	90.3%	---	---	---	---
Conc. (Cv)	ppm	14.9	7.8	8.2	---	---	---	---

Trial 4.3.7 Ultrasound Power: 2 W, Air Flow: 20 lpm

Droplet size distributions - Effect of Ultrasound

U/S Power: **2 W**
Air flow: **20 lpm**

Droplet size distributions - Expt. and Model

U/S Power: **2 W**
Air flow: **20 lpm**
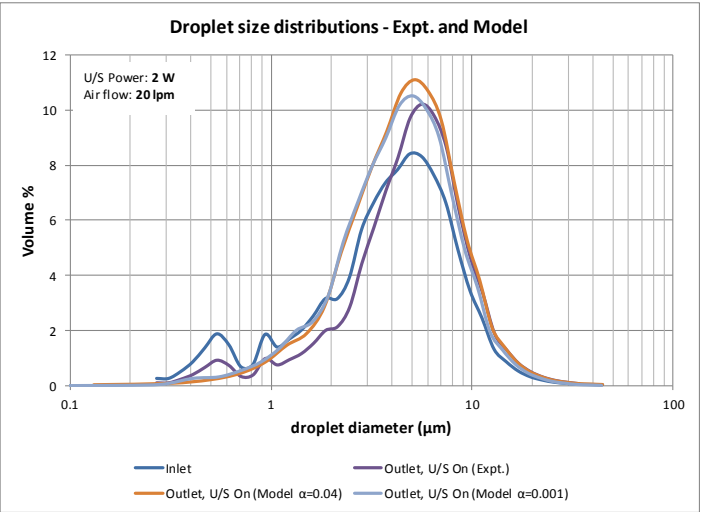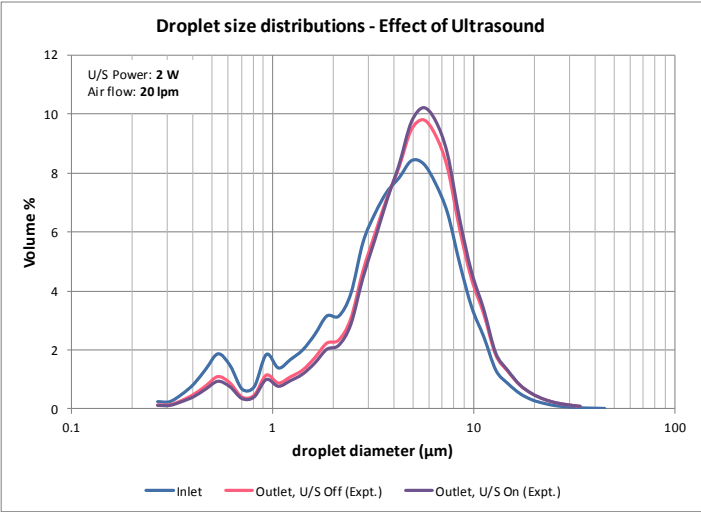
| Experiment Date | 9/06/2014 |
| Time | 16:25:36 - 16:29:59 |

Conduit Properties	Unit	Value
Diameter	mm	100
Length	mm	300

U/S Field	Unit	Value
Frequency	kHz	21.7
Power	W	2

Parameter	Unit	INLET	Experimental Results at OUTLET		Model Results at OUTLET			
					U/S Off		U/S On	
			U/S Off	U/S On	α = 0.04	α = 0.001	α = 0.04	α = 0.001
Air Properties								
Flow rate	lpm	20.15	---	---	19.39	19.39	19.49	19.49
Temp.	°C	21.8	14.3	14.3	8.8	8.8	8.9	8.9
Rel. Hum.		0.08855	0.917	0.921	1.000	1.000	1.000	1.000
Sp. Humidity	g/kg	1.43	9.35	9.39	7.08	7.08	7.09	7.09
Water Droplet Properties								
Flow rate	ml/min	0.323	---	---	0.188	0.188	0.187	0.187
Temp.	°C	24.5	---	---	8.8	8.8	8.9	8.8
Length to end of calculation					3	80	3	74

Parameter	Unit	INLET	Experimental Results at OUTLET		Model Results at OUTLET			
					U/S Off		U/S On	
			U/S Off	U/S On	α = 0.04	α = 0.001	α = 0.04	α = 0.001
Dv(10)	(µm)	1.02	1.63	1.81	2.14	1.93	2.13	1.91
Dv(50)	(µm)	4.19	4.96	5.12	4.77	4.58	4.76	4.56
Dv(90)	(µm)	8.91	9.95	10.04	10.25	10.10	10.25	10.09
Span		1.88	1.68	1.61	1.70	1.79	1.71	1.79
D[3][2]	(µm)	2.34	3.03	3.22	3.95	3.57	3.91	3.53
D[4][3]	(µm)	4.78	5.58	5.72	5.74	5.44	5.72	5.41
% Transm.		76.9%	91.2%	91.6%	---	---	---	---
Conc. (Cv)	ppm	14.9	6.9	7.0	---	---	---	---

Trial 4.3.8 Ultrasound Power: 5 W, Air Flow: 6.5 lpm

Droplet size distributions - Effect of Ultrasound

U/S Power: **5 W**
Air flow: **6.5 lpm**

— Inlet — Outlet, U/S Off (Expt.) — Outlet, U/S On (Expt.)

Droplet size distributions - Expt. and Model

U/S Power: **5 W**
Air flow: **6.5 lpm**

— Inlet — Outlet, U/S On (Expt.)
— Outlet, U/S On (Model α=0.04) — Outlet, U/S On (Model α=0.001)
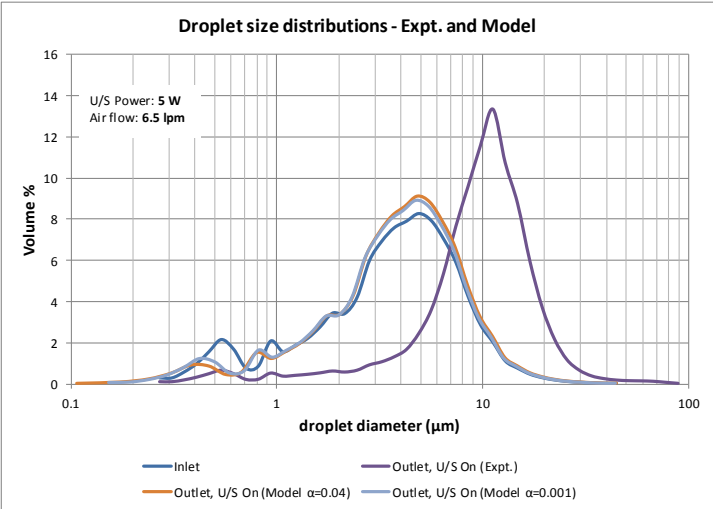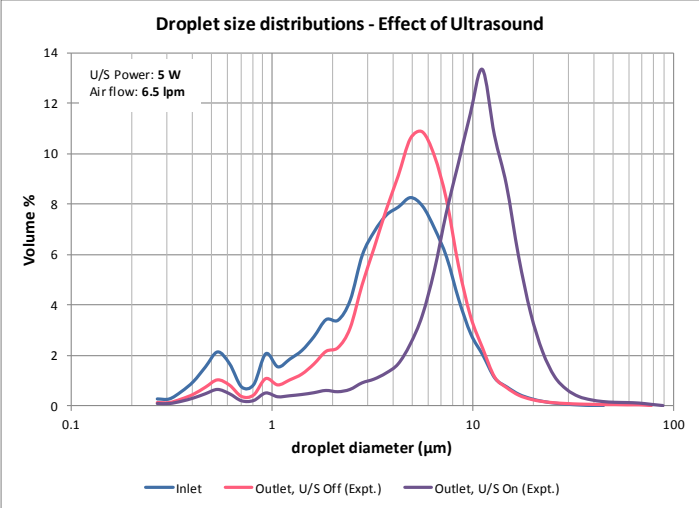
Experiment Date	29/05/2014
Time	11:31:13 - 11:36:00

Conduit Properties	Unit	Value
Diameter	mm	100
Length	mm	300

U/S Field	Unit	Value
Frequency	kHz	21.7
Power	W	5

Parameter	Unit	INLET	Experimental Results at OUTLET		Model Results at OUTLET			
			U/S Off	U/S On	U/S Off		U/S On	
					α = 0.04	α = 0.001	α = 0.04	α = 0.001
Air Properties								
Flow rate	lpm	6.55	---	---	6.34	6.34	6.34	6.34
Temp.	°C	21	18.65	19.6	9.0	9.0	9.1	9.1
Rel. Hum.		0.0952	0.932	0.936	1.003	1.001	1.003	1.000
Sp. Humidity	g/kg	1.46	12.60	13.45	7.15	7.16	7.21	7.22
Water Droplet Properties								
Flow rate	ml/min	0.3	---	---	0.255	0.255	0.255	0.255
Temp.	°C	21.75	---	---	9.0	9.0	9.1	9.1
Length to end of calculation		0			1	5	1	4

Parameter	Unit	INLET	Experimental Results at OUTLET		Model Results at OUTLET			
			U/S Off	U/S On	U/S Off		U/S On	
					α = 0.04	α = 0.001	α = 0.04	α = 0.001
Dv(10)	(µm)	0.93	1.70	3.88	1.34	1.20	1.32	1.18
Dv(50)	(µm)	3.90	4.83	10.19	4.31	4.24	4.31	4.23
Dv(90)	(µm)	8.51	8.90	17.76	8.87	8.83	8.86	8.82
Span		1.94	1.49	1.36	1.74	1.80	1.75	1.80
D[3][2]	(µm)	2.17	3.03	5.38	2.65	2.44	2.61	2.42
D[4][3]	(µm)	4.53	5.35	10.93	4.88	4.76	4.86	4.75
% Transm.		71.1%	62.6%	88.3%	---	---	---	---
Conc. (Cv)	ppm	17.8	35.1	17.2	---	---	---	---

Trial 4.3.9 Ultrasound Power: 5 W, Air Flow: 8 lpm

Droplet size distributions - Effect of Ultrasound

Droplet size distributions - Expt. and Model
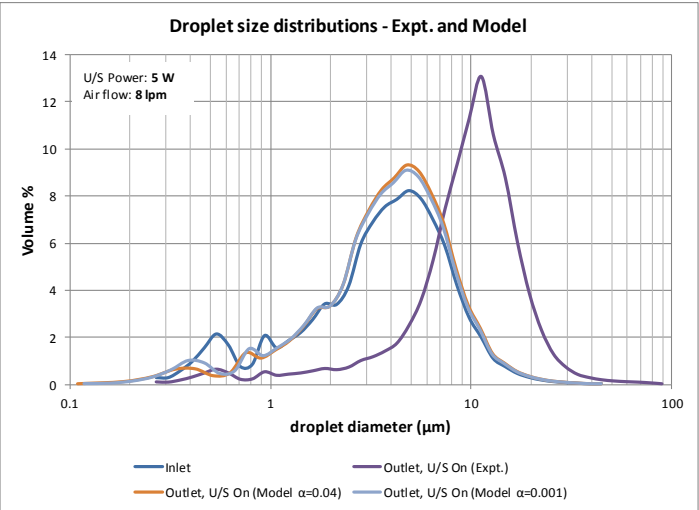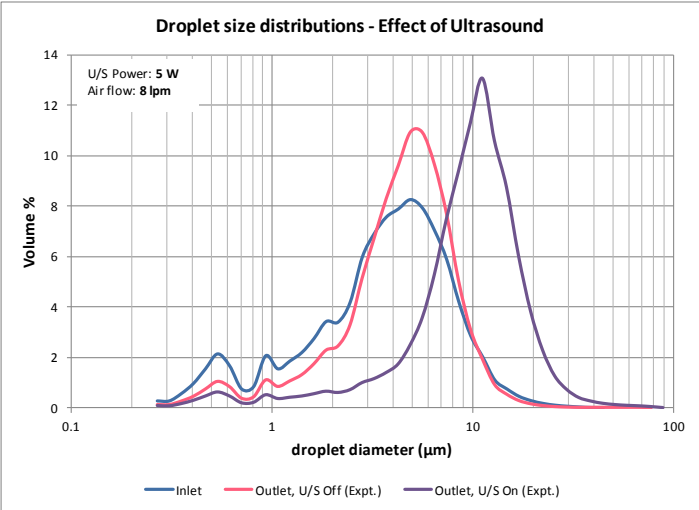
Experiment Date 29/05/2014
Time 11:51:54 - 11:55:14

Conduit Properties	Unit	Value
Diameter	mm	100
Length	mm	300

U/S Field	Unit	Value
Frequency	kHz	21.7
Power	W	5

Parameter	Unit	INLET	Experimental Results at OUTLET		Model Results at OUTLET			
			U/S Off	U/S On	U/S Off		U/S On	
					α = 0.04	α = 0.001	α = 0.04	α = 0.001
Air Properties								
Flow rate	lpm	8.055	---	---	7.80	7.80	7.80	7.80
Temp.	°C	21.2	17.8	19.11	9.2	9.2	9.3	9.3
Rel. Hum.		0.0973	0.937	0.939	1.003	1.000	1.003	1.000
Sp. Humidity	g/kg	1.51	12.00	13.08	7.27	7.27	7.31	7.31
Water Droplet Properties								
Flow rate	ml/min	0.3	---	---	0.245	0.245	0.244	0.245
Temp.	°C	25.95	---	---	9.2	9.2	9.3	9.3
Length to end of calculation		0			1	7	1	6

Parameter	Unit	INLET	Experimental Results at OUTLET		Model Results at OUTLET			
			U/S Off	U/S On	U/S Off		U/S On	
					α = 0.04	α = 0.001	α = 0.04	α = 0.001
Dv(10)	(µm)	0.93	1.66	3.71	1.46	1.31	1.44	1.29
Dv(50)	(µm)	3.90	4.65	10.21	4.41	4.32	4.40	4.31
Dv(90)	(µm)	8.51	8.45	17.96	8.95	8.90	8.95	8.89
Span		1.94	1.46	1.40	1.70	1.76	1.71	1.76
D[3][2]	(µm)	2.17	2.95	5.39	2.80	2.52	2.75	2.50
D[4][3]	(µm)	4.53	5.03	10.95	4.95	4.82	4.93	4.80
% Transm.		71.1%	66.8%	87.4%	---	---	---	---
Conc. (Cv)	ppm	17.8	29.4	18.6	---	---	---	---

Trial 4.3.10 Ultrasound Power: 5 W, Air Flow: 10 lpm

Droplet size distributions - Effect of Ultrasound

U/S Power: **5 W**
Air flow: **10 lpm**

Legend: Inlet — Outlet, U/S Off (Expt.) — Outlet, U/S On (Expt.)

Droplet size distributions - Expt. and Model

U/S Power: **5 W**
Air flow: **10 lpm**

Legend: Inlet — Outlet, U/S On (Expt.) — Outlet, U/S On (Model α=0.04) — Outlet, U/S On (Model α=0.001)
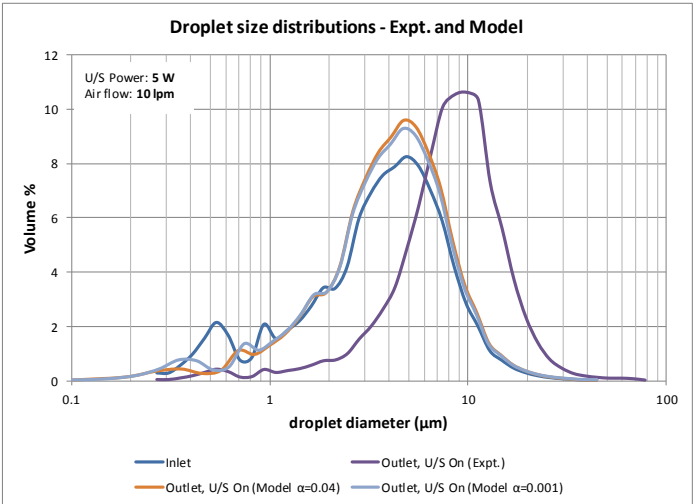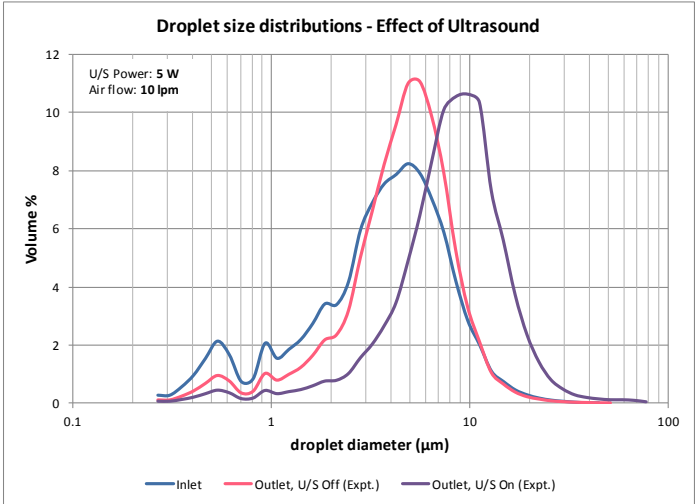
Experiment Date	29/05/2014	
Time	12:26:49 - 12:31:23	

Conduit Properties	Unit	Value
Diameter	mm	100
Length	mm	300

U/S Field	Unit	Value
Frequency	kHz	21.7
Power	W	5

Parameter	Unit	INLET	Experimental Results at OUTLET		Model Results at OUTLET			
			U/S Off	U/S On	U/S Off		U/S On	
					α = 0.04	α = 0.001	α = 0.04	α = 0.001
Air Properties								
Flow rate	lpm	10	---	---	9.67	9.67	9.67	9.67
Temp.	°C	21.35	17.3	18	9.2	9.2	9.1	9.1
Rel. Hum.		0.101	0.933	0.934	1.002	1.000	1.002	1.000
Sp. Humidity	g/kg	1.59	11.57	12.12	7.23	7.23	7.23	7.23
Water Droplet Properties								
Flow rate	ml/min	0.3	---	---	0.233	0.233	0.233	0.233
Temp.	°C	24.15	---	---	9.2	9.1	9.1	9.1
Length to end of calculation		0			2	11	1	10

Parameter	Unit	INLET	Experimental Results at OUTLET		Model Results at OUTLET			
			U/S Off	U/S On	U/S Off		U/S On	
					α = 0.04	α = 0.001	α = 0.04	α = 0.001
Dv(10)	(μm)	0.93	1.77	3.42	1.61	1.44	1.58	1.41
Dv(50)	(μm)	3.90	4.76	8.37	4.53	4.43	4.52	4.41
Dv(90)	(μm)	8.51	8.67	15.70	9.06	9.00	9.05	8.99
Span		1.94	1.45	1.47	1.64	1.71	1.65	1.72
D[3][2]	(μm)	2.17	3.08	5.30	3.01	2.66	2.94	2.62
D[4][3]	(μm)	4.53	5.15	9.36	5.06	4.90	5.03	4.87
% Transm.		71.1%	73.8%	85.4%	---	---	---	---
Conc. (Cv)	ppm	17.8	23.1	21.4	---	---	---	---

Trial 4.3.11 Ultrasound Power: 5 W, Air Flow: 12 lpm

Droplet size distributions - Effect of Ultrasound

Droplet size distributions - Expt. and Model
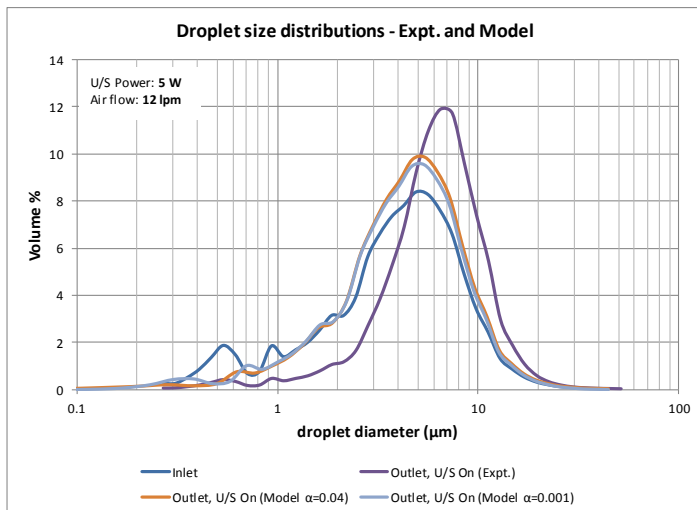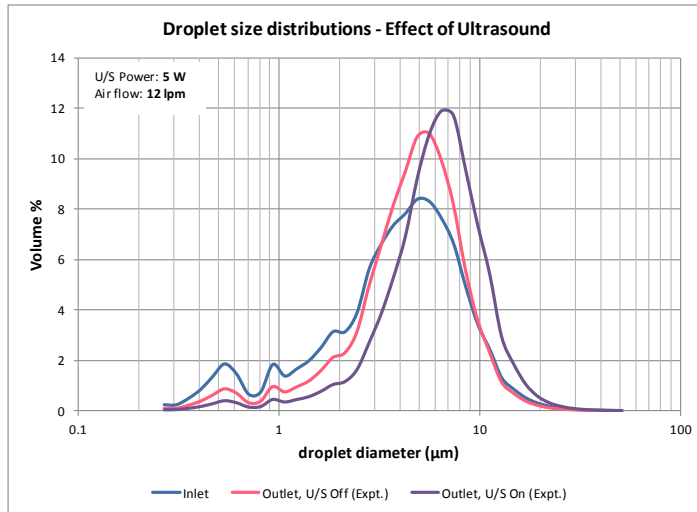
Experiment Date	9/06/2014
Time	12:19:24 - 12:26:07

Conduit Properties	Unit	Value
Diameter	mm	100
Length	mm	300

U/S Field	Unit	Value
Frequency	kHz	21.7
Power	W	5

Parameter	Unit	INLET	Experimental Results at OUTLET		Model Results at OUTLET			
			U/S Off	U/S On	U/S Off		U/S On	
					α = 0.04	α = 0.001	α = 0.04	α = 0.001
Air Properties								
Flow rate	lpm	12.05	---	---	11.60	11.60	11.70	11.70
Temp.	°C	21.5	16.9	17.4	9.3	9.3	9.2	9.2
Rel. Hum.		0.109	0.916	0.921	1.002	1.000	1.002	1.000
Sp. Humidity	g/kg	1.73	11.07	11.49	7.30	7.30	7.27	7.27
Water Droplet Properties								
Flow rate	ml/min	0.323	---	---	0.244	0.244	0.243	0.243
Temp.	°C	23.2	---	---	9.3	9.2	9.2	9.2
Length to end of calculation		0			2	17	1	16

Parameter	Unit	INLET	Experimental Results at OUTLET		Model Results at OUTLET			
			U/S Off	U/S On	U/S Off		U/S On	
					α = 0.04	α = 0.001	α = 0.04	α = 0.001
Dv(10)	(µm)	1.02	1.84	2.90	1.86	1.66	1.83	1.63
Dv(50)	(µm)	4.19	4.83	6.24	4.91	4.79	4.89	4.77
Dv(90)	(µm)	8.91	8.82	11.16	9.64	9.54	9.63	9.53
Span		1.88	1.45	1.33	1.59	1.65	1.59	1.66
D[3][2]	(µm)	2.34	3.17	4.46	3.39	3.00	3.33	2.95
D[4][3]	(µm)	4.78	5.22	6.77	5.37	5.19	5.35	5.16
% Transm.		76.9%	83.4%	87.1%	---	---	---	---
Conc. (Cv)	ppm	14.9	14.3	15.5	---	---	---	---

Trial 4.3.12 Ultrasound Power: 5 W, Air Flow: 15 lpm

Droplet size distributions - Effect of Ultrasound

U/S Power: **5 W**
Air flow: **15 lpm**

Droplet size distributions - Expt. and Model

U/S Power: **5 W**
Air flow: **15 lpm**
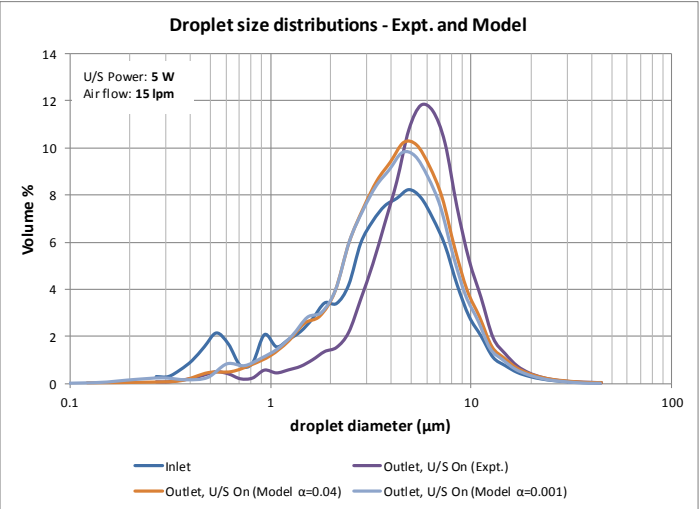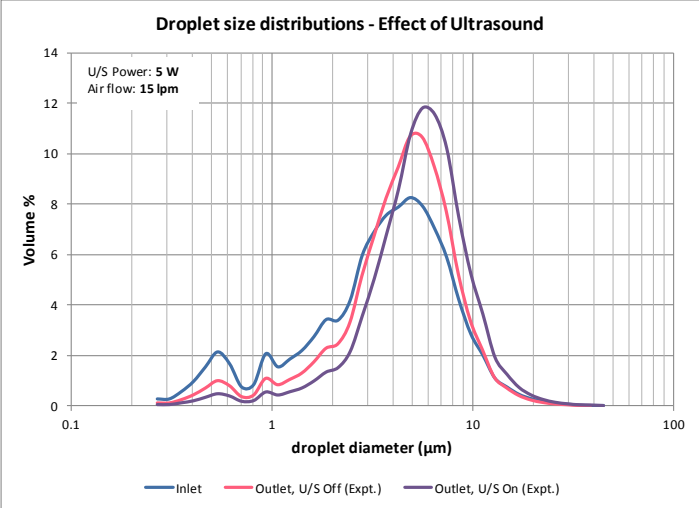
Experiment Date	29/05/2014
Time	13:19:35 - 13:24:30

Conduit Properties	Unit	Value
Diameter	mm	100
Length	mm	300

U/S Field	Unit	Value
Frequency	kHz	21.7
Power	W	5

Parameter	Unit	INLET	Experimental Results at OUTLET		Model Results at OUTLET			
			U/S Off	U/S On	U/S Off		U/S On	
					α = 0.04	α = 0.001	α = 0.04	α = 0.001
Air Properties								
Flow rate	lpm	15	---	---	14.49	14.49	14.49	14.49
Temp.	°C	21.1	16.1	16.7	8.6	8.6	8.6	8.6
Rel. Hum.		0.0926	0.918	0.922	1.001	1.000	1.001	1.000
Sp. Humidity	g/kg	1.43	10.53	11.00	6.97	6.97	6.98	6.98
Water Droplet Properties								
Flow rate	ml/min	0.3	---	---	0.201	0.201	0.201	0.201
Temp.	°C	23.5	---	---	8.6	8.6	8.6	8.6
Length to end of calculation		0			2	33	2	30

Parameter	Unit	INLET	Experimental Results at OUTLET		Model Results at OUTLET			
			U/S Off	U/S On	U/S Off		U/S On	
					α = 0.04	α = 0.001	α = 0.04	α = 0.001
Dv(10)	(µm)	0.93	1.70	2.58	1.99	1.76	1.94	1.72
Dv(50)	(µm)	3.90	4.69	5.55	4.54	4.10	4.51	4.09
Dv(90)	(µm)	8.51	8.74	10.07	9.49	9.35	9.48	9.33
Span		1.94	1.50	1.35	1.65	1.85	1.67	1.86
D[3][2]	(µm)	2.17	3.01	3.98	3.45	3.07	3.40	3.00
D[4][3]	(µm)	4.53	5.11	6.07	5.30	5.08	5.27	5.05
% Transm.		71.1%	83.7%	86.4%	---	---	---	---
Conc. (Cv)	ppm	17.8	13.2	14.6	---	---	---	---

Trial 4.3.13 Ultrasound Power: 5 W, Air Flow: 18 lpm

Droplet size distributions - Effect of Ultrasound

U/S Power: **5 W**
Air flow: **18 lpm**

Legend: Inlet — Outlet, U/S Off (Expt.) — Outlet, U/S On (Expt.)

Droplet size distributions - Expt. and Model

U/S Power: **5 W**
Air flow: **18 lpm**

Legend: Inlet — Outlet, U/S On (Expt.) — Outlet, U/S On (Model α=0.04) — Outlet, U/S On (Model α=0.001)
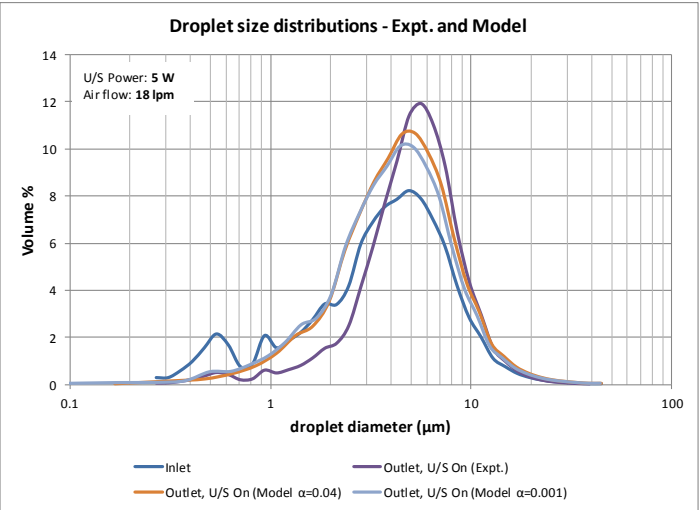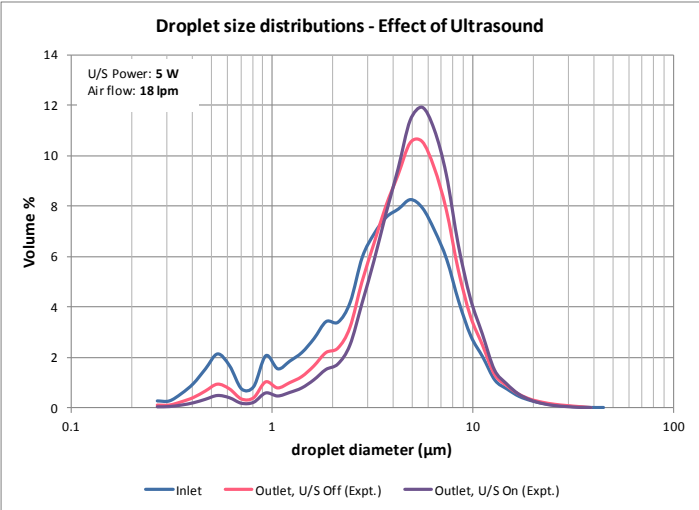
| Experiment Date | 29/05/2014 |
| Time | 13:33:25 - 13:38:32 |

Conduit Properties	Unit	Value
Diameter	mm	100
Length	mm	300

U/S Field	Unit	Value
Frequency	kHz	21.7
Power	W	5

Parameter	Unit	INLET	Experimental Results at OUTLET		Model Results at OUTLET			
			U/S Off	U/S On	U/S Off		U/S On	
					α = 0.04	α = 0.001	α = 0.04	α = 0.001
Air Properties								
Flow rate	lpm	18	---	---	17.37	17.37	17.38	17.38
Temp.	°C	21.25	15	15.3	8.5	8.5	8.5	8.5
Rel. Hum.		0.0856	0.917	0.919	1.000	1.000	1.000	1.000
Sp. Humidity	g/kg	1.34	9.79	10.01	6.93	6.92	6.92	6.92
Water Droplet Properties								
Flow rate	ml/min	0.3	---	---	0.180	0.180	0.181	0.181
Temp.	°C	24.3	---	---	8.5	8.5	8.5	8.5
Length to end of calculation		0			3	60	2	53

Parameter	Unit	INLET	Experimental Results at OUTLET		Model Results at OUTLET			
			U/S Off	U/S On	U/S Off		U/S On	
					α = 0.04	α = 0.001	α = 0.04	α = 0.001
Dv(10)	(µm)	0.93	1.77	2.41	1.96	1.74	1.92	1.69
Dv(50)	(µm)	3.90	4.80	5.22	4.43	4.28	4.41	4.25
Dv(90)	(µm)	8.51	9.05	9.42	9.80	9.63	9.77	9.59
Span		1.94	1.52	1.34	1.77	1.85	1.78	1.86
D[3][2]	(µm)	2.17	3.10	3.77	3.64	3.30	3.59	3.23
D[4][3]	(µm)	4.53	5.30	5.70	5.45	5.19	5.41	5.14
% Transm.		71.1%	87.8%	88.5%	---	---	---	---
Conc. (Cv)	ppm	17.8	10.0	11.5	---	---	---	---

Trial 4.3.14 Ultrasound Power: 5 W, Air Flow: 20 lpm

Droplet size distributions - Effect of Ultrasound

U/S Power: **5 W**
Air flow: **20 lpm**

Droplet size distributions - Expt. and Model

U/S Power: **5 W**
Air flow: **20 lpm**
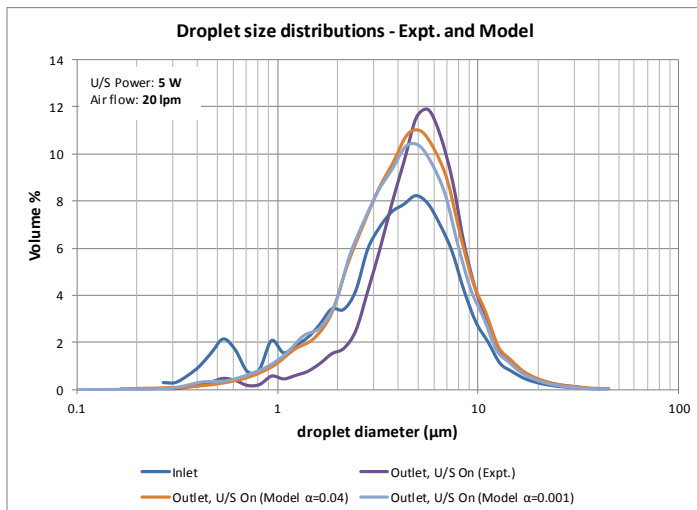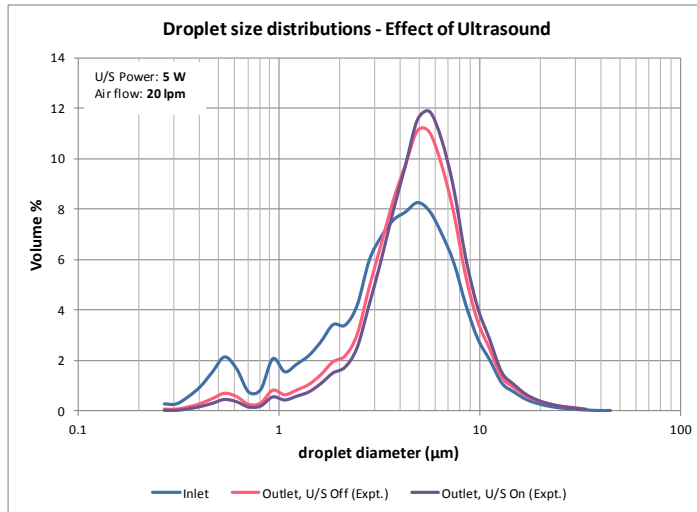
Experiment Date	29/05/2014	
Time	13:44:42 - 13:49:08	

Conduit Properties	Unit	Value
Diameter	mm	100
Length	mm	300

U/S Field	Unit	Value
Frequency	kHz	21.7
Power	W	5

Parameter	Unit	INLET	Experimental Results at OUTLET		Model Results at OUTLET			
			U/S Off	U/S On	U/S Off		U/S On	
					α = 0.04	α = 0.001	α = 0.04	α = 0.001
Air Properties								
Flow rate	lpm	20.1	---	---	19.40	19.40	19.40	19.40
Temp.	°C	21.2	14.4	14.6	8.5	8.5	8.6	8.6
Rel. Hum.		0.0915	0.914	0.918	1.000	1.000	1.000	1.000
Sp. Humidity	g/kg	1.42	9.38	9.55	6.94	6.94	6.94	6.94
Water Droplet Properties								
Flow rate	ml/min	0.3	---	---	0.168	0.168	0.168	0.168
Temp.	°C	24.35	---	---	8.5	8.5	8.5	8.5
Length to end of calculation		0			4	83	3	74

Parameter	Unit	INLET	Experimental Results at OUTLET		Model Results at OUTLET			
			U/S Off	U/S On	U/S Off		U/S On	
					α = 0.04	α = 0.001	α = 0.04	α = 0.001
Dv(10)	(µm)	0.93	2.01	2.44	2.07	1.84	2.04	1.81
Dv(50)	(µm)	3.90	4.88	5.18	4.55	4.38	4.53	4.35
Dv(90)	(µm)	8.51	9.11	9.58	9.97	9.79	9.96	9.76
Span		1.94	1.45	1.38	1.74	1.82	1.75	1.83
D[3][2]	(µm)	2.17	3.36	3.80	3.76	3.39	3.71	3.33
D[4][3]	(µm)	4.53	5.45	5.78	5.54	5.24	5.51	5.20
% Transm.		71.1%	89.0%	89.8%	---	---	---	---
Conc. (Cv)	ppm	17.8	9.8	10.2	---	---	---	---

Trial 4.3.15 Ultrasound Power: 7 W, Air Flow: 6.5 lpm

Droplet size distributions - Effect of Ultrasound

U/S Power: **7 W**
Air flow: **6.5 lpm**

Legend: Inlet — Outlet, U/S Off (Expt.) — Outlet, U/S On (Expt.)

Droplet size distributions - Expt. and Model

U/S Power: **7 W**
Air flow: **6.5 lpm**

Legend: Inlet — Outlet, U/S On (Expt.) — Outlet, U/S On (Model α=0.04) — Outlet, U/S On (Model α=0.001)
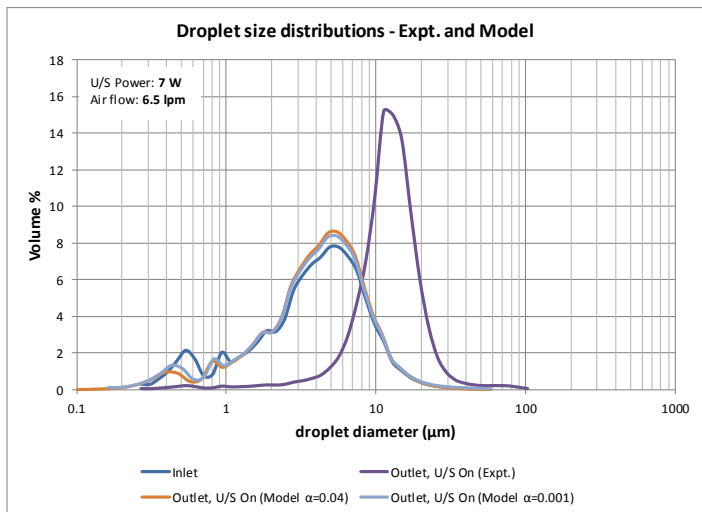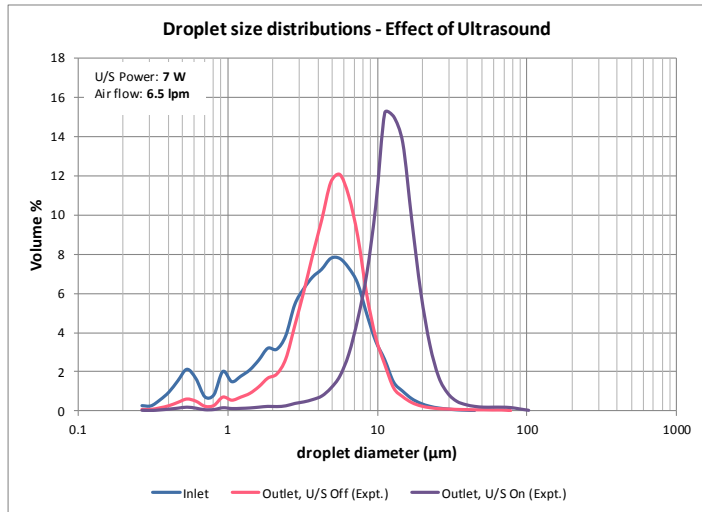
| Experiment Date | 27/06/2014 |
| Time | 09:17:51 - 09:23:33 |

Conduit Properties	Unit	Value
Diameter	mm	100
Length	mm	300

U/S Field	Unit	Value
Frequency	kHz	21.7
Power	W	7

Parameter	Unit	INLET	Experimental Results at OUTLET		Model Results at OUTLET			
			U/S Off	U/S On	U/S Off		U/S On	
					α = 0.04	α = 0.001	α = 0.04	α = 0.001
Air Properties								
Flow rate	lpm	6.545	---	---	6.34	6.34	6.35	6.35
Temp.	°C	21	18.2	19.9	9.3	9.3	9.3	9.3
Rel. Hum.		0.09065	0.932	0.935	1.003	1.003	1.003	1.002
Sp. Humidity	g/kg	1.39	12.25	13.69	7.29	7.29	7.28	7.29
Water Droplet Properties								
Flow rate	ml/min	0.339	---	---	0.293	0.293	0.293	0.293
Temp.	°C	24.05	---	---	9.3	9.3	9.3	9.3
Length to end of calculation					2	8	1	5

Parameter	Unit	INLET	Experimental Results at OUTLET		Model Results at OUTLET			
			U/S Off	U/S On	U/S Off		U/S On	
					α = 0.04	α = 0.001	α = 0.04	α = 0.001
Dv(10)	(µm)	0.93	2.25	6.82	1.38	1.18	1.32	1.16
Dv(50)	(µm)	4.14	5.07	12.28	4.56	4.49	4.55	4.48
Dv(90)	(µm)	9.31	8.97	19.93	9.74	9.70	9.74	9.69
Span		2.02	1.32	1.07	1.83	1.90	1.85	1.90
D[3][2]	(µm)	2.22	3.57	8.85	2.75	2.49	2.69	2.46
D[4][3]	(µm)	4.90	5.60	13.33	5.28	5.16	5.26	5.14
% Transm.		69.6%	64.5%	91.4%	---	---	---	---
Conc. (Cv)	ppm	19.4	39.1	20.6	---	---	---	---

Trial 4.3.16 Ultrasound Power: 7 W, Air Flow: 8 lpm

Droplet size distributions - Effect of Ultrasound

U/S Power: **7 W**
Air flow: **8 lpm**

Legend: Inlet — Outlet, U/S Off (Expt.) — Outlet, U/S On (Expt.)

Droplet size distributions - Expt. and Model

U/S Power: **7 W**
Air flow: **8 lpm**

Legend: Inlet — Outlet, U/S On (Expt.) — Outlet, U/S On (Model α=0.04) — Outlet, U/S On (Model α=0.001)
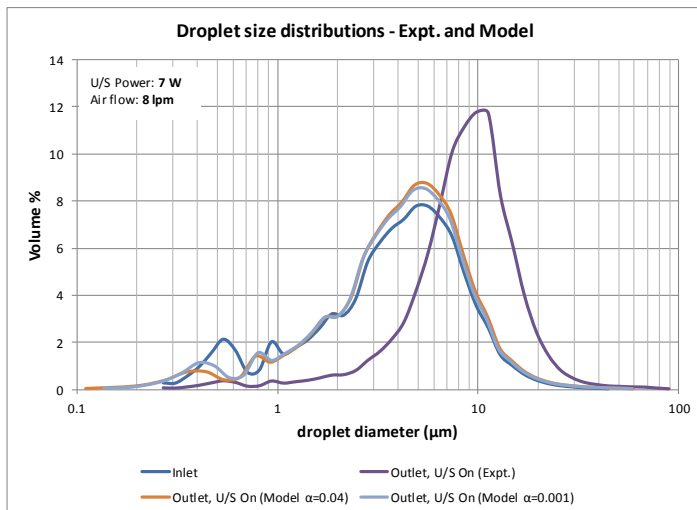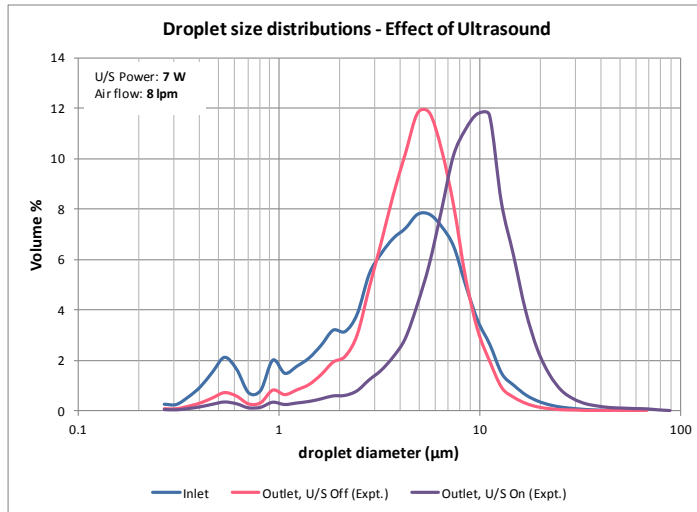
Experiment Date 27/06/2014
Time 09:32:43 - 09:38:13

Conduit Properties	Unit	Value
Diameter	mm	100
Length	mm	300

U/S Field	Unit	Value
Frequency	kHz	21.7
Power	W	7

Parameter	Unit	INLET	Experimental Results at OUTLET		Model Results at OUTLET			
					U/S Off		U/S On	
			U/S Off	U/S On	α = 0.04	α = 0.001	α = 0.04	α = 0.001
Air Properties								
Flow rate	lpm	8.05	---	---	7.80	7.80	7.80	7.80
Temp.	°C	20.5	17.2	18.9	8.7	8.7	8.8	8.8
Rel. Hum.		0.09005	0.928	0.934	1.003	1.002	1.003	1.001
Sp. Humidity	g/kg	1.34	11.43	12.84	7.00	7.00	7.07	7.07
Water Droplet Properties								
Flow rate	ml/min	0.339	---	---	0.284	0.284	0.284	0.284
Temp.	°C	23.55	---	---	8.7	8.7	8.8	8.8
Length to end of calculation					2	9	2	6

Parameter	Unit	INLET	Experimental Results at OUTLET		Model Results at OUTLET			
					U/S Off		U/S On	
			U/S Off	U/S On	α = 0.04	α = 0.001	α = 0.04	α = 0.001
Dv(10)	(µm)	0.93	2.02	3.93	1.45	1.27	1.42	1.25
Dv(50)	(µm)	4.14	4.82	8.88	4.65	4.56	4.64	4.55
Dv(90)	(µm)	9.31	8.48	15.83	9.84	9.78	9.83	9.77
Span		2.02	1.34	1.34	1.80	1.87	1.81	1.87
D[3][2]	(µm)	2.22	3.32	5.86	2.88	2.56	2.81	2.53
D[4][3]	(µm)	4.90	5.17	9.75	5.36	5.22	5.34	5.19
% Transm.		69.6%	68.1%	84.4%	---	---	---	---
Conc. (Cv)	ppm	19.4	31.7	25.5	---	---	---	---

Trial 4.3.17 Ultrasound Power: 7 W, Air Flow: 10 lpm

Droplet size distributions - Effect of Ultrasound

U/S Power: **7 W**
Air flow: **10 lpm**

— Inlet — Outlet, U/S Off (Expt.) — Outlet, U/S On (Expt.)

Droplet size distributions - Expt. and Model

U/S Power: **7 W**
Air flow: **10 lpm**

— Inlet — Outlet, U/S On (Expt.) — Outlet, U/S On (Model α=0.04) — Outlet, U/S On (Model α=0.001)
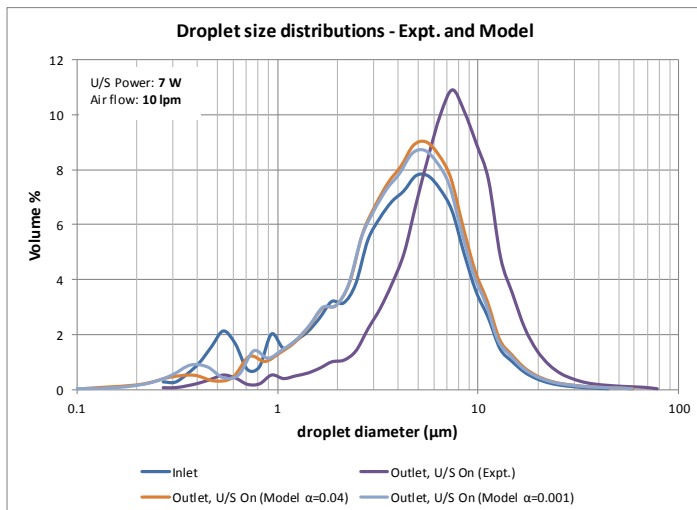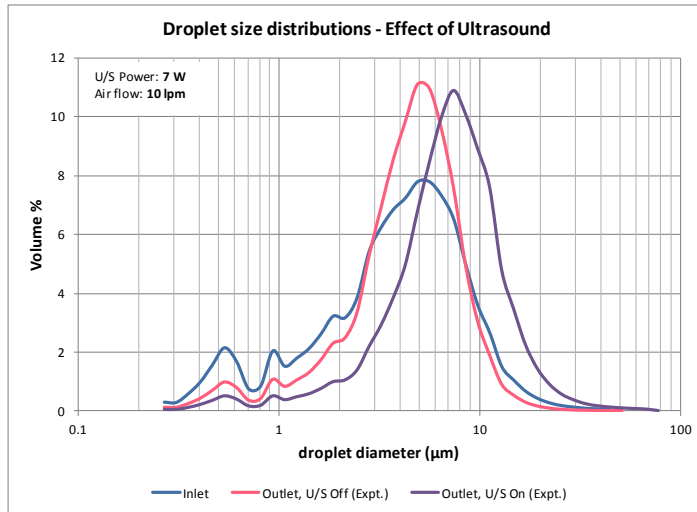
Experiment Date	27/06/2014
Time	09:45:25 - 09:50:44

Conduit Properties	Unit	Value
Diameter	mm	100
Length	mm	300

U/S Field	Unit	Value
Frequency	kHz	21.7
Power	W	7

Parameter	Unit	INLET	Experimental Results at OUTLET		Model Results at OUTLET			
			U/S Off	U/S On	U/S Off		U/S On	
					α = 0.04	α = 0.001	α = 0.04	α = 0.001
Air Properties								
Flow rate	lpm	9.99	---	---	9.67	9.67	9.67	9.67
Temp.	°C	20.5	16.6	17.5	8.4	8.4	8.6	8.6
Rel. Hum.		0.08685	0.926	0.931	1.002	1.001	1.003	1.000
Sp. Humidity	g/kg	1.29	10.98	11.70	6.88	6.88	6.95	6.95
Water Droplet Properties								
Flow rate	ml/min	0.339	---	---	0.272	0.272	0.272	0.272
Temp.	°C	23.3	---	---	8.4	8.4	8.6	8.6
Length to end of calculation					3	11	2	9

Parameter	Unit	INLET	Experimental Results at OUTLET		Model Results at OUTLET			
			U/S Off	U/S On	U/S Off		U/S On	
					α = 0.04	α = 0.001	α = 0.04	α = 0.001
Dv(10)	(µm)	0.93	1.71	2.88	1.58	1.40	1.56	1.37
Dv(50)	(µm)	4.14	4.63	7.11	4.78	4.67	4.77	4.65
Dv(90)	(µm)	9.31	8.40	13.76	9.96	9.90	9.96	9.89
Span		2.02	1.44	1.53	1.75	1.82	1.76	1.83
D[3][2]	(µm)	2.22	3.00	4.57	3.08	2.68	3.00	2.65
D[4][3]	(µm)	4.90	4.98	8.15	5.46	5.30	5.44	5.27
% Transm.		69.6%	75.9%	83.1%	---	---	---	---
Conc. (Cv)	ppm	19.4	20.4	21.5	---	---	---	---

Trial 4.3.18 Ultrasound Power: 7 W, Air Flow: 12 lpm

Droplet size distributions - Effect of Ultrasound

U/S Power: **7 W**
Air flow: **12 lpm**

Droplet size distributions - Expt. and Model

U/S Power: **7 W**
Air flow: **12 lpm**
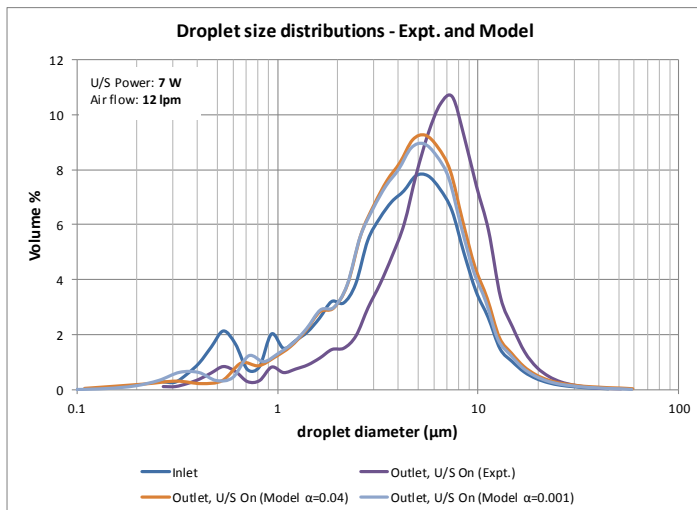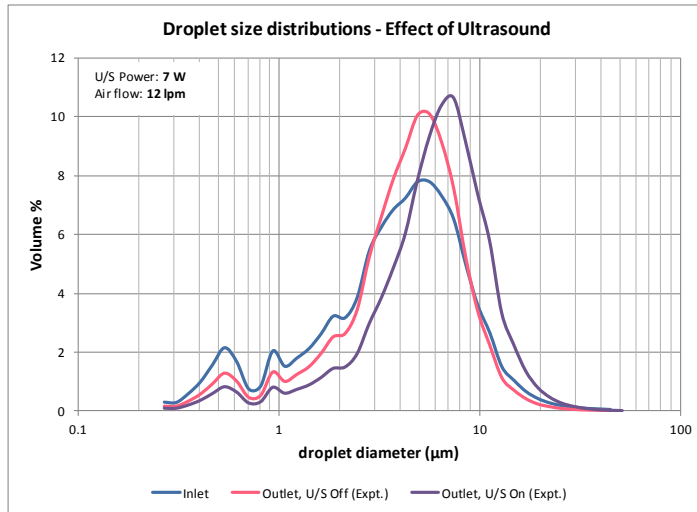
Experiment Date	27/06/2014	
Time	09:58:25 - 10:03:43	

Conduit Properties	Unit	Value
Diameter	mm	100
Length	mm	300

U/S Field	Unit	Value
Frequency	kHz	21.7
Power	W	7

Parameter	Unit	INLET	Experimental Results at OUTLET		Model Results at OUTLET			
					U/S Off		U/S On	
			U/S Off	U/S On	α = 0.04	α = 0.001	α = 0.04	α = 0.001
Air Properties								
Flow rate	lpm	11.95	---	---	11.60	11.60	11.50	11.50
Temp.	°C	20.85	16	17	8.6	8.6	8.6	8.6
Rel. Hum.		0.08715	0.922	0.927	1.002	1.000	1.002	1.000
Sp. Humidity	g/kg	1.33	10.51	11.28	6.94	6.94	6.98	6.98
Water Droplet Properties								
Flow rate	ml/min	0.339	---	---	0.259	0.259	0.259	0.259
Temp.	°C	23.85	---	---	8.6	8.5	8.6	8.6
Length to end of calculation					3	15	2	14

Parameter	Unit	INLET	Experimental Results at OUTLET		Model Results at OUTLET			
					U/S Off		U/S On	
			U/S Off	U/S On	α = 0.04	α = 0.001	α = 0.04	α = 0.001
Dv(10)	(µm)	0.93	1.44	2.14	1.73	1.53	1.69	1.50
Dv(50)	(µm)	4.14	4.58	6.21	4.91	4.79	4.90	4.77
Dv(90)	(µm)	9.31	8.73	11.71	10.10	10.02	10.09	10.00
Span		2.02	1.59	1.54	1.70	1.77	1.72	1.78
D[3][2]	(µm)	2.22	2.76	3.70	3.30	2.84	3.21	2.78
D[4][3]	(µm)	4.90	5.00	6.81	5.57	5.38	5.55	5.35
% Transm.		69.6%	80.7%	85.3%	---	---	---	---
Conc. (Cv)	ppm	19.4	14.5	14.7	---	---	---	---

Trial 4.3.19 Ultrasound Power: 7 W, Air Flow: 15 lpm

Droplet size distributions - Effect of Ultrasound

U/S Power: **7 W**
Air flow: **15 lpm**

— Inlet — Outlet, U/S Off (Expt.) — Outlet, U/S On (Expt.)

Droplet size distributions - Expt. and Model

U/S Power: **7 W**
Air flow: **15 lpm**

— Inlet — Outlet, U/S On (Expt.)
— Outlet, U/S On (Model α=0.04) — Outlet, U/S On (Model α=0.001)
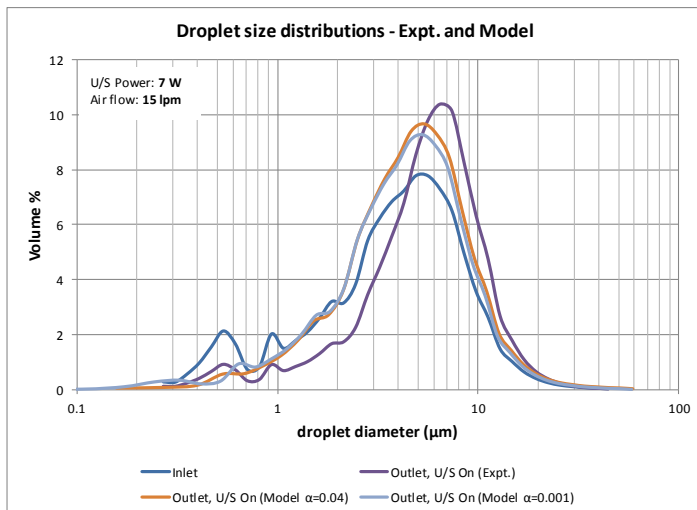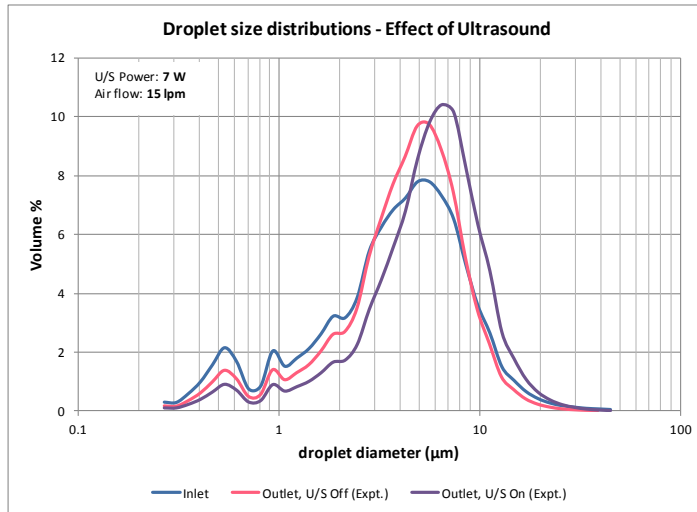
Experiment Date	27/06/2014
Time	10:23:19 - 10:28:36

Conduit Properties	Unit	Value
Diameter	mm	100
Length	mm	300

U/S Field	Unit	Value
Frequency	kHz	21.7
Power	W	7

Parameter	Unit	INLET	Experimental Results at OUTLET		Model Results at OUTLET			
					U/S Off		U/S On	
			U/S Off	U/S On	α = 0.04	α = 0.001	α = 0.04	α = 0.001
Air Properties								
Flow rate	lpm	15.1	---	---	14.59	14.59	14.58	14.58
Temp.	°C	21.05	15.6	16.2	8.5	8.5	8.5	8.5
Rel. Hum.		0.08485	0.918	0.924	1.002	1.000	1.002	1.000
Sp. Humidity	g/kg	1.31	10.19	10.67	6.91	6.91	6.94	6.94
Water Droplet Properties								
Flow rate	ml/min	0.339	---	---	0.238	0.238	0.238	0.238
Temp.	°C	23.75	---	---	8.5	8.5	8.5	8.5
Length to end of calculation					4	29	3	26

Parameter	Unit	INLET	Experimental Results at OUTLET		Model Results at OUTLET			
					U/S Off		U/S On	
			U/S Off	U/S On	α = 0.04	α = 0.001	α = 0.04	α = 0.001
Dv(10)	(μm)	0.93	1.35	1.94	1.98	1.73	1.95	1.70
Dv(50)	(μm)	4.14	4.54	5.77	5.12	4.75	5.11	4.71
Dv(90)	(μm)	9.31	8.79	11.05	10.31	10.22	10.31	10.20
Span		2.02	1.64	1.58	1.63	1.79	1.64	1.81
D[3][2]	(μm)	2.22	2.68	3.45	3.58	3.11	3.52	3.04
D[4][3]	(μm)	4.90	4.98	6.34	5.74	5.51	5.71	5.48
% Transm.		69.6%	84.7%	87.3%	---	---	---	---
Conc. (Cv)	ppm	19.4	10.9	11.7	---	---	---	---

Trial 4.3.20 Ultrasound Power: 7 W, Air Flow: 18 lpm

Droplet size distributions - Effect of Ultrasound

U/S Power: **7 W**
Air flow: **18 lpm**

Legend: Inlet — Outlet, U/S Off (Expt.) — Outlet, U/S On (Expt.)

Droplet size distributions - Expt. and Model

U/S Power: **7 W**
Air flow: **18 lpm**

Legend: Inlet — Outlet, U/S On (Expt.) — Outlet, U/S On (Model α=0.04) — Outlet, U/S On (Model α=0.001)
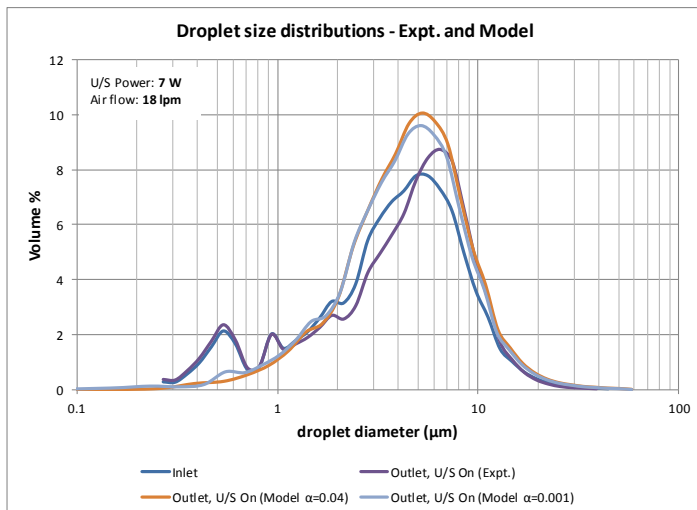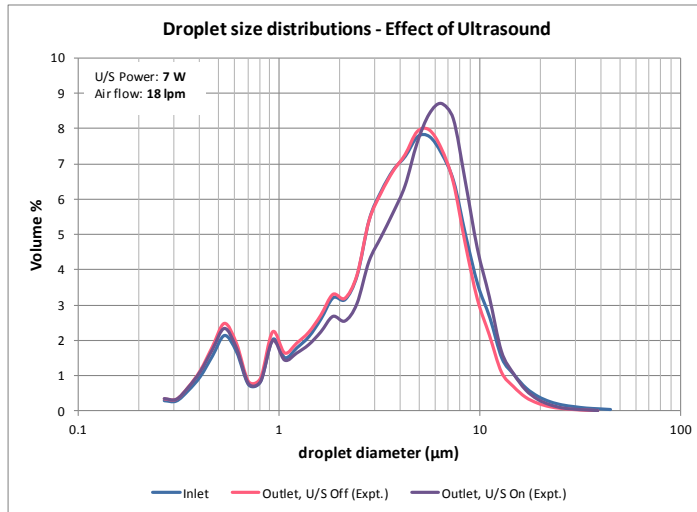
| Experiment Date | 27/06/2014 |
| Time | 10:38:15 - 10:43:38 |

Conduit Properties	Unit	Value
Diameter	mm	100
Length	mm	300

U/S Field	Unit	Value
Frequency	kHz	21.7
Power	W	7

Parameter	Unit	INLET	Experimental Results at OUTLET		Model Results at OUTLET			
			U/S Off	U/S On	U/S Off		U/S On	
					α = 0.04	α = 0.001	α = 0.04	α = 0.001
Air Properties								
Flow rate	lpm	18	---	---	17.37	17.37	17.38	17.38
Temp.	°C	21.3	14.7	15.2	8.5	8.5	8.6	8.6
Rel. Hum.		0.08205	0.917	0.921	1.001	1.000	1.001	1.000
Sp. Humidity	g/kg	1.28	9.60	9.97	6.94	6.94	6.96	6.97
Water Droplet Properties								
Flow rate	ml/min	0.339	---	---	0.217	0.218	0.218	0.218
Temp.	°C	25.6	---	---	8.5	8.5	8.6	8.6
Length to end of calculation					5	50	3	43

Parameter	Unit	INLET	Experimental Results at OUTLET		Model Results at OUTLET			
			U/S Off	U/S On	U/S Off		U/S On	
					α = 0.04	α = 0.001	α = 0.04	α = 0.001
Dv(10)	(µm)	0.93	0.80	0.87	2.15	1.91	2.07	1.82
Dv(50)	(µm)	4.14	3.96	4.68	4.76	4.49	4.71	4.46
Dv(90)	(µm)	9.31	8.62	9.64	10.57	10.41	10.55	10.38
Span		2.02	1.97	1.87	1.77	1.89	1.80	1.92
D[3][2]	(µm)	2.22	2.05	2.22	3.78	3.37	3.72	3.28
D[4][3]	(µm)	4.90	4.51	5.12	5.90	5.63	5.86	5.58
% Transm.		69.6%	86.8%	89.7%	---	---	---	---
Conc. (Cv)	ppm	19.4	7.0	5.9	---	---	---	---

Trial 4.3.21 Ultrasound Power: 7 W, Air Flow: 20 lpm

Droplet size distributions - Effect of Ultrasound

U/S Power: **7 W**
Air flow: **20 lpm**

Droplet size distributions - Expt. and Model

U/S Power: **7 W**
Air flow: **20 lpm**
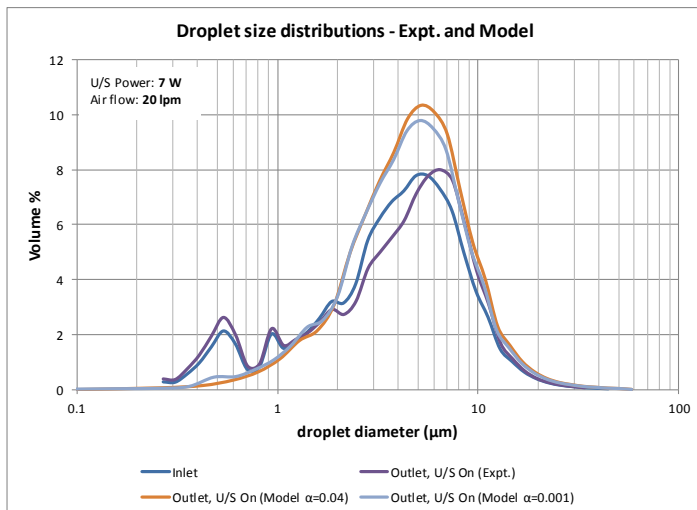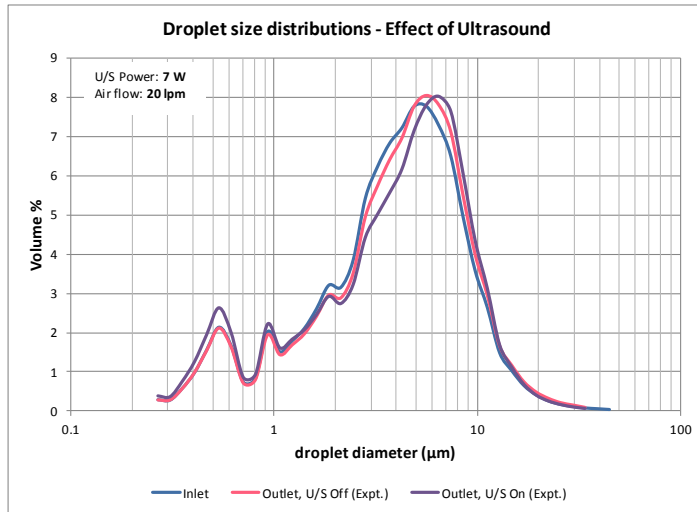
Experiment Date	27/06/2014	
Time	10:47:27 - 10:51:00	

Conduit Properties	Unit	Value
Diameter	mm	100
Length	mm	300

U/S Field	Unit	Value
Frequency	kHz	21.7
Power	W	7

Parameter	Unit	INLET	Experimental Results at OUTLET		Model Results at OUTLET			
			U/S Off	U/S On	U/S Off		U/S On	
					α = 0.04	α = 0.001	α = 0.04	α = 0.001
Air Properties								
Flow rate	lpm	20.1	---	---	19.40	19.40	19.40	19.40
Temp.	°C	21.35	14.3	14.5	8.6	8.6	8.7	8.7
Rel. Hum.		0.08575	0.917	0.919	1.001	1.000	1.001	1.000
Sp. Humidity	g/kg	1.35	9.35	9.50	6.97	6.97	7.00	7.00
Water Droplet Properties								
Flow rate	ml/min	0.339	---	---	0.204	0.205	0.204	0.204
Temp.	°C	26.7	---	---	8.6	8.6	8.7	8.6
Length to end of calculation					6	69	4	62

Parameter	Unit	INLET	Experimental Results at OUTLET		Model Results at OUTLET			
			U/S Off	U/S On	U/S Off		U/S On	
					α = 0.04	α = 0.001	α = 0.04	α = 0.001
Dv(10)	(µm)	0.93	0.93	0.73	2.11	1.81	2.06	1.77
Dv(50)	(µm)	4.14	4.39	4.42	4.78	4.60	4.77	4.57
Dv(90)	(µm)	9.31	9.71	9.71	10.78	10.58	10.77	10.55
Span		2.02	2.00	2.03	1.81	1.91	1.83	1.92
D[3][2]	(µm)	2.22	2.27	2.07	3.90	3.49	3.84	3.43
D[4][3]	(µm)	4.90	5.10	5.02	6.00	5.70	5.96	5.65
% Transm.		69.6%	90.1%	91.4%	---	---	---	---
Conc. (Cv)	ppm	19.4	5.7	4.5	---	---	---	---

Trial 4.3.22 Ultrasound Power: 10 W, Air Flow: 6.5 lpm

Droplet size distributions - Effect of Ultrasound

Droplet size distributions - Expt. and Model
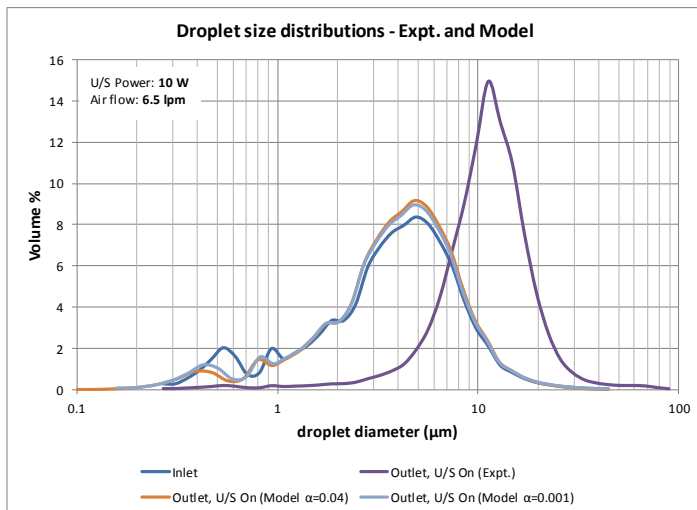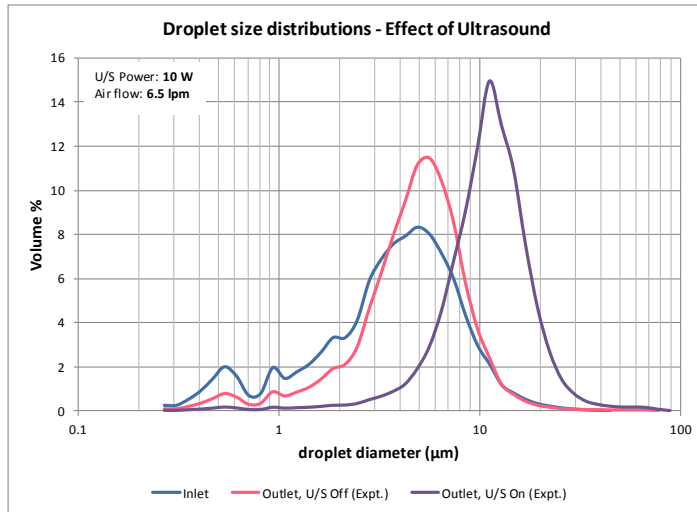
| Experiment Date | 30/05/2014 |
| Time | 10:39:13 - 10:44:17 |

Conduit Properties	Unit	Value
Diameter	mm	100
Length	mm	300

U/S Field	Unit	Value
Frequency	kHz	21.7
Power	W	10

Parameter	Unit	INLET	Experimental Results at OUTLET		Model Results at OUTLET			
			U/S Off	U/S On	U/S Off		U/S On	
					α = 0.04	α = 0.001	α = 0.04	α = 0.001
Air Properties								
Flow rate	lpm	6.52	---	---	6.31	6.31	6.32	6.32
Temp.	°C	21.75	18.9	20.5	9.4	9.4	9.5	9.5
Rel. Hum.		0.0867	0.934	0.937	1.003	1.002	1.003	1.000
Sp. Humidity	g/kg	1.40	12.84	14.25	7.38	7.38	7.41	7.41
Water Droplet Properties								
Flow rate	ml/min	0.331	---	---	0.284	0.285	0.284	0.284
Temp.	°C	22.9	---	---	9.4	9.4	9.5	9.5
Length to end of calculation					1	5	1	4

Parameter	Unit	INLET	Experimental Results at OUTLET		Model Results at OUTLET			
			U/S Off	U/S On	U/S Off		U/S On	
					α = 0.04	α = 0.001	α = 0.04	α = 0.001
Dv(10)	(µm)	0.96	1.98	5.91	1.37	1.23	1.35	1.21
Dv(50)	(µm)	3.99	4.96	11.22	4.37	4.30	4.36	4.29
Dv(90)	(µm)	8.68	8.96	18.79	9.00	8.96	9.00	8.96
Span		1.93	1.41	1.15	1.75	1.80	1.75	1.80
D[3][2]	(µm)	2.24	3.32	8.22	2.71	2.50	2.66	2.48
D[4][3]	(µm)	4.65	5.47	12.17	4.97	4.87	4.96	4.85
% Transm.		72.1%	66.2%	92.2%	---	---	---	---
Conc. (Cv)	ppm	17.7	34.1	17.3	---	---	---	---

Trial 4.3.23 Ultrasound Power: 10 W, Air Flow: 8 lpm

Droplet size distributions - Effect of Ultrasound

U/S Power: **10 W**
Air flow: **8 lpm**

Legend: Inlet — Outlet, U/S Off (Expt.) — Outlet, U/S On (Expt.)

Droplet size distributions - Expt. and Model

U/S Power: **10 W**
Air flow: **8 lpm**

Legend: Inlet — Outlet, U/S On (Expt.) — Outlet, U/S On (Model α=0.04) — Outlet, U/S On (Model α=0.001)
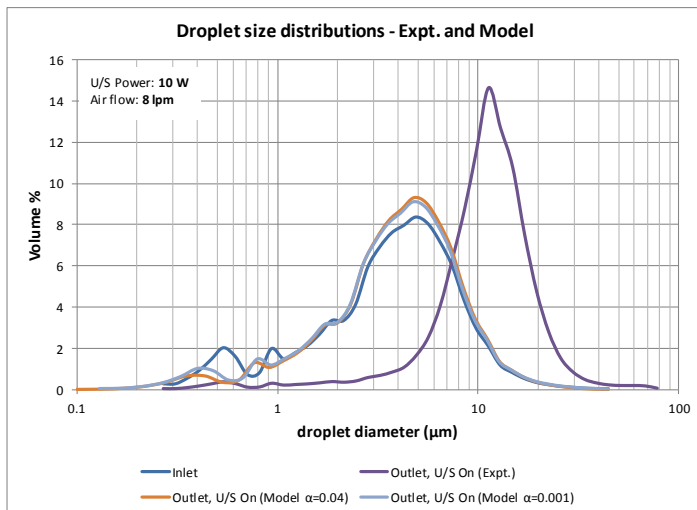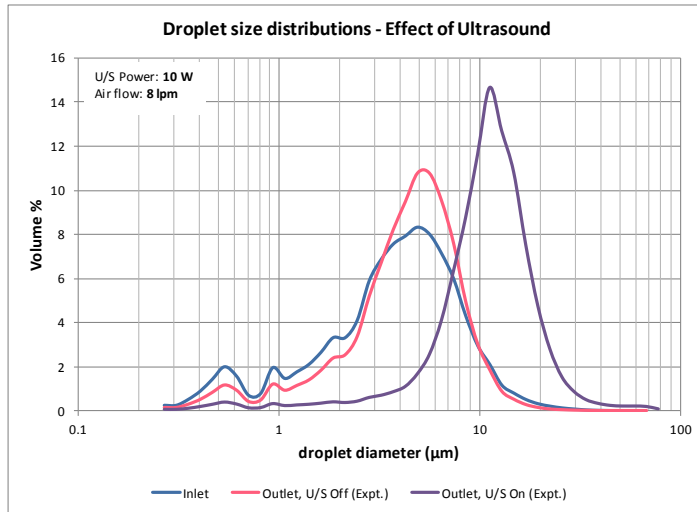
| Experiment Date | 30/05/2014 |
| Time | 10:56:30 - 11:01:36 |

Conduit Properties	Unit	Value
Diameter	mm	100
Length	mm	300

U/S Field	Unit	Value
Frequency	kHz	21.7
Power	W	10

Parameter	Unit	INLET	Experimental Results at OUTLET		Model Results at OUTLET			
					U/S Off		U/S On	
			U/S Off	U/S On	α = 0.04	α = 0.001	α = 0.04	α = 0.001
Air Properties								
Flow rate	lpm	8	---	---	7.74	7.74	7.74	7.74
Temp.	°C	21.55	18.4	20.3	9.2	9.2	9.4	9.4
Rel. Hum.		0.0918	0.93	0.938	1.003	1.001	1.003	1.000
Sp. Humidity	g/kg	1.46	12.38	14.09	7.28	7.27	7.36	7.36
Water Droplet Properties								
Flow rate	ml/min	0.331	---	---	0.275	0.276	0.275	0.275
Temp.	°C	23.7	---	---	9.2	9.2	9.4	9.4
Length to end of calculation					1	6	1	5

Parameter	Unit	INLET	Experimental Results at OUTLET		Model Results at OUTLET			
					U/S Off		U/S On	
			U/S Off	U/S On	α = 0.04	α = 0.001	α = 0.04	α = 0.001
Dv(10)	(µm)	0.96	1.55	5.47	1.47	1.32	1.45	1.30
Dv(50)	(µm)	3.99	4.59	11.23	4.45	4.37	4.44	4.36
Dv(90)	(µm)	8.68	8.37	19.13	9.07	9.02	9.07	9.02
Span		1.93	1.49	1.22	1.71	1.76	1.71	1.77
D[3][2]	(µm)	2.24	2.84	6.88	2.83	2.57	2.78	2.54
D[4][3]	(µm)	4.65	4.94	12.17	5.04	4.91	5.02	4.89
% Transm.		72.1%	68.0%	92.6%	---	---	---	---
Conc. (Cv)	ppm	17.7	27.0	13.7	---	---	---	---

Trial 4.3.24 Ultrasound Power: 10 W, Air Flow: 10 lpm

Droplet size distributions - Effect of Ultrasound

U/S Power: **10 W**
Air flow: **10 lpm**

Droplet size distributions - Expt. and Model

U/S Power: **10 W**
Air flow: **10 lpm**

Experiment Date	30/05/2014	
Time	11:16:45 - 11:18:53	

Conduit Properties	Unit	Value
Diameter	mm	100
Length	mm	300

U/S Field	Unit	Value
Frequency	kHz	21.7
Power	W	10

Parameter	Unit	INLET	Experimental Results at OUTLET		Model Results at OUTLET			
			U/S Off	U/S On	U/S Off		U/S On	
					α = 0.04	α = 0.001	α = 0.04	α = 0.001
Air Properties								
Flow rate	lpm	10	---	---	9.67	9.67	9.67	9.67
Temp.	°C	21.85	18	19.9	9.4	9.4	9.6	9.6
Rel. Hum.		0.09925	0.931	0.934	1.002	1.000	1.002	1.000
Sp. Humidity	g/kg	1.61	12.08	13.68	7.35	7.35	7.44	7.44
Water Droplet Properties								
Flow rate	ml/min	0.331	---	---	0.263	0.263	0.262	0.262
Temp.	°C	24.55	---	---	9.4	9.4	9.6	9.6
Length to end of calculation					2	10	1	9

Parameter	Unit	INLET	Experimental Results at OUTLET		Model Results at OUTLET			
			U/S Off	U/S On	U/S Off		U/S On	
					α = 0.04	α = 0.001	α = 0.04	α = 0.001
Dv(10)	(µm)	0.96	1.83	7.46	1.61	1.44	1.59	1.42
Dv(50)	(µm)	3.99	4.81	12.79	4.56	4.47	4.55	4.45
Dv(90)	(µm)	8.68	8.76	21.02	9.21	9.12	9.21	9.11
Span		1.93	1.44	1.06	1.67	1.72	1.67	1.73
D[3][2]	(µm)	2.24	3.15	10.56	3.02	2.69	2.96	2.66
D[4][3]	(µm)	4.65	5.22	14.14	5.13	4.98	5.11	4.96
% Transm.		72.1%	75.7%	94.7%	---	---	---	---
Conc. (Cv)	ppm	17.7	21.7	15.2	---	---	---	---

Trial 4.3.25 Ultrasound Power: 10 W, Air Flow: 12 lpm

Droplet size distributions - Effect of Ultrasound

U/S Power: **10 W**
Air flow: **12 lpm**

Legend: Inlet — Outlet, U/S Off (Expt.) — Outlet, U/S On (Expt.)

Droplet size distributions - Expt. and Model

U/S Power: **10 W**
Air flow: **12 lpm**

Legend: Inlet — Outlet, U/S On (Expt.) — Outlet, U/S On (Model α=0.04) — Outlet, U/S On (Model α=0.001)
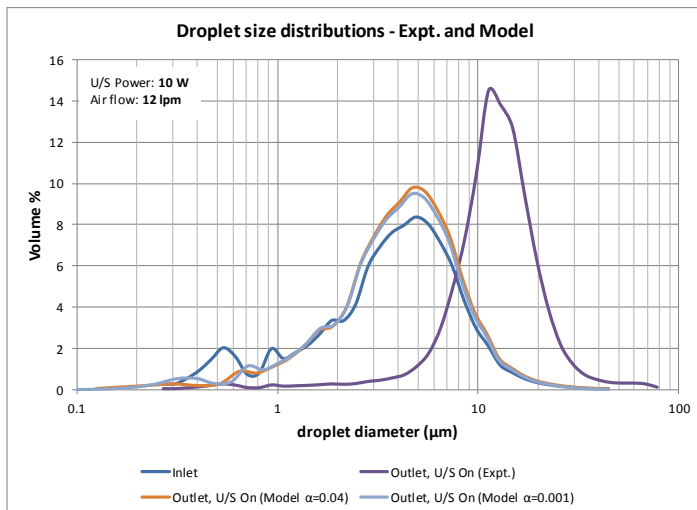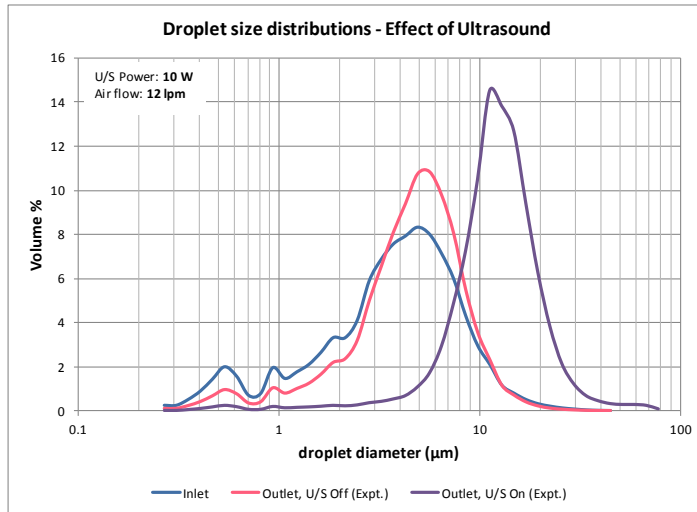
Experiment Date	30/05/2014
Time	11:35:05 - 11:40:15

Conduit Properties	Unit	Value
Diameter	mm	100
Length	mm	300

U/S Field	Unit	Value
Frequency	kHz	21.7
Power	W	10

Parameter	Unit	INLET	Experimental Results at OUTLET		Model Results at OUTLET			
			U/S Off	U/S On	U/S Off		U/S On	
					α = 0.04	α = 0.001	α = 0.04	α = 0.001
Air Properties								
Flow rate	lpm	12	---	---	11.59	11.59	11.59	11.59
Temp.	°C	21.75	17.4	19.3	9.1	9.1	9.3	9.3
Rel. Hum.		0.09745	0.926	0.929	1.002	1.000	1.002	1.000
Sp. Humidity	g/kg	1.57	11.56	13.09	7.22	7.22	7.30	7.30
Water Droplet Properties								
Flow rate	ml/min	0.331	---	---	0.250	0.250	0.249	0.250
Temp.	°C	23.2	---	---	9.1	9.1	9.3	9.3
Length to end of calculation					2	16	1	14

Parameter	Unit	INLET	Experimental Results at OUTLET		Model Results at OUTLET			
			U/S Off	U/S On	U/S Off		U/S On	
					α = 0.04	α = 0.001	α = 0.04	α = 0.001
Dv(10)	(µm)	0.96	1.75	6.65	1.74	1.56	1.72	1.54
Dv(50)	(µm)	3.99	4.77	12.25	4.68	4.56	4.67	4.55
Dv(90)	(µm)	8.68	8.80	20.75	9.37	9.27	9.37	9.25
Span		1.93	1.48	1.15	1.63	1.69	1.64	1.70
D[3][2]	(µm)	2.24	3.07	8.21	3.21	2.83	3.14	2.79
D[4][3]	(µm)	4.65	5.17	13.52	5.23	5.05	5.21	5.03
% Transm.		72.1%	79.2%	93.8%	---	---	---	---
Conc. (Cv)	ppm	17.7	17.7	13.7	---	---	---	---

Trial 4.3.26 Ultrasound Power: 10 W, Air Flow: 15 lpm

Droplet size distributions - Effect of Ultrasound

U/S Power: **10 W**
Air flow: **15 lpm**

Legend: Inlet — Outlet, U/S Off (Expt.) — Outlet, U/S On (Expt.)

Droplet size distributions - Expt. and Model

U/S Power: **10 W**
Air flow: **15 lpm**

Legend: Inlet — Outlet, U/S On (Expt.) — Outlet, U/S On (Model α=0.04) — Outlet, U/S On (Model α=0.001)
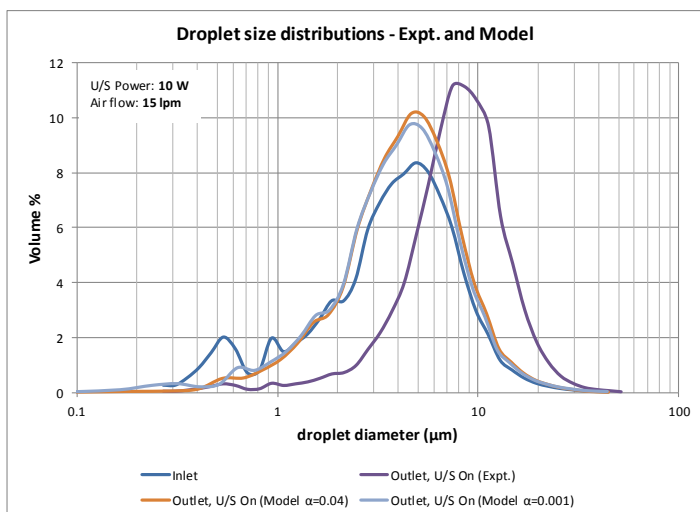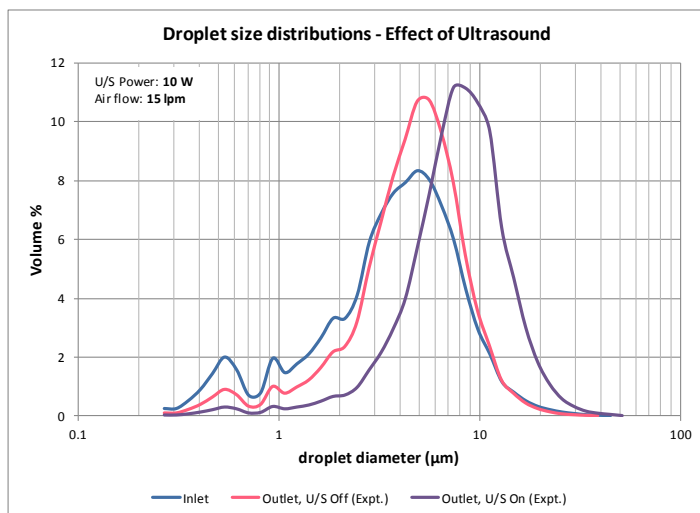
Experiment Date	30/05/2014	
Time	11:51:59 - 11:57:39	

Conduit Properties	Unit	Value
Diameter	mm	100
Length	mm	300

U/S Field	Unit	Value
Frequency	kHz	21.7
Power	W	10

Parameter	Unit	INLET	Experimental Results at OUTLET		Model Results at OUTLET			
			U/S Off	U/S On	U/S Off		U/S On	
					α = 0.04	α = 0.001	α = 0.04	α = 0.001
Air Properties								
Flow rate	lpm	15.1	---	---	14.58	14.58	14.59	14.59
Temp.	°C	21.75	16.5	17.8	9.1	9.1	9.3	9.3
Rel. Hum.		0.0983	0.919	0.926	1.001	1.000	1.001	1.000
Sp. Humidity	g/kg	1.58	10.82	11.86	7.19	7.19	7.28	7.28
Water Droplet Properties								
Flow rate	ml/min	0.331	---	---	0.229	0.230	0.230	0.230
Temp.	°C	25	---	---	9.1	9.0	9.2	9.2
Length to end of calculation					2	30	2	26

Parameter	Unit	INLET	Experimental Results at OUTLET		Model Results at OUTLET			
			U/S Off	U/S On	U/S Off		U/S On	
					α = 0.04	α = 0.001	α = 0.04	α = 0.001
Dv(10)	(µm)	0.96	1.79	3.60	1.96	1.75	1.89	1.71
Dv(50)	(µm)	3.99	4.78	7.91	4.87	4.30	4.85	4.24
Dv(90)	(µm)	8.68	8.89	14.59	9.63	9.50	9.61	9.47
Span		1.93	1.49	1.39	1.57	1.80	1.59	1.83
D[3][2]	(µm)	2.24	3.11	5.54	3.46	3.07	3.39	3.00
D[4][3]	(µm)	4.65	5.22	8.70	5.37	5.16	5.33	5.12
% Transm.		72.1%	85.6%	91.1%	---	---	---	---
Conc. (Cv)	ppm	17.7	12.0	13.1	---	---	---	---

Trial 4.3.27 Ultrasound Power: 10 W, Air Flow: 18 lpm

Droplet size distributions - Effect of Ultrasound

U/S Power: **10 W**
Air flow: **18 lpm**

Inlet — Outlet, U/S Off (Expt.) — Outlet, U/S On (Expt.)

Droplet size distributions - Expt. and Model

U/S Power: **10 W**
Air flow: **18 lpm**

Inlet — Outlet, U/S On (Expt.) — Outlet, U/S On (Model α=0.04) — Outlet, U/S On (Model α=0.001)
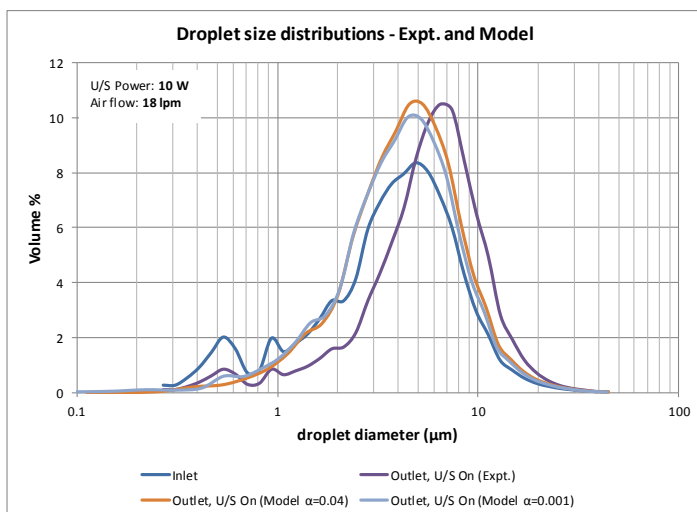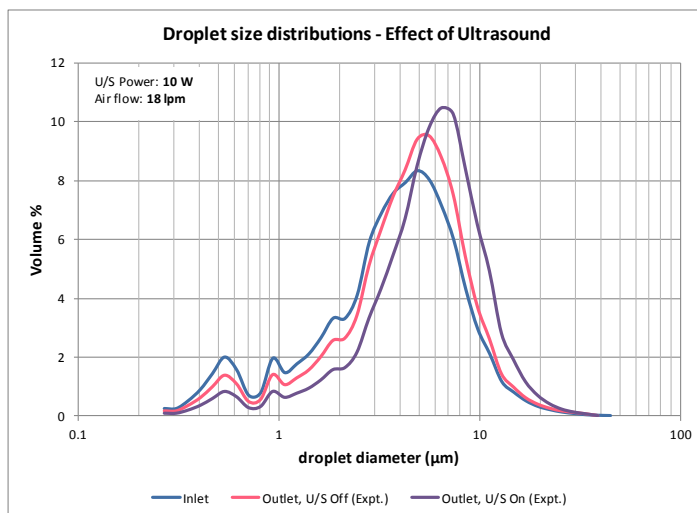
Experiment Date	30/05/2014
Time	12:04:51 - 12:09:34

Conduit Properties	Unit	Value
Diameter	mm	100
Length	mm	300

U/S Field	Unit	Value
Frequency	kHz	21.7
Power	W	10

Parameter	Unit	INLET	Experimental Results at OUTLET		Model Results at OUTLET			
					U/S Off		U/S On	
			U/S Off	U/S On	α = 0.04	α = 0.001	α = 0.04	α = 0.001
Air Properties								
Flow rate	lpm	18.15	---	---	17.47	17.47	17.57	17.57
Temp.	°C	21.95	15.6	16.5	9.1	9.1	9.3	9.3
Rel. Hum.		0.09925	0.915	0.92	1.001	1.000	1.000	1.000
Sp. Humidity	g/kg	1.62	10.16	10.83	7.22	7.22	7.28	7.28
Water Droplet Properties								
Flow rate	ml/min	0.331	---	---	0.210	0.210	0.209	0.209
Temp.	°C	24.55	---	---	9.1	9.1	9.2	9.2
Length to end of calculation					3	51	2	45

Parameter	Unit	INLET	Experimental Results at OUTLET		Model Results at OUTLET			
					U/S Off		U/S On	
			U/S Off	U/S On	α = 0.04	α = 0.001	α = 0.04	α = 0.001
Dv(10)	(µm)	0.96	1.36	2.05	2.10	1.69	2.04	1.83
Dv(50)	(µm)	3.99	4.63	5.87	4.40	4.26	4.39	4.24
Dv(90)	(µm)	8.68	9.24	11.25	9.88	9.73	9.87	9.70
Span		1.93	1.70	1.57	1.77	1.89	1.78	1.86
D[3][2]	(µm)	2.24	2.72	3.57	3.63	3.28	3.58	3.21
D[4][3]	(µm)	4.65	5.19	6.46	5.50	5.25	5.47	5.21
% Transm.		72.1%	88.7%	91.2%	---	---	---	---
Conc. (Cv)	ppm	17.7	8.0	8.2	---	---	---	---

Trial 4.3.28 Ultrasound Power: 10 W, Air Flow: 20 lpm

Droplet size distributions - Effect of Ultrasound

U/S Power: **10 W**
Air flow: **20 lpm**

Inlet — Outlet, U/S Off (Expt.) — Outlet, U/S On (Expt.)

Droplet size distributions - Expt. and Model

U/S Power: **10 W**
Air flow: **20 lpm**

Inlet — Outlet, U/S On (Expt.) — Outlet, U/S On (Model α=0.04) — Outlet, U/S On (Model α=0.001)
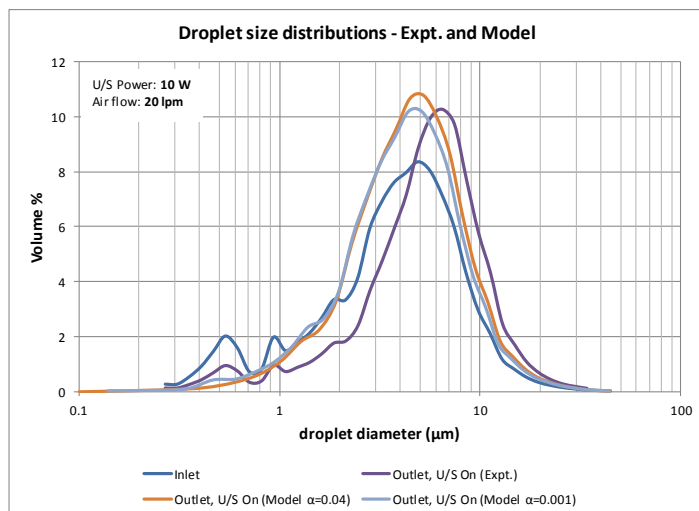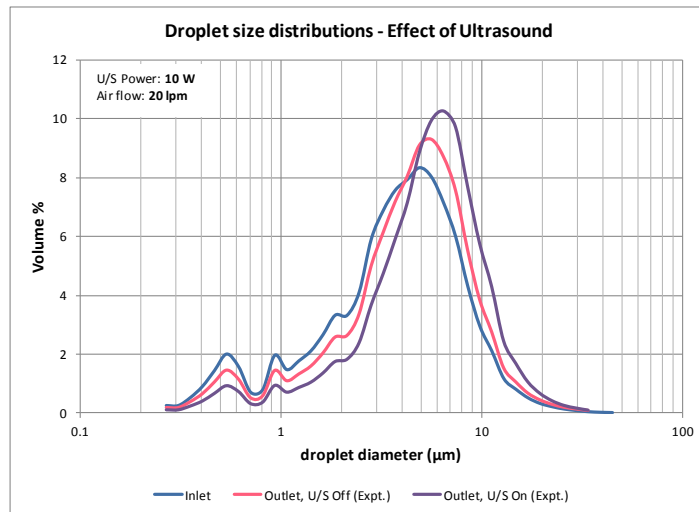
| Experiment Date | 30/05/2014 |
| Time | 12:16:47 - 12:21:57 |

Conduit Properties	Unit	Value
Diameter	mm	100
Length	mm	300

U/S Field	Unit	Value
Frequency	kHz	21.7
Power	W	10

Parameter	Unit	INLET	Experimental Results at OUTLET		Model Results at OUTLET			
					U/S Off		U/S On	
			U/S Off	U/S On	α = 0.04	α = 0.001	α = 0.04	α = 0.001
Air Properties								
Flow rate	lpm	20.05	---	---	19.40	19.40	19.29	19.29
Temp.	°C	22	15.1	15.9	9.2	9.2	9.1	9.1
Rel. Hum.		0.09575	0.915	0.921	1.000	1.000	1.000	1.000
Sp. Humidity	g/kg	1.57	9.83	10.43	7.25	7.25	7.19	7.19
Water Droplet Properties								
Flow rate	ml/min	0.331	---	---	0.197	0.197	0.196	0.196
Temp.	°C	24.95	---	---	9.2	9.2	9.0	9.0
Length to end of calculation					3	70	3	61

Parameter	Unit	INLET	Experimental Results at OUTLET		Model Results at OUTLET			
					U/S Off		U/S On	
			U/S Off	U/S On	α = 0.04	α = 0.001	α = 0.04	α = 0.001
Dv(10)	(µm)	0.96	1.30	1.89	2.06	1.80	2.02	1.77
Dv(50)	(µm)	3.99	4.65	5.60	4.51	4.36	4.50	4.33
Dv(90)	(µm)	8.68	9.47	10.88	10.04	9.88	10.04	9.86
Span		1.93	1.76	1.61	1.77	1.86	1.78	1.87
D[3][2]	(µm)	2.24	2.67	3.38	3.74	3.39	3.69	3.33
D[4][3]	(µm)	4.65	5.25	6.21	5.59	5.31	5.56	5.26
% Transm.		72.1%	90.1%	91.6%	---	---	---	---
Conc. (Cv)	ppm	17.7	6.8	7.4	---	---	---	---

Trial 4.3.29 Ultrasound Power: 12 W, Air Flow: 6.5 lpm

Droplet size distributions - Effect of Ultrasound

U/S Power: **12 W**
Air flow: **6.5 lpm**

Legend: Inlet — Outlet, U/S Off (Expt.) — Outlet, U/S On (Expt.)

Droplet size distributions - Expt. and Model

U/S Power: **12 W**
Air flow: **6.5 lpm**

Legend: Inlet — Outlet, U/S On (Expt.) — Outlet, U/S On (Model α=0.04) — Outlet, U/S On (Model α=0.001)
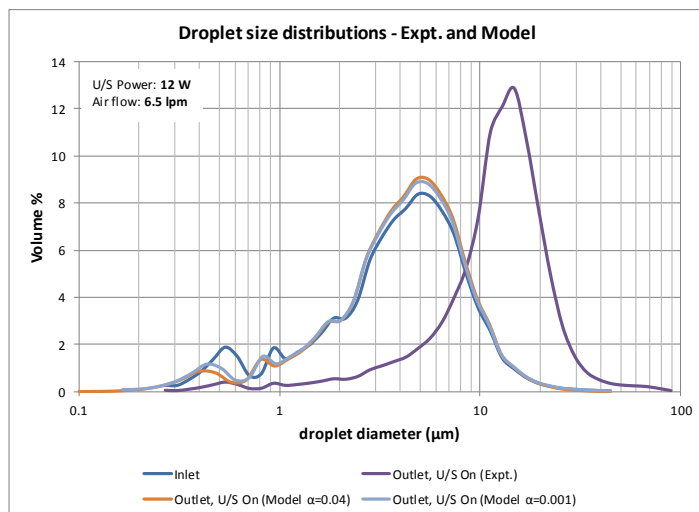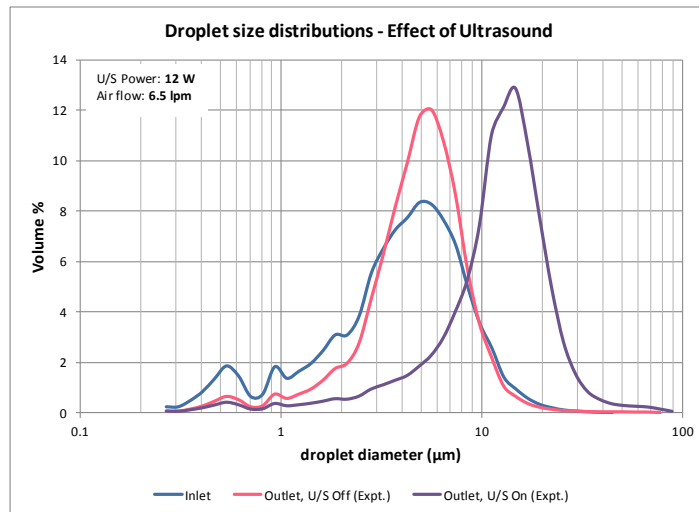
Experiment Date 26/06/2014
Time 10:02:28 - 10:08:08

Conduit Properties	Unit	Value
Diameter	mm	100
Length	mm	300

U/S Field	Unit	Value
Frequency	kHz	21.7
Power	W	12

Parameter	Unit	INLET	Experimental Results at OUTLET		Model Results at OUTLET			
			U/S Off	U/S On	U/S Off		U/S On	
					α = 0.04	α = 0.001	α = 0.04	α = 0.001
Air Properties								
Flow rate	lpm	6.5	---	---	6.30	6.30	6.30	6.30
Temp.	°C	21.75	18.8	20.8	9.9	9.9	9.9	9.9
Rel. Hum.		0.09515	0.931	0.934	1.003	1.002	1.003	1.001
Sp. Humidity	g/kg	1.53	12.71	14.48	7.59	7.59	7.63	7.63
Water Droplet Properties								
Flow rate	ml/min	0.366	---	---	0.319	0.319	0.319	0.319
Temp.	°C	25	---	---	9.9	9.9	9.9	9.9
Length to end of calculation					1	5	1	3

Parameter	Unit	INLET	Experimental Results at OUTLET		Model Results at OUTLET			
			U/S Off	U/S On	U/S Off		U/S On	
					α = 0.04	α = 0.001	α = 0.04	α = 0.001
Dv(10)	(µm)	1.03	2.15	4.56	1.53	1.28	1.39	1.26
Dv(50)	(µm)	4.23	4.99	12.77	4.59	4.52	4.58	4.51
Dv(90)	(µm)	9.05	8.83	22.03	9.43	9.38	9.42	9.37
Span		1.90	1.34	1.37	1.72	1.79	1.76	1.80
D[3][2]	(µm)	2.36	3.47	6.90	2.81	2.61	2.76	2.58
D[4][3]	(µm)	4.86	5.49	13.61	5.16	5.06	5.14	5.04
% Transm.		76.0%	63.4%	92.6%	---	---	---	---
Conc. (Cv)	ppm	15.7	39.3	13.8	---	---	---	---

Trial 4.3.30 Ultrasound Power: 12 W, Air Flow: 8 lpm

Droplet size distributions - Effect of Ultrasound

U/S Power: **12 W**
Air flow: **8 lpm**

Legend: Inlet — Outlet, U/S Off (Expt.) — Outlet, U/S On (Expt.)

Droplet size distributions - Expt. and Model

U/S Power: **12 W**
Air flow: **8 lpm**

Legend: Inlet — Outlet, U/S On (Expt.) — Outlet, U/S On (Model α=0.04) — Outlet, U/S On (Model α=0.001)
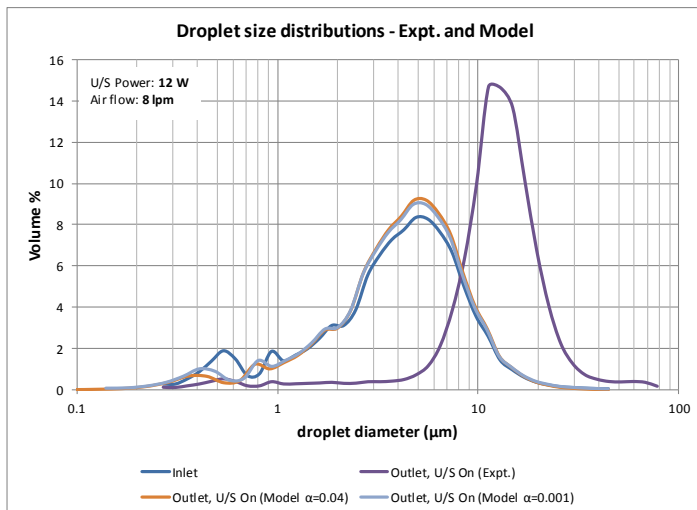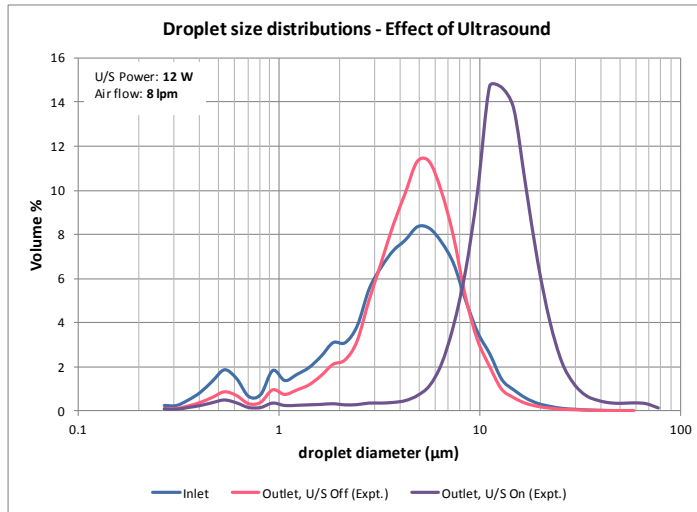
| Experiment Date | 26/06/2014 |
| Time | 10:20:08 - 10:23:37 |

Conduit Properties	Unit	Value
Diameter	mm	100
Length	mm	300

U/S Field	Unit	Value
Frequency	kHz	21.7
Power	W	12

Parameter	Unit	INLET	Experimental Results at OUTLET		Model Results at OUTLET			
			U/S Off	U/S On	U/S Off		U/S On	
					α = 0.04	α = 0.001	α = 0.04	α = 0.001
Air Properties								
Flow rate	lpm	8.09	---	---	7.84	7.84	7.83	7.83
Temp.	°C	21.3	18.4	20.9	9.4	9.4	9.4	9.4
Rel. Hum.		0.09755	0.932	0.933	1.003	1.001	1.003	1.000
Sp. Humidity	g/kg	1.53	12.40	14.55	7.36	7.35	7.34	7.34
Water Droplet Properties								
Flow rate	ml/min	0.366	---	---	0.310	0.310	0.310	0.310
Temp.	°C	23.85	---	---	9.4	9.4	9.4	9.3
Length to end of calculation					1	6	1	5

Parameter	Unit	INLET	Experimental Results at OUTLET		Model Results at OUTLET			
			U/S Off	U/S On	U/S Off		U/S On	
					α = 0.04	α = 0.001	α = 0.04	α = 0.001
Dv(10)	(µm)	1.03	1.85	6.95	1.52	1.37	1.49	1.35
Dv(50)	(µm)	4.23	4.76	12.65	4.67	4.59	4.66	4.58
Dv(90)	(µm)	9.05	8.58	20.96	9.52	9.46	9.51	9.45
Span		1.90	1.41	1.11	1.71	1.76	1.72	1.77
D[3][2]	(µm)	2.36	3.15	7.18	2.93	2.68	2.88	2.65
D[4][3]	(µm)	4.86	5.15	13.81	5.22	5.10	5.21	5.09
% Transm.		76.0%	69.7%	94.6%	---	---	---	---
Conc. (Cv)	ppm	15.7	28.1	10.3	---	---	---	---

264

Trial 4.3.31 Ultrasound Power: 12 W, Air Flow: 10 lpm

Droplet size distributions - Effect of Ultrasound

U/S Power: **12 W**
Air flow: **10 lpm**

Legend: Inlet — Outlet, U/S Off (Expt.) — Outlet, U/S On (Expt.)

Droplet size distributions - Expt. and Model

U/S Power: **12 W**
Air flow: **10 lpm**

Legend: Inlet — Outlet, U/S On (Expt.) — Outlet, U/S On (Model α=0.04) — Outlet, U/S On (Model α=0.001)
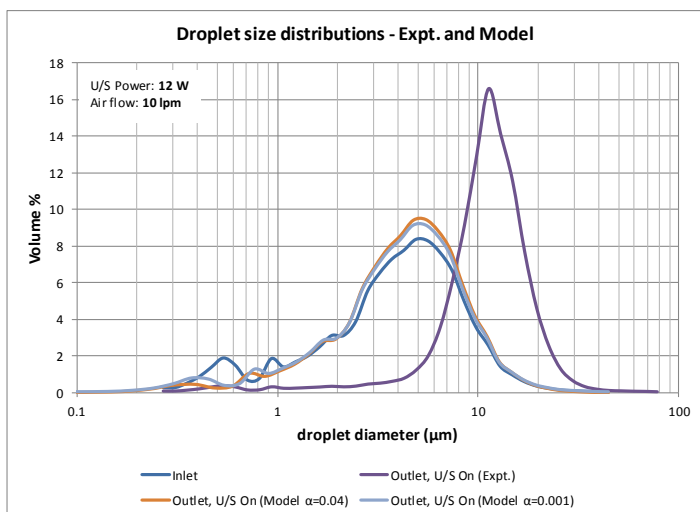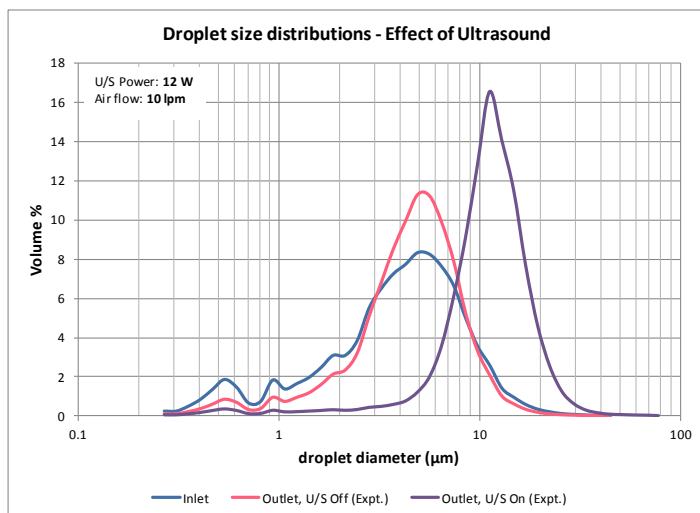
| Experiment Date | 26/06/2014 |
| Time | 10:34:05 - 10:39:19 |

Conduit Properties	Unit	Value		U/S Field	Unit	Value
Diameter	mm	100		Frequency	kHz	21.7
Length	mm	300		Power	W	12

Parameter	Unit	INLET	Experimental Results at OUTLET		Model Results at OUTLET			
					U/S Off		U/S On	
			U/S Off	U/S On	α = 0.04	α = 0.001	α = 0.04	α = 0.001
Air Properties								
Flow rate	lpm	9.99	---	---	9.67	9.67	9.66	9.66
Temp.	°C	21.45	17.8	20.6	9.2	9.2	9.3	9.3
Rel. Hum.		0.0937	0.926	0.932	1.002	1.000	1.002	1.000
Sp. Humidity	g/kg	1.48	11.86	14.27	7.25	7.25	7.33	7.33
Water Droplet Properties								
Flow rate	ml/min	0.366	---	---	0.297	0.298	0.296	0.296
Temp.	°C	24.85	---	---	9.2	9.2	9.3	9.3
Length to end of calculation					2	9	1	8

Parameter	Unit	INLET	Experimental Results at OUTLET		Model Results at OUTLET			
					U/S Off		U/S On	
			U/S Off	U/S On	α = 0.04	α = 0.001	α = 0.04	α = 0.001
Dv(10)	(μm)	1.03	1.86	6.25	1.64	1.48	1.62	1.46
Dv(50)	(μm)	4.23	4.74	11.32	4.77	4.68	4.77	4.67
Dv(90)	(μm)	9.05	8.56	18.03	9.64	9.57	9.64	9.56
Span		1.90	1.41	1.04	1.67	1.73	1.68	1.73
D[3][2]	(μm)	2.36	3.17	7.29	3.11	2.79	3.05	2.76
D[4][3]	(μm)	4.86	5.10	11.88	5.31	5.17	5.29	5.14
% Transm.		76.0%	76.7%	94.5%	---	---	---	---
Conc. (Cv)	ppm	15.7	20.8	10.8	---	---	---	---

Trial 4.3.32 Ultrasound Power: 12 W, Air Flow: 12 lpm

Droplet size distributions - Effect of Ultrasound

U/S Power: **12 W**
Air flow: **12 lpm**

Legend: Inlet — Outlet, U/S Off (Expt.) — Outlet, U/S On (Expt.)

Droplet size distributions - Expt. and Model

U/S Power: **12 W**
Air flow: **12 lpm**

Legend: Inlet — Outlet, U/S On (Expt.) — Outlet, U/S On (Model α=0.04) — Outlet, U/S On (Model α=0.001)
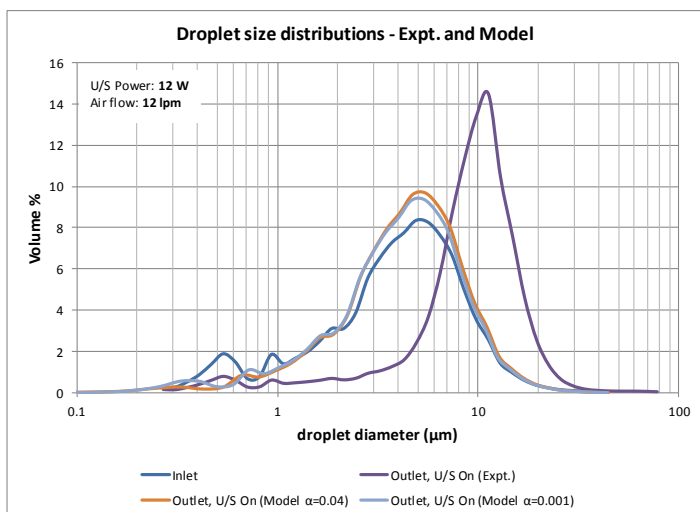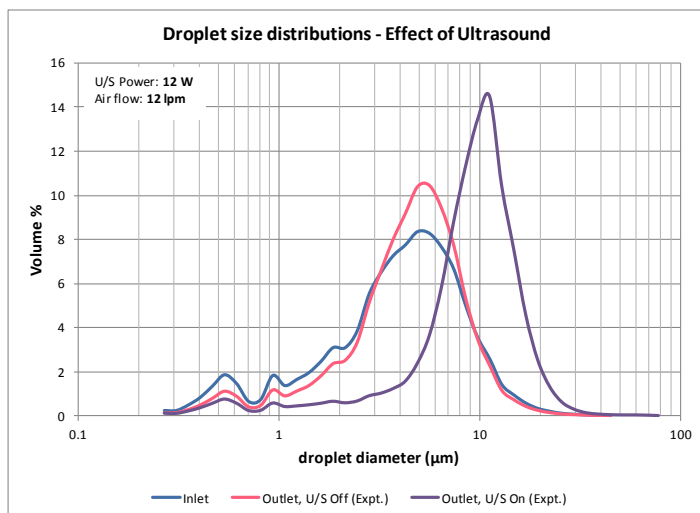
Experiment Date   26/06/2014
Time   10:48:08 - 10:53:18

Conduit Properties	Unit	Value
Diameter	mm	100
Length	mm	300

U/S Field	Unit	Value
Frequency	kHz	21.7
Power	W	12

Parameter	Unit	INLET	Experimental Results at OUTLET		Model Results at OUTLET			
					U/S Off		U/S On	
			U/S Off	U/S On	α = 0.04	α = 0.001	α = 0.04	α = 0.001
Air Properties								
Flow rate	lpm	12	---	---	11.60	11.60	11.60	11.60
Temp.	°C	21.45	17.5	20.1	9.0	9.0	9.2	9.2
Rel. Hum.		0.09205	0.922	0.932	1.002	1.000	1.002	1.000
Sp. Humidity	g/kg	1.45	11.58	13.82	7.16	7.16	7.26	7.26
Water Droplet Properties								
Flow rate	ml/min	0.366	---	---	0.284	0.284	0.283	0.283
Temp.	°C	25.1	---	---	9.0	9.0	9.2	9.2
Length to end of calculation					2	15	1	13

Parameter	Unit	INLET	Experimental Results at OUTLET		Model Results at OUTLET			
					U/S Off		U/S On	
			U/S Off	U/S On	α = 0.04	α = 0.001	α = 0.04	α = 0.001
Dv(10)	(µm)	1.03	1.60	3.62	1.78	1.60	1.76	1.57
Dv(50)	(µm)	4.23	4.67	9.66	4.88	4.78	4.88	4.76
Dv(90)	(µm)	9.05	8.77	15.74	9.76	9.68	9.76	9.67
Span		1.90	1.54	1.25	1.63	1.69	1.64	1.70
D[3][2]	(µm)	2.36	2.92	5.00	3.31	2.93	3.24	2.88
D[4][3]	(µm)	4.86	5.09	9.93	5.40	5.23	5.38	5.20
% Transm.		76.0%	81.2%	91.7%	---	---	---	---
Conc. (Cv)	ppm	15.7	15.0	11.1	---	---	---	---

Trial 4.3.33 Ultrasound Power: 12 W, Air Flow: 15 lpm
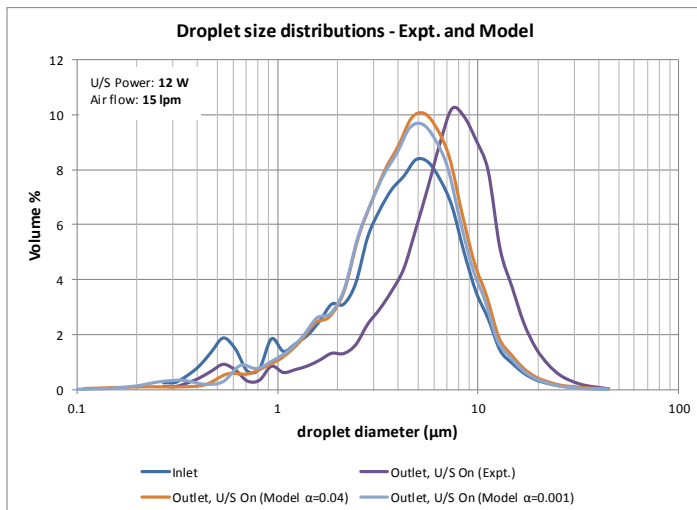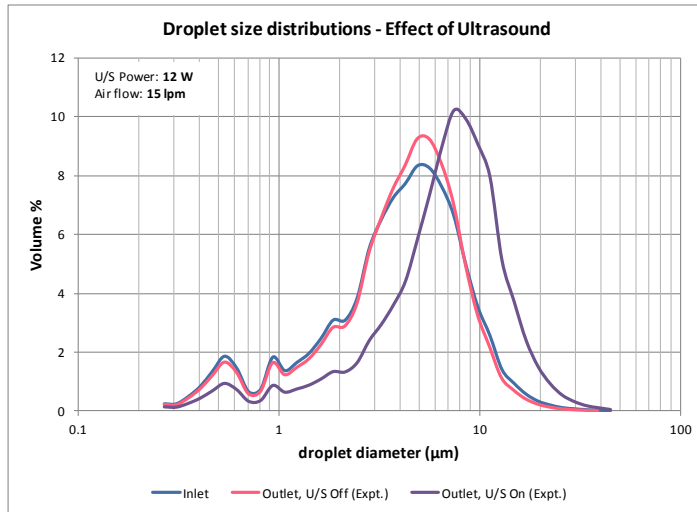
| Experiment Date | 26/06/2014 |
| Time | 10:59:05 - 11:04:22 |

Conduit Properties	Unit	Value
Diameter	mm	100
Length	mm	300

U/S Field	Unit	Value
Frequency	kHz	21.7
Power	W	12

Parameter	Unit	INLET	Experimental Results at OUTLET		Model Results at OUTLET			
					U/S Off		U/S On	
			U/S Off	U/S On	α = 0.04	α = 0.001	α = 0.04	α = 0.001
Air Properties								
Flow rate	lpm	15	---	---	14.49	14.49	14.49	14.49
Temp.	°C	21.6	16.3	17.5	9.0	9.0	9.1	9.1
Rel. Hum.		0.094	0.917	0.925	1.002	1.000	1.001	1.000
Sp. Humidity	g/kg	1.50	10.66	11.62	7.16	7.16	7.22	7.22
Water Droplet Properties								
Flow rate	ml/min	0.366	---	---	0.265	0.265	0.264	0.264
Temp.	°C	25.05	---	---	9.0	9.0	9.1	9.1
Length to end of calculation					2	26	2	23

Parameter	Unit	INLET	Experimental Results at OUTLET		Model Results at OUTLET			
					U/S Off		U/S On	
			U/S Off	U/S On	α = 0.04	α = 0.001	α = 0.04	α = 0.001
Dv(10)	(µm)	1.03	1.15	2.11	2.00	1.77	1.97	1.73
Dv(50)	(µm)	4.23	4.37	7.10	5.05	4.92	5.04	4.61
Dv(90)	(µm)	9.05	8.69	13.67	9.95	9.85	9.94	9.83
Span		1.90	1.73	1.63	1.57	1.64	1.58	1.76
D[3][2]	(µm)	2.36	2.48	3.82	3.56	3.15	3.49	3.08
D[4][3]	(µm)	4.86	4.82	7.76	5.53	5.33	5.50	5.29
% Transm.		76.0%	86.3%	90.5%	---	---	---	---
Conc. (Cv)	ppm	15.7	8.9	9.5	---	---	---	---

Trial 4.3.34 Ultrasound Power: 12 W, Air Flow: 18 lpm

Droplet size distributions - Effect of Ultrasound

U/S Power: **12 W**
Air flow: **18 lpm**

Inlet — Outlet, U/S Off (Expt.) — Outlet, U/S On (Expt.)

Droplet size distributions - Expt. and Model

U/S Power: **12 W**
Air flow: **18 lpm**

Inlet — Outlet, U/S On (Expt.)
Outlet, U/S On (Model α=0.04) — Outlet, U/S On (Model α=0.001)
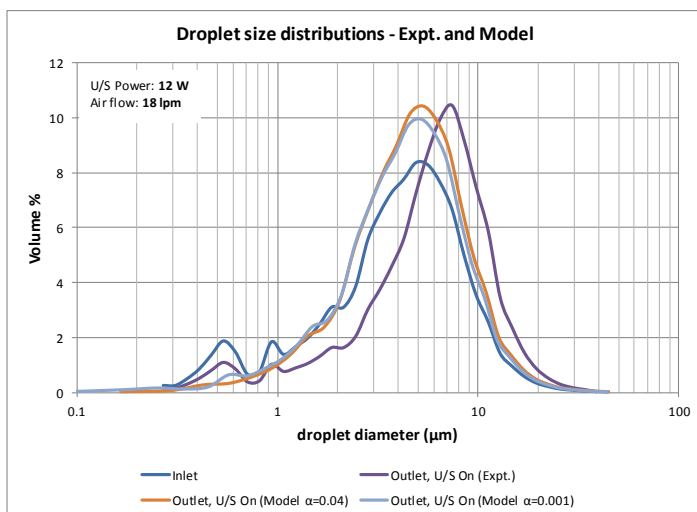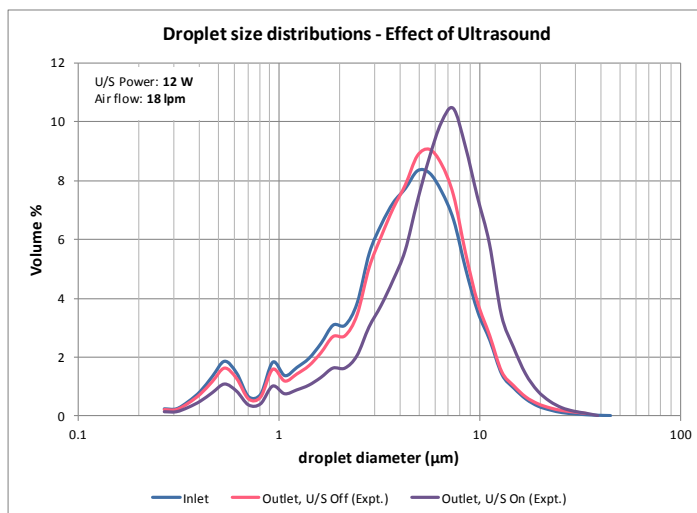
Experiment Date	26/06/2014	
Time	11:10:08 - 11:15:23	

Conduit Properties	Unit	Value
Diameter	mm	100
Length	mm	300

U/S Field	Unit	Value
Frequency	kHz	21.7
Power	W	12

Parameter	Unit	INLET	Experimental Results at OUTLET		Model Results at OUTLET			
			U/S Off	U/S On	U/S Off		U/S On	
					α = 0.04	α = 0.001	α = 0.04	α = 0.001
Air Properties								
Flow rate	lpm	18.1	---	---	17.47	17.47	17.47	17.47
Temp.	°C	21.9	15.5	16.5	9.0	9.0	9.1	9.1
Rel. Hum.		0.08875	0.915	0.924	1.001	1.000	1.000	1.000
Sp. Humidity	g/kg	1.44	10.09	10.88	7.16	7.16	7.19	7.19
Water Droplet Properties								
Flow rate	ml/min	0.366	---	---	0.243	0.243	0.243	0.243
Temp.	°C	25	---	---	9.0	9.0	9.0	9.0
Length to end of calculation					3	46	2	40

Parameter	Unit	INLET	Experimental Results at OUTLET		Model Results at OUTLET			
			U/S Off	U/S On	U/S Off		U/S On	
					α = 0.04	α = 0.001	α = 0.04	α = 0.001
Dv(10)	(µm)	1.03	1.19	1.78	2.17	1.98	2.09	1.88
Dv(50)	(µm)	4.23	4.58	6.19	5.24	4.43	4.55	4.40
Dv(90)	(µm)	9.05	9.38	11.77	10.16	10.04	10.14	10.01
Span		1.90	1.79	1.61	1.52	1.82	1.77	1.85
D[3][2]	(µm)	2.36	2.56	3.37	3.76	3.39	3.70	3.30
D[4][3]	(µm)	4.86	5.16	6.72	5.66	5.42	5.62	5.37
% Transm.		76.0%	88.8%	91.2%	---	---	---	---
Conc. (Cv)	ppm	15.7	7.4	7.7	---	---	---	---

Trial 4.3.35 Ultrasound Power: 12 W, Air Flow: 20 lpm

Droplet size distributions - Effect of Ultrasound

U/S Power: **12 W**
Air flow: **20 lpm**

- Inlet
- Outlet, U/S Off (Expt.)
- Outlet, U/S On (Expt.)

Droplet size distributions - Expt. and Model

U/S Power: **12 W**
Air flow: **20 lpm**

- Inlet
- Outlet, U/S On (Expt.)
- Outlet, U/S On (Model α=0.04)
- Outlet, U/S On (Model α=0.001)
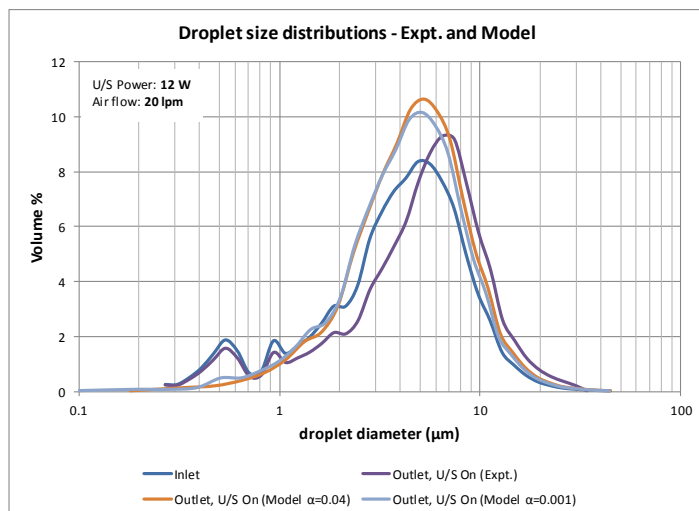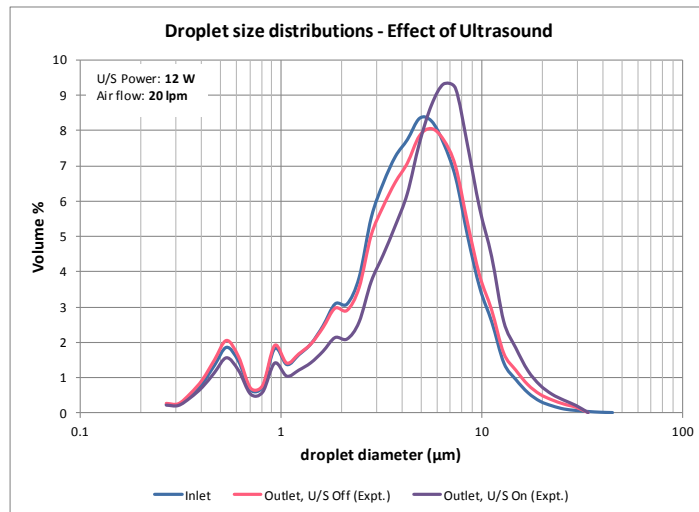
Experiment Date	26/06/2014	
Time	11:19:52 - 11:25:24	

Conduit Properties	Unit	Value
Diameter	mm	100
Length	mm	300

U/S Field	Unit	Value
Frequency	kHz	21.7
Power	W	12

Parameter	Unit	INLET	Experimental Results at OUTLET		Model Results at OUTLET			
			U/S Off	U/S On	U/S Off		U/S On	
					α = 0.04	α = 0.001	α = 0.04	α = 0.001
Air Properties								
Flow rate	lpm	20.1	---	---	19.40	19.40	19.40	19.40
Temp.	°C	21.95	15	16.1	9.1	9.1	9.1	9.1
Rel. Hum.		0.0937	0.914	0.921	1.000	1.000	1.000	1.000
Sp. Humidity	g/kg	1.53	9.76	10.57	7.20	7.20	7.22	7.22
Water Droplet Properties								
Flow rate	ml/min	0.366	---	---	0.231	0.231	0.230	0.230
Temp.	°C	25.3	---	---	9.1	9.1	9.1	9.1
Length to end of calculation					3	62	2	54

Parameter	Unit	INLET	Experimental Results at OUTLET		Model Results at OUTLET			
			U/S Off	U/S On	U/S Off		U/S On	
					α = 0.04	α = 0.001	α = 0.04	α = 0.001
Dv(10)	(µm)	1.03	0.95	1.28	2.09	1.91	2.03	1.84
Dv(50)	(µm)	4.23	4.38	5.46	4.80	4.51	4.76	4.48
Dv(90)	(µm)	9.05	9.76	11.13	10.27	10.15	10.26	10.12
Span		1.90	2.01	1.81	1.71	1.83	1.73	1.85
D[3][2]	(µm)	2.36	2.30	2.79	3.85	3.49	3.80	3.42
D[4][3]	(µm)	4.86	5.11	6.06	5.73	5.47	5.70	5.42
% Transm.		76.0%	91.5%	93.2%	---	---	---	---
Conc. (Cv)	ppm	15.7	5.0	4.8	---	---	---	---

Trial 4.3.36 Ultrasound Power: 15 W, Air Flow: 6.5 lpm

Droplet size distributions - Effect of Ultrasound

U/S Power: **15 W**
Air flow: **6.5 lpm**

Legend: Inlet — Outlet, U/S Off (Expt.) — Outlet, U/S On (Expt.)

Droplet size distributions - Expt. and Model

U/S Power: **15 W**
Air flow: **6.5 lpm**

Legend: Inlet — Outlet, U/S On (Expt.) — Outlet, U/S On (Model α=0.04) — Outlet, U/S On (Model α=0.001)
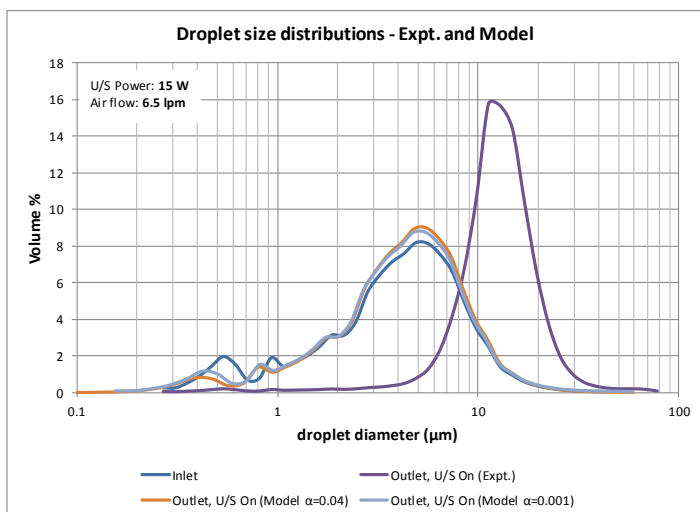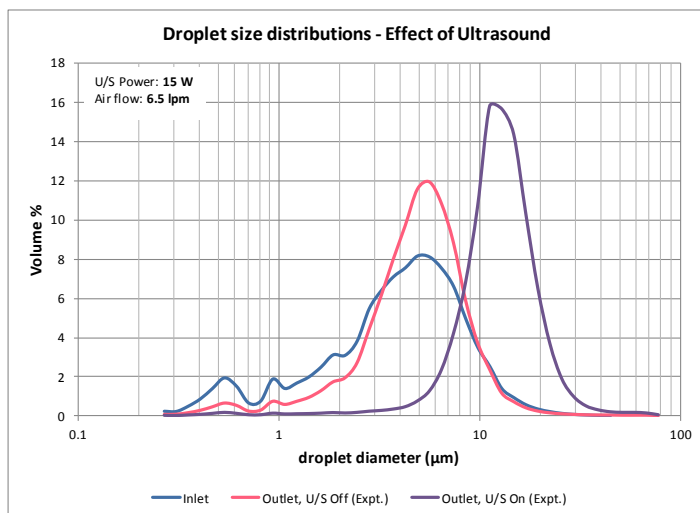
| Experiment Date | 10/06/2014 |
| Time | 13:35:58 - 13:41:56 |

Conduit Properties	Unit	Value
Diameter	mm	100
Length	mm	300

U/S Field	Unit	Value
Frequency	kHz	21.7
Power	W	15

Parameter	Unit	INLET	Experimental Results at OUTLET		Model Results at OUTLET			
					U/S Off		U/S On	
			U/S Off	U/S On	α = 0.04	α = 0.001	α = 0.04	α = 0.001
Air Properties								
Flow rate	lpm	6.585	---	---	6.37	6.37	6.38	6.38
Temp.	°C	21.15	18.7	20.9	9.1	9.1	9.2	9.2
Rel. Hum.		0.07965	0.933	0.939	1.003	1.002	1.003	1.002
Sp. Humidity	g/kg	1.24	12.66	14.65	7.18	7.18	7.24	7.24
Water Droplet Properties								
Flow rate	ml/min	0.339	---	---	0.292	0.292	0.292	0.292
Temp.	°C	23.45	---	---	9.1	9.1	9.2	9.2
Length to end of calculation					2	8	1	5

Parameter	Unit	INLET	Experimental Results at OUTLET		Model Results at OUTLET			
					U/S Off		U/S On	
			U/S Off	U/S On	α = 0.04	α = 0.001	α = 0.04	α = 0.001
Dv(10)	(µm)	0.98	2.17	7.49	1.44	1.28	1.40	1.25
Dv(50)	(µm)	4.21	5.04	12.56	4.61	4.54	4.60	4.52
Dv(90)	(µm)	9.12	8.93	20.08	9.57	9.52	9.57	9.51
Span		1.93	1.34	1.00	1.76	1.82	1.77	1.83
D[3][2]	(µm)	2.31	3.50	9.35	2.87	2.59	2.80	2.56
D[4][3]	(µm)	4.90	5.53	13.50	5.27	5.15	5.25	5.13
% Transm.		66.8%	64.9%	93.5%	---	---	---	---
Conc. (Cv)	ppm	22.5	37.7	16.4	---	---	---	---

Trial 4.3.37 Ultrasound Power: 15 W, Air Flow: 8 lpm

Droplet size distributions - Effect of Ultrasound

U/S Power: **15 W**
Air flow: **8 lpm**

Inlet — Outlet, U/S Off (Expt.) — Outlet, U/S On (Expt.)

Droplet size distributions - Expt. and Model

U/S Power: **15 W**
Air flow: **8 lpm**

Inlet — Outlet, U/S On (Expt.) — Outlet, U/S On (Model α=0.04) — Outlet, U/S On (Model α=0.001)
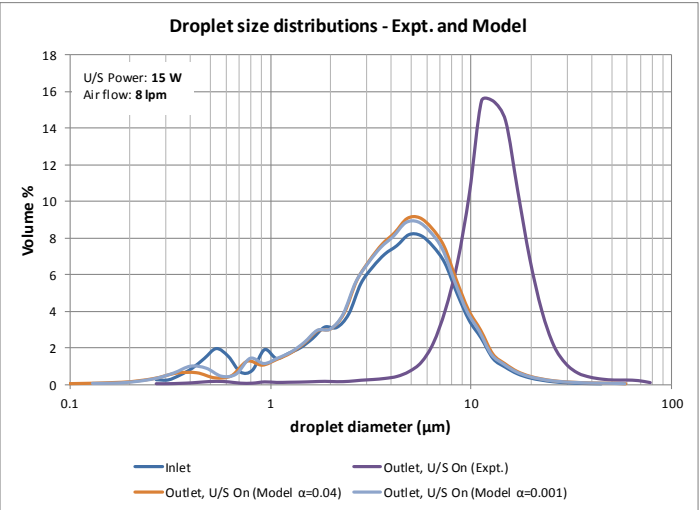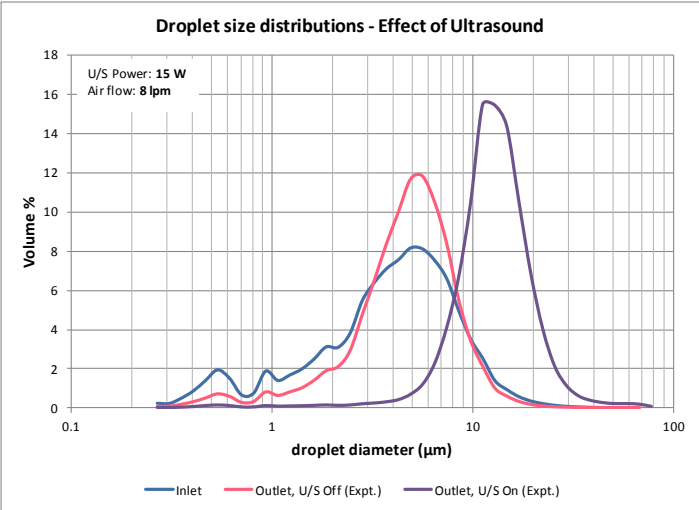
| Experiment Date | 10/06/2014 |
| Time | 13:56:31 - 14:01:57 |

Conduit Properties	Unit	Value
Diameter	mm	100
Length	mm	300

U/S Field	Unit	Value
Frequency	kHz	21.7
Power	W	15

Parameter	Unit	INLET	Experimental Results at OUTLET		Model Results at OUTLET			
			U/S Off	U/S On	U/S Off		U/S On	
					α = 0.04	α = 0.001	α = 0.04	α = 0.001
Air Properties								
Flow rate	lpm	8.095	---	---	7.83	7.83	7.84	7.84
Temp.	°C	20.65	18.2	20.9	8.6	8.6	8.8	8.8
Rel. Hum.		0.0801	0.934	0.939	1.003	1.002	1.003	1.000
Sp. Humidity	g/kg	1.20	12.27	14.65	6.96	6.96	7.04	7.05
Water Droplet Properties								
Flow rate	ml/min	0.339	---	---	0.283	0.283	0.282	0.283
Temp.	°C	23.8	---	---	8.6	8.6	8.8	8.8
Length to end of calculation					2	9	1	6

Parameter	Unit	INLET	Experimental Results at OUTLET		Model Results at OUTLET			
			U/S Off	U/S On	U/S Off		U/S On	
					α = 0.04	α = 0.001	α = 0.04	α = 0.001
Dv(10)	(μm)	0.98	2.05	7.67	1.54	1.37	1.51	1.34
Dv(50)	(μm)	4.21	4.89	12.73	4.70	4.61	4.69	4.59
Dv(90)	(μm)	9.12	8.63	20.53	9.66	9.60	9.66	9.59
Span		1.93	1.35	1.01	1.73	1.79	1.74	1.80
D[3][2]	(μm)	2.31	3.36	9.72	3.00	2.67	2.92	2.64
D[4][3]	(μm)	4.90	5.25	13.82	5.34	5.20	5.32	5.18
% Transm.		66.8%	69.4%	93.9%	---	---	---	---
Conc. (Cv)	ppm	22.5	30.5	16.1	---	---	---	---

Trial 4.3.38 Ultrasound Power: 15 W, Air Flow: 10 lpm

Droplet size distributions - Effect of Ultrasound

U/S Power: **15 W**
Air flow: **10 lpm**

Legend: Inlet — Outlet, U/S Off (Expt.) — Outlet, U/S On (Expt.)

Droplet size distributions - Expt. and Model

U/S Power: **15 W**
Air flow: **10 lpm**

Legend: Inlet — Outlet, U/S On (Expt.) — Outlet, U/S On (Model α=0.04) — Outlet, U/S On (Model α=0.001)
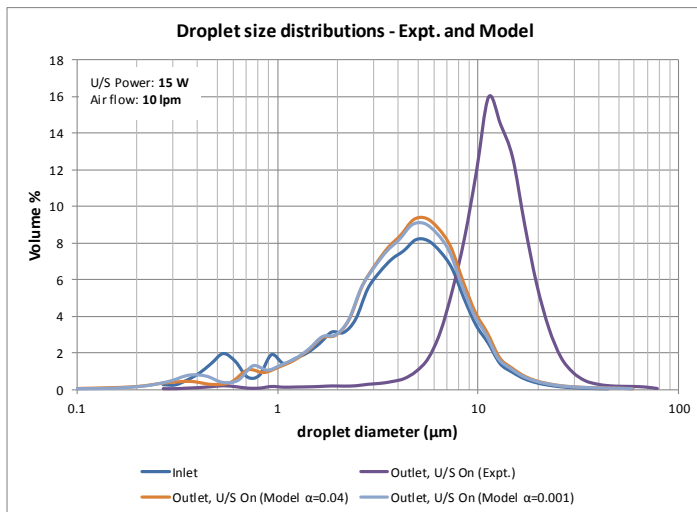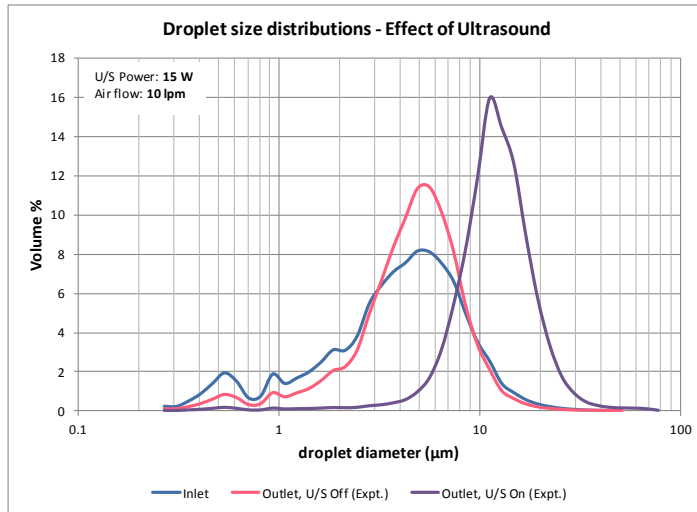
Experiment Date	10/06/2014	
Time	14:12:37 - 14:16:47	

Conduit Properties	Unit	Value
Diameter	mm	100
Length	mm	300

U/S Field	Unit	Value
Frequency	kHz	21.7
Power	W	15

Parameter	Unit	INLET	Experimental Results at OUTLET		Model Results at OUTLET			
					U/S Off		U/S On	
			U/S Off	U/S On	α = 0.04	α = 0.001	α = 0.04	α = 0.001
Air Properties								
Flow rate	lpm	10	---	---	9.67	9.67	9.67	9.67
Temp.	°C	20.5	17.5	20.5	8.3	8.3	8.4	8.4
Rel. Hum.		0.0782	0.929	0.935	1.002	1.001	1.002	1.000
Sp. Humidity	g/kg	1.17	11.67	14.22	6.83	6.83	6.88	6.88
Water Droplet Properties								
Flow rate	ml/min	0.339	---	---	0.271	0.271	0.270	0.271
Temp.	°C	23.5	---	---	8.3	8.3	8.4	8.4
Length to end of calculation					3	11	2	9

Parameter	Unit	INLET	Experimental Results at OUTLET		Model Results at OUTLET			
					U/S Off		U/S On	
			U/S Off	U/S On	α = 0.04	α = 0.001	α = 0.04	α = 0.001
Dv(10)	(µm)	0.98	1.89	7.02	1.67	1.48	1.64	1.46
Dv(50)	(µm)	4.21	4.81	11.91	4.81	4.71	4.80	4.69
Dv(90)	(µm)	9.12	8.65	19.63	9.79	9.72	9.79	9.70
Span		1.93	1.40	1.06	1.69	1.75	1.70	1.76
D[3][2]	(µm)	2.31	3.20	8.85	3.20	2.79	3.11	2.75
D[4][3]	(µm)	4.90	5.19	12.91	5.44	5.27	5.41	5.24
% Transm.		66.8%	74.7%	93.4%	---	---	---	---
Conc. (Cv)	ppm	22.5	23.2	15.6	---	---	---	---

Trial 4.3.39 Ultrasound Power: 15 W, Air Flow: 12 lpm

Droplet size distributions - Effect of Ultrasound

U/S Power: **15 W**
Air flow: **12 lpm**

Legend: Inlet — Outlet, U/S Off (Expt.) — Outlet, U/S On (Expt.)

Droplet size distributions - Expt. and Model

U/S Power: **15 W**
Air flow: **12 lpm**

Legend: Inlet — Outlet, U/S On (Expt.) — Outlet, U/S On (Model α=0.04) — Outlet, U/S On (Model α=0.001)
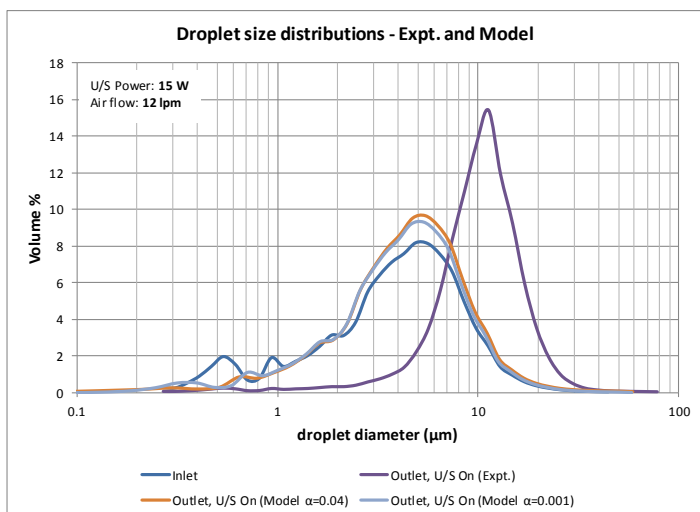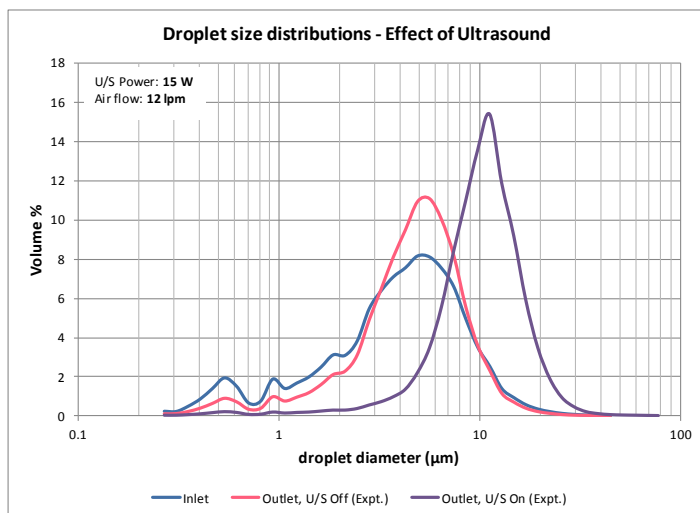
Experiment Date	10/06/2014
Time	14:31:52 - 14:37:42

Conduit Properties	Unit	Value
Diameter	mm	100
Length	mm	300

U/S Field	Unit	Value
Frequency	kHz	21.7
Power	W	15

Parameter	Unit	INLET	Experimental Results at OUTLET		Model Results at OUTLET			
			U/S Off	U/S On	U/S Off		U/S On	
					α = 0.04	α = 0.001	α = 0.04	α = 0.001
Air Properties								
Flow rate	lpm	12	---	---	11.60	11.60	11.60	11.60
Temp.	°C	20.75	16.9	19.6	8.4	8.4	8.5	8.5
Rel. Hum.		0.0814	0.926	0.936	1.002	1.000	1.002	1.000
Sp. Humidity	g/kg	1.23	11.19	13.45	6.87	6.87	6.91	6.91
Water Droplet Properties								
Flow rate	ml/min	0.339	---	---	0.258	0.258	0.257	0.257
Temp.	°C	23.95	---	---	8.4	8.4	8.5	8.4
Length to end of calculation					3	16	2	14

Parameter	Unit	INLET	Experimental Results at OUTLET		Model Results at OUTLET			
			U/S Off	U/S On	U/S Off		U/S On	
					α = 0.04	α = 0.001	α = 0.04	α = 0.001
Dv(10)	(μm)	0.98	1.83	5.55	1.81	1.61	1.78	1.58
Dv(50)	(μm)	4.21	4.82	10.40	4.93	4.81	4.92	4.79
Dv(90)	(μm)	9.12	8.79	17.06	9.92	9.84	9.92	9.82
Span		1.93	1.44	1.11	1.64	1.71	1.65	1.72
D[3][2]	(μm)	2.31	3.15	7.49	3.40	2.94	3.31	2.88
D[4][3]	(μm)	4.90	5.21	10.97	5.54	5.35	5.51	5.31
% Transm.		66.8%	77.8%	91.9%	---	---	---	---
Conc. (Cv)	ppm	22.5	19.5	16.3	---	---	---	---

Trial 4.3.40 Ultrasound Power: 15 W, Air Flow: 15 lpm

Droplet size distributions - Effect of Ultrasound

U/S Power: **15 W**
Air flow: **15 lpm**

Legend: Inlet — Outlet, U/S Off (Expt.) — Outlet, U/S On (Expt.)

Droplet size distributions - Expt. and Model

U/S Power: **15 W**
Air flow: **15 lpm**

Legend: Inlet — Outlet, U/S On (Expt.) — Outlet, U/S On (Model α=0.04) — Outlet, U/S On (Model α=0.001)
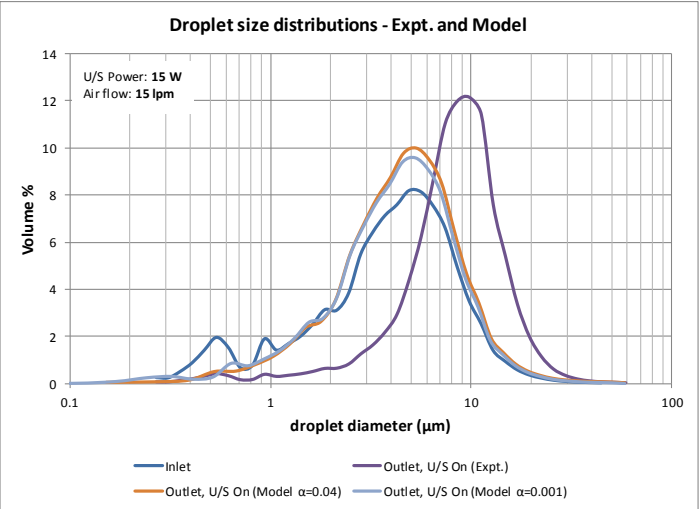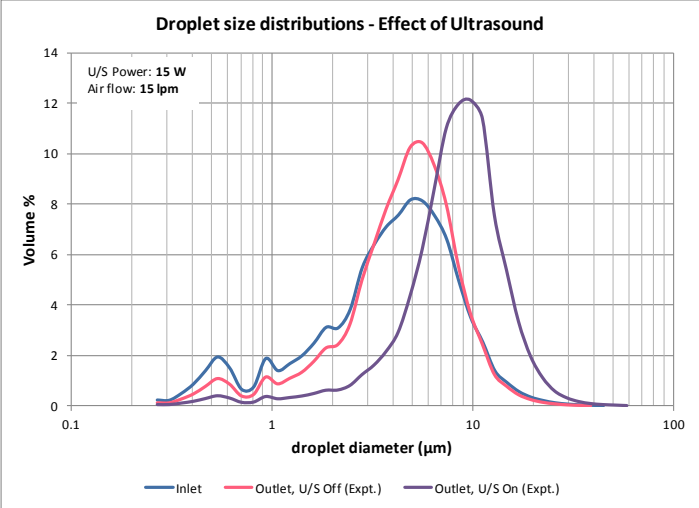
| Experiment Date | 10/06/2014 |
| Time | 14:46:53 - 14:52:13 |

Conduit Properties	Unit	Value
Diameter	mm	100
Length	mm	300

U/S Field	Unit	Value
Frequency	kHz	21.7
Power	W	15

Parameter	Unit	INLET	Experimental Results at OUTLET		Model Results at OUTLET			
					U/S Off		U/S On	
			U/S Off	U/S On	α = 0.04	α = 0.001	α = 0.04	α = 0.001
Air Properties								
Flow rate	lpm	14.9	---	---	14.39	14.39	14.39	14.39
Temp.	°C	20.65	16.1	17.6	8.1	8.1	8.2	8.2
Rel. Hum.		0.07585	0.923	0.933	1.001	1.000	1.002	1.000
Sp. Humidity	g/kg	1.14	10.59	11.80	6.74	6.74	6.79	6.79
Water Droplet Properties								
Flow rate	ml/min	0.339	---	---	0.239	0.239	0.239	0.239
Temp.	°C	24.2	---	---	8.1	8.1	8.2	8.2
Length to end of calculation					4	29	3	25

Parameter	Unit	INLET	Experimental Results at OUTLET		Model Results at OUTLET			
					U/S Off		U/S On	
			U/S Off	U/S On	α = 0.04	α = 0.001	α = 0.04	α = 0.001
Dv(10)	(µm)	0.98	1.62	3.82	2.04	1.79	2.00	1.75
Dv(50)	(µm)	4.21	4.75	8.53	5.11	4.74	5.10	4.69
Dv(90)	(µm)	9.12	8.93	14.95	10.12	10.02	10.11	10.00
Span		1.93	1.54	1.30	1.58	1.73	1.59	1.76
D[3][2]	(µm)	2.31	2.96	5.59	3.63	3.18	3.56	3.10
D[4][3]	(µm)	4.90	5.18	9.13	5.67	5.45	5.64	5.41
% Transm.		66.8%	84.3%	90.8%	---	---	---	---
Conc. (Cv)	ppm	22.5	12.5	13.8	---	---	---	---

Trial 4.3.41 Ultrasound Power: 15 W, Air Flow: 18 lpm

Droplet size distributions - Effect of Ultrasound

U/S Power: **15 W**
Air flow: **18 lpm**

Legend: Inlet — Outlet, U/S Off (Expt.) — Outlet, U/S On (Expt.)

Droplet size distributions - Expt. and Model

U/S Power: **15 W**
Air flow: **18 lpm**

Legend: Inlet — Outlet, U/S On (Expt.) — Outlet, U/S On (Model α=0.04) — Outlet, U/S On (Model α=0.001)
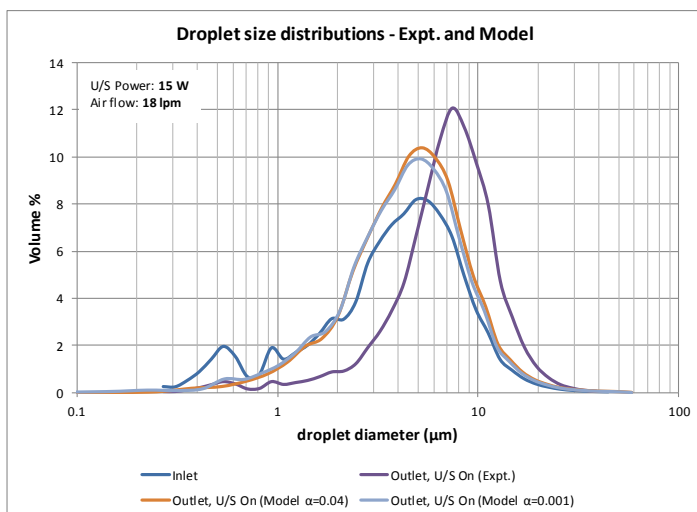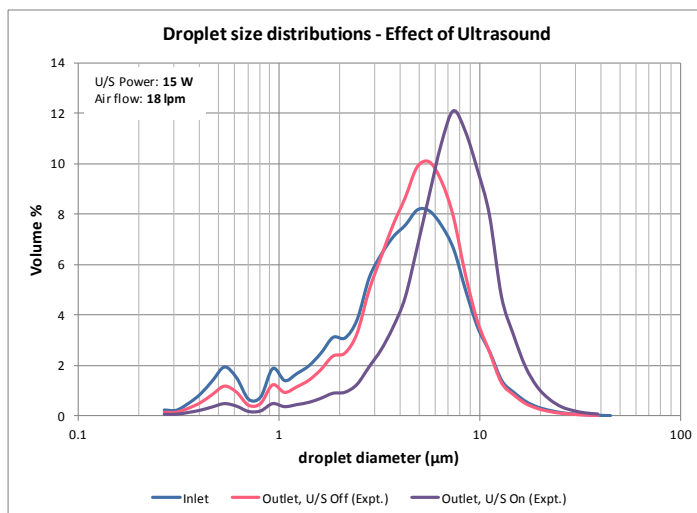
| Experiment Date | 10/06/2014 |
| Time | 14:59:02 - 15:03:47 |

Conduit Properties	Unit	Value
Diameter	mm	100
Length	mm	300

U/S Field	Unit	Value
Frequency	kHz	21.7
Power	W	15

Parameter	Unit	INLET	Experimental Results at OUTLET		Model Results at OUTLET			
			U/S Off	U/S On	U/S Off		U/S On	
					α = 0.04	α = 0.001	α = 0.04	α = 0.001
Air Properties								
Flow rate	lpm	18.15	---	---	17.58	17.58	17.48	17.48
Temp.	°C	20.8	14.9	16	8.3	8.3	8.2	8.2
Rel. Hum.		0.0803	0.922	0.929	1.001	1.000	1.001	1.000
Sp. Humidity	g/kg	1.22	9.78	10.59	6.81	6.81	6.78	6.78
Water Droplet Properties								
Flow rate	ml/min	0.339	---	---	0.218	0.219	0.218	0.218
Temp.	°C	24.65	---	---	8.3	8.2	8.2	8.2
Length to end of calculation					5	52	3	45

Parameter	Unit	INLET	Experimental Results at OUTLET		Model Results at OUTLET			
			U/S Off	U/S On	U/S Off		U/S On	
					α = 0.04	α = 0.001	α = 0.04	α = 0.001
Dv(10)	(µm)	0.98	1.53	3.09	2.26	1.77	2.18	1.94
Dv(50)	(µm)	4.21	4.74	7.19	4.73	4.48	4.68	4.45
Dv(90)	(µm)	9.12	9.04	12.89	10.34	10.22	10.33	10.19
Span		1.93	1.58	1.36	1.71	1.89	1.74	1.85
D[3][2]	(µm)	2.31	2.87	4.73	3.82	3.42	3.75	3.34
D[4][3]	(µm)	4.90	5.20	7.77	5.82	5.56	5.78	5.51
% Transm.		66.8%	88.1%	92.7%	---	---	---	---
Conc. (Cv)	ppm	22.5	9.0	9.1	---	---	---	---

Trial 4.3.42 Ultrasound Power: 15 W, Air Flow: 20 lpm

Droplet size distributions - Effect of Ultrasound

U/S Power: **15 W**
Air flow: **20 lpm**

Legend: Inlet — Outlet, U/S Off (Expt.) — Outlet, U/S On (Expt.)

Droplet size distributions - Expt. and Model

U/S Power: **15 W**
Air flow: **20 lpm**

Legend: Inlet — Outlet, U/S On (Expt.) — Outlet, U/S On (Model α=0.04) — Outlet, U/S On (Model α=0.001)
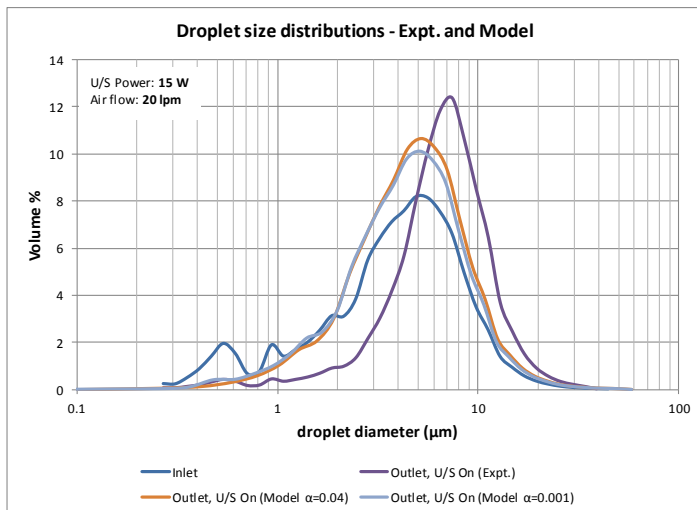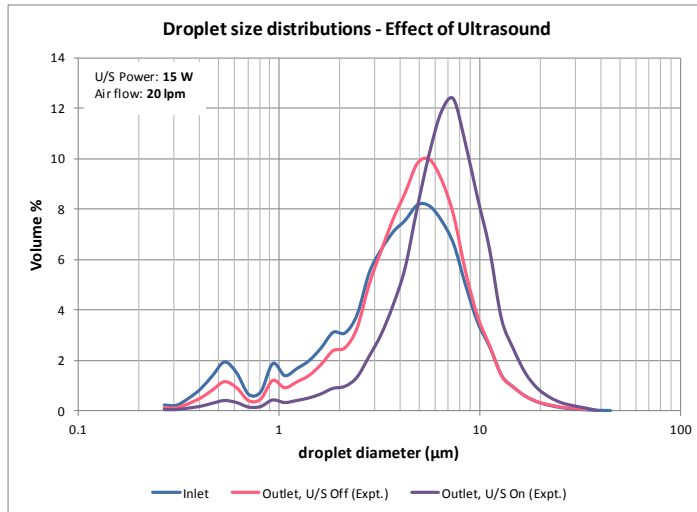
Experiment Date: 10/06/2014
Time: 15:09:54 - 15:14:37

Conduit Properties	Unit	Value
Diameter	mm	100
Length	mm	300

U/S Field	Unit	Value
Frequency	kHz	21.7
Power	W	15

Parameter	Unit	INLET	Experimental Results at OUTLET		Model Results at OUTLET			
			U/S Off	U/S On	U/S Off		U/S On	
					α = 0.04	α = 0.001	α = 0.04	α = 0.001
Air Properties								
Flow rate	lpm	20.1	---	---	19.40	19.40	19.40	19.40
Temp.	°C	20.8	14.4	15.4	8.1	8.1	8.2	8.2
Rel. Hum.		0.0784	0.918	0.926	1.001	1.000	1.001	1.000
Sp. Humidity	g/kg	1.19	9.42	10.15	6.74	6.74	6.76	6.76
Water Droplet Properties								
Flow rate	ml/min	0.339	---	---	0.205	0.206	0.206	0.206
Temp.	°C	24.3	---	---	8.1	8.1	8.2	8.1
Length to end of calculation					6	72	3	61

Parameter	Unit	INLET	Experimental Results at OUTLET		Model Results at OUTLET			
			U/S Off	U/S On	U/S Off		U/S On	
					α = 0.04	α = 0.001	α = 0.04	α = 0.001
Dv(10)	(µm)	0.98	1.53	3.09	2.19	1.86	2.12	1.81
Dv(50)	(µm)	4.21	4.73	6.72	4.76	4.58	4.73	4.54
Dv(90)	(µm)	9.12	9.21	11.91	10.50	10.35	10.47	10.31
Span		1.93	1.62	1.31	1.74	1.85	1.77	1.87
D[3][2]	(µm)	2.31	2.88	4.69	3.94	3.54	3.86	3.46
D[4][3]	(µm)	4.90	5.27	7.32	5.92	5.63	5.87	5.57
% Transm.		66.8%	89.9%	93.0%	---	---	---	---
Conc. (Cv)	ppm	22.5	7.5	8.6	---	---	---	---

Trial 4.3.43 Ultrasound Power: 17 W, Air Flow: 6.5 lpm

Droplet size distributions - Effect of Ultrasound

U/S Power: 17 W
Air flow: 6.5 lpm

Droplet size distributions - Expt. and Model

U/S Power: 17 W
Air flow: 6.5 lpm
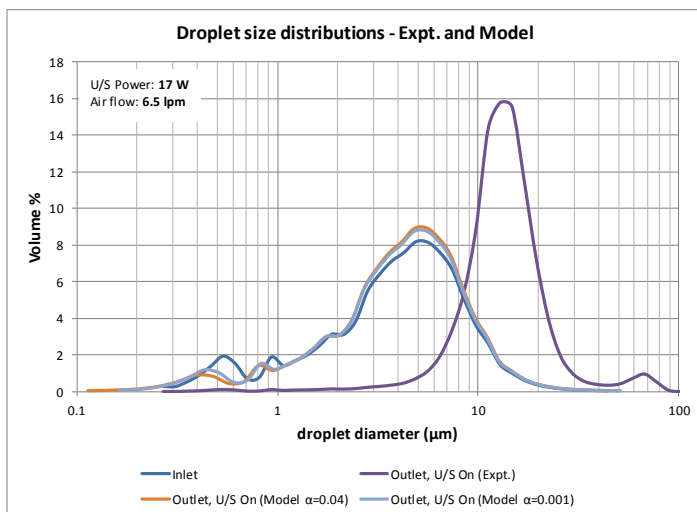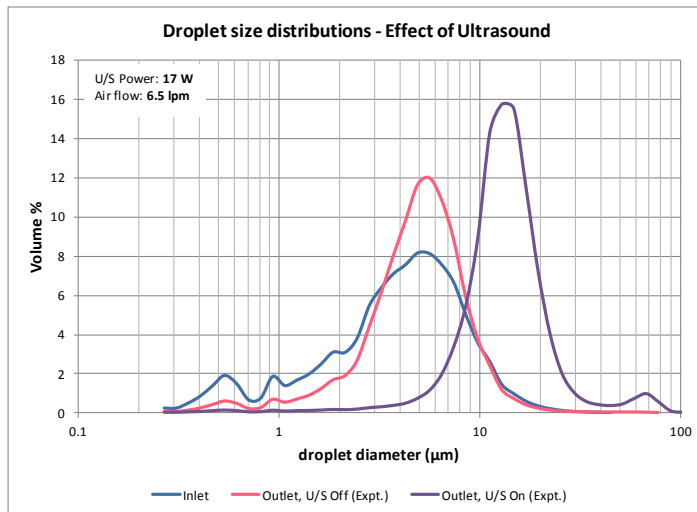
| Experiment Date | 26/06/2014 |
| Time | 11:47:58 - 11:53:29 |

Conduit Properties	Unit	Value
Diameter	mm	100
Length	mm	300

U/S Field	Unit	Value
Frequency	kHz	21.7
Power	W	17

Parameter	Unit	INLET	Experimental Results at OUTLET		Model Results at OUTLET			
					U/S Off		U/S On	
			U/S Off	U/S On	α = 0.04	α = 0.001	α = 0.04	α = 0.001
Air Properties								
Flow rate	lpm	6.505	---	---	6.32	6.32	6.27	6.27
Temp.	°C	22.9	19.7	22.3	10.4	10.4	10.3	10.3
Rel. Hum.		0.0866	0.932	0.938	1.003	1.002	1.003	1.001
Sp. Humidity	g/kg	1.50	13.48	15.98	7.88	7.88	7.83	7.83
Water Droplet Properties								
Flow rate	ml/min	0.368	---	---	0.319	0.319	0.319	0.319
Temp.	°C	25.35	---	---	10.4	10.4	10.3	10.3
Length to end of calculation					1	6	1	4

Parameter	Unit	INLET	Experimental Results at OUTLET		Model Results at OUTLET			
					U/S Off		U/S On	
			U/S Off	U/S On	α = 0.04	α = 0.001	α = 0.04	α = 0.001
Dv(10)	(µm)	1.00	2.24	7.87	1.42	1.27	1.39	1.25
Dv(50)	(µm)	4.23	5.07	13.25	4.61	4.54	4.60	4.53
Dv(90)	(µm)	9.15	8.99	21.71	9.57	9.52	9.56	9.51
Span		1.93	1.33	1.04	1.77	1.82	1.78	1.82
D[3][2]	(µm)	2.33	3.57	10.17	2.83	2.60	2.77	2.57
D[4][3]	(µm)	4.89	5.60	15.18	5.22	5.11	5.20	5.09
% Transm.		71.1%	63.1%	94.1%	---	---	---	---
Conc. (Cv)	ppm	19.2	41.0	16.3	---	---	---	---

Trial 4.3.44 Ultrasound Power: 17 W, Air Flow: 8 lpm

Droplet size distributions - Effect of Ultrasound

U/S Power: **17 W**
Air flow: **8 lpm**

— Inlet — Outlet, U/S Off (Expt.) — Outlet, U/S On (Expt.)

Droplet size distributions - Expt. and Model

U/S Power: **17 W**
Air flow: **8 lpm**

— Inlet — Outlet, U/S On (Expt.)
— Outlet, U/S On (Model α=0.04) — Outlet, U/S On (Model α=0.001)
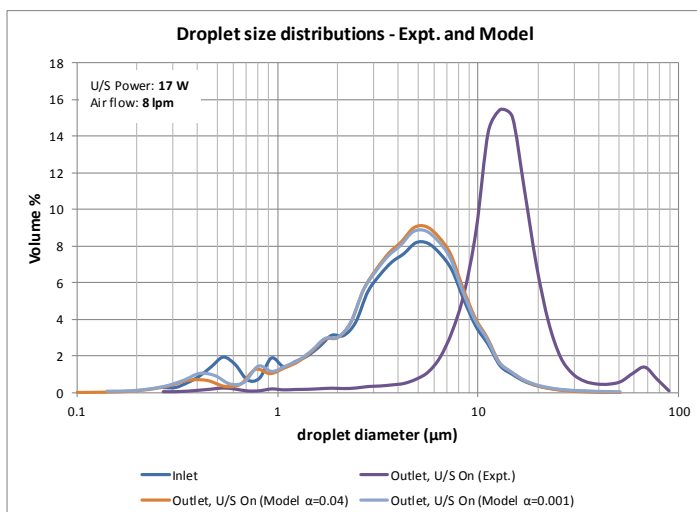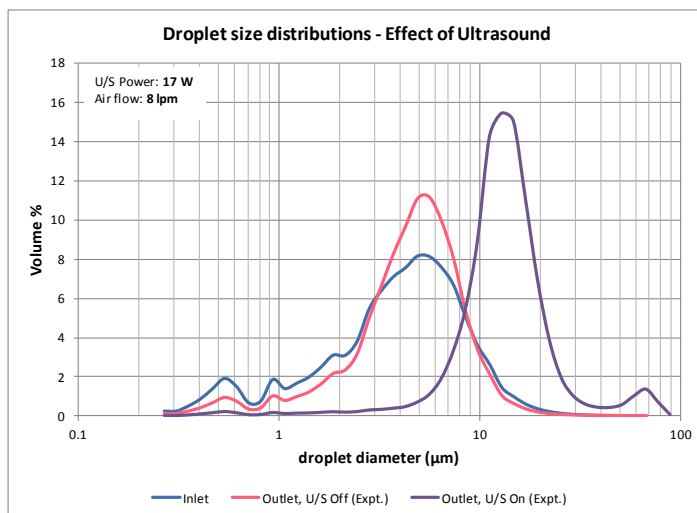
Experiment Date	26/06/2014	
Time	12:07:27 - 12:13:38	

Conduit Properties	Unit	Value
Diameter	mm	100
Length	mm	300

U/S Field	Unit	Value
Frequency	kHz	21.7
Power	W	17

Parameter	Unit	INLET	Experimental Results at OUTLET		Model Results at OUTLET			
					U/S Off		U/S On	
			U/S Off	U/S On	α = 0.04	α = 0.001	α = 0.04	α = 0.001
Air Properties								
Flow rate	lpm	8.015	---	---	7.76	7.76	7.75	7.75
Temp.	°C	21.95	20.3	23.1	9.8	9.8	9.9	9.9
Rel. Hum.		0.0979	0.932	0.939	1.003	1.002	1.003	1.000
Sp. Humidity	g/kg	1.60	14.00	16.81	7.54	7.54	7.59	7.59
Water Droplet Properties								
Flow rate	ml/min	0.368	---	---	0.311	0.311	0.311	0.311
Temp.	°C	24.9	---	---	9.8	9.8	9.9	9.8
Length to end of calculation					2	7	1	5

Parameter	Unit	INLET	Experimental Results at OUTLET		Model Results at OUTLET			
					U/S Off		U/S On	
			U/S Off	U/S On	α = 0.04	α = 0.001	α = 0.04	α = 0.001
Dv(10)	(µm)	1.00	1.79	7.61	1.50	1.35	1.47	1.32
Dv(50)	(µm)	4.23	4.76	13.20	4.68	4.60	4.67	4.59
Dv(90)	(µm)	9.15	8.65	22.49	9.64	9.58	9.64	9.57
Span		1.93	1.44	1.13	1.74	1.79	1.75	1.80
D[3][2]	(µm)	2.33	3.10	9.19	2.94	2.66	2.87	2.63
D[4][3]	(µm)	4.89	5.16	15.57	5.28	5.15	5.26	5.13
% Transm.		71.1%	69.2%	93.9%	---	---	---	---
Conc. (Cv)	ppm	19.2	28.2	15.2	---	---	---	---

Trial 4.3.45 Ultrasound Power: 17 W, Air Flow: 10 lpm

Droplet size distributions - Effect of Ultrasound

U/S Power: **17 W**
Air flow: **10 lpm**

Legend: Inlet — Outlet, U/S Off (Expt.) — Outlet, U/S On (Expt.)

Droplet size distributions - Expt. and Model

U/S Power: **17 W**
Air flow: **10 lpm**

Legend: Inlet — Outlet, U/S On (Expt.) — Outlet, U/S On (Model α=0.04) — Outlet, U/S On (Model α=0.001)
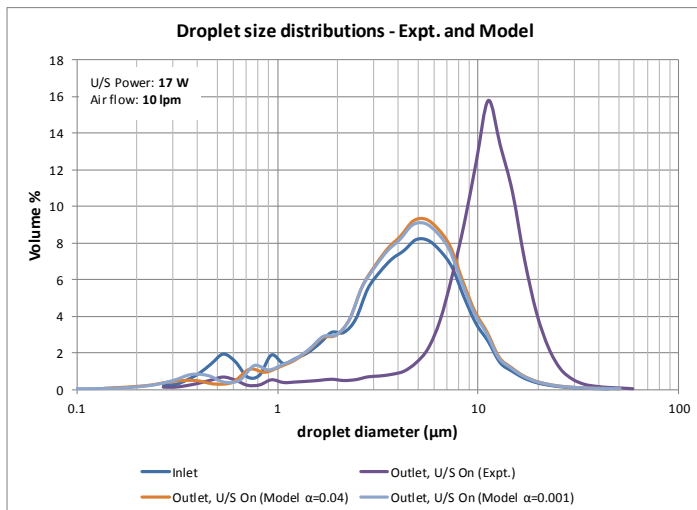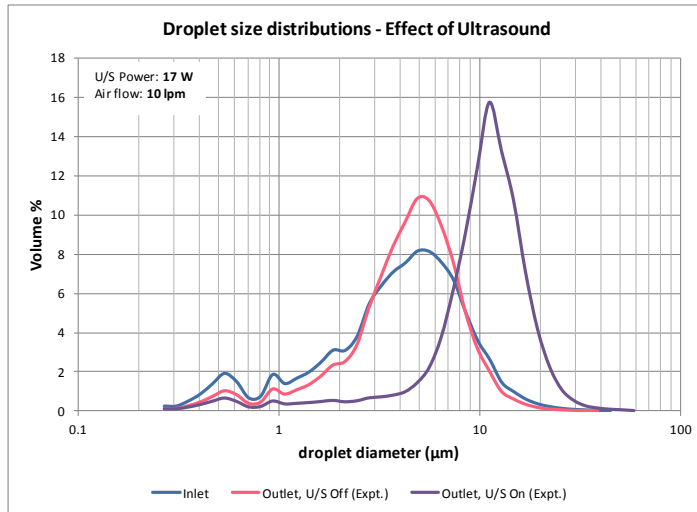
Experiment Date   26/06/2014
Time   12:20:46 - 12:27:14

Conduit Properties	Unit	Value
Diameter	mm	100
Length	mm	300

U/S Field	Unit	Value
Frequency	kHz	21.7
Power	W	17

Parameter	Unit	INLET	Experimental Results at OUTLET		Model Results at OUTLET			
			U/S Off	U/S On	U/S Off		U/S On	
					α = 0.04	α = 0.001	α = 0.04	α = 0.001
Air Properties								
Flow rate	lpm	10	---	---	9.67	9.67	9.67	9.67
Temp.	°C	22.15	19.1	22.4	9.6	9.6	9.8	9.8
Rel. Hum.		0.09485	0.927	0.938	1.002	1.000	1.002	1.000
Sp. Humidity	g/kg	1.56	12.90	16.08	7.46	7.46	7.55	7.55
Water Droplet Properties								
Flow rate	ml/min	0.368	---	---	0.298	0.298	0.297	0.297
Temp.	°C	25.5	---	---	9.6	9.6	9.8	9.8
Length to end of calculation					2	9	1	8

Parameter	Unit	INLET	Experimental Results at OUTLET		Model Results at OUTLET			
			U/S Off	U/S On	U/S Off		U/S On	
					α = 0.04	α = 0.001	α = 0.04	α = 0.001
Dv(10)	(µm)	1.00	1.67	4.79	1.64	1.47	1.61	1.44
Dv(50)	(µm)	4.23	4.63	10.98	4.80	4.70	4.79	4.68
Dv(90)	(µm)	9.15	8.52	17.68	9.76	9.70	9.76	9.69
Span		1.93	1.48	1.17	1.69	1.75	1.70	1.76
D[3][2]	(µm)	2.33	2.96	5.74	3.13	2.78	3.06	2.74
D[4][3]	(µm)	4.89	4.99	11.27	5.38	5.22	5.35	5.19
% Transm.		71.1%	78.1%	94.7%	---	---	---	---
Conc. (Cv)	ppm	19.2	18.1	8.0	---	---	---	---

Trial 4.3.46 Ultrasound Power: 17 W, Air Flow: 12 lpm

Droplet size distributions - Effect of Ultrasound

U/S Power: **17 W**
Air flow: **12 lpm**

Legend: Inlet — Outlet, U/S Off (Expt.) — Outlet, U/S On (Expt.)

Droplet size distributions - Expt. and Model

U/S Power: **17 W**
Air flow: **12 lpm**

Legend: Inlet — Outlet, U/S On (Expt.) — Outlet, U/S On (Model α=0.04) — Outlet, U/S On (Model α=0.001)
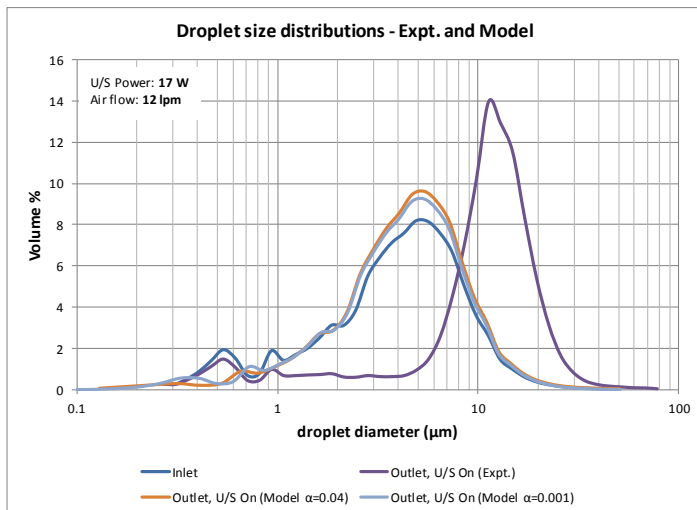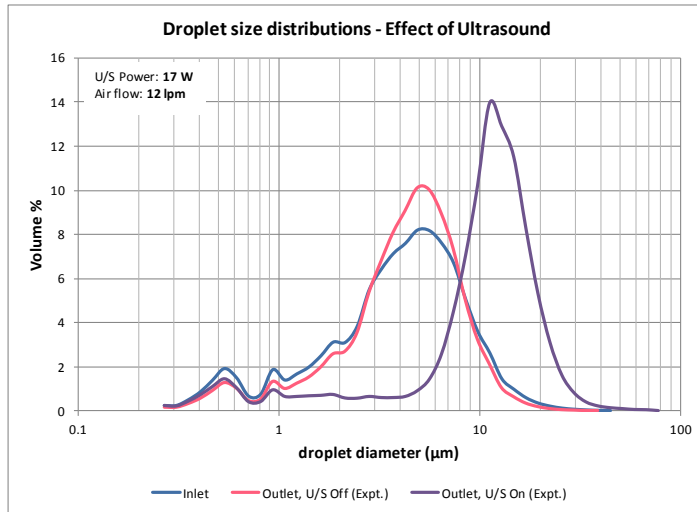
Experiment Date	26/06/2014	
Time	12:33:39 - 12:40:34	

Conduit Properties	Unit	Value
Diameter	mm	100
Length	mm	300

U/S Field	Unit	Value
Frequency	kHz	21.7
Power	W	17

Parameter	Unit	INLET	Experimental Results at OUTLET		Model Results at OUTLET			
			U/S Off	U/S On	U/S Off		U/S On	
					α = 0.04	α = 0.001	α = 0.04	α = 0.001
Air Properties								
Flow rate	lpm	12	---	---	11.59	11.59	11.59	11.59
Temp.	°C	22.3	18.2	21.7	9.4	9.4	9.6	9.6
Rel. Hum.		0.08735	0.924	0.935	1.002	1.000	1.002	1.000
Sp. Humidity	g/kg	1.45	12.14	15.34	7.36	7.36	7.47	7.47
Water Droplet Properties								
Flow rate	ml/min	0.368	---	---	0.284	0.284	0.282	0.283
Temp.	°C	25.95	---	---	9.4	9.4	9.6	9.6
Length to end of calculation					3	15	2	13

Parameter	Unit	INLET	Experimental Results at OUTLET		Model Results at OUTLET			
			U/S Off	U/S On	U/S Off		U/S On	
					α = 0.04	α = 0.001	α = 0.04	α = 0.001
Dv(10)	(µm)	1.00	1.43	1.74	1.78	1.59	1.76	1.57
Dv(50)	(µm)	4.23	4.51	11.42	4.92	4.81	4.91	4.79
Dv(90)	(µm)	9.15	8.58	19.20	9.90	9.82	9.90	9.81
Span		1.93	1.59	1.53	1.65	1.71	1.66	1.72
D[3][2]	(µm)	2.33	2.74	3.97	3.34	2.92	3.26	2.87
D[4][3]	(µm)	4.89	4.90	11.65	5.47	5.29	5.45	5.26
% Transm.		71.1%	82.8%	95.8%	---	---	---	---
Conc. (Cv)	ppm	19.2	12.7	4.3	---	---	---	---

Trial 4.3.47 Ultrasound Power: 17 W, Air Flow: 15 lpm

Droplet size distributions - Effect of Ultrasound

U/S Power: **17 W**
Air flow: **15 lpm**

Legend: Inlet — Outlet, U/S Off (Expt.) — Outlet, U/S On (Expt.)

Droplet size distributions - Expt. and Model

U/S Power: **17 W**
Air flow: **15 lpm**

Legend: Inlet — Outlet, U/S On (Expt.) — Outlet, U/S On (Model α=0.04) — Outlet, U/S On (Model α=0.001)
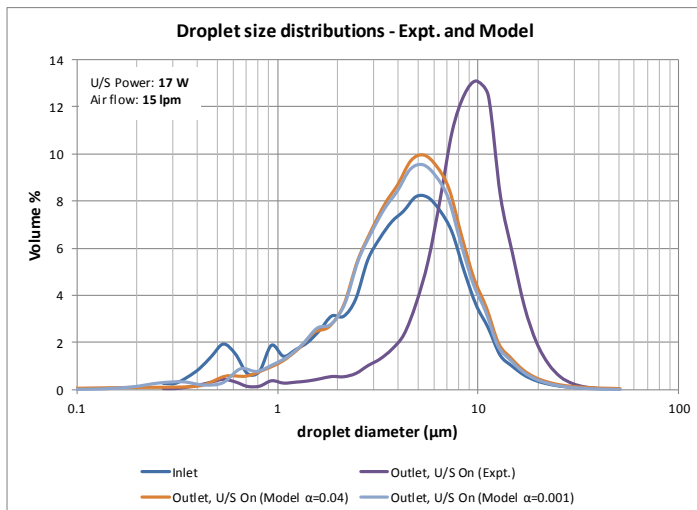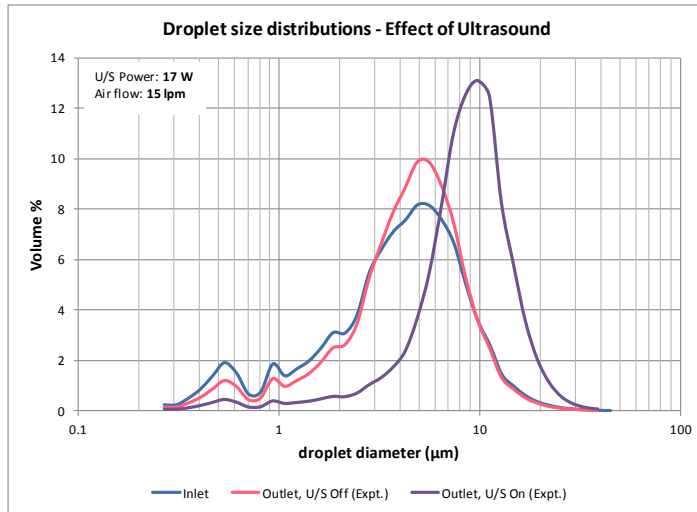
Experiment Date	26/06/2014
Time	12:47:40 - 12:52:53

Conduit Properties	Unit	Value
Diameter	mm	100
Length	mm	300

U/S Field	Unit	Value
Frequency	kHz	21.7
Power	W	17

Parameter	Unit	INLET	Experimental Results at OUTLET		Model Results at OUTLET			
					U/S Off		U/S On	
			U/S Off	U/S On	α = 0.04	α = 0.001	α = 0.04	α = 0.001
Air Properties								
Flow rate	lpm	15	---	---	14.48	14.48	14.47	14.47
Temp.	°C	22.3	17.2	19.7	9.3	9.3	9.4	9.4
Rel. Hum.		0.0867	0.918	0.931	1.002	1.000	1.002	1.000
Sp. Humidity	g/kg	1.44	11.31	13.46	7.30	7.30	7.37	7.37
Water Droplet Properties								
Flow rate	ml/min	0.368	---	---	0.263	0.264	0.263	0.263
Temp.	°C	26.1	---	---	9.3	9.3	9.4	9.4
Length to end of calculation					3	26	2	23

Parameter	Unit	INLET	Experimental Results at OUTLET		Model Results at OUTLET			
					U/S Off		U/S On	
			U/S Off	U/S On	α = 0.04	α = 0.001	α = 0.04	α = 0.001
Dv(10)	(µm)	1.00	1.51	4.05	2.01	1.77	1.98	1.73
Dv(50)	(µm)	4.23	4.62	8.84	5.10	4.72	5.08	4.68
Dv(90)	(µm)	9.15	8.99	14.99	10.09	9.99	10.08	9.97
Span		1.93	1.62	1.24	1.59	1.74	1.59	1.76
D[3][2]	(µm)	2.33	2.83	5.61	3.59	3.15	3.52	3.08
D[4][3]	(µm)	4.89	5.12	9.31	5.61	5.40	5.58	5.35
% Transm.		71.1%	88.0%	94.5%	---	---	---	---
Conc. (Cv)	ppm	19.2	8.9	8.2	---	---	---	---

Trial 4.3.48 Ultrasound Power: 17 W, Air Flow: 18 lpm

Droplet size distributions - Effect of Ultrasound

U/S Power: **17 W**
Air flow: **18 lpm**

Inlet — Outlet, U/S Off (Expt.) — Outlet, U/S On (Expt.)

Droplet size distributions - Expt. and Model

U/S Power: **17 W**
Air flow: **18 lpm**

Inlet — Outlet, U/S On (Expt.) — Outlet, U/S On (Model α=0.04) — Outlet, U/S On (Model α=0.001)
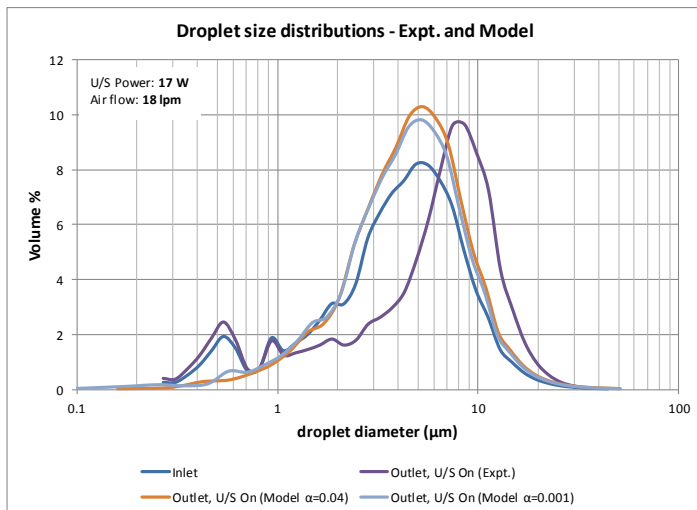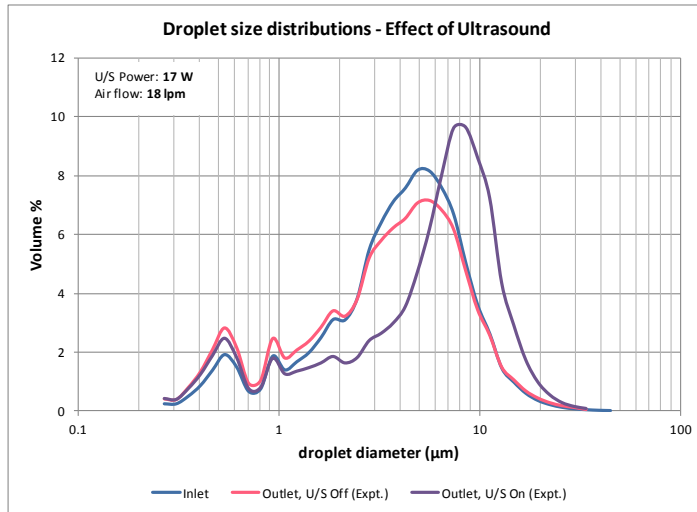
| Experiment Date | 26/06/2014 |
| Time | 12:58:57 - 13:04:46 |

Conduit Properties	Unit	Value
Diameter	mm	100
Length	mm	300

U/S Field	Unit	Value
Frequency	kHz	21.7
Power	W	17

Parameter	Unit	INLET	Experimental Results at OUTLET		Model Results at OUTLET			
					U/S Off		U/S On	
			U/S Off	U/S On	α = 0.04	α = 0.001	α = 0.04	α = 0.001
Air Properties								
Flow rate	lpm	18	---	---	17.37	17.37	17.37	17.37
Temp.	°C	22.45	16.2	17.4	9.4	9.4	9.5	9.5
Rel. Hum.		0.09325	0.913	0.929	1.001	1.000	1.001	1.000
Sp. Humidity	g/kg	1.57	10.54	11.60	7.37	7.37	7.40	7.40
Water Droplet Properties								
Flow rate	ml/min	0.368	---	---	0.244	0.244	0.244	0.244
Temp.	°C	26.15	---	---	9.4	9.4	9.5	9.5
Length to end of calculation					4	45	2	38

Parameter	Unit	INLET	Experimental Results at OUTLET		Model Results at OUTLET			
					U/S Off		U/S On	
			U/S Off	U/S On	α = 0.04	α = 0.001	α = 0.04	α = 0.001
Dv(10)	(µm)	1.00	0.66	0.79	2.14	1.93	2.07	1.84
Dv(50)	(µm)	4.23	3.88	6.47	5.27	4.45	4.59	4.42
Dv(90)	(µm)	9.15	9.22	12.41	10.27	10.15	10.26	10.13
Span		1.93	2.21	1.80	1.54	1.85	1.78	1.87
D[3][2]	(µm)	2.33	1.94	2.39	3.76	3.37	3.70	3.28
D[4][3]	(µm)	4.89	4.66	6.69	5.73	5.49	5.69	5.44
% Transm.		71.1%	91.6%	95.4%	---	---	---	---
Conc. (Cv)	ppm	19.2	4.0	2.7	---	---	---	---

Trial 4.3.49 Ultrasound Power: 17 W, Air Flow: 20 lpm

Droplet size distributions - Effect of Ultrasound

Droplet size distributions - Expt. and Model
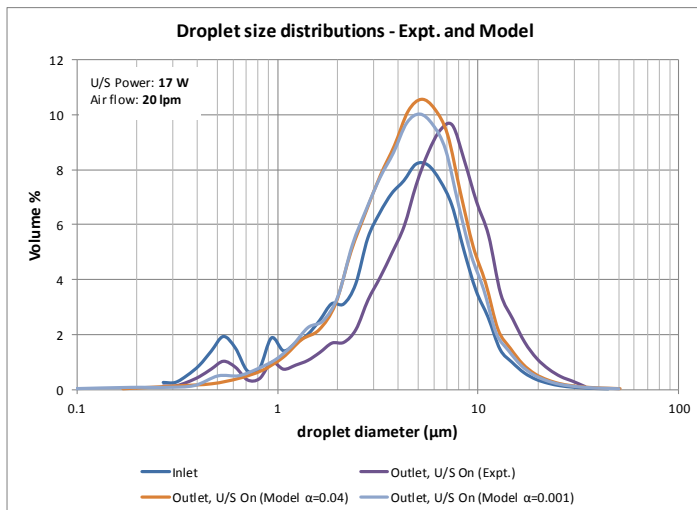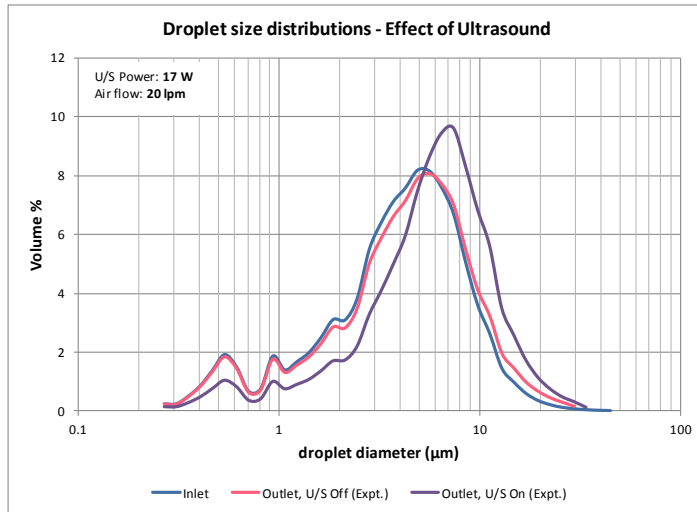
Experiment Date	26/06/2014
Time	13:09:25 - 13:13:54

Conduit Properties	Unit	Value
Diameter	mm	100
Length	mm	300

U/S Field	Unit	Value
Frequency	kHz	21.7
Power	W	17

Parameter	Unit	INLET	Experimental Results at OUTLET		Model Results at OUTLET			
			U/S Off	U/S On	U/S Off		U/S On	
					α = 0.04	α = 0.001	α = 0.04	α = 0.001
Air Properties								
Flow rate	lpm	19.95	---	---	19.29	19.29	19.18	19.18
Temp.	°C	22.5	15.7	16.6	9.4	9.4	9.2	9.2
Rel. Hum.		0.0864	0.916	0.924	1.001	1.000	1.000	1.000
Sp. Humidity	g/kg	1.46	10.24	10.95	7.34	7.34	7.27	7.27
Water Droplet Properties								
Flow rate	ml/min	0.368	---	---	0.230	0.230	0.229	0.230
Temp.	°C	25.95	---	---	9.4	9.3	9.2	9.2
Length to end of calculation					4	61	3	52

Parameter	Unit	INLET	Experimental Results at OUTLET		Model Results at OUTLET			
			U/S Off	U/S On	U/S Off		U/S On	
					α = 0.04	α = 0.001	α = 0.04	α = 0.001
Dv(10)	(μm)	1.00	1.04	1.80	2.10	1.91	2.04	1.83
Dv(50)	(μm)	4.23	4.52	6.05	4.90	4.55	4.86	4.52
Dv(90)	(μm)	9.15	10.20	12.30	10.41	10.28	10.40	10.25
Span		1.93	2.03	1.74	1.70	1.84	1.72	1.87
D[3][2]	(μm)	2.33	2.43	3.39	3.88	3.50	3.81	3.42
D[4][3]	(μm)	4.89	5.31	6.81	5.82	5.55	5.78	5.49
% Transm.		71.1%	92.8%	94.5%	---	---	---	---
Conc. (Cv)	ppm	19.2	4.4	4.8	---	---	---	---

Trial 4.3.50 Ultrasound Power: 20 W, Air Flow: 6.5 lpm

Droplet size distributions - Effect of Ultrasound

U/S Power: 20 W
Air flow: 6.5 lpm

— Inlet — Outlet, U/S Off (Expt.) — Outlet, U/S On (Expt.)

Droplet size distributions - Expt. and Model

U/S Power: 20 W
Air flow: 6.5 lpm

— Inlet — Outlet, U/S On (Expt.)
— Outlet, U/S On (Model α=0.04) — Outlet, U/S On (Model α=0.001)
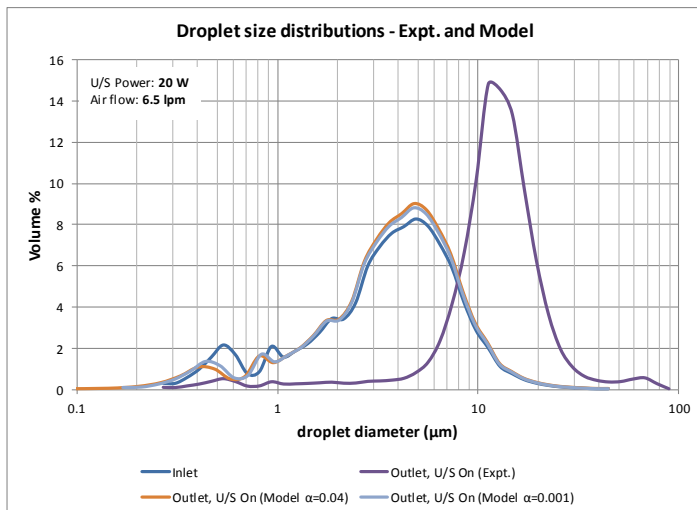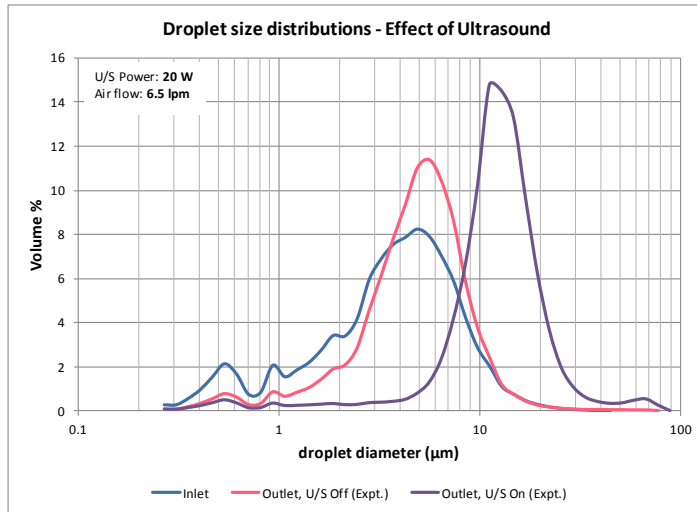
| Experiment Date | 29/05/2014 |
| Time | 14:06:40 - 14:13:12 |

Conduit Properties	Unit	Value
Diameter	mm	100
Length	mm	300

U/S Field	Unit	Value
Frequency	kHz	21.7
Power	W	20

Parameter	Unit	INLET	Experimental Results at OUTLET		Model Results at OUTLET			
					U/S Off		U/S On	
			U/S Off	U/S On	α = 0.04	α = 0.001	α = 0.04	α = 0.001
Air Properties								
Flow rate	lpm	6.55	---	---	6.34	6.34	6.35	6.35
Temp.	°C	22	18.2	20.5	9.7	9.7	9.9	9.9
Rel. Hum.		0.0824	0.939	0.941	1.003	1.002	1.003	1.001
Sp. Humidity	g/kg	1.35	12.34	14.32	7.52	7.52	7.60	7.60
Water Droplet Properties								
Flow rate	ml/min	0.359	---	---	0.311	0.311	0.310	0.310
Temp.	°C	25.3	---	---	9.7	9.7	9.9	9.9
Length to end of calculation					1	5	1	3

Parameter	Unit	INLET	Experimental Results at OUTLET		Model Results at OUTLET			
					U/S Off		U/S On	
			U/S Off	U/S On	α = 0.04	α = 0.001	α = 0.04	α = 0.001
Dv(10)	(µm)	0.93	1.97	6.61	1.28	1.15	1.25	1.13
Dv(50)	(µm)	3.90	4.99	12.42	4.26	4.20	4.25	4.19
Dv(90)	(µm)	8.51	9.03	20.73	8.82	8.79	8.82	8.78
Span		1.94	1.42	1.14	1.77	1.82	1.78	1.83
D[3][2]	(µm)	2.17	3.32	6.97	2.58	2.40	2.53	2.37
D[4][3]	(µm)	4.53	5.55	13.81	4.83	4.73	4.81	4.71
% Transm.		71.1%	62.5%	94.8%	---	---	---	---
Conc. (Cv)	ppm	17.8	38.8	9.7	---	---	---	---

Trial 4.3.51 Ultrasound Power: 20 W, Air Flow: 8 lpm

Droplet size distributions - Effect of Ultrasound

U/S Power: **20 W**
Air flow: **8 lpm**

Legend: Inlet — Outlet, U/S Off (Expt.) — Outlet, U/S On (Expt.)

Droplet size distributions - Expt. and Model

U/S Power: **20 W**
Air flow: **8 lpm**

Legend: Inlet — Outlet, U/S On (Expt.) — Outlet, U/S On (Model α=0.04) — Outlet, U/S On (Model α=0.001)
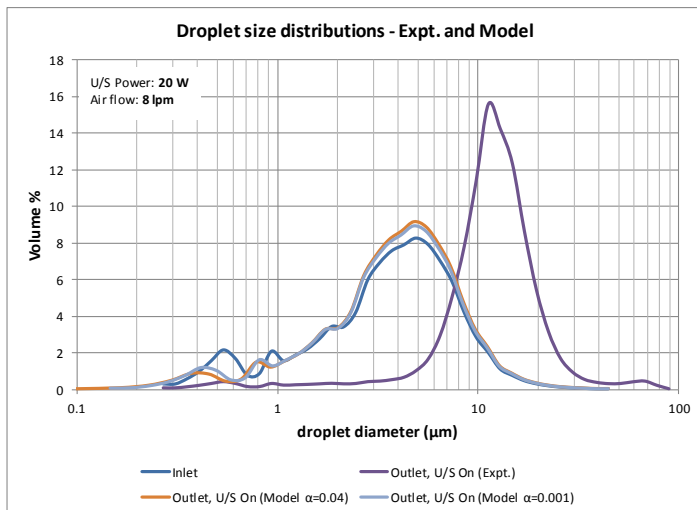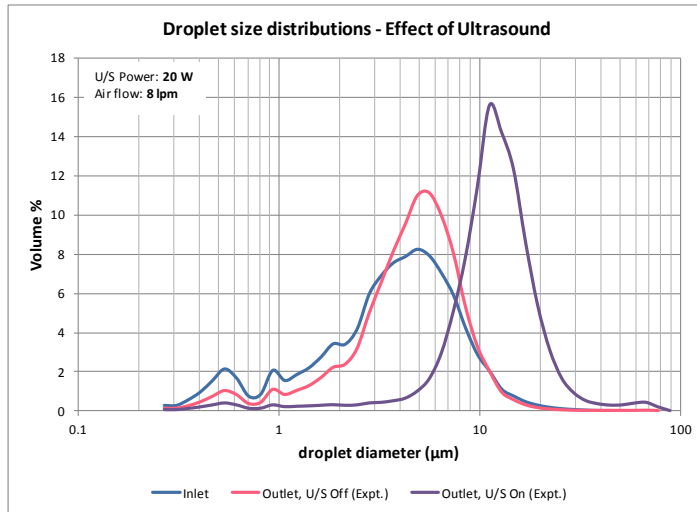
Experiment Date   29/05/2014
Time   14:41:08 - 14:47:17

Conduit Properties	Unit	Value
Diameter	mm	100
Length	mm	300

U/S Field	Unit	Value
Frequency	kHz	21.7
Power	W	20

Parameter	Unit	INLET	Experimental Results at OUTLET		Model Results at OUTLET			
			U/S Off	U/S On	U/S Off		U/S On	
					α = 0.04	α = 0.001	α = 0.04	α = 0.001
Air Properties								
Flow rate	lpm	8.02	---	---	7.76	7.76	7.76	7.76
Temp.	°C	21.6	18.4	21.3	9.2	9.2	9.4	9.4
Rel. Hum.		0.0845	0.933	0.939	1.003	1.001	1.003	1.000
Sp. Humidity	g/kg	1.35	12.42	15.02	7.26	7.26	7.36	7.36
Water Droplet Properties								
Flow rate	ml/min	0.359	---	---	0.303	0.303	0.301	0.302
Temp.	°C	23.7	---	---	9.2	9.2	9.4	9.4
Length to end of calculation					1	6	1	5

Parameter	Unit	INLET	Experimental Results at OUTLET		Model Results at OUTLET			
			U/S Off	U/S On	U/S Off		U/S On	
					α = 0.04	α = 0.001	α = 0.04	α = 0.001
Dv(10)	(µm)	0.93	1.69	6.47	1.37	1.22	1.35	1.21
Dv(50)	(µm)	3.90	4.73	11.87	4.33	4.26	4.33	4.25
Dv(90)	(µm)	8.51	8.55	19.96	8.88	8.84	8.88	8.84
Span		1.94	1.45	1.14	1.73	1.79	1.74	1.80
D[3][2]	(µm)	2.17	3.00	7.31	2.68	2.46	2.63	2.43
D[4][3]	(µm)	4.53	5.11	13.17	4.89	4.78	4.87	4.76
% Transm.		71.1%	66.9%	94.2%	---	---	---	---
Conc. (Cv)	ppm	17.8	29.7	11.3	---	---	---	---

Trial 4.3.52 Ultrasound Power: 20 W, Air Flow: 10 lpm

Droplet size distributions - Effect of Ultrasound

U/S Power: **20 W**
Air flow: **10 lpm**

Legend: Inlet — Outlet, U/S Off (Expt.) — Outlet, U/S On (Expt.)

Droplet size distributions - Expt. and Model

U/S Power: **20 W**
Air flow: **10 lpm**

Legend: Inlet — Outlet, U/S On (Expt.) — Outlet, U/S On (Model α=0.04) — Outlet, U/S On (Model α=0.001)
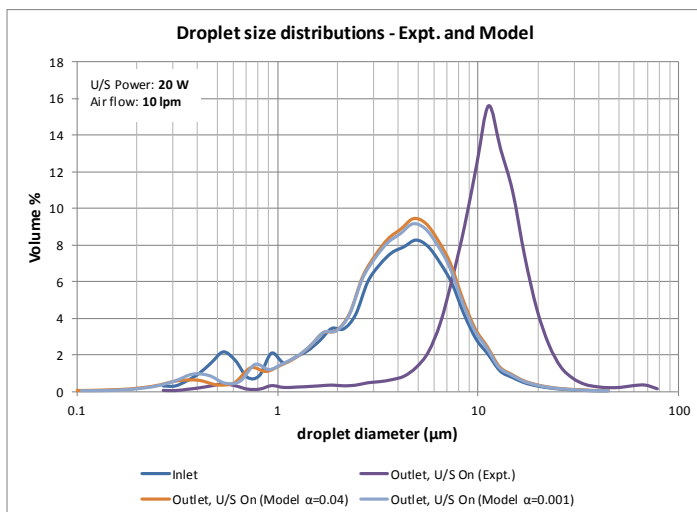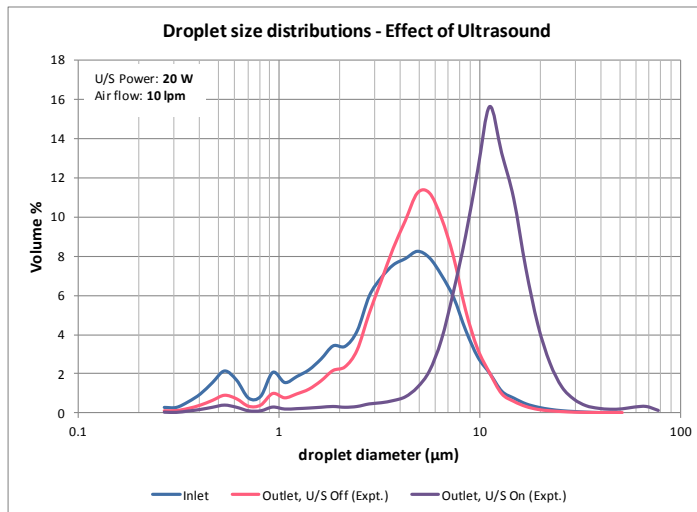
Experiment Date 29/05/2014
Time 15:01:40 - 15:07:55

Conduit Properties	Unit	Value
Diameter	mm	100
Length	mm	300

U/S Field	Unit	Value
Frequency	kHz	21.7
Power	W	20

Parameter	Unit	INLET	Experimental Results at OUTLET		Model Results at OUTLET			
			U/S Off	U/S On	U/S Off		U/S On	
					α = 0.04	α = 0.001	α = 0.04	α = 0.001
Air Properties								
Flow rate	lpm	10.1	---	---	9.76	9.76	9.76	9.76
Temp.	°C	21.7	18.4	21.3	9.1	9.1	9.3	9.3
Rel. Hum.		0.0852	0.934	0.938	1.003	1.000	1.003	1.000
Sp. Humidity	g/kg	1.37	12.43	15.01	7.22	7.22	7.33	7.33
Water Droplet Properties								
Flow rate	ml/min	0.359	---	---	0.289	0.289	0.287	0.287
Temp.	°C	25	---	---	9.1	9.1	9.3	9.3
Length to end of calculation					2	9	1	8

Parameter	Unit	INLET	Experimental Results at OUTLET		Model Results at OUTLET			
			U/S Off	U/S On	U/S Off		U/S On	
					α = 0.04	α = 0.001	α = 0.04	α = 0.001
Dv(10)	(µm)	0.93	1.82	5.89	1.51	1.35	1.49	1.33
Dv(50)	(µm)	3.90	4.74	11.27	4.44	4.35	4.44	4.34
Dv(90)	(µm)	8.51	8.55	18.85	8.98	8.93	8.98	8.92
Span		1.94	1.42	1.15	1.68	1.74	1.69	1.75
D[3][2]	(µm)	2.17	3.12	6.84	2.86	2.56	2.80	2.53
D[4][3]	(µm)	4.53	5.10	12.35	4.98	4.84	4.96	4.82
% Transm.		71.1%	75.9%	95.0%	---	---	---	---
Conc. (Cv)	ppm	17.8	21.3	9.1	---	---	---	---

Trial 4.3.53 Ultrasound Power: 20 W, Air Flow: 12 lpm

Droplet size distributions - Effect of Ultrasound

U/S Power: **20 W**
Air flow: **12 lpm**

Legend: Inlet — Outlet, U/S Off (Expt.) — Outlet, U/S On (Expt.)

Droplet size distributions - Expt. and Model

U/S Power: **20 W**
Air flow: **12 lpm**

Legend: Inlet — Outlet, U/S On (Expt.) — Outlet, U/S On (Model α=0.04) — Outlet, U/S On (Model α=0.001)
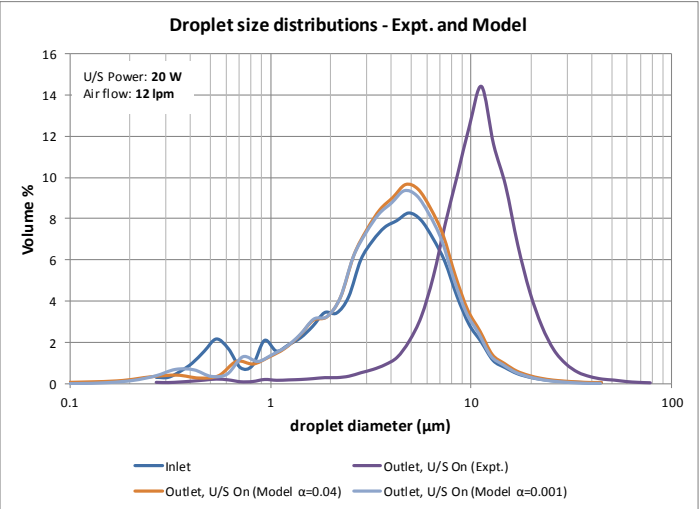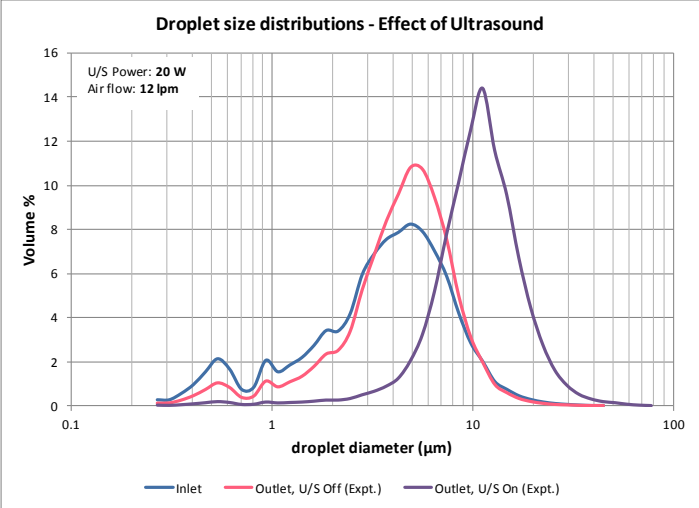
| Experiment Date | 29/05/2014 |
| Time | 15:19:22 - 15:27:25 |

Conduit Properties	Unit	Value
Diameter	mm	100
Length	mm	300

U/S Field	Unit	Value
Frequency	kHz	21.7
Power	W	20

Parameter	Unit	INLET	Experimental Results at OUTLET		Model Results at OUTLET			
			U/S Off	U/S On	U/S Off		U/S On	
					α = 0.04	α = 0.001	α = 0.04	α = 0.001
Air Properties								
Flow rate	lpm	12	---	---	11.59	11.59	11.59	11.59
Temp.	°C	21.75	17.1	20.8	8.8	8.8	9.2	9.3
Rel. Hum.		0.08215	0.927	0.94	1.002	1.000	1.002	1.000
Sp. Humidity	g/kg	1.32	11.35	14.57	7.08	7.08	7.28	7.28
Water Droplet Properties								
Flow rate	ml/min	0.359	---	---	0.276	0.277	0.274	0.274
Temp.	°C	24.45	---	---	8.8	8.8	9.3	9.2
Length to end of calculation					2	14	1	12

Parameter	Unit	INLET	Experimental Results at OUTLET		Model Results at OUTLET			
			U/S Off	U/S On	U/S Off		U/S On	
					α = 0.04	α = 0.001	α = 0.04	α = 0.001
Dv(10)	(µm)	0.93	1.65	5.75	1.63	1.46	1.61	1.44
Dv(50)	(µm)	3.90	4.62	10.80	4.55	4.44	4.55	4.44
Dv(90)	(µm)	8.51	8.48	18.77	9.07	9.01	9.08	9.01
Span		1.94	1.48	1.21	1.64	1.70	1.64	1.71
D[3][2]	(µm)	2.17	2.95	7.90	3.03	2.68	2.97	2.64
D[4][3]	(µm)	4.53	4.99	11.77	5.07	4.91	5.05	4.88
% Transm.		71.1%	81.4%	95.2%	---	---	---	---
Conc. (Cv)	ppm	17.8	15.0	10.2	---	---	---	---

Trial 4.3.54 Ultrasound Power: 20 W, Air Flow: 15 lpm

Droplet size distributions - Effect of Ultrasound

U/S Power: **20 W**
Air flow: **15 lpm**

Legend: Inlet — Outlet, U/S Off (Expt.) — Outlet, U/S On (Expt.)

Droplet size distributions - Expt. and Model

U/S Power: **20 W**
Air flow: **15 lpm**

Legend: Inlet — Outlet, U/S On (Expt.) — Outlet, U/S On (Model α=0.04) — Outlet, U/S On (Model α=0.001)
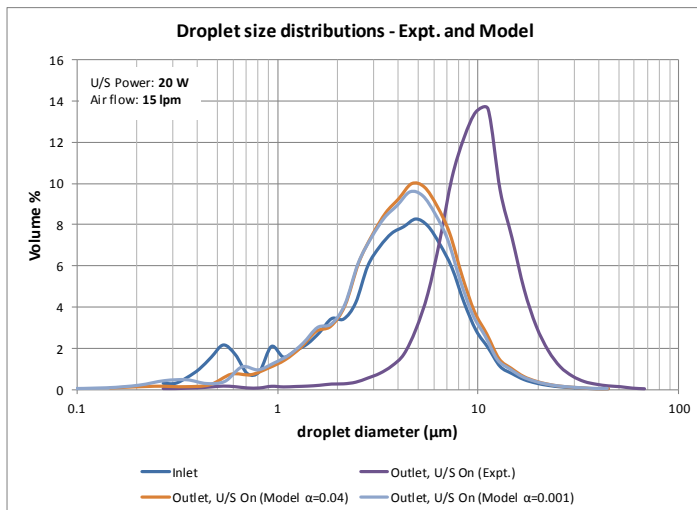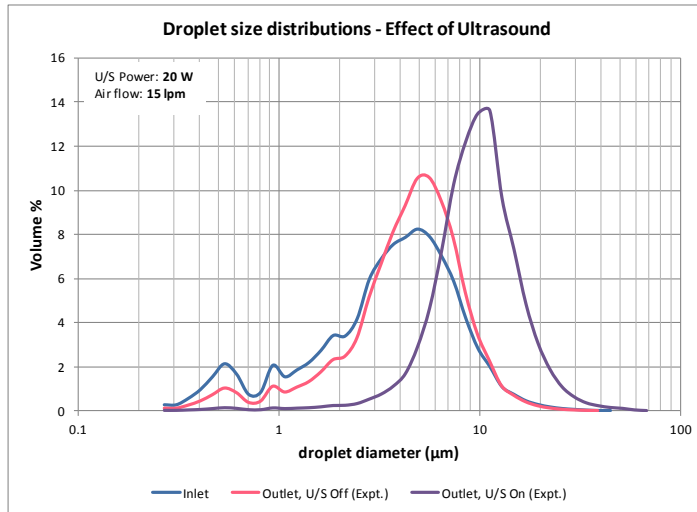
| Experiment Date | 29/05/2014 |
| Time | 15:41:11 - 15:44:05 |

Conduit Properties	Unit	Value
Diameter	mm	100
Length	mm	300

U/S Field	Unit	Value
Frequency	kHz	21.7
Power	W	20

Parameter	Unit	INLET	Experimental Results at OUTLET		Model Results at OUTLET			
					U/S Off		U/S On	
			U/S Off	U/S On	α = 0.04	α = 0.001	α = 0.04	α = 0.001
Air Properties								
Flow rate	lpm	14.9	---	---	14.39	14.39	14.38	14.38
Temp.	°C	21.55	16.6	19.6	8.6	8.6	8.9	8.9
Rel. Hum.		0.0789	0.924	0.935	1.002	1.000	1.002	1.000
Sp. Humidity	g/kg	1.25	10.95	13.43	6.97	6.97	7.11	7.11
Water Droplet Properties								
Flow rate	ml/min	0.359	---	---	0.257	0.257	0.255	0.256
Temp.	°C	24.7	---	---	8.6	8.6	8.9	8.9
Length to end of calculation					2	24	2	21

Parameter	Unit	INLET	Experimental Results at OUTLET		Model Results at OUTLET			
					U/S Off		U/S On	
			U/S Off	U/S On	α = 0.04	α = 0.001	α = 0.04	α = 0.001
Dv(10)	(µm)	0.93	1.67	5.39	1.82	1.62	1.79	1.59
Dv(50)	(µm)	3.90	4.70	9.75	4.71	4.58	4.71	4.57
Dv(90)	(µm)	8.51	8.77	16.96	9.28	9.16	9.29	9.15
Span		1.94	1.51	1.19	1.58	1.65	1.59	1.66
D[3][2]	(µm)	2.17	2.99	7.66	3.28	2.88	3.21	2.82
D[4][3]	(µm)	4.53	5.11	10.68	5.19	5.00	5.17	4.96
% Transm.		71.1%	86.8%	94.2%	---	---	---	---
Conc. (Cv)	ppm	17.8	10.4	11.8	---	---	---	---

Trial 4.3.55 Ultrasound Power: 20 W, Air Flow: 18 lpm

Droplet size distributions - Effect of Ultrasound

U/S Power: **20 W**
Air flow: **18 lpm**

Legend: Inlet — Outlet, U/S Off (Expt.) — Outlet, U/S On (Expt.)

Droplet size distributions - Expt. and Model

U/S Power: **20 W**
Air flow: **18 lpm**

Legend: Inlet — Outlet, U/S On (Expt.) — Outlet, U/S On (Model α=0.04) — Outlet, U/S On (Model α=0.001)
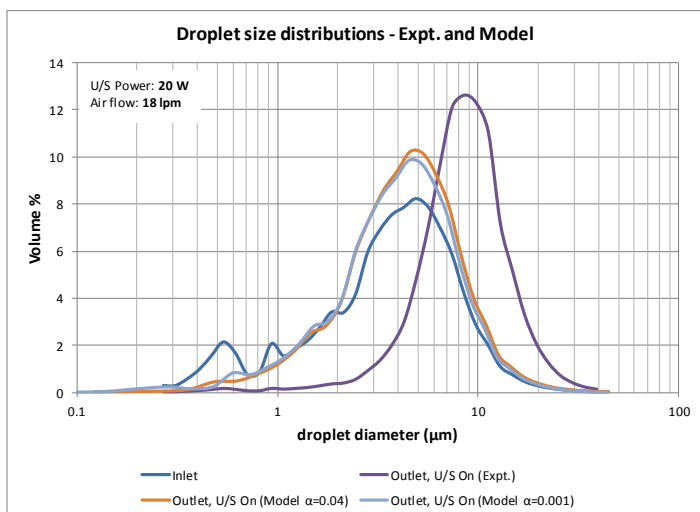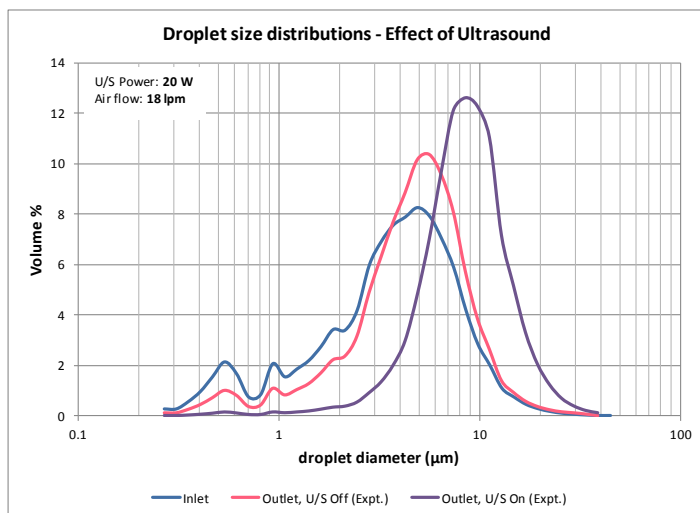
Experiment Date	29/05/2014	
Time	15:59:10 - 16:04:04	

Conduit Properties	Unit	Value
Diameter	mm	100
Length	mm	300

U/S Field	Unit	Value
Frequency	kHz	21.7
Power	W	20

Parameter	Unit	INLET	Experimental Results at OUTLET		Model Results at OUTLET			
			U/S Off	U/S On	U/S Off		U/S On	
					α = 0.04	α = 0.001	α = 0.04	α = 0.001
Air Properties								
Flow rate	lpm	17.9	---	---	17.28	17.28	17.28	17.28
Temp.	°C	21.35	15.9	17.9	8.6	8.6	8.7	8.7
Rel. Hum.		0.08355	0.918	0.93	1.001	1.000	1.001	1.000
Sp. Humidity	g/kg	1.31	10.40	11.99	6.96	6.96	7.00	7.00
Water Droplet Properties								
Flow rate	ml/min	0.359	---	---	0.238	0.239	0.238	0.238
Temp.	°C	25	---	---	8.6	8.6	8.7	8.7
Length to end of calculation					3	40	2	35

Parameter	Unit	INLET	Experimental Results at OUTLET		Model Results at OUTLET			
			U/S Off	U/S On	U/S Off		U/S On	
					α = 0.04	α = 0.001	α = 0.04	α = 0.001
Dv(10)	(µm)	0.93	1.70	4.53	2.01	1.78	1.96	1.73
Dv(50)	(µm)	3.90	4.84	8.51	4.57	4.12	4.53	4.09
Dv(90)	(µm)	8.51	9.23	15.04	9.51	9.37	9.50	9.34
Span		1.94	1.55	1.24	1.64	1.84	1.66	1.86
D[3][2]	(µm)	2.17	3.05	6.66	3.46	3.08	3.40	3.00
D[4][3]	(µm)	4.53	5.36	9.31	5.31	5.09	5.27	5.04
% Transm.		71.1%	89.4%	94.5%	---	---	---	---
Conc. (Cv)	ppm	17.8	8.5	9.7	---	---	---	---

Trial 4.3.56 Ultrasound Power: 20 W, Air Flow: 20 lpm

Droplet size distributions - Effect of Ultrasound

U/S Power: **20 W**
Air flow: **20 lpm**

Legend: Inlet — Outlet, U/S Off (Expt.) — Outlet, U/S On (Expt.)

Droplet size distributions - Expt. and Model

U/S Power: **20 W**
Air flow: **20 lpm**

Legend: Inlet — Outlet, U/S On (Expt.) — Outlet, U/S On (Model α=0.04) — Outlet, U/S On (Model α=0.001)
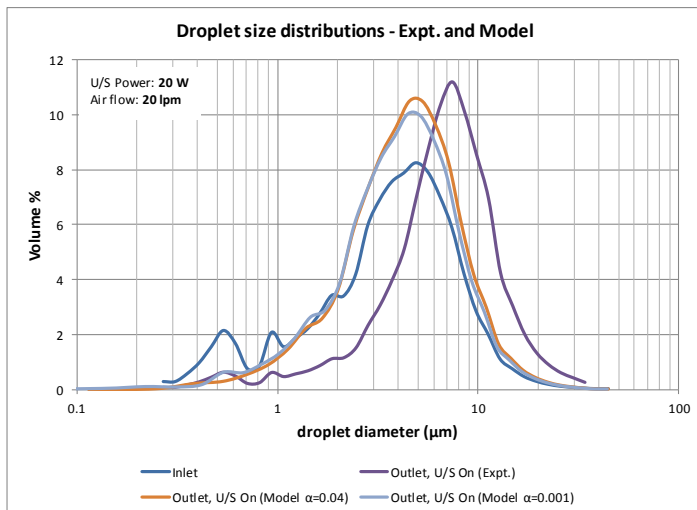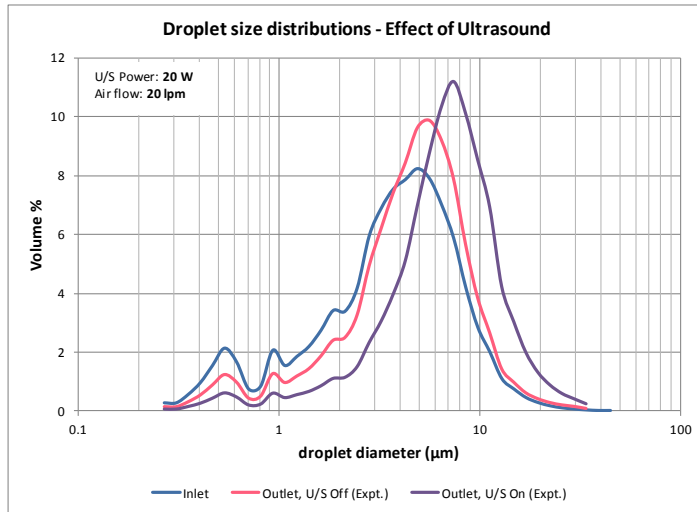
| Experiment Date | 29/05/2014 |
| Time | 16:11:14 - 16:16:30 |

Conduit Properties	Unit	Value
Diameter	mm	100
Length	mm	300

U/S Field	Unit	Value
Frequency	kHz	21.7
Power	W	20

Parameter	Unit	INLET	Experimental Results at OUTLET		Model Results at OUTLET			
			U/S Off	U/S On	U/S Off		U/S On	
					α = 0.04	α = 0.001	α = 0.04	α = 0.001
Air Properties								
Flow rate	lpm	20.1	---	---	19.39	19.39	19.39	19.39
Temp.	°C	21.6	15.2	16.2	8.7	8.7	8.7	8.7
Rel. Hum.		0.08355	0.919	0.925	1.001	1.000	1.000	1.000
Sp. Humidity	g/kg	1.33	9.94	10.68	7.02	7.02	7.02	7.02
Water Droplet Properties								
Flow rate	ml/min	0.359	---	---	0.223	0.223	0.223	0.223
Temp.	°C	24.75	---	---	8.7	8.7	8.7	8.7
Length to end of calculation					3	58	2	50

Parameter	Unit	INLET	Experimental Results at OUTLET		Model Results at OUTLET			
			U/S Off	U/S On	U/S Off		U/S On	
					α = 0.04	α = 0.001	α = 0.04	α = 0.001
Dv(10)	(µm)	0.93	1.49	2.68	2.06	1.67	1.98	1.62
Dv(50)	(µm)	3.90	4.76	6.87	4.37	4.22	4.35	4.19
Dv(90)	(µm)	8.51	9.35	13.18	9.70	9.54	9.68	9.51
Span		1.94	1.65	1.53	1.75	1.86	1.77	1.88
D[3][2]	(µm)	2.17	2.85	4.28	3.58	3.23	3.52	3.15
D[4][3]	(µm)	4.53	5.33	7.64	5.40	5.15	5.36	5.10
% Transm.		71.1%	91.1%	94.4%	---	---	---	---
Conc. (Cv)	ppm	17.8	6.5	6.3	---	---	---	---

Bibliography

1.   Mayo-Clinic-Staff. *Sleep, Sleep Apnea*. 2007 [cited 2009 15 Feb]; Available from: http://www.mayoclinic.com/health/obstructive-sleep-apnea/DS00968.
2.   America-Sleep-Apnea-Association. *Sleep Apnea Information*. 2008 [cited 2009 15 Feb]; Available from: http://www.sleepapnea.org/info/index.html.
3.   Esmond, G.M.C., *Non-invasive respiratory support techniques : oxygen therapy, non-invasive ventilation, and CPAP*. 2009, Chichester, West Sussex; Ames, Iowa: Wiley-Blackwell.
4.   Massie, C.A., et al., *Effects of humidification on nasal symptoms and compliance in sleep apnea patients using continuous positive airway pressure.* Chest, 1999. **116**(2): p. 403-408.
5.   Leonelli, C. and T.J. Mason, *Microwave and ultrasonic processing: Now a realistic option for industry.* Chemical Engineering and Processing: Process Intensification, 2010. **49**(9): p. 885-900.
6.   Legay, M., et al., *Enhancement of heat transfer by ultrasound: Review and recent advances.* International Journal of Chemical Engineering, 2011.
7.   Yarin, A.L., et al., *Evaporation of acoustically levitated droplets.* Journal of Fluid Mechanics, 1999. **399**: p. 151-204.
8.   Sabarez, H.T., J.A. Gallego-Juarez, and E. Riera, *Ultrasonic-Assisted Convective Drying of Apple Slices.* Drying Technology, 2012. **30**(9): p. 989-997.
9.   Javaheri, E. and W.H. Finlay, *Size manipulation of hygroscopic saline droplets: Application to respiratory drug delivery.* International Journal of Heat and Mass Transfer, 2013. **67**: p. 690-695.
10.   Wood, E.W. and A.L. Loomis, *XXXVIII. <i>The physical and biological effects of high-frequency sound-waves of great intensity</i>.* Philosophical Magazine Series 7, 1927. **4**(22): p. 417 - 436.
11.   Giovannini, A., et al. *Evaluation and design of new piezoelectrical droplets generator*. in *Proceedings of IEEE Ultrasonics Symposium, 1-4 Nov. 1994*. 1994. New York, NY, USA: IEEE.
12.   Al-Suleimani, Y., A.J. Yule, and A.P. Collins. *How orderly is ultrasonic atomization?* in *ILASS-Europe '99*. 1999. Toulouse.
13.   Ghazanfari, T., et al., *The influence of fluid physicochemical properties on vibrating-mesh nebulization.* International Journal of Pharmaceutics, 2007. **339**(1-2): p. 103-111.
14.   Toda, K. and Y. Akimura, *An ultrasonic atomizing device using coupled-mode vibration.* Review of Scientific Instruments, 1994. **65**(10): p. 3276-3278.
15.   Waldrep, J.C. and R. Dhand, *Advanced nebulizer designs employing vibrating mesh/aperture plate technologies for aerosol generation.* Current Drug Delivery, 2008. **5**(2): p. 114-119.
16.   Harada, T., et al., *Droplet generation using a torsional Langevin-type transducer and a micropore plate.* Sensors and Actuators, A: Physical, 2009. **155**(1): p. 168-174.
17.   Shen, S.C., *A new cymbal-shaped high power microactuator for nebulizer application.* Microelectronic Engineering, 2010. **87**(2): p. 89-97.
18.   Tsai, S.C., P. Childs, and P. Luu, *Ultrasound-modulated two-fluid atomization of a water jet.* AIChE Journal, 1996. **42**(Compendex): p. 3340-3350.

19.   Kurosawa, M., A. Futami, and T. Higuchi. *Characteristics of liquids atomization using surface acoustic wave*. in *Proceedings of the 1997 International Conference on Solid-State Sensors and Actuators. Part 2 (of 2), June 16, 1997 - June 19, 1997*. 1997. Chicago, IL, USA: IEEE.

20.   Tokumitsu, K., D. Koyama, and K. Nakamura. *Efficient ultrasonic atomization using a vibrating small gap*. in *2009 IEEE International Ultrasonics Symposium, IUS 2009, September 20, 2009 - September 23, 2009*. 2009. Rome, Italy: Institute of Electrical and Electronics Engineers Inc.

21.   Lang, R.J., *Ultrasonic Atomization of Liquids.* The Journal of the Acoustical Society of America, 1962. **34**(1): p. 6-8.

22.   Yasuda, K., et al. *Analysis of concentration characteristics in ultrasonic atomization by droplet diameter distribution*. 2005. Elsevier.

23.   Barreras, F., H. Amaveda, and A. Lozano, *Transient high-frequency ultrasonic water atomization.* Experiments in Fluids, 2002. **33**(3): p. 405-13.

24.   Dobre, M. and L. Bolle, *Practical design of ultrasonic spray devices: experimental testing of several atomizer geometries.* Experimental Thermal and Fluid Science, 2002. **26**(2-4): p. 205-211.

25.   Tsai, S.C., et al., *Silicon-based megahertz ultrasonic nozzles for production of monodisperse micrometer-sized droplets.* IEEE Transactions on Ultrasonics, Ferroelectrics and Frequency Control, 2009. **56**(9): p. 1968-79.

26.   Topp, M.N., *Ultrasonic atomization-a photographic study of the mechanism of disintegration.* Journal of Aerosol Science, 1973. **4**(1): p. 17-20, IN1-IN7, 21-25.

27.   Boguslavskii, Y. and O.K. Eknadiosyants, *PHYSICAL MECHANISM OF ACOUSTIC ATOMIZATION OF LIQUID.* Akusticheskij Zhurnal, 1969. **15**(1): p. 17-24.

28.   Pandit, A.B., et al., *Ultrasonic atomization: Effect of liquid phase properties.* Ultrasonics, 2006. **44**(Copyright 2006, The Institution of Engineering and Technology): p. 146-58.

29.   Yule, A.J. and Y. Al-Suleimani, *On droplet formation from capillary waves on a vibrating surface.* Proceedings of the Royal Society A: Mathematical, Physical and Engineering Sciences, 2000. **456**(1997): p. 1069-1085.

30.   Rajan, R. and A.B. Pandit, *Correlations to predict droplet size in ultrasonic atomisation.* Ultrasonics, 2001. **39**(4): p. 235-55.

31.   Söllner, K., *Experiments to demonstrate cavitation caused by ultrasonic waves.* Transactions of the Faraday Society, 1936. **32**: p. 1537-1539.

32.   Perron, R.R., *The Design and Application of a Reliable Ultrasonic Atomizer.* Sonics and Ultrasonics, IEEE Transactions on, 1967. **14**(4): p. 149-152.

33.   Dumouchel, C., D. Sindayihebura, and L. Bolle, *Application of the maximum entropy formalism on sprays produced by ultrasonic atomizers.* Particle and Particle Systems Characterization, 2003. **20**(2): p. 150-161.

34.   Lozano, A., et al., *High-frequency ultrasonic atomization with pulsed excitation.* Journal of Fluids Engineering, Transactions of the ASME, 2003. **125**(Compendex): p. 941-945.

35.   Maehara, N., S. Ueha, and E. Mori, *Influence of the vibrating system of a multipinhole-plate ultrasonic nebulizer on its performance.* Review of Scientific Instruments, 1986. **57**(Copyright 1987, IEE): p. 2870-6.

36.   Meacham, J.M., et al., *Droplet formation and ejection from a micromachined ultrasonic droplet generator: Visualization and scaling.* Physics of Fluids, 2005. **17**(10).

37.	Toda, K. and J. Ishii, *Operation performance of self-oscillation ultrasonic vibrating device for liquid atomization.* Japanese Journal of Applied Physics, Part 1: Regular Papers & Short Notes & Review Papers, 1995. **34**(9 B): p. 5332-5334.

38.	Percin, G. and B.T. Khuri-Yakub, *Piezoelectrically actuated flextensional micromachined ultrasound droplet ejectors.* Ultrasonics, Ferroelectrics and Frequency Control, IEEE Transactions on, 2002. **49**(6): p. 756-766.

39.	Chang, R. and E.J. Davis, *Knudsen aerosol evaporation.* Journal of Colloid and Interface Science, 1976. **54**(3): p. 352-363.

40.	G.A, F., *The size of soluble aerosol particles as a function of the humidity of the air. Application to the human respiratory tract.* Journal of Aerosol Science, 1977. **8**(4): p. 251-267.

41.	Porstendorfer, J., G. Robig, and J. Gebhart, *Effect of evaporation on the size distribution of nebulized aerosols.* Journal of Aerosol Science, 1977. **8**(6): p. 371-80.

42.	Eisner, A.D., R.C. Graham, and T.B. Martonen, *Coupled mass and energy transport phenomena in aerosol/vapor-laden gases-I. theory of the hygroscopic aerosol effects on temperature and relative humidity patterns of inspired air.* Journal of Aerosol Science, 1990. **21**(7): p. 833-848.

43.	Ferron, G.A. and S.C. Soderholm, *Estimation of the times for evaporation of pure water droplets and for stabilization of salt solution particles.* Journal of Aerosol Science, 1990. **21**(3): p. 415-429.

44.	Graham, R.C. and A.D. Eisner, *Coupled mass and energy transport phenomena in aerosol/vapor-laden gases-II. computer modeling of water vapor/droplet interaction and entrainment.* Journal of Aerosol Science, 1990. **21**(7): p. 849-858.

45.	Tsang, T.H., S.M. Cook, and M.E. Marra, *Dynamic behavior of condensation and evaporation of polydisperse volatile aerosols.* Aerosol science and technology : the journal of the American Association for Aerosol Research, 1990. **12**(2): p. 386-398.

46.	Tsang, T.H. and L.K. Huang, *On a Petrov-Galerkin finite element method for evaporation of polydisperse aerosols.* Aerosol Science and Technology, 1990. **12**(3): p. 578-597.

47.	Reist, P.C., *Aerosol science and technology.* 1993, New York: McGraw-Hill.

48.	Vesala, T., et al., *Models for condensational growth and evaporation of binary aerosol particles.* Journal of Aerosol Science, 1997. **28**(4): p. 565-598.

49.	Miller, R.S., K. Harstad, and J. Bellan, *Evaluation of equilibrium and non-equilibrium evaporation models for many-droplet gas-liquid flow simulations.* International Journal of Multiphase Flow, 1998. **24**(6): p. 1025-55.

50.	Hinds, W.C., *Aerosol technology: properties, behavior, and measurement of airborne particles* 2nd ed. ed. 1999, New York: Wiley Interscience. 483.

51.	Finlay, W.H., *The Mechanics of Inhaled Pharmaceutical Aerosols : An Introduction.* 2001, San Diego: Academic Press.

52.	Moyle, A.M., P.M. Smidansky, and D. Lamb, *Laboratory Studies of Water Droplet Evaporation Kinetics*, in *12th Conference on Cloud Physics.* 2006: Madison, WI.

53.	Sazhin, S.S., *Advanced models of fuel droplet heating and evaporation.* Progress in Energy and Combustion Science, 2006. **32**(2): p. 162-214.

54.	McDermott, R., *A formulation and numerical method for treating droplet evaporation*, B.a.F.R. Laboratory, Editor. 2007.

55.	Saleh, R. and A. Shihadeh, *Hygroscopic growth and evaporation in an aerosol with boundary heat and mass transfer.* Journal of aerosol science, 2007. **38**(1): p. 1-16.

56.	Dushin, V.R., et al., *Mathematical simulation for non-equilibrium droplet evaporation.* Acta Astronautica, 2008. **63**(11-12): p. 1360-1371.

57.	Cochet, M., et al., *Evaporation of polydispersed droplets in a highly turbulent channel flow.* Experiments in Fluids, 2009. **47**(3): p. 379-394.

58.	Tonini, S., *Heat and mass transfer modeling of submicrometer droplets under atmospheric pressure conditions.* Atomization and Sprays, 2009. **19**(9): p. 833-846.

59.	Rao, N., N. Kadrichu, and B. Ament, *Application of a droplet evaporation model to aerodynamic size measurement of drug aerosols generated by a vibrating mesh nebulizer.* Journal of Aerosol Medicine and Pulmonary Drug Delivery, 2010. **23**(5): p. 295-302.

60.	Yongyingsakthavorn, P., et al., *Prediction of evaporation time and rate of water sprays from their local drop diameter distributions and liquid volume concentration.* 2011. **21**(2): p. 159-165.

61.	Kim, K.H., et al., *Analysis of water droplet evaporation in a gas turbine inlet fogging process.* Applied Thermal Engineering, 2012. **33–34**(0): p. 62-69.

62.	Nilius, G., et al., *Impact of a controlled heated breathing tube humidifier on sleep quality during CPAP therapy in a cool sleeping environment.* The European respiratory journal : official journal of the European Society for Clinical Respiratory Physiology, 2008. **31**(4): p. 830-836.

63.	Hiromitsu, N. and O. Kawaguchi, *Evaporation rate of a suspended droplet in hot air flow containing water vapor (1st report, droplet of water and water-soluble liquid).* Nippon Kikai Gakkai Ronbunshu, B Hen/Transactions of the Japan Society of Mechanical Engineers, Part B, 1997. **63**(609): p. 1680-1686.

64.	Sheu, W.J. and N.C. Liou, *Effect of temporal variation of pressure on vaporization of liquid droplets.* International Journal of Heat and Mass Transfer, 1999. **42**(21): p. 4043-54.

65.	Belarbi, R., C. Ghiaus, and F. Allard, *Modeling of water spray evaporation: Application to passive cooling of buildings.* Solar Energy, 2006. **80**(12): p. 1540-1552.

66.	Smolík, J., et al., *Evaporation of ventilated water droplet: connection between heat and mass transfer.* Journal of Aerosol Science, 2001. **32**(6): p. 739-748.

67.	Martin, A.R., et al., *An in vitro assessment of aerosol delivery through patient breathing circuits used with medical air or a helium-oxygen mixture.* Journal of Aerosol Medicine and Pulmonary Drug Delivery, 2011. **24**(5): p. 225-234.

68.	Tate, R.W., *Immersion sampling of spray droplets.* AIChE Journal, 1961. **7**(4): p. 574-577.

69.	Azzopardi, B.J., *Measurement of drop sizes.* International Journal of Heat and Mass Transfer, 1979. **22**(9): p. 1245-1279.

70.	Lee Black, D., M.Q. McQuay, and M.P. Bonin, *Laser-based techniques for particle-size measurement: A review of sizing methods and their industrial applications.* Progress in Energy and Combustion Science, 1996. **22**(3): p. 267-306.

71.   Corcoran, T.E., et al., *Optical measurement of nebulizer sprays: A quantitative comparison of diffraction, phase Doppler interferometry, and time of flight techniques.* Journal of Aerosol Science, 2000. **31**(1): p. 35-50.

72.   Lim, E.W.C., et al., *Experimental and computational studies of liquid aerosol evaporation.* Journal of Aerosol Science, 2008. **39**(7): p. 618-634.

73.   Finlay, W.H. and K.W. Stapleton, *The effect on regional lung deposition of coupled heat and mass transfer between hygroscopic droplets and their surrounding phase.* Journal of Aerosol Science, 1995. **26**(4): p. 655-670.

74.   Xu, Z., Y. Xiao, and Y. Wang, *Experimental and theoretical studies on air humidification by a water spray at elevated pressure.* Applied Thermal Engineering, 2007. **27**(14-15): p. 2549-2558.

75.   Packirisamy, M., et al., *A polyimide based resistive humidity sensor.* Sensor Review, 2005. **25**(Copyright 2005, IEE): p. 271-6.

76.   Lang, W., et al. *Humidity measurement by dynamic dew-point detection*. in *IEEE International Solid-State Sensors and Actuators Conference, 8-12 June 2003*. 2003. Piscataway, NJ, USA: IEEE.

77.   Qiu, Y.Y., et al. *A CMOS humidity sensor with on-chip calibration*. in *Proceedings of EUROSENSORS. 14th European Conference, 27-30 Aug. 2000*. 2001. Switzerland: Elsevier.

78.   Frazier, G.C., *Water droplet vaporization in humid atmospheres.* Canadian Journal of Chemical Engineering, 1977. **55**(6): p. 678-82.

79.   Kincaid, D.C. and T.S. Longley, *A WATER DROPLET EVAPORATION AND TEMPERATURE MODEL.* Transactions of the Asae, 1989. **32**(2): p. 457-463.

80.   Fuchs, N.A. and A.G. Sutugin, *Highly dispersed aerosols*. 1970, Ann Arbor: Ann Arbor Science Publishers.

81.   Amani, E. and M.R.H. Nobari, *A calibrated evaporation model for the numerical study of evaporation delay in liquid fuel sprays.* International journal of heat and mass transfer, 2013. **56**(1–2): p. 45-58.

82.   Jangi, M. and H. Kobayashi, *Heat and mass transfer of a fuel droplet evaporating in oscillatory flow.* International Journal of Heat and Fluid Flow, 2009. **30**(4): p. 729-740.

83.   Worth Longest, P. and M. Hindle, *CFD simulations of enhanced condensational growth (ECG) applied to respiratory drug delivery with comparisons to in vitro data.* Journal of aerosol science, 2010. **41**(8): p. 805-820.

84.   Dickinson, D.R. and W.R. Marshall, *The rates of evaporation of sprays.* AIChE Journal, 1968. **14**(4): p. 541-552.

85.   Mezhericher, M., A. Levy, and I. Borde, *Modeling of droplet drying in spray chambers using 2D and 3D computational fluid dynamics.* Drying Technology, 2009. **27**(3): p. 359-370.

86.   Mezhericher, M., A. Levy, and I. Borde, *Spray drying modelling based on advanced droplet drying kinetics.* Chemical Engineering and Processing: Process Intensification, 2010. **49**(11): p. 1205-1213.

87.   Kuz, V.A., *Evaporation of small drops.* Journal of Applied Physics, 1991. **69**(Copyright 1991, IEE): p. 7034-6.

88.   Crowe, C.T. *Conservation equations for vapor-droplet flows*. in *Proceedings of the 1976 Heat Transfer and Fluid Mechanics Institute, 21-23 June 1976*. 1976. Stanford, CA, USA: Stanford Univ. Press.

89. Kulmala, M., et al., *Mass transfer from a drop--II. Theoretical analysis of temperature dependent mass flux correlation.* International Journal of Heat and Mass Transfer, 1995. **38**(9): p. 1705-1708.

90. Levenspiel, O., *Chemical reaction engineering*. 1972, New York: Wiley.

91. Mason, T.J., *Developments in ultrasound—Non-medical.* Progress in biophysics and molecular biology, 2007. **93**(1–3): p. 166-175.

92. Harvey, A.P., M.R. Mackley, and T. Seliger. *Process intensification of biodiesel production using a continuous oscillatory flow reactor*. 2003. John Wiley and Sons Ltd.

93. Trinh, E.H., *Compact acoustic levitation device for studies in fluid dynamics and material science in the laboratory and microgravity.* Review of Scientific Instruments, 1985. **56**(11): p. 2059.

94. Yarin, A.L., et al., *Acoustically levitated drops: Drop oscillation and break-up driven by ultrasound modulation.* International Journal of Multiphase Flow, 2002. **28**(6): p. 887-910.

95. Rayleigh, L., *On the Capillary Phenomena of Jets.* Proceedings of the Royal Society of London, 1879. **29**(196-199): p. 71-97.

96. Foote, G.B., *A numerical method for studying liquid drop behavior: simple oscillation.* Journal of Computational Physics, 1973. **11**(4): p. 507-530.

97. Lundgren, T.S. and N.N. Mansour, *OSCILLATIONS OF DROPS IN ZERO GRAVITY WITH WEAK VISCOUS EFFECTS.* Journal of Fluid Mechanics, 1988. **194**(Compendex): p. 479-510.

98. Patzek, T.W., et al., *Nonlinear oscillations of inviscid free drops.* Journal of Computational Physics, 1991. **97**(2): p. 489-515.

99. Basaran, O.A., *Nonlinear oscillations of viscous liquid drops.* Journal of Fluid Mechanics, 1992. **241**: p. 169-198.

100. Becker, E., W.J. Hiller, and T.A. Kowalewski, *Experimental and theoretical investigation of large-amplitude oscillations of liquid droplets.* Journal of Fluid Mechanics, 1991. **231**: p. 189-210.

101. Tang, H.H.K. and C.Y. Wong, *Vibration of a viscous liquid sphere.* Journal of Physics A: General Physics, 1974. **7**(9): p. 1038-1050.

102. Mashayek, F. and N. Ashgriz, *Nonlinear oscillations of drops with internal circulation.* Physics of Fluids, 1998. **10**(5): p. 1071-1082.

103. Trinh, E. and T.G. Wang, *LARGE-AMPLITUDE FREE AND DRIVEN DROP-SHAPE OSCILLATIONS: EXPERIMENTAL OBSERVATIONS.* Journal of Fluid Mechanics, 1982. **122**(Compendex): p. 315-338.

104. Anilkumar, A.V., C.P. Lee, and T.G. Wang, *Stability of an acoustically levitated and flattened drop: an experimental study.* Physics of Fluids A (Fluid Dynamics), 1993. **5**(11): p. 2763-74.

105. Shi, W.T., R.E. Apfel, and R.G. Holt, *INSTABILITY OF A DEFORMED LIQUID-DROP IN AN ACOUSTIC FIELD.* Physics of Fluids, 1995. **7**(11): p. 2601-2607.

106. Rein, M., *Phenomena of liquid drop impact on solid and liquid surfaces.* Fluid Dynamics Research, 1993. **12**(2): p. 61-93.

107. Rioboo, R., C. Tropea, and M. Marengo, *Outcomes from a drop impact on solid surfaces.* Atomization and Sprays, 2001. **11**(2): p. 155-165.

108. Yarin, A.L., *Drop impact dynamics: Splashing, spreading, receding, bouncing*. 2006. p. 159-192.

109. Moreira, A.L.N., et al., *Secondary atomization of water and isooctane drops impinging on tilted heated surfaces.* Experiments in Fluids, 2007. **43**(2-3): p. 297-313.

110. Burdukov, A.P. and V.E. Nakoryakov, *On mass transfer in an acoustic field.* Journal of Applied Mechanics and Technical Physics, 1966. **6**(2): p. 51-55.

111. Larsen, P.S. and J.W. Jensen, *Evaporation rates of drops in forced convection with superposed transverse sound field.* International Journal of Heat and Mass Transfer, 1978. **21**(4): p. 511-517.

112. Temkin, S., *Gasdynamic agglomeration of aerosols. I. Acoustic waves.* Physics of Fluids, 1994. **6**(7): p. 2294.

113. Sujith, R.I., et al., *An experimental investigation of the behavior of droplets in axial acoustic fields.* Journal of Vibration and Acoustics, Transactions of the ASME, 1997. **119**(3): p. 285-292.

114. Sujith, R.I., et al., *A theoretical investigation of the behavior of droplets in axial acoustic fields.* Journal of Vibration and Acoustics, Transactions of the ASME, 1999. **121**(3): p. 286-294.

115. Sujith, R.I., et al., *Experimental investigation of the evaporation of droplets in axial acoustic fields.* Journal of Propulsion and Power, 2000. **16**(2): p. 278-285.

116. García-Pérez, J.V., et al., *Modeling Ultrasonically Assisted Convective Drying of Eggplant.* Drying Technology, 2011. **29**(13): p. 1499-1509.

117. Ozuna, C., et al., *Improvement of water transport mechanisms during potato drying by applying ultrasound.* Journal of the science of food and agriculture, 2011. **91**(14): p. 2511-2517.

118. García-Pérez, J.V., et al., *Influence of the Applied Acoustic Energy on the Drying of Carrots and Lemon Peel.* Drying Technology, 2009. **27**(2): p. 281-287.

119. Garcia-Perez, J., et al., *Enhancement of Water Transport and Microstructural Changes Induced by High-Intensity Ultrasound Application on Orange Peel Drying.* Food and Bioprocess Technology, 2012. **5**(6): p. 2256-2265.

120. Gamboa-Santos, J., et al., *Air-borne ultrasound application in the convective drying of strawberry.* Journal of Food Engineering, 2014. **128**: p. 132-139.

121. Gopinath, A. and A.F. Mills, *Convective heat transfer from a sphere due to acoustic streaming.* Journal of Heat Transfer, 1993. **115**(2): p. 332-339.

122. Tian, Y. and R.E. Apfel, *A novel multiple drop levitator for the study of drop arrays.* Journal of Aerosol Science, 1996. **27**(5): p. 721-737.

123. Brenn, G., et al., *Investigation of droplet drying characteristics using an acoustic-aerodynamic levitator.* International Journal of Fluid Mechanics Research, 1997. **24**(Copyright 2001, IEE): p. 633-42.

124. Kawahara, N., et al., *Effect of acoustic streaming on the mass transfer from a sublimating sphere.* Physics of Fluids, 2000. **12**(4): p. 912-23.

125. Yarin, A.L., et al., *Drying of acoustically levitated droplets of liquid-solid suspensions: Evaporation and crust formation.* Physics of Fluids, 2002. **14**(7): p. 2289-98.

126. Bachalo, W.D. *Droplet Analysis Techniques: Their Selection and Applications*. in *ASTM Special Technical Publication*. 1984. Kansas City, MO, USA: ASTM.

127. Hedrih, K., V. Babovi, and D. Sarkovi, *An auxiliary size distribution model for the ultrasonically produced water droplets.* Experimental Thermal and Fluid Science, 2006. **30**(6): p. 559-564.

128. Yuan, J., et al., *Measurement and analysis of water mist droplet size based on machine vision.* Guangxue Xuebao/Acta Optica Sinica, 2009. **29**(10): p. 2842-2847.

129. Alderliesten, M., *MEAN PARTICLE DIAMETERS. FROM STATISTICAL DEFINITION TO PHYSICAL UNDERSTANDING.* Journal of biopharmaceutical statistics, 2005. **15**(2): p. 295-325.

130. Eischeid, T., *RE: NCU Transducers*. 2011, The Ultran Group: State College PA. p. 1.

131. Zahnd, J., *RE: High frequency air transducers*. 2011, APC International Ltd. p. 1.

132. Schindel, D.W., *RE: BAT Transducers*. 2013, MicroAcoustic Instruments Inc.: Quebec, Canada. p. 1.

133. ISO/IEC, *Acoustics -- Attenuation of sound during propagation outdoors -- Part 1: Calculation of the absorption of sound by the atmosphere*. 1993, ISO. p. 26.

134. Kinsler, L.E., *Fundamentals of acoustics*. 4 ed. 2000, New York: Wiley.

135. Arai, M., A. Ishii, and M. Saito, *Atomization behavior and energy analysis for a single droplet impinged on a surface oscillating with ultrasonic frequency.* Atomization and Sprays, 2007. **17**(Copyright 2009, The Institution of Engineering and Technology): p. 601-20.

136. Manzello, S.L. and J.C. Yang, *An experimental study of high Weber number impact of methoxy-nonafluorobutane C4F9OCH3 (HFE-7100) and n-heptane droplets on a heated solid surface.* International Journal of Heat and Mass Transfer, 2002. **45**(Copyright 2002, IEE): p. 3961-71.

137. Sikalo, S., C. Tropea, and E.N. Ganic, *Impact of droplets onto inclined surfaces.* Journal of Colloid and Interface Science, 2005. **286**(2): p. 661-669.

138. Moita, A.S. and A.L.N. Moreira, *Drop impacts onto cold and heated rigid surfaces: Morphological comparisons, disintegration limits and secondary atomization.* International Journal of Heat and Fluid Flow, 2007. **28**(4): p. 735-752.

139. Lewis, E.R., *The effect of surface tension (Kelvin effect) on the equilibrium radius of a hygroscopic aqueous aerosol particle.* Journal of Aerosol Science, 2006. **37**(Compendex): p. 1605-1617.

140. Cengel, Y.A., *Heat and mass transfer: a practical approach*. 2007, Boston: McGraw-Hill.

141. Çengel, Y.A. and M.A. Boles, *Thermodynamics : an engineering approach*. 6th ed. McGraw-Hill series in mechanical engineering. 2008, Boston: McGraw-Hill Higher Education. xxxi, 1018 p.

142. Enright, W.H., T.E. Hull, and B. Lindberg, *Comparing numerical methods for stiff systems of O.D.E:s.* BIT Numerical Mathematics, 1975. **15**(1): p. 10-48.

143. Herrmann, S., H.-J. Kretzschmar, and D.P. Gatley, *Thermodynamic properties of real moist air, dry air, steam, water, and ice (RP-1485).* HVAC and R Research, 2009. **15**(5): p. 961-986.

144. Wagner, W., et al., *The IAPWS Industrial Formulation 1997 for the thermodynamic properties of water and steam.* Transactions of the ASME. Journal of Engineering for Gas Turbines and Power, 2000. **122**(1): p. 150-82.

145. Fatkin, J., *The Particle Size Measurement of Sprays by Laser Diffraction*. Malvern Instruments. p. 8.

146. Feng, H., W. Yang, and T. Hielscher, *Power Ultrasound.* Food Science and Technology International, 2008. **14**(5): p. 433-436.

147. Cárcel, J.A., et al., *Influence of High-Intensity Ultrasound on Drying Kinetics of Persimmon.* Drying Technology, 2007. **25**(1): p. 185-193.

148. Carcel, J.A., et al., *Improvement of Convective Drying of Carrot by Applying Power UltrasoundInfluence of Mass Load Density.* Drying Technology, 2011. **29**(2): p. 174-182.

149. Riera, E., et al., *Computational Study of Ultrasound-Assisted Drying of Food Materials*, in *Innovative Food Processing Technologies: Advances in Multiphysics Simulation*, K. Knoerzer, et al., Editors. 2011, Blackwell Publishing Ltd. p. 265-301.

150. Marek, R. and J. Straub, *Analysis of the evaporation coefficient and the condensation coefficient of water.* International Journal of Heat and Mass Transfer, 2001. **44**(1): p. 39-53.

151. Deguchi, S., et al., *Enhancement of heat transfer rate in a falling film layer by ultrasonic irradiation.* Journal of Chemical Engineering of Japan, 1995. **28**(5): p. 570-575.

152. Ondas, M.S. and D.A. Santavicca. *Study of droplet vaporization in a longitudinal acoustic field using exciplex vapor/liquid visualization*. in *American Society of Mechanical Engineers, Fluids Engineering Division (Publication) FED*. 1997. Dallas, TX, USA: ASME.

153. Yao, Y., *Using power ultrasound for the regeneration of dehumidizers in desiccant air-conditioning systems: A review of prospective studies and unexplored issues.* Renewable and Sustainable Energy Reviews, 2010. **14**(7): p. 1860-1873.

154. Guan, G., et al., *Simulation of mass transfer from an oscillating microdroplet.* International journal of heat and mass transfer, 2005. **48**(9): p. 1705-1715.